AN EXPERIMENTAL TECHNIQUE FOR DETERMINING CYCLE-RESOLVED PRE-COMBUSTION IN-CYLINDER COMPOSITION AND ITS APPLICATION TOWARDS THE UNDERSTANDING OF DIESEL ENGINE EMISSIONS DURING TRANSIENT OPERATION

by

Jonathan Ray Hagena

A dissertation submitted in partial fulfillment
of the requirements for the degree of
Doctor of Philosophy
(Mechanical Engineering)
in The University of Michigan
2008

Doctoral Committee:

Professor Dionissios N. Assanis, Co-Chair
Research Associate Professor Zoran S. Filipi, Co-Chair
Professor Huei Peng
Associate Professor Jing Sun

To my Grandparents

Ben and Frieda Hagena

and

Wilmer and Beverly Nelson

Your lives of faith, family, and farming
sowed the seeds of my future

ACKNOWLEDGMENTS

Numerous people have contributed to this work their inputs, whether direct or indirect, are most appreciated and make this work what it is.

I first wish to thank Professor Dennis Assanis for giving me the opportunity to further my education at the University of Michigan and for providing such an exceptional facility for research. His vision, leadership, and guidance have been instrumental in the completion of this work.

Dr. Zoran Filipi has been an outstanding technical mentor to me throughout my years here at Michigan. I appreciate his willingness to discuss technical matters and share his deep insight into engine phenomena. I also admire his unbridled enthusiasm toward his work.

This project was made possible through funding from the US Army/RDECom through the Automotive Research Center. I specifically thank Walter Bryzik and Peter Schil for their continued support of graduate education.

My fellow labmates have made this adventure at Michigan truly a time I will never forget. Alexander Knafl's contributions to the lab and toward my abilities as a researcher are invaluable. I especially appreciate his wisdom, candor, and friendship. Rob Prucka and I lived together for four years and during that time spent many an evening on the porch at 800 S. Main. When we did decide to talk about research, his work with residual fraction measurement in a gasoline engine really sparked the ideas that became the centerpiece of my research. Thanks, mmkay. Ashwin Salvi provided assistance in configuring the instrumentation used in this research and helped me gather

the data. Many others have contributed to this work; I especially want to acknowledge Tim Jacobs, Guntram Lechner, Orgun Guralp, Steve Busch, and Matt Leustek.

The machinists and technicians in the Mechanical Engineering department are first-rate and have assisted in numerous crucial times. Thanks to Kent Pruss, John Mears, Warren Eaton, Bill Kirkpatrick, and Steve Emmanuel.

While I greatly appreciate the assistance and input from this large group of people, I am more thankful for the relationships that we have built. Knowledge is fleeting and I truly believe that my largest gain from this pursuit is not the degree, but the relationships that have been forged through it. Thank you all for making the past six and a half years a joy for me.

Finally I wish to thank my family for their continual love and support. Tara and I have been only married a few months and even though we have both been writing our dissertations most of the time; they have been the most wonderful in my life. I love you more every day. I truly could not ask for better parents. They have given me all the opportunities in the world, the freedom to pursue the ones I desired, and the encouragement to follow through. I am blessed to have Holly, Heidi and Lee, and Thomas as siblings and I cherish the relationships that we have.

TABLE OF CONTENTS

LIST OF FIGURES

LIST OF TABLES

LIST OF APPENDICES

LIST OF ABBREVIATIONS

CO_2	Carbon Dioxide
BTU	British Thermal Unit
NO_X	Oxides of Nitrogen ($NO + NO_2$)
EGR	Exhaust Gas Recirculation
NO	Nitrogen Monoxide
NO_2	Nitrogen Dioxide
FTP	Federal Test Procedure
EPA	Environmental Protection Agency
THC	Total Hydrocarbons
CO	Carbon Monoxide
NMHC	Non-Methane Hydrocarbons
PM	Particulate Matter
SFTP	Supplemental Federal Test Procedure
NMOG	Non-Methane Organic Gases
ASI	After Start of Injection
PAH	Polycyclic Aromatic Hydrocarbons
O_2	Diatomic Oxygen
N_2	Diatomic Nitrogen
PCM	Powertrain Control Module
VGT	Variable Geometry Turbocharger
HEUI	Hydraulic Electric Unit Injector
IPR	Injection Pressure Regulator
FICM	Fuel Injection Control Module
FSO	Full Scale Output
LFE	Laminar Flow Element
NIST	National Institute of Standards and Technology

H_2O	Water
RTD	Resistance Thermal Detector
POI	PUMA Operating Interface
ARC	Automotive Research Center
F-FEM	Fast Front End Module
IFEM	Indicating Front End Module
FID	Flam Ionization Detector
DC	Direct Current
CLD	Chemiluminescent Detector
O_3	Ozone
NDIR	Non-Dispersive Infrared Detector
DMS	Differential Mobility Spectrometer
CSV	Cambustion Sampling Valve
y	Ratio of hydrogen to carbon in fuel
H_2	Hydrogen
ϕ	Equivalence Ratio
TDC	Top Dead Center
BDC	Bottom Dead Center
C_d	Fuel Injector Flow Discharge Coefficient
SOI	Start of Injection
EOI	End of Injection
CA	Crank Angle
COV	Coefficient of Variance
BMEP	Brake Mean Effective Pressure
rpm	Revolutions Per Minute
MFB	Mass Fraction Burned
SCP	Stoichiometric Combustion Products
EVO	Exhaust Valve Opening
UMHR	University of Michigan Heat Release Code
GUI	Graphical User Interface

ABSTRACT

This study introduces an experimental technique to quantify cycle-resolved values of pre-combustion in-cylinder compositions during transient engine operation. The work is motivated by increased particulate and NO_X emissions during transient engine operation, which contribute significantly to overall cumulative diesel emissions. The study is divided into three major tasks: technique development, validation, and application to demonstrate its capability to provide new insight into transient engine behavior.

One cylinder of a 6.0L V-8 diesel engine is instrumented to obtain cycle-resolved masses of three in-cylinder pre-combustion constituents: fuel, air, and stoichiometric combustion products. Fuel is determined through use of an instrumented fuel injector and cylinder pressure. The mass of air is determined through calculation of the air/fuel ratio of each cycle from measurements of CO_2 concentrations in the exhaust and in the cylinder. Stoichiometric combustion product mass is quantified through the pre-combustion in-cylinder measurement of CO_2.

Validation of the technique is accomplished by first determining that the methodology does not significantly alter combustion. Error and sensitivity analysis confirm that the technique provides accurate results. The masses of fuel, air, and stoichiometric combustion products are known to ±0.74%, ±2.82%, and ±3.93%, respectively, with a 95^{th} percentile confidence interval. The technique provides data on a cycle-by-cycle basis, a resolution that is unattainable with traditional test cell hardware. This allows insight into engine behavior that was previously impossible, especially during transient operation.

Engine data is taken in three separate investigations: steady-state conditions, constant-speed load sweeps, and realistic in-vehicle engine behavior during an FTP 75 driving schedule. Cycle-resolved NO emissions and fast particulate measurements are also made to characterize transient emissions. During the first few cycles of intense accelerations, excessive levels of over-fueling occur, resulting in cycles with equivalence ratios as high as 1.4. These cycles cause extremely high particulate emissions. High levels of NO emissions occur 3-4 cycles into strong accelerations and are attributed to intensely-premixed combustion with high levels of in-cylinder oxygen. In summary, this study demonstrates that tighter cycle-resolved control of fuel injection and EGR systems, including internal residual, are necessary prerequisites for realizing the full potential of low-emissions transient engine operation strategies.

CHAPTER 1

INTRODUCTION

1.1 Motivation

Modern civilization has been built upon and is currently enabled by the combustion of fossil fuels. Every aspect of life in the developed world, from the production and distribution of the necessities of life: food, clothing, and shelter, to the ways in which humans spend their leisure time are made possible by the consumption of fossil fuels. Every day, 84.5 million barrels of petroleum, 288.8 billion cubic feet of natural gas, and 17.7 million tons of coal are consumed to support human civilization on earth [1]. These fossil fuels account for 95% of all the energy consumed in the world [2].

Not only is the consumption of fossil fuels staggeringly large; it is also increasing. Between 1995 and 2005, world fossil fuel consumption rates increased by an average of 2.3% per year [2]. Future growth rates are expected to remain at or near these levels [2].

Such continually growing rates of fossil fuel consumption are not sustainable, as their quantity on earth is finite. Numerous studies have been conducted on the amount of known obtainable worldwide fossil fuel reserves. Typical values are 1,317 billion barrels of petroleum [3,4], 6,381 trillion cubic feet of natural gas [4,5], and 997,748 million tons of coal [6]. Assuming no increase in consumption rates, these reserves result in about 43 years of petroleum, 60 years of natural gas, and 154 years of coal before proven reserves are depleted. Factoring in estimates for the amount of fossil fuels that have not yet been discovered, it is likely that there are 50-150 years of oil, 200-600 years of natural gas, and 200-2000 years of coal left on earth at current consumption rates [7].

The burning of fossil fuels produces emissions which are harmful to human and environmental health. Predominant is the generation of carbon dioxide (CO_2); at 2005 rates, 84.9 million tons of CO_2 were created and released into the environment every day from the combustion of fossil fuels [6]. CO_2 in the atmosphere behaves as a greenhouse gas, which allows heat from the sun to impact the earth's surface but acts to traps heat in the atmosphere that is being radiated by the earth, resulting in increasing temperatures on the earth's surface. This so-called global warming has the potential to significantly alter the delicate balance of the earth's ecosystems and is currently a widely-debated topic. Much disagreement exists about how much human activity, especially the burning of fossil fuels, has contributed to global warming. Three facts, however, are undeniable:

1. The earth's temperature is rising and impacting the environment.
2. Increased levels of CO_2 in the atmosphere are contributing to this temperature rise.
3. The burning of fossil fuels produces significant levels of atmospheric CO_2.

Irrefutable scientific proof that human activity is causing significant alterations to the environment may be decades away. By that time, however, the changes may be irreversible. Therefore, we as a human race cannot take the chance that our way of living is not impacting the earth and must make significant strides towards reducing our consumption of fossil fuels and production of atmospheric CO_2.

Because of the current high fossil fuel consumption rate, the finite supplies of coal, petroleum, and natural gas on the earth, and the potentially irreversible environmental impacts of burning fossil fuels, there is an urgent need to develop and implement more efficient energy conversion technologies. To assess areas in which improvements are viable, it is helpful to understand how energy is used. Analyzing the demand side of energy flow typically involves breaking consumption into four major sectors: industrial, commercial, residential, and transportation. Figure 1.1, adapted from

[2], demonstrates the flow of all energy into the United States in 2006 and how that energy was utilized.

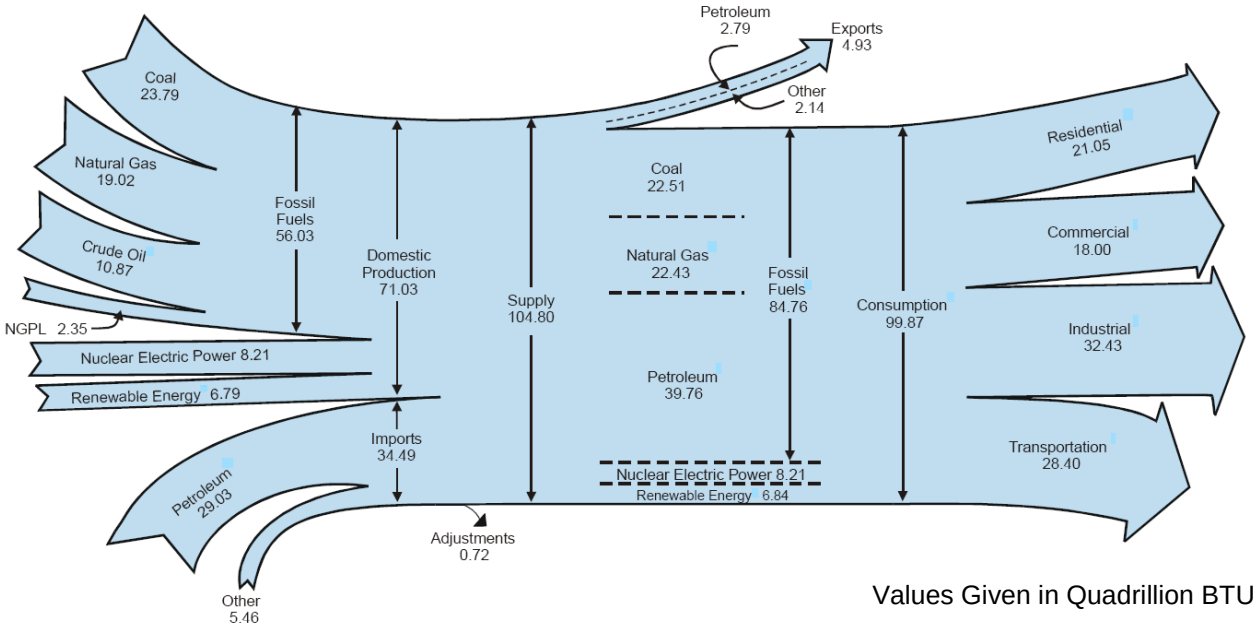

Figure 1.1: Energy Flow In to and Out of United States in 2006

Of the nearly 100 quadrillion BTUs (29.3 trillion kW-hr) of fossil fuels consumed, 28.4% were used to fuel the transportation sector. About two-thirds of the energy consumed in the transportation sector is in the form of gasoline [2], which is typically used to propel light-duty automobiles. This means that about 20% of all the energy consumed in the U.S. is in the form of gasoline, and demonstrates that developing more efficient methods to power automobiles is integral to reducing overall fossil fuel consumption.

One viable method of improving automobile fuel economy is to equip these vehicles with diesel engines. Diesel engines are a proven and available technology that is inherently more efficient than gasoline engines and typically improve the fuel economy of an automobile by between 20-50%. Hindering the implementation of diesel engines is their greater cost and their higher emissions. Diesel combustion is a complex process due to turbulent mixing, three-dimensional heterogeneity, and unsteadiness. These

characteristics, coupled with the high-temperature and high-pressure combustion chamber environment, lead to conditions that are favorable to the formation of regulated emissions—particularly oxides of nitrogen (NO_X) and particulates.

Significant research efforts are currently being undertaken to reduce the emissions from diesel engines, including: in-cylinder combustion development, the use of alternative fuels, the development of aftertreatment, implementation of sophisticated electrically-controlled hardware, and the development of novel combustion modes. Typically these experimental and simulation studies are conducted at steady-state conditions, where engine speed and load are fixed. These efforts have undoubtedly been invaluable to the significant improvement in fuel economy and reduction in emissions that diesel-powered vehicles have experienced in the last 30 years.

When considering actual in-vehicle operation, however, the engine almost never experiences steady-state conditions [8]. Typical engine behavior includes frequent and sudden changes in engine speed and torque and is referred to as transient operation. Transient engine behavior is characterized by a transition between operating states such that quantities of in-cylinder components (fuel, air, EGR, and residual) and their mixing processes are not well-controlled. When these inputs to combustion are not well controlled, neither are the emissions formed from them. Because of this, transient engine operation contributes much more to the total amount of emissions during in-vehicle use than steady-state engine operation [9].

Preliminary data taken for this study confirms that transient engine behavior contributes significantly to overall drive cycle emissions. Test cell facilities at the W.E. Lay Automotive Laboratory permit an engine to be tested as though it is in a vehicle. During these tests, time-resolved concentrations of NO and particulate are measured, which permits the identification the portions of the cycle that result in high emissions. To assess the impact that transient engine behavior has on emissions, a steady-state emissions map is made from engine data and then the engine commands and speeds

experienced in the driving cycle are input to the map. The output of the map is emissions levels if the engine were to experience driving cycle speeds and loads at steady-state operation. The emissions values from the transient test and the quasi-steady approximation are then compared to determine the influence of transient engine behavior.

Representative data from this comparison for NO and particulate emissions are shown in Figure 1.2 and Figure 1.3. From these graphs it is clear that there are discernable differences in the quasi-steady predictions and the measured emissions values. Further, the greatest discrepancies and the highest levels of absolute emissions occur during the periods when the greatest vehicle acceleration is taking place. Under these conditions, the engine is drastically changing speed and load. This confirms that the engine emissions are especially sensitive to transient engine behavior. Considering cumulative emissions over a driving cycle, the transient engine behavior alone accounts for about 19% of total NO emissions and 53% of total particulate emissions.

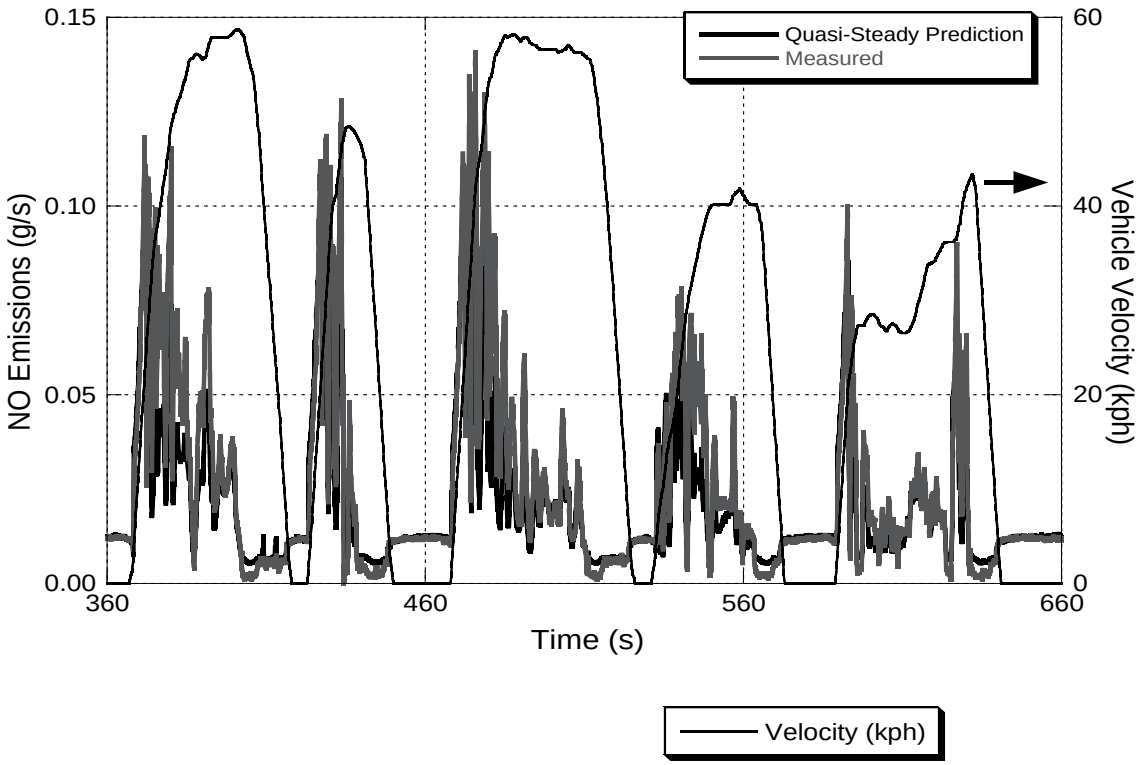

Figure 1.2: Measured and Quasi-Steady NO Emissions during In-Vehicle Engine Behavior

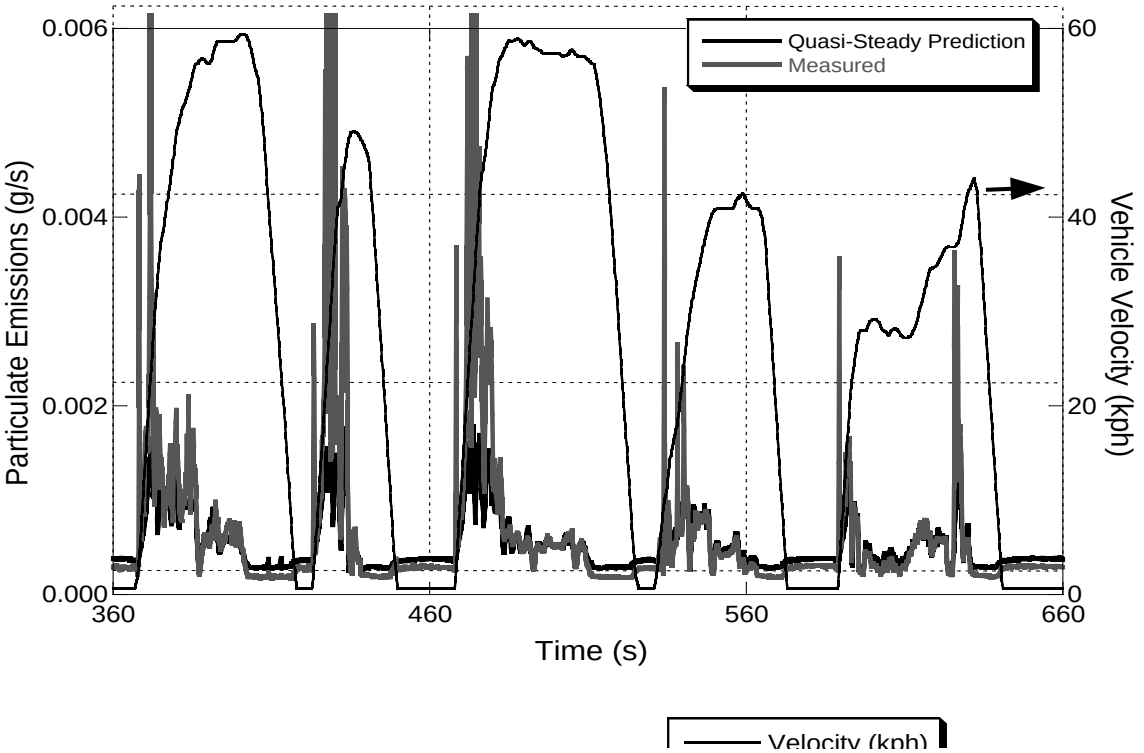

Figure 1.3: Measured and Quasi-Steady Particulate Emissions during In-Vehicle Engine Behavior

A great deal remains to be discovered about emissions formation during transient engine operation. Past work does reveal, however, that engine transient emissions are extremely complicated [8], vary significantly with each particular driving cycle [10 and 11], and are highly-dependent upon the configuration and use of the engine's subsystems [10 and 12].

Because transient emissions production is not well understood, accurate models of their formation do not exist. Models that predict emissions formation during transient engine operation can originate from two sources: physics and engine phenomena. Diesel combustion is extremely complex by nature and involves turbulent mixing, three-dimensional heterogeneity, and unsteadiness. Thus modeling the physics and developing the governing equations that describe emissions formation is incredibly difficult. Much of the complexity of diesel combustion can be avoided by using phenomenological models, which quantify emissions relative to the engine inputs that govern their behavior.

In this sense, diesel combustion is relatively simple: fuel, air, and some exhaust gases enter the cylinder, the fuel and air burn, and emissions are formed. This occurs repeatedly in the cylinder in discreet events that last anywhere from 30-200 ms. Traditional test cell instrumentation and techniques, however, are unable to resolve the inputs and outputs of combustion to these levels. Therefore it is impossible to develop links between the inputs and outputs of combustion, which prevents the identification of the primary drivers of emissions formation during transient engine operation.

Considering that transient engine operation is a significant source of regulated exhaust emissions and that the formation of these pollutants is not well understood, a need exists to conduct further studies into the nature of emissions formation during transient engine operation. Understanding the conditions under which these emissions are created and the factors that contribute their formation have numerous benefits, including: reduced overall emissions during transient engine operation due to better control of engine subsystems, improvements to the refinement and accuracy of transient emissions models, and an increase in the longevity of aftertreatment devices since fewer engine-out emissions are produced.

1.2 Objectives

The first step to gaining an understanding about emissions formation during realistic engine operation is to identify when and why emissions are formed. This means having knowledge about the products and reactants of individual engine cycles, which becomes difficult because of the time scales involved with individual engine events and the relatively slow response of traditional test cell instrumentation. Flow meters for fuel and air and emissions measurement devices all respond on the order of seconds, while engine cycles occur in the realm of milliseconds.

Recent developments in experimental equipment, however, have led to instrumentation that has response times well below one millisecond. When used properly, these devices can provide cycle-resolved data from the engine. Such equipment is instrumental to this research effort and is used extensively throughout.

The objectives of this study are four-fold:

1. To develop an experimental technique that can quantify the amount of fuel, air, EGR, and residual trapped for each combustion cycle and to measure cycle-resolved NO and particulate emissions during realistic engine behavior.
2. To validate the experimental technique by performing a comprehensive error and sensitivity analysis and by comparing its results to those obtained with traditional test cell instrumentation.
3. To apply the technique by using it to investigate transient engine behavior in which high concentrations of emissions are formed and explain why these occur in light of knowledge of the amount of fuel, air, EGR, and residual that went into each cycle.
4. To provide insight into how to manage the engine during transients to reduce emissions.

1.3 Approach

One cylinder of a 6.0L V-8 diesel engine is instrumented to acquire complete data from it during realistic engine operation. Cycle-resolved measurements of the individual components of the trapped mass inside this cylinder are made possible through use of unique fast-response experimental equipment. Fuel mass is determined by using an instrumented injector that measures needle lift and injection pressure. When combined with cylinder pressure, this information is used with an orifice flow equation and a lookup table of flow discharge coefficient to measure fuel mass.

Estimations for the mass of air and EGR and residual are made by combining the knowledge of fuel mass with CO_2 gas concentration measurements. In-cylinder CO_2 is measured during the compression stroke to determine the quantity of EGR and residual prior to combustion. Exhaust manifold CO_2 concentration is measured to determine the air/fuel ratio of the previous combustion event.

Emissions of NO and particulate generated during engine operation are measured with fast-response devices that sample exhaust gases from the exhaust manifold immediately outside of the instrumented cylinder. This proximity to the cylinder allows measurements from these emissions devices to be linked as closely as possible to individual cycles.

To operate the engine in a realistic manner, it is used in a test cell which incorporates a state-of-the-art dynamometer and a vehicle simulation to make the engine experience in-vehicle conditions. The vehicle simulation exists in a MATLAB/SIMULINK environment and simulates the driver and all vehicle components from the engine flywheel to the ground. This simulation is incorporated into the test cell so that pedal position signals from the virtual driver pass to the engine, which responds by making torque. Torque is measured by the dynamometer and fed back into the model, which alters the vehicle velocity. Thus the engine experiences speed and load combinations and driver inputs which are representative of in-vehicle operation.

1.4 Document Outline

This document is divided into nine chapters. Chapter One is an introductory chapter that presents the motivation for the research, demonstrates its need, summarizes the objectives, and outlines its approach. Chapter Two is a literature review that explores previously published work in related research fields. The experimental setup and instrumentation is described in Chapter Three.

Chapter Four introduces and develops the experimental methodology used to determine the cycle-resolved in-cylinder masses. First in-cylinder conceptualizations are introduced, then equations are developed relating gas concentration measurements to pre-combustion in-cylinder composition. In-cylinder measurement techniques are then introduced, followed by a description of the determination of cycle-resolved fuel measurement. An iterative methodology is then presented that incorporates fuel mass and in-cylinder and exhaust manifold gas measurements to calculate the trapped air and stoichiometric combustion product mass.

Chapter Five quantifies the validity of the experimental technique by performing an error and sensitivity analysis. First the influence of instrumenting the cylinder and removing mass during the compression stroke is examined to determine how the combustion process is impacted. Then confidence intervals are developed for the determined pre-combustion in-cylinder masses. A comparison between results obtained using the experimental technique and traditional test cell instrumentation is then conducted. Finally, engine operating conditions in which the technique yields results with high uncertainty are discussed.

Chapters Six, Seven, and Eight investigate the data obtained with the developed experimental technique and demonstrate the insight it provides. Steady-state engine conditions are explored in Chapter Six and highlight how cycle-to-cycle variances impact engine emissions. Chapter Seven examines how the technique gives insight into engine emissions constant-speed load steps. Chapter Eight then studies engine behavior representative of in-vehicle operation, where it experiences conditions that span its performance envelope.

Chapter Nine is a summary chapter that reviews the motivation and objectives of the study, highlights the major findings, presents the conclusions formed from these results, and makes suggestions for future work.

CHAPTER 2

BACKGROUND

This chapter is a summary of the literature reviewed for this research effort. Topics have fallen into four major categories and are discussed separately as follows:

1. Review of Diesel Emissions Regulations
2. Conceptual Model of Diesel Combustion.
2. NO_X and Soot Formation in Diesel Combustion.
3. Transient Diesel Emissions Characteristics.

2.1 Diesel Emissions Regulations

The United States Environmental Protection Agency (EPA) was founded with the mission to protect human health and to safeguard the natural environment by preserving the quality of air, water, and land—those natural resources upon which life depends [13]. The agency was formed and given legislative authority through the Clean Air Act of 1970, which also set statutory deadlines for reducing automobile emission levels. These regulations were focused on limiting the production of three harmful tailpipe pollutants: total hydrocarbons (THC), carbon monoxide (CO), and oxides of nitrogen (NO_X) [14].

Further automobile emissions regulations were imposed under the Clean Air Act Amendments of 1990 where two sets of standards, Tier 1 and Tier 2, were defined for new light-duty non-commercial vehicles. The Tier 1 regulations were adopted in 1991

and began to take effect in 1994. Tier 2 standards were passed in their final form in 1999 and a phase-in implementation began on all model year 2004 vehicles [13].

Tier 1 standards were phased in progressively between 1994 and 1997. These regulations not only further reduced the allowable emission levels of THC, CO, and NO_X set forth in the original 1970 legislation, but also set standards for non-methane hydrocarbons (NMHC) and particulate matter (PM). They applied to all new light-duty vehicles such as passenger cars, light duty trucks, sport utility vehicles, minivans, and pickup trucks with a gross vehicle weight rating, i.e., vehicle weight plus rated cargo capacity of less than 8500 pounds.

Vehicles produced under Tier 1 were divided by weight class, and heavier vehicles had standards appropriate for their engine size. In the lightest weight class, diesel-powered vehicles had more lenient NO_X standards than their gasoline counterparts. The limitations were effective over a full vehicle life of 100,000 miles and also required that an intermediate standard be met at 50,000 miles. Emissions were measured and regulated on a grams per mile basis over the Federal Test Procedure (FTP 75) test, as well as a Supplemental Federal Test Procedure (SFTP) which includes additional test cycles that reflect aggressive highway driving (US06 cycle) and urban driving with the air conditioning system operating (SC03 cycle).

Tier 2 standards began to take effect on all model year 2004 vehicles and will be progressively phased in through 2009. In addition to the pollutants regulated in Tier 1, Tier 2 also limits the formation of aldehydes and regulates the emission of non-methane organic gases (NMOG) rather than NMHC. For the species that were regulated previously in Tier 1, the permissible levels allowed by Tier 2 have decreased drastically—in some cases ten-fold.

Allowable emissions levels in Tier 2 are structured into eight certification bins of different stringency. Vehicle manufacturers can choose to certify any particular vehicle in any bin, but the average NO_X emissions of a manufacturer's entire vehicle fleet must

meet an average value of 0.07 grams per mile. Tier 2 standards also lengthen the useful vehicle life and therefore the period over which the emissions are regulated to 120,000 miles. Figure 2.1 shows the relative change of particulate and NO_X emissions regulations from Tier 1 to Tier 2 standards. Tier 2 Bin 5 is shown and represents the fleet-wide average emissions levels under the Tier 2 standards.

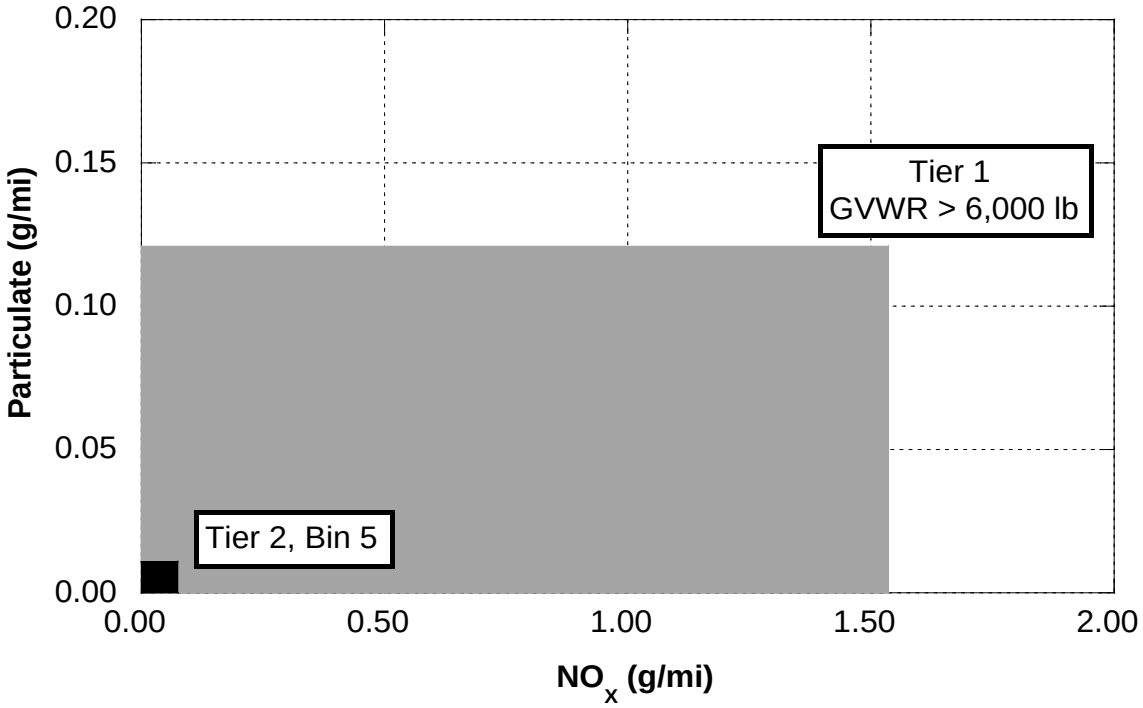

Figure 2.1: EPA NO_X and Particulate Matter Regulation Trends

As in Tier 1, vehicles with a GVWR below 8500 pounds are regulated, but a new class of medium-duty passenger vehicles between 8500 and 10,000 pounds has also been formed. This new weight class assures that large sport utility vehicles, passenger vans, and pickup trucks are covered under the legislation. Distinctions are no longer made between vehicles in different weight categories; discrepancy exists solely through the afore-mentioned certification bins. Since emissions levels are regulated to the grams of pollutants per mile, larger engines must incorporate more advanced emissions control technologies than smaller engines in order to meet the standard.

2.2 Conceptual Model of Diesel Combustion

Even though this research is not focused specifically on the intricacies of diesel combustion, an understanding of its basic nature is important for any investigation that targets emissions formation. Thus a brief overview of steady state diesel combustion and emissions formation is presented.

In 1997 Dec presented his conceptual model [16] of diesel combustion based on numerous laser-sheet imaging studies. The publication was a culmination of his previous investigations [17, 18] and new findings that detailed the events that occur during the ignition delay, start of combustion, premixed burn, and the mixing controlled burn including the transition to the quasi-steady period. Findings of later studies by Dec [19] and Flynn et al [20] further supported this conceptual model. The transition from the quasi-steady burn period to the later burnout stages was explained by Dec [21] where he discussed how combustion changes and then burns out after injection ends. These papers provide a foundational understanding of diesel combustion. Following is a summary of the model and the conclusions found in the afore-mentioned papers.

Figure 2.2 presents a temporal sequence of schematics showing the development of a diesel fuel jet from the start of injection, through the premixed burn, and into the first part of the mixing-controlled burn. Images were obtained from a 2.34 L single-cylinder research engine with a compression ratio of 10 operating at 1200 rpm (139μs/degree) and are denoted by the crank angle degrees after the start of injection (ASI). These crank angle values are retained in this discussion merely to correlate the text with the diagrams in the figure. Variations in engine design, speed, load, injection parameters, swirl, wall interactions, and turbocharging will undoubtedly effect the spatial and absolute temporal development of the jet; however, the relative temporal stages presented generally hold true for direct injection diesel combustion.

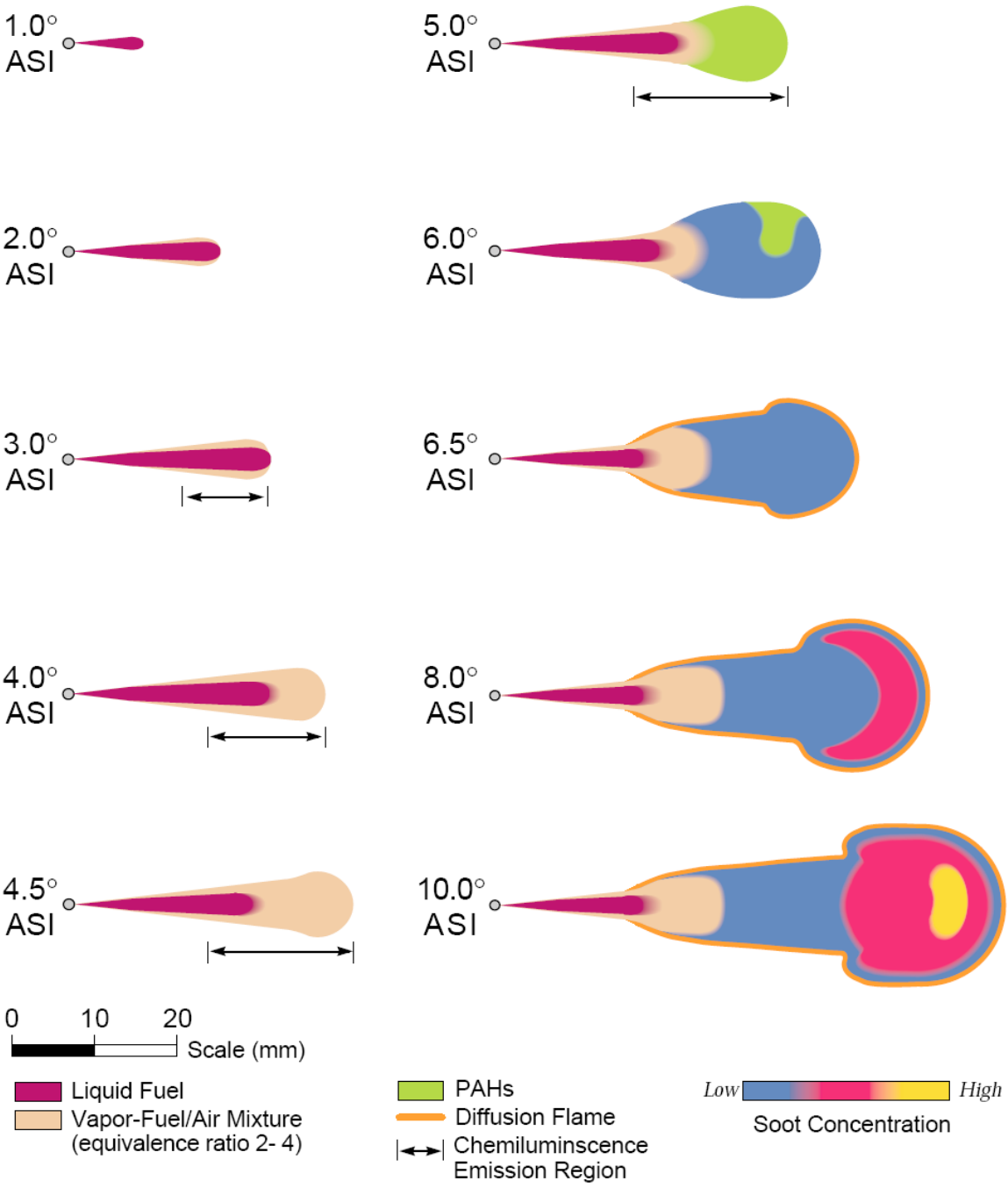

Figure 2.2: Evolution of Diesel Combustion (Dec)

2.2.1 Initial Jet Development (1.0°-4.5° ASI)

The first three images in Figure 2.2 show the jet penetration to the point where all the fuel is vaporized. At the injector, the fuel exists as a liquid (1.0° ASI) but as the fuel moves downstream along the jet, some air is entrained and a fuel vapor sheath forms around the liquid fuel core (2.0° ASI). The liquid fuel jet continues to penetrate until 3.0° ASI, where the jet reaches its greatest penetration length. At this point, the entrainment of hot air has fully vaporized all the fuel. The fuel vapor region continues to thicken and extends beyond the liquid fuel core (4.0° ASI) and eventually a head vortex forms (4.5° ASI). This vortex region contains a well-mixed and generally uniform mixture of air and fuel vapor with equivalence ratios ranging from 2 to 4.

2.2.2 Autoignition (3.0° to 5.0° ASI)

Although the autoignition point is commonly defined as the crank angle when the apparent heat release rate reverses direction or first goes positive, natural flame emission has been detected prior to this time [17]. One component of natural flame emission is chemiluminescence, which arises from combustion radicals that are raised to an excited state by chemical reactions and then decay back to lower energy levels by emitting a photon. The occurrence of chemiluminescence is the first indication of fuel energy release and is therefore considered as the point of autoignition. As early as 3.5° ASI, chemiluminescence was detected at various locations in the vapor portions of the jets. Thus ignition must be occurring at multiple points nearly simultaneously throughout the vapor region of the jet. The intensity of the chemiluminescence increases progressively and by 4.5° ASI it occurs volumetrically throughout the head vortex and the leading edge of the fuel spray. The portion of the spray denoted by the arrows from 3.0° to 5.0° ASI indicates the regions where chemiluminescence was detected.

2.2.3 First Part of Premixed Burn Spike (4.0° to 6.5° ASI)

Chemical heat release, indicated by chemiluminescence, causes the heat release curve to begin moving upward at 4.0° ASI and then it increases sharply after 4.5° ASI. At this time, chemiluminescence engulfs the leading edge of the vapor jet but there is little indication of fuel breakdown. By 5.0° ASI, the fuel has broken down and large polycyclic aromatic hydrocarbons (PAH) form across the entire cross section of the leading portion of the jet where the equivalence ratio ranges from 2 to 4. This timing coincides with the rapid rise in the heat release rate. By 6.0° ASI, soot occurs as very small particles throughout large portions of the cross section of the downstream portion of the fuel jet. These particles are formed by the fuel-rich premixed burn that is occurring throughout the cross section. At 6.5° ASI, small soot particles are present throughout the entire cross section of the downstream region of the jet.

2.2.4 Onset of Diffusion Flame (5.5° to 6.5° ASI)

Between 5.5° and 6.5° ASI, a diffusion flame forms at the outer edge of the fuel jet between the products of premixed combustion and the surrounding air. By 6.5° ASI, the leading portion of the reacting fuel jet is completely surrounded by the thin (approximately 120 μm) diffusion flame. This flame also extends back to the injector to just upstream of the penetrating fuel jet tip. Heat from this flame accelerates the fuel vaporization process, causing the liquid fuel jet to decrease in penetration length. Also at 6.5° ASI, large soot particles begin to appear around the periphery of the fuel jet; they arise from the combustion taking place between the products of premixed combustion and the surrounding air on the rich side of the diffusion flame front (these particles are not shown in Figure 2.2). These events occur just prior to the midpoint of the premixed spike in the apparent heat release rate curve.

2.2.5 Last Part of Premixed Burn Spike (7.0° to 9.0° ASI)

The fuel vapor jet continues to grow outward throughout the remainder of the premixed burn. Soot concentrations throughout the jet increase, with the soot levels becoming the highest in the head vortex region. The diffusion flame sheath around the periphery of the fuel vapor jet remains, forming large soot particles around the edges of the premixed jet and even larger particles in the head vortex zone. Imaging has shown that the soot particles appear abruptly after the fuel vapor region (see 8.0° ASI schematic), suggesting the existence of a thin soot-formation zone across the cross-section of the jet just inside the diffusion flame between the tip of the liquid fuel and the main soot-formation zone.

2.2.6 First Part of the Mixing-Controlled Burn (9.0° ASI to Quasi-Steady)

The overall appearance of the jet changes very little as the combustion transitions to purely mixing controlled. The jet continues to grow outward and the head vortex becomes more well-formed. Soot concentrations have increased in the head vortex region due to the particles increasing in size. Soot particles remain present around the diffusion flame upstream of the head vortex and throughout the sooting region just downstream of the liquid fuel jet. This pattern continues through the mixing-controlled burn stage until the end of injection.

2.2.7 Mixing-Controlled Combustion (Quasi-Steady to End of Injection)

Figure 2.3 shows a schematic of the fully-developed quasi-steady mixing-controlled burn. The term quasi-steady is used because the general shape of the combustion remains unchanged. Turbulence, however, contributes to spatial variations in the outer and inner regions of the jet. Figure 2.3 does not take into account the effect of wall interactions or charge motion. Depending on the size and speed of the engine, the

vapor jet will eventually reach the combustion chamber wall and become distorted from the ideal schematic sometime before or during the quasi-steady burn period. This schematic is a more mature version of the 10° ASI diagram shown in Figure 2.2. A liquid fuel jet penetrates into the combustion chamber while hot air begins to entrain the fuel, thus forming a vapor sheath around the downstream portions of the liquid fuel. The liquid penetrates until the turbulent entrainment vaporizes all of the fuel and a uniformly-mixed fuel vapor region is formed. Downstream from this region the first soot appears as small particles across the entire cross-section of the jet due to a standing fuel-rich premixed flame. As these particles move toward the head vortex region, they increase in size and number and at the head vortex they accumulate and continue to grow. A thin diffusion flame forms around the vapor region, encompassing the head vortex region and the main soot-producing region in the center of the penetrating jet. As the soot particles move to the outer portions of the jet, they can be oxidized by the diffusion flame wall. Conditions on the outside of this diffusion area are ideal for thermal NO_X production because flame temperatures are the hottest due to a nearly stoichiometric equivalence ratio and an abundance of oxygen.

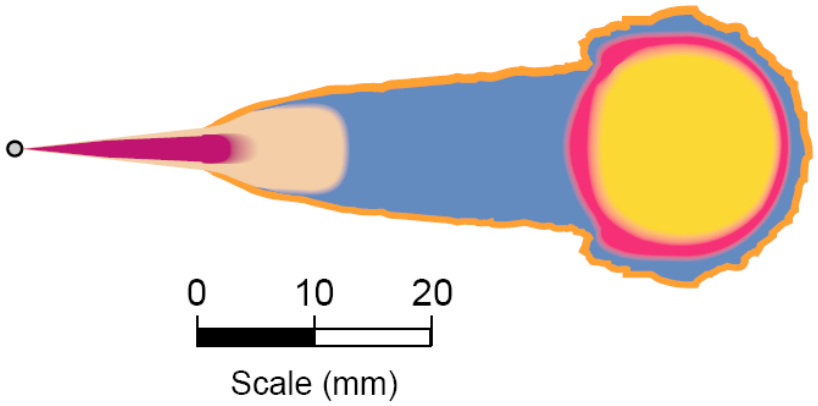

Figure 2.3: Fully-Developed Quasi-Steady Mixing-Controlled Burn (Dec)

2.2.8 Burnout Period (End of Injection to End of Combustion)

The quasi-steady burn period continues as long as fuel is injected into the cylinder. Once injection ceases, the burnout period begins. Combustion spreads quickly back to the injector when fuel injection ends, and soot forms in this upstream region. The reacting jet now consists of the diffusion flame surrounding the sooty products of rich premixed combustion. Momentum of the upstream portion of the jet carries it downstream to the leading portion of the jet along the combustion chamber wall and then back towards the center of the combustion chamber as it folds back on itself. The diffusion flame surrounds the jet as it moves, oxidizing soot particles as they reach the jet periphery, thus reducing the size of the jet. This results in the formation of separate pockets of combustion that continue to get smaller until the soot is consumed by the diffusion flame or the flame is quenched by the relatively cool walls of the combustion chamber.

Using this conceptual model as a guide to understanding the diesel combustion process will provide more insight into combustion phenomena. Observations made, trends explained, and conclusions drawn from the data obtained in this research effort will be more accurate and reliable because of the fundamental understanding facilitated by the model.

2.3 NO_X and Soot Formation in Diesel Combustion

As briefly mentioned above, the nature of diesel combustion produces conditions that are favorable for the production of NO_X and particulates. Many sources have shown that a general relationship exists between NO_X and soot emissions in diesel engine, and the so-called soot-NO_X tradeoff is well documented. Figure 2.4 demonstrates a typical soot-NO_X tradeoff curve that was generated by varying injection pressure on a 6.0 L V-8 diesel engine while keeping all other inputs constant.

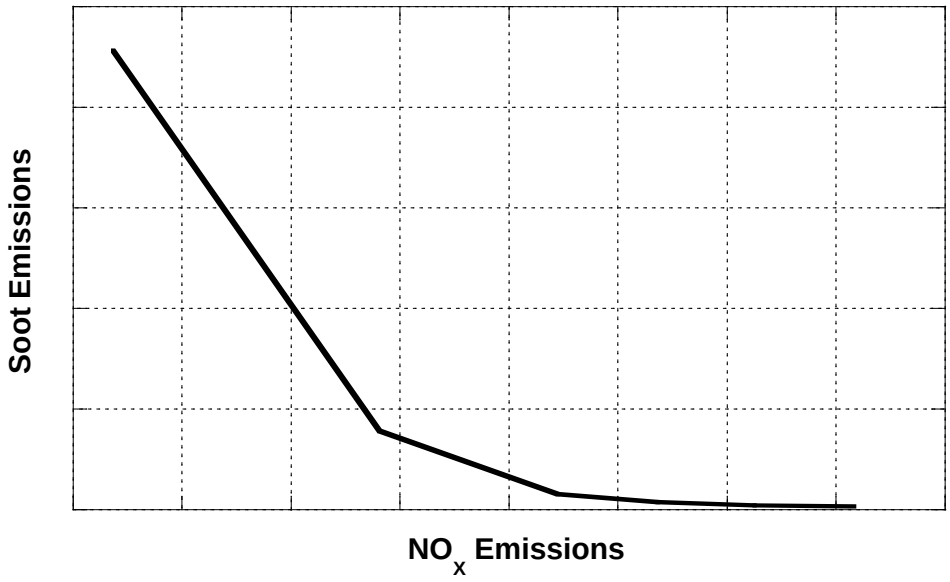

Figure 2.4: Soot-NO_X Tradeoff

When a diesel engine is operating on this curve, methods to reduce NO_X emissions result in an increase in particulate emissions. Similarly, schemes to decrease particulate production cause NO_X emissions to increase.

Because NO_X and particulate emissions are regulated by government standards, an understanding of how these two pollutants form is necessary. Following is a summary of the mechanisms of NO_X and soot formation and a description of their production in diesel engine combustion.

2.3.1 NOx Formation Mechanisms

Although NO and NO_2 are usually grouped together as NO_X emissions, the production of NO is predominant in diesel combustion [8]. Two different mechanisms of NO formation have been proposed for diesel combustion: thermal NO and prompt NO. Experimental investigations have shown that in diesel combustion, nearly all of the NO is formed in the thermal manner [8]. This is accomplished through the oxidation of atmospheric nitrogen at elevated temperatures. The equations governing the formation of

NO via the oxidation of atmospheric nitrogen are known as the extended Zeldovich mechanism and are shown in Figure 2.5.

$$O + N_2 = NO + N$$
$$N + O_2 = NO + O$$
$$N + OH = NO + H$$

Figure 2.5: Extended Zeldovich Mechanism

The rate of formation of NO via the extended Zeldovich mechanism yields

$$\frac{d[NO]}{dt} = k_1^+[O][N_2] + k_2^+[N][O_2] + k_3^+[N][OH] \cdots \\ \cdots - k_1^-[NO][N] - k_2^-[NO][O] - k_3^-[NO][H] \tag{2.1}$$

where [ ] denotes species concentrations. Similarly, the rate of formation of N from the extended Zeldovich mechanism gives

$$\frac{d[N]}{dt} = k_1^+[O][N_2] - k_2^+[N][O_2] - k_3^+[N][OH] \cdots \\ \cdots - k_1^-[NO][N] + k_2^-[NO][O] + k_3^-[NO][H] \tag{2.2}$$

By using the steady-state approximation for N and setting the above Equation (2.2) to zero, an expression for [N] can be found.

$$[N] = \frac{k_1^+[O][N_2] + k_2^-[NO][O] + k_3^-[NO][H]}{k_2^+[O_2] + k_3^+[OH] + k_1^-[NO]} \tag{2.3}$$

Substituting this back into Equation (2.1) results in

$$\frac{d[NO]}{dt} = 2k_1^+[O][N_2] + \frac{1 - \frac{[NO]^2}{K[O_2][N_2]}}{1 + \frac{k_1^-[NO]}{k_2^+[O_2] + k_3^+[OH]}} \tag{2.4}$$

where

$$K = \left(\frac{k_1^+}{k_1^-}\right)\left(\frac{k_2^+}{k_2^-}\right) \tag{2.5}$$

Further substitution and assumptions for rate constants and equilibrium concentrations, denoted by $[\ ]_e$, results in an equation for the initial value of $d[NO]/dt$.

$$\frac{d[NO]}{dt} = \frac{6 \times 10^{16}}{\sqrt{T}} \cdot exp\left(\frac{-69{,}090}{T}\right)[O_2]_e^{1/2}[N_2]_e \tag{2.6}$$

Equation (2.6) shows the strong temperature and oxygen concentration dependence of $d[NO]/dt$. According to this equation, high temperatures and high oxygen concentrations result in large NO formation rates.

Experimental data show that for diesel engines, NO_2 can be up to 30% of total NO_X emissions [8]. Thus the formation mechanism of NO_2 is briefly discussed. NO formed in the cylinder can be converted to NO_2 by reactions such as

$$NO + HO_2 \rightarrow NO_2 + OH \tag{2.7}$$

The NO_2 can be converted back to NO by

$$NO_2 + O \rightarrow NO + O_2 \tag{2.8}$$

2.3.2 NOx Formation in Diesel Engines

NO_X formation rates were shown above to increase as the temperature and oxygen concentration increase. This has significant implications when considering NO_X formation during diesel combustion because of high flame temperatures and an overall oxygen-rich environment. When fuel is first injected into the cylinder, temperatures and pressures are high due to the compression process. As the injected fuel breaks down and begins to combust, temperatures and pressures go up even further, and when the temperature increases beyond 2100 K, NO_X formation rates become significant.

Local temperature variations throughout the cylinder lead to heterogeneous spatial and temporal NO_X formation. The premixed burn just after autoignition is fuel-rich, with an equivalence ratio in the range of four and with adiabatic flame temperatures around 1600 K [16]. These conditions are not conducive to NO production due to the lack of oxygen and the low temperatures. After the premixed combustion, the subsequently injected fuel passes through the rich premixed flame and then burns as a diffusion flame at the periphery of the fuel jet, see Figure 2.6. Temperatures are high at the diffusion flame as the fuel burns stoichiometrically and oxygen is plentiful. These conditions are ideal for thermal NO production. NO may also be produced in the latter part of the mixing-controlled burn or in the hot-gas regions after the end of combustion. While temperatures are not as high as around the periphery of the fuel jet, oxygen is still available and the time scales are much longer; these conditions are favorable for NO formation.

Much of the NO formed would decompose back into nitrogen and oxygen if sufficient time were available to allow equilibrium conditions to be established. But the sudden cooling of cylinder gases essentially freezes NO chemistry. When the cylinder gas temperatures drop the rate constants that govern the formation of NO decrease drastically and the Zeldovich mechanism and the corresponding rate equations cease to affect NO production. As the piston moves away from top dead center, expansion cooling causes cylinder gas temperatures to drop rapidly. High-temperature cylinder gases are also cooled as they mix with cooler burned gases or fresh air. Thus actual NO emissions are higher than they would be if more time was available to let the system move further toward equilibrium.

2.3.3 Particulate Formation in Diesel Engines

Particulates consist principally of organic compounds absorbed onto combustion generated carbonaceous material (soot). In diesel combustion, most particulates are generated from the incomplete combustion of fuel hydrocarbons and some is formed from the engine oil. During the combustion process, soot particles first form and then grow in size. Some of these particulates are oxidized to CO or CO_2; the balance of this formation and destruction of particulates results in overall emission levels. But due to the turbulent, unsteady, and three-dimensional complexity of diesel combustion, much about the particulate generation process is poorly and incompletely understood.

Particle formation is thought to initiate with the pyrolysis, or breaking down without oxygen, of fuel into soot nucleation sites. These sites typically include acetylene and its higher analogues (C_{2n} H_2) and polycyclic aromatic hydrocarbons. Pyrolysis is highly sensitive to temperature and prior studies have found that below 1600 K, this process does not occur to hydrocarbons. Around 1700 K, only aromatics and highly unsaturated hydrocarbons pyrolyze. Between 1800 K and 2400 K, most hydrocarbon fuels will produce soot when burned sufficiently rich. Above 2400 K, commonly used fuels will decompose into smaller gaseous hydrocarbon fragments and burn faster than they can pyrolize into soot nucleation sites. Additional local variables, such as equivalence ratio and pressure, also impact soot formation. Soot production becomes significant at C/O ratios of 0.8 and grows rapidly as the C/O ratio increases beyond this value. Higher pressures tend to produce greater soot emissions, but this relationship is relatively weak.

Surface growth and particle aggregation both contribute to the particle growth process. After the nucleation sites are formed through fuel pyrolysis, gaseous hydrocarbon fragments condense on them and become incorporated into the particle. This surface growth process generates the majority of the solid-phase material.

Aggregation occurs when two or more particles collide and combine to form one larger particle. Rates of aggregation go up as the particulate sizes initially increase due to the higher frequency of particle collisions. As combustion progresses, however, aggregation becomes less frequent because the number of particles has been diminished. As with particle formation, the particle growth process is also a function of local cylinder gas temperature, pressure, and equivalence ratio throughout the combustion event.

Oxidation of the particles can take place any time during their formation and growth processes. Various species contribute to the oxidation of particulate matter, but attack by OH appears to be the most important [18]. Oxidation is a surface area phenomenon, so the shape of a particle plays a large role in its consumption rate. The smaller the surface area to volume ratio, the longer it takes for a particle to be consumed. How tightly the particles are compacted also impacts oxidation rates; more dense particles take longer to combust. Thus densely-packed, spherically-shaped particles require the most time to oxidize.

The diesel combustion conceptual model proposed by Dec and described above provides an explanation for the soot formation process. Pyrolysis and the initial soot nucleation process is attributed to a hypothesized standing fuel-rich premixed flame located just downstream of the maximum liquid penetration. In this region, sufficient oxygen and an excess of fuel provide a sufficiently hot environment for pyrolysis and soot formation. These particles grow in size as they move downstream toward the head vortex. Oxidation then occurs as these particles move into the diffusion flame sheath that surrounds the entire jet plume. Figure 2.6 is identical to Figure 2.3, but the discussed emissions formation features have been added.

Due to the technical nature of this paper, the terms “soot”, “smoke” and “particulate matter” are used very precisely. Considering soot as the portion of particulate matter that consists of elemental carbon, “soot” and “smoke” are used interchangeably throughout the rest of this paper. However, the term “particulate matter”

is reserved for the total amount of emitted solids, which are a combination of soot, soluble organic compounds, and sulfates.

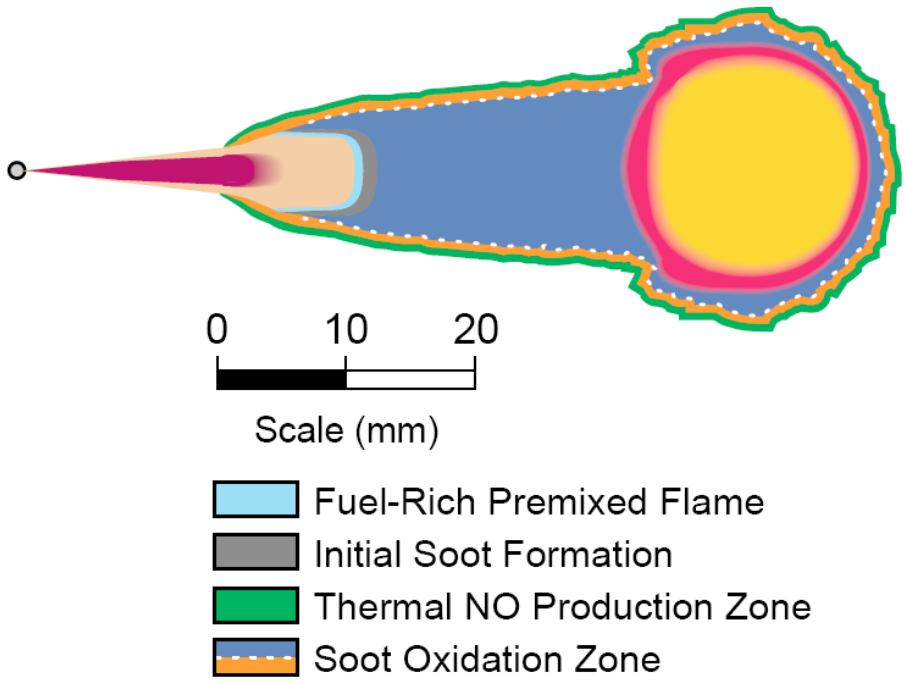

Figure 2.6: Emissions Formation Features in Combustion Plume (Dec)

2.4 Transient Diesel Engine Emissions Characteristics

The previous sections focused specifically on the nature of diesel combustion and emissions formation during steady-state engine operation to establish a foundation upon which the understanding of transient emissions behavior can be built. While the chemistry that forms transient emissions is no different than that at steady state, the entire process becomes much more complex experimentally and phenomenologically due to constantly-changing combustion environments and engine subsystem interactions.

As speed and load fluctuate, the settings of the engine's fuel injection system, turbocharger, and EGR circuit adjust according to the embedded powertrain control module (PCM) calibration. Modulations in the action of these systems alter manifold

dynamics, which impact fresh air and burned gas flow fields and lead to variations in charge composition and turbulence. Engine speed changes result in different time scales during combustion which significantly impacts the fuel atomization, vaporization, and mixing as well as the heat transfer processes. In particular, the response of the fuel injection system is very fast, while time scales associated with the intake air and EGR systems are much longer.

Fluctuations in charge composition, charge motion, and time scales lead to thermodynamic changes within the cylinder; temperatures and pressures, and therefore the properties of charge components are continually inconsistent. Thus on a cycle-to-cycle basis, heat release rates and emissions formation rates are constantly changing [22] and consequently, steady state characterization of engine emissions cannot be applied to transient behavior [8].

While the overwhelming majority of diesel engine emissions research has focused on steady state conditions, some researchers have studied transient emissions behavior. Experimental transient emissions testing generally falls into two categories: those that instrument vehicles with emissions equipment to investigate realistic engine behavior and those that occur in a laboratory setting. The tests from the former group tend to be less analytical; raw numbers are given but little or no explanation for the reasons behind the observed trends is included. This is because performing controlled, repeatable tests is difficult and detailed data from the engine is typically not collected. The latter group provides more insight into engine and transient emissions behavior, but the engine operation does not replicate in-vehicle conditions. That is, the transients investigated occur at constant-speed conditions. These two categories and their findings are reviewed separately.

2.4.1 Laboratory Engine Emissions During Simplified Transients

To conduct these tests, a traditional engine test cell is used and load sweeps are performed at constant speed while engine subsystem and/or emissions data are recorded. This type of research focuses specifically on the actions of engine subsystems and their impact on performance and emissions. A number of the sources came to the conclusion that the most important engine parameter during a transient event is the air-fuel ratio, which indicates the quality of combustion and hence dictates emissions behavior, fuel consumption, and performance [22, 23, and 24].

During a load sweep, both soot and NO_X emissions spike upwards in the initial portion of the transient before settling to steady state values [25]. These short bursts are attributed to air-fuel ratios that promote emissions production. Because modern fuel injection systems respond to inputs rapidly, the EGR and VGT systems were identified as the primary cause of transient air-fuel ratio excursions [8]. When coupled together, the EGR and VGT have a relatively long response time due to flow dynamics and turbocharger rotor inertia; therefore they cannot instantaneously produce the air and EGR flow rates demanded by the PCM [26]. As an example, Green [12] found that purging of EGR from the intake manifold took 6-8 cycles upon valve closure. Furthermore, when the EGR valve was opened suddenly, 15 engine cycles were required to achieve 90% of the EGR flow and nearly 100 additional cycles were necessary to achieve the remaining 10% of the steady state EGR flow rate. In addition, mixing can be significantly altered during transients leading to reduced air/fuel ratio.

As a transient load step is initiated the EGR valve closes rapidly to increase the amount of fresh air ingested by the engine [27], which leads to a significant increase in NO_X emissions [28]. Sudden closure of the EGR valve also results in a pressure spike in the exhaust manifold, thus increasing residual fraction and reducing air-fuel ratio [25]. Contributing to low air-fuel ratios during the onset of a load step is the time required for

the turbocharger to create adequate boost pressure [29]. While the use of a VGT greatly eliminates the effect of turbocharger lag, time is still required for the vanes to adjust and the rotor to speed up. These high residual fractions and low air fuel ratios are likely to be the cause of the particulate spike observed at the onset of a load step [24].

The period over which the EGR valve remains closed during a load step affects the relative intensity of the soot and NO_X spikes. Shorter valve closer periods tend to reduce NO_X and increase particulate bursts, while as the time the valve is closed lengthens the opposite trend occurs [25].

Maldistribution of EGR is well-documented at steady-state conditions and this problem is only exacerbated during transient events [12]. Large variations are seen on a cylinder-to-cylinder and cycle-to-cycle basis and these discrepancies contribute significantly to the soot bursts observed during engine transients [25]. Thus accurate control of EGR throughout transient processes is critical to emissions reduction [30].

2.4.2 In-Vehicle Engine Emissions During Real World Driving

A number of studies were reviewed which investigated the transient emissions characteristics of vehicles as they were operated in real-world driving conditions. These vehicles are typically equipped with instrumentation to record vehicle motion, driver action, and tailpipe emissions production. Except for engine speed, little or no information about engine operation is documented. Thus results tend to focus on analyzing driver behavior and their impact on emissions, as well as variance between vehicle configurations.

Small differences in driving style were found to profoundly impact particulate emissions from diesel engines, while NO_X emissions were less sensitive. Aggressive driving was found to increase particulate production by a factor of two when compared to

non-aggressive driving [11]. This is attributed to particulate bursts that occur during rapid engine accelerations, which tend to occur more often with aggressive drivers.

NO_X emissions were found to be more sensitive to vehicle weight and tended to reflect fuel economy trends; as more fuel is burned, more NO_X are formed. Particulate emissions are not as influenced by vehicle weight, but more impacted by the number and intensity of engine accelerations [23]. NO_X emissions are also dependent upon the rate at which the change in engine speed takes place. Slower engine accelerations lead to lower NO_X emissions [32].

2.4.3 Transient Engine Simulations

Simulations of transient diesel engine performance have been around for over 30 years [33] and have modeled the impact of various engine parameters and subsystems on power and fuel economy. While some studies focused on the potential performance gains with new technology [34], others used varied the characteristics of engine components to optimize engine response and fuel economy [35-37]. Some studies emphasized the determination of important in-cylinder quantities, such as air-fuel ratio and gas temperatures [38 and 39]. Knowledge of these parameters can provide valuable insight to emissions formation.

CHAPTER 3

EXPERIMENTAL SETUP

This chapter describes the engine, test cell, and instrumentation that are used in this research effort. Included are specifications and capabilities of the hardware and software, as well as figures and tables to aid in the description of the setup. Special attention will be focused on those components which make this setup especially suited to the type of testing that will occur during this investigation.

3.1 Engine Systems and Instrumentation

The engine used in this investigation is a 6.0 L V-8 direct-injection diesel engine manufactured by the International Truck and Engine Corporation. Known as the Power Stroke, this medium-duty engine is most commonly used in three-quarter ton and greater Ford F-series pickup trucks. It incorporates numerous advanced technologies to reduce exhaust emissions and provide outstanding engine performance. Primary engine specifications are given in Table 3.1.

A hydraulically-actuated electrically-controlled unit injection (HEUI) system provides precise control of fuel injection timing, pressure, and quantity. The force required to inject the fuel is generated by a high pressure oil system. Lubricating oil from the crankcase is compressed by a gear-driven pump and then supplied to oil rails located directly above both banks of injectors. This oil comes into contact with the injectors and

Table 3.1: Engine Specifications

Engine Type	Diesel, 4 Cycle
Configuration	4 Overhead Valves, Cam-in-Crankcase 90° V-8
Displacement	6.0 L (365 in^3)
Bore and Stroke	95 x 105 mm (3.74 x 4.134 in)
Compression Ratio	18.0:1
Aspiration	Variable Geometry Turbocharger/Charge Air Cooler
Rated Power @ RPM	242 kW (325 hp) @ 3300 RPM
Rated Torque @ RPM	760 N-m (560 ft-lb) @ 2000 RPM
Combustion System	Digital Direct Injection
Total Engine Weight	438 kg (966 lb)

provides the force necessary for the fuel injection process. Pressure in this system is electronically controlled by the injection pressure regulator (IPR), which is governed by the powertrain control module (PCM). Since the fuel injection pressure is linked directly to oil rail pressure, modulation of the oil rail pressure results in a change in the fuel injection pressure. Electronics spool valves on the injectors are then actuated to control the timing of the injection event. This system is capable of injection pressures in excess of 2000 bar and also permits the limited use of pilot injection. A schematic demonstrating the fuel injection system components is shown in Figure 3.1.

An exhaust gas recirculation (EGR) circuit is used to introduce cooled exhaust gases into the intake manifold in order to decrease NO_X emissions. EGR flow rate is controlled through modulation of the EGR valve and the setting of the variable geometry turbocharger (VGT). The VGT is also used to enhance engine performance, as it reduces turbocharger lag and allows control of the intake manifold pressure.

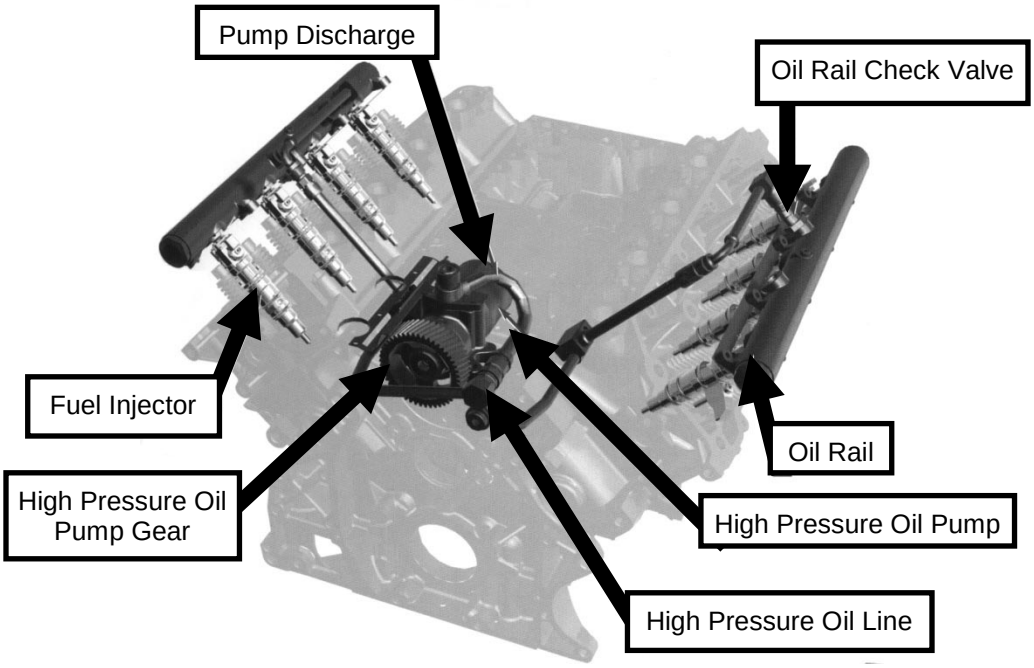

Figure 3.1: Fuel Injection System Schematic

To optimize the effectiveness of these electronically-controlled devices, a sophisticated engine control system is utilized. The control system's basic function is to acquire data from numerous sensors located on the engine and to use that information to determine the best settings for all of the engine's controllable devices. A schematic of the engine control system is shown in Figure 3.2. Signals from engine sensors are input into the PCM and used in algorithms that calculate the desired settings of the EGR control valve, the VGT control valve, and the IPR. The PCM forwards some sensor signals (rpm, engine oil temperature, etc.) and some calculated values (desired mass of fuel, injection control pressure, etc.) to the fuel injection control module (FICM) where the timing of the electrical signals that correlate to start of injection and injection duration are determined. Once these values have been calculated, the FICM distributes the electrical signals that fire the injectors.

The algorithms used to calculate the orientation of the electrically-controlled devices at all operating conditions are collectively known as the engine calibration. The

engine calibration must strike an acceptable balance between engine performance, economy, emissions levels, and drivability.

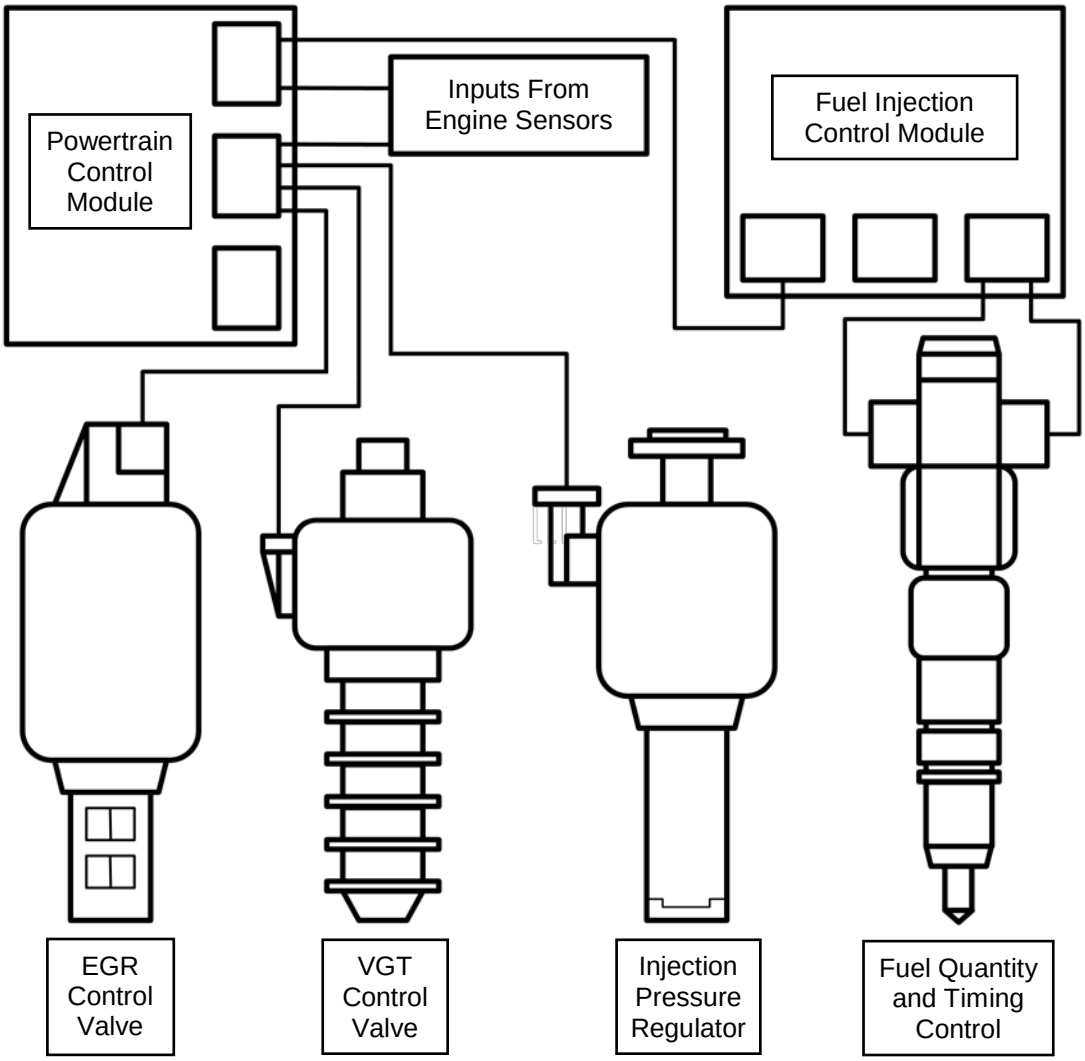

Figure 3.2: Engine Control System Schematic

3.1.1 INCA

Software and hardware from ETAS, Incorporated allows the monitoring and modulation of all electronically-controllable engine systems including: EGR flow rate, VGT setting, injection pressure, injection quantity, injection timing, and pilot injection

characteristics. The flow rate of EGR is adjusted by changing the position of the EGR valve or by changing the exhaust manifold backpressure via the VGT setting. Boost pressure in the intake manifold is also controlled by modulating the VGT. The VGT can be controlled by demanding a particular vane setting or by requesting a constant backpressure in the exhaust manifold. Fuel injection pressure is regulated by altering the oil rail pressure via the IPR. The PCM uses lookup tables to determine the amount of fuel that is injected at any particular operating condition; modification of these values changes the quantity of fuel injected. Injection timing is advanced or retarded by inputting an offset to the standard calibration's timing. Pilot injection parameters are controlled by specifying the pilot quantity and timing.

3.1.2 Engine Instrumentation

The engine has been fully instrumented to capture the necessary temperatures, pressures, and flow rates necessary to characterize its behavior. Following is a discussion that details the specifications of the instrumentation that are the most critical to this study.

Crank Angle

Crank angle signals are provided by an AVL 364C Angle Encoder mounted to the crankshaft pulley on the front of the engine. The opto-electronic device has a crank angle resolution of 0.1°; this high resolution provides the accuracy necessary for diesel combustion analysis.

Needle Lift and Injection Pressure

To obtain a better understanding of the injection process, a injector has been instrumented to measure needle lift height and fuel injection pressure. The injector was instrumented and modified in a joint effort between Siemens and Wolff Controls

Corporation. Needle lift is measured using a Hall Effect sensor mounted inside of the nozzle needle valve spring. A small magnet is brazed to the spring guide and moves up and down with the needle. The magnet's motion is detected by the stationary Hall Effect sensor, which outputs a voltage that is proportional to the distance that the needle has moved. A full bridge strain gage circuit is used to measure the hoop strain around the nozzle needle spring cage. This deformation is a result of fluctuating fuel injection pressures. As the cage expands and contracts, the resistance of strain gage circuit changes and the bridge becomes unbalanced. This alters the circuit's output voltage, which can be related directly to the fuel injection pressure. Accuracy of the injection pressure is reported as <±0.3% of the reported value. Data from the injector is acquired on a crank-angle basis at a resolution of 0.1 crank angle degrees.

Cylinder Pressure

Cylinder pressure transducers have been inserted into each engine cylinder through the existing glow plug holes. The glow plugs have been removed and replaced with adapters that permit transducer mounting without modification to the cylinder heads. The uncooled cylinder pressure transducers are AVL model GU12P and are capable of measuring cylinder pressures in the range of 0-200 bar with a linearity of $\leq \pm 0.3\%$ full scale output (FSO). These piezo-electric devices use a quartz crystal to generate an electrical charge when a change in cylinder pressure is sensed. Charge amplifiers are used to magnify the transducer signal and convert it to a voltage, which linear with the measured pressure. Cylinder pressure data is taken every 0.1 degrees of crankshaft rotation.

Crank-Angle Resolved Intake and Exhaust Manifold Pressures

To better understand flow dynamics during engine operation, both intake and exhaust manifolds have been instrumented with pressure transducers to capture crank-angle resolved data. These sensors are located as close to the instrumented cylinder as physically possible to give an accurate reading of the conditions in the manifolds during the cylinder filling and emptying processes. The sensors used are Kistler 4045A2 piezoelectric pressure transducers with a functional range of 0-2 bar and a nonlinearity and hysteresis of $<\pm 0.3\%$ of full-scale operation. They are connected to Kistler 4618A0 charge amplifiers which produce a 0-10 volt dc signal that is proportional to the pressures measured. To extend the life of the sensor in the exhaust manifold and to minimize the effects of sensor temperature drift, it is mounted in a Kistler 7511 cooling adapter, which circulates cooling water around the transducer. Under high-power conditions, the pressures in the exhaust manifold exceed 2 bar, and the sensor saturates. This makes the transducer outputs under these conditions inaccurate.

Air Flow

A Meriam laminar flow element (LFE) model 50MC2-6F is used to measure the mass flow of air into the engine. Air first enters the LFE through a filter and then is passed through a diffuser and a section of honeycombs, where the air flow is straightened and slowed down. These conditions produce a laminar flow of air, which is then passed through an orifice. The pressure drop across the orifice is measured and used to calculate, along with other inputs, the mass flow rate of air into the engine. The LFE is calibrated and correlated at several flow rates using a Meriam Standard, which is controlled per the calibration requirements of ANSI Z540-1 and is traceable to the National Institute of Standards and Technology (NIST). The particular model used has less than 0.40% error from actual air flow rate in the calibrated working range of 2.83

m^3/min to 27.18 m^3/min; this spans nearly every operating condition except at engine speeds near idle.

Pressure drop across the LFE is measured using an LPM 9381 Druck differential pressure transducer. The gauge has a measurement range of 0-10 in-H_2O with an accuracy of ±0.1% of full scale output. Differential pressure is measured by exposing a diaphragm to the pressure difference, which causes the diaphragm to deflect. The sensor implements an eddy current measurement system to quantify the deflection and output a voltage that is linear to the pressure drop.

Additional inputs to the air mass flow rate calculation from the Meriam LFE are ambient air pressure, temperature, and humidity. The atmospheric pressure in the test cell is obtained from a Druck RPT 410V barometric pressure sensor. With an operating range of 59.3 to 110.1 kPa, the transducer has an accuracy of ±0.05 kPa. A resonator and pressure-sensitive diaphragm machined from single-crystal silicon form the multi-layer sensor structure. Ambient air temperature and relative humidity are measured by a HX93A Omega transmitter. The sensor provides a temperature-compensated output signal of 4-20 mA for both temperature and relative humidity measurement. Output signals are calibrated and scaled 0-100% for relative humidity and -20 to 75°C for temperature. A thin film polymer capacitor senses relative humidity and is accurate to within ±2.5% at 75°C, while a 100 ohm resistance temperature detector (RTD) measures temperature to within ±0.6°C.

Fuel Flow

A Micro Motion model CMF025 coriolis flow meter is used to measure fuel mass flow rate values that are independent of fluid temperature or composition. Sensor capacity is 377.8 g/s with an error resolution of ±0.5% of flow rate. It is powered by 24 V DC and outputs a 4-20 mA signal that is linear to mass flow rate.

3.2 Test Cell Systems and Instrumentation

The devices and systems used to monitor, control, and evaluate the engine during testing is known collectively as the test cell. This includes the dynamometer, test cell control hardware and software, low speed and high speed data acquisition systems, and emissions measurement equipment. This section will explore these components in detail.

3.2.1 Dynamometer

A dynamometer is a device that absorbs the rotational energy from an engine and determines the output power by measuring the engine's speed and torque. The dynamometer used in this experimental effort is an AVL ELIN series 100 APA Asynchronous Dynamometer. Dynamometer performance specifications are shown in Figure 3.3, as is the dynamometer itself. This dynamometer is especially suited to perform transient testing, as it has the capability for very rapid changes in torque and has a wide bandwidth over the entire operating speed range.

Speed Range	±8000 rpm
Torque Range	-1273 to +1400 N-m
Power (Absorbing)	330 kW
Power (Motoring)	300 kW
Power Consumption	400 Amps @ 400 Volts
Rotational Inertia	2.91 kg-m^2
Rotor Mass	271 kg
Total Mass	1750 kg
Torque Response	5 ms
Torque Reversal	10 ms (-100% to +100%)
Overload Capacity	25% for 1 minute
Shaft Centerline	0.8 m

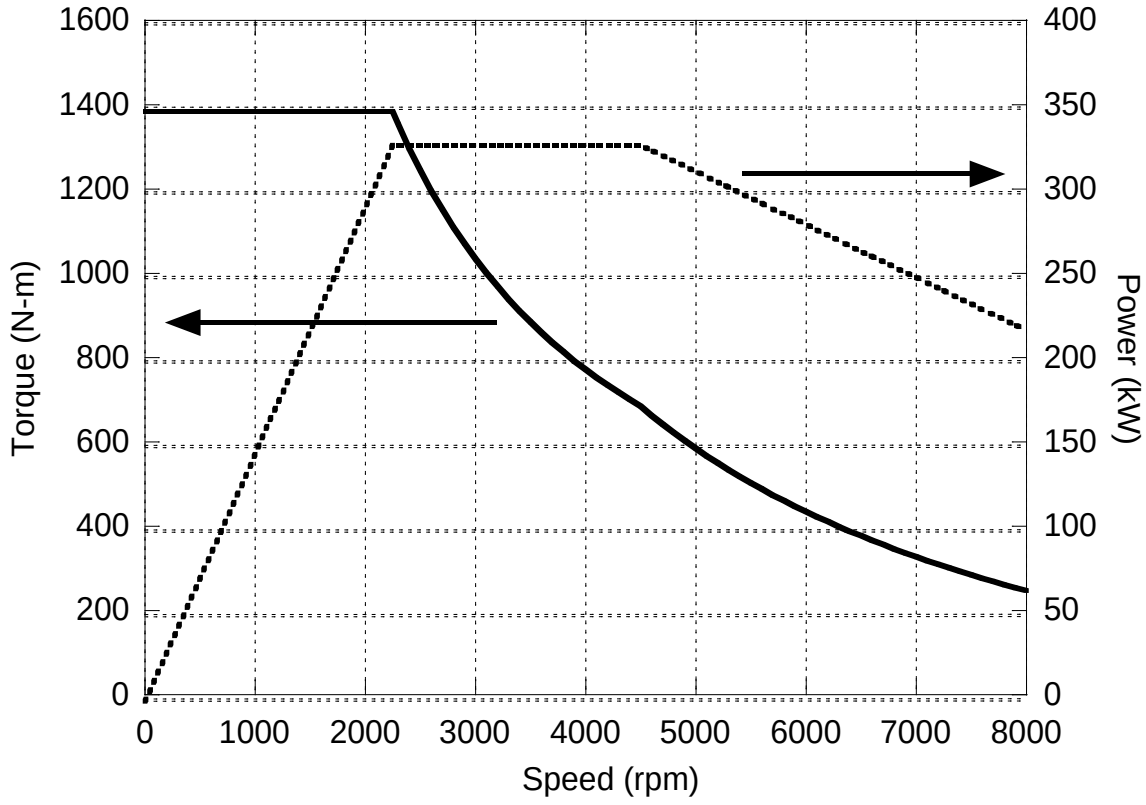

Figure 3.3: Dynamometer Specifications and Performance

3.2.2 Test Cell Control Software

Control of the dynamometer, engine, measurement, and auxiliary devices is orchestrated by PUMA Open software from AVL. A schematic of the test cell control hierarchy is shown in Figure 3.4.

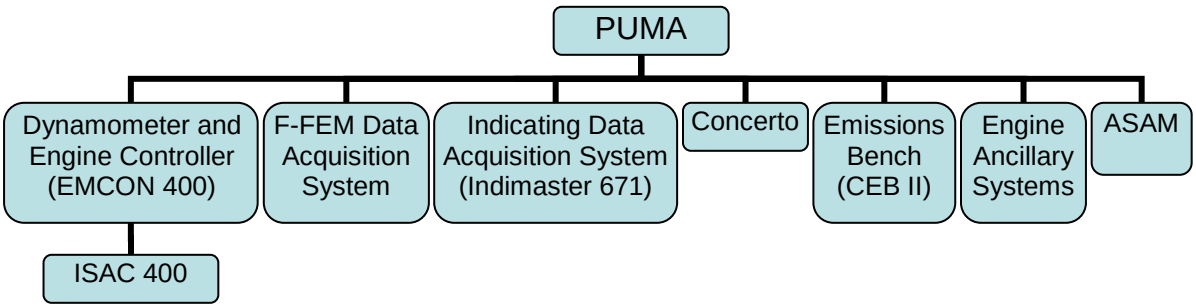

Figure 3.4: Test Cell Control Software Hierarchy

At its core, PUMA provides an automation environment where a single operator can control and monitor all test cell functions. It allows seamless communication between input/output systems and computation processes with high throughputs, real time processing for automation and measurement, and data management. A database management option permits administration of test cell parameters and result data. A test preparation feature allows the programming and editing of predefined experiments. While tests can be programmed and run automatically, flexibility remains to operate the system manually.

Data can be recorded continuously and stored permanently due to the large buffer and high system throughput. This data can also be accessed real-time in graphical and tabular form. Multi-level safety monitoring continually observes predefined variables and their assigned limits (such as oil pressure or coolant temperature) and issues progressive warnings if these limits are approached or exceeded. A formula calculation device operates cyclically or on demand and contains a formula editor with arithmetic, logical, and statistical functions and provides continual or on-demand calculation of important engine metrics.

Test order, automation functions, process quantities, user dialogues, and system messages are visualized with the PUMA Operator Interface (POI). This Windows operating environment includes a complete set of predefined operating windows that can be customized and modified to meet relevant test requirements.

The PUMA system is housed in the aptly-named PUMA cabinet in the control room. Next to the cabinet is the operator's station, where all PUMA and test cell control functions are monitored and executed. Four 19 inch monitors display the POI, as well as information from the high speed data acquisition and ETAS systems. This hardware is shown in Figure 3.5.

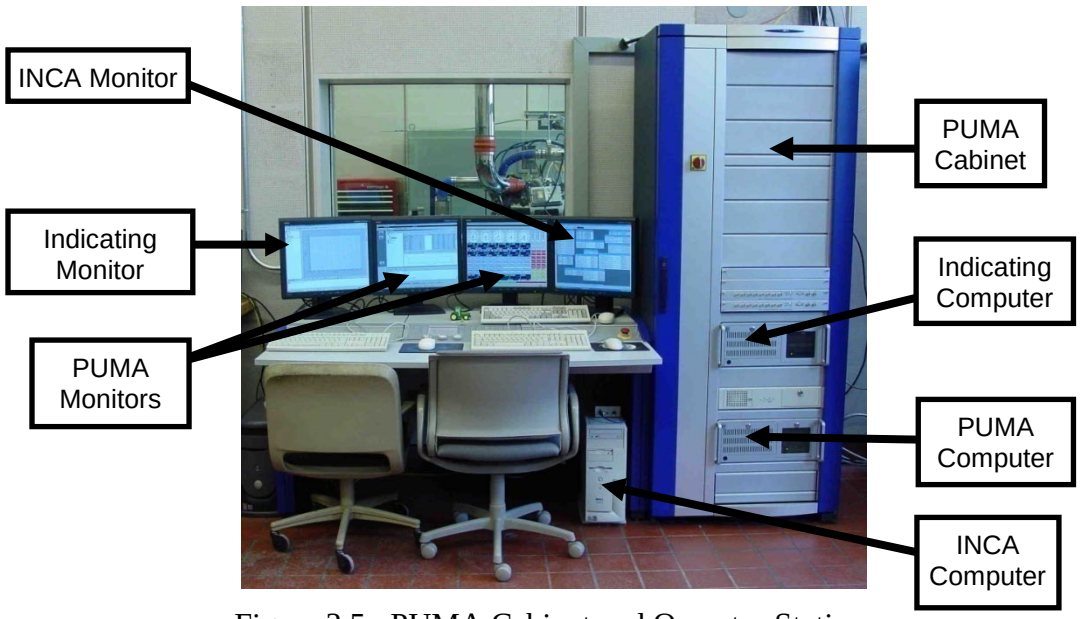

Figure 3.5: PUMA Cabinet and Operator Station

3.2.3 Engine and Dynamometer Control

Manual and automatic control of the engine and dynamometer is achieved through use of an EMCON 400 controller. This system consists of tunable PID controllers that govern dynamometer and engine operation. Two controllable metrics define the dynamometer operation: its rotational speed and the torque it generates.

Engine operation is defined by three parameters including engine speed, torque, and pedal position. Control over the engine is exercised only through the pedal position; a throttle controller inputs a 0-5 V signal into the engine wiring harness that corresponds to 0-100% of pedal position. To manage engine speed and torque output, EMCON modulates the pedal position until the commanded torque or speed value is attained.

An operating mode is defined when one metric from the dynamometer and the engine are controlled by EMCON. Four operating modes are commonly used. These four modes can be incorporated into a manual or an automatic testing strategy and are detailed below.

1. Dynamometer Speed/Engine Pedal—This is the most frequently used mode, as the speed and pedal position are directly commanded.
2. Dynamometer Speed/Engine Torque—Similar to mode one, but used when a specific torque output at a determined speed is required.
3. Dynamometer Torque/Engine Speed—This mode is like mode two, but the engine pedal position will be modulated to try and maintain a particular speed.
4. Dynamometer Torque/Engine Pedal—The dynamometer provides a set resistance torque and the engine will have a specific pedal position. Engine speed will adjust depending on its torque curve.

The system also has the capability to operate the engine and dynamometer over a prescribed transient cycle. This is an especially powerful tool, as engine operation over any desired driving cycle can be evaluated. When operating in this manner, the controller also has the capability to control engine subsystems on a transient basis.

3.2.4 ISAC 400

ISAC 400 is an extension of the EMCON 400 that allows for the complete simulation of drivetrain components, vehicle driver, and the road. This system has

numerous submodels that can be specified by the user to build a virtual vehicle. Models that exist for the wheel, axle, differential, and drive shaft are combined with a selected transmission and road simulation to calculate the torque experienced by the engine. The vehicle driver simulation can account for shifting gears, driving hills, and overall driver behavior.

The ISAC module also has the capability of linking with Matlab to accept user-defined vehicle, powertrain, and driver models written in Simulink. A large degree of flexibility in the system allows various combinations of components to be simulated. Past work [40] through the Automotive Research Center (ARC) at the University of Michigan has linked an existing vehicle dynamics simulation (VESIM) with the hardware in the test cell to create a hardware-in-the-loop system; this configuration is demonstrated in Figure 3.6. This system functions to allow the engine performance to be evaluated in definable vehicles with various powertrain arrangements.

VESIM runs in parallel as the engine operates and contains submodels for the driver, driveline, and vehicle. The input to the system is a drive cycle within VESIM, which contains a user-defined vehicle speed profile. At each time step, the driver compares the demanded drive cycle speed and the actual vehicle speed and then outputs a commanded pedal position signal to the engine. The engine responds by making more or less torque and this signal is passed on to the vehicle dynamics model thus causing a change in vehicle speed. The engine works against resistance dynamometer's resistance, which is determined by VESIM and intended to mimic the road load of the defined vehicle. Dynamometer speed is also controlled by VESIM and is a direct calculation from simulated vehicle velocity and transmission states.

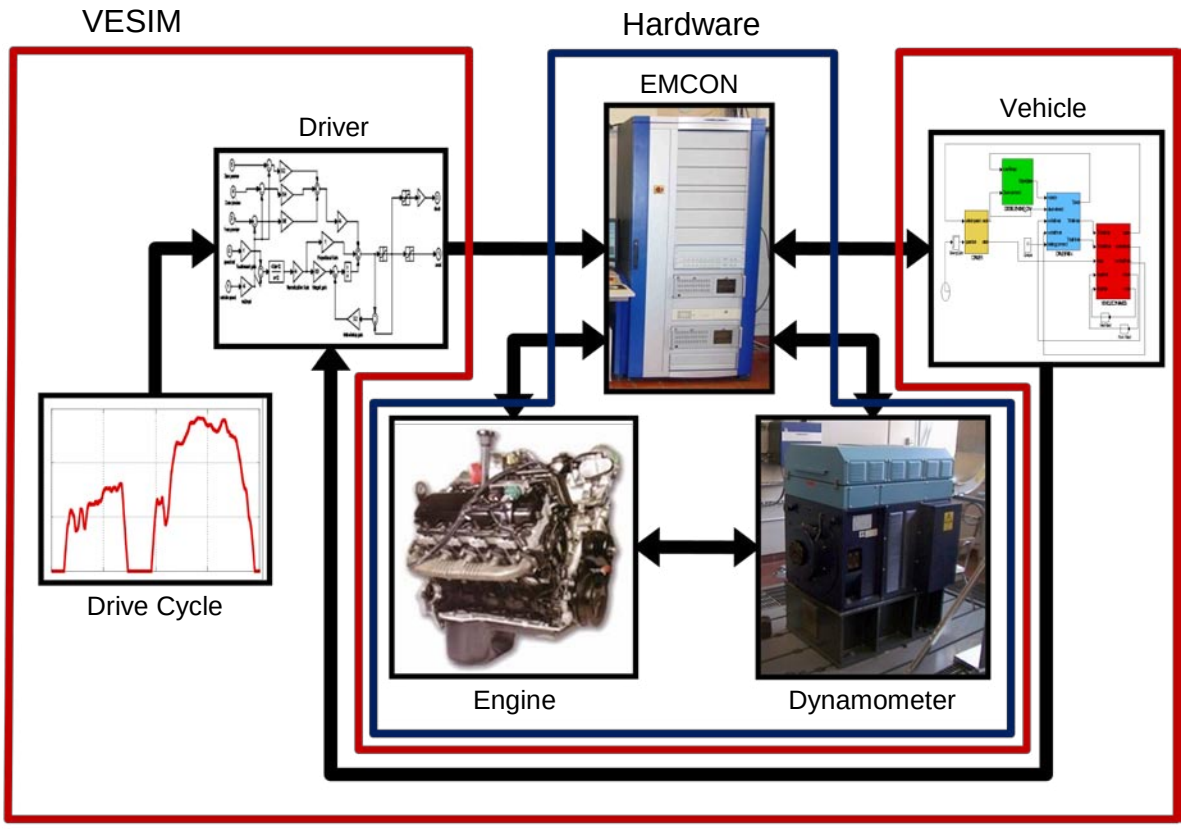

Figure 3.6: Engine-in-the-Loop Test Cell Configuration

3.2.5 F-FEM Data Acquisition System

AVL Fast Front End Modules (F-FEMs) constitute a modular input/output system for high precision measurement and demand value output and control. They have the ability to measure temperature signals from thermocouples and RTDs, voltages, currents, resistances, measuring bridges, and frequencies. All signal conditioning and conversion to engineering units is done inside the F-FEMs before the data is transferred to PUMA. Five kinds of F-FEMs are used in the test cell; each is described in Table 3.2.

Table 3.2: Fast Front End Module Specifications

Number	Type	Description	Channel / Function
1	F-FEM CON	Analog and digital I/O as well as frequency and strain gage channels to control engine, dynamometer and accessories in the test bed	4 analog input channels, 5 kHz data acquisition rate 4 analog output channels, 5 kHz data acquisition rate 2 counter inputs 2 frequency outputs 4 digital I/O
4	F-FEM AI	Analog input measurement device for temperature, voltage, current, resistance and measurement bridges	16 channels, up to 200 Hz data acquisition rate per channel
2	F-FEM DIO	Digital I/O for relays and opto-inputs	16 I/O channels, 200 Hz data acquisition rate
1	F-FEM DAC	Analog output for voltage and current	4 channels, up to 1 kHz data acquisition rate
1	F-FEM CNT	Measurement device for digital signals: speed, period, frequency, duration, TDC, duty cycle, or ignition point	6 channels, 5 kHz data acquisition rate

3.2.6 Indicating Data Acquisition System

An AVL Indimaster Advanced 671 indicating system is used to obtain crank-angle-resolved signals and perform combustion analysis. The signals include crank angle, cylinder pressure, needle lift, and injection pressure. Two Micro Indicating Front End Modules (Micro IFEMs), in conjunction with imbedded piezo and voltage amplifiers, obtain the signals from the eight cylinder pressure transducers and provide the conditioned and amplified signals to the IndiCom software. An additional Micro IFEM has the capability to acquire two more piezo electric signals as well as two multi-purpose signals. These devices have a 14-bit amplitude resolution with a maximum sampling frequency of 800 kHz per channel.

IndiCom software operates on a Windows platform, facilitates parameter management, and provides test specific data and combustion analysis results. A graphical assistant presents displays all system parameters, permits hardware set up, and

allows access to measurement definitions. A graphical formula editor performs real-time calculation of such combustion metrics as start of combustion, heat release rate, total heat release, and fuel injection rate allowing visualization of these parameters as experiments are conducted. The indicating system can be controlled through the PUMA software or it can operate as a stand-alone program.

3.2.7 ASAM Interface

ASAM is communications protocol developed by a body of automotive manufacturers who formed an association in Europe in an effort to standardize the various interfaces made at various levels to a test bed. U. S. manufacturers are embracing the standard and are producing products that are ASAM compliant. PUMA uses this ASAM standard to communicate with non-AVL test cell components.

An ASAM-compliant interface is used between PUMA and the INCA software that is connected to the PCM. Through this connection, PUMA is able to acquire specified engine data as well as exert control over engine operating parameters.

3.2.8 Emissions Bench

An AVL Combustion Emissions Bench II (CEB-II) is used to sample, condition, and measure exhaust gas constituents. The cabinet stands in the control room next to the PUMA cabinet and is shown in Figure 3.7. Analyzers in the cabinet quantify the amount of CO, CO_2, O_2, total hydrocarbons (THC), NO and NO_X in the exhaust gases and the CO_2 levels in the intake manifold.

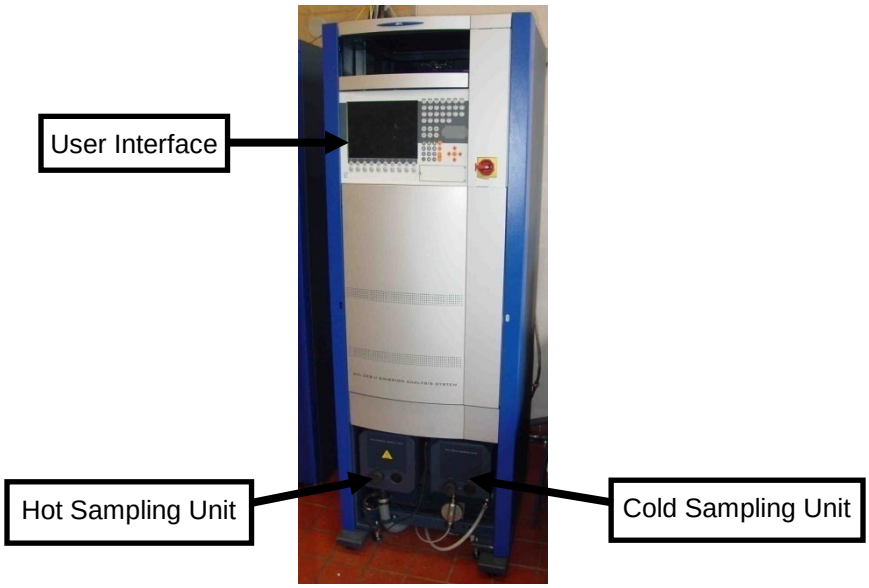

Figure 3.7: CEB-II Emissions Bench

Total Hydrocarbon Analyzer

An ABB Advance Optima Multi-FID 14 EGA is used to measure the total hydrocarbon emissions. This flame ionization detector (FID) determines the mass of carbon in the sample which is converted to a hydrocarbon-mass basis by assuming a specific carbon to hydrogen ratio. A FID uses a burner to combust a stream of hydrogen/helium fuel as a diffusion flame in air. The hydrocarbon-containing sample gas is premixed with the fuel and is also consumed in the burner. Combustion of these hydrocarbons increases the concentrations of ions within the flame. This increase in ionization is directly proportional to the mass flow rate of carbon atoms into the flame. A DC voltage between the burner tip and a collector electrode, which surrounds the flame, collects the ions within the flame, causing current to flow through the associated electronic circuits. This current is measured and associated to the total hydrocarbon emissions.

Oxides of Nitrogen Analyzer

NO and NO_X emissions are quantified with an Eco-Physics CLD 700 chemiluminescent detector (CLD). This analyzer can only measure the concentration of NO, but incorporates a high-efficiency converter to change any NO_2 present to NO to determine the total NO_X emissions. Light is emitted from the chemiluminescent reaction of NO and ozone (O_3) and when excess O_3 is present, the amount of light emitted is proportional to the concentration of NO. This light is detected by an optical filter-photomultiplier combination that produces an output that is linear to the concentration of NO in the sample.

Carbon Monoxide and Carbon Dioxide Analyzers

Two ABB Advance Optima URAS 14 EGA nondispersive infrared (NDIR) analyzers are used to determine the amount of CO and CO_2 in the samples. One measures the amount of CO and CO_2 in the exhaust gas, while the other measures the amount of CO_2 in the intake manifold.

The NDIR analyzers detect the infrared energy absorption differential between two gas-filled columns. The gas concentration that is to be determined flows through the sample column while the reference column is filled with a non-absorbing gas such as dry air. Infrared radiation is passed through the sample and reference columns into a detector that has two cells which are filled with gas and physically separated by a flexible, metal diaphragm. The infrared radiation collected by each cell heats up its gas and increases the cell pressure.

When a sample gas flows through the sample column, some of the infrared energy is absorbed by the gas and less energy will arrive at the sample cell side of the detector. This causes a gas in the sample cell side to heat up less and therefore have a lower pressure than the reference cell. The pressure difference causes a deflection in the metal

diaphragm, which is used as one plate of a variable plate capacitor in a tuned electric circuit. Detector output is generated by oscillating the diaphragm and measuring its amplitude, which is correlated to the amount of CO and CO_2.

Oxygen Analyzer

An ABB Advance Optima Magnos 16 paramagnetic oxygen analyzer is used to determine the amount of oxygen in the exhaust gas sample. This instrument operates by quantifying the magnetic susceptibility of the sample, which can be thought of as a measure of the ability of a molecule to become a temporary magnet when placed in a magnetic field. Since oxygen is the only exhaust gas constituent that is strongly paramagnetic, its quantity is readily obtained by using this method. A dumbbell-shaped test body mounted on a quartz fiber is suspended in a nonuniform magnetic field. As the partial pressure of oxygen in the gas sample surrounding the test body changes, the body will rotate. An optical system that senses this rotation causes a voltage to be applied to the test body to maintain it in a stationary position. This voltage is output signal of the amplifier circuit, and is then correlated to the oxygen concentration in the gas sample.

3.2.9 Fast NO Analyzer

Transient NO emissions are measured by a CLD 500 Fast NO analyzer made by Cambustion, Limited. It is a chemiluminescent detector that is used for measuring NO and NO_X concentration in a sample gas and has a 90%→10% response time of less than 2 ms. This is achieved by locating the detectors in remote sample heads that are positioned very close to the sample point in the engine and conveying the sample gas to the detectors under the influence of a vacuum through narrow heated capillaries. Data from this device is provided every 3 milliseconds. At an engine speed of 3000 rpm, this results in NO

values updated every 6 crank angle degrees, which gives a good picture of concentrations during the blowdown process.

3.2.10 Fast Particulate Spectrometer

Temporally resolved particulate concentrations are provided by a differential mobility spectrometer (DMS) 500 manufactured by Cambustion, Limited. This instrument measures the number of particles and their spectral weighting in the 5 nm to 1000 nm size range with a time response of 200 ms. Data from this device is provided at 10 Hz; at engine speeds over 1200 rpm, this means that the readings are updated less than once per cycle. Therefore linking particulate emissions to specific cycles is not possible. This data rate, however, represents the fastest particulate measurements available from any device on the market.

The instrument provides aerosol size spectral data by using a corona discharge to place a prescribed charge on each particle. The charged sample is then introduced into a strong electrical field inside a classifier column as shown in Figure 3.8. This field causes particles to drift through a sheath flow to the electrometer detectors. Particles are detected at different points throughout the column depending on their aerodynamic drag/charge ratio. Outputs from the electrometers are then processed to provide spectral data and other desired parameters. Conversion of aerosol spectral size data into particulate mass is performed by using a correlation developed by Park, et. al. [40].

3.2.12 Fast Sampling Valve System

To permit accurate in-cylinder gas measurements, a Cambustion CSV500 Fast-Sampling Valve System is used. The system uses rapidly-actuating solenoid valves to sample gases from the combustion chamber over a well-defined crank-angle window independent of engine speed. This eliminates the need for transient time corrections and maintains gas sensor accuracy by providing a constant-pressure sampling environment.

This CSV500 valve system consists of a control computer, a main control unit, a valve driver unit, and a valve assembly. The control computer runs software that is used to define and monitor system performance, specifically the crank angle window over which the sampling takes place. Settings from the control computer are then passed to the main control unit, which provides timing signals to the valve driver unit, drives for the heaters, and vacuum levels for the sampling system. Valve timing signals are passed into the valve driver unit, which develops and sends the appropriate pulses to the solenoids on the valve assembly that control sample flow.

The valve assembly, shown in Figure 3.9, consists of four components: the sample line, a sample distribution block, a purge solenoid valve, and a sampling solenoid valve. The sample line is inserted into the engine and provides access to the cylinder gases. See Section 4.3 for further details regarding instrumentation of the cylinder. The sample distribution block directs the in-cylinder gases to either the atmosphere through the purge valve or into a storage tube, which is plumbed in parallel with the gas analyzer. The solenoid valves function to control the directional flow of the sampled in-cylinder gases.

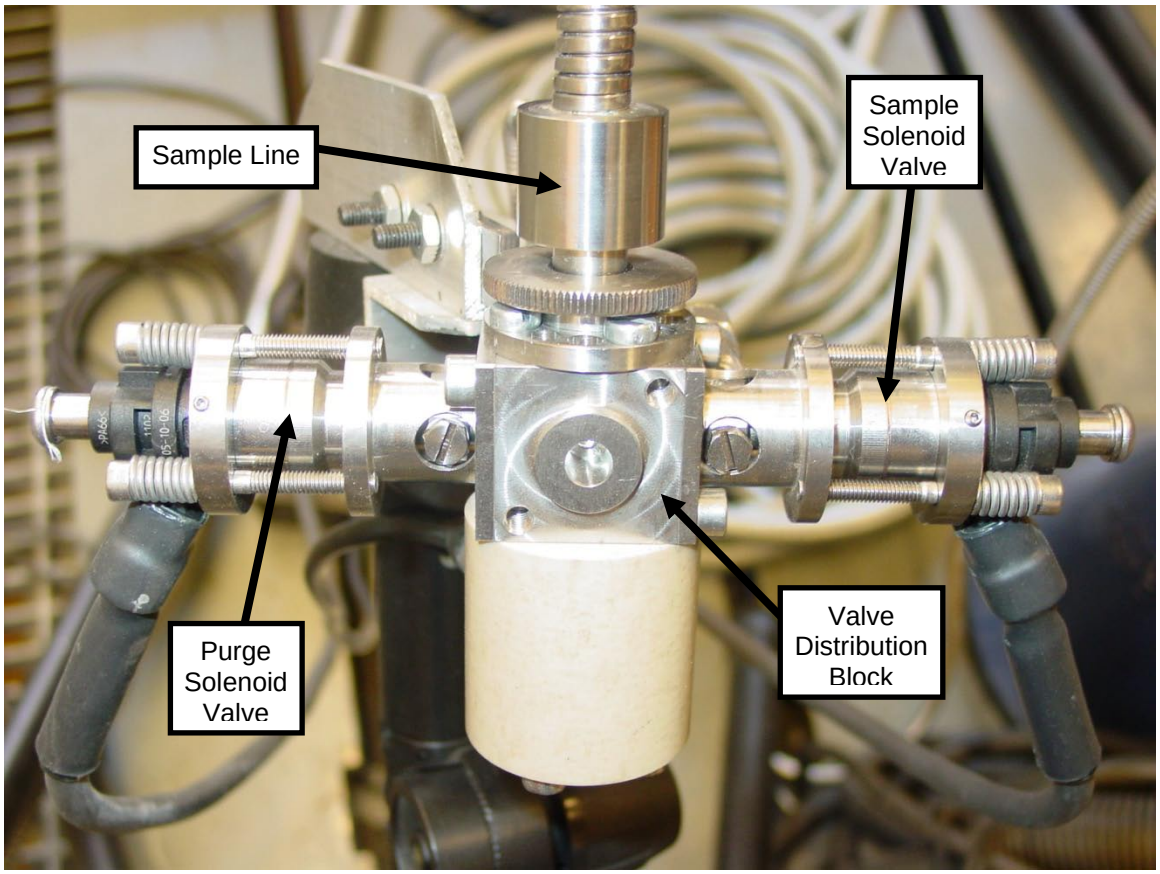

Figure 3.9: CSV500 Valve Assembly

As a test is being conducted, the gas analyzer draws a sample continuously and the solenoid valves open and close to change the source of the gas pulled through the analyzer. When both solenoid valves are closed, the system is sealed and no sample is taken from the cylinder. Instead, the analyzer draws gas from the open-ended storage tube, which provides a constant-pressure sampling environment; this is demonstrated in Figure 3.10(a). When a measurement of in-cylinder gases is made, the purge solenoid valve opens and cylinder pressure drives the gases in the length of the sample line to purge to the atmosphere and fills the sample line with fresh in-cylinder gases, as shown inFigure 3.10(b). This solenoid valve closes and then the valve connected to the gas analyzer and storage tube opens to allow the fresh sample from in the cylinder to flow into the storage tube as shown in Figure 3.10(c). Once a sufficient volume of gas has been provided to the storage tube, the solenoid valve closes to once again seal up the

cylinder. The gas analyzer then draws the in-cylinder sample from the storage tube to generate a reading from the configuration displayed in Figure 3.10(a), and the system has returned to its original state.

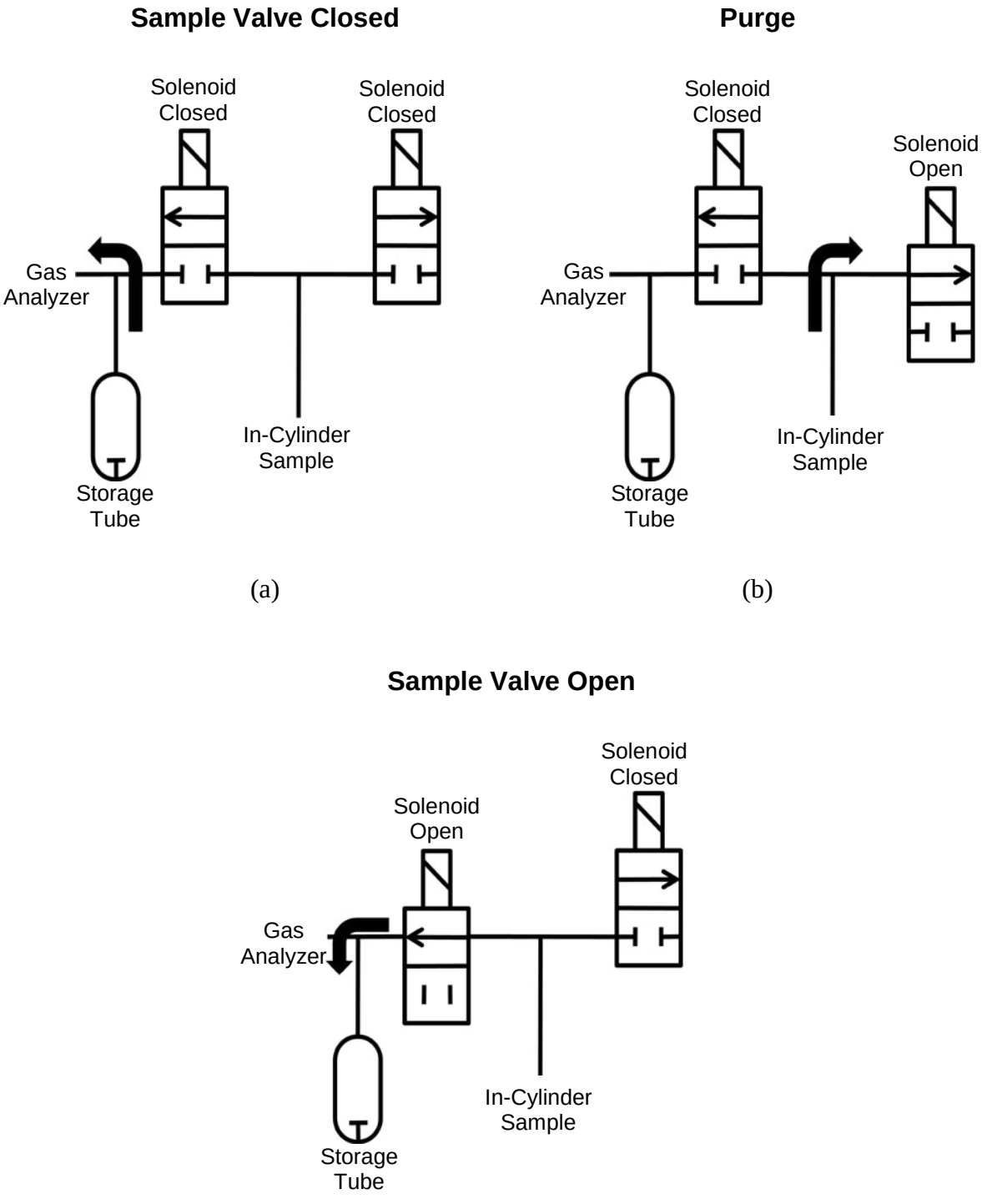

Figure 3.10: Pneumatic Schematic of CSV500 Fast Sampling Valve

CHAPTER 4

EXPERIMENTAL TECHNIQUE TO DETERMINE CYCLE-RESOLVED IN-CYLINDER MIXTURE COMPOSITION

Knowledge of cycle-resolved in-cylinder trapped masses is necessary to understand why and how transient emissions are formed. To facilitate this, an experimental and analytical technique is developed to determine the mass of fuel, air, and stoichiometric combustion product gases trapped in the cylinder. This chapter describes in detail the employed methodology and includes the assumptions, equations, and implemented iterative procedure. First, in-cylinder conceptualizations before and after combustion are presented. Next, equations are developed that relate exhaust gas measurements to pre-combustion in-cylinder composition and establish the need to perform in-cylinder and exhaust manifold gas measurements. Then cycle-resolved in-cylinder and exhaust manifold measurement techniques are developed, which is followed by the determination of cycle-resolved fuel mass. Finally, an iterative technique that incorporates the fuel mass and in-cylinder and exhaust manifold gas measurements is then presented to calculate the trapped air and stoichiometric combustion product mass.

4.1 In-Cylinder Conceptualization

A conceptualization of in-cylinder conditions before and after combustion is facilitated through use of hydrocarbon combustion equations.

4.1.1 Governing Equations

The combustion reaction for one mole of a typical hydrocarbon fuel with air [42] is expressed in Equation (4.1).

$$CH_y + (j)(O_2 + 3.773N_2) \rightarrow (a)CO_2 + (b)H_2O + (c)C_3H_8 + \cdots \\ \cdots + (d)NO + (e)H_2 + (f)CO + (g)O_2 + (h)N_2 \tag{4.1}$$

Where: y = Atomic H-C ratio of fuel

( ) = Moles of constituent per mole of fuel

By assuming complete and stoichiometric combustion, Equation (4.1) becomes

$$CH_y + (j)(O_2 + 3.773N_2) \rightarrow (a)CO_2 + (b)H_2O + (h)N_2 \tag{4.2}$$

Now the only unknowns are the concentrations of air, carbon dioxide, water, and nitrogen. By balancing the atoms of carbon, hydrogen, oxygen, and nitrogen, four equations are written to solve for the unknowns, and Equation (4.2) is written as

$$CH_y + \left(1 + \frac{y}{4}\right)(O_2 + 3.773N_2) \rightarrow CO_2 + \left(\frac{y}{2}\right)H_2O + \left(1 + \frac{y}{4}\right)N_2 \tag{4.3}$$

In Equation (4.3), the coefficient in front of the air term represents the number of moles of air that are needed for stoichiometric combustion, $(n_{AIR})_{Stoich}$. To develop a relationship between the number of air moles in stoichiometric and non-stoichiometric combustion, the equivalence ratio, ϕ, is introduced as

$$\phi = \frac{(A/F)_{Stoich}}{(A/F)_{Actual}} = \frac{\left(\frac{m_{Air}}{m_{Fuel}}\right)_{Stoich}}{\left(\frac{m_{Air}}{m_{Fuel}}\right)_{Actual}} = \frac{\left(\frac{n_{Air}\,MW_{Air}}{n_{Fuel}\,MW_{Fuel}}\right)_{Stoich}}{\left(\frac{n_{Air}\,MW_{Air}}{n_{Fuel}\,MW_{Fuel}}\right)_{Actual}} \tag{4.4}$$

Where: ϕ = Equivalence Ratio (-)

$(A/F)_{Stoich}$ = Stoichiometric air/fuel ratio (-)

$(A/F)_{Actual}$ = Actual air/fuel ratio (-)

m_{Air} = Mass of air (kg)

m_{Fuel} = Mass of fuel (kg)

n_{Air} = Moles of air (-)

n_{Fuel} = Moles of fuel (-)

MW_{Air} = Molecular weight of air (kg/kmole)

MW_{Fuel} = Molecular weight of fuel (kg/kmole)

When Equation (4.4) is written for one mole of fuel and solved for the moles of air in the actual combustion process, it simplifies to

$$(A/F)_{Stoic\,h} = \left(\frac{n_{Air}\,MW_{Air}}{n_{Fuel}\,MW_{Fuel}}\right)_{Stoic\,h} = 4.773\left(1+\frac{y}{4}\right)\left(\frac{MW_{Air}}{MW_{Fuel}}\right) \tag{4.5}$$

Using the terms from the numerator in Equation (4.4) and the coefficients in Equation (4.3), the stoichiometric air/fuel ratio is calculated.

$$(n_{Air})_{Actual} = \frac{(n_{Air})_{Stoic\,h}}{\phi} \tag{4.6}$$

By substituting Equation (4.5) into Equation (4.3) and rewriting the equation with all the unknowns from Equation (4.1), the combustion reaction becomes

$$CH_y + \frac{1}{\phi}\left(1+\frac{y}{4}\right)(O_2 + 3.773N_2) \rightarrow (a)CO_2 + (b)H_2O + (c)C_3H_8 + \cdots \tag{4.7}$$
$$\cdots + (d)NO + (e)H_2 + (f)CO + (g)O_2 + (h)N_2$$

For equivalence ratios less than one, excess air is present and the amount of unburned fuel, nitrogen monoxide, hydrogen, and carbon monoxide are negligible. This type is typical for direct injection diesel combustion, where the process is typically lean. Thus Equation (4.7) is rewritten as

$$CH_y + \frac{1}{\phi}\left(1+\frac{y}{4}\right)(O_2 + 3.773N_2) \rightarrow (a)CO_2 + (b)H_2O + (g)O_2 + (h)N_2 \tag{4.8}$$

The unknown terms on the right-hand-side of Equation (4.8) can now be written in terms of ϕ by balancing the individual atoms, which yields

$$CH_y + \frac{1}{\phi}\left(1+\frac{y}{4}\right)(O_2 + 3.773N_2) \rightarrow CO_2 + \left(\frac{y}{2}\right)H_2O + \left(\frac{1}{\phi}-1\right)\left(1+\frac{y}{4}\right)O_2 + \frac{3.773}{\phi}\left(1+\frac{y}{4}\right)N_2 \quad (4.9)$$

Rearranging the oxygen and nitrogen on the right-hand-side so that the oxygen and nitrogen are grouped together in the ratio that exists in air, Equation (4.9) becomes

$$CH_y + \frac{1}{\phi}\left(1+\frac{y}{4}\right)(O_2 + 3.773N_2) \rightarrow CO_2 + \left(\frac{y}{2}\right)H_2O + \cdots \quad (4.10)$$
$$\cdots + 3.773\left(1+\frac{y}{4}\right)N_2 + \underbrace{\left(\frac{1}{\phi}-1\right)\left(1+\frac{y}{4}\right)O_2 + 3.773\left(\frac{1}{\phi}-1\right)\left(1+\frac{y}{4}\right)N_2}_{Air}$$

The stoichiometric combustion reaction shown in Equation (4.3) and the lean combustion reaction in Equation (4.10) are very similar and aid in the formation of an in-cylinder conceptualization. Because the coefficients of the products in the stoichiometric reaction match the coefficients of the non-air products in the lean reaction, it follows that lean combustion produces two distinct components: the products of combustion of a stoichiometric mixture of air and fuel, and excess air which does not participate in combustion. This distinction is shown clearly in Equation (4.11).

$$CH_y + \frac{1}{\phi}\left(1+\frac{y}{4}\right)(O_2 + 3.773N_2) \rightarrow \quad (4.11)$$
$$\underbrace{CO_2 + \left(\frac{y}{2}\right)H_2O + 3.773\left(1+\frac{y}{4}\right)N_2^{SC}}_{Stiochiometric\ Combustion\ Products} + \cdots$$
$$\cdots + \underbrace{\left(\frac{1}{\phi}-1\right)\left(1+\frac{y}{4}\right)O_2 + 3.773\left(\frac{1}{\phi}-1\right)\left(1+\frac{y}{4}\right)N_2}_{Excess\ Air}$$

Two important conclusions can be made from Equation (4.11). First, for the complete combustion of one mole of fuel, the amount of CO_2, H_2O, and N_2 from stoichiometric combustion remains fixed. Therefore, knowledge of the concentration of one of these three individual components results in knowing the concentrations of all

three. When these products are recycled into the cylinder in the form of residual gas or EGR, they act as an inert diluent and are denoted in equations by the SC script.

Second, the proportion of stoichiometric combustion products is independent of the equivalence ratio. Thus for any combustion event, if the amount of fuel is known, so is the amount of the stoichiometric combustion products. These conclusions have further implications which are discussed in the next section, where conceptualizations of in-cylinder conditions before and after combustion are introduced.

4.1.2 In-Cylinder Conceptualization Prior to Combustion

During the intake process of a four-stroke engine, the piston moves from top dead center (TDC) to bottom dead center (BDC). As the piston begins to move downward, the exhaust valve typically remains open for a few crank angles into the intake stroke so that the maximum amount of exhaust gas from the previous cycle is expelled from the cylinder. Not all of this exhaust is removed, however, so there is some amount of this residual gas present in every cycle.

Most of the gas drawn into the cylinder during the intake stroke comes from the intake manifold through the intake valve. The gas in the intake manifold typically consists of a mixture of fresh air and EGR. Engines that use external EGR route the gases from the exhaust manifold to the intake manifold and generally use a heat exchanger to cool the gases. Therefore the EGR in the intake manifold is a mixture of exhaust gases from multiple cylinders and multiple cycles. When the intake stroke is completed and the intake valve closes, the cylinder charge thus consists of fresh air, residual gas and EGR. This is demonstrated on a molar basis in Equation (4.12) and with a diagram in Figure 4.1(a).

$$n^{Pre-Comb} = \sum_i n_i = n_{Air} + n_{EGR} + n_{Residual} \tag{4.12}$$

Where: $n^{Pre-Comb}$ = Moles prior to combustion and fuel injection

n_i = Moles of the i^{th} gas component

n_{Air} = Moles of air

n_{EGR} = Moles of EGR

$n_{Residual}$ = Moles of residual

As concluded above from Equation (4.11), the products of lean combustion consist only of excess air and stoichiometric combustion products. While the relative proportion of these two components is dependent upon the equivalence ratio of the combustion event in which they were formed, they remain distinct. Because both EGR and residual gas are the products of lean combustion, they are considered to be made up of air and the products of stoichiometric combustion. Therefore the terms for the moles of EGR and residual in Equation (4.12) are changed to moles of air and stoichiometric combustion products in Equation (4.13). This is also represented in Figure 4.1(b).

$$n^{Pre-Comb} = \sum_i n_i = n_{Air} + \underbrace{(n_{Air} + n_{SC})}_{From\ EGR} + \underbrace{(n_{Air} + n_{SC})}_{From\ Residual} \tag{4.13}$$

Where: $n^{Pre-Comb}$ = Moles prior to combustion and fuel injection

n_i = Moles of the i^{th} gas component

n_{Air} = Moles of air

n_{SC} = Moles from stoichiometric combustion

Chemically there is no distinction between fresh air and the air present in exhaust gases. Likewise, because the ratios of the components of the products of stoichiometric combustion are fixed and independent of the combustion conditions, there is no chemical difference between the stoichiometric combustion products from different combustion cycles. Thus Equation (4.13) is simplified to Equation (4.14), which is represented in Figure 4.1(c).

$$n^{Pre-Comb} = \sum_i n_i = n_{Air} + n_{SC} \tag{4.14}$$

Once fuel injection has occurred and the fuel has vaporized, the total number of gas moles changes to account for the additional moles of fuel vapor. Thus the total number of moles in the cylinder increases, as shown in Equation (4.15), which is written according to the in-cylinder conceptualization shown in Figure 4.1(d).

$$n^{Pre-Comb,F} = \sum_i n_i = n_{Air} + n_{SC} + n_{Fuel} \tag{4.15}$$

Where: $n^{Pre-Comb,F}$ = Moles prior to combustion and after fuel injection

n_i = Moles of the i^{th} gas component

n_{Air} = Moles of air

n_{SC} = Moles from stoichiometric combustion

n_{Fuel} = Moles of fuel

4.1.3 In-Cylinder Conceptualization After Combustion

During the combustion process, chemical reactions take place between the molecules represented in Equation (4.15) and thus the number of moles in the cylinder change continuously. Once the reactions subside, however, the number of moles in the cylinder remains fixed. Since the moles from stoichiometric combustion in the cylinder from EGR and residual do not participate in the combustion reaction, they are carried through from Equation (4.15). Fuel and air, however, are consumed and new combustion products are formed; to account for this, the term $n_{Exhaust}^{AFR}$ is introduced. Therefore the post-combustion mixture is written as Equation (4.16), which is also shown schematically in Figure 4.2(a).

$$n^{Post-Comb} = \sum_i n_i = n_{Exhaust}^{AFR} + n_{SC} \tag{4.16}$$

Where: $n^{Post-Comb}$ = Moles of gas after combustion

n_i = Moles of i^{th} gas component

$n_{Exhaust}^{AFR}$ = Moles formed from combustion

n_{SC} = Moles from stoichiometric combustion in EGR and residual gas

By referring to Equation (4.11), the products of lean combustion are composed entirely of the products of stoichiometric combustion and air. Therefore the molecules represented by the $n_{Exhaust}^{AFR}$ term can be replaced by air and stoichiometric combustion moles. Thus the molecules of gas after combustion can are represented by Equation (4.17) and Figure 4.2(b).

$$n^{Post-Comb} = \sum_i n_i = \underbrace{n_{Air} + n_{SC}}_{From\ Combustion} + \underbrace{n_{SC}}_{From\ EGR\ and\ Residual} \tag{4.17}$$

As in the pre-combustion case, there is no chemical difference between the stoichiometric combustion moles formed by combustion and those that came from previous combustion cycles in the form of EGR and residual. Therefore the conceptualization becomes as shown in Equation (4.18) and Figure 4.2(c).

$$n^{Post-Comb} = \sum_i n_i = n_{Air} + n_{SC} \tag{4.18}$$

The in-cylinder conceptualizations before and after combustion presented in Equations (4.12) through (4.18) and Figure 4.1 and Figure 4.2 are used when developing an understanding of gas measurements taken from the cylinder before combustion and the exhaust manifold after combustion. These are described in further detail in Section 4.3.2.

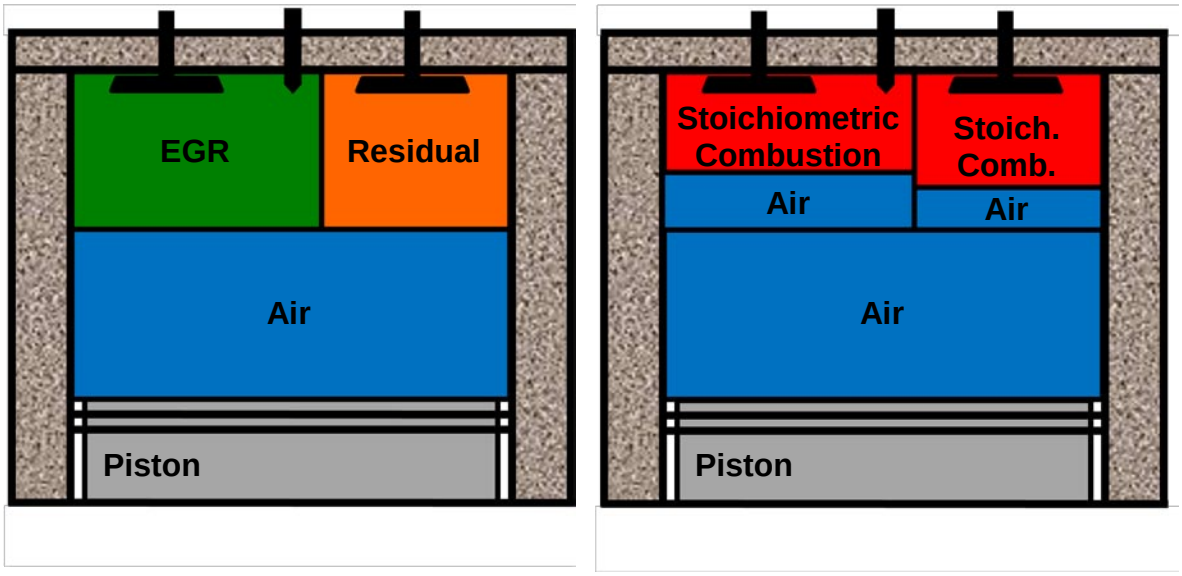

(a) (b)

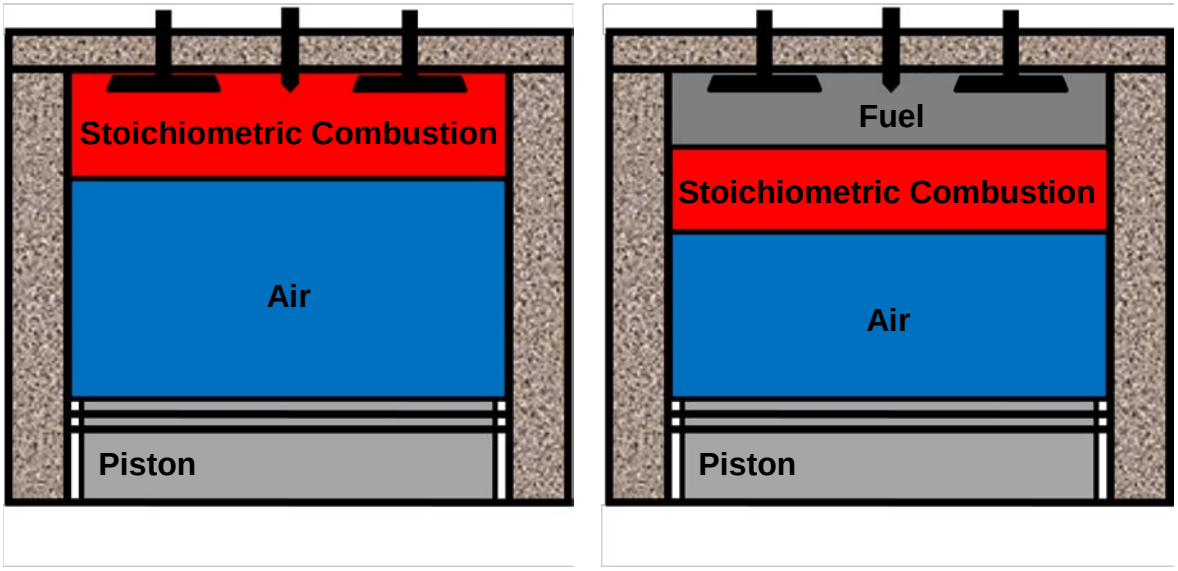

(c) (d)

Figure 4.1: Pre-Combustion In-Cylinder Conceptualization

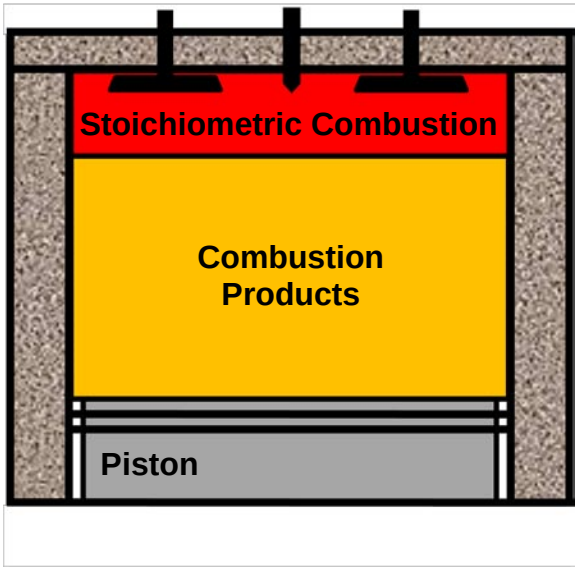

(a)

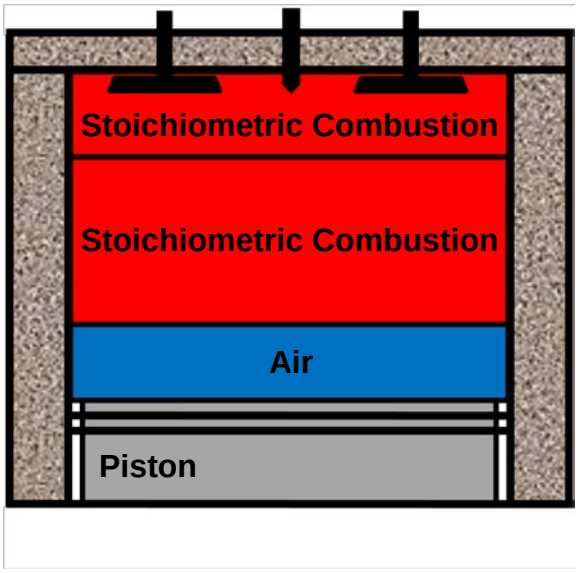

(b)

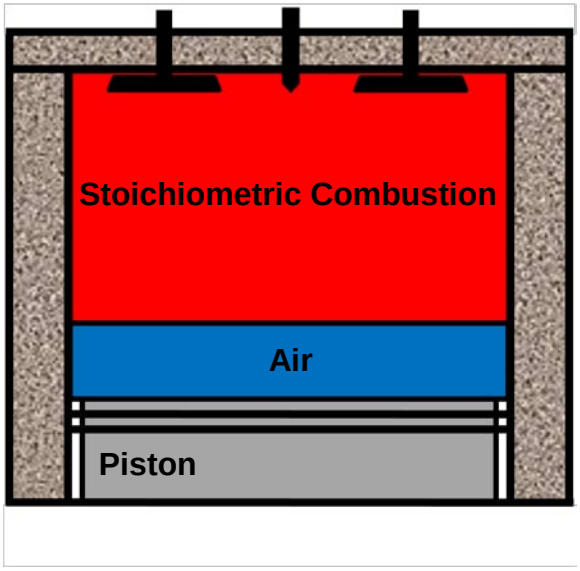

(c)

Figure 4.2: Post-Combustion In-Cylinder Conceptualization

4.2 Exhaust Mass Emissions and Air/Fuel Ratio Determination on a Fuel Basis

Exhaust gas measurement techniques have long been recognized as straight-forward and reliable means to obtain information about combustion processes [43]. When used in conjunction with combustion equations, exhaust gas measurements can also be used to determine pre-combustion conditions.

In order to determine how much mass of a particular compound an engine is forming, two parameters are needed: the concentration of that compound in the exhaust stream and the mass of one component of the exhaust. The mass can be of the air or fuel prior to combustion, or of the exhaust formed by combustion. Generally fuel flow is used because it is the most readily and accurately determined. To use fuel flow, however, the observed exhaust concentrations must be converted to their production on a fuel basis.

Once exhaust concentrations are known on a fuel basis, combustion equations can be used to convert the quantities of the products of combustion into quantities of the reactants prior to combustion on a fuel basis. With knowledge of fuel mass, this technique can be used to determine the amount of air in the cylinder prior to combustion.

4.2.1 Exhaust Mass Emissions on a Fuel Basis

To determine exhaust mass emissions on a fuel basis, the combustion equation for one mole of a hydrocarbon fuel is rewritten from Equation (4.1)

$$CH_y + (j)(O_2 + 3.773N_2) \rightarrow (a)CO_2 + (b)H_2O + (c)C_3H_8 + \cdots \\ \cdots + (d)NO + (e)H_2 + (f)CO + (g)O_2 + (h)N_2 \tag{4.19}$$

Where: y = Atomic H-C ratio of fuel

( ) = Moles of constituent per mole of fuel

To reduce the number of unknowns, the number of C, H, O, and N atoms in the reactants and products are balanced. Thus Equation (4.19) becomes

$$CH_y + (j)(O_2 + 3.773N_2) \rightarrow (a)CO_2 + (b)H_2O + (c)C_3H_8 + \cdots \quad (4.20)$$
$$\cdots + (d)NO + \left(\frac{y}{2} - b - 4c\right)H_2 + (1 - a - 3c)CO + \cdots$$
$$\cdots + \left(j - a - \frac{b}{2} - \frac{d}{2} - \frac{1 - a - 3c}{2}\right)O_2 + \left(3.773j - \frac{d}{2}\right)N_2$$

Since the above equation is written for one mole of fuel which is represented on a C_1 basis, it follows that only one mole of carbon atoms is present on both sides of the equation. Therefore, balancing the number of carbon atoms yields

$$1 = a + (1 - a - 6c) + 3c \quad (4.21)$$

By assuming ideal gas behavior, the concentration, or mole fraction, is proportional to the number of moles prescribed in Equation (4.20) and thus when written in terms of moles and molar concentrations, Equation (4.21) becomes

$$n_{Fuel} = \chi_{CO_2} + \chi_{CO} + 3\chi_{C_3H_8} \quad (4.22)$$

Where: n_{Fuel} = Moles of fuel

χ_{CO_2} = Mole fraction of CO_2 in exhaust

χ_{CO} = Mole fraction of CO in exhaust

$\chi_{C_3H_8}$ = Mole fraction of C_3H_8 in exhaust

Therefore the number of moles of any component X from Equation (4.20) per mole of fuel can be represented by Equation (4.23).

$$\frac{n_X}{n_{Fuel}} = \frac{\chi_X}{\chi_{CO_2} + \chi_{CO} + 3\chi_{C_3H_8}} \quad (4.23)$$

Where: n_X = Moles of X

n_{Fuel} = Moles of fuel

χ_X = Mole fraction of component X in exhaust

χ_{CO_2} = Mole fraction of CO_2 in exhaust

χ_{CO} = Mole fraction of CO in exhaust

$\chi_{C_3H_8}$ = Mole fraction of C_3H_8 in exhaust

Using this molar ratio, the mass of any constituent of Equation (4.20) relative to the mass of fuel is determined via Equation (4.24).

$$\frac{m_X}{m_{Fuel}} = \left(\frac{MW_X}{MW_{Fuel}}\right)\frac{\chi_X}{\chi_{CO_2} + \chi_{CO} + 3\chi_{C_3H_8}} \tag{4.24}$$

Where: m_X = Mass of X

m_{Fuel} = Mass of fuel

MW_X = Molecular weight of X

MW_{Fuel} = Molecular weight of fuel

χ_X = Mole fraction of component X in exhaust

χ_{CO_2} = Mole fraction of CO_2 in exhaust

χ_{CO} = Mole fraction of CO in exhaust

$\chi_{C_3H_8}$ = Mole fraction of C_3H_8 in exhaust

4.2.2 Air/Fuel Ratio Determination from Exhaust Concentration Measurements

Determination of air/fuel ratio from exhaust concentration measurements is accomplished through a method introduced by Stivender [42]. Using Equation (4.20), he introduces a fuel conversion factor, N, which is defined as

$$N = \frac{n_{Exhaust}}{n_{Fuel}} = \frac{100}{\chi_{CO_2} + \chi_{CO} + 3\chi_{C_3H_8}} \tag{4.25}$$

Where: $n_{Exhaust}$ = Moles of exhaust

n_{Fuel} = Moles of fuel

χ_{CO_2} = Mole fraction of CO_2 in exhaust (%)

χ_{CO} = Mole fraction of CO in exhaust (%)

$\chi_{C_3H_8}$ = Mole fraction of C_3H_8 in exhaust

Equation (4.20) also provides the molar air to fuel ratio, which is defined as

$$\frac{n_{Air}}{n_{Fuel}} = j + 3.773j = 4.773j \tag{4.26}$$

Where: n_{Air} = Moles of air

n_{Fuel} = Moles of fuel

To determine the number of moles formed from the combustion of one mole of fuel, the coefficients of the products in Equation (4.20) are summed together.

$$N = a + b + c + d + \left(\frac{y}{2} - b - 4c\right) + (1 - a - 3c) + \cdots \tag{4.27}$$
$$\cdots + \left(j - a - \frac{b}{2} - \frac{d}{2} - \frac{1 - a - 3c}{2}\right) + \left(3.773j - \frac{d}{2}\right)$$

By simplifying, rearranging, and assuming that no water is condensed, the number of exhaust moles simplifies to

$$N = 4.773j - 3c + \left(\frac{1 - a - 3c}{2}\right) - \frac{b}{2} + \frac{y}{2} \tag{4.28}$$

Combining Equations (4.26) and (4.28) and solving for the molar air to fuel ratio yields

$$\frac{n_{Air}}{n_{Fuel}} = N + 3c - \left(\frac{1 - a - 3c}{2}\right) + \frac{b}{2} - \frac{y}{2} \tag{4.29}$$

In Equation (4.29) the terms c, $(1 - a - 3c)$, and b represent the coefficients of unburned fuel, carbon monoxide, and water, respectively, from Equation (4.20). To express these coefficients in terms of molar percent concentrations, the fuel conversion factor is used in the identity

$$\frac{n_X}{n_{Fuel}} = \frac{n_X}{n_{Exhaust}} \cdot \frac{n_{Exhaust}}{n_{Fuel}} = \frac{\chi_X}{100} \cdot N \tag{4.30}$$

Thus the individual terms in Equation (4.29) where the coefficients are present are replaced with the identity in Equation (4.30), which results in

$$\frac{n_{Air}}{n_{Fuel}} = N + \frac{3\chi_{C_3H_8}}{100}N - \frac{\chi_{CO}}{200}N + \frac{\chi_{H_2O}}{200}N - \frac{y}{2} \tag{4.31}$$

By grouping terms and multiplying by the ratio of molecular weights of air and fuel, an equation for the air/fuel ratio based on exhaust gas concentration measurements is derived.

$$\frac{m_{Air}}{m_{Fuel}} = \frac{MW_{Air}}{MW_{Fuel}}\left[N + \frac{N}{100}\left(3\chi_{C_3H_8} - \frac{1}{2}\chi_{CO} + \frac{1}{2}\chi_{H_2O}\right) - \frac{y}{2}\right] \tag{4.32}$$

Using the assumptions from the development of Equation (4.11) and the in-cylinder conceptualizations, lean combustion has negligible levels of hydrocarbon and CO emissions. Therefore, Equations (4.25) and (4.32) are respectively rewritten as

$$N = \frac{100}{\chi_{CO_2}} \tag{4.33}$$

$$\frac{m_{Air}}{m_{Fuel}} = \frac{MW_{Air}}{MW_{Fuel}}\left[\frac{100}{\chi_{CO_2}} + \frac{1}{\chi_{CO_2}}\left(\frac{1}{2}\chi_{H_2O}\right) - \frac{y}{2}\right] \tag{4.34}$$

Furthermore, using the relationships presented in Equation (4.11), for each mole of fuel burned, the ratio of water and carbon dioxide formed during combustion is fixed at

$$\chi_{H_2O} = \frac{y}{2}\chi_{CO_2} \tag{4.35}$$

By substituting Equation (4.35) into (4.34), the air/fuel ratio becomes

$$\frac{m_{Air}}{m_{Fuel}} = \frac{MW_{Air}}{MW_{Fuel}}\left[\frac{100}{\chi_{CO_2}^{AFR}} - \frac{y}{4}\right] \tag{4.36}$$

The CO_2 concentration in Equation (4.36), $\chi_{CO_2}^{AFR}$, represents the amount of CO_2 formed from combustion. Therefore if any CO_2 was present in the cylinder prior to combustion in the form of residual or EGR, it should not be included in this equation. To know how much CO_2 was formed from combustion when EGR and residual are existent, both the pre- and post-combustion CO_2 levels must be known. This is accomplished

through in-cylinder and exhaust manifold measurements, which are detailed in the next section.

4.3 In-Cylinder and Exhaust Manifold Measurements

This section describes the gas concentration measurements made in the cylinder and in the exhaust manifold. First, the locations used to sample and measure the concentration of gases in the cylinder and in the exhaust manifold are described. Then typical data from these measurements are demonstrated as well as the procedures used to determine cycle-resolved values. Finally, equations are presented that link the in-cylinder and exhaust manifold measurements to the in-cylinder conceptualizations developed in Section 4.1.

4.3.1 Measurement Locations

One cylinder of the engine used in this study is instrumented to permit the sampling of gases from the combustion chamber. The exhaust manifold adjacent to the outlet of the cylinder is also instrumented to allow exhaust gas measurement. The front right cylinder was chosen because gases measured at this location during the exhaust stroke almost certainly come from that particular cylinder and engine layout affords easy access.

In-cylinder measurements are facilitated by an L-shaped port drilled into the head. The presence of cooling jackets, oil galleries, and valve ports in the head presented limited options to access the cylinder. This configuration was chosen to minimize the potential of oil and coolant leaks and to simplify the machining process by excluding any compound angles. A cross-section of the head demonstrating the relative positioning of the measurement probe and the piston is shown in Figure 4.3 and a picture of the port itself as seen from the bottom of the cylinder head is shown in Figure 4.4.

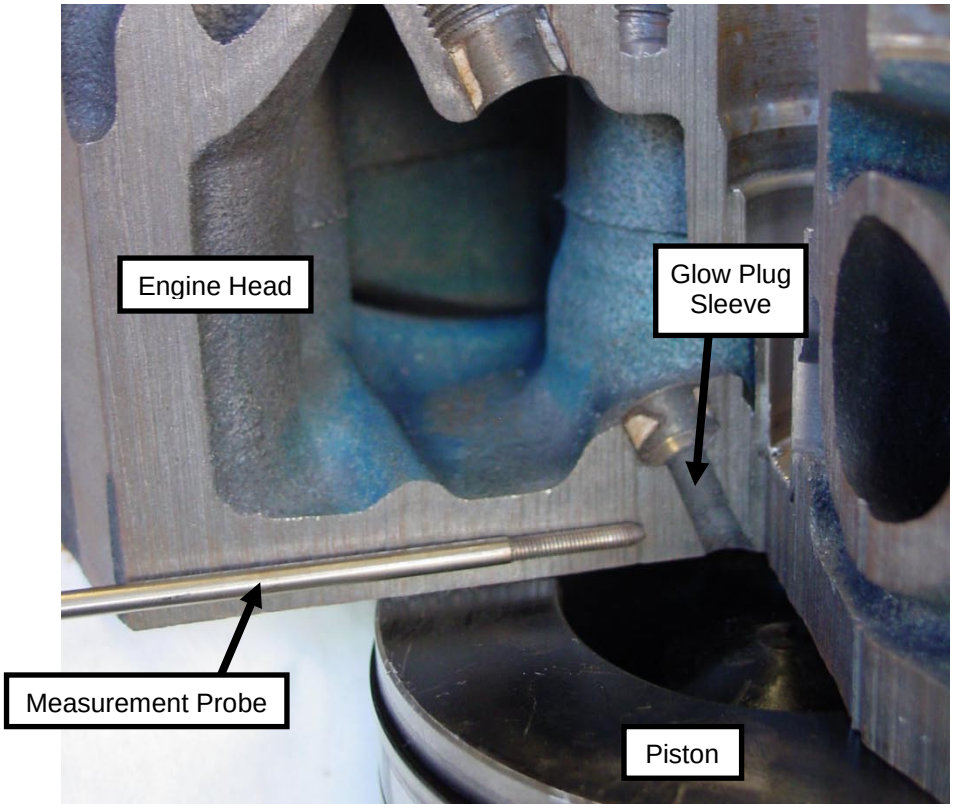

Figure 4.3: Cross-Section of Head and Measurement Port

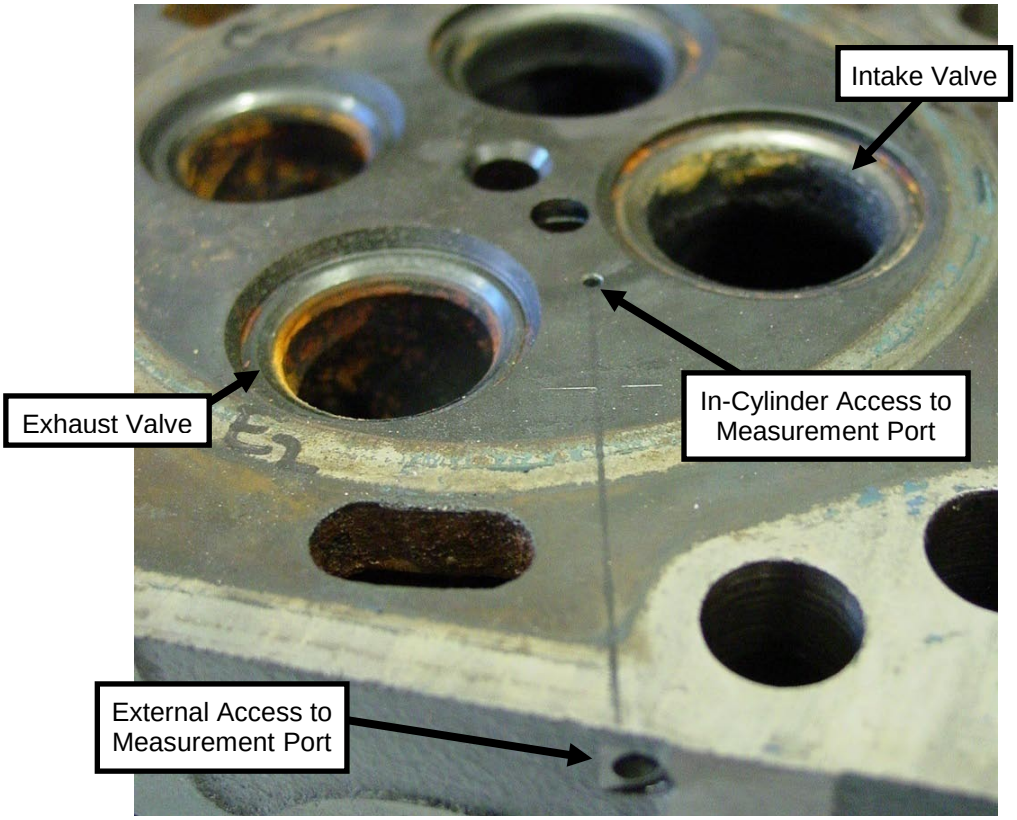

Figure 4.4: In-Cylinder Measurement Port

The corresponding location in the exhaust manifold has been instrumented to allow measurement of exhaust gases. This configuration with all accompanying instrumentation is shown in Figure 4.5.

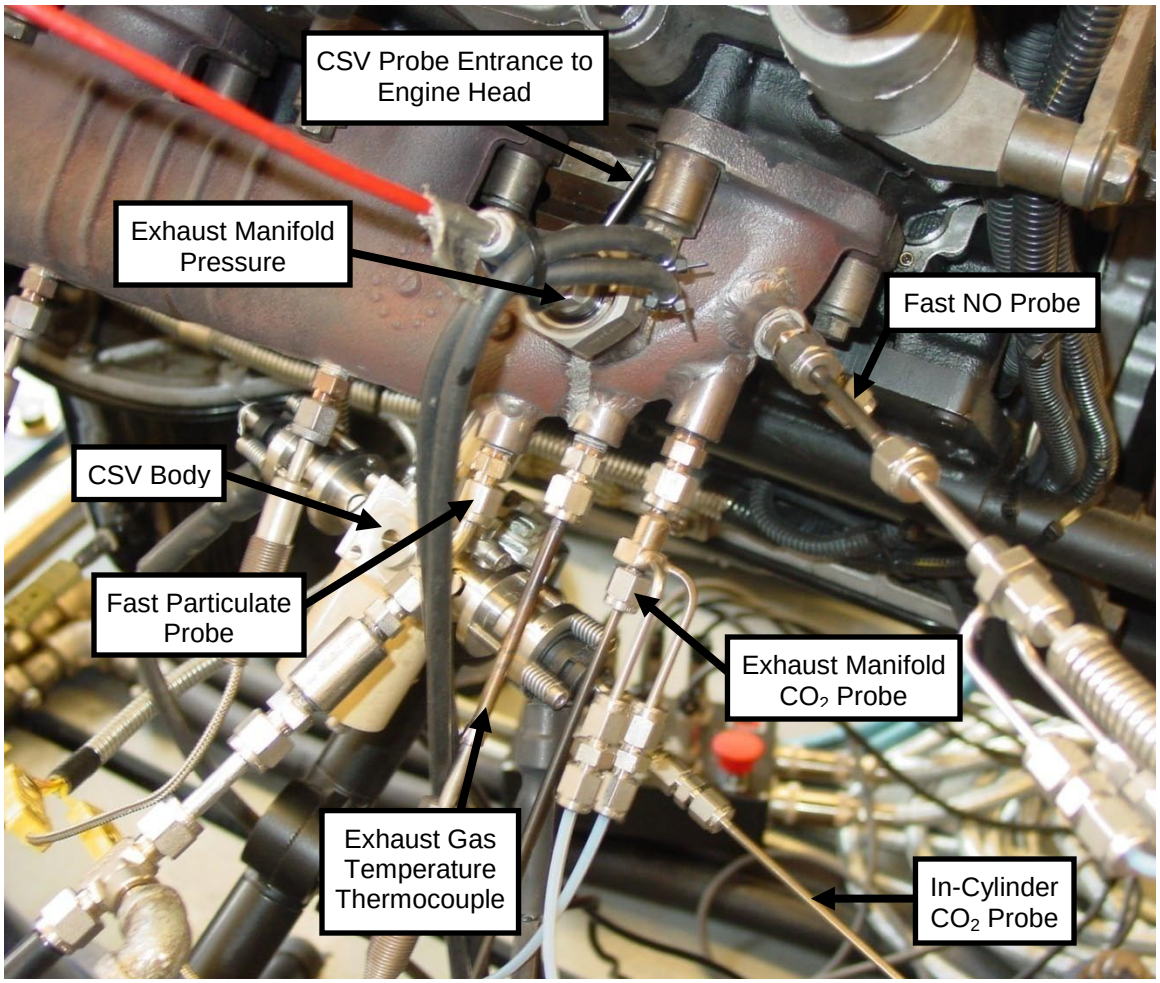

Figure 4.5: Exhaust Manifold Instrumentation

Data from the Fast CO/CO_2 sensor and the Fast NO sensor are obtained on a crank-angle resolved basis. These data must be distilled down to cycle-resolved values, which is accomplished with routines in MATLAB and is described in detail in Appendix B.

4.3.2 CO_2 Measurement Equations

For this study, an NDIR gas analyzer is used to measure the concentration of carbon dioxide in the cylinder and in the exhaust manifold. This analyzer measures the molar fraction of CO_2 in the mixture, and typically reports its output on a percentage or a parts-per-million (ppm) basis. The molar fraction of CO_2, χ_{CO_2}, is given in Equation (4.37).

$$\chi_{CO_2} = \frac{Moles\ CO_2}{Total\ Moles} = \frac{n_{CO_2}}{\sum_i n_i} \tag{4.37}$$

Where: n_{CO_2} = Moles of CO_2

n_i = Moles of i^{th} gas constituent

For in-cylinder measurements of CO_2 made prior to fuel injection, the conceptualization shown in Figure 4.1(a) is applicable and the reading from the sensor is given by Equation (4.38).

$$\chi_{CO_2}^{Pre-Comb} = \frac{Moles\ CO_2}{Total\ Moles} = \frac{n_{CO_2}}{n_{Air} + n_{EGR} + n_{Residual}} \tag{4.38}$$

Where: $\chi_{CO_2}^{Pre-Comb}$ = Mole fraction of CO_2 before combustion

n_{CO_2} = Moles of CO_2 prior to combustion

n_{Air} = Moles of air

n_{EGR} = Moles of EGR

$n_{Residual}$ = Moles of residual

When Equation (4.38) is written according to the in-cylinder conceptualization prior to combustion demonstrated in Figure 4.1(c), the measurement of CO_2 becomes

$$\chi_{CO_2}^{Pre-Comb} = \frac{n_{CO_2}}{n_{Air} + n_{SC}} \tag{4.39}$$

Where: $\chi_{CO_2}^{Pre-Comb}$ = Mole fraction of CO_2 before combustion

n_{CO_2} = Moles of CO_2 prior to combustion and fuel injection

n_{Air} = Moles of air

n_{SC} = Moles from stoichiometric combustion

The number of moles of CO_2 in cylinder prior to combustion can also be thought of as the sum of the mole fractions of CO_2 in each component of the gas mixture. Thus Equation (4.39) is rewritten as

$$\chi_{CO_2}^{Pre-Comb} = \frac{\chi_{CO_2}^{Air} n_{Air} + \chi_{CO_2}^{SC} n_{SC}}{n_{Air} + n_{SC}} \tag{4.40}$$

Where: $\chi_{CO_2}^{Pre-Comb}$ = Mole fraction of CO_2 before combustion

$\chi_{CO_2}^{Air}$ = Mole fraction of CO_2 in air

n_{Air} = Moles of air

$\chi_{CO_2}^{SC}$ = Mole fraction of CO_2 in gas from stoichiometric combustion

n_{SC} = Moles from stoichiometric combustion

By assuming the mole fraction of CO_2 in the fresh air is zero, the first term in the numerator disappears. The mole fraction of CO_2 in the gas from stoichiometric combustion is a fixed value as demonstrated in Equation (4.11) and is shown in Equation (4.41).

$$\chi_{CO_2}^{SC} = \frac{n_{CO_2}}{n_{CO_2} + n_{H_2O} + n_{N_2}^{SC}} = \frac{1}{1 + \frac{y}{2} + 3.773\left(1 + \frac{y}{4}\right)} \tag{4.41}$$

Where: $\chi_{CO_2}^{SC}$ = Mole fraction of CO_2 in gas from stoichiometric combustion

n_{CO_2} = Moles of CO_2

n_{H_2O} = Moles of H_2O

$n_{N_2}^{SC}$ = Moles of N_2 from stoichiometric combustion

Using these simplifications, Equation (4.40) becomes

$$\chi_{CO_2}^{Pre-Comb} = \frac{\chi_{CO_2}^{SC} n_{SC}}{n_{Air} + n_{SC}} \tag{4.42}$$

Measurements taken in the exhaust manifold during the exhaust stroke capture the gas concentrations present after combustion has subsided. The concentration of CO_2

after combustion, $\chi_{CO_2}^{Post-Comb}$, is written according to the post-combustion, in-cylinder conceptualization shown in Figure 4.2(a).

$$\chi_{CO_2}^{Post-Comb} = \frac{Moles\ CO_2}{Total\ Moles} = \frac{n_{CO_2}}{n_{Exhaust}^{AFR} + n_{SC}} \tag{4.43}$$

Where: $\chi_{CO_2}^{Post-Comb}$ = Mole fraction of CO_2 after combustion

n_{CO_2} = Moles of CO_2 after combustion

$n_{Exhaust}^{AFR}$ = Moles of combustion products

n_{SC} = Moles from stoichiometric combustion

The moles from stoichiometric combustion in Equation (4.43) are the same number of moles that were present prior to combustion; that is, n_{SC} from Equation (4.42). The moles of combustion products appear because of the reactions of air and fuel. A portion of these products is CO_2, which represents the amount of CO_2 formed during combustion. This is precisely the quantity needed to calculate the air/fuel ratio in Equation (4.36). By rewriting the number of moles of CO_2 as the sum of the mole fractions of the components of the mixture, Equation (4.43) becomes

$$\chi_{CO_2}^{Post-Comb} = \frac{\chi_{CO_2}^{AFR} n_{Exhaust}^{AFR} + \chi_{CO_2}^{SC} n_{SC}}{n_{Exhaust}^{AFR} + n_{SC}} \tag{4.44}$$

Where: $\chi_{CO_2}^{Post-Comb}$ = Mole fraction of CO_2 after combustion

$\chi_{CO_2}^{AFR}$ = Mole fraction of CO_2 in combustion products

$n_{Exhaust}^{AFR}$ = Moles of combustion products

$\chi_{CO_2}^{SC}$ = Mole fraction of CO_2 in products of stoichiometric combustion

n_{SC} = Moles from stoichiometric combustion

Equations (4.42) and (4.44) are used in an iteration technique to calculate in-cylinder trapped masses of air and inert gases from stoichiometric combustion. These calculations, however, are predicated on knowledge of the fuel mass in the cylinder. The next section describes the cyclical determination of injected fuel mass.

4.4 Fuel Mass Determination

Calculation of the mass of fuel injected into the cylinder on a cyclical basis is accomplished through use of injector and fuel properties, tabulated steady-state data, and crank-angle resolved data from an instrumented fuel injector.

4.4.1 Governing Equations

Assuming that the fuel flow is inviscid, steady, and incompressible and that the nozzle holes act as an orifice, the fuel velocity through the injector holes can be approximated by using the Bernoulli equation.

$$\frac{1}{\rho_{Fuel}} P_{Cyl} + \frac{1}{2} {V_{Cyl}}^2 + g h_{Cyl} = \frac{1}{\rho_{Fuel}} P_{Inj} + \frac{1}{2} {V_{Inj}}^2 + g h_{Inj} \tag{4.45}$$

Where: P_{Cyl} = Cylinder pressure (N/m^2)

ρ_{Fuel} = Fuel density (kg/m^3)

V_{Cyl} = Velocity of fuel inside the injector (m/s)

h_{Cyl} = Vertical location of fuel inside the injector (m)

P_{Inj} = Injection pressure (N/m^2)

V_{Inj} = Injection velocity (m/s)

h_{Inj} = Vertical location of fuel outlet of injector (m)

By neglecting the effects of gravity and assuming that the area inside the injector is much greater than the nozzle hole area and solving for the injection velocity, Equation (4.45) becomes

$$V_{Inj} = \sqrt{\frac{2\left(P_{Cyl} - P_{Inj}\right)}{\rho_{Fuel}}} \text{ (m/s)} \tag{4.46}$$

Alternatively, by using the conservation of mass during the injection process, the fuel flow rate can be written as

$$\frac{dm_{Fuel}}{dt} = \rho_{Fuel} A_{Inj} V_{Inj} \text{ (kg/s)} \tag{4.47}$$

Where: $\frac{dm_{Fuel}}{dt}$ =Differential fuel mass flow rate (kg/s)

ρ_{Fuel} = Fuel density (kg/m^3)

A_{Inj} = Flow area of injector (m^2)

V_{Inj} = Injection velocity (m/s)

Substituting Equation (4.46) into Equation (4.47) yields

$$\frac{dm_{Fuel}}{dt} = A_{Inj}\sqrt{2\rho_{Fuel}\left(P_{Cyl} - P_{Inj}\right)} \text{ (kg/s)} \tag{4.48}$$

Friction losses during the fuel injection process result in energy dissipation, which reduces the actual mass flow rate from its theoretical limit. This phenomenon is typically accounted for by introducing a discharge coefficient, C_d, which is defined as

$$C_d = \frac{\left(\frac{dm_{Fuel}}{dt}\right)_{Actual}}{\left(\frac{dm_{Fuel}}{dt}\right)_{Theoretical}} \tag{4.49}$$

Where: C_d = Discharge coefficient

$\left(\frac{dm_{Fuel}}{dt}\right)_{Actual}$ = Differential actual fuel mass flow rate (kg/s)

$\left(\frac{dm_{Fuel}}{dt}\right)_{Theoretical}$ = Differential theoretical fuel mass flow rate (kg/s)

When Equation (4.49) is inserted into Equation (4.48), frictional losses are accounted for and the fuel flow rate becomes

$$\frac{dm_{Fuel}}{dt} = A_{Inj}\,C_d\sqrt{2\rho_{Fuel}\left(P_{Cyl} - P_{Inj}\right)} \text{ (kg/s)} \tag{4.50}$$

Both cylinder pressure and injection pressure are measured on a crank angle basis, and therefore the left hand side of Equation (4.48) must be rewritten in terms of crank angle,

$$\frac{dm_{Fuel}}{dCA} = A_{Inj}\,C_d\sqrt{2\rho_{Fuel}\left(P_{Cyl} - P_{Inj}\right)} \text{ (kg/CA)} \tag{4.51}$$

By multiplying both sides by dCA and integrating over the crank angle interval during which there is fuel flow Equation (4.51) takes the form

$$\int_{SOI}^{EOI} \frac{dm_{Fuel}}{dCA}\, dCA = \int_{SOI}^{EOI} \left[A_{Inj}\, C_d \sqrt{2\rho_{Fuel}\left(P_{Cyl} - P_{Inj}\right)} \right] dCA \ \text{(kg)} \tag{4.52}$$

Since fuel density and flow area of the injector do not change as a function of crank angle, they are moved outside of the integrand. Discharge coefficient, however, is a strong function of crank angle and its value is dependent upon needle lift height [44], fuel injection pressure [45], and is very sensitive to cavitation [46]. Start and end of injection processes when the injector needle is very near its seat are especially critical and cause significant changes to the discharge coefficient [47]. To account for the relationship between discharge coefficient and crank angle, the integral analogue of Equation (4.49) is written on a crank angle basis and used to introduce an average discharge coefficient term, $\overline{C_d}$, in Equation (4.53).

$$\overline{C_d} = \frac{\int_{SOI}^{EOI} \left(\frac{dm_{Fuel}}{dCA}\right)_{Actual} dCA}{\int_{SOI}^{EOI} \left(\frac{dm_{Fuel}}{dCA}\right)_{Theoretical} dCA} \tag{4.53}$$

Where: $\overline{C_d}$ = Discharge coefficient

$\left(\frac{dm_{Fuel}}{dCA}\right)_{Actual}$ = Differential actual fuel mass flow rate (kg/CA)

$\left(\frac{dm_{Fuel}}{dCA}\right)_{Theoretical}$ = Differential theoretical fuel mass flow rate (kg/CA)

Using the relationship established in Equation (4.49), Equation (4.53) can be rewritten as

$$\overline{C_d} = \frac{\int_{SOI}^{EOI} C_d \left(\frac{dm_{Fuel}}{dCA}\right)_{Theoretical} dCA}{\int_{SOI}^{EOI} \left(\frac{dm_{Fuel}}{dCA}\right)_{Theoretical} dCA} \tag{4.54}$$

Equation (4.54) shows that for a particular fuel injection event, the discharge coefficient essentially acts as a weighting function to the injected fuel mass. Furthermore, one value can be used to represent the discharge coefficient for an injection process. Therefore, Equation (4.52) can be rewritten as

$$\int_{SOI}^{EOI} \frac{dm_{Fuel}}{dCA}\, dCA = \sqrt{2\rho_{Fuel}}\, A_{Inj}\, \overline{C_d} \int_{SOI}^{EOI} \sqrt{\left(P_{Cyl} - P_{Inj}\right)}\, dCA \text{ (kg)} \tag{4.55}$$

The term on the right hand side of Equation (4.55) can be computed numerically with knowledge about fuel and injector properties and by using crank angle-resolved pressure data. The term on the left hand side is simply the total amount of fuel injected into each cylinder per cycle, m_{Fuel}. This mass of fuel can be determined experimentally in the test cell under steady state conditions by using the fuel flow rate measured with the fuel flow meter and assuming that an equal amount of fuel is distributed to each cylinder.

$$m_{Fuel} = \frac{60\dot{m}_{Fuel}\, n_R}{N n_C} \text{ (kg)} \tag{4.56}$$

Where: m_{Fuel} = Fuel mass (kg)

$\dot{m}_{Fuel}$ = Mass flow rate of fuel (kg/s)

n_R = Engine revolutions per power stroke

N = Engine speed (rpm)

n_C = Number of cylinders

Now the only unknown in Equation (4.55) is $\overline{C_d}$. Substituting Equation (4.56) into Equation (4.55) and solving for the average discharge coefficient yields

$$\overline{C_d} = \frac{60\dot{m}_{Fuel}\, n_R}{N n_C \sqrt{2\rho_{Fuel}}\, A_{Inj} \int_{SOI}^{EOI} \sqrt{\left(P_{Cyl} - P_{Inj}\right)}\, dCA} \tag{4.57}$$

Determining $\overline{C_d}$ in this manner with steady state data accounts for any inaccuracies incurred by approximation and forces the cumulative mass in an injection event to exactly match the fuel flow rate measured by the flow meter. This essentially

tunes the model for a particular operating condition by finding an average discharge coefficient that can be used throughout the fuel injection event.

4.4.2 Cyclic Determination of Average Discharge Coefficient

Cyclic determination of average discharge coefficient is accomplished by interpolation of steady state engine data. Three specific components are necessary: average discharge coefficients over the entire engine operating envelope, the proper inputs that will be used to look up each average discharge coefficient, and an appropriate interpolation method.

Steady State Average Discharge Coefficient

To obtain average discharge coefficients, experimental data was taken that spans the entire capability of the injection system. Specifically, engine speed, torque and nominal injection pressure were varied to produce 363 data points. At each condition, 100 cycles of data were used to calculate the average discharge coefficient using Equation (4.57). A visualization of the generated data is displayed in Figure 4.6.

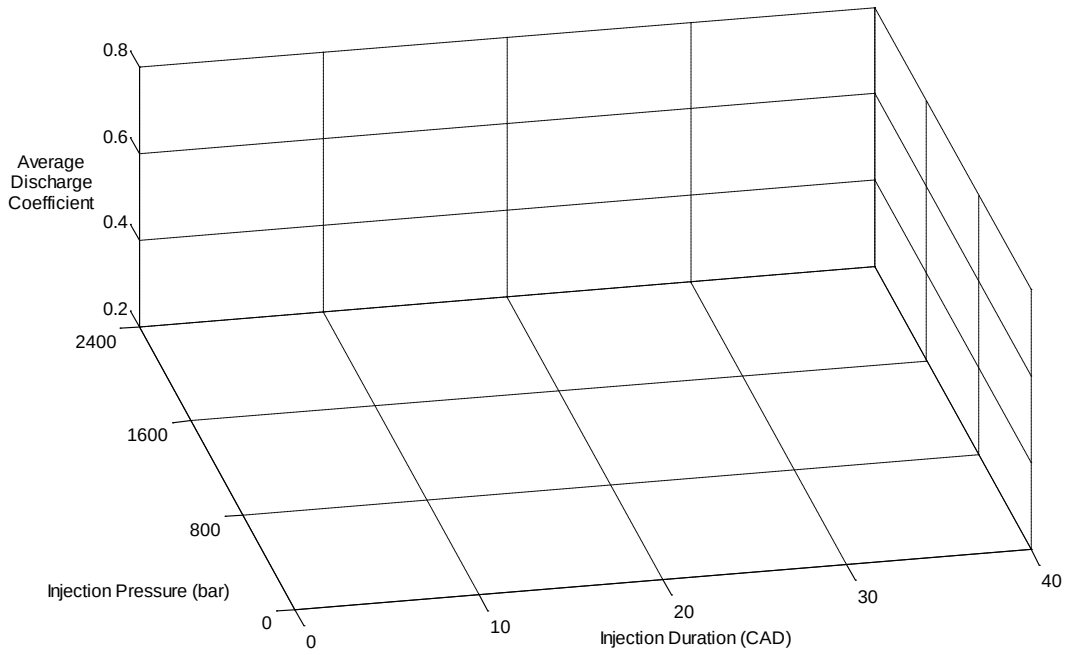

Figure 4.6: Experimentally-Obtained Average Discharge Coefficient

Inputs to Determine Cyclic Average Discharge Coeffcient

Analysis of the data and review of literature resulted in two variables that most directly impact the average discharge coefficient: the length of time during the injection event and the fuel injection pressure. Injection time is critical because it indicates the relative impact of the effects the opening and closing of the injector needle. When the needle is near its seat, C_d values are very low; conversely, C_d values are the highest when the needle is fully open. Since motion of the needle is governed by needle spring force and fuel injection pressure, the time for the needle to open and close is independent of the overall length of the injection event. Thus the effect of low C_d values as the needle is near its seat is much more prevalent during shorter injections; this is demonstrated in Figure 4.7. Rather than use injection time directly, engine speed in rpm and injection duration in crank angle are used because they are directly measured from the engine and they also take into account the engine operating condition.

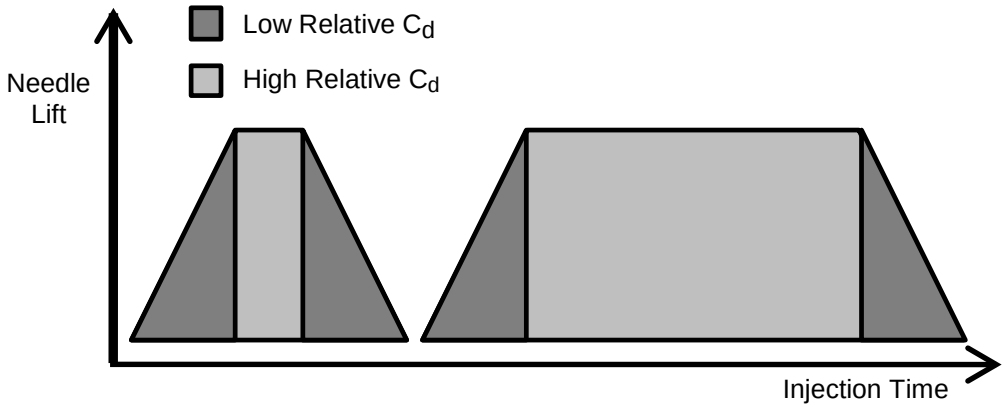

Figure 4.7: Influence of Injection Time on Average Discharge Coefficient

Injection pressure impacts the average discharge coefficient because it governs fluid velocity through the nozzle and the amount of cavitation. Nominal injection pressure can be represented in numerous ways, and its value must be accurate on a cycle-resolved basis and repeatable from cycle to cycle. Three different methods were considered in this study: the demanded injection pressure from the engine's PCM, the maximum injection pressure, and the average injection pressure during an injection event.

As engine operation remains steady, the demanded injection pressure from the engine's PCM provides repeatable values, but is not able to be obtained on a cycle-resolved basis and does not account for the actual behavior of the injector. The remaining two options, maximum and average fuel injection pressures, are both obtained from the instrumented injector. Using the maximum injection pressure, more emphasis is placed on repeatable cycle-to-cycle maximum pressure values. The average injection pressure, however, places more importance on consistent injector behavior over the entire injection event.

To determine which of the two variables best represents nominal injection pressure, two metrics were considered. First, the coefficient of variation (COV) of both the maximum and average injection pressure over 100 cycles was determined for each engine operating condition to determine which was the most repeatable. The average

COV of the maximum injection pressure was 1.78%, while the average COV of the average injection pressure was 1.89%. Second, another comparison was made to evaluate how these values correlate to the demanded pressure from the engine's PCM. The metric with the greatest squared correlation coefficient is more precisely controlled by the engine calibration. The maximum injection pressure values have a squared correlation coefficient of 0.95, while the average injection pressure values are 0.92. These results are shown in Figure 4.8. Because the maximum injection pressure values have lower COVs and are more precisely controlled by the engine's demanded injection pressure, it is used as the third input to look up the average discharge coefficients.

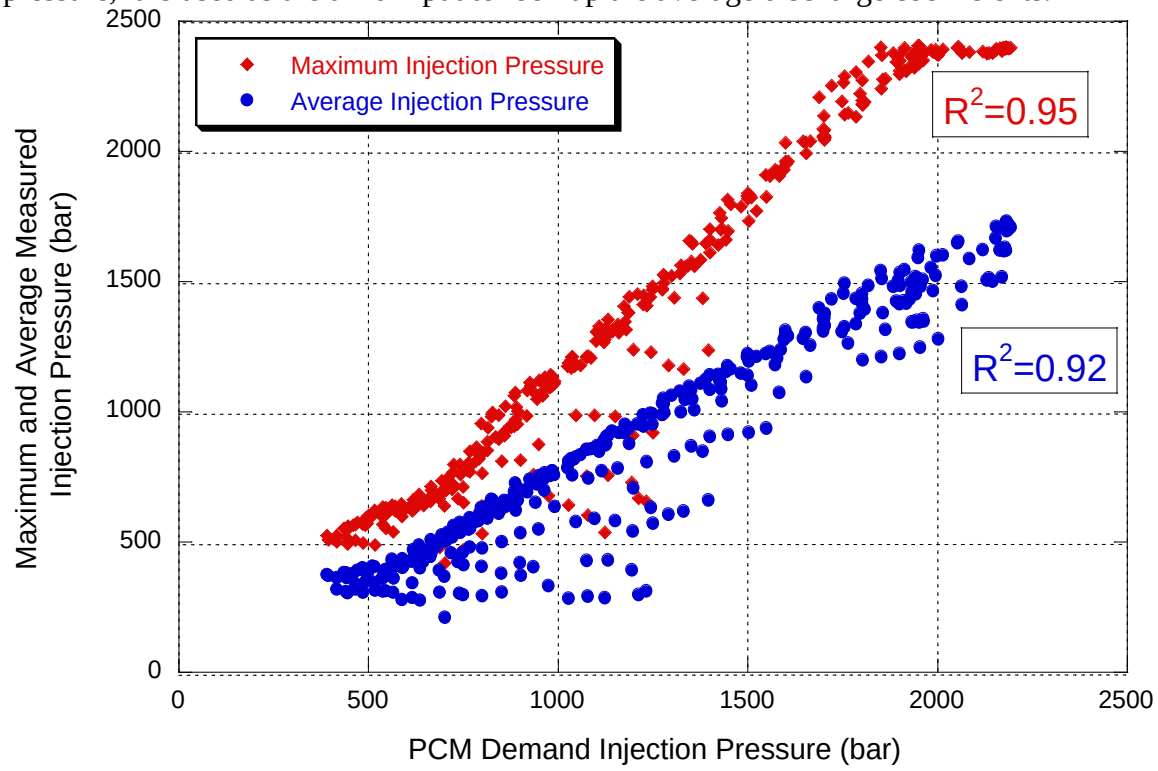

Figure 4.8: Correlation between PCM Demand Injection Pressure and Maximum and Average Measured Injection Pressure

Interpolation Method

Interpolation of the average discharge coefficient data is not trivial because the data is sparse and multi-dimensional. MATLAB was chosen to perform this task and the

details of this process are located in Appendix A. First injection pressure, injection duration, and engine speed are normalized to equalize the influence of each input; a visualization of the input data is shown in Figure 4.9. Then the *delaunay3* function is used to create tetrahedrons such that the data points are vertices of the tetrahedrons and no data point is contained within any tetrahedron. Therefore when any combination of engine speed, maximum injection pressure, and injection duration are used as inputs to be interpolated, it falls into a particular tetrahedron. The data points that define the vertices of that tetrahedron are then used to linearly interpolate a value of average discharge coefficient.

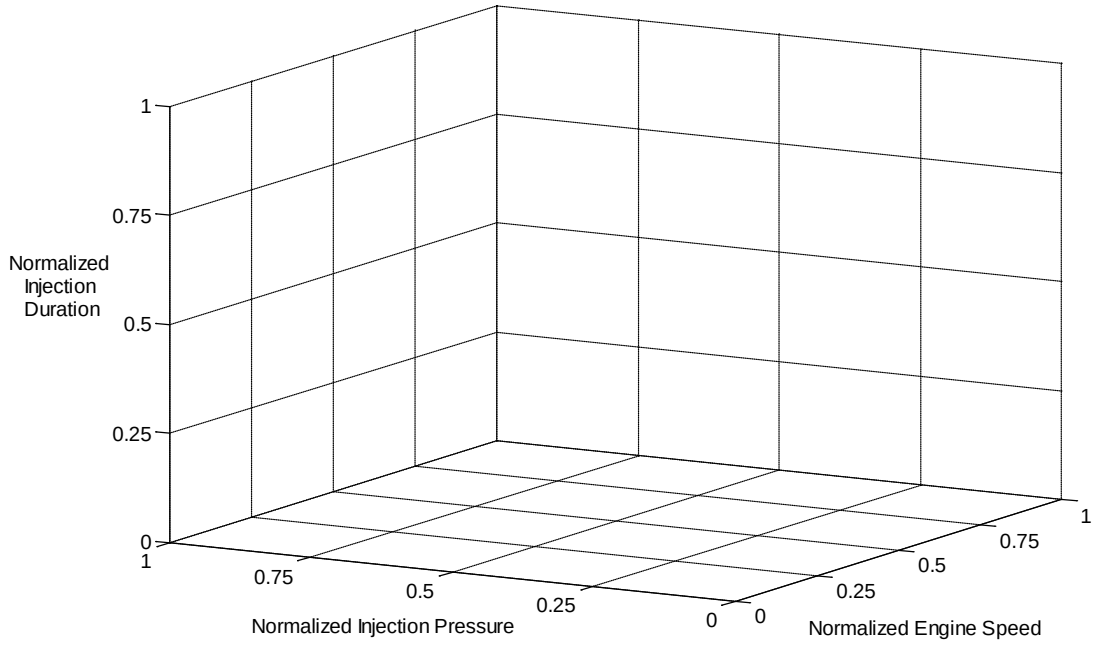

Figure 4.9: Normalized Average Discharge Coefficient Data Points

The relative proximity of the point to be interpolated to each one of the vertices is also accounted for by using a weighting function, which gives closer points a greater influence over the final value of average discharge coefficient. Figure 4.10 demonstrates the interpolation scheme within the tetrahedron, while Equation (4.58) is used to calculate the interpolated average discharge coefficient data.

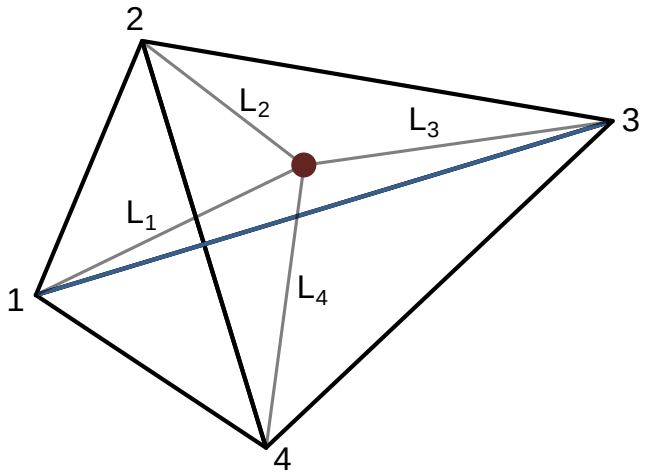

Figure 4.10: Interpolation of Average Discharge Coefficient Data

$$\overline{C_d}_{Interpolated} = \frac{\sum_{i=1}^{4}(\overline{C_d})_i \cdot L_i}{\sum_{i=1}^{4} L_i} \tag{4.58}$$

Where: $\overline{C_d}_{Interpolated}$ = Interpolated average discharge coefficient

$(\overline{C_d})_i$ = Average discharge coefficient of i^{th} tetrahedron vertex

L_i = Distance from point to be interpolated and i^{th} tetrahedron vertex

4.4.3 Cyclic Determination of Fuel Mass

When the fuel mass is to be evaluated on a cyclical basis, cylinder pressure, injection pressure, start of injection, end of injection, and engine speed are measured and used to calculate the mass of injected fuel. Because cylinder pressure and injection pressure are known only at discreet points, numerical integration must be used to approximate the integral in Equation (4.55). The composite trapezoid rule is used to numerically integrate the term under the integrand and thus the statement becomes as shown in Equation (4.59) where the term ΔCA represents the crank angle resolution of the pressure data.

$$m_{Fuel} = \sqrt{2\rho_{Fuel}}\, A_{Inj}\, \overline{C_d} \sum_{i=SOI}^{EOI-1} \left[\frac{\Delta CA}{2}\left\{\left(\sqrt{P_{Cyl} - P_{Inj}}\right)_i + \left(\sqrt{P_{Cyl} - P_{Inj}}\right)_{i+1}\right\}\right] \text{ (kg)} \tag{4.59}$$

The first two terms on the left-hand-side of Equation (4.59) remain constant for all engine cycles, while the average discharge coefficient is determined via the procedure developed in Section 4.4.2 using the engine speed, maximum injection pressure, and injection duration for that cycle. An error and sensitivity analysis of this technique is presented in Chapter 5.

4.5 Iterative Technique to Calculate Air and Inert Mass

Using the equations described in this chapter, an iterative technique is developed to calculate the cycle-resolved mass of air and mass of inert gases from stoichiometric combustion trapped in the cylinder. Iterations are necessary because the mass of air during combustion is first estimated to calculate other quantities, while successive loops converge on a final air mass value. The steps are as follows.

1. Determine fuel mass using the technique outlined in Section 4.4. Convert the mass of fuel to moles of fuel with

$$n_{Fuel} = \frac{m_{Fuel}}{MW_{Fuel}} \tag{4.60}$$

Where: n_{Fuel} = Moles of fuel
m_{Fuel} = Mass of fuel (kg)
MW_{Fuel} = Molecular weight of fuel (kg/kmol)

2. Estimate air mass with the flow rate value from the laminar flow element. Use the mass of fuel and mass of air to calculate an air/fuel ratio with

$$\left({}^{A}/_{F}\right)_{Actual} = \frac{m_{Air}}{m_{Fuel}} \tag{4.61}$$

Where: $\left({}^{A}/_{F}\right)_{Actual}$ = Actual air/fuel ratio
m_{Air} = Mass of air (kg)
m_{Fuel} = Mass of fuel (kg)

3. Determine the moles of air by using the air/fuel ratio and the moles of fuel via

$$n_{Air} = n_{Fuel} \frac{MW_{Fuel}}{MW_{Air}} \left(A/F\right)_{Actual} \tag{4.62}$$

Where: n_{Air} = Moles of air

n_{Fuel} = Moles of fuel

MW_{Fuel} = Molecular weight of fuel (kg/kmol)

MW_{Air} = Molecular weight of air (kg/kmol)

$\left(A/F\right)_{Actual}$ = Actual air/fuel ratio

4. Measure the CO_2 concentration in-cylinder, $\chi_{CO_2}^{Pre-Comb}$. This quantity is restated from Equation (4.42) as

$$\chi_{CO_2}^{Pre-Comb} = \frac{\chi_{CO_2}^{SC} n_{SC}}{n_{Air} + n_{SC}} \tag{4.63}$$

Where: $\chi_{CO_2}^{Pre-Comb}$ = Mole fraction of CO_2 before combustion

$\chi_{CO_2}^{SC}$ = Mole fraction of CO_2 in products of stoichiometric combustion

n_{SC} = Moles from stoichiometric combustion

n_{Air} = Moles of air

The mole fraction of CO_2 in the inert gases from stoichiometric combustion is fixed and given in Equation (4.41). Therefore the only unknown in Equation (4.63) is the number of moles of inert; solving for n_{SC} yields

$$n_{SC} = \frac{\chi_{CO_2}^{Pre-Comb} n_{Air}}{\chi_{CO_2}^{SC} - \chi_{CO_2}^{Pre-Comb}} \tag{4.64}$$

5. Calculate the equivalence ratio of the combustion process using the stoichiometric and actual air/fuel ratios. The stoichiometric air/fuel ratio is taken from Equation (4.5), while the actual air/fuel ratio is calculated in Equation (4.61).

$$\phi = \frac{\left(A/F\right)_{Stoich}}{\left(A/F\right)_{Actual}} = \frac{4.773\left(1 + \frac{y}{4}\right)\left(\frac{MW_{Air}}{MW_{Fuel}}\right)}{\left(A/F\right)_{Actual}} \tag{4.65}$$

Where: $\left(A/F\right)_{Stoich}$ = Stoichiometric air/fuel ratio

$\left(A/F\right)_{Actual}$ = Actual air/fuel ratio

y = Molar H-C ratio

MW_{Air} = Molecular weight of air (kg/kmol)

MW_{Fuel} = Molecular weight of fuel (kg/kmol)

6. Determine the number of moles of products formed from combustion. This is accomplished by summing the coefficients of the products in Equation (4.9) and then multiplying by the number of moles of fuel calculated in Equation (4.60).

$$n_{Exhaust}^{AFR} = n_{Fuel}\left[\frac{y}{4} + \frac{4.773}{\phi}\left(1 + \frac{y}{4}\right)\right] \tag{4.66}$$

Where: $n_{Exhaust}^{AFR}$ = Moles of exhaust formed during combustion

n_{Fuel} = Moles of fuel

y = Molar H-C ratio

ϕ = Equivalence ratio

7. Measure the CO_2 concentration in the exhaust manifold, $\chi_{CO_2}^{Post-Comb}$. This quantity is restated from Equation (4.44) as

$$\chi_{CO_2}^{Post-Comb} = \frac{\chi_{CO_2}^{AFR} n_{Exhaust}^{AFR} + \chi_{CO_2}^{SC} n_{SC}}{n_{Exhaust}^{AFR} + n_{SC}} \tag{4.67}$$

Where: $\chi_{CO_2}^{Post-Comb}$ = Mole fraction of CO_2 after combustion

$\chi_{CO_2}^{AFR}$ = Mole fraction of CO_2 in combustion products

$n_{Exhaust}^{AFR}$ = Moles of combustion products

$\chi_{CO_2}^{SC}$ = Mole fraction of CO_2 in gas from stoichiometric combustion

n_{SC} = Moles from stoichiometric combustion

The only unknown term in Equation (4.67) is $\chi_{CO_2}^{AFR}$, the mole fraction of CO_2 in the products of combustion. Rearranging this equation yields

$$\chi_{CO_2}^{AFR} = \frac{\chi_{CO_2}^{Post-Comb}\left(n_{Exhaust}^{AFR} + n_{SC}\right) - \chi_{CO_2}^{SC} n_{SC}}{n_{Exhaust}^{AFR}} \tag{4.68}$$

8. Calculate the actual air/fuel ratio using Equation (4.36), which is rewritten below

$$\left(A/F\right)_{Actual} = \frac{MW_{Air}}{MW_{Fuel}}\left[\frac{100}{\chi_{CO_2}^{AFR}} - \frac{y}{4}\right] \tag{4.69}$$

Where: $\left(A/F\right)_{Actual}$ = Actual air/fuel ratio

MW_{Air} = Molecular weight of air (kg/kmole)

MW_{Fuel} = Molecular weight of fuel (kg/kmole)

$\chi_{CO_2}^{AFR}$ = Mole fraction of CO_2 in combustion products

y = Molar H-C ratio

9. Check for convergence by determining the difference between the air/fuel ratio calculated in Step 8 and the one determined in Step 2. This is shown in Equation (4.70). If the difference between the two is less than δ, then the process has converged. For this study, a δ of *1E-9* is used.

$$\delta \leq \left(A/F\right)_{Actual}^{Step\ 8} - \left(A/F\right)_{Actual}^{Step\ 2} \tag{4.70}$$

Where: δ = Small value, *1E-9*

$\left(A/F\right)_{Actual}^{Step\ 8}$ = Actual air/fuel ratio from Step 8

$\left(A/F\right)_{Actual}^{Step\ 2}$ = Actual air/fuel ratio from Step 2

10. If the process has converged, calculate the final air mass by rearranging Equation (4.61) to get

$$m_{Air} = m_{Fuel}\left(A/F\right)_{Actual} \tag{4.71}$$

11. The mass of inert gases from stoichiometric combustion from EGR and residual is determined by using a form of Equation (4.64),

$$m_{SC} = \left(\frac{MW_{SC}}{MW_{Air}}\right)\frac{\chi_{CO_2}^{Pre-Comb}\, m_{Air}}{\chi_{CO_2}^{SC} - \chi_{CO_2}^{Pre-Comb}} \tag{4.72}$$

Where: m_{SC} = Mass of inert gases from stoichiometric combustion (kg)

MW_{SC} = Molecular weight of inert fraction (kg/kmole)

MW_{Air} = Molecular weight of air (kg/kmole)

$\chi_{CO_2}^{Pre-Comb}$ = Mole fraction of CO_2 before combustion

m_{Air} = Mass of air (kg)

$\chi_{CO_2}^{SC}$ = Mole fraction of CO_2 in gases from stoichiometric combustion

The molecular weight of the gases from stoichiometric combustion is readily determined because its components are known and occur in a fixed ratio.

$$MW_{SC} = \frac{\sum_i MW_i \cdot n_i}{\sum_i n_i} = \frac{MW_{CO_2} n_{CO_2} + MW_{H_2O} n_{H_2O} + MW_{N_2} n_{N_2}^{SC}}{n_{CO_2} + n_{H_2O} + n_{N_2}^{SC}} \tag{4.73}$$

$$= \frac{MW_{CO_2}(1) + MW_{H_2O}\left(\frac{y}{2}\right) + MW_{N_2}\left(3.773\left(1+\frac{y}{4}\right)\right)}{1 + \frac{y}{2} + 3.773\left(1+\frac{y}{4}\right)}$$

Where: MW_{SC} = Molecular weight of inert fraction (kg/kmole)

MW_i = Molecular weight i^{th} component of inert fraction (kg/kmole)

n_i = Number of moles of i^{th} component of inert fraction

MW_{CO_2} = Molecular weight of CO_2 (kg/kmole)

n_{CO_2} = Number of moles of CO_2

MW_{H_2O} = Molecular weight of H_2O (kg/kmole)

n_{H_2O} = Number of moles of H_2O

MW_{N_2} = Molecular weight of N_2 (kg/kmole)

$n_{N_2}^{SC}$ = Number of moles of excess N_2

If the process has not converged, the air/fuel ratio calculated in Step 8 is passed back to Step 2 and the quantities from Step 3 through Step 9 are recalculated. This iteration occurs until the convergence criterion is met. A flow chart representing this iteration scheme is shown in Figure 4.11. The numbers in the upper left corner of each box correspond to the steps above. An error and sensitivity analysis of this technique is also conducted in Chapter 5.

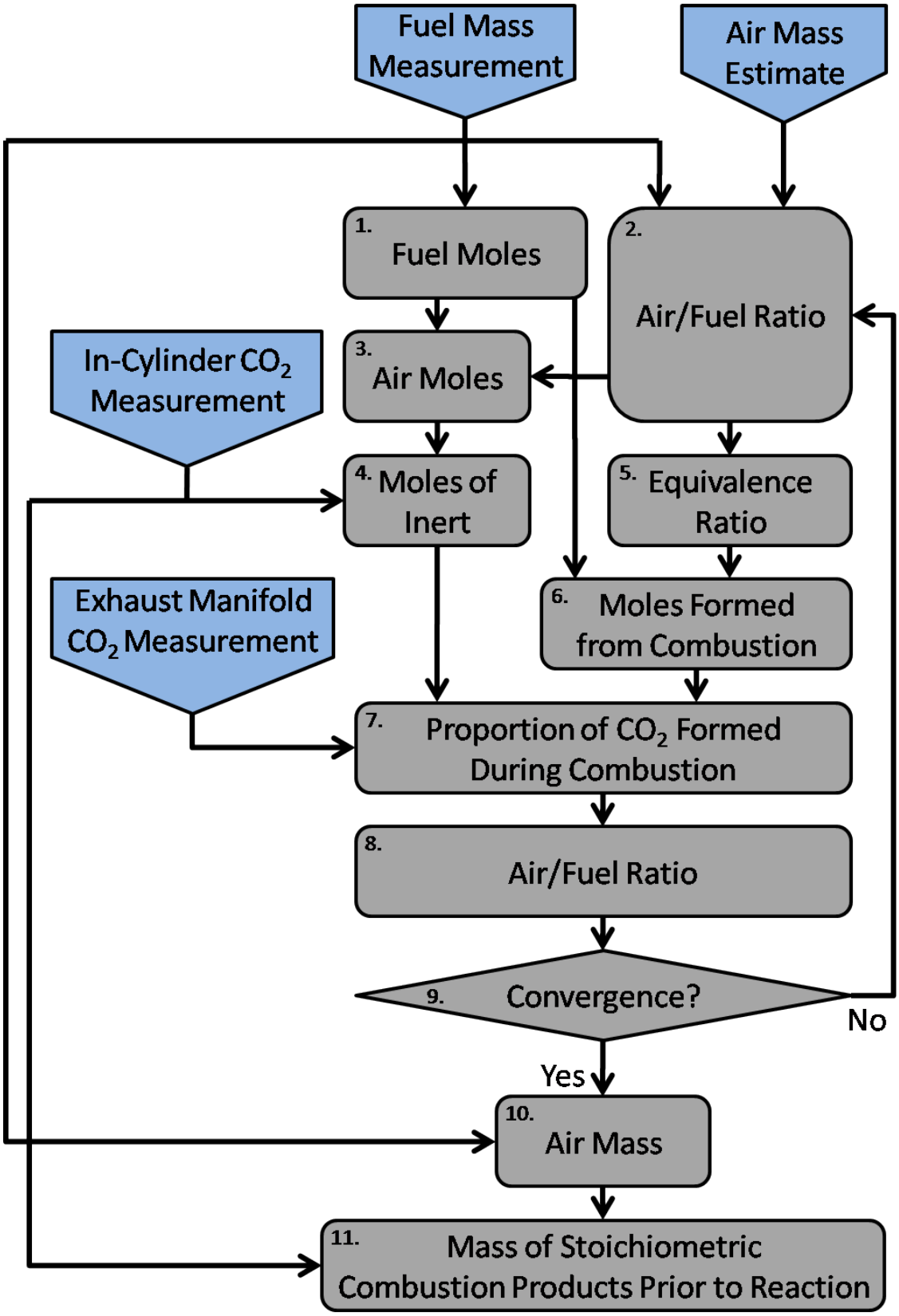

Figure 4.11: Iteration Technique for Air and Inert Mass Determination

CHAPTER 5

VALIDATION OF EXPERIMENTAL TECHNIQUE

This research effort develops and introduces a new technique to quantify the mass of fuel, air, and stoichiometric combustion products on a cyclic basis over a wide range of engine operating conditions during transient behavior. To quantify the validity of this technique three issues are addressed: the degree to which measurements change the nature of combustion, the error associated with the reported cylinder mass values, and a comparison of the results of this technique to results obtained with traditional test cell instrumentation. This chapter performs an in-depth analysis on the experimental technique to address the first two topics. First the influence of instrumenting the cylinder and removing mass during the compression stroke is studied to understand how combustion is impacted. Then an error and sensitivity analysis on the technique is performed to generate confidence intervals for the reported masses of fuel, air, and stoichiometric combustion products. The third topic is addressed by using the technique and traditional test cell instrumentation to gather data from the engine. This data is then compared and contrasted. Finally, this chapter wraps up with a discussion that focuses on the limitations of the experimental methodology and identifies the engine operating conditions in which the technique provides information with high levels of uncertainty.

5.1 Impact of Measurements on In-Cylinder Conditions and Engine Performance

The addition of instrumentation and the sampling of gases from the cylinder and exhaust manifold impact the combustion process. This section assesses the degree to which in-cylinder conditions are altered and combustion is affected.

5.1.1 Compression Ratio Decrease

The addition of in-cylinder measurement instrumentation increases the clearance volume of the cylinder, which reduces the cylinder's effective compression ratio. Three specific components contribute to the increased volume: the machined port, the sampling line, and the valve distribution block.

The machined port that allows access to the combustion chamber is located directly above the piston bowl and positioned between an intake and exhaust valve to provide a gas sample that is representative of the entire mixture. A #46 drill bit, which has a diameter of 2.1 mm, was used to machine the hole to a depth of 6.8 mm. Thus the total volume of the vertical portion of the port is 23.6 mm^2. The sampling line that carries gas from the cylinder to the valve body has a 1.0 mm diameter and is 150.0 mm long. This contributes an additional 117.8 mm^2 to the clearance volume. The valve distribution block has an internal volume of 50.9 mm^2. In total, the instrumentation of the cylinder adds 0.44% to the clearance volume and lowers the overall compression ratio by 0.41%. The effect of these three volumes on the cylinder clearance volume and compression ratio is summarized in Table 5.1.

Table 5.1: In-Cylinder Instrumentation Impact on Clearance Volume and Compression Ratio

	Original	Instrumented
In-Cylinder Clearance Volume	43780.1 mm^2	43780.1 mm^2
Machined Port Volume	-	23.6 mm^2
Instrument Probe Volume	-	117.8 mm^2
Valve Distribution Block Volume	-	50.9 mm^2
Total Clearance Volume	43780.1 mm^2	43972.4 mm^2
Clearance Volume Change	-	0.44%
Compression Ratio	18.00	17.93
Compression Ratio Change	-	0.41%

5.1.2 Cylinder Gas Mass Removal

The effect of reduced compression ratio due to in-cylinder gas measurement is further increased by the removal of mass from the cylinder as the sampling occurs. While the additional clearance volume introduced by the instrumentation cannot be avoided, the amount of mass removed during sampling can be minimized through careful configuration of the sampling system. This involves two distinct processes: removing the all of the gas in the CSV probe from the previous combustion cycle but no more, and directing just enough fresh gas to the analyzer to produce a stable and reliable signal.

CSV settings are dictated by the physical limitations of the system and by gas flow phenomena. While gas behavior is dependent upon engine operation, the physical limitations in the CSV system are a characteristic of the device and cannot be changed. To ensure that the solenoid valves open consistently and reliably, they must have a commanded opening signal with a duration of at least 0.8 ms. This amount of time translates to 3 degrees of crankshaft rotation at idle (625 rpm) and about 16 degrees at full engine load (3300 rpm). Thus these values are the minimums that can be used at

these engine speeds. Considering gas flow, a combination of simulation estimations and experiments are conducted to arrive at the proper CSV settings that can be used over the for all the investigated engine operating conditions.

To determine the proper purge valve opening and closing crank angles, a simulation exercise is conducted by using software from Cambustion that estimates the gas flows through the system depending on valve configurations and in-cylinder conditions. This simulation is further explored in Appendix D. Cylinder pressures measured from engine operation are input to determine the driving potential of the in-cylinder gases, and sample line conditions are used to estimate the state of gases as they are stored in the sampling tube. Because these conditions change significantly with engine speed and load, they impact the mass stored in the sample tube and the crank angle window necessary to purge the sample line. The opening of the purge valve, or beginning of the sampling from the cylinder, was defined to be 45º before combustion TDC to permit enough time for the cylinder charge to become homogeneously mixed and to allow all of the sampling to take place prior to fuel injection. The results from the simulation serve as a starting point for the rest of the configuration procedure.

Two characteristics govern the crank angle duration necessary to purge the sample line: in-cylinder conditions and engine speed. As cylinder pressures go up, the driving potential of the cylinder gases to purge the sample line increases, and a shorter duration is necessary. As engine speed increases, the timescale for a given crank angle window goes down and a longer duration is required to purge the line. These two characteristics have a counteracting effect because at lower engine speeds, cylinder pressures tend to be lower and vice versa. Therefore the crank angle duration necessary to purge the sample line does not change linearly with engine speed or load. At idling conditions, the simulation determines that 5 crank angle degrees are necessary to purge the sample line. At full engine power, 20 degrees are required to empty the line. Because full engine power conditions cause overpressures in the sampling system, a

purge valve duration of 15 degrees is used throughout the experiments, as it is the value necessary at the peak experimental conditions. This value also falls within the constraints imposed by the physical limitations of the valve and provides complete and reliable purging up to 3125 rpm.

Using a purge valve opening of 45º before TDC and closing of 30º before TDC, engine experiments are conducted to define the crank angle window over which to open and close the sampling solenoid valve. Opening of the sample valve is set to be 28º before TDC, which permits a small amount of time between the purging and sampling process. Determination of the crank angle of sampling valve closing must satisfy two constraints: the total time the valve is open must be no shorter than 0.8 ms and it must provide a large enough volume of gas to the CO_2 analyzer to provide a well-defined signal.

Because the CO_2 analyzer typically samples ambient air, its output during the majority of the cycle is essentially zero. When in-cylinder gases are sampled, the presence of EGR and residual gas causes a once-per-cycle plateau. The high level of this plateau is defined as two consecutive data points from the analyzer that are within 5% of one another. The CO_2 analyzer provides data every 3 ms, so the shortest time length of a plateau is 6 ms. At idle, this translates to 22.5 degrees of crankshaft rotation and at 3300 rpm is represents 118.8 degrees of crankshaft rotation.

During the experiment, the duration of the sampling valve is adjusted and the plateau length is observed and recorded. It is found that at idling conditions, a sample valve duration of 10 degrees is necessary to provide enough gas to the CO_2 analyzer to register a plateau of at least 22.5 degrees. At the upper envelope of investigated points, a 15 degree sample valve duration is required. Therefore to satisfy the physical constraints of the CSV and CO_2 analyzer and the gas flow constraints, a sample valve duration of 15 degrees is used throughout the entire engine operation range.

The conditions measured on the engine with the final purge and sample valve opening and closing intervals is then re-entered into the simulation code to estimate the total mass removed from the cylinder. This value is then compared to the experimentally-obtained in-cylinder mass. Table 5.2 below demonstrates the settings of the CSV500 at various engine operating conditions and the percentage of mass removed. The values shown here are the average of the results obtained from 100 engine cycles operating at each steady-state condition.

Table 5.2: Impact of In-Cylinder Sampling on Trapped Mass

Engine Speed and Load Condition	Purge Valve Opening Interval	Sample Valve Opening Interval	Estimated Percentage of Mass Removal
Idle, 625 rpm	-45º to -30º	-28º to -23º	1.89%
750 rpm, 1 bar BMEP	-45º to -30º	-28º to -23º	1.76%
750 rpm, 5.7 bar BMEP	-45º to -30º	-28º to -23º	1.76%
1750 rpm, 1 bar BMEP	-45º to -30º	-28º to -23º	0.70%
1750 rpm, 10 bar BMEP	-45º to -30º	-28º to -23º	0.76%
2750 rpm, 1 bar BMEP	-45º to -30º	-28º to -23º	0.50%
2750 rpm, 9 bar BMEP	-45º to -30º	-28º to -23º	0.51%

As mentioned earlier, two characteristics govern the mass removed from the cylinder: the time interval that the valves are open and the pressure differential between the cylinder and the atmosphere. When using the fixed purge and sample valve timings shown in Table 5.2, the estimated amount of cylinder mass removal never goes above 1.9%. This condition occurs at engine idle, when engine speed is low and the crank-angle based valve intervals are the longest on a time basis. As engine speed increases, the time elapsed during the valve opening and closing goes down, and less mass is removed on a percentage basis. When speed is held constant and load is increased, the

higher cylinder pressures cause a greater proportion of mass to be removed. From this data, it is clear that the valve opening interval has an impact on percentage of mass removal that is an order of magnitude greater than the influence of cylinder pressure.

Lowering of the cylinder's effective compression ratio and removal of mass from the cylinder impact pre-combustion in-cylinder conditions by lowering peak compression pressures and temperatures. This in turn affects ignition delay and consequently the entire combustion process. To assess the degree to which the pre-combustion environment is altered, experimental data from the original and instrumented cylinder at operating conditions that span the engine's performance envelope are examined.

The overall impact of instrumenting the cylinder and removing mass during the compression stroke is determined by comparing cylinder pressures and bulk gas temperatures at the beginning of the fuel injection process for both the original and instrumented cylinder at various operating conditions. Pressures are measured from experiments, while bulk gas temperatures are determined with the ideal gas law. For the instrumented cylinder, the amount of mass removed is determined from Table 5.2. Mixture molecular weights are also taken to be equivalent for original and uninstrumented cases.

Table 5.3 shows the magnitude of change in pre-combustion in-cylinder conditions for various operating conditions between the original and instrumented cylinder. Not surprisingly, those engine operating conditions that had the greatest proportion of mass removal also saw the greatest impact on cylinder pressure reduction. At idle, pre-injection cylinder pressures are reduced by just over five percent, while at 2750 rpm and 9 bar BMEP, pressures are lowered by 1.17%. Pre-injection temperatures are also lessened, and the degree to which this occurs is dependent upon the ratio of pressure loss and mass loss. As pressures are decreased, the calculated temperatures also go down. With less mass, however, the cylinder temperature goes up for a given pressure

level. Calculated pre-injection bulk temperature dropped 3.24% at idle and 0.66% at 2750 rpm, 9 bar BMEP.

Table 5.3: Experimental Comparison of Pre-Injection In-Cylinder Conditions for Original and Instrumented Cylinder at Various Engine Operating Conditions with Optimal Purge Valve and Sample Valve Timings

		Original		**Instrumented**	
Engine Speed and Load Condition	Start of Injection (ºaTDC)	Pre-Injection Pressure (bar)	Pre-Injection Temperature (K)	Percent Reduction of Pre-Injection Pressure	Percent Reduction of Pre-Injection Temperature
625 rpm Idle	2.9	44.09	968.4	5.07%	3.24%
750 rpm 1 bar BMEP	3	45.25	986.1	4.12%	2.40%
750 rpm 5.7 bar BMEP	3.2	47.33	1116.5	2.46%	0.71%
1750 rpm 1 bar BMEP	-3.7	49.59	1082.8	2.31%	1.62%
1750 rpm 10 bar BMEP	4.5	89.40	1161.1	1.42%	0.67%
2750 rpm 1 bar BMEP	-2.6	62.42	1228.9	1.52%	0.98%
2750 rpm 9 bar BMEP	3.8	106.24	1251.6	1.17%	0.66%

To identify the impact that instrumenting the cylinder has on combustion, heat release analysis is performed for both the original and instrumented cylinder at various operating conditions. The results of the average of 100 cycles at each condition are displayed in Table 5.4. In all cases, use of the CSV lengthens the ignition delay, which is attributed to the lower cylinder temperatures and pressures at the onset of fuel injection. At conditions in which more mass is removed and temperatures and pressures are reduced the most, ignition delays are lengthened the furthest. At idle, the ignition delay

increases from two to three degrees. Under higher speed and load conditions, however, ignition delay changes by only 0.1 or 0.2 degrees.

Table 5.4: Comparison of Combustion Parameters for Original and Instrumented Cylinder at Various Engine Operating Conditions

		Original				**Instrumented**			
Engine Speed and Load Condition	Start of Injection (ºaTDC)	Ignition Delay	10% MFB angle	50% MFB angle	90% MFB angle	Ignition Delay	10% MFB angle	50% MFB angle	90% MFB angle
625 rpm Idle	2.9	2.0	1.2	1.8	2.7	3.0	1.3	1.9	2.7
750 rpm 1 bar BMEP	3	2.8	1.5	2.3	4.4	3.8	1.6	2.3	4.2
750 rpm 5.7 bar BMEP	3.2	2.3	1.3	3.0	11.6	2.4	1.4	3.3	11.9
1750 rpm 1 bar BMEP	-3.7	5.3	1.6	3.2	9.2	5.6	1.7	3.2	9.0
1750 rpm 10 bar BMEP	4.5	3.3	2.4	9.8	20.0	3.4	2.4	9.7	20.0
2750 rpm 1 bar BMEP	-2.6	6.4	2.3	5.2	13.4	6.6	2.3	5.2	13.6
2750 rpm 9 bar BMEP	3.8	4.4	4.1	13.2	26.0	4.5	4.0	13.0	25.4

The mass fraction burned angles do not change significantly, and the greatest variation in any of the values investigated was 0.6 degrees. At a couple of lighter load conditions (750 rpm, 1 bar BMEP and 1750 rpm, 1 bar BMEP) combustion actually progresses more quickly with use of the CSV. These conditions are characterized by premixed burning, and the longer ignition delay times result in a more pronounced premixed burn, which promotes more rapid combustion. At the higher load conditions, the mass fraction burned crank angles are negligibly impacted.

Engine idle is the condition most significantly impacted. While the overall shape and burn rate at this condition do not change, combustion occurs so quickly (less than three degrees) that a one degree change in ignition delay essentially shifts the curve to later crank angles. This change is clearly seen in Figure 5.1, which is a contrast to the 2750 rpm, 9 bar BMEP case in Figure 5.2 that shows little change in the combustion process. These figures present singular engine cycles that are representative of the average heat release curves at these conditions, and are displayed to convey the degree to which combustion is impacted at both conditions.

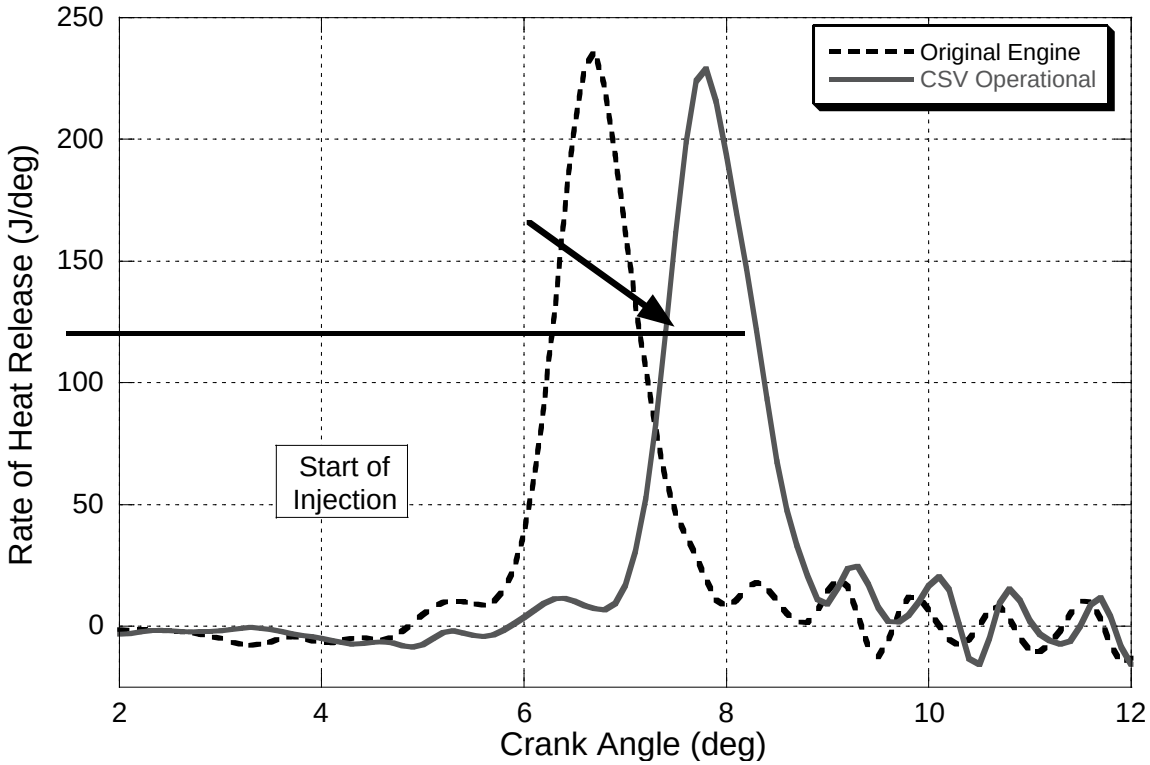

Figure 5.1: Rate of Heat Release at Engine Idle With Original Uninstrumented Engine and with CSV Operational

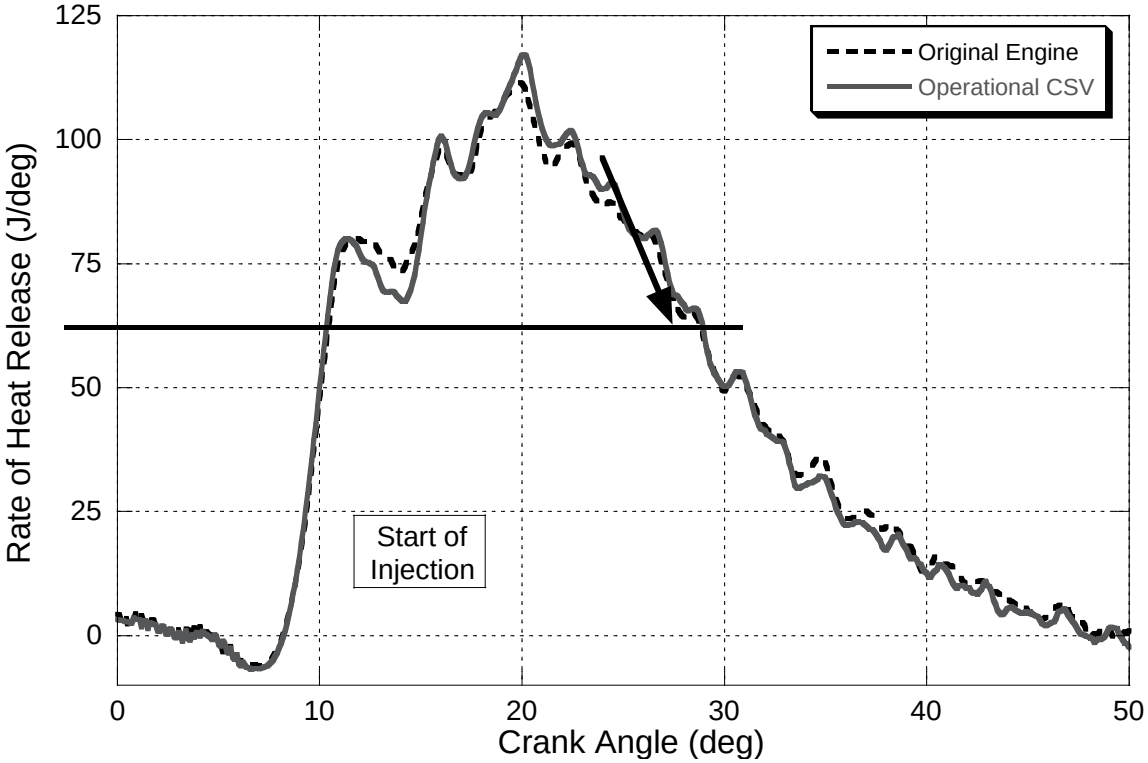

Figure 5.2: Rate of Heat Release at 2750 rpm and 9 Bar BMEP With Original Uninstrumented Engine and with CSV Operational

5.1.3 Exhaust Manifold Measurements

Sampling exhaust gases from the exhaust manifold reduces the mass flow rate of the exhaust through the turbocharger turbine. To quantify this effect, the standard engine exhaust flow rate is determined by converting the measured air and fuel mass flow rates into volumetric units and compared with total analyzer flow rate. This relationship is demonstrated for a variety of operating points in Table 5.5. At engine idle, the lightest speed and load condition tested, about one percent of the total exhaust flow rate is sampled. As engine speed and load increase, the proportion of exhaust gas sampled goes down appropriately. At 2750 rpm and 9 bar BMEP, less than two-tenths of one percent is sampled.

As the exhaust flow through the turbine of the turbocharger decreases, the energy available for boosting the intake air decreases; this is evidenced by a reduction in boost

pressure. The maximum observed value is 1.54% the minimum is 0.10%, and the proportional reduction in boost pressure tends to decrease as engine speed and load increase.

Table 5.5: Exhaust Flow Rate and Gas Analyzer Flow Rate at Various Engine Operating Conditions

Engine Speed and Load Condition	Engine Exhaust Flow Rate (Std L/min)	Total Gas Analyzer Flow Rate (Std L/min)	Percent of Exhaust Sampled	Percent Change in Boost Pressure
625 rpm, Idle	1482	15.0	1.01%	-0.50%
750 rpm, 1 bar BMEP	1794	15.0	0.84%	-0.49%
750 rpm, 5.7 bar BMEP	1823	15.0	0.82%	-1.54%
1750 rpm, 1 bar BMEP	3581	15.0	0.42%	-0.48%
1750 rpm, 10 bar BMEP	7195	15.0	0.21%	-0.11%
2750 rpm, 1 bar BMEP	6354	15.0	0.24%	-0.41%
2750 rpm, 9 bar BMEP	11768	15.0	0.13%	-0.10%

In summary, the removal of gases from the cylinder and the exhaust manifold has a slight, but measureable impact on engine behavior. Sampling gases during the compression stroke slightly alters combustion phasing due to lengthened ignition delays, with lower speeds and loads impacted more than higher operating conditions. Removing gases from the exhaust manifold reduces boost pressure, but levels never exceed more than around 1.5%.

Regardless of the impact on combustion, the measurement technique and the data gathered with it remain legitimate. All the measurements, both in the cylinder and in the exhaust manifold, are made on the gases from the instrumented cylinder. Therefore the effects of any changes in pressures or gas concentrations caused by the instrumentation

are measured and the observed trends and relationships due to transient engine operation are valid.

5.2 Error and Sensitivity Analysis

An error and sensitivity analysis is conducted to determine the accuracy of the values obtained by the experimental technique. Errors are incurred through use of the laboratory instrumentation, the assumptions made to simplify combustion equations, and the data analysis. The goal of this section is to develop confidence intervals for the reported cyclic mass of fuel, air, and stoichiometric combustion products. Also examined is the influence of these errors on heat release analysis.

5.2.1 Fuel Mass Error

Typically fuel flow rate is determined directly from a fuel flow meter. In this investigation, fuel flow rate is determined though use of crank angle resolved cylinder pressure and instrumented injector measurements, as well as discharge coefficient data developed under steady-state conditions. The injected fuel mass for each cycle is given by Equation (5.1), which is rewritten from Equation (4.59). The portion shown behind the sigma is the composite trapezoid rule, which is used to approximate an integral.

$$m_{Fuel} = \sqrt{2\rho_{Fuel}}\, A_{Inj}\, \overline{C_d} \sum_{i=SOI}^{EOI-1} \left[\frac{\Delta CA}{2} \left\{ \left(\sqrt{P_{Cyl} - P_{Inj}} \right)_i + \left(\sqrt{P_{Cyl} - P_{Inj}} \right)_{i+1} \right\} \right] \text{ (kg)} \tag{5.1}$$

Where: m_{Fuel} = Fuel mass (kg)

ρ_{Fuel} = Fuel density (kg/m^3)

A_{Inj} = Injector flow area (m^2)

$\overline{C_d}$ = Injector flow discharge coefficient (-)

CA = Crank angle (degrees)

P_{Cyl} = Cylinder pressure (N/m^2)

P_{Inj} = Injection pressure (N/m^2)

The discharge coefficient can be rewritten from Equation (4.57) as

$$\overline{C_d} = \frac{60\dot{m}_{Fuel}\, n_R}{N n_C \sqrt{2\rho_{Fuel}}\, A_{Inj} \int_{SOI}^{EOI} \sqrt{\left(P_{Cyl} - P_{Inj}\right)}\, dCA} \tag{5.2}$$

Where: $\overline{C_d}$ = Injector flow discharge coefficient (-)

$\dot{m}_{Fuel}$ = Fuel mass flow rate (kg/s)

n_R = Engine revolutions per power stroke (-)

N = Engine speed (rpm)

n_C = Number of cylinders (-)

ρ_{Fuel} = Fuel density (kg/m^3)

A_{Inj} = Injector flow area (m^2)

SOI = Start of injection (degrees)

EOI = End of injection (degrees)

P_{Cyl} = Cylinder pressure (N/m^2)

P_{Inj} = Injection pressure (N/m^2)

dCA = Crank angle differential

By substituting Equation (5.2) into (5.1) and cancelling terms, the expression for fuel mass becomes

$$m_{Fuel} = \underbrace{\frac{60 n_R}{N n_C}}_{1} \underbrace{\dot{m}_{Fuel}}_{2} \underbrace{\frac{\sum_{i=SOI}^{EOI-1} \left[\frac{\Delta CA}{2}\left\{\left(\sqrt{P_{Cyl} - P_{Inj}}\right)_i + \left(\sqrt{P_{Cyl} - P_{Inj}}\right)_{i+1}\right\}\right]}{\int_{SOI}^{EOI} \sqrt{\left(P_{Cyl} - P_{Inj}\right)}\, dCA}}_{3} \text{ (kg)} \tag{5.3}$$

Engine speed is quantified with a crank angle encoder, which uses a disk with 720 evenly-spaced markings to discern rotation and then measures the elapsed time between the markings. Since the accuracy of speed measurement only limited by the ability to machine markings in the disk and measure time, engine speed is assumed to be constant. Therefore the leading term in Equation (5.3), denoted by (1) is a constant term. The second portion, (2), is the reading from the mass flow meter. Term (3) is the ratio of the approximation to an integral from numerical integration to the definite value of the same

integral. When considering Equation (5.3), the estimation of error in fuel mass must take into account the error from the fuel flow meter, the error from the cylinder pressure and injection pressure measurements, the error in using the composite trapezoid rule to approximate the integral in the denominator of term (3), and the fact that these three are multiplied together. This is accomplished by taking the root sum of the squares of the individual fractional errors and is represented by Equation (5.4).

$$e_{FM} = \sqrt{{e_{FMF}}^2 + {e_{\Delta P}}^2 + {e_{CTR}}^2} \tag{5.4}$$

Where: e_{FM} = Fractional error in fuel mass (%)

e_{FMF} = Fractional error in fuel mass flow rate (%)

$e_{\Delta P}$ = Fractional error from pressure differential (%)

e_{CTR} = Fractional error in composite trapezoid rule (%)

The error in the fuel mass flow rate is obtained from the manufacturer of the flow meter and stated to be 0.5% of the measured value. This value is defined as e_{FMF} and is readily plugged into Equation (5.4). Fractional error from the difference in injection and cylinder pressure is obtained from the manufacturers of the sensors, and both are stated as 0.3% of the measured value. When computing the uncertainty in subtracting the two pressure values, the relationship in Equation (5.5) is used.

$$e_{\Delta P} = \frac{\sqrt{\left(P_{Cyl}\, e_{PCyl}\right)^2 + \left(P_{Inj}\, e_{PInj}\right)^2}}{P_{Inj} - P_{Cyl}} \tag{5.5}$$

Where: $e_{\Delta P}$ = Fractional error from pressure differential (%)

P_{Cyl} = Cylinder pressure measurement (bar)

e_{PCyl} = Fractional error in cylinder pressure measurement (%)

P_{Inj} = Injection pressure measurement (bar)

e_{PInj} = Fractional error in injection pressure measurement (%)

Considering all of the data obtained in this research effort, the maximum differential error observed in pressure difference over an entire injection process is

0.70%. Assuming a normal distribution of the error, 95% of the data has an uncertainty of less than 0.55%.

Error incurred from the composite trapezoid rule is given by [48] and shown in Equation (5.6).

$$E_{CTR} = \frac{-(b-a)\cdot f''(c)\cdot h^2}{12} \tag{5.6}$$

Where: E_{CTR} = Error in composite trapezoid rule (kg)

b = Ending point of integration (-)

a = Beginning point of integration (-)

$f''(c)$ = The second derivative of the function to be integrated at any point c between a and b (-)

h = Step size of integration (-)

The beginning and ending points of integration are simply the start and end of injection. In this case, the step size of integration is the crank angle resolution of the data. Because the function is only known at discrete data points, the second derivative at any location cannot be determined. This value can, however, be approximated at each known point by using the centered difference formula, shown in Equation (5.7).

$$f''(c) = \frac{f(c+h) - 2f(c) + f(c-h)}{h^2} \tag{5.7}$$

To determine the amount of error incurred by using the composite trapezoid rule for each fuel injection process, the second derivative is determined at each point between SOI and EOI using Equation (5.7) and then the maximum absolute value over the injection event is used in Equation (5.6). This value is then divided by the quantity of fuel injected to arrive at the fractional error, e_{CTR}, which is plugged directly into Equation (5.4). Using this method gives a good approximation of the upper bound of integration error.

All experimental data taken is investigated to determine the level of error incurred by using the composite trapezoid rule to perform the numerical integration, which includes thousands of cycles of engine data that encompass the entire operating regime of the engine. The average level of error in the composite trapezoid rule is -0.03%, the maximum observed error is -0.05%, and by assuming a normal distribution of the error about the mean, 95% of the points are within -0.04%. These levels of error are extremely low and attributed to the fine crank angle resolution (0.1°) of the data.

When combining the levels of fuel flow meter error, pressure differential measurement error, and composite trapezoidal numerical integration error, suitable fractional errors are established for the fuel mass values obtained in this investigation. Considering the maximum levels of error observed, fuel mass values are within 0.86% of their actual values. Assuming a normal distribution of the error, 95% of the fuel mass values are within 0.74% of their true levels.

5.2.2 Error Incurred from Neglecting CO and HC Emissions

Calculating the mass of air and stoichiometric combustion products is accomplished through use of the carbon balance method outlined in Section 4.2.2. This procedure functions by keeping track of all of the carbon atoms involved in the combustion reaction. During the compression stroke, carbon atoms are present in the burned gases and in the fuel. Carbon atoms exit the cylinder in the form of carbon dioxide, unburned hydrocarbons, and carbon dioxide. Because the production of carbon monoxide and hydrocarbons in conventional diesel combustion is typically two orders of magnitude less than carbon dioxide, they are neglected.

Since carbon dioxide and unburned hydrocarbons contain carbon and a carbon balance is used to calculate the air/fuel ratio, not accounting for them results in errors when reporting the measured air/fuel ratio. To account for this error, data from multiple

driving cycles are considered while using emissions measurements from the CEB II emissions bench. Air fuel ratios are determined with realistic values of CO_2, CO and HC. When all three compounds are considered, the air fuel ratio is given by Equation (5.8), which is rewritten from Equation (4.32).

$$\frac{m_{Air}}{m_{Fuel}} = \frac{MW_{Air}}{MW_{Fuel}}\left[N + \frac{N}{100}\left(3\chi_{C_3H_8} - \frac{1}{2}\chi_{CO} + \frac{1}{2}\chi_{H_2O}\right) - \frac{y}{2}\right] \tag{5.8}$$

In this equation, $N$is defined as

$$N = \frac{100}{\chi_{CO_2} + \chi_{CO} + 3\chi_{C_3H_8}} \tag{5.9}$$

and the concentration of water in the exhaust is determined by

$$\chi_{H_2O} = \frac{y}{2} \cdot \frac{\chi_{CO_2} + \chi_{CO}}{\frac{\chi_{CO}}{3.8\chi_{CO_2}} + 1} \tag{5.10}$$

The same data is used to calculate the air/fuel ratio when carbon monoxide and unburned hydrocarbons are neglected. Equations (5.8) and (5.9) simplify and combine to become

$$\frac{m_{Air}}{m_{Fuel}} = \frac{MW_{Air}}{MW_{Fuel}}\left[\frac{100}{\chi_{CO_2}^{AFR}} - \frac{y}{4}\right] \tag{5.11}$$

Data from a total of thirteen 20-minute long FTP 75 driving cycles are considered when comparing air/fuel ratio measurements. These tests are conducted using the engine-in-the-loop capability with a variety of powertrain configurations, including a conventional four-speed automatic transmission, a parallel electric hybrid, and a series hydraulic hybrid. This diverse group of powertrains functioning over a relative aggressive driving cycle provides a broad range of engine speed and load combinations that span its operation envelope.

Neglecting carbon monoxide and unburned hydrocarbons will always over-predict the air/fuel ratio, so an average value of error can be determined. For all conditions investigated, the average error in air/fuel ratio calculation is 1.02%. The maximum error observed is 3.40% and 95% of the investigated data points have an error of less than 2.0%.

5.2.3 Air Mass Error

Air mass for each cycle is determined by multiplying the air/fuel ratio by the fuel mass and is shown in a manipulated form of Equation (5.11).

$$m_{Air} = \frac{MW_{Air}}{MW_{Fuel}}\left[\frac{100}{\chi_{CO_2}^{AFR}} - \frac{y}{4}\right] m_{Fuel} \tag{5.12}$$

When calculating the error in the air mass, it is clear from Equation (5.12) that the error in the fuel mass must be considered. Because this calculation does not take into account the emissions of carbon monoxide and unburned hydrocarbons, this error must also be included. Additional error is incurred through determination of the $\chi_{CO_2}^{AFR}$ term, which represents the amount of CO_2 formed during combustion and stems from inaccuracy in the measurement of CO_2 both in the cylinder and the exhaust manifold. The fractional error in the mass of air in each cycle is therefore written as

$$e_{AM} = \sqrt{{e_{FM}}^2 + {e_{A/F}}^2 + {e_{co_2}}^2} \tag{5.13}$$

Where: e_{AM} = Fractional error in air mass (%)

e_{FM} = Fractional error in fuel mass (%)

$e_{A/F}$ = Fractional error in air/fuel ratio from neglecting CO and HC emissions

e_{CO_2} = Fractional error due to CO_2 measurement

The first two terms are quantified in Section 5.2.1 and Section 5.2.2. To examine the impact of the $\chi_{CO_2}^{AFR}$ term, the equation to determine this quantity is rewritten below from Equation (4.68).

$$\chi_{CO_2}^{AFR} = \frac{\chi_{CO_2}^{Post-Comb}\left(n_{Exhaust}^{AFR} + n_{SC}\right) - \chi_{CO_2}^{SC} n_{SC}}{n_{Exhaust}^{AFR}} \tag{5.14}$$

Where: $\chi_{CO_2}^{AFR}$ = Mole fraction of CO_2 in combustion products

$\chi_{CO_2}^{Post-Comb}$ = Mole fraction of CO_2 after combustion

$n_{Exhaust}^{AFR}$ = Moles of combustion products

n_{SC} = Moles from stoichiometric combustion

$\chi_{CO_2}^{SC}$ = Mole fraction of CO_2 in gas from stoichiometric combustion

The terms in Equation (5.14) are either measured directly from the Fast CO/CO_2 sensor or calculated from the readings obtained with the device. Because of this complex relationship, a sensitivity analysis is conducted to evaluate the impact of CO_2 measurement error. To perform this analysis, readings from the device are compared against the known concentrations of calibration gases. A total of twenty readings are taken from the manufacturer's calibration sheet and maximum error of ±2.0% and a relative standard deviation of 0.73% are established. These values serve as the step increments to the CO_2 data for the sensitivity analysis.

Data from the seven steady-state load and speed combinations introduced in Section 5.1 are used since these points encompass a broad range of engine operating conditions. In-cylinder and exhaust manifold CO_2 data from these engine experiments are taken and varied by ±2.0% to establish maximum error bounds. The original CO_2 data are then varied by twice the relative standard deviation, or 1.45%, to determine the error levels for the 95th percentile confidence interval. This analysis results in nine different scenarios at each error level with low, normal, and high levels of both in-cylinder and exhaust manifold CO_2. Results for engine idle with maximum CO_2 error and 95% confidence interval are shown in Table 5.6 and Table 5.7, while results for the 2750 rpm, 9 bar BMEP condition at both error levels are shown in Table 5.8 and Table 5.9.

Table 5.6: Variance in Air Mass from Maximum Levels of In-Cylinder and Exhaust Manifold CO_2 Measurement Error at Engine Idle

		In-Cylinder CO_2 Level					
		Low		Normal		High	
		Air Mass	% Error	Air Mass	% Error	Air Mass	% Error
Exhaust Manifold CO_2 Level	Low	733.4	2.06%	733.8	2.12%	734.2	2.18%
	Normal	718.2	-0.05%	**718.6**		719.0	0.05%
	High	703.6	-2.09%	703.9	-2.04%	704.3	-1.98%

Table 5.7: Variance in Air Mass from 95th Percentile Levels of In-Cylinder and Exhaust Manifold CO_2 Measurement Error at Engine Idle

		In-Cylinder CO_2 Level					
		Low		Normal		High	
		Air Mass	% Error	Air Mass	% Error	Air Mass	% Error
Exhaust Manifold CO_2 Level	Low	729.3	1.49%	729.6	1.53%	729.9	1.57%
	Normal	718.3	-0.04%	**718.6**		718.9	0.04%
	High	707.6	-1.52%	707.9	-1.49%	708.2	-1.45%

Table 5.8: Variance in Air Mass from Maximum Levels of In-Cylinder and Exhaust Manifold CO_2 Measurement Error at 2750 rpm and 9 Bar BMEP

		In-Cylinder CO_2 Level					
		Low		Normal		High	
		Air Mass	% Error	Air Mass	% Error	Air Mass	% Error
Exhaust Manifold CO_2 Level	Low	1273.2	2.18%	1273.9	2.23%	1274.6	2.29%
	Normal	1245.4	-0.05%	**1246.0**		1246.7	0.05%
	High	1218.8	-2.19%	1219.3	-2.14%	1219.9	-2.10%

Table 5.9: Variance in Air Mass from 95th Percentile Levels of In-Cylinder and Exhaust Manifold CO_2 Measurement Error at 2750 rpm and 9 Bar BMEP

		In-Cylinder CO_2 Level					
		Low		Normal		High	
		Air Mass	% Error	Air Mass	% Error	Air Mass	% Error
Exhaust Manifold CO_2 Level	Low	1265.6	1.57%	1266.1	1.61%	1266.6	1.65%
	Normal	1245.6	-0.04%	**1246.0**		1246.5	0.04%
	High	1226.1	-1.60%	1226.6	-1.56%	1227.0	-1.53%

In general, CO_2 measurement errors have the same impact on air mass at both operating conditions. Variances in exhaust manifold CO_2 change the reported air mass by the same order of magnitude, with lower levels of CO_2 resulting in higher values of air. Errors in in-cylinder CO_2 have negligible impact on air mass, as the percentage in air mass changes are two orders of magnitude less than the error percentage. Maximum variances in air mass occur when exhaust manifold error causes CO_2 to be reported low and in-cylinder values are reported high. Changes, however, remain on the same level as the error in the exhaust manifold measurement.

Although the results from only two operating conditions are shown, all nine responded in the same manner. The maximum observed sensitivity to CO_2 measurement error is at the 2750 rpm, 1 bar BMEP operating condition. When the exhaust manifold CO_2 levels are reported low and the in-cylinder CO_2 levels are reported high at this operating condition, the error in the air mass at this condition is 2.55%. When assuming a normal error distribution, 95% of the data at this condition has an error of 1.84% or less. These low levels of error demonstrate the low sensitivity of air mass to CO_2

measurement error and give significant confidence to the air mass measurement technique.

By using Equation (5.13), the total error in air mass is determined. Maximum levels of error are calculated using the greatest observed error for all three components. Specifically, these values are 0.86% for the fuel mass, 3.40% for neglecting the presence of carbon monoxide and unburned hydrocarbons, and ±2.55% from error in the in-cylinder and exhaust manifold CO_2 measurements. This results in a maximum overall air mass error of ±4.34%. The 95th percentile error values for these components are 0.74% for the fuel mass, 2.00% for neglecting carbon monoxide and unburned hydrocarbons, and ±1.84% for in-cylinder and exhaust manifold CO_2 measurements. Therefore 95% of air mass values have an error of ±2.82% or less.

5.2.4 Stoichiometric Combustion Products Mass Error

The mass of stoichiometric combustion products in the cylinder for each cycle prior to combustion is determined by

$$m_{SC} = \left(\frac{MW_{SC}}{MW_{Air}}\right)\frac{\chi_{CO_2}^{Pre-Comb}}{\chi_{CO_2}^{SC} - \chi_{CO_2}^{Pre-Comb}} m_{Air} \tag{5.15}$$

Where: m_{SC} = Mass of inert gases from stoichiometric combustion (kg)

MW_{SC} = Molecular weight of inert fraction (kg/kmole)

MW_{Air} = Molecular weight of air (kg/kmole)

$\chi_{CO_2}^{Pre-Comb}$ = Mole fraction of CO_2 before combustion

$\chi_{CO_2}^{SC}$ = Mole fraction of CO_2 in gases from stoichiometric combustion

m_{Air} = Mass of air (kg)

By substituting the expression for air mass given in Equation (5.12), Equation (5.15) reduces to

$$m_{SC} = \left(\frac{MW_{SC}}{MW_{Fuel}}\right)\frac{\chi_{CO_2}^{Pre-Comb}}{\chi_{CO_2}^{SC} - \chi_{CO_2}^{Pre-Comb}}\left[\frac{100}{\chi_{CO_2}^{AFR}} - \frac{y}{4}\right] m_{Fuel} \tag{5.16}$$

This statement is very similar to the expression for air mass given in Equation (5.12), with the addition of a CO_2 concentration ratio. Therefore the error in the mass of stoichiometric combustion products is similarly dependent upon fuel mass measurement error, the error incurred by neglecting carbon monoxide and unburned hydrocarbon emissions, and in-cylinder and exhaust manifold CO_2 concentration error. Thus the fractional error in the stoichiometric combustion products mass for each cycle is stated as

$$e_{SCPM} = \sqrt{{e_{FM}}^2 + {e_{A/F}}^2 + {e_{co_2}}^2} \tag{5.17}$$

Where: e_{SCPM} = Fractional error in stoichiometric combustion product mass (%)

e_{FM} = Fractional error in fuel mass (%)

$e_{A/F}$ = Fractional error in air/fuel ratio from neglecting CO and HC emissions

e_{CO_2} = Fractional error due to CO_2 measurement

The presence of the additional CO_2 ratio indicates a greater degree of dependence on CO_2 measurement error. To assess this relationship, the sensitivity analysis outlined in the discussion of air mass error in Section 5.2.3 is also conducted for the mass of stoichiometric combustion products. Nine steady-state points are investigated, with low, normal, and high levels of CO_2 measurement for both maximum error levels and the 95th percentile confidence interval. Results for the sensitivity analysis at engine idle with maximum error are shown in Table 5.10 and with 95th percentile error levels in Table 5.11. Results for the same error levels at 2750 rpm and 9 bar BMEP are shown in Table 5.12 and Table 5.13.

Table 5.10: Variance in Stoichiometric Combustion Product Mass from Maximum Levels of In-Cylinder and Exhaust Manifold CO_2 Measurement Error at Engine Idle

		In-Cylinder CO_2 Level					
		Low		Normal		High	
		SCP Mass	% Error	SCP Mass	% Error	SCP Mass	% Error
Exhaust Manifold CO_2 Level	Low	2.77	-0.02%	2.83	2.09%	2.89	4.19%
	Normal	2.72	-2.06%	**2.77**		2.83	2.06%
	High	2.66	-4.02%	2.72	-2.00%	2.77	0.02%

Table 5.11: Variance in Stoichiometric Combustion Product Mass from 95th Percentile Levels of In-Cylinder and Exhaust Manifold CO_2 Measurement Error at Engine Idle

		In-Cylinder CO_2 Level					
		Low		Normal		High	
		SCP Mass	% Error	SCP Mass	% Error	SCP Mass	% Error
Exhaust Manifold CO_2 Level	Low	2.77	-0.01%	2.82	1.51%	2.86	3.02%
	Normal	2.73	-1.49%	**2.77**		2.82	1.50%
	High	2.69	-2.93%	2.73	-1.46%	2.77	0.01%

Table 5.12: Variance in Stoichiometric Combustion Product Mass from Maximum Levels of In-Cylinder and Exhaust Manifold CO_2 Measurement Error at 2750 rpm and 9 Bar BMEP

		In-Cylinder CO_2 Level					
		Low		Normal		High	
		SCP Mass	% Error	SCP Mass	% Error	SCP Mass	% Error
Exhaust Manifold CO_2 Level	Low	43.51	-0.08%	44.45	2.07%	45.39	4.23%
	Normal	42.63	-2.11%	**43.54**		44.47	2.11%
	High	41.78	-4.05%	42.68	-1.98%	43.58	0.08%

Table 5.13: Variance in Stoichiometric Combustion Product Mass from 95th Percentile Levels of In-Cylinder and Exhaust Manifold CO_2 Measurement Error at 2750 rpm and 9 Bar BMEP

		In-Cylinder CO_2 Level					
		Low		Normal		High	
		SCP Mass	% Error	SCP Mass	% Error	SCP Mass	% Error
Exhaust Manifold CO_2 Level	Low	43.52	-0.06%	44.20	1.49%	44.87	3.05%
	Normal	42.88	-1.53%	**43.54**		44.21	1.53%
	High	42.26	-2.96%	42.91	-1.45%	43.57	0.06%

Variance in in-cylinder and exhaust manifold CO_2 concentration has a relatively linear impact on stoichiometric combustion product mass at both operating conditions. This relationship is nearly one-to-one, as for every percent change in CO_2 error, there is a one percent change in stoichiometric combustion product mass. High levels of exhaust manifold CO_2 result in a reduction of stoichiometric combustion product mass, and vice versa. As in-cylinder levels of CO_2 concentration go up, so does the reported stoichiometric combustion product mass. Errors in in-cylinder and exhaust manifold CO_2 concentrations are also roughly additive, so that if exhaust manifold CO_2 is low by 1% and in-cylinder CO_2 is high by 1%, the reported stoichiometric combustion mass increases by about 2%.

All nine operating conditions responded in the same manner as the two conditions shown. The maximum error for all the speed load combinations is 4.58%, which occurs at the 2750 rpm, 1 bar BMEP operating condition when the exhaust manifold CO_2 is low and the in-cylinder CO_2 is high. The 95th percentile error in stoichiometric combustion product mass at this condition is 3.30%.

The extra CO_2 ratio term in Equation (5.16) results in stoichiometric combustion product mass to be much more sensitive to in-cylinder CO_2 concentration than air mass. Because they are both equally sensitive to exhaust manifold CO_2 concentration error, the

errors observed in the mass of stoichiometric combustion products are roughly twice as high as those in the air mass. This relationship exists at both error levels investigated.

When considering all the fractional error terms presented in Equation (5.17), the maximum fuel error is ±0.86%, the error from neglecting carbon monoxide and unburned hydrocarbon emissions is ±3.40% and the error incurred from CO_2 measurement is ±4.58%. This results in a maximum error of ±5.77% in stoichiometric combustion product mass. When 95^{th} percentile errors are considered, the fuel error is ±0.74%, the error from neglecting carbon monoxide and unburned hydrocarbon emissions is ±2.00% and the error from CO_2 concentration measurement is ±3.30%. This results in 95% of the data points having an error of ±3.93% or less.

5.2.5 Measurement Error Impact on Heat Release Analysis

To assess the impact of fuel, air and stoichiometric combustion product mass errors on combustion analysis, heat release is performed with the maximum levels of errors. All seven operating conditions are investigated with combinations of high and low fuel mass, air mass, and stoichiometric combustion product mass to evaluate the impact on combustion characteristics.

Minor variations are observed in the rate of heat release curve and the integrated heat release curve. While fuel mass variation had virtually no impact, the mass of air and stoichiometric combustion products had a discernable effect on heat release. The more air and stoichiometric combustion products in the cylinder, the smaller the amount of energy required to produce the cylinder pressures measured, and for a given cylinder pressure curve, the calculated rate of heat release decreases. Over all cases considered, the most the peak rate of heat release changed with maximum cylinder mass error is ±0.26%. The integrated heat release varied by ±0.23% under the same conditions. These differences occur at the 2750 rpm 9 bar BMEP condition, which are shown in Figure 5.3.

The graph must be magnified substantially to observe the difference induced by cylinder mass errors.

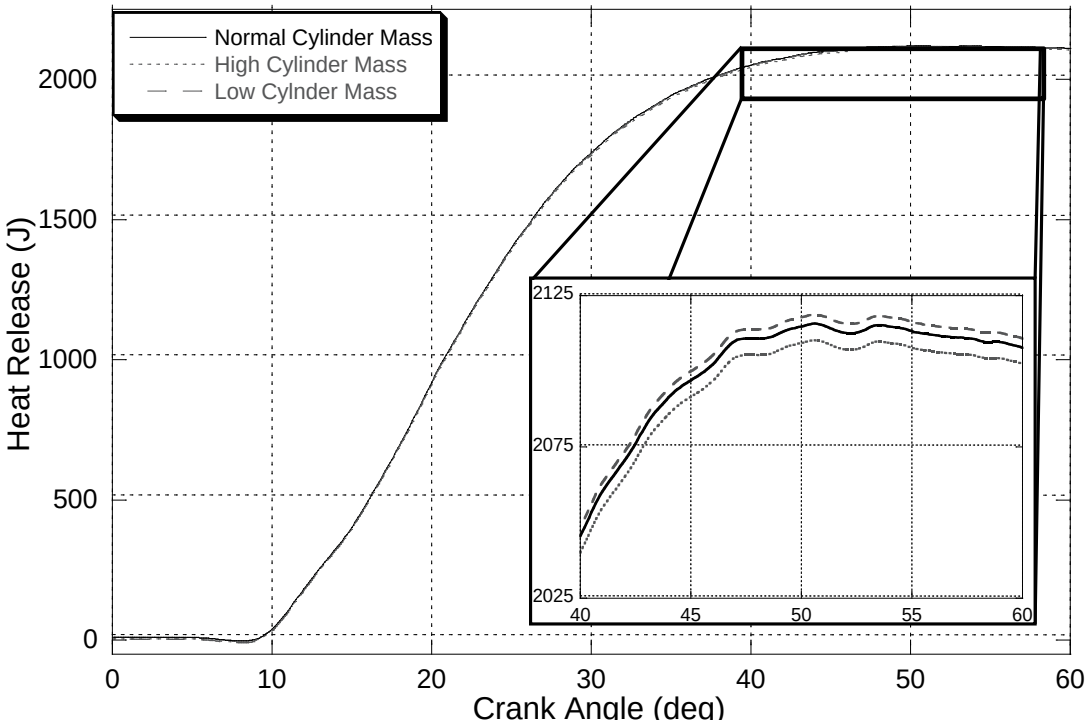

Figure 5.3: Heat Release Sensitivity to Errors in Fuel Mass, Air Mass and Stoichiometric Combustion Product Mass at 2750 rpm, 9 Bar BMEP

For the maximum error levels expected from the techniques used to quantify fuel mass, air mass, and stoichiometric combustion product mass, the impact on combustion is negligible. Ignition delays and burn rates remain unchanged for all of the conditions investigated, indicating that any errors in cylinder mass will not affect the heat release analysis or conclusions made from heat release results.

5.3 Comparison of Data Obtained with the Experimental Technique and Traditional Test Cell Instrumentation

Traditional engine test cell instrumentation for measurement of fuel flow, air flow, and emissions concentrations are very accurate but are unable to respond to rapid changes in the data they measure. The reasons for this inability to quantify fast variances are two-fold: the devices are typically located a considerable distance from the engine

and the measurement principles they incorporate are slow to react. Thus delays arise from the time it takes for the sampled quantity to reach the device, or transport, and the time it takes for the instrument to react to the change. These devices are therefore very well-suited to data collection during steady-state engine operation but they are not able to provide accurate measurements at cycle-resolved levels.

The primary motivation for developing the proposed experimental technique is to be able to determine cycle-resolved values of in-cylinder components. To assess the potential for this methodology to provide unique insight into engine behavior, a comparison is made between data gathered with traditional test cell instrumentation and data measured and calculated by the proposed experimental technique.

The comparison is made by gathering data from the engine simultaneously with the instrumentation for both methods. Data from the traditional test cell instrumentation is gathered on a 10 Hz basis, but then is interpolated to yield one value per engine cycle. During the test, the engine is operated as though it is in a vehicle that is performing the FTP 75 driving cycle. Specifically, attention is focused on an acceleration event where the vehicle goes from a standing start to 40 km/hr in 10.2 seconds. This event encompasses engine behavior between cycles 1640 and 1790 of the FTP 75. Engine command and vehicle velocity for this event are shown in Figure 5.4 and the engine speed and torque are displayed in Figure 5.5.

Discussion focuses on the differences in the trends of the output produced by these devices and does not go into detail about why the trends occur themselves. That analysis is provided in Chapter 8. It should be noted that the prior to the cycles shown in this comparison that the engine is not operating at steady-state. Therefore an offset in the measurements of the investigated metrics is expected at the beginning of the displayed cycles.

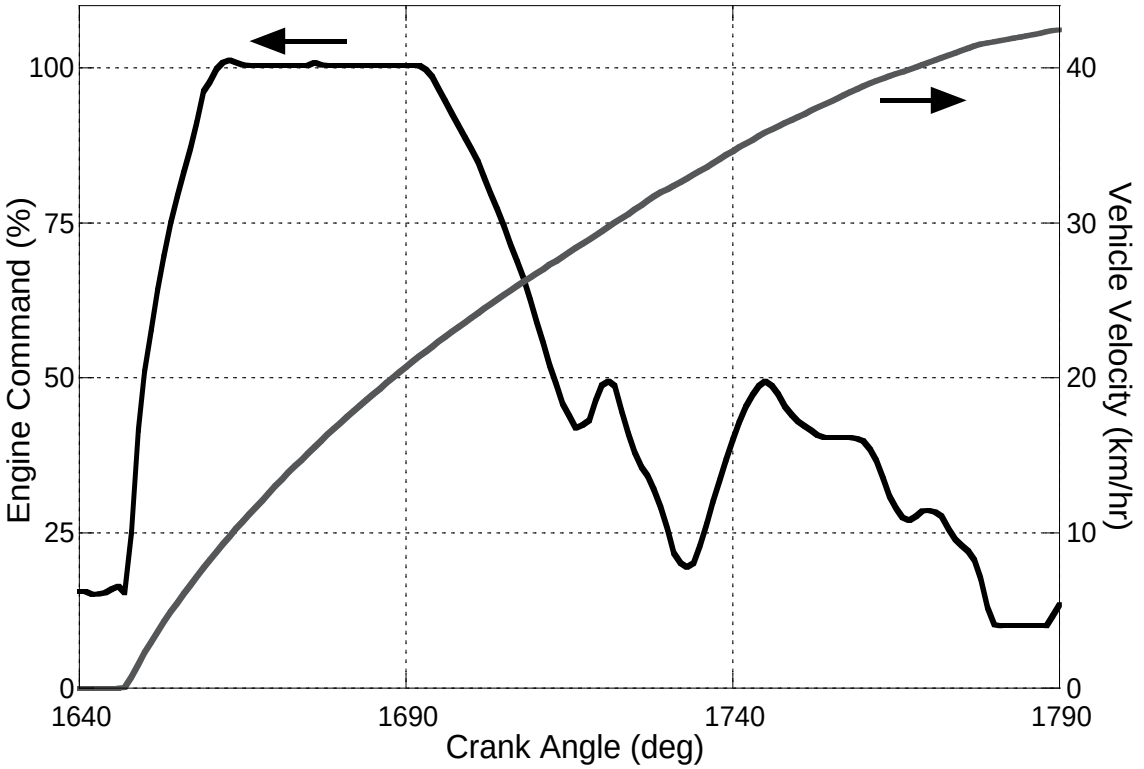

Figure 5.4: Engine Command and Vehicle Velocity during Vehicle Acceleration

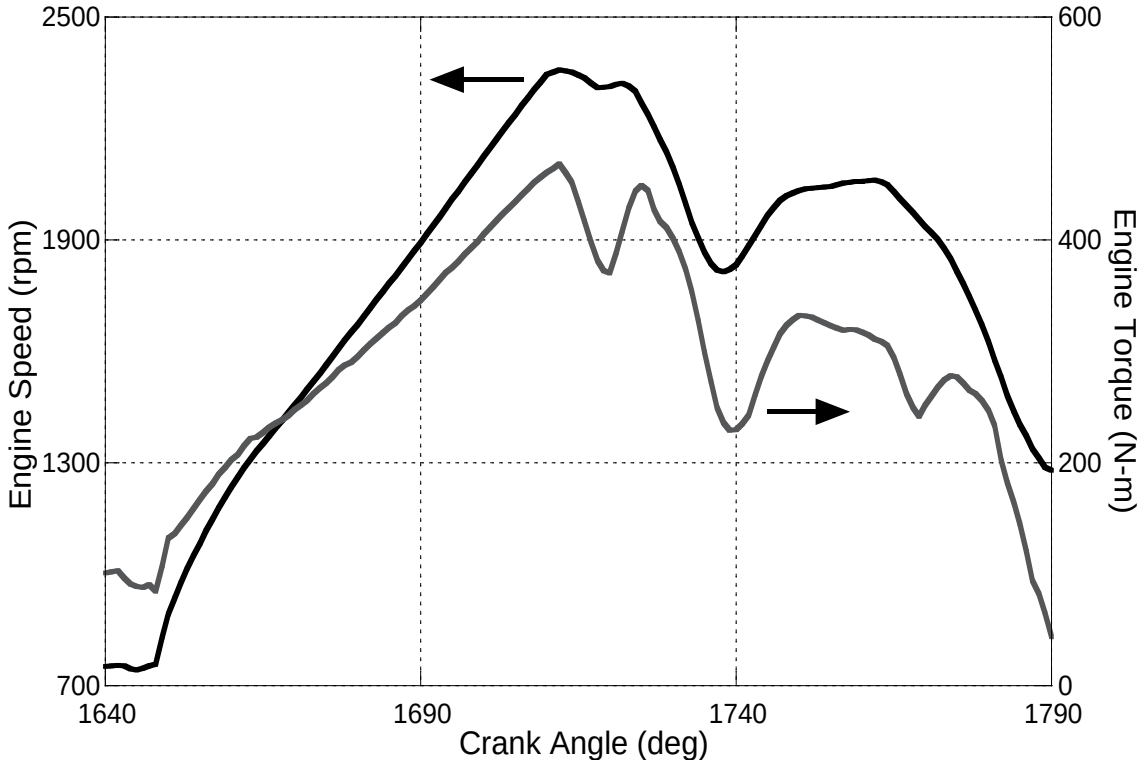

Figure 5.5: Engine Speed and Engine Torque during Vehicle Acceleration

5.3.1 Fuel Measurement Comparison

The fuel flow meter used in this study is described in detail in Section 3.1.2. It is located about 5 meters behind the engine and measures the mass of fuel that flows into a loop that continuously circulates fuel to the engine. This arrangement results in measurements that have a significant transport time. The output signal from this device is grams of fuel per second. By using the engine speed during each cycle and assuming that fuel is distributed evenly to all eight engine cylinders, this rate value is converted into a mass value per cycle per cylinder. As described in Section 4.4, fuel mass in the experimental technique is determined by crank angle resolved injection pressure and cylinder pressure data, as well as cycle-resolved start and end of injection timings from the instrumented injector.

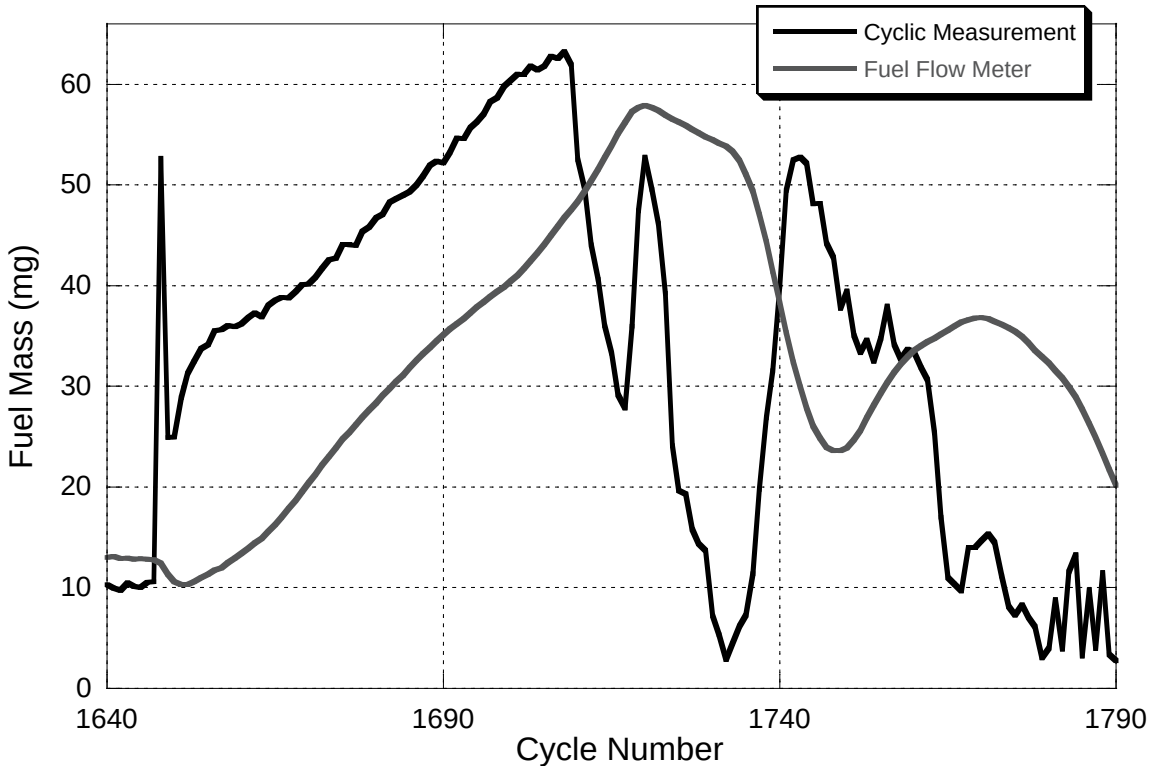

Figure 5.6: Cycle-Resolved Fuel Mass Measurement from Experimental Technique and Fuel Flow Meter during Cycles 1640-1790 of FTP 75

Fuel flow results obtained from the coriolis flow meter and the experimental technique are shown in Figure 5.6. It is clear that an increase in fuel consumption takes place during these cycles in two separate events as both methods show two rises and falls in fuel mass. The first encompasses more cycles and has a higher fueling rate. Beyond this, however, there is very little agreement between the two readings. The reading from the flow meter shows significant lag and completely misses features of the fuel injection mass that the experimental technique captures with crisp and clear fidelity.

5.3.2 Air Measurement Comparison

Air flow is determined in the test cell by two methods: through use of the laminar flow element (LFE) and the emissions bench. While the LFE produces results in grams per second, the emissions bench uses gas measurements to calculate an emissions-based air/fuel ratio. By using the fuel flow rate from the fuel flow meter, an air flow rate is calculated. The LFE is located directly above the engine and sits approximately 2 meters upstream of the turbocharger compressor; it is detailed in Section 3.1.2. The emissions bench, described in Section 3.2.8, samples exhaust gases about 2 meters downstream of the turbocharger, and the bench itself is another 10 meters away. Transport delays for the measurements of the emissions analyzers have been quantified and the data is shifted appropriately. Therefore the only delay in emissions results from the emissions bench should occur due to the response time of the individual gas analyzers.

Air mass from the experimental technique is determined by calculating the air/fuel ratio by using cycle-resolved CO_2 measurements from the exhaust manifold and inside the cylinder. This value is then multiplied by the fuel mass to arrive at air mass in the cylinder prior to combustion. Note should be taken that the air mass calculated from this technique includes any air that is recycled to the cylinder through EGR or residual, where the LFE only measures fresh air flow into the engine and the bench assumes that

all the CO_2, CO, and hydrocarbons in the exhaust are generated during combustion, which results in a slight under-estimation of air/fuel ratio.

The results of the determination of air mass from the LFE, emissions bench, and experimental technique are shown in Figure 5.7. For the first 60 cycle of the transient, the LFE and experimental technique provide results that agree very well with one another. After that, the two methods provide similar trends but different absolute values. Air mass values from the emissions bench are significantly lower than the other two processes near the beginning but much higher near the end. This result's error and lag is compounded with the error and lag of the fuel flow meter. All three results capture two separate increases and decreases in air flow. There are periods in which the experimental technique does not provide a reading of air flow; the reason for this is discussed in Section 5.4.

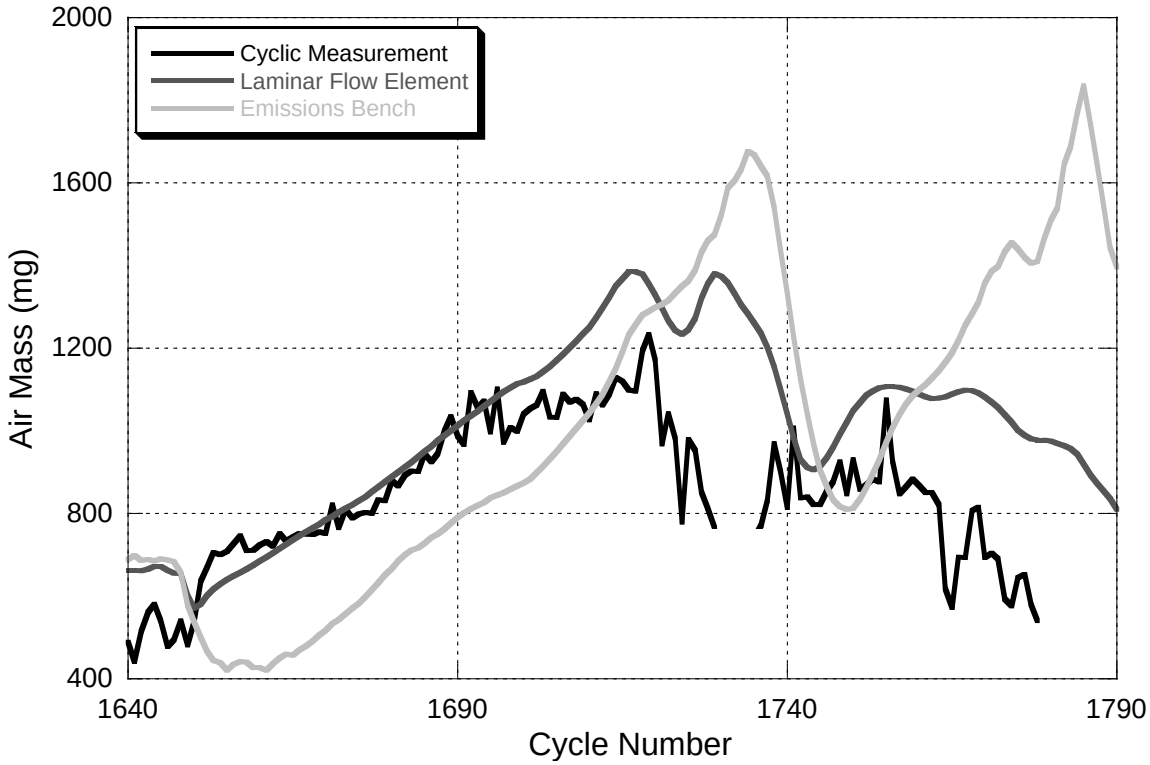

Figure 5.7: Cycle-Resolved Air Mass Measurement from Experimental Technique, LFE, and Emissions Bench during Cycles 1640-1790 of FTP 75

5.3.3 Air/Fuel Ratio Calculation Comparison

Air/fuel ratio is determined by taking the ratio of air mass to fuel mass. The emissions bench reports this value directly, while when combined with the data from the fuel flow meter, the LFE can also provide an air/fuel ratio measurement. Air/fuel ratio from the experimental technique is calculated by using cycle-resolved CO_2 measurements from the exhaust manifold and inside the cylinder. The air/fuel ratio from these three methods is shown in Figure 5.8.

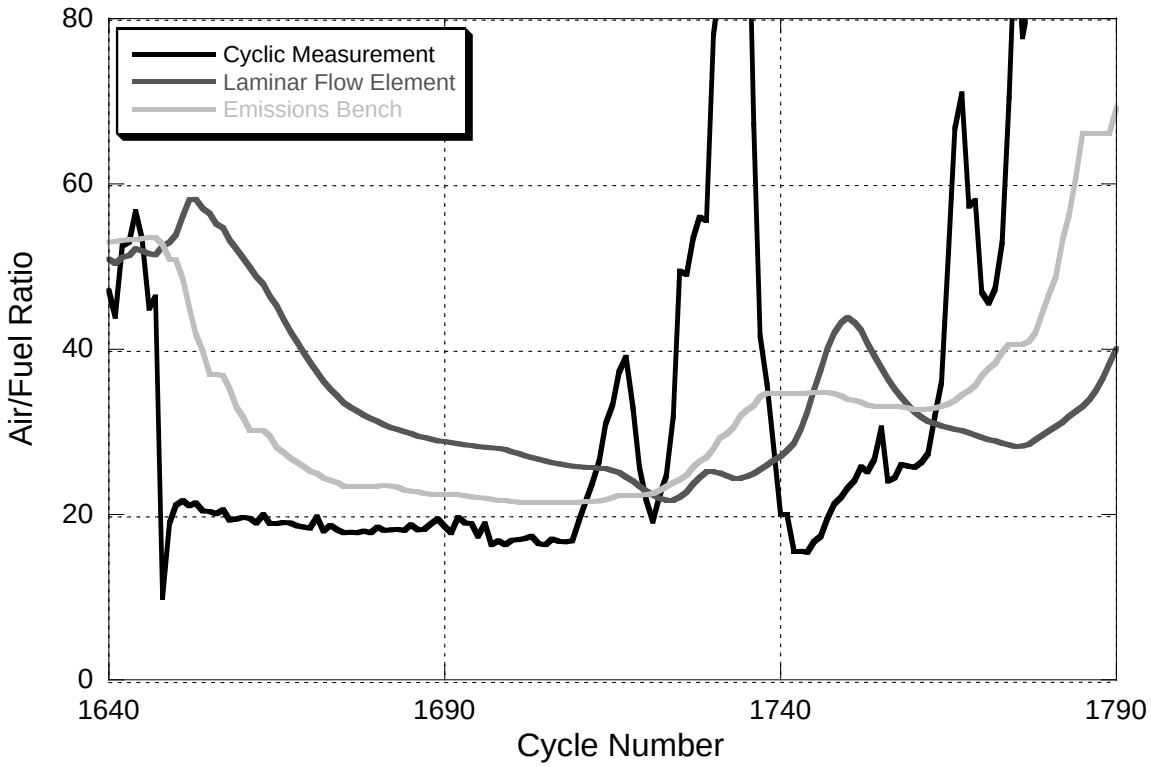

Figure 5.8: Cycle-Resolved Air/Fuel Ratio Calculation from Experimental Technique, LFE, and Emissions Bench during Cycles 1640-1790 of FTP 75

The trends obtained in air/fuel ratio from these three methods are quite different. While they all start out close to one another and move downward in the fifty cycles, they do not agree after that. Results from the LFE and emissions bench follow one another generally but quantitatively are quite different.

5.3.4 In-Cylinder/Intake Manifold CO_2 Comparison

The concentration of CO_2 in the intake manifold is measured by the emissions bench and used to quantify the amount of exhaust gases that the engine is recirculating. One probe of the fast CO_2 sensor is mounted in-cylinder to sample gases during the compression stroke. While these devices will read different absolute values, their behavior should have relatively similar trends, especially when EGR is flowing. Figure 5.9 demonstrates the signals obtained from these two devices.

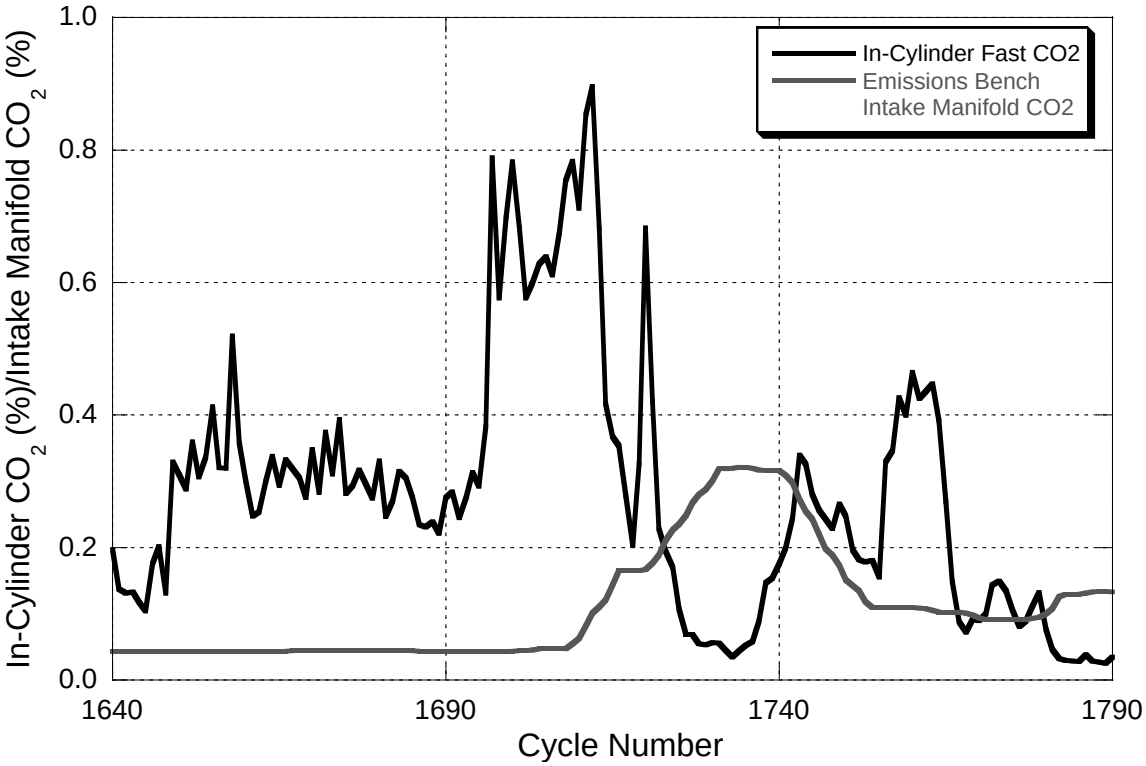

Figure 5.9: Cycle-Resolved Intake Manifold and In-Cylinder CO_2 Measurements from Fast CO_2 Sensor and Emissions Bench during Cycles 1640-1790 of FTP 75

Results from the sensors are quite different. Intake manifold CO_2 remains consistently low during the first 70 cycles which indicates that EGR flow is low and suggests that the EGR valve is closed. In-cylinder CO_2 readings during this period confirm the assumption. Starting around cycle 1690, however, in-cylinder CO_2 jumps up by a factor of nearly four. Around 20 cycles later, a pulse in the intake manifold CO_2 is

reported and these two waveforms are probably the measurement of the same event as the EGR valve opens. For the final 50 cycles of the transient, the readings are in general agreement with one another.

5.3.5 EGR/Stoichiometric Combustion Product Percentage Comparison

The percentage of EGR and stoichiometric combustion products in the cylinder is not a direct comparison. These two quantities are closely related to one another, however, as the percentage of EGR is a component of the fraction of stoichiometric combustion products. Their trends are demonstrated in Figure 5.10.

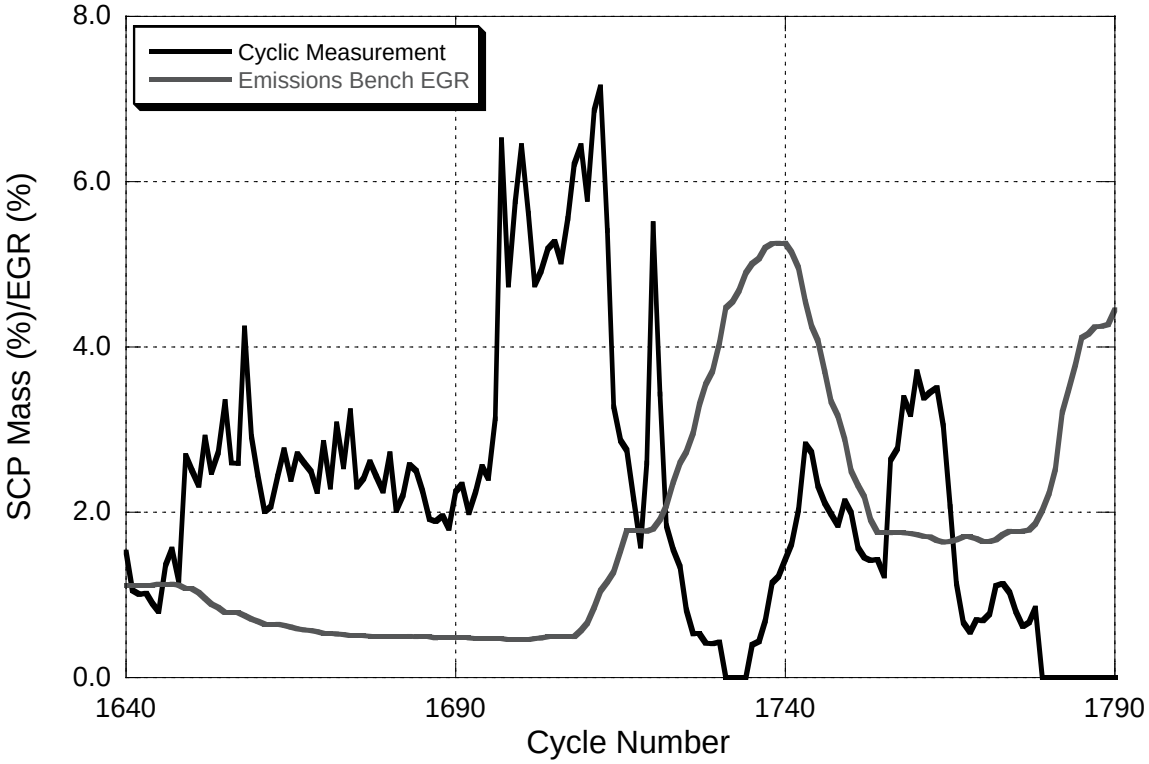

Figure 5.10: Cycle-Resolved EGR and Stoichiometric Combustion Product Percentage during Cycles 1640-1790 of FTP 75

These quantities are derivatives of the signals shown in Figure 5.9, so it follows that their relationship should follow the one established between the in-cylinder and intake manifold CO_2 signals. While EGR rate remains low for the first 70 cycles, the

stoichiometric combustion product mass hovers above 2%. Around cycle 1690, a large pulse in the fraction of stoichiometric combustion products forms and this value exceeds 6%. Just as this pulse is ending, the EGR percentage begins rising and peaks at around 5% before falling back down. These two waveforms are likely the same event and demonstrate that at this condition, the EGR signal lags the stoichiometric combustion signal by about 30 cycles and does not capture the rapid changes that occur.

5.3.6 Exhaust CO_2 Comparison

Measurements of CO_2 in the exhaust are made by the Fast CO_2 sensor which is measuring gases as they exit the exhaust valve. The emissions bench is also quantifying the concentration of CO_2 in the exhaust. Transport time delays for the CO_2 sensor in the emissions bench are known and the data is shifted so that the only lag is due to sensor response.

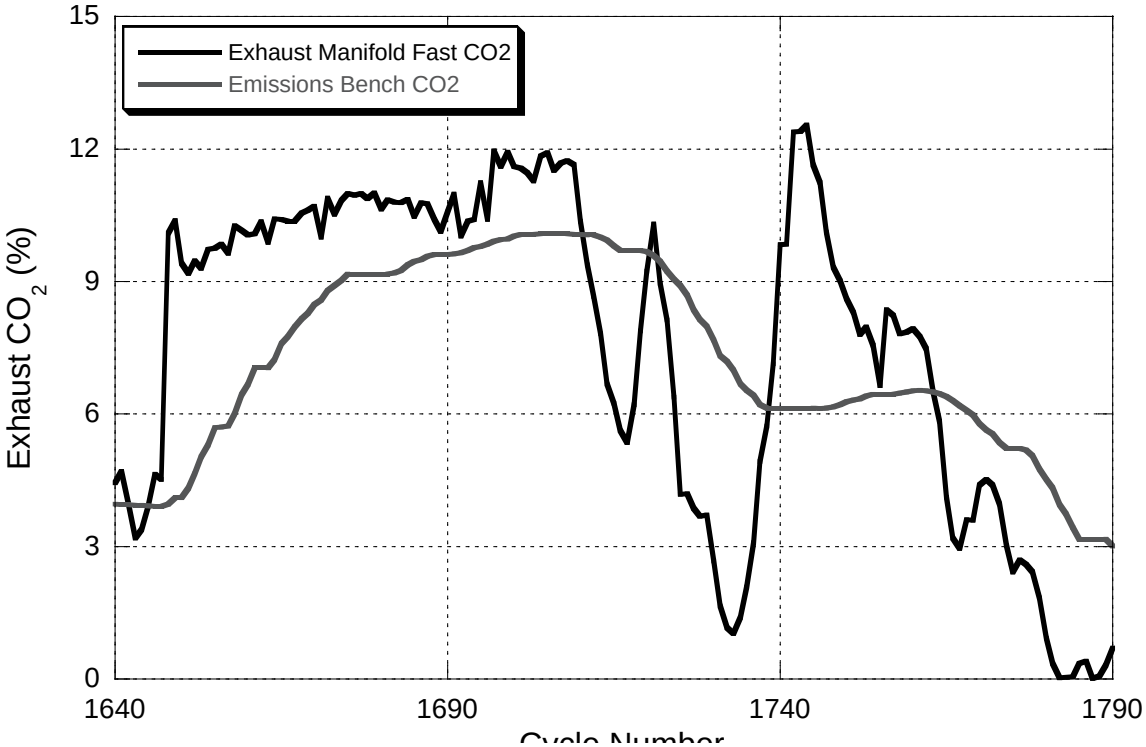

Figure 5.11: Cycle-Resolved Exhaust CO_2 Measurements from Fast CO_2 Sensor and Emissions Bench during Cycles 1640-1790 of FTP 75

The signals fit each other quite well quantitatively, as the concentrations reported by the two devices is generally in good agreement. The slow response of the sensor in the emissions bench is visible; however, as it fails to capture the rapid changes in exhaust CO_2. A good example of this is considering the signal from the bench CO_2 sensor around cycle 1715. While the fast-response device quickly drops and increases again by cycle 1740, the bench sensor reacts slowly and misses both the valley of CO_2 formation and the following peak and provides a signal that is somewhere in between the two extremes. Another factor which contributes to this behavior is mixing of gases from different cycles during the transport of the sample from the exhaust line to the emissions bench. This would tend to average out the concentrations of individual cycles and provide a more averaged gas concentration to the analyzer.

5.3.7 Exhaust NO Comparison

To quantify the amount of NO in the exhaust, one channel of the Fast NO analyzer is placed in the exhaust manifold near the exhaust valve. Another NO analyzer is located in the emissions bench. The signals from these two devices are displayed in Figure 5.12. As in the case of the other analyzers, the transport time is known and accounted for in this figure.

Quantitatively, the devices agree quite well. The poor response time of the bench's NO analyzer is evident, however, when examining the figure. The peaks and valleys that appear in the Fast NO signal are not detected, and the entire waveform is shifted rightward. Mixing of the sample as it is transported through the 10 meters of sampling line is undoubtedly occurring, which results in a gas sample that is averaged and contributes to the bench's much more smooth output. Discerning NO emissions to cycle-resolved values is impossible from such a signal.

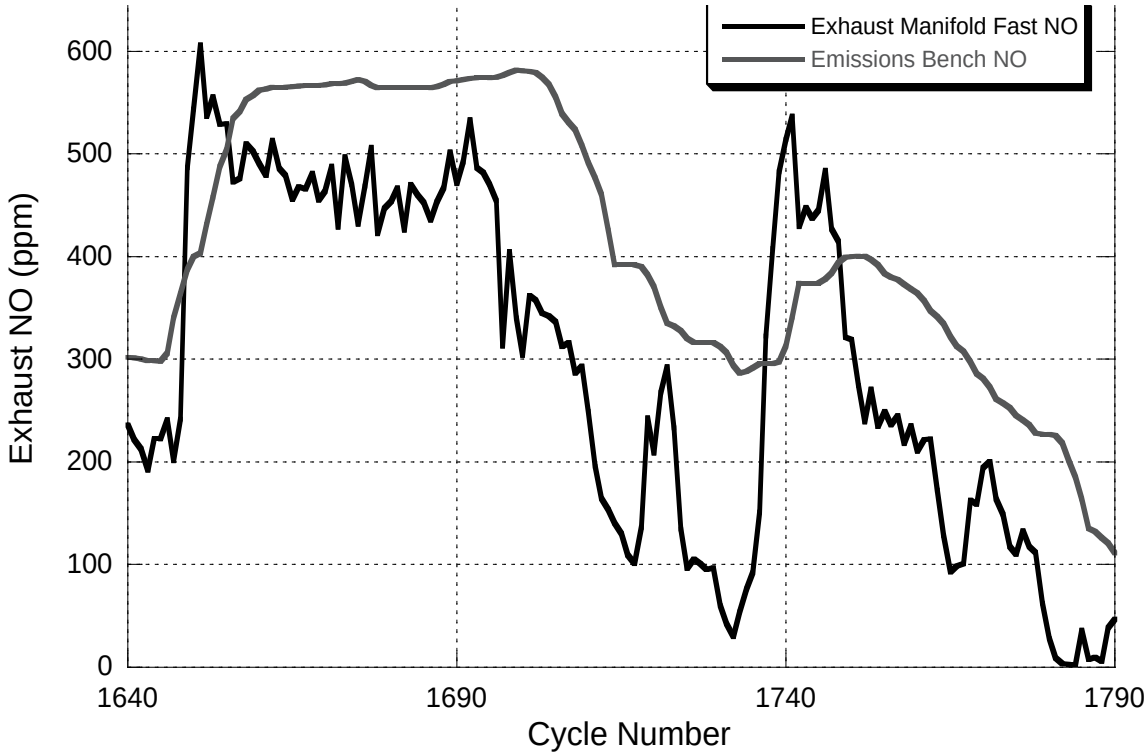

Figure 5.12: Cycle-Resolved Exhaust NO Measurements from Fast NO Sensor and Emissions Bench during Cycles 1640-1790 of FTP 75

5.3.8 Data Comparison Summary

When considering the data gathered from traditional test cell information and the experimental technique developed in this study, the differences between the two are distinct. Typical test cell instrumentation cannot resolve engine output to cyclic values. There are two main reasons for this. First, the devices have relatively long response times. Second, the design or configuration of the device is such that it cannot measure the sample medium at the required locations. The fuel flow meter cannot possibly be located within the injection system to measure fuel flow. The LFE or emissions bench has no way to account for maldistribution of EGR or air to the cylinders. Since these devices are located a far distance from the measurement point, any cyclic variance is erased as the sample is transported to the instrument.

Conversely, the experimental technique developed and presented in this research has the capability to measure cycle-resolved values of fuel, air, and stoichiometric

combustion products over a wide range of engine operating conditions. The insight it provides into cycle-resolved engine behavior during transient engine operation is significantly more meaningful than the data provided by traditional test cell instrumentation.

5.4 Limitations of Experimental Technique

There are particular engine operating conditions in which the experimental technique provides results which have a high level of uncertainty. These conditions exist at the very upper and lower regions of the engine's performance envelope and impact the fuel calculation technique and the exhaust manifold CO_2 measurement.

5.4.1 Fuel Mass Measurement Uncertainty

At very low-load conditions, especially when the engine is coasting down in speed, very little fuel is injected. Typical needle lifts have a magnitude of 0.4 mm, but when engine coast-down occurs no needle lift may take place at all. In these cases, the needle lift signal is reduced to nothing but noise and the algorithm that calculates the start and end of injection timing may report SOI and EOI crank angles that are completely incorrect which leads to a reported fuel mass that is simply not occurring. Figure 5.13 demonstrates a normal needle lift, in which the SOI is -3.6º after TDC and the EOI is 1.0º after TDC. It also shows the needle lift for an event of non-combustion. In this cycle, the algorithm reports a SOI of -7.1º after TDC and an EOI of 13.5º after TDC. By inspection, this injection event is obviously not occurring. Evaluation of the data is therefore necessary during engine coast-down to ensure that the reported fuel mass values are reasonable.

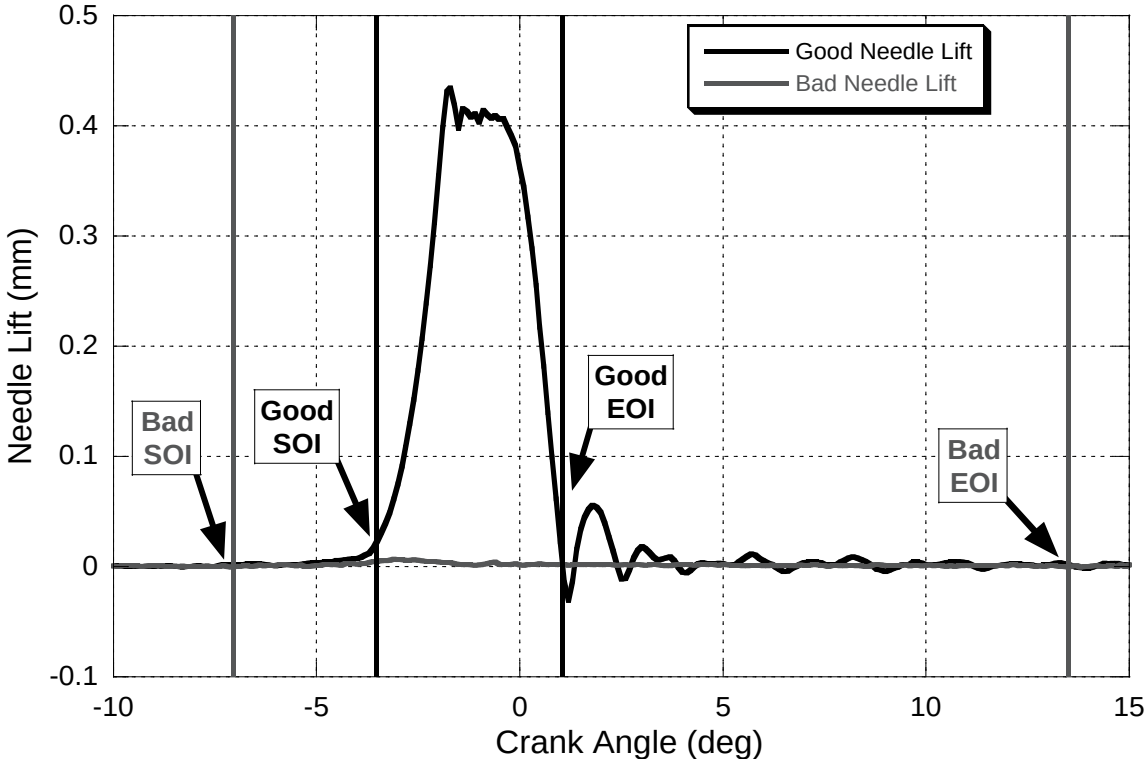

Figure 5.13: Needle Lift for Typical Injection Event and for Zero-Combustion Case During Engine Coast-Down

Fuel mass data from engine conditions that have fueling rates of less than 5.5 mg/cycle must be examined very carefully, as this is the fuel consumption during engine idle. In the tests conducted for this study, any injection event that reports a fuel mass less than this value is ignored, and the mass of fuel, air, and stoichiometric combustion products for that cycle are not calculated. This is evident when considering some of the figures in this document, especially in Chapter 8 where engine behavior experiences frequent and significant periods of engine coast-down.

Under certain operating conditions at low loads and speeds, the fuel injector experiences a significant proportion of needle bounce. This behavior is also captured in the measurement of fuel injection pressure, and suggests that fuel is injected both in the true needle lift event and the bounce as well. The algorithm that determines the end of injection may define EOI after the needle closes for the first time or after the first bounce. This significantly impacts the overall duration of injection, which plays a major role in

calculating the mass of injected fuel. Figure 5.14 demonstrates the needle lift and injection pressure in such a condition.

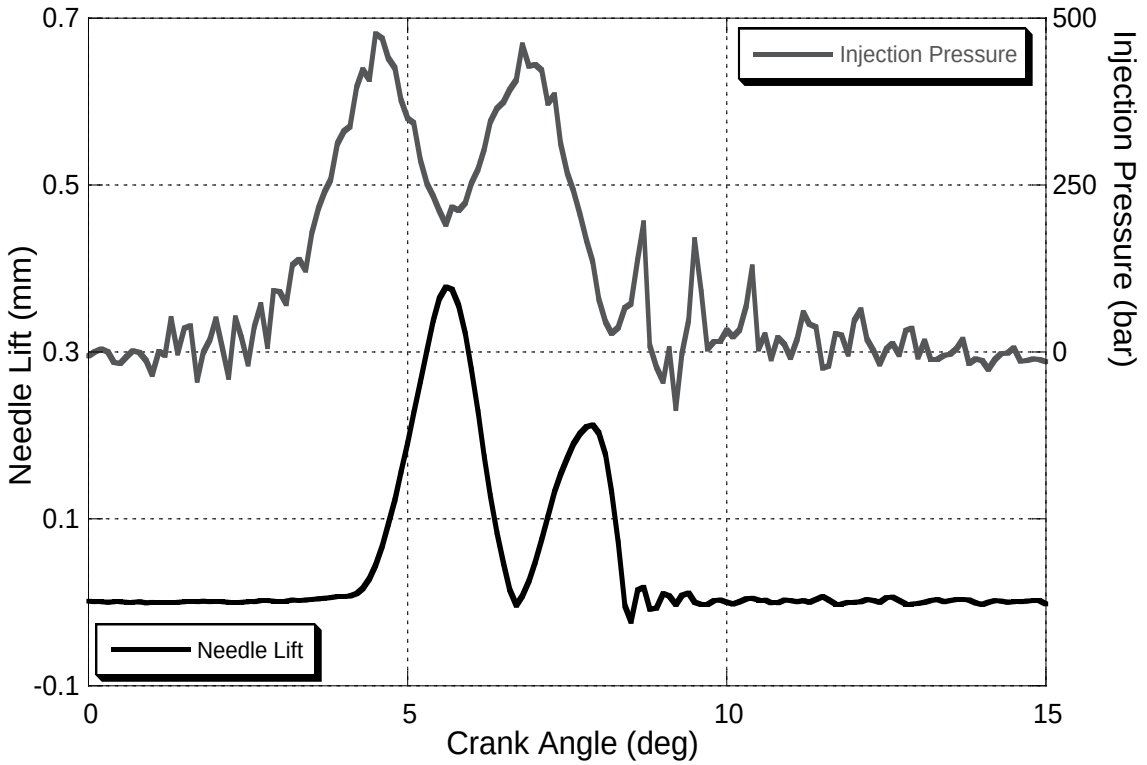

Figure 5.14: Needle Lift and Injection Pressure at 755 rpm, 2.1 Bar BMEP

Using the shorter EOI results in a calculated fuel mass of 10.9 mg, and with the longer EOI the reported fuel mass is 17.9 mg. The actual fuel mass probably falls somewhere between the two. It is less than the value reported with the longer EOI because the action of the closing and reopening of the needle results in an actual average discharge coefficient that is less than it would be in a normal injection event. Most likely the actual fuel mass is greater than the amount calculated with the shorter EOI because fuel is injected during the needle bounce.

Errors in the fuel measurement under such conditions propagate through the experimental technique, as the determination of air mass and stoichiometric combustion product mass are calculated using fuel mass. Fortunately such conditions only occur at very light engine loads when emissions formation is very low and engine behavior is less

critical. Needle lift at engine conditions below 1000 rpm and under 2 Bar BMEP must be scrutinized to identify the presence and degree of injector needle bounce and to assess the impact on the reported mass of injected fuel.

5.4.2 Exhaust Manifold CO_2 Measurement Uncertainty

Under very low load conditions when the engine is coasting down, the concentration of CO_2 in the exhaust falls to levels near zero. In such situations, the blowdown process is very weak and may not even exist; a typical CO_2 signal from such an exhaust event is shown in Figure 5.15 along with a CO_2 trace from a normal combustion event. Therefore the algorithm to locate the crank angle at which blowdown begins may completely misinterpret the data, which results in an error in the amount of CO_2 in the exhaust manifold. Absolute values of CO_2 are very low at such conditions, and small absolute errors at such a condition results in large relative error. Additionally, these conditions occur when fuel flow is also very low and the technique to determine the amount of fuel mass reports values with a high level of uncertainty. These errors propagate through to the mass of air and stoichiometric combustion products. Thus CO_2 concentrations that are reported from engine coast-downs are typically ignored and for these cycles no air or stoichiometric combustion product masses are calculated. This is evident in a number of figures in Chapter 8, where the engine experiences numerous periods of coasting-down.

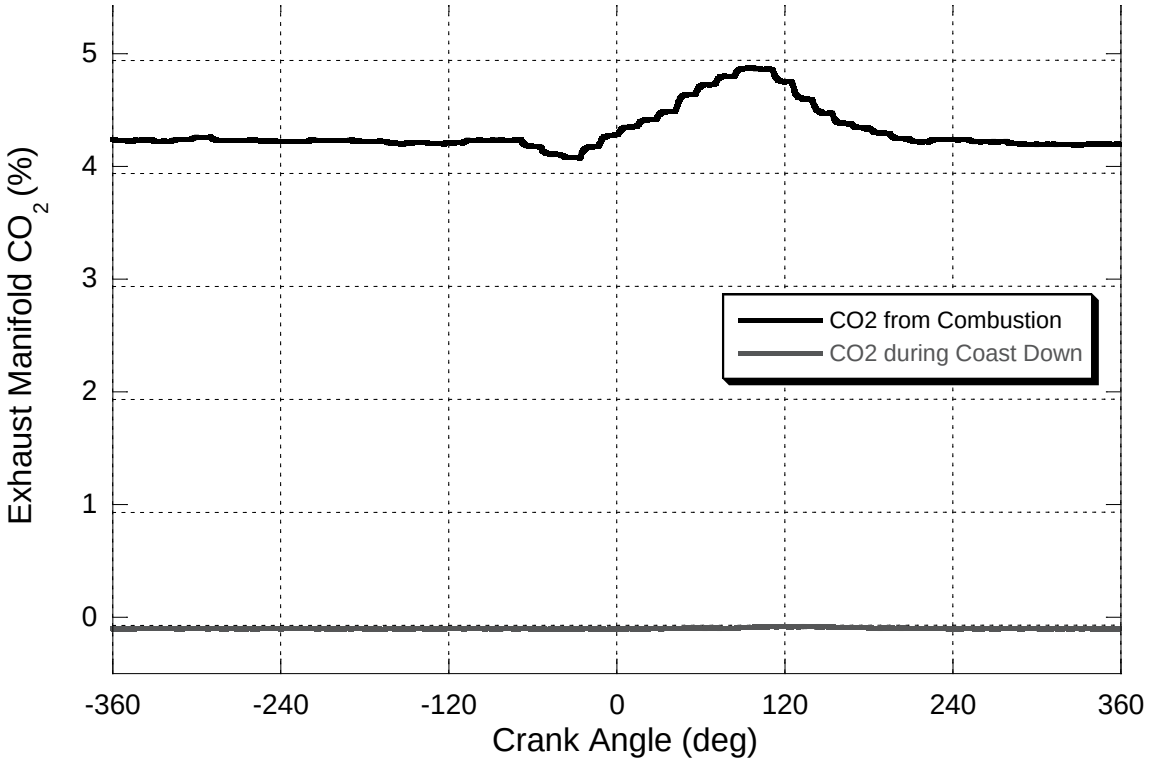

Figure 5.15: Exhaust Manifold CO_2 Measurement during a Normal Combustion Cycle and during Engine Coast-Down

Under very high engine loads, the pressures in the exhaust manifold climb to levels that are greater than the chamber pressure in the Fast CO_2 exhaust probe in the exhaust manifold. The output of this device is very sensitive to pressure, and increasing the chamber pressure above the pressure that is used to calibrate the device results in erroneous readings. Fortunately these conditions only exist when the engine is generating exhaust manifold pressures in excess of 200 kPa, which occurs only when the engine is producing high levels of power. During the driving cycle investigated in this study and examined in Chapter 8, such conditions are only experienced very briefly and therefore this type of error does not significantly impact the results presented in this study. Care must be taken, however, when using the Fast CO_2 sensor to ensure that it is able to maintain a consistent chamber pressure throughout the test.

5.5 Validation of Experimental Technique Summary

This chapter explores the impact of the experimental technique on the combustion process and establishes confidence intervals on the measured values of the mass of fuel, air, and stoichiometric combustion products. Adding volume to the combustion chamber and removing mass from the cylinder during the compression stroke affect combustion by lowering cylinder temperatures and pressures and prior to fuel injection, thereby increasing the ignition delay. The effect is noticeable at lower engine operating conditions but negligible at higher engine speeds and loads. At engine idle, ignition delay increases from 2.0 to 3.0 degrees, while at 1750 rpm 1 bar BMEP, the ignition delay goes up by 0.3 degrees. Burn rates, however, remain unchanged and those conditions that experience a larger increase in ignition delay have burn rate curves that are essentially shifted to the right by the increment in ignition delay.

Analysis of errors in the instrumentation used in the experiments, the assumptions made to simplify calculations, and the techniques implemented to determine cylinder charge component masses reveal high confidence in the data. Error levels are consistently low over the full range of engine operating conditions examined. Using a 95% confidence interval, fuel mass is determined to within 0.74%, air mass is known to within ±2.82%, and the mass of stoichiometric combustion products is measured to within ±3.93%. These error values are very low and demonstrate the robustness of the experimental technique.

This technique incorporates instrumentation that has a fast enough response time to respond to cycle-resolved changes in the engine. Traditional test cell instrumentation cannot provide data at this high level of fidelity due to slow instrument response times, transport delays, and the mixing that occurs during the transport period.

Engine operation at the outer edges of its performance envelope creates conditions in which the technique provides results with high levels of uncertainty. This is

especially true as the engine transitions from a high-load condition to a low-load point. During such behavior, no fuel is injected and very little, if any, CO_2 is measured in the exhaust. With no fuel injection, the needle lift signal is erroneously interpreted into bogus SOI and EOI values, which are then used to calculate an injected fuel mass that does not exist. Extremely low values of CO_2 in the exhaust amplify the impact of measurement errors, and when combined with the error incurred by the fuel flow calculation, the results develop a very high level of uncertainty. Errors are also incurred during low-speed low-load conditions in which the fuel injector exhibits needle bounce. This results in injection durations that are too long or short and directly impacts the fuel mass calculation. Under extremely high-load conditions, exhaust manifold pressures overwhelm the ability of the fast CO_2 sensor to maintain a constant internal chamber pressure, which results in sensor inaccuracies. Fortunately these conditions are not encountered frequently in the investigated driving cycles.

CHAPTER 6

CYCLE-RESOLVED MEASUREMENTS DURING STEADY STATE ENGINE OPERATION

To examine the insight provided by the experimental technique, data is taken while the engine is operating at steady state conditions. Because all inputs to the engine are fixed, data taken while the engine is operating constantly will reveal cycle-to-cycle variances in in-cylinder trapped masses and the influence on these variances in emissions. First the experimental procedure is described, followed by a discussion of engine behavior at both of the investigated operating conditions. Finally a summary of the steady-state data is presented.

6.1 Steady-State Experimental Procedure

Three different operating conditions are evaluated while the engine operates at steady state. Mid-speed low-load behavior is examined at 2000 rpm, 1 bar BMEP. Mid-speed mid-load conditions are studied at 2000 rpm, 9 bar BMEP. During the testing process in both cases, the engine is operated using the standard calibration from the PCM and dynamometer speed and engine command are held constant. If any of the inputs to combustion change: injection timing, injection pressure, fueling rate, EGR valve position, or VGT vane position, it is because the engine's controller is making the variations. This arrangement most closely mimics steady-state operation in a vehicle.

6.2 2000 rpm, 1 bar BMEP

At the 2000 rpm, 1 bar BMEP operating condition, the engine is experiencing a light load condition. Fuel injection quantities, and therefore injection durations are relatively small, boost pressure is negligible, and the EGR valve is opened for NO_X emissions control. To establish the true steadiness of this operation condition, Figure 6.1 shows the variance of PCM-controlled engine parameters, including the desired fuel injection mass, the fuel injection timing, the fuel injection pressure, the EGR valve position and the VGT vane position.

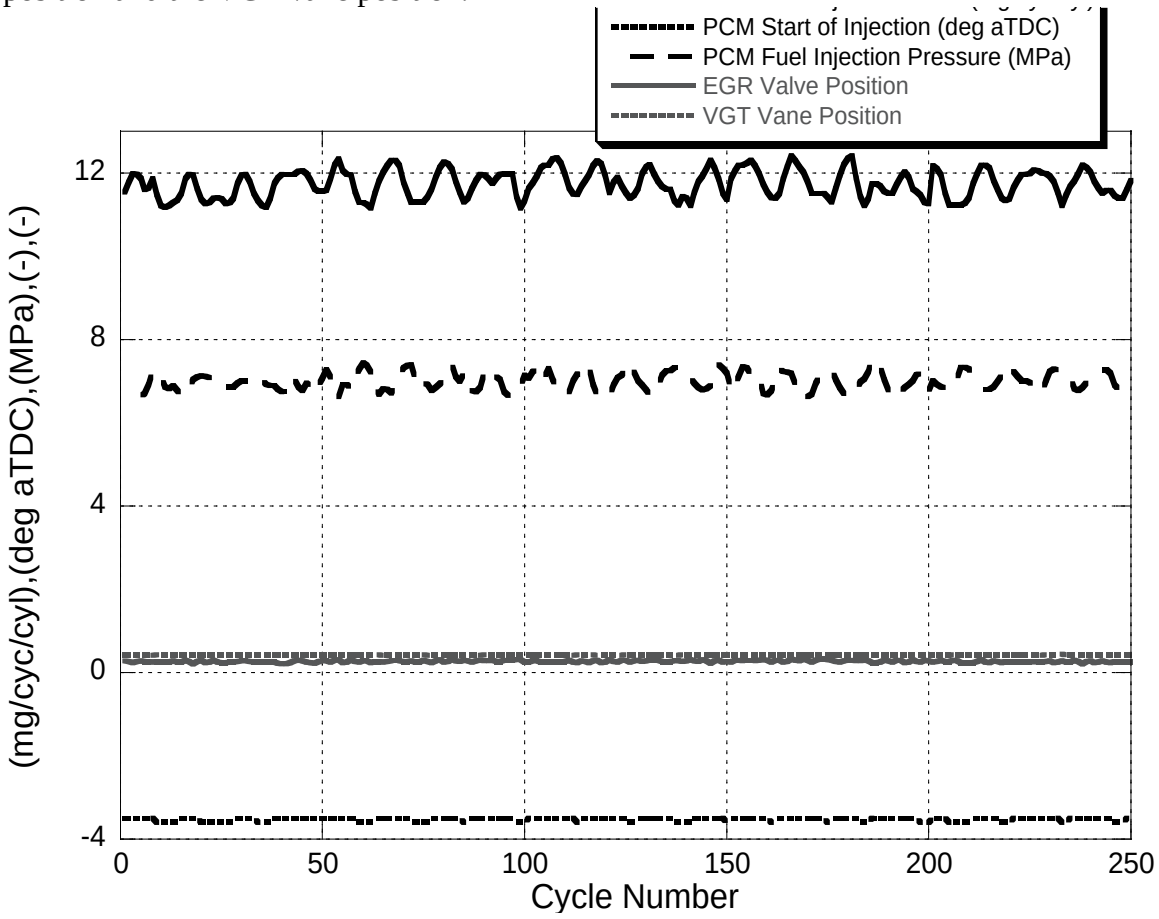

Figure 6.1: PCM Desired Fuel Injection Mass, Start of Injection, Injection Pressure, EGR Valve Position, and VGT Vane Position at 2000 rpm, 1 Bar BMEP

While the desired fuel injection mass seems to vary the most in Figure 6.1, it actually does not when considering variance on a relative basis. A more fair comparison of these input values is given in Table 6.1. All engine-controlled inputs have a COV of

less than 5% except for the EGR valve position, indicating the setpoints of these variables remain quite constant. Variances between the maximum and minimum values of these variables are also displayed and demonstrate that significantly different engine operating conditions might well be encountered during so-called steady-state operation.

Table 6.1: Mean Value, Coefficient of Variance, and Percent Difference Between the Maximum and Minimum Values of PCM-Controlled Engine Inputs at 2000 rpm, 1 Bar BMEP

Variable	Mean Value	Coefficient Of Variance	Percent Difference Between Maximum and Minimum Values
Fuel Injection Mass	11.7 mg	2.8%	10.8%
Fuel Injection Timing	-3.5º aTDC	1.3%	2.8%
Fuel Injection Pressure	6.99 MPa	3.1%	12.7%
EGR Valve Position	0.27	8.5%	41.0%
VGT Vane Position	0.43	1.2%	7.1%

6.2.1 Fuel Injection Mass

Actual fuel injection mass is during steady-state operation is shown in Figure 6.2. It is readily evident that this value has much more variance than the demanded fuel injection mass by the PCM shown in Figure 6.1. The COV for the measured fuel injection mass is 6.4% and the percent difference between the maximum and minimum values is 40.0%; these values are 2.3 and 3.7 times greater than their counterparts for the demanded fuel injection mass. These differences are attributed to the inability of the injection to perform identical injection events. This is confirmed by evaluation of the COV of the injection duration and injection pressure, which are on the order of the COV of the measured fuel injection mass. At this condition, fueling rates are relatively low and engine speeds are high, resulting in a narrow window (5.3º) for fuel injection in

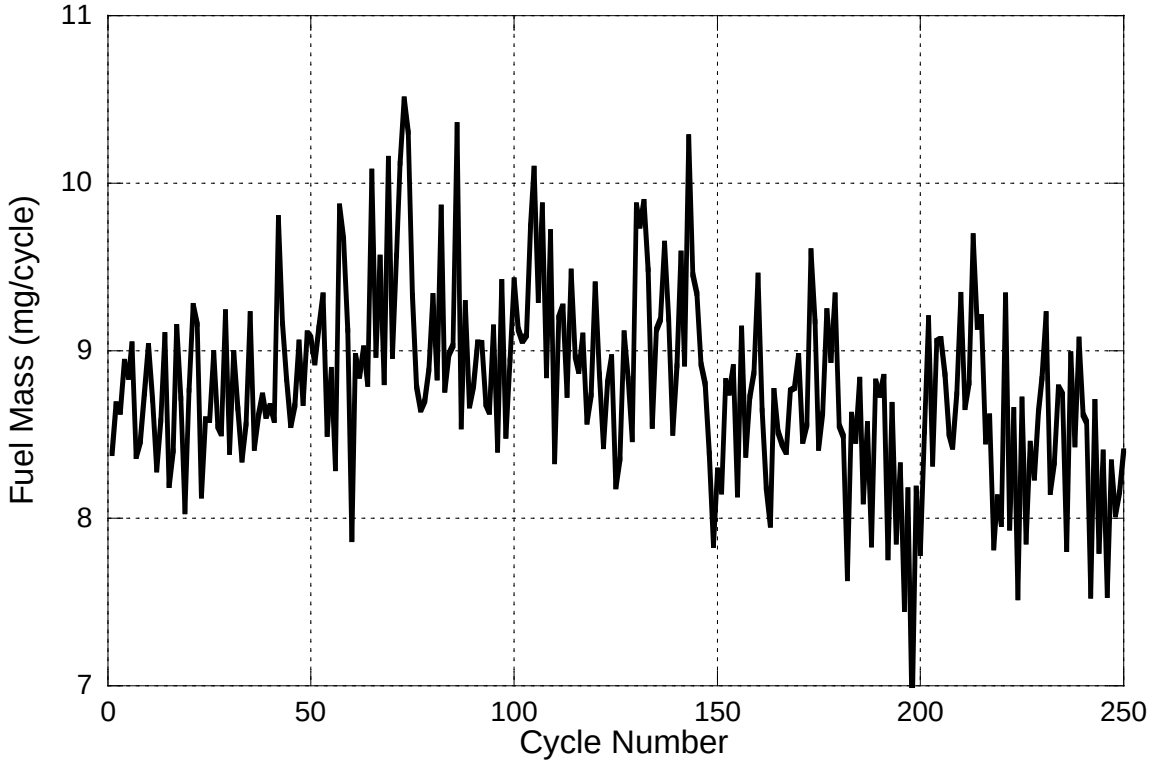

Figure 6.2: Cycle-Resolved Fuel Mass at 2000 rpm, 1 Bar BMEP

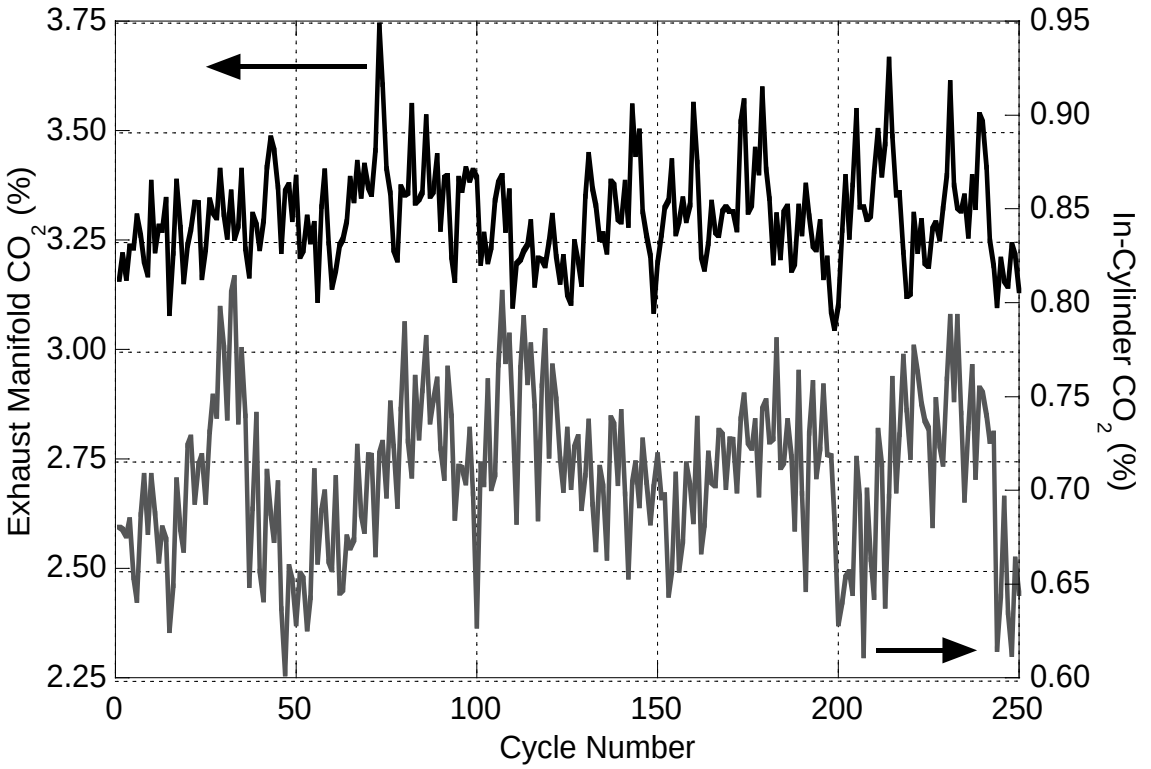

Figure 6.3: Cycle-Resolved Exhaust Manifold and In-Cylinder CO_2 Concentrations at 2000 rpm, 1 Bar BMEP

terms of crank angle degrees. Thus a fuel injection event that lasts one-half of a degree longer results in a much greater mass of injected fuel mass.

6.2.2 CO_2 Measurements

Cycle-resolved values for in-cylinder and exhaust manifold CO_2 are shown in Figure 6.3. COV for the in-cylinder CO_2 is 5.9% and for the exhaust manifold CO_2 is 3.4%. The percent differences between the maximum and minimum values are 29.8% and 21.0%, indicating significant differences in combustion cycles as the engine operates. These values are put through the iterative technique to determine cycle-resolved air and stoichiometric combustion product masses, which are shown in Figure 6.4.

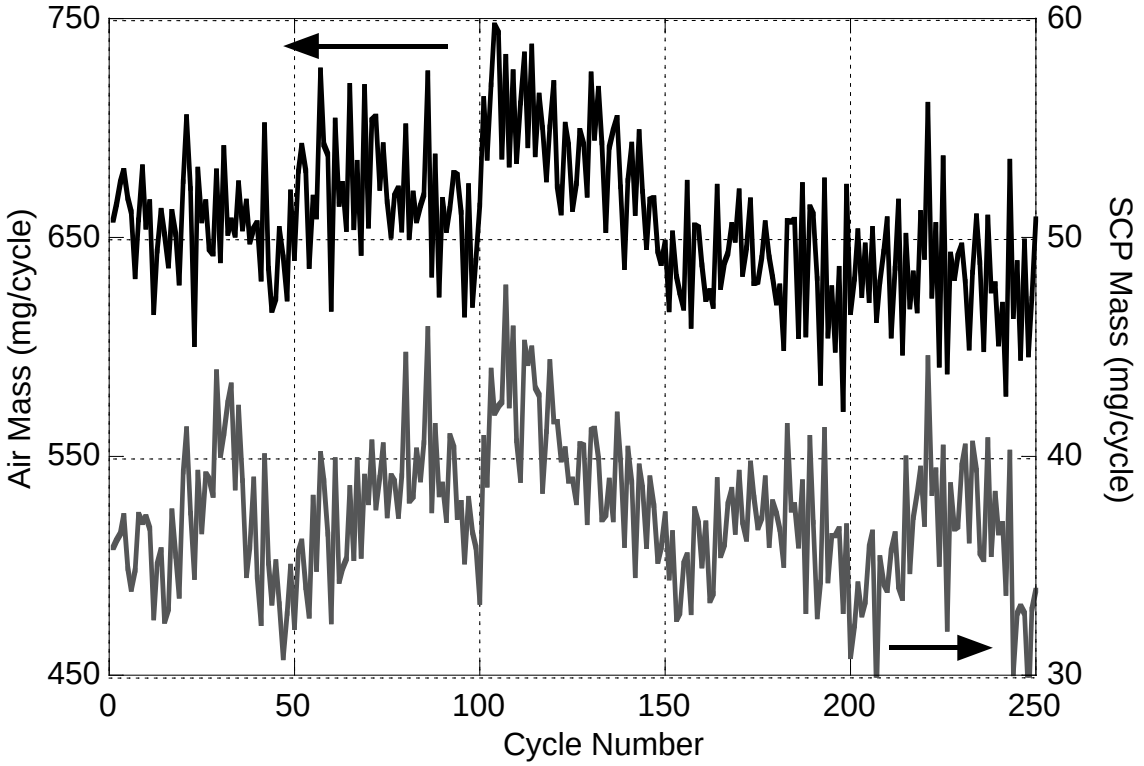

Figure 6.4: Cycle-Resolved Air and Stoichiometric Combustion Product Mass at 2000 rpm, 1 Bar BMEP

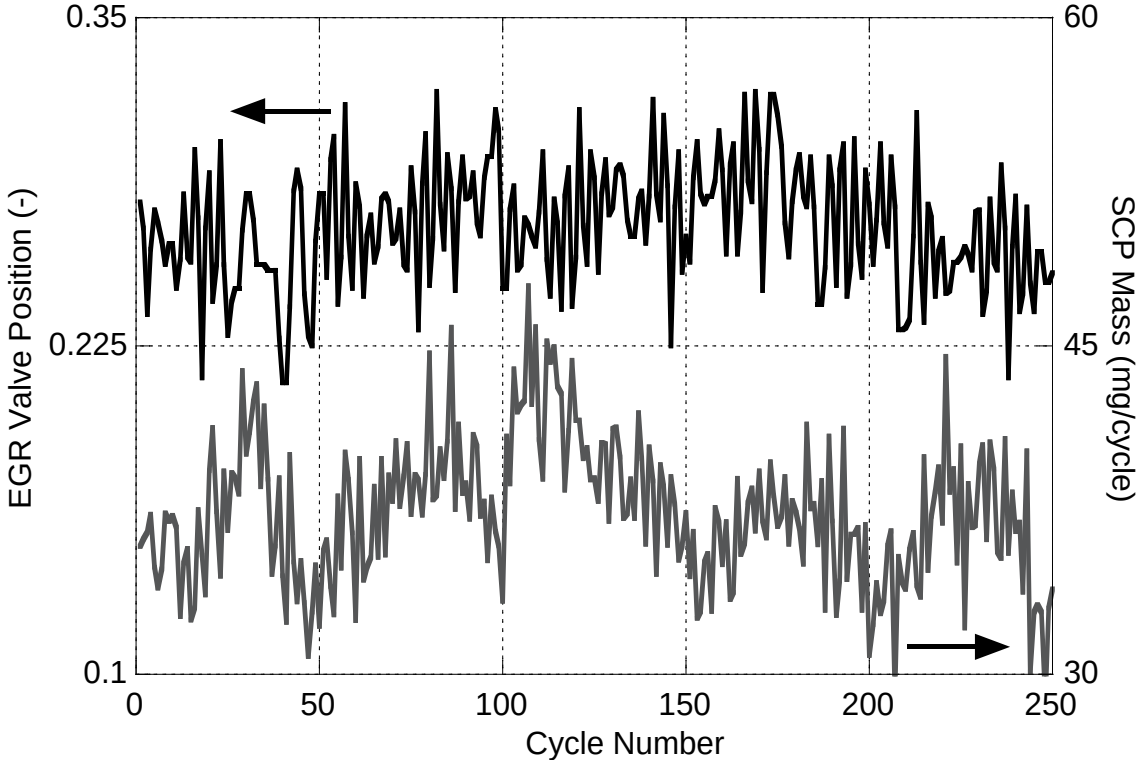

Figure 6.5: EGR Valve Position and Stoichiometric Combustion Product Mass at 2000 rpm, 1 Bar BMEP

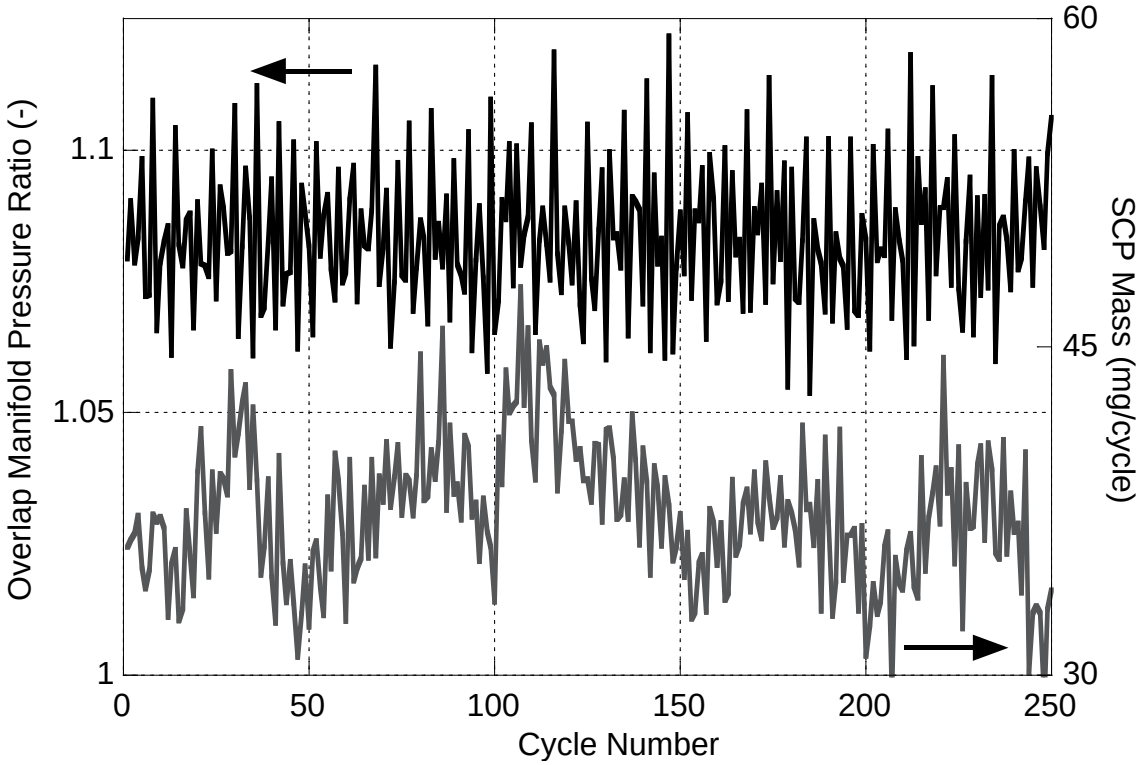

Figure 6.6: Manifold Pressure Ratio During Valve Overlap Period and Stoichiometric Combustion Product Mass at 2000 rpm, 1 Bar BMEP

6.2.3 Stoichiometric Combustion Products Mass

The variation of stoichiometric combustion product mass trapped in the cylinder is a function of three things: the pressure ratio between the exhaust manifold and the intake manifold during the valve overlap process, the opening of the EGR valve, and the degree to which fresh air and the EGR are mixed in the intake manifold. Figure 6.5 displays EGR valve position and stoichiometric combustion product mass.

Analysis of the relationship between EGR valve position and stoichiometric combustion product mass in Figure 6.5 reveals that the variation in SCP mass is not due to the motion of the EGR valve. The ratio of exhaust manifold pressure to intake manifold pressure during the valve overlap period is also not related to the variation in stoichiometric combustion product mass as demonstrated in Figure 6.6. Therefore variations in the trapped mass of stoichiometric combustion products in the cylinder must occur because of poor mixing of air and EGR in the intake manifold.

6.2.4 Air Mass

Trapped air mass is a function of boost level, manifold pressure ratios during the valve overlap period, and flow dynamics in the intake manifold. Figure 6.7 demonstrates the relationship between air mass and the average intake manifold pressure during the valve overlap period. While they do not track together perfectly, there is a correlation in how they change during the investigated 250 cycles. Turbocharger surging at this condition could certainly be taking place, as air flow rates and boost pressures are relatively low. Investigation of manifold pressure ratios are inconclusive and do not demonstrate a marked relationship to air flow rate. Intake manifold dynamics could definitely contribute to the variation in air flow rates. The unsteady rate of stoichiometric combustion products shown in Figure 6.4 and the fact that air mass roughly tracks with it support this possibility.

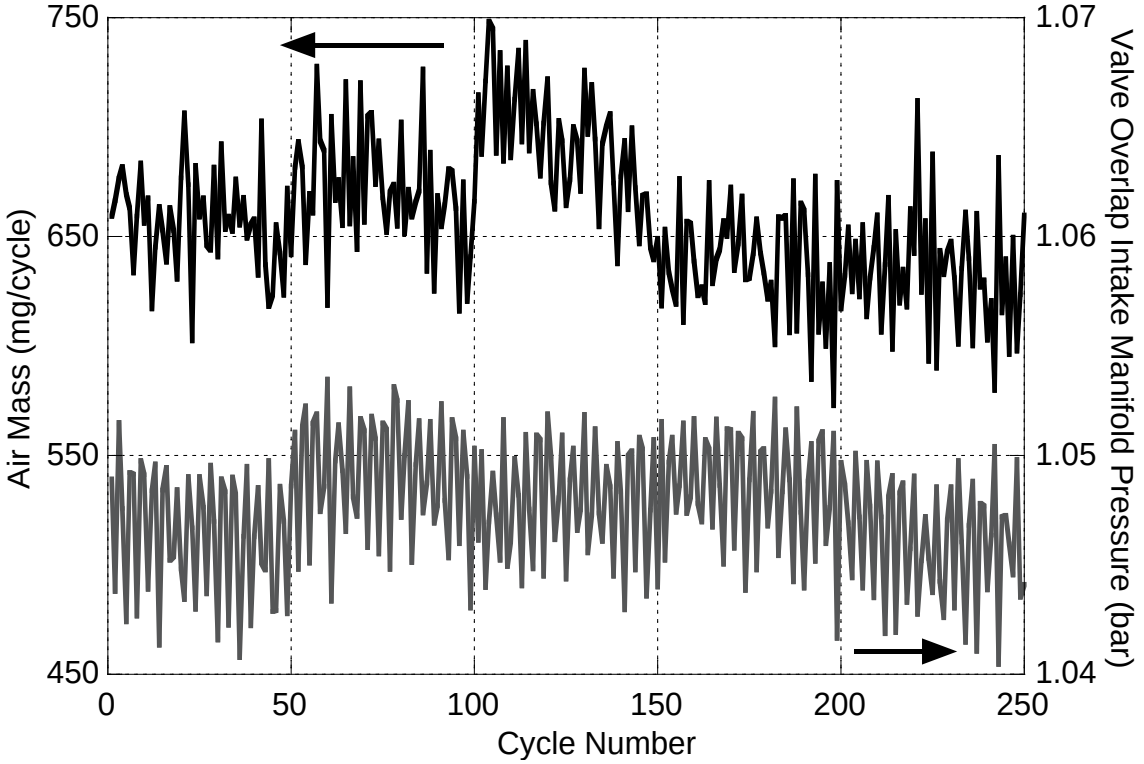

Figure 6.7: Air Mass and Average Intake Manifold Pressure During Valve Overlap at 2000 rpm, 1 Bar BMEP

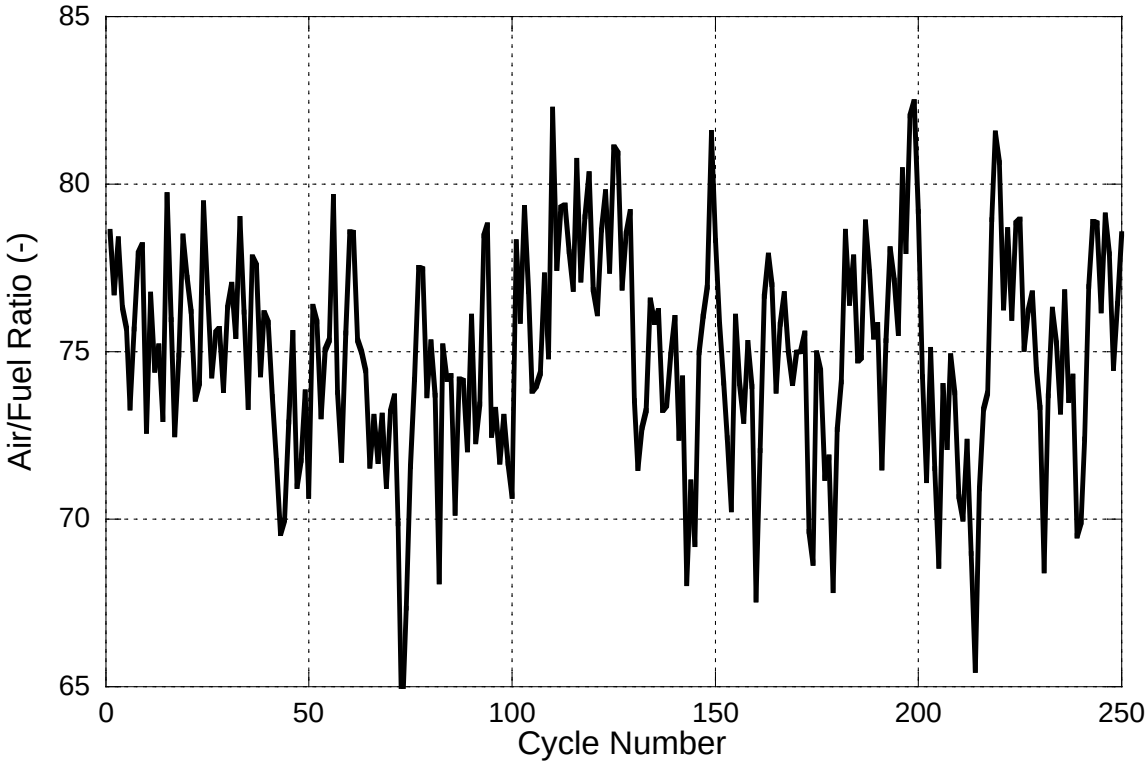

Figure 6.8: Cycle-Resolved Air/Fuel Ratio at 2000 rpm, 1 Bar BMEP

6.2.5 Air/Fuel Ratio

Air/fuel ratio variations during the test are shown in Figure 6.8. The COV of the air/fuel ratio for the test is 4.2% and the percent difference between the maximum and minimum values is 24.4%. These deviations are due to cyclical changes in fuel mass and air mass.

6.2.6 Combustion Analysis

Rate of heat release analysis is conducted on the data to establish an understanding of the cyclic consistency of the combustion process. The results are summarized in Table 6.2. The COV for the ignition delay is quite low at 3.2%. The COVs for the mass fraction burned crank angle duration begins above 11% for the 0-5% MFB and then goes below 5% for the total 0-90% MFB. This indicates that the beginning portion of combustion has larger variances than the end. The percent differences in the maximum and minimum values follow the same trend and go from a value of 59.8% for 0-5% MFB to 27.7% for 0-90% MFB.

Table 6.2: Mean Value, Coefficient of Variance, and Percent Difference Between Maximum and Minimum Values for Combustion Characteristics at 2000 rpm, 1 Bar BMEP

Variable	Mean Value	Coefficient Of Variance	Percent Difference Between Maximum and Minimum Values
Ignition Delay	5.7º	3.2%	19.3%
0-5% MFB Duration	1.2º	11.2%	59.8%
0-10% MFB Duration	1.6º	9.6%	57.8%
0-50% MFB Duration	3.3º	4.9%	30.5%
0-90% MFB Duration	9.8º	4.7%	27.7%

6.2.7 NO Emissions

NO emissions trends at this steady-state condition are a function of a number of factors that fall into one of three categories: injection parameters, the proportion of fresh air and stoichiometric combustion products in the cylinder, and the variation of the first two. A number of these causes are considered, and the trend that most clearly impacts NO emissions is injection pressure. Higher injection pressures produce higher NO emissions, and vice versa. Individual cycles where injection pressures are far above or below the mean produce NO emissions that are also markedly high or low. Charge composition, especially the mole fraction of O_2 before combustion also impacts NO emissions, but its influence is much less pronounced than injection pressure

6.2.8 Particulate Emissions

As with NO emissions, a number of different factors contribute to the amount of particulates formed. Considering all of the engine electronics and in-cylinder charge constituents, the one most likely influencing particulate emissions is the combustion duration. The relationship between these two is shown in Figure 6.10. As the combustion is lengthened, fuel burned near the end of the process does so at much cooler temperatures which reduces particulate oxidation rates and contributes to overall higher particulate formation.

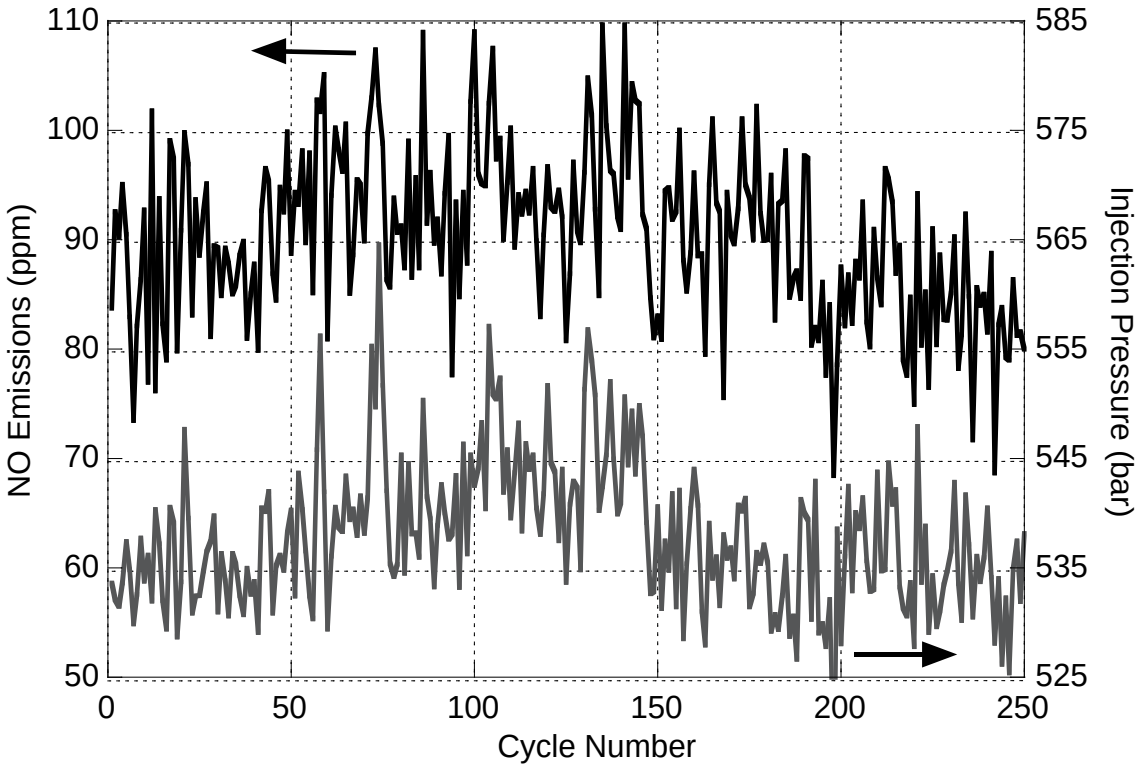

Figure 6.9: NO Emissions and Injection Pressure at 2000 rpm, 1 Bar BMEP

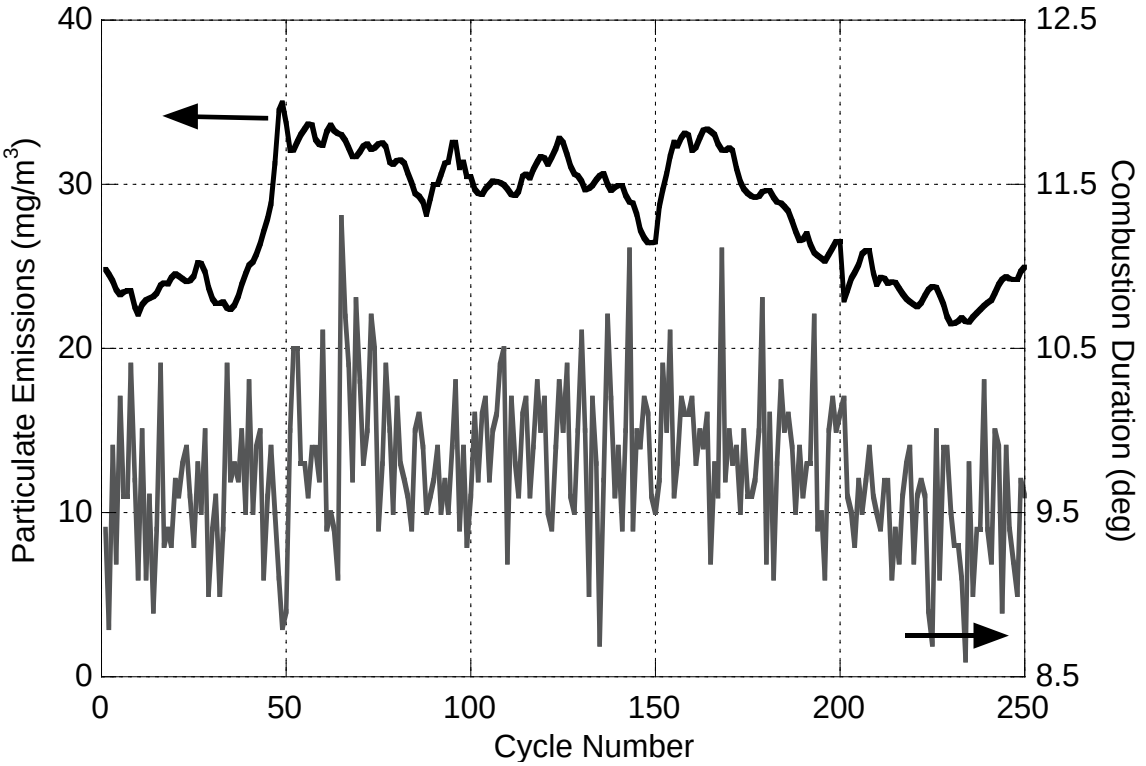

Figure 6.10: Particulate Emissions and Combustion Duration at 2000 rpm, 1 Bar BMEP

6.3 2000 rpm, 9 bar BMEP

The 2000 rpm, 9 bar BMEP condition represents a mid-range load and speed point for this engine. Fuel injection quantities are relatively high, as are boost pressures. For NO_X mitigation, the EGR valve is opened just slightly. To establish the consistency of the engine-controlled electronics, Figure 6.11 presents the PCM demanded fuel injection mass, start of injection, injection pressure, EGR valve position and VGT vane position.

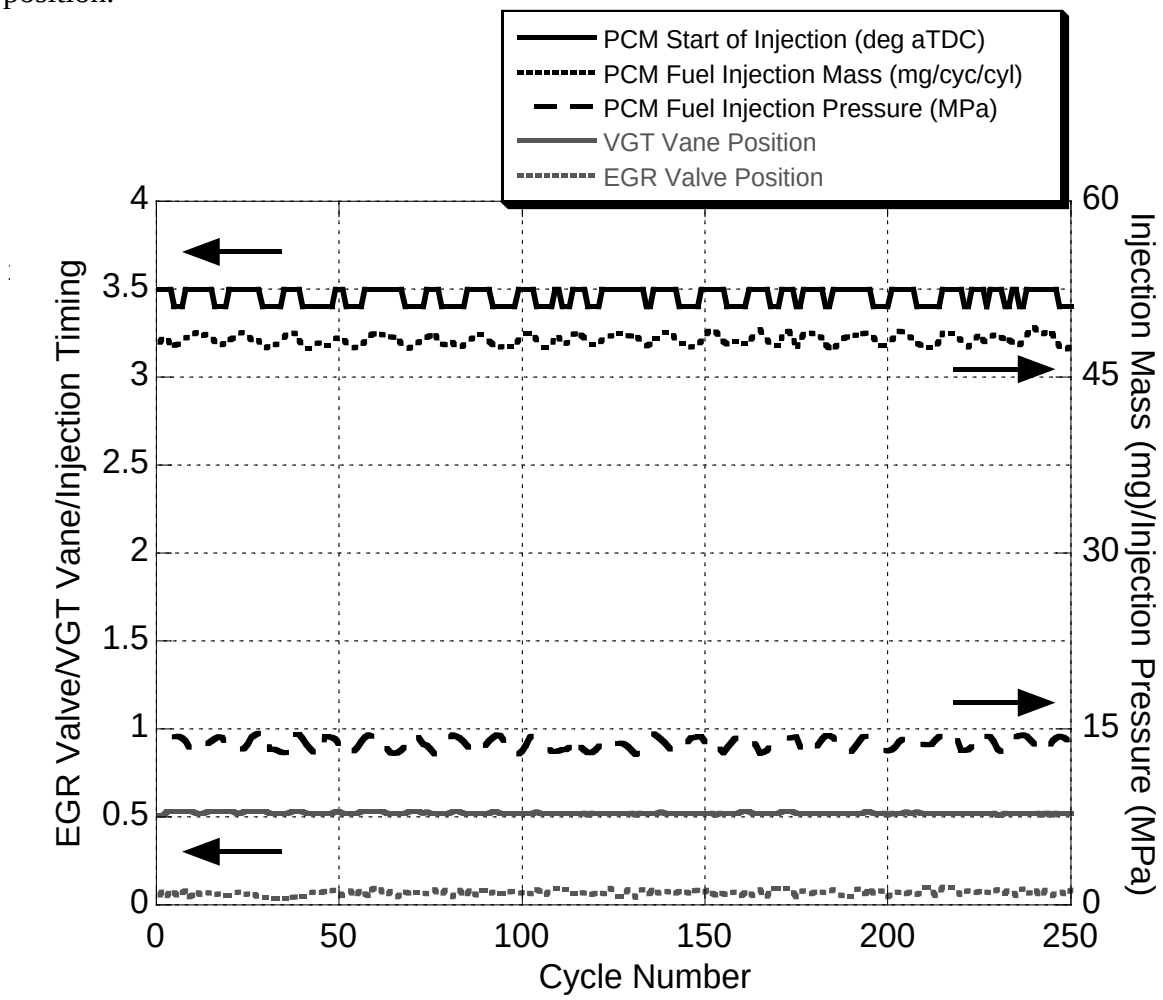

Figure 6.11: PCM-Controlled Start of Injection, Fuel Injection Mass, Fuel Injection Pressure, VGT Vane Position and EGR Valve Position at 2000 rpm, 9 Bar BMEP

Table 6.3: Mean Value, Coefficient of Variance, and Percent Difference Between Maximum and Minimum Values of Engine-Controlled Parameters at 2000 rpm, 9 Bar BMEP

Variable	Mean Value	Coefficient Of Variance	Percent Difference Between Maximum and Minimum Values
Fuel Injection Mass	48.2 mg	0.9%	4.0%
Fuel Injection Timing	3.5º aTDC	1.4%	2.9%
Fuel Injection Pressure	13.7 MPa	3.9%	13.8%
EGR Valve Position	0.07	21.7%	93.6%
VGT Vane Position	0.52	0.9%	3.8%

The quantities shown in Figure 6.11 seem to remain quite constant, but to give a fair comparison of how these terms deviate the coefficient of variance and the percent difference between maximum and minimum values are summarized in Table 6.3. All metrics have a COV below 4% except for the EGR valve position, which is over 20%. The relative spread of the data for the fuel injection mass, injection timing and VGT vane position is very narrow, as the percent difference between the maximum and minimum values is less than 4%. Fuel injection pressure is around 14%, while there is over a 90% difference between the maximum and minimum values of EGR position. Part of this is because the EGR valve is nearly closed, with an average duty position of 7%. Thus any small change on an absolute basis is amplified on a relative basis. The excellent consistency of the demand fuel injection mass, fuel injection timing, VGT vane position and the respectable consistency of the fuel injection pressure indicate that the engine might very well be operating at steady-state, with any variations able to be attributed to flow dynamics or EGR valve position.

6.3.1 Fuel Injection Mass

Both the demanded fuel mass from the PCM and the measured fuel injection mass at this operating condition are shown in Figure 6.12. Absolute differences in these two lines are irrelevant, but deviations in the relative shapes demonstrate that injector behavior does not necessarily follow what is demanded of it. Every fifty cycles or so, the injector seems to experience some higher-order level of resonance. Any impact that this has on combustion or emissions is discussed below. It should be noted, however, that the percent difference between the maximum and minimum values for the injected fuel mass is less than 8%, and narrow window used in Figure 6.12 might be suggesting deviant behavior when none is really present.

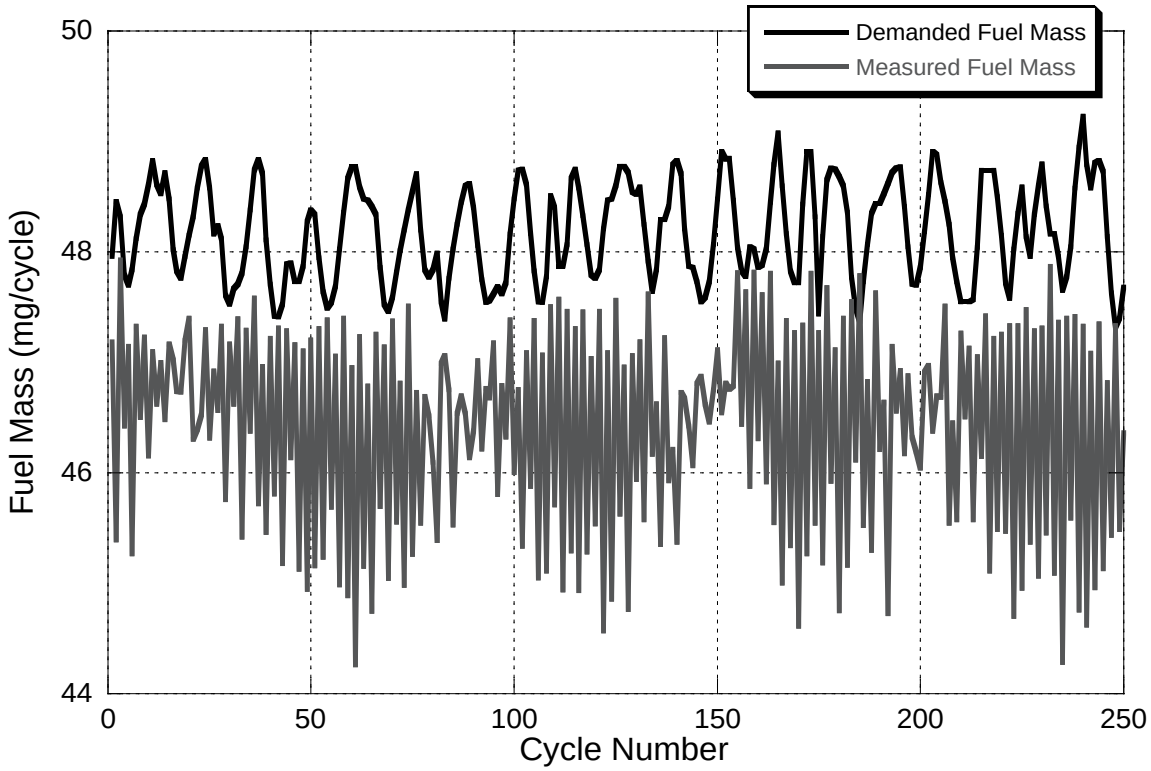

Figure 6.12: PCM-Demanded Fuel Injection Mass and Measured Fuel Injection Mass at 2000 rpm, 9 Bar BMEP

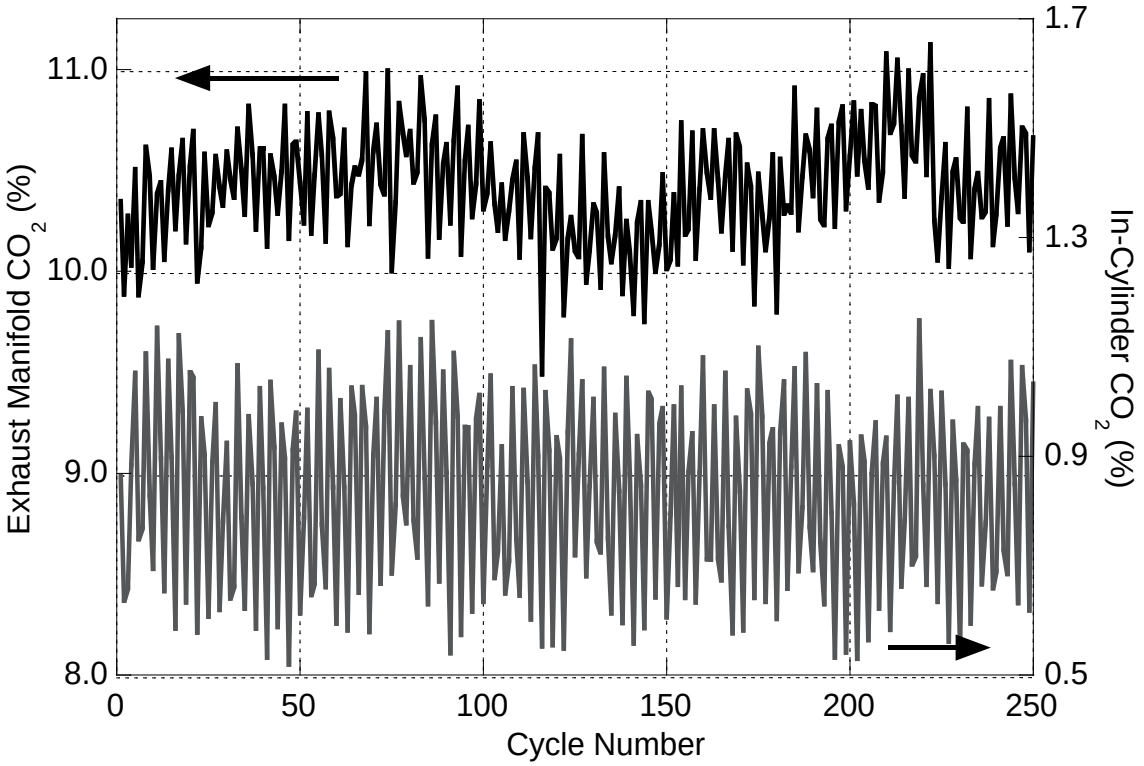

Figure 6.13: Exhaust Manifold and In-Cylinder CO_2 Concentrations at 2000 rpm, 9 Bar BMEP

6.3.2 CO_2 Measurements

In-cylinder and exhaust manifold CO_2 concentration is shown in Figure 6.13. COV for the exhaust manifold CO_2 is 2.7%, indicating a reasonable level of consistency in combustion cycles. COV of the in-cylinder CO_2, however, is 20.8% and demonstrates a large amount of cyclic variability. These trends have a marked impact on cycle-resolved air and stoichiometric combustion product mass, which are shown in Figure 6.14. The behavior of air mass is essentially the inverse of the exhaust manifold CO_2 curve in Figure 6.13, while the stoichiometric combustion product mass very closely resembles the in-cylinder CO_2 trace in Figure 6.13.

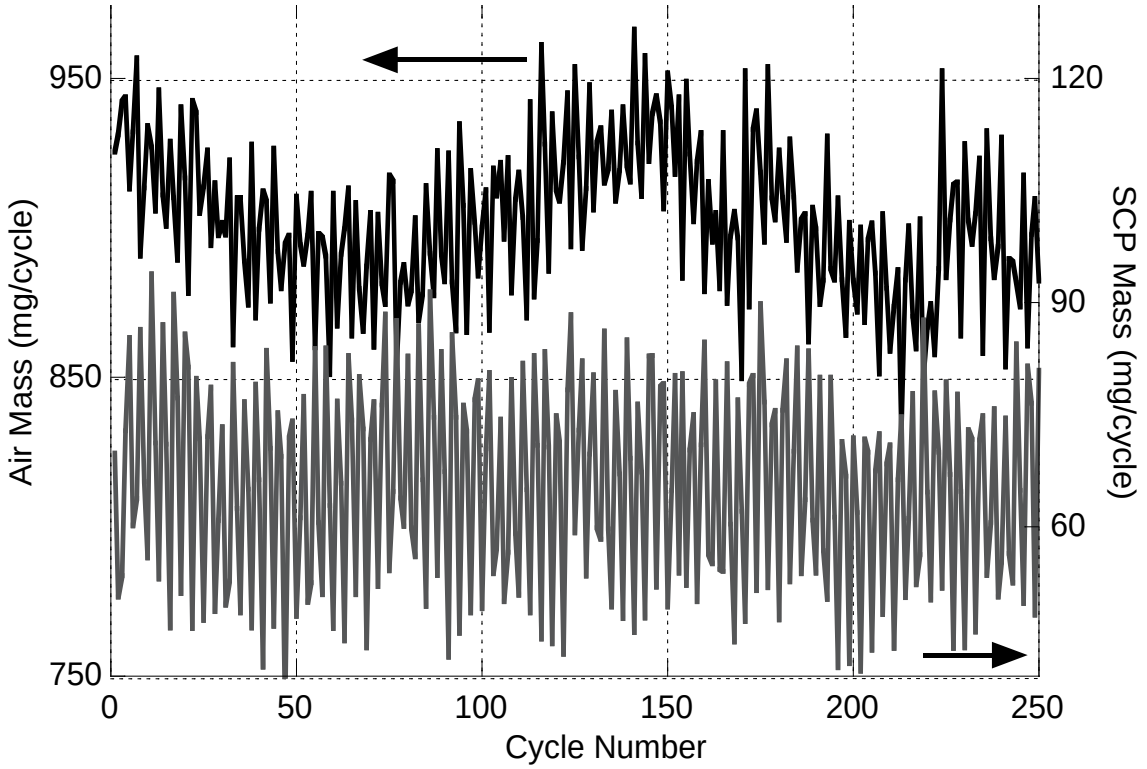

Figure 6.14: Air Mass and Stoichiometric Combustion Product Mass at 2000 rpm, 9 Bar BMEP

6.3.3 Stoichiometric Combustion Product Mass

As mentioned in the previous section, the amount of stoichiometric combustion products in the cylinder is a function of EGR valve position, manifold pressure ratio during the valve overlap period, and the degree of mixing of fresh air and exhaust gas in the intake manifold. The relationship between manifold pressure ratio and stoichiometric combustion product is inconclusive. EGR valve position and stoichiometric combustion product mass is shown in Figure 6.15. This graph demonstrates that while these two values change at about the same frequency, the stoichiometric combustion product mass is not being driven by EGR valve position. The EGR valve is sometimes more closed with high levels of stoichiometric combustion product mass and sometimes more open. Therefore poor mixing in the intake manifold is most likely the cause of the large oscillations in the stoichiometric combustion product mass.

6.3.4 Air Mass

Air mass behavior is a function of boost levels, manifold pressure ratios during the valve overlap process, and intake manifold dynamics. Investigation of boost pressures and manifold pressure ratios are inconclusive and do not track with air mass. Thus variation in trapped air mass is most likely due to poor mixing in the intake manifold and flow dynamics.

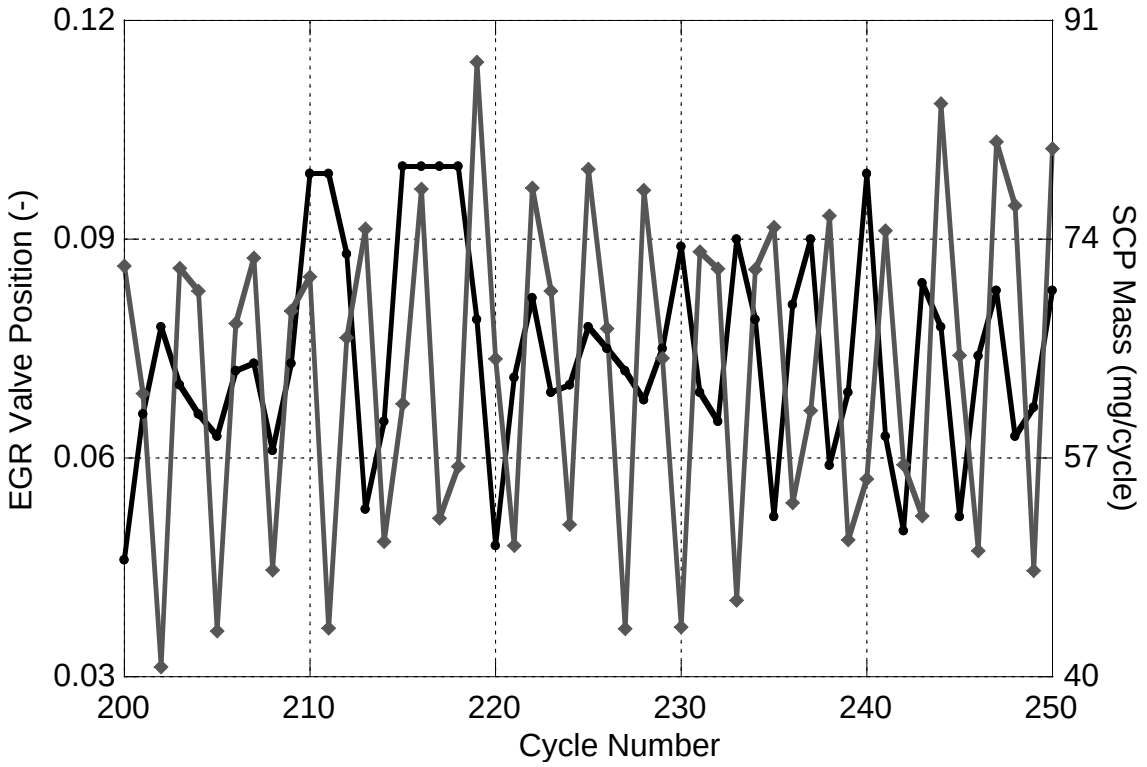

Figure 6.15: EGR Valve Position and Stoichiometric Combustion Product Mass at 2000 rpm, 1 Bar BMEP

6.3.5 Air/Fuel Ratio

Air/fuel ratios at this condition are shown in Figure 6.16; the shape of this curve is governed by the air mass flow, as they follow the same trend. COV for the air/fuel ratio is 2.8%, indicating relative consistency throughout the test.

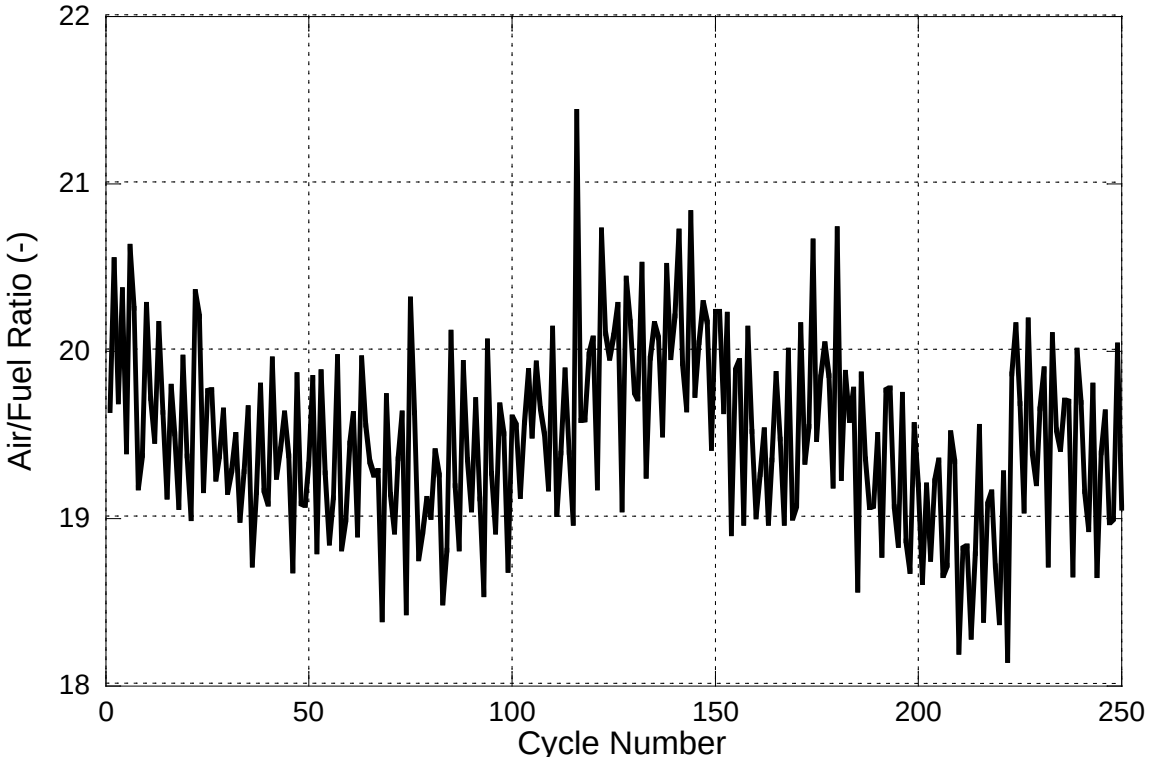

Figure 6.16: Air/Fuel Ratio at 2000 rpm, 9 Bar BMEP

6.3.6 Combustion Analysis

Rate of heat release analysis is conducted on the individual cycles at the 2000 rpm, 9 bar BMEP operating condition to assess the consistency of the combustion process. The results are summarized in Table 6.4. The ignition delay at this condition is quite consistent, with a COV of 2.6% and less than 15% separating the overall maximum and minimum values. MFB crank angle durations also demonstrate little variability, as the COV for every span is less than 4%, and these values tend to get lower for the 0-50% and 0-90% durations. The same trend is observed when considering the percent differences between the maximum and minimum values. As the MFB duration gets longer, the difference between the extreme values gets lower.

Table 6.4: Mean Value, Coefficient of Variance, and Percent Difference Between Maximum and Minimum Values for Combustion Characteristics at 2000 rpm, 9 Bar BMEP

Variable	Mean Value	Coefficient Of Variance	Percent Difference Between Maximum and Minimum Values
Ignition Delay	4.4º	2.6%	14.8%
0-5% MFB Duration	1.7º	3.9%	17.3%
0-10% MFB Duration	2.5º	3.3%	20.3%
0-50% MFB Duration	10.2º	1.9%	10.8%
0-90% MFB Duration	21.8º	2.1%	11.0%

6.3.7 NO Emissions

NO emissions during this steady-state test are typically governed by: injection parameters, charge composition, and the variance of these two. When considering NO production as a whole, as shown in Figure 6.17, two characteristics stand out. First is that NO emissions oscillate at a high frequency and vary by a significant amount. The smallest NO value is 171 ppm and the largest is 346 ppm; a percentage difference of 67.9%. Second is that there is no higher-order trend with NO emissions. The cycle-resolved values move up and down frequently but the mean of the curve stays very constant.

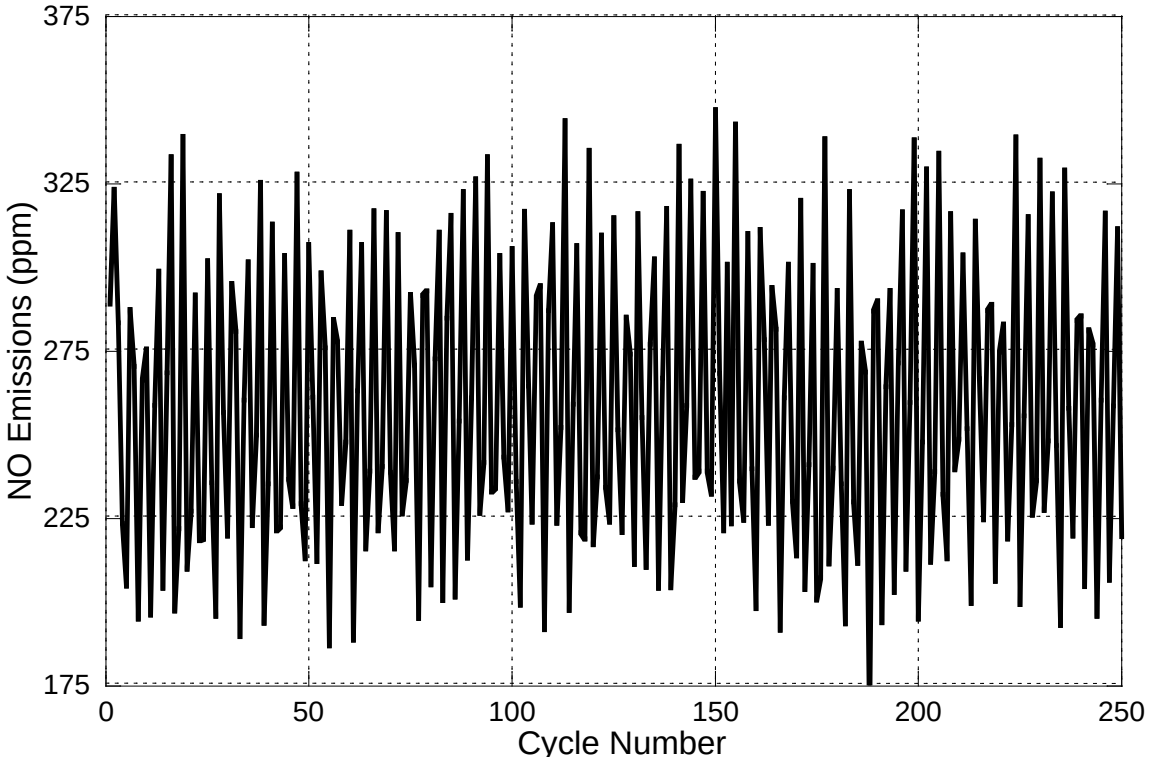

Figure 6.17: NO Emissions at 2000 rpm, 9 Bar BMEP

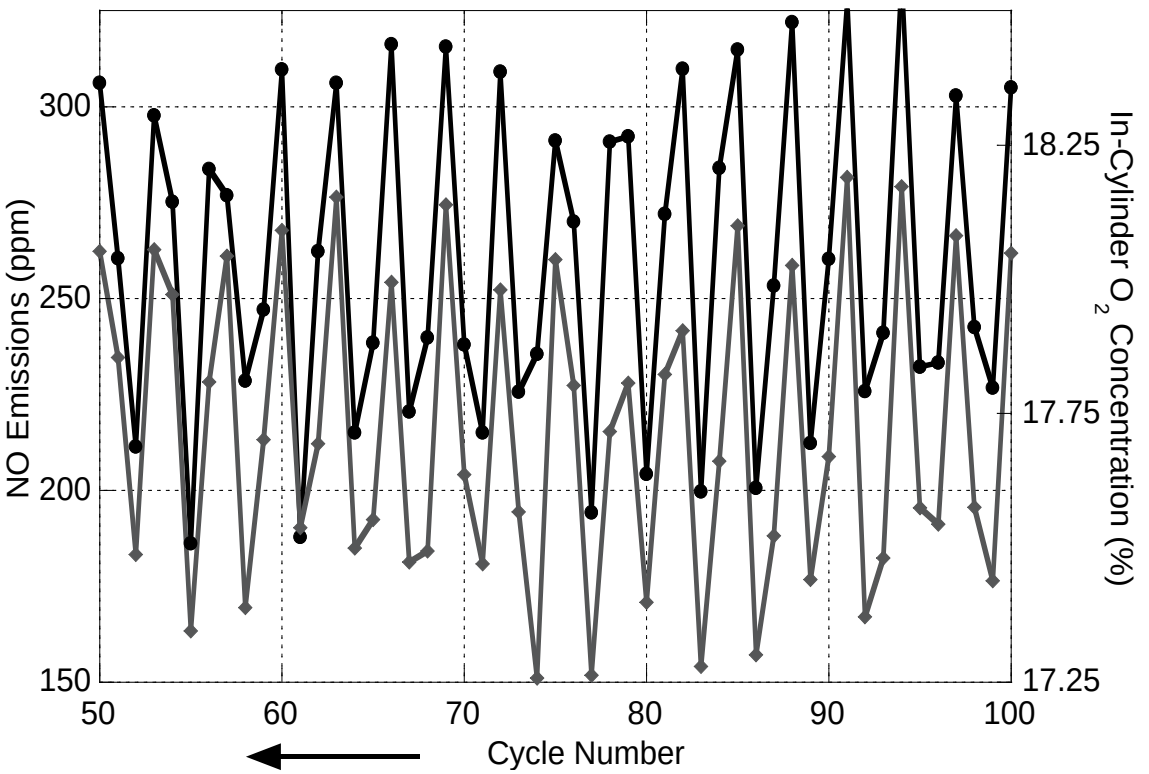

Figure 6.18: NO Emissions and In-Cylinder Pre-Combustion O_2 Concentration at 2000 rpm, 9 Bar BMEP

Examination of the NO data reveals that it is very closely related to the amount of oxygen in the cylinder prior to combustion. Pre-combustion O_2 is the most accurate method of determining the degree to which fresh air has been diluted by EGR and residual gases and also accounts for the individual gas components in the EGR and residual. Figure 6.18 reveals that for combustion cycles in which higher levels of O_2 are present (less EGR and residual) higher NO emissions are formed. Conversely, for those cycles in which O_2 levels are lower (more EGR and residual) lower NO emissions are produced. This trend is no surprise, but the frequency at which in-cylinder O_2 concentration changes and the impact that it has on NO emissions is significant.

6.3.8 Particulate Emissions

Particulate emissions data gathered during this test are consistently very low. The signals obtained were so little, in fact, that the readings were below the noise level of the DMS 500. Therefore the only conclusion that can be made from the data is that the particulate produced at this condition is consistently lower than what the instrument can accurately measure.

6.4 Steady-State Measurement Summary

Steady-state engine operating conditions at 2000 rpm, 1 and 9 bar BMEP are investigated using cycle-resolved measurements to determine pre-combustion in-cylinder gas composition and the emissions that form from these cycles. The degree to which the engine operates in a consistent manner is evaluated by calculating the COV for each engine-controlled combustion input, and the maximum deviations in these values relative to their mean are quantified by determining the percent difference between their largest and smallest measured values. Engine operation is found to be more consistent at the 9

bar BMEP condition, as COV's for injection parameters and VGT vane position are much more steady. EGR valve changes, however, are relatively larger at this condition.

The consistency of the injection parameters and VGT vane position at the 9 bar BMEP condition result in injected fuel masses and trapped air masses that have a much smaller deviance from their mean than those same quantities at the 1 bar BMEP condition. The COV for fuel and air mass at 9 bar BMEP is 2.0% and 2.9%, respectively, while at the 1 bar BMEP condition these values are 6.4% and 5.1%. The COV of stoichiometric combustion product mass at the 9 bar BMEP condition is nearly 2.5 times higher than the COV at the 1 bar BMEP condition. This difference is attributed to mixing inconsistencies in the intake manifold and EGR valve position fluctuation.

The variation in the crank angle duration of mass fraction burned points was much lower at 9 bar BMEP than at the 1 bar BMEP condition. COV levels and the percent difference between maximum and minimum values at 9 bar BMEP are roughly half of those observed at 1 bar BMEP. This demonstrates that the combustion processes themselves are more repeatable when the inputs to combustion are more consistent.

Significant variations in NO emissions are observed on a cycle-resolved basis. At the 1 bar BMEP condition, this is attributed to fuel injection parameters. Fueling rates are very low at this point and small absolute deviations in fuel injection pressures cause large relative changes in combustion which directly impact NO formation. At the 9 bar BMEP condition, fuel injection is more consistent and gas composition changes more strongly influence NO production. In-cylinder pre-combustion oxygen concentration is found to be the dominating determinant of NO formation, as a change of O_2 concentration by 0.5% can cut NO emissions by half. Such changes are observed frequently and occur in the span of consecutive cycles.

Particulate emissions results are less conclusive, as the relatively low levels of emissions make it difficult to reasonably conclude that observed trends are physical or noise in the device. This situation is encountered at the 9 bar BMEP condition. At 1 bar

BMEP, particulate production levels are higher, and variations here are most likely due to combustion variations that are caused by in-cylinder mass deviations that lead to differing combustion characteristics, such as combustion duration.

The technique presented in this work gives unique insight into engine behavior during so-called steady-state conditions. Traditional test cell instrumentation is unable to capture the cycle-resolved differences that occur in fuel mass, air mass, and stoichiometric combustion product mass or the emissions that are formed during these combustion processes. Manifold flow dynamics and poor fresh air and EGR mixing are found to be the primary culprits to these variations. NO emissions are observed to be especially sensitive to the in-cylinder fluctuations of charge composition on a cyclic level. The experimental technique presented by this research makes this behavior measureable and facilitates its understanding.

CHAPTER 7

CYCLE-RESOLVED MEASUREMENTS DURING CONSTANT-SPEED LOAD SWEEPS

The experimental technique presented in this study is used to analyze engine behavior during constant speed load sweeps. These sweeps are transient in nature, as the inputs to the engine (engine command) and outputs from the engine (torque and emissions) are changing with time. By keeping speed constant, however, these transients are more well-controlled and simplified because time scales are fixed. This chapter is broken into three sections: a description of the experimental procedure, a discussion of the results, and presentation of the summary.

7.1 Constant-Speed Load Sweep Experimental Procedure

During this series of tests, engine speed is held constant at 2000 rpm while engine command changes so that the engine experiences a load increase from 1 bar to 9 bar BMEP. The amount of time over which engine command changes is also swept, and five different times are tested: 0 seconds (instantaneous), 1, 2, 3, and 5 seconds. Engine command for these conditions changes from a nominal value of 17% to 40%. The engine command input for this series of tests is shown in Figure 7.1 and reveals the only variation from case to case is the amount of time it takes the engine command to change from its minimum to maximum value. Analysis of the results considered data from all

five cases, but only results from the 0, 2, and 5 second cases are examined in detail to simplify graphs and streamline analysis.

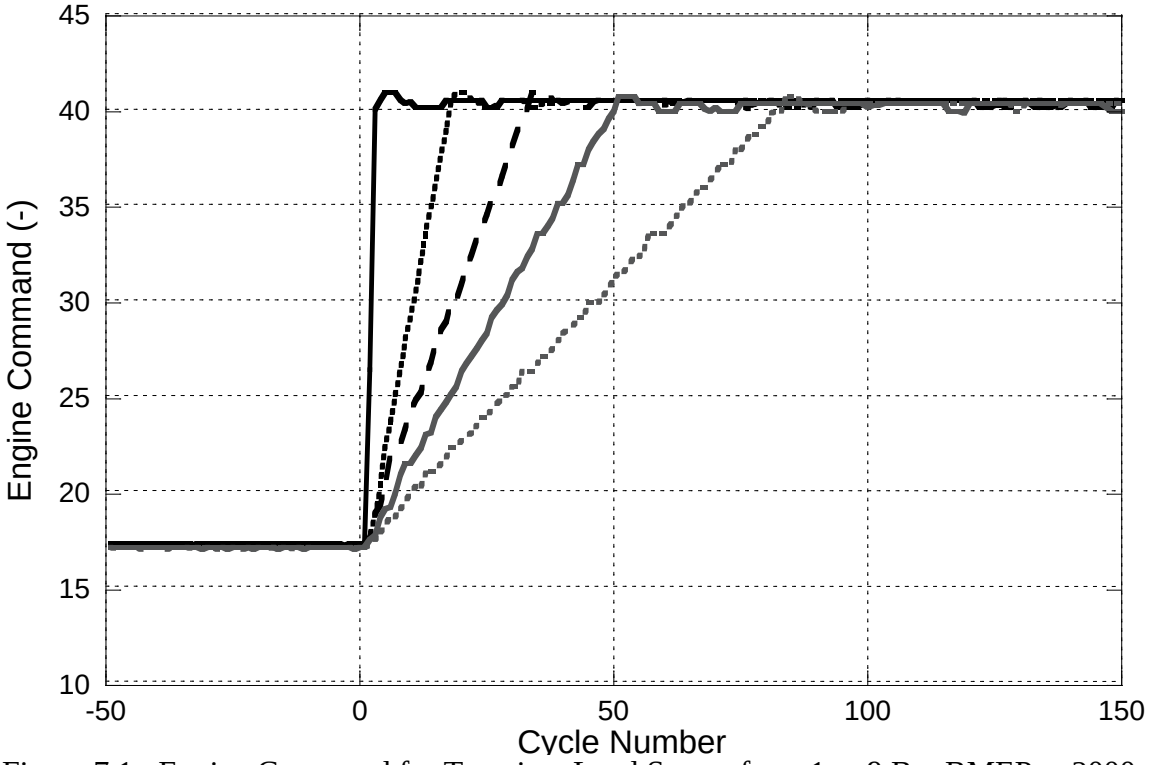

Figure 7.1: Engine Command for Transient Load Sweep from 1 to 9 Bar BMEP at 2000 rpm

7.2 Constant-Speed Load Sweep Results

7.2.1 Torque Response

Engine torque for the 0, 2, and 5 second engine command change is shown in Figure 7.2. Response for the engine in the 2 and 5 second cases is quite linear and torque is generated nearly as quickly as it is demanded. For the 0 second case, however, there is a noticeable kink in the torque response curve. This is not a limitation of the engine's capability to produce torque; rather, it is the result of a fueling rate limiter imposed by the PCM.

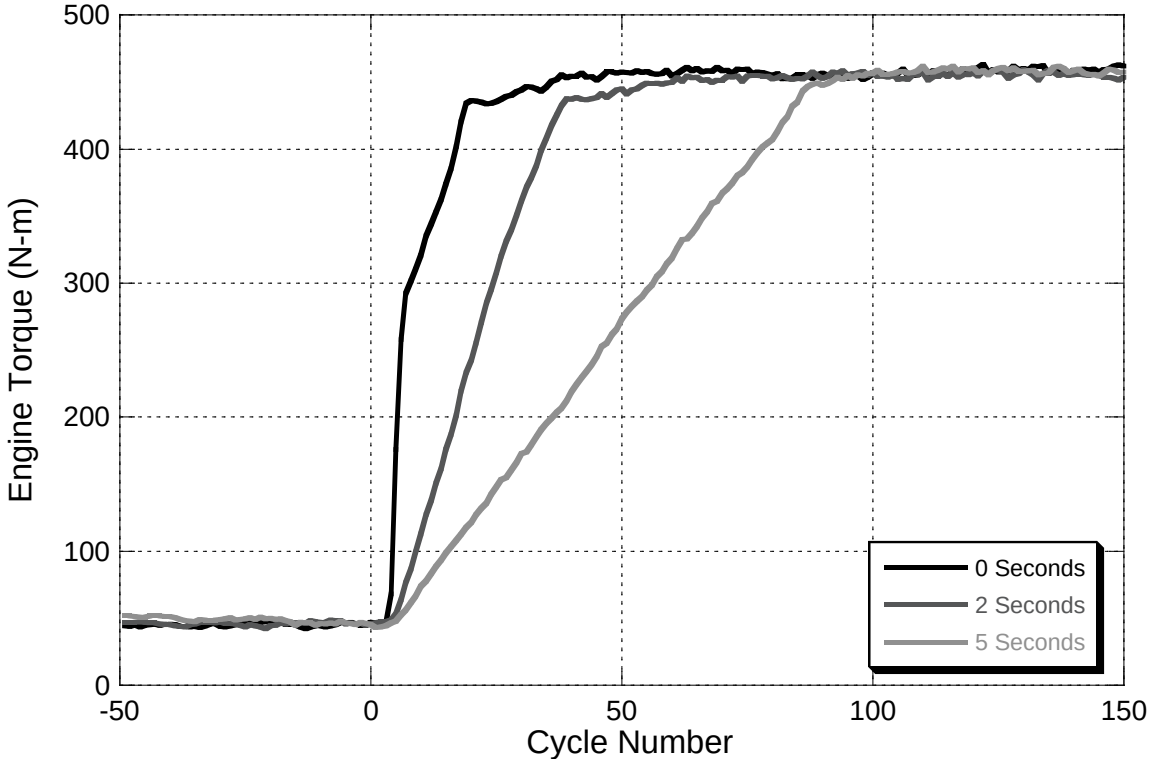

Figure 7.2: Engine Torque during Transient Load Sweep from 1 to 9 bar BMEP at 2000 rpm

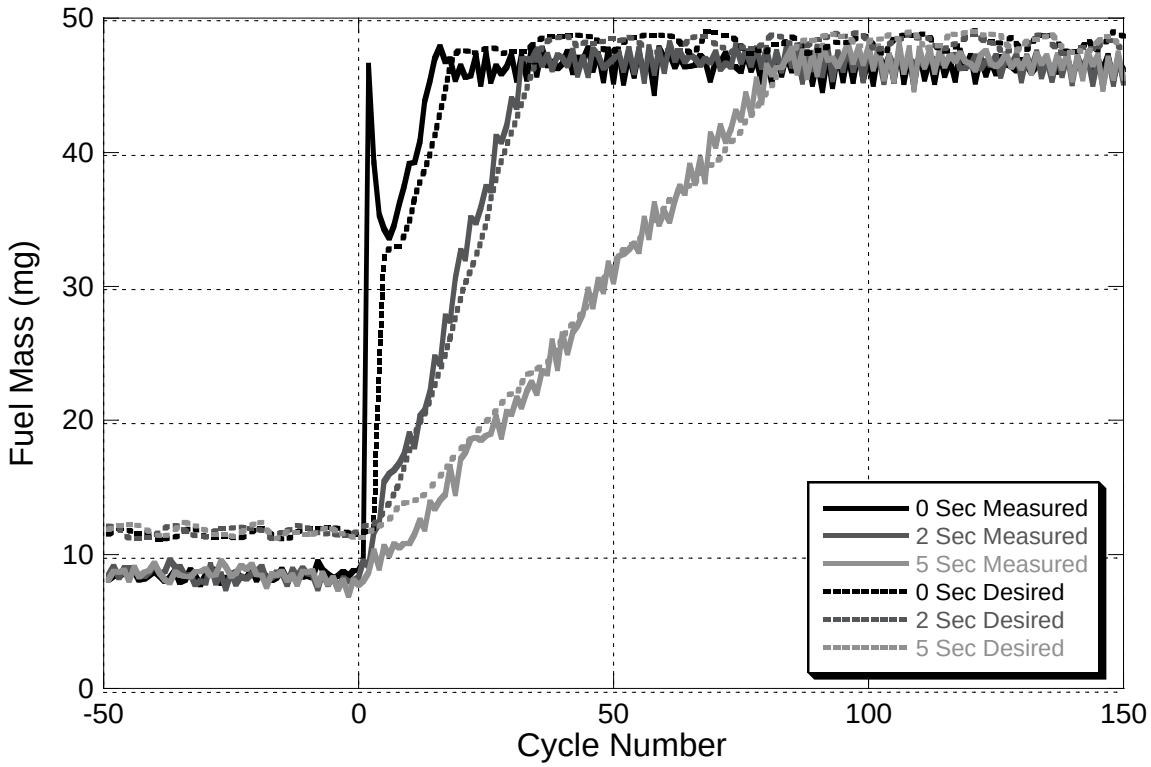

Figure 7.3: Measured and Desired Fuel Injection Mass during Transient Load Sweep from 1 to 9 Bar BMEP at 2000 rpm

7.2.2 Measured and Desired Fuel Injection Rate

The presence of the fueling rate limiter is evident when considering Figure 7.3, which demonstrates the desired and measured fuel injection masses during the load sweep. The 2 and 5 second cases show a very linear transition from the lower fueling rate to the higher one, but the 0 second case displays a marked flattening of the curve halfway through the load increase process.

Another noticeable aspect of Figure 7.3 is the measured overshoot of fuel mass in the 0 second load sweep condition. Closer examination of the data reveal that this overshoot involves a step change in fuel rate from 9.7 mg to 46.8 mg in consecutive cycles and then a gradual reduction in fueling rate for three cycles to match the desired fuel injection mass. The overshoot occurs because the injection duration makes a step change from 5.6 crank angle degrees to 16.0 crank angle degrees and the maximum fuel injection pressures increase from 546 bar to 1284 bar. In the ensuing cycles over which the fuel injection mass is decreased, injection pressures remain relatively constant, while injection duration goes down.

7.2.3 In-Cylinder CO_2 Measurement

In-cylinder CO_2 concentration is dependent upon the quantity of EGR and internal residual trapped in the cylinder, as well as the CO_2 concentrations in those gases. Figure 7.4 displays the in-cylinder CO_2 values gathered during this study and demonstrates that the three cases behaved very differently. The causes of these differences are discussed in Section 7.2.5, so only shapes of the curves are examined here. In all cases, in-cylinder CO_2 values before the transient are about 0.7% and after the transient average around 0.8%. During the transient, however, very different behavior is observed.

For the 0 Second case, in-cylinder CO_2 first drops immediately down to 0.25% before moving back up to 0.5% by cycle 25. From there, the value gradually moves upward to the steady-state value and achieves that value of 0.8% by about cycle 75.

At the onset of the transient in the 2 Second case, in-cylinder CO_2 moves up to 0.95% during the first 10 cycles and then for the next 10 cycles goes down to 0.55%. After cycle 25, the in-cylinder CO_2 begins to move towards the steady-state value of 0.8% and reaches this level around cycle 75, the same time as the 0 Second case.

The 5 Second condition moves gradually upward at the beginning of the transient to a value of around 1.3% by cycle 30. It stays above 1% until about cycle 75, at which time it gradually transitions to the steady-state value of 0.8% by cycle 100. Understanding the behavior of in-cylinder CO_2 is necessary when examining the measurements of exhaust manifold CO_2, which is discussed in the following section.

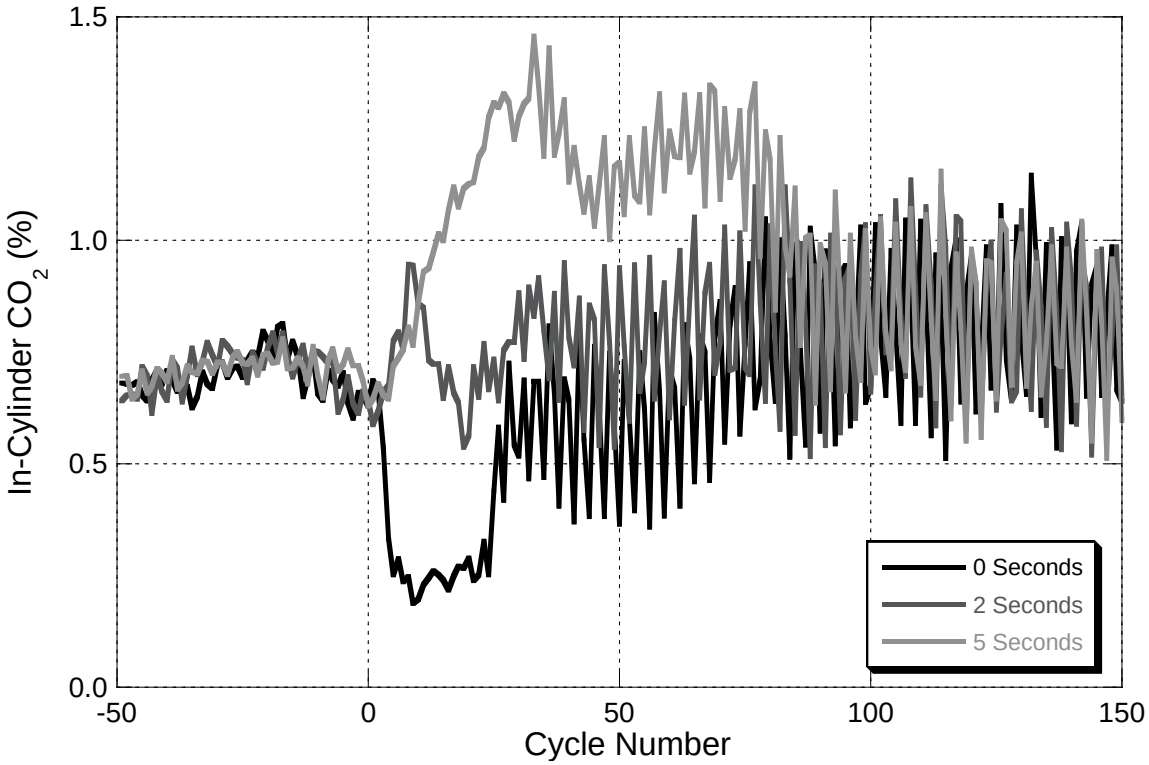

Figure 7.4: In-Cylinder CO_2 Measurements during Transient Load Sweep from 1 to 9 Bar BMEP at 2000 rpm

7.2.4 Exhaust Manifold CO_2 Measurement

Carbon dioxide in the exhaust manifold has two origins: the CO2 that is in the cylinder prior to combustion, and the CO_2 generated from the previous cycle's combustion. Therefore when interpreting exhaust manifold CO_2 data, both the amount of fuel combusted and the pre-combustion CO_2 level must be considered. The CO_2 measured during the transient load sweeps is shown in Figure 7.5.

0 Second Exhaust CO_2 Concentration

The shapes of these curves are very similar to the measured fuel mass curves in Figure 7.3, demonstrating the influence of the quantity of fuel combusted on CO_2 formation. The 0 Second case experiences a very rapid spike in CO_2 concentration immediately after the onset of the transient from the overshoot of fuel injection. As the fuel injection mass falls back down to the demand value, so does the exhaust CO_2 concentration. Another peak is present when the engine reaches its full fueling rate at cycle 11. CO_2 concentrations fall again after cycle 11 because at this state, the contribution of CO_2 from pre-combustion is small (see Figure 7.4) and the turbocharger boost pressure increasing rapidly, as shown in Figure 7.6, which results in lower CO_2 concentrations. This trend continues until around cycle 25, at which time in-cylinder CO_2 concentrations begin rising and add to the CO_2 generated from combustion. CO_2 concentrations continue to rise to their steady-state value of 10.5%, which is reached around cycle 125.

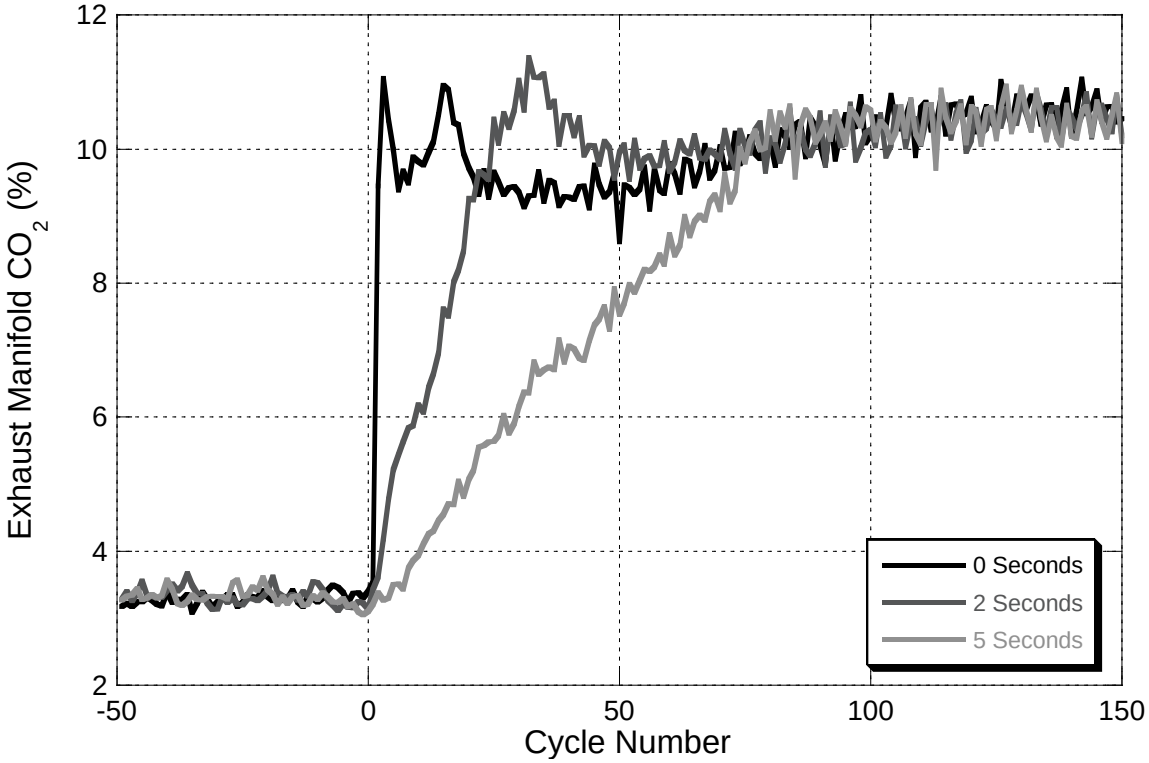

Figure 7.5: Exhaust Manifold CO_2 Measurement during Transient Load Sweep from 1 to 9 Bar BMEP at 2000 rpm

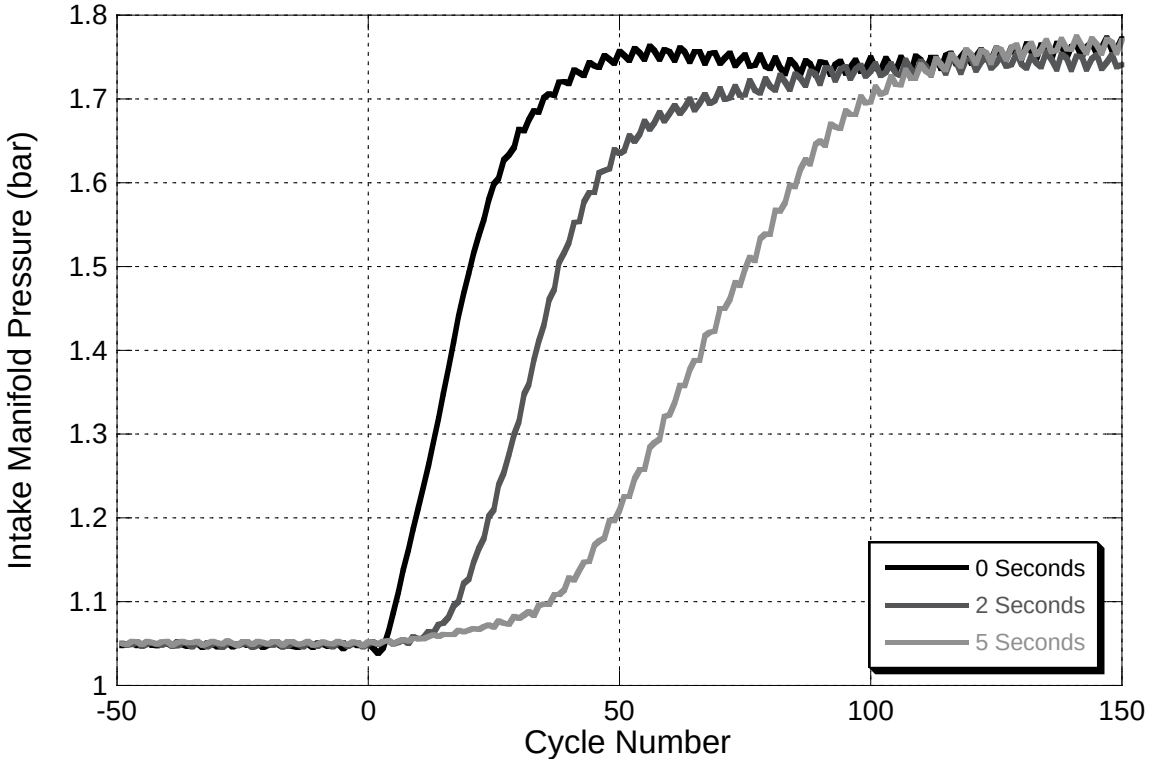

Figure 7.6: Intake Manifold Pressure during Transient Load Sweep from 1 to 9 Bar BMEP at 2000 rpm

2 Second Exhaust CO_2 Concentration

The 2 Second case moves upward gradually from its original steady-state condition of around 3.4% and the trend follows the fuel mass injection until it reaches a peak around cycle 32. At this point, fuel injection mass has reached a maximum and, as in the 0 Second case, the turbocharger is not yet providing full boost, which causes CO_2 concentrations to be above their steady-state value. During cycles 32-50, the turbo catches up and provides more air to the cylinder, causing CO_2 concentrations to fall below 10%. At about the same time, in-cylinder CO_2 concentrations are rising and after cycle 50, contribute to overall exhaust CO_2 readings such that the values increase to their final steady state levels of 10.5%.

5 Second Exhaust CO_2 Concentration

Unlike the other conditions, the CO_2 concentrations during the 5 Second sweep transition gradually throughout the transient process. Boost levels track quite well with the fuel injection quantity, resulting in CO_2 measurements that do not overshoot or undershoot the final steady state value. Additionally, the effect of in-cylinder pre-combustion CO_2 is ever present, eliminating the increase in exhaust CO_2 concentration that occurs in the other two cases after cycle 50.

7.2.5 Stoichiometric Combustion Product Mass

The presence of stoichiometric combustion product gases in the cylinder is quantified by the concentration of CO_2 in-cylinder prior to combustion and originates from either external EGR, internal residual, or a combination of the two. Strongly influencing the quantity of internal residual is the ratio of the exhaust manifold pressure to the intake manifold pressure during the valve overlap period. During the crank angles near exhaust TDC, both intake and exhaust valves are open. If higher pressures are in the

exhaust manifold, gases will backflow from the exhaust manifold into the cylinder and intake manifold. When the exhaust valves close, the gases that have backflowed are trapped in the cylinder. External EGR is facilitated by the opening of the EGR valve and the cycle-averaged exhaust manifold-to-intake manifold pressure ratio, which provides the pressure differential to flow EGR.

The mass of stoichiometric combustion products trapped in the cylinder for all three cases is shown in Figure 7.7. Since each case behaves differently, each one is discussed separately.

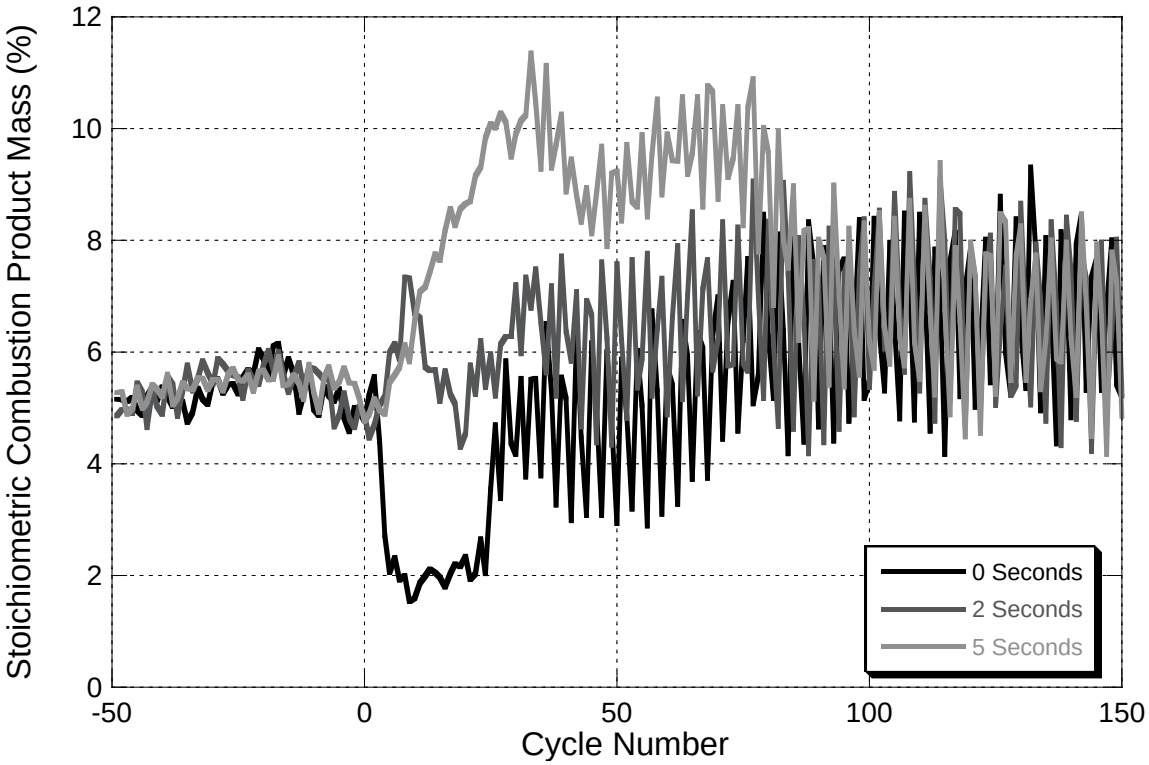

Figure 7.7: Percentage of Stoichiometric Combustion Product Mass during Transient Load Sweep from 1 to 9 Bar BMEP at 2000 rpm

0 Second Stoichiometric Combustion Product Mass

This condition is denoted by the black line in Figure 7.7. Prior to the load sweep, the quantity of stoichiometric combustion product in the cylinder before combustion is

roughly 5% of the trapped cylinder mass. When engine command increases instantaneously, the EGR valve begins to close immediately, and takes about 10 cycles (or 0.6 seconds) to close. This behavior, along with the EGR position for the other two cases, is demonstrated in Figure 7.8. Closing of the EGR valve causes stoichiometric combustion product mass to fall immediately, and as quickly as the valve is closed, the stoichiometric combustion product mass reaches a minimum. This value does not go to zero, however, due to the presence of internal residual. Although the manifold pressure ratio during the valve overlap period is very high at this condition, as shown in Figure 7.9, the stoichiometric combustion product mass remains low.

Once the engine begins to stabilize its operation around cycle 25, the EGR valve begins to open gradually until it reaches its steady-state condition at about cycle 75. The stoichiometric combustion product mass increases in value as well to its steady-state condition, but its value oscillates cyclically to values ±50% of the mean. The average value of the stoichiometric combustion product mass at the final steady state condition is about 6.5% of the total trapped mass.

2 Second Stoichiometric Combustion Product Mass

The stoichiometric combustion product mass for the 2 Second case is the medium gray line in Figure 7.7. When this transient begins, the engine conditions are practically identical to the conditions in the 0 Second load sweep. But when the load is increased, the EGR valve remains open and even increases its opening for 8 cycles. During this period, the driving potential of EGR increases rapidly, as exhaust manifold pressures are rising much more quickly than intake manifold pressures. This trend is observable in Figure 7.10. Exhaust backpressure is also increasing the amount of internal residual and when combined with the EGR behavior, stoichiometric combustion product mass increases by nearly 50% on an absolute basis over the first 8 cycles.

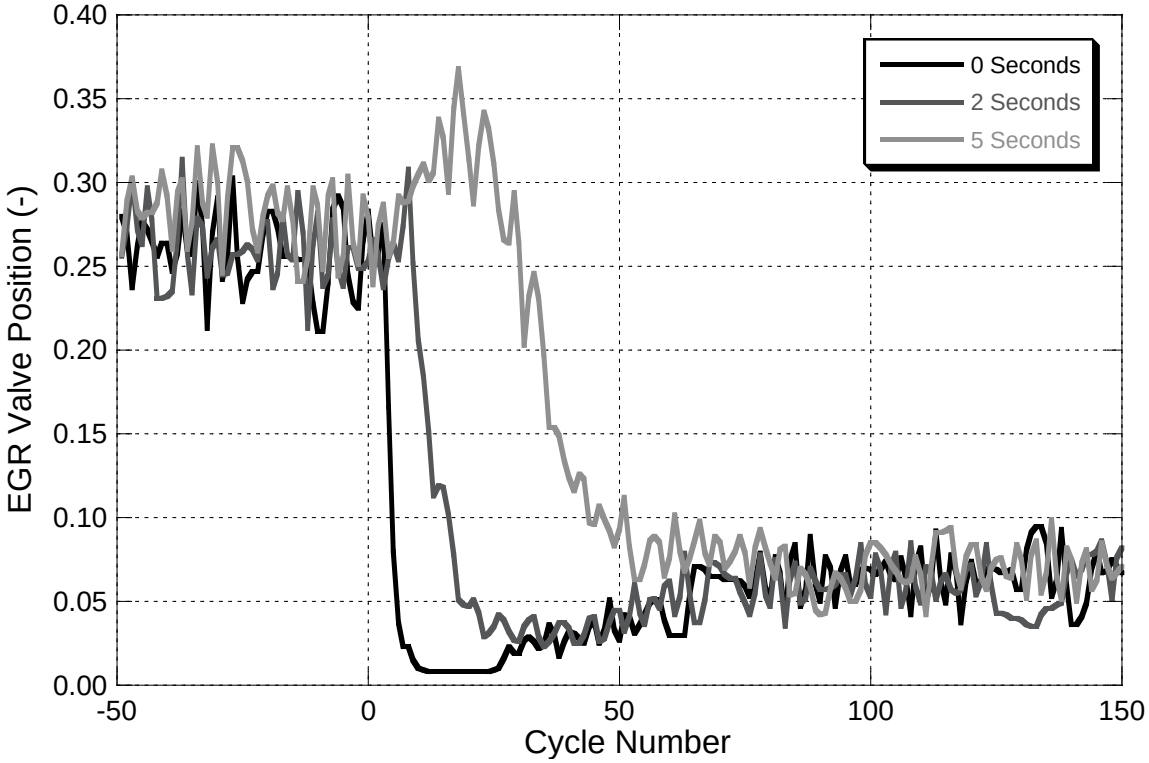

Figure 7.8: EGR Valve Position during Transient Load Sweep from 1 to 9 Bar BMEP at 2000 rpm

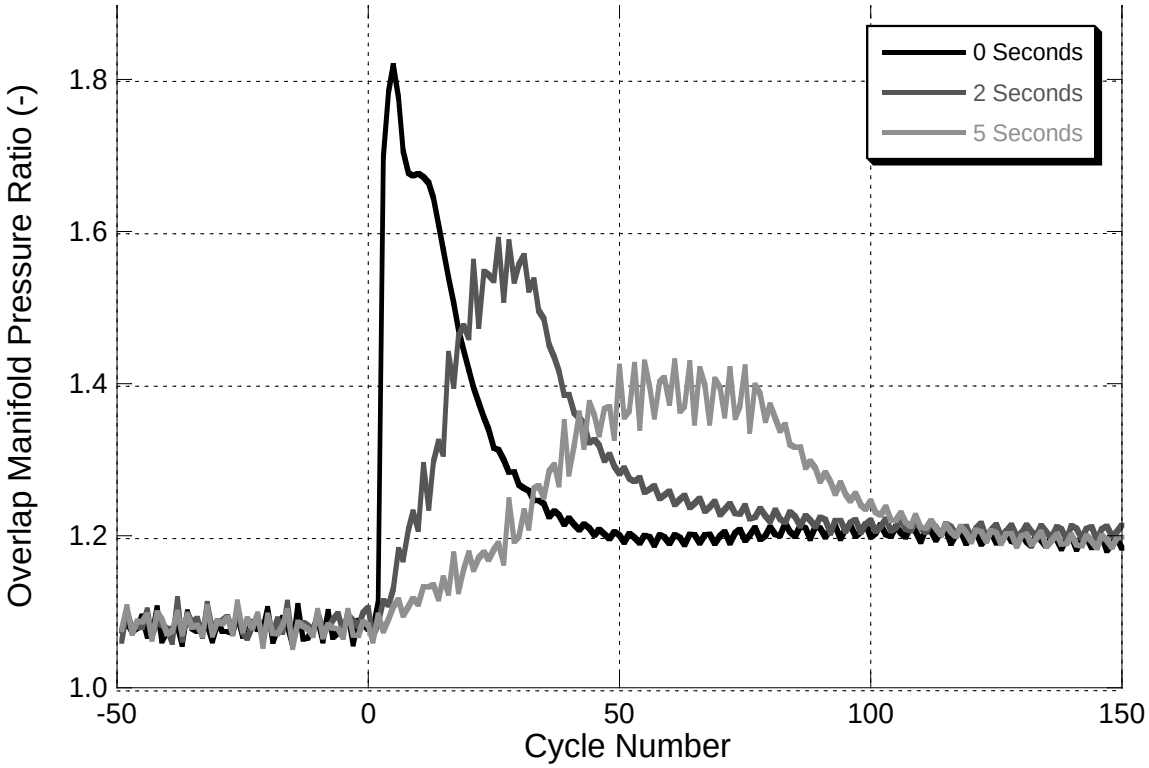

Figure 7.9: Manifold Pressure Ratio throughout the Valve Overlap Period during Transient Load Sweep from 1 to 9 Bar BMEP at 2000 rpm

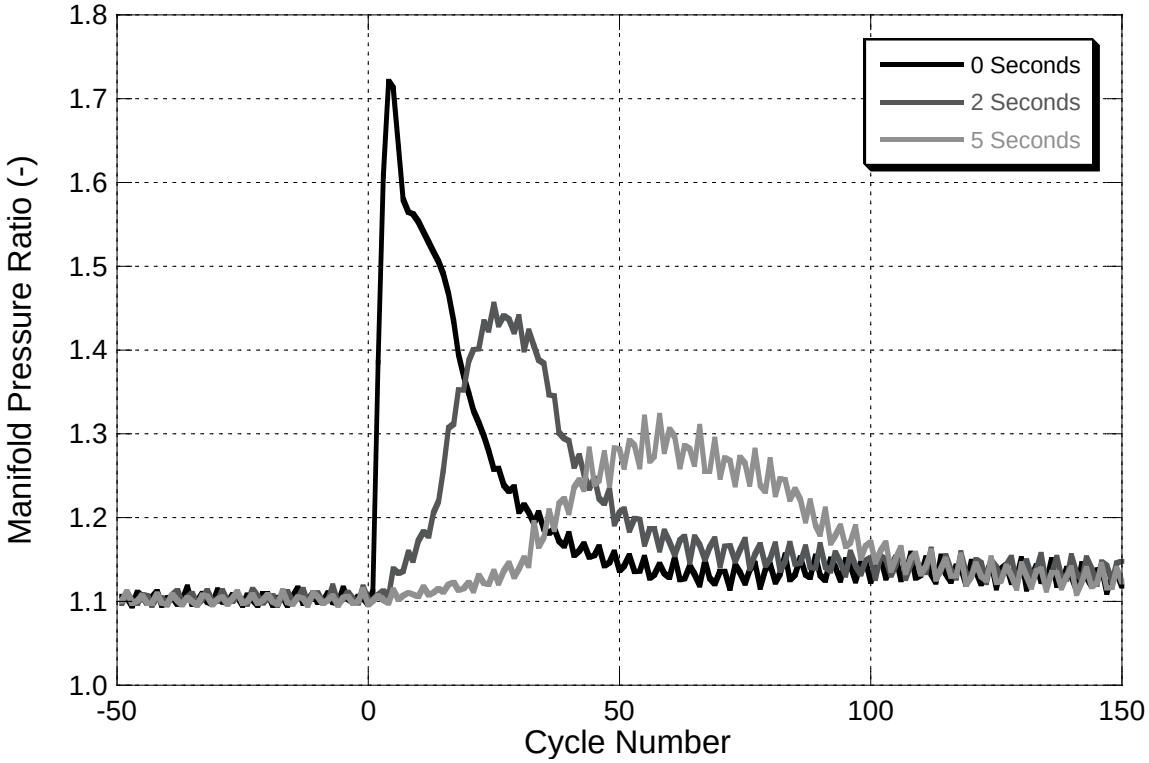

Figure 7.10: Average Manifold Pressure Ratio during Transient Load Sweep from 1 to 9 Bar BMEP at 2000 rpm

After cycle 8, however, the EGR valve begins to close quickly, and by cycle 40 the valve reaches its minimum position before settling to steady state around cycle 75. Stoichiometric combustion product mass behaves similarly during this period and decreases slightly as the EGR valve closes before settling upward to its steady state value of 6.5%.

5 Second Stoichiometric Combustion Product Mass

The lightest line in Figure 7.7 represents the stoichiometric combustion product mass for the 5 Second load sweep case. Upon the onset of the load change, the EGR valve opens up further than its original position and remains at or above this level until cycle 30. During this period the relative value of the stoichiometric combustion products rises until it reaches around 10% at cycle 30. The EGR valve then gradually closes until it reaches its steady state value around cycle 100.

While the EGR valve flow area is decreasing from cycles 30-75, the driving potential of the EGR and the manifold pressure ratio during the overlap period reach their peak values, which contribute to keep stoichiometric combustion products around 10% of the trapped mass during this period. After cycle 75, intake manifold pressures rise as the turbo begins building boost and the manifold pressure ratios decrease, dropping EGR driving potential and also internal residual. These factors, in addition to the smaller EGR valve flow area, cause the relative stoichiometric combustion gas mass to drop to its final steady-state value of around 6.5% by cycle 100.

7.2.6 Air Mass

Air mass trapped in the cylinder is a function of a number of factors such as: intake manifold pressure, EGR flow, the makeup of the EGR, and the manifold pressure ratio during the valve overlap period. The net influence of these factors is shown in Figure 7.11, which demonstrates the air mass for the three load sweeps.

As the load increases for each case, the air flow goes up. This is strongly a function of intake manifold pressure, shown in Figure 7.6, and as the turbocharger creates boost, more air flows into the cylinder when the intake valves are open. For both the 0 Second and 2 Second cases, air flow increases gradually to a maximum; this occurs at about cycle 40 and cycle 55, respectively. After this time, the EGR valve opens back up, introducing hot exhaust gases with relatively high levels of CO_2 into the intake manifold. This EGR displaces some of the air that could flow into the cylinder, and the trapped air mass decreases gradually until it reaches its steady-state value around cycle 150. This behavior agrees well with EGR valve motion and stoichiometric combustion product mass numbers.

The air mass flow trend observed in the 5 Second load sweep case, however, acts differently than the other two cases. At the onset of the transient, its air mass increases,

but does so faster than in the 2 Second case. When considering the intake manifold pressures alone between cycles 0-20, this fact seems to defy logic, as the intake manifold pressure in the 2 Second sweep is 14% greater than in the 5 Second sweep at cycle 20. Following cycle 20, the 5 Second sweep air mass decreases until cycle 35, after which it increases in accordance with intake manifold pressure until it reaches its steady state value around cycle 100.

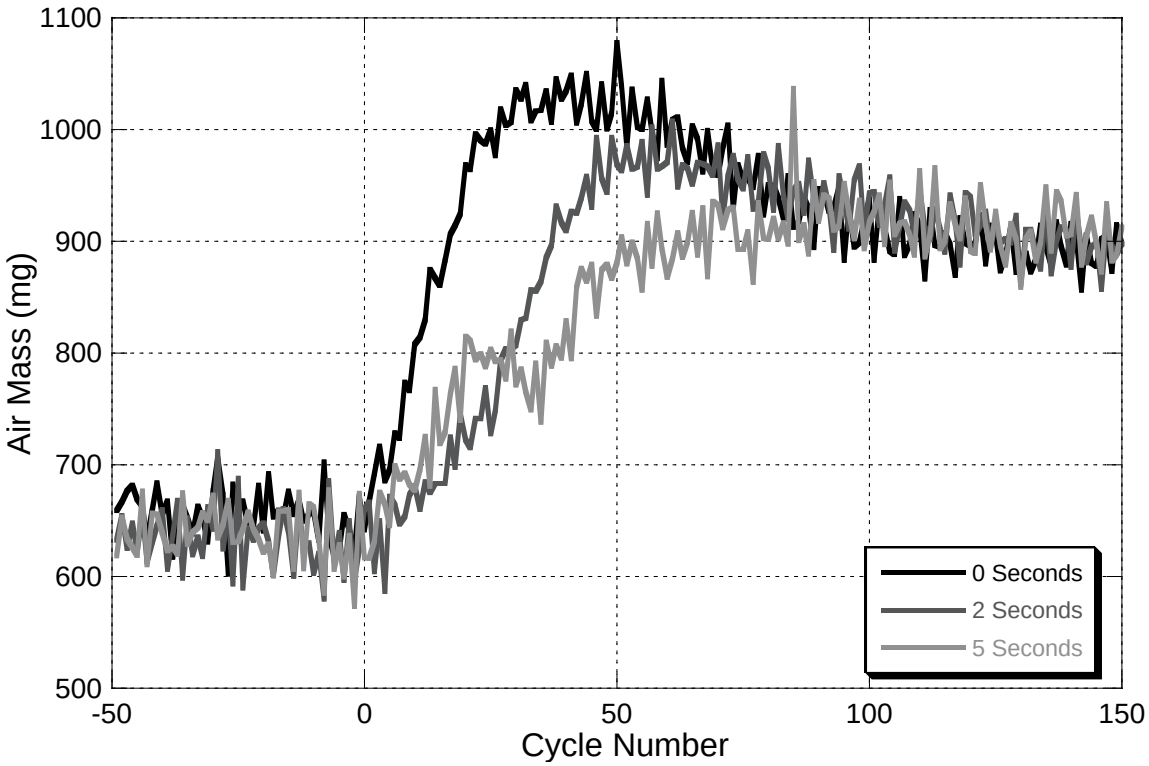

Figure 7.11: Air Mass during Transient Load Sweep from 1 to 9 Bar BMEP at 2000 rpm

To understand why more air is trapped in the cylinder in the 5 Second case than in the 2 Second case during the first 25 cycles of the transient, further investigation into the data is necessary. In the 2 Second sweep, the EGR valve first opens for 8 cycles but then closes rapidly. The net result of this movement is that the overall proportion of stoichiometric combustion mass remains relatively unchanged during the first 25 cycles. During the 5 Second sweep, the EGR valve opens during the first 25 cycles, essentially doubling the proportion of stoichiometric combustion products. The gases recycled into

the cylinder during this period come from combustion cycles that are very lean; therefore these gases are mostly air—see Equation (4.11). Since the trapped air mass shown in Figure 7.11 consists of both fresh air and air that comes from the recycled exhaust gases and residual, better understanding of the trends is obtained by calculating these two components separately. This is done by first approximating that the exhaust gases in the cylinder and the exhaust manifold have equal ratios of air and stoichiometric combustion products. Therefore the CO_2 in the cylinder prior to combustion is assumed to be a diluted form of the exhaust gases. For this exercise, this approximation is a reasonable one considering that CO_2 concentrations in the exhaust do not change drastically cycle-to-cycle. Using this relationship, it is possible to know the ratio of the mass of air and mass of stoichiometric combustion products in the exhaust gases, which is presented in Equation (7.1).

$$\frac{m_{Air}^{SC}}{m_{SC}} = [CO_2\ Dilution\ Ratio]\left[\frac{MW_{Air}}{MW_{SC}}\right]\left[\frac{n_{Air}}{n_{SC}}\right] \tag{7.1}$$

Where: m_{Air}^{SC} = Mass of air from stoichiometric combustion

m_{SC} = Mass of stoichiometric combustion products

MW_{Air} = Molecular weight of air

MW_{SC} = Molecular weight of stoichiometric combustion products

n_{Air} = Number of moles of air

n_{SC} = Number of moles of stoichiometric combustion products

The ratio of air moles to stoichiometric combustion product moles (Equation (7.2)) is determined by first dividing the numerator and denominator by the total number of moles of exhaust (Equation (7.2)). These terms are re-written as the molar fractions of air and stoichiometric combustion products in the exhaust (Equation (7.2)). According to the conceptualization of in-cylinder constituents after combustion presented in Figure 4.2, diesel exhaust consists entirely of air and the products of stoichiometric combustion.

Therefore the mole fraction of air in the exhaust can be re-written as one minus the mole fraction of stoichiometric combustion products in the exhaust (Equation (7.2)).

$$\underbrace{\left[\frac{n_{Air}}{n_{SC}}\right]}_{a} = \underbrace{\left[\frac{\frac{n_{Air}}{n_{Exh}}}{\frac{n_{SC}}{n_{Exh}}}\right]}_{b} = \underbrace{\left[\frac{\chi_{Air}}{\chi_{SC}}\right]}_{c} = \underbrace{\left[\frac{1-\chi_{SC}}{\chi_{SC}}\right]}_{d} \tag{7.2}$$

Where: n_{Air} = Number of moles of air

n_{SC} = Number of moles of stoichiometric combustion products

n_{Exh} = Number of moles of exhaust

χ_{Air} = Mole fraction of air in the exhaust

χ_{SC} = Mole fraction of stoichiometric combustion products in the exhaust

The makeup of the stoichiometric combustion products is first stated in Equation (4.11). Each mole of stoichiometric combustion products consists of one mole of CO_2, $y/2$ moles of H_2O and $3.773\left(1+\frac{y}{4}\right)$ moles of N_2. Substitution of this relationship into Equations (7.2), expansion of the ratios in Equation (7.1) , and solving for the mass of air in the stoichiometric combustion products results in

$$m_{Air}^{SC} = [m_{SC}]\left[\frac{\chi_{CO_2}^{In-Cyl}}{\chi_{CO_2}^{Exh}}\right]\left[\frac{MW_{Air}}{MW_{SC}}\right]\left[\frac{1-\left\{1+\frac{y}{2}+3.773\left(1+\frac{y}{4}\right)\right\}\chi_{CO_2}^{Exh}}{\left\{1+\frac{y}{2}+3.773\left(1+\frac{y}{4}\right)\right\}\chi_{CO_2}^{Exh}}\right] \tag{7.3}$$

Where: m_{Air}^{SC} = Mass of air from stoichiometric combustion

m_{SC} = Mass of stoichiometric combustion products

$\chi_{CO_2}^{In-Cyl}$ = Percentage of CO_2 in the cylinder

$\chi_{CO_2}^{Exh}$ = Percentage of CO_2 in the exhaust manifold

MW_{Air} = Molecular weight of air

MW_{SC} = Molecular weight of stoichiometric combustion products

y = C-H ratio in fuel

All of the terms on the right hand side of Equation (7.3) are known, making the quantity of air that comes from residual and EGR gases straightforward. By taking the total quantity of ingested air and subtracting off the air that comes from EGR and residual, the fresh air is calculated. The results of this effort are shown in Figure 7.12.

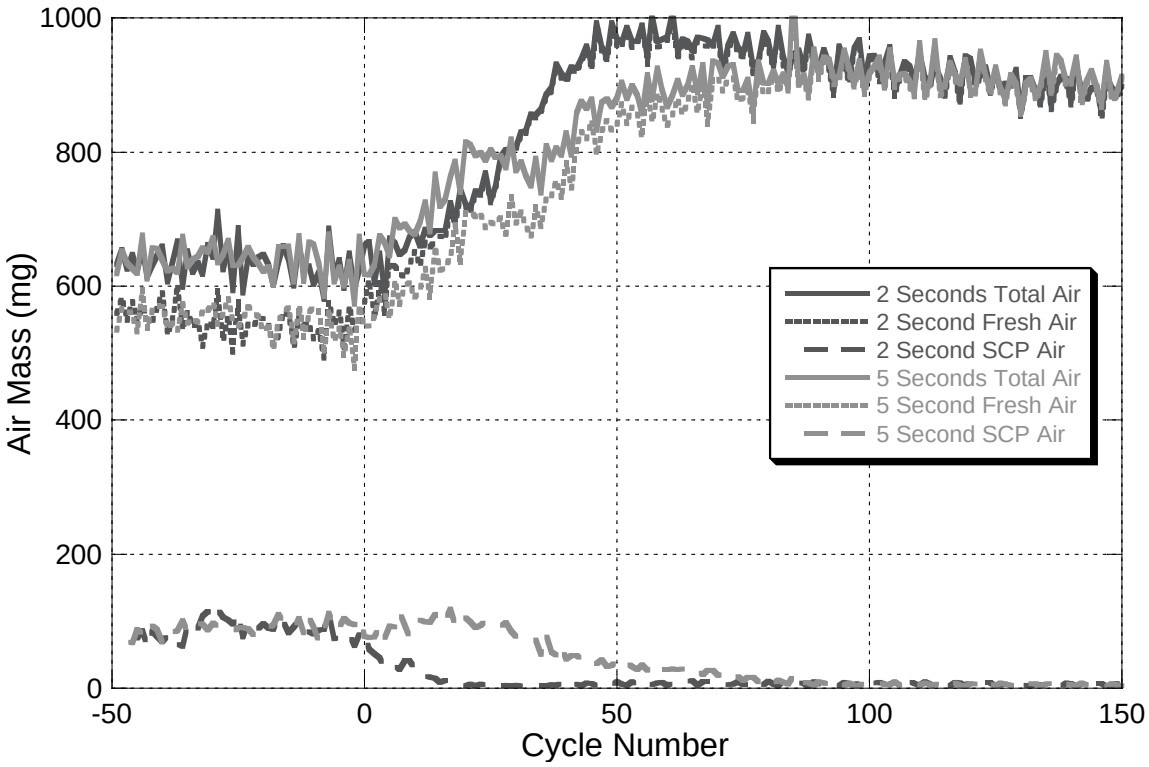

Figure 7.12: Total Air Mass, Fresh Air Mass, Air Mass From Exhaust Gases during Load Sweep from 1 to 9 Bar BMEP at 2000 rpm

Considering only the flow of fresh air into the cylinder, represented by the fine dashed lines, the trend exhibited during the load sweep demonstrates that the flow of fresh air is controlled by the intake manifold pressure for both the 2 Second and 5 Second load sweeps. This behavior is in accordance with expectations.

The observed behavior of the air that is ingested from EGR and residual gases also behaves as expected and is displayed as the coarsely dashed lines in Figure 7.12. During the steady-state portion 50 cycles prior to the transient, the amount of air in the cylinder that comes from recycled gases is about 13% of all the air trapped in the

cylinder. When the transient begins, the EGR valve closes in the 2 Second case, which causes the air from the recycled gases to go to near zero. In the 5 Second sweep, however, this value remains constant until the EGR valve begins closing around cycle 25. This confirms that the bulge in air flow observed in the 5 second case from the beginning of the transient to cycle 25 is due to the high rates of EGR and residual that are mostly made up of air.

After cycle 100 in the tests, as the engine settles to its new steady-state operating point at 9 bar BMEP, the EGR valve is open and approximately 6.5% of the trapped mass consists of stoichiometric combustion products. Combustion conditions at this state, however, are producing exhaust with CO_2 concentrations of around 10.5%, and the exhaust contains very little air. This is demonstrated by the near-zero values of air from stoichiometric combustion products in Figure 7.12 after cycle 100.

7.2.7 Air/Fuel Ratio

Now that the trends of fuel mass and air mass have been explored separately, the air/fuel ratio is examined because this value typically has a large influence on emissions production. Air/fuel ratio for 0, 2, and 5 second load sweeps are shown in Figure 7.13. For all cases observed, the air/fuel ratio begins at around 75 prior to the transient and ends around 20 after the load sweep. What happens in between, however, is very different for each case.

0 Second Air/Fuel Ratio

As expected, the mass of fuel overshoot in the 0 Second sweep causes a very low dip in the air/fuel ratio. The value goes down to 14.8, which is essentially a stoichiometric combustion event and represents a much richer mixture than the engine would ever produce at steady-state. In fact, the lowest air/fuel ratio achievable with the

engine's standard calibration is 18.4 at 750 rpm and 7.9 bar BMEP; which is the maximum engine torque at this speed.

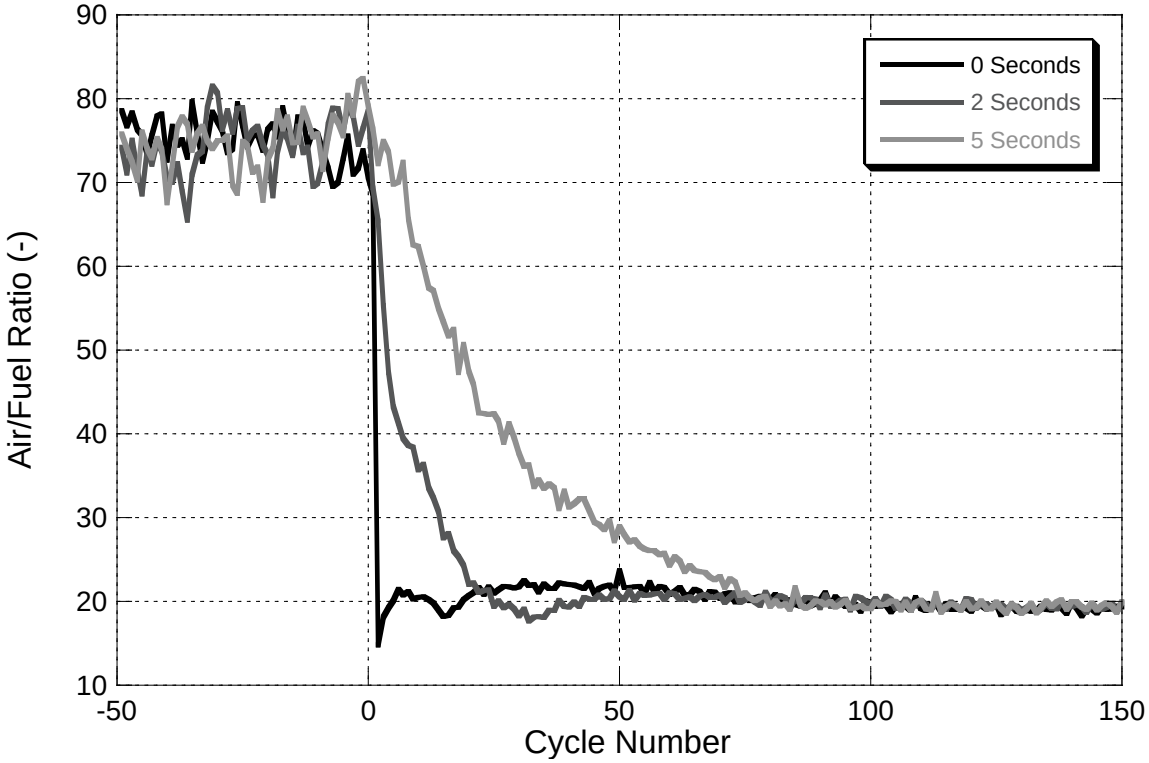

Figure 7.13: Air/Fuel Ratio during Transient Load Sweep from 1 to 9 Bar BMEP at 2000 rpm

This extremely low air/fuel ratio is the result of how the engine responds to a sudden load demand from the driver. When the engine command increases, the fuel injection system responds by immediately injecting more fuel into the cylinder. This takes place into a mixture of air, EGR, and residual that is unchanged from the previous combustion event. The result is a step change in air/fuel ratio because the components that control the amount of air in the cylinder (the turbocharger and EGR system) have not yet responded to the change in engine command.

After the cycle with the lowest air/fuel ratio, two more cycles take place that are below the final steady state value. From there, air/fuel ratio behavior tends to mirror the

trends observed with the measured mass of injected fuel. By cycle 50, the air/fuel ratio in the 0 Second sweep has settled to within 5% of its final steady-state value.

2 Second Air/Fuel Ratio

In the 2 Second load sweep, the air fuel ratio moves downward at the onset of the transient, but much less sharply than in the 0 Second case. The minimum air/fuel ratio experienced is 17.7, which occurs at cycle 32, a time in which fueling rates are maximum and air flow rate is low due to turbocharger lag. By cycle 50, however, air/fuel ratios have settled down to the steady-state level.

5 Second Air/Fuel Ratio

The 5 Second load sweep experiences a very gradual drop in air/fuel ratio from the initial value to the final value. In fact, by cycle 83, the cycle in which the engine command reaches its final position, the air/fuel ratio has also attained its final steady-state value. This demonstrates that in this load sweep, the air charging system can respond quickly enough to provide the demanded amount of air for each cycle.

7.2.8 Combustion Analysis

To better characterize the combustion events that occur during the constant-speed load sweeps, rate of heat release analysis is conducted on each one of the cycles. Since all three sweeps begin and end at the equivalent operating conditions, the rate of heat release curves for cycles before and after the transient load sweep are equivalent. Figure 7.14 demonstrates two rate of heat release curves that are representative of combustion cycles before and after the transient load sweep.

At the initial condition of the transient, the combustion is completely premixed. The ignition delay at this point is 5.8º, and the combustion duration is 9.6º. At the final

operating point of the transient, the rate of heat release curve exhibits both premixed and diffusion burning. The ignition delay is 4.0º and the combustion duration is 22.0º.

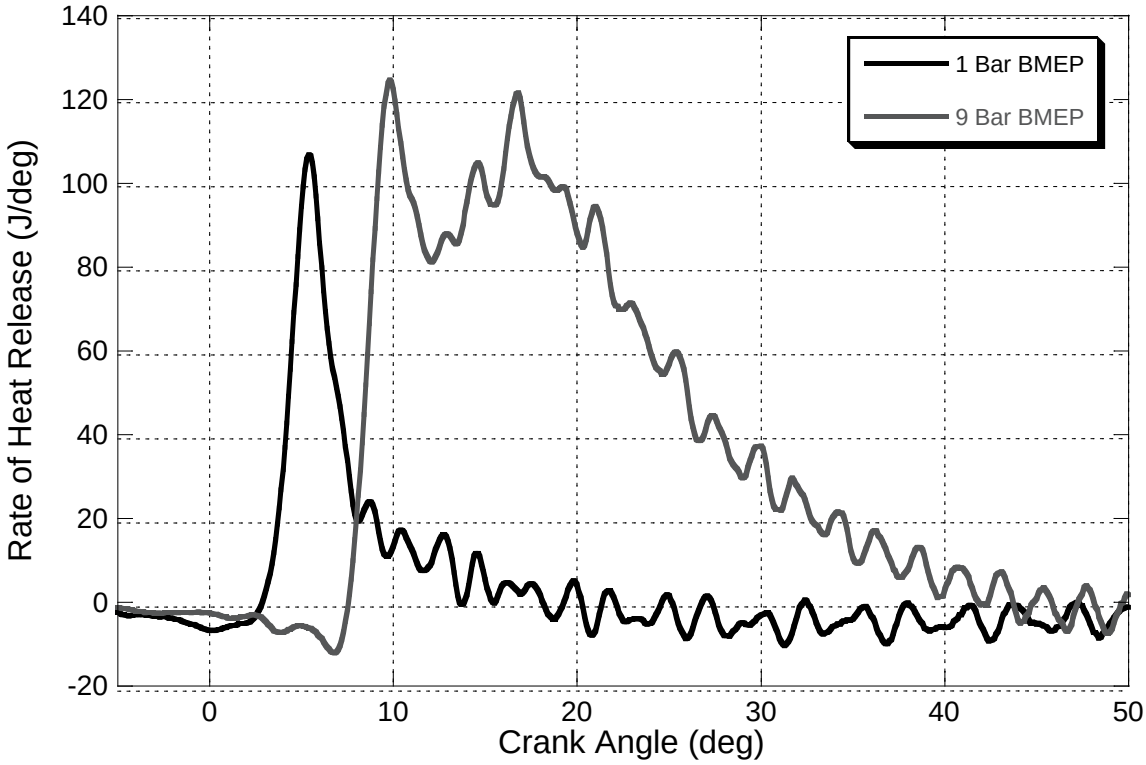

Figure 7.14: Typical Rate of Heat Release Curves at 1 Bar and 9 Bar BMEP, 2000 rpm

The previous sections examine very carefully the differences in trapped masses of fuel, air, and stoichiometric combustion product and explain why these variances are observed. To understand how the combustion process itself develops during the transient sweep, a number of figures are presented.

0 Second Rate of Heat Release Analysis

To visualize how the combustion events evolve during the 0 Second case, two graphs are used because as the transient proceeds, the combustion process first retards and increases in premixed combustion intensity and then advances and develops into a premixed and diffusion burn process. Figure 7.15 shows the first portion of this process;

rate of heat release curves are shown for every five cycles, and the third curve from the left represents the cycle with the very low air/fuel ratio. Prior to the transient, the combustion is entirely premixed, and during the first 17 cycles of the transient, the intensity of the premixed spike doubles and its crank angle location retards 7º. By cycle 17, the presence of some diffusion burning is detectable.

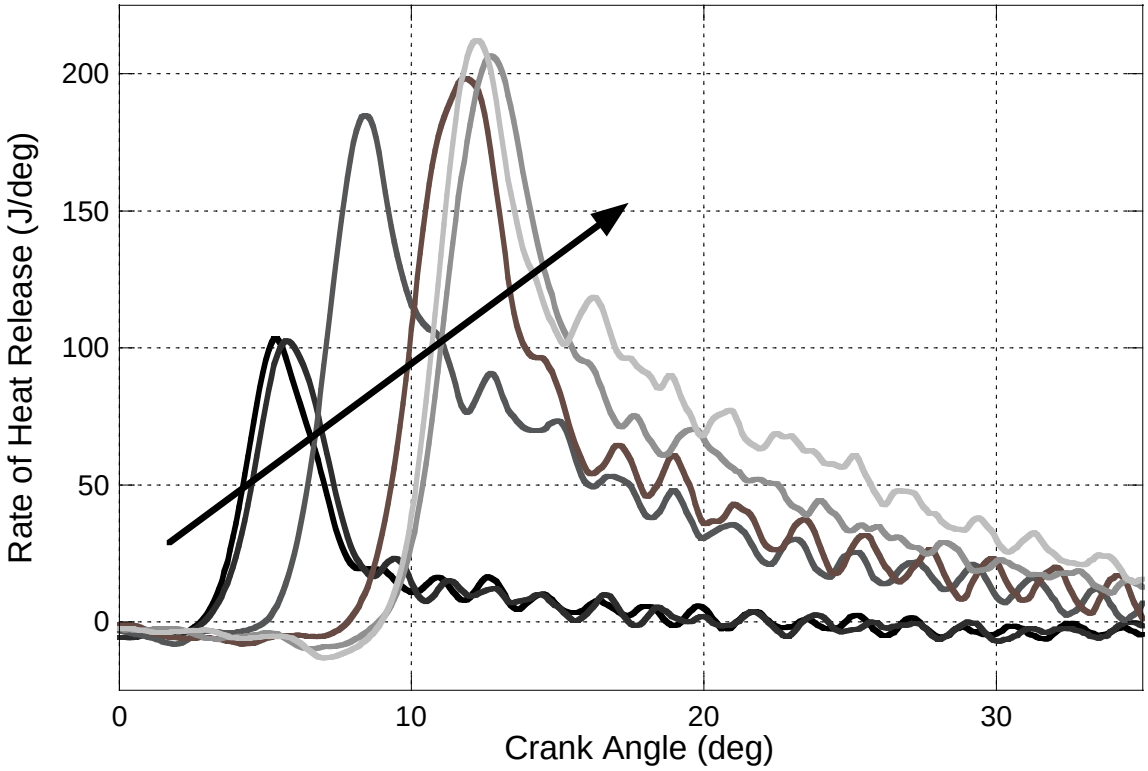

Figure 7.15: Rate of Heat Release for Initial Portion of 0 Second Transient Load Sweep from 1 Bar to 9 Bar BMEP at 2000 rpm

Figure 7.16 shows how the combustion progresses after cycle 17 until the engine has reached steady-state operation at cycle 147, which is represented by a medium gray line. As seen on the previous graph, cycle 17 consists almost entirely of premixed combustion with very little diffusion burning. As the engine settles toward steady-state operation, the intensity of the premixed spike decreases and the amount of energy released as diffusion burning increases. The start of combustion also advances slightly, as does the overall combustion phasing.

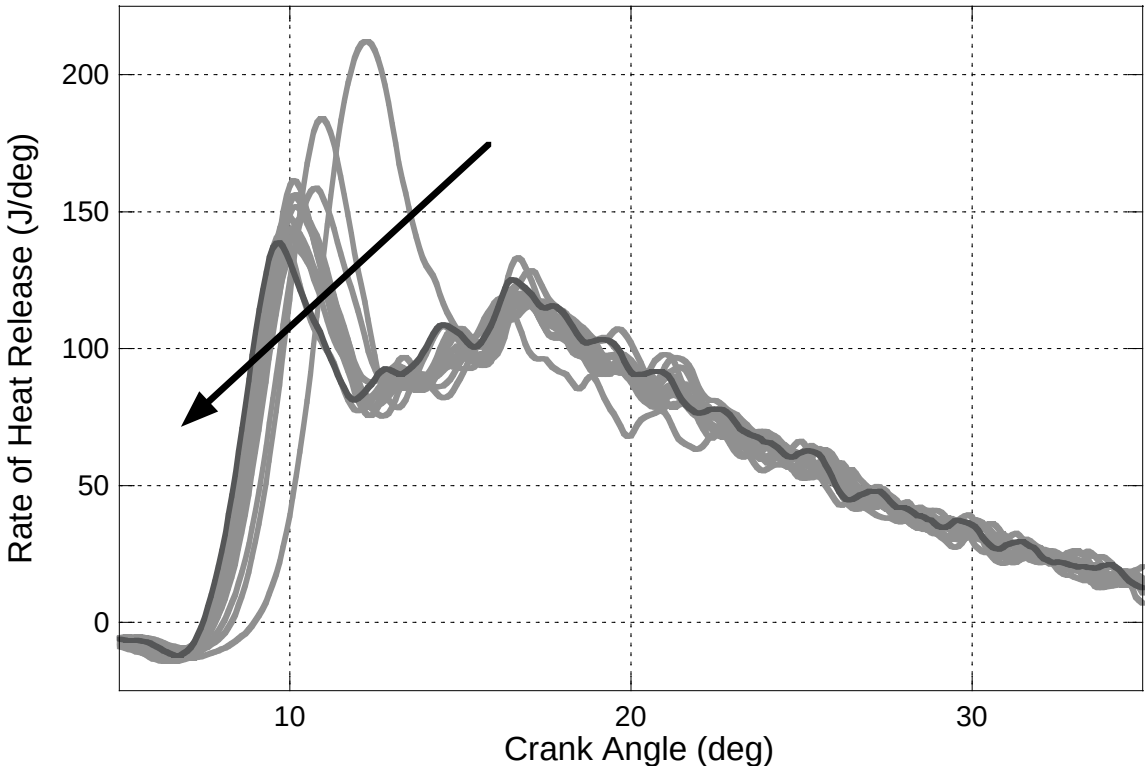

Figure 7.16: Rate of Heat Release for Cycles 17-147 during 0 Second Transient Load Sweep from 1 Bar to 9 Bar BMEP at 2000 rpm

Two factors are controlling the trends observed in the phasing and the type of combustion processes observed in Figure 7.15 and Figure 7.16: the injection timing and in-cylinder conditions. The start of injection for all three load sweeps is shown in Figure 7.17. At the beginning of the transient, the start of injection is around -2.7º after TDC. By cycle 17, the injection timing has retarded to 3.6º after TDC, and is the main cause for the retarding of the location of the premixed spike observed in Figure 7.15. The time elapsed for these cycles to occur is about one second, and in that time, the temperature in the combustion chamber remains relatively unchanged. Therefore the later injection timings result in longer ignition delays and more intense premixed combustion. This is evidenced by considering the ignition delay, as shown in Figure 7.18. During the first 17 cycles of the transient, the ignition delay goes from 5.7º before the transient to a maximum of 6.6º at cycle 3 back down to 5.4º by cycle 17.

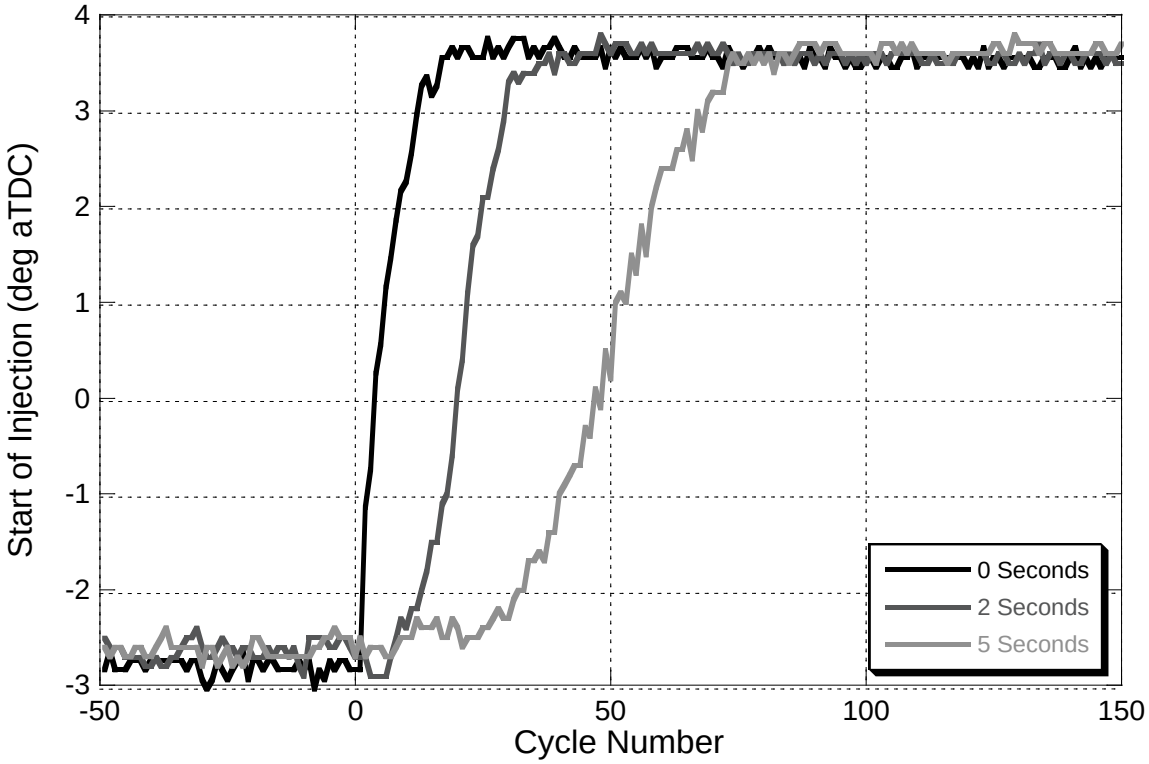

Figure 7.17: Measured Start of Injection Timing during Transient Load Sweep from 1 to 9 Bar BMEP at 2000 rpm

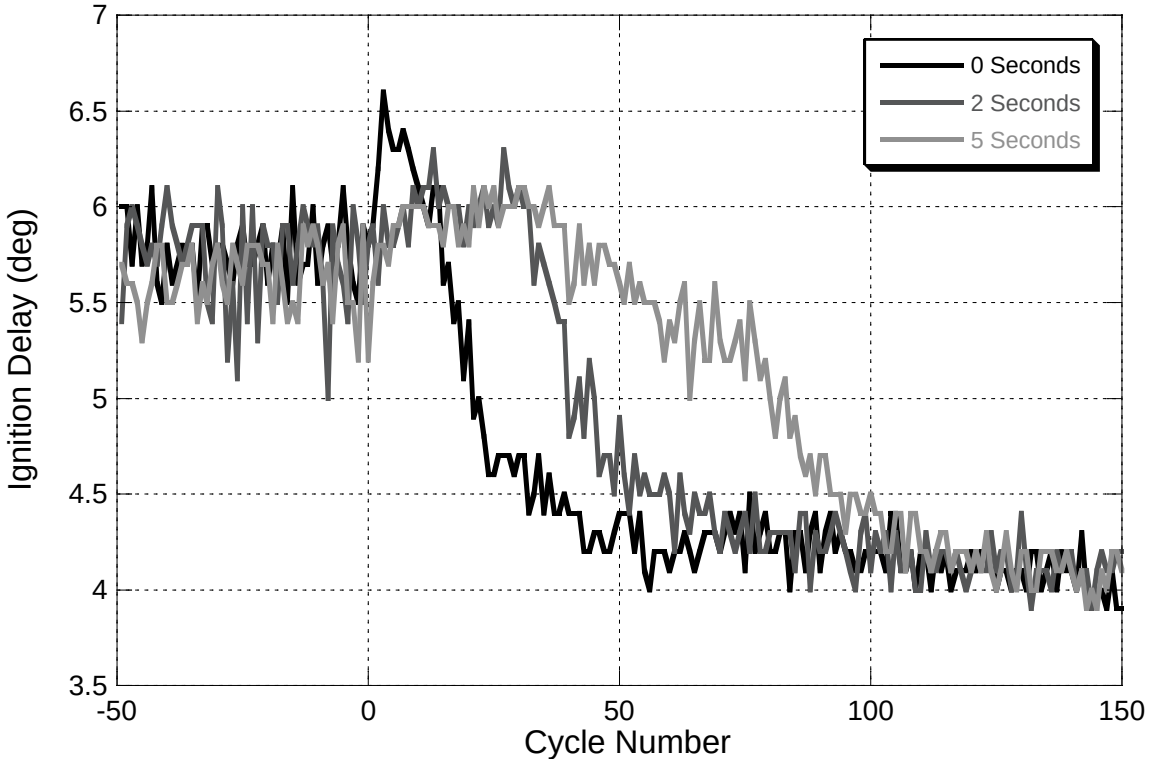

Figure 7.18: Ignition Delay during Transient Load Sweep from 1 to 9 Bar BMEP at 2000 rpm

After cycle 17, the ignition delay keeps reducing without any change in injection timing. By this time, cylinder temperatures are beginning to rise from higher air flow rates and more energy being released from greater volumes of fuel. Therefore the time necessary for the injected fuel to atomize, vaporize, and become entrained with the air in the cylinder reduces and ignition delays decrease. This reduces the amount of energy released during the premixed spike and shifts more combustion to be diffusion in nature. This is evident when studying the evolution of combustion after cycle 17 as shown in Figure 7.16.

Combustion phasing during the 0 Second case is evaluated by considering the mass fraction burned curves and the crank angle occurrence duration of the 0-5%, 0-50% and 0-90% burn intervals, the latter is also known as the combustion duration. The 0-5% duration changes very little; this is because is amount of energy is typically encompassed by the initial portion of the premixed spike. The degree of change in the 0-50% duration is more pronounced, as a step change occurs at cycle 2 that doubles the crank angles necessary to burn the fuel. This only makes sense, as the quantity of fuel consumed is also increased greatly. From this point, as the intensity of the premixed spike increases, the 0-50% MFB duration decreases. As the combustion transitions so that more energy is released as diffusion combustion, the 0-50% MFB duration lengthens to its final steady-state value. Combustion duration also experiences significant change. Prior to the transient, the combustion duration is around 10º. When the transient sweep begins, a step change in the duration of combustion at cycle 2 increases the length of combustion by a factor of 2.5. As the engine stabilizes, the combustion duration settles to a length of about 22º.

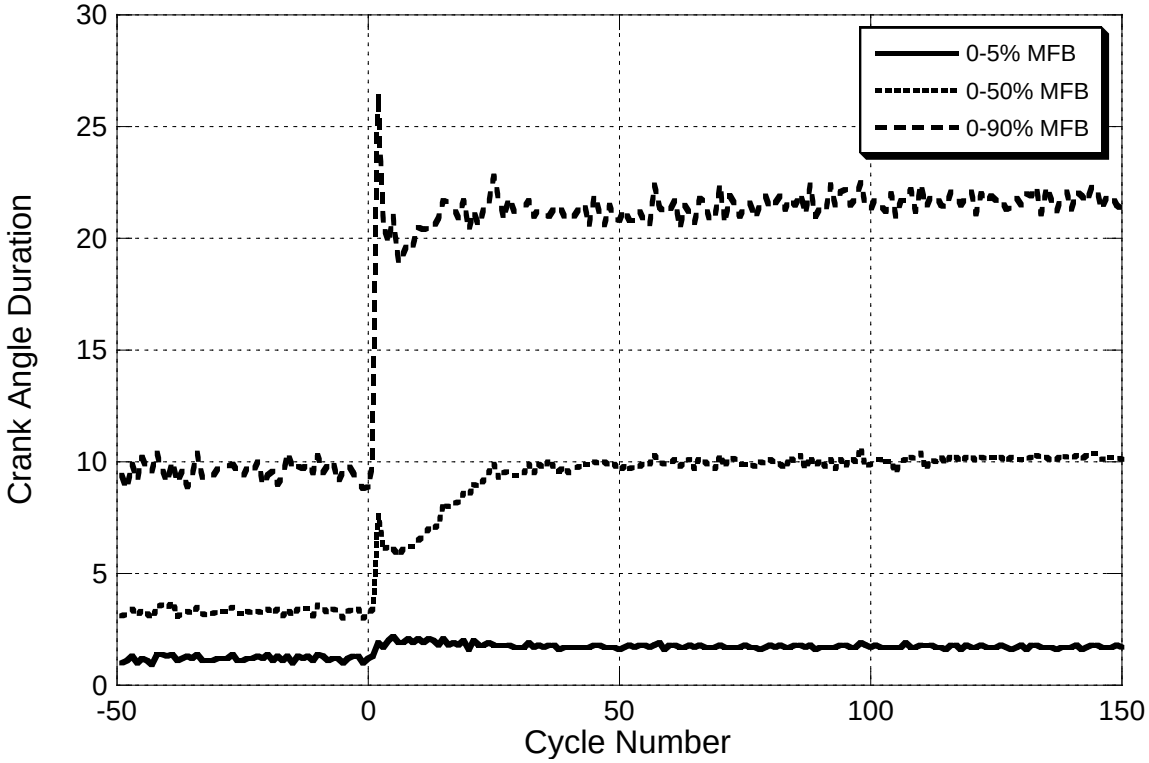

Figure 7.19: Mass Fraction Burn Durations: 0-5%, 0-50%, and 0-90% during 0 Second Transient Load Sweep from 1 to 9 Bar BMEP at 2000 rpm

2 Second Rate of Heat Release Analysis

As in the 0 Second transient, the 2 second transient undergoes an evolution of combustion. This transition is represented in Figure 7.20, which shows 12 cycles of heat release during the 2 Second sweep. Black lines represent the heat release as it is increasing in premixed intensity and retarding in timing. The premixed combustion reaches its maximum level at cycle 33. From that point, the start of combustion begins advancing and the combustion begins to transition to less premixed burning and more diffusion burning. This is represented by the light gray lines in Figure 7.20. The medium gray line is cycle 142, and represents the combustion in its steady-state form.

The transitions in combustion observed during the 2 Second sweep occur for the same reasons the same transitions occurred in the 0 Second case. Retarded injection timing (see Figure 7.17) after the transient begins intensifies premixed combustion. As

the cylinder begins to get hotter, the ignition delay decreases (see Figure 7.18) and diminishes the intensity of premixed combustion, causing more fuel to burn in a diffusion-controlled manner.

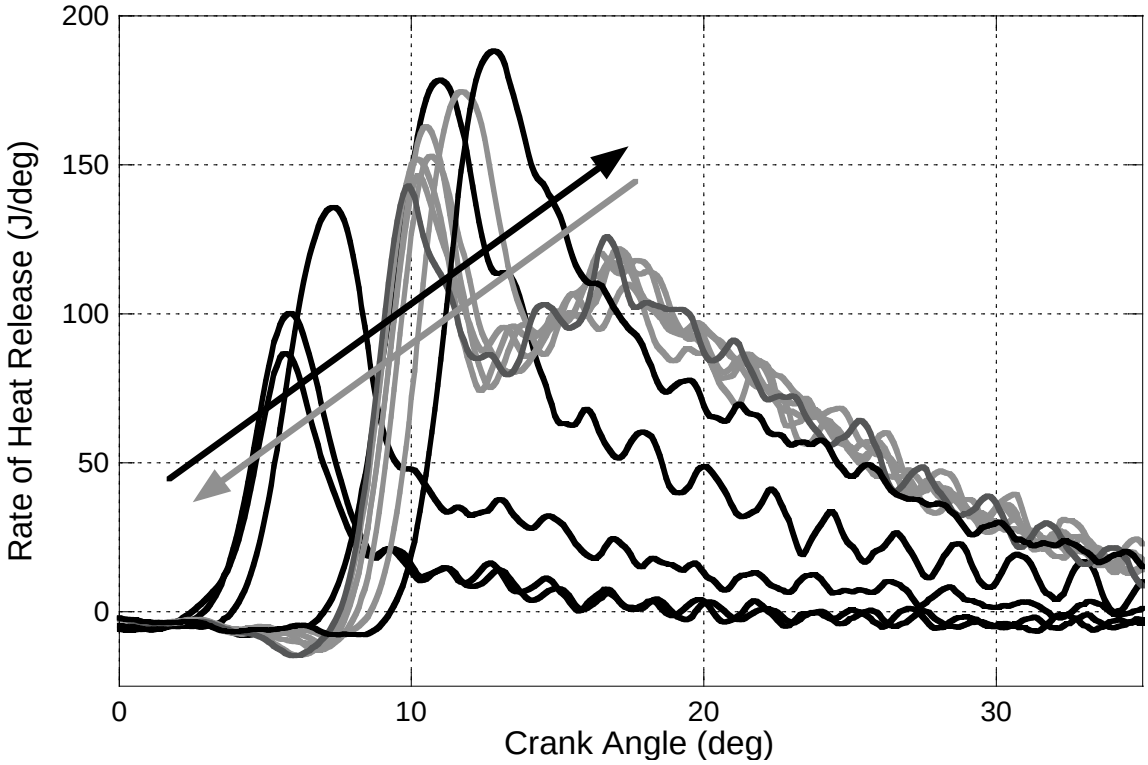

Figure 7.20: Rate of Heat Release for Cycles -12-142 during 2 Second Transient Load Sweep from 1 to 9 Bar BMEP at 2000 rpm

Combustion phasing for the 2 Second case is studied by examining the crank angle durations to necessary to achieve 0-5% MFB, 0-50% MFB, and 0-90% MFB. These trends are displayed in Figure 7.21. For all mass fraction burned durations, a gradual transition from one steady state condition to another is demonstrated. This indicates that combustion is changed incrementally during this transient.

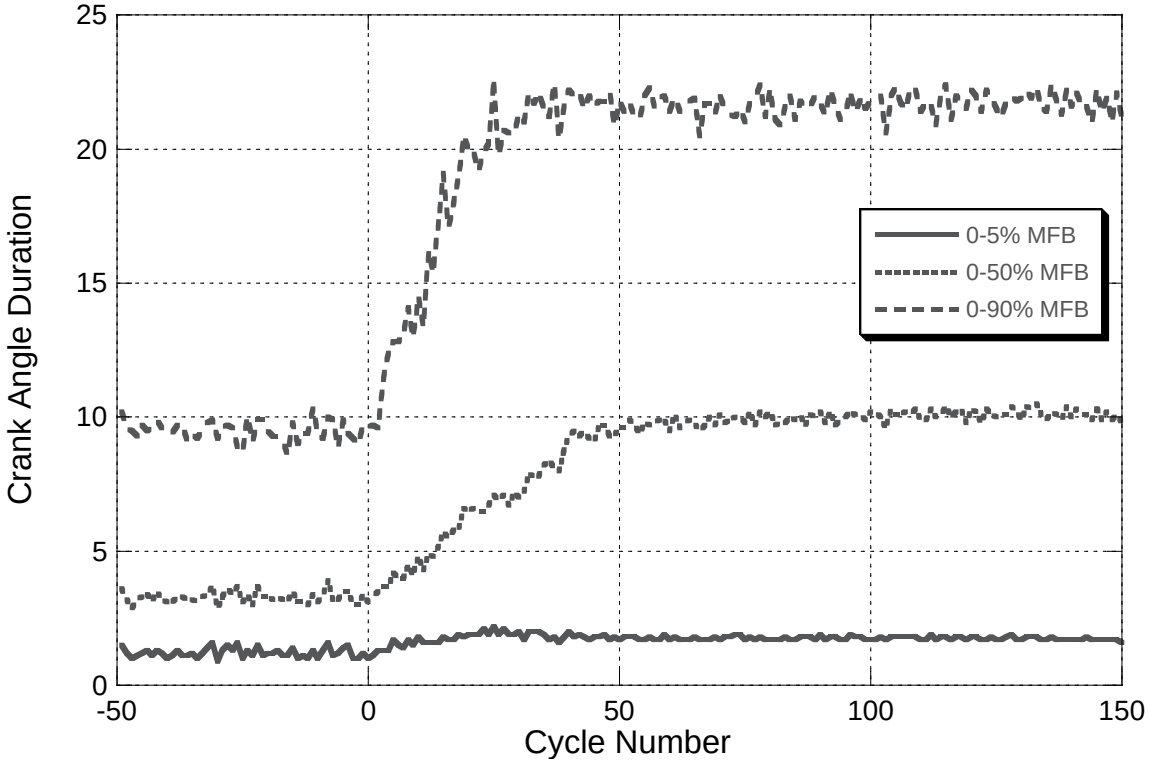

Figure 7.21: Mass Fraction Burn Durations: 0-5%, 0-50%, and 0-90% during 2 Second Transient Load Sweep from 1 to 9 Bar BMEP at 2000 rpm

5 Second Rate of Heat Release Analysis

Heat release curves for the 5 Second sweep are shown in Figure 7.22. As in the other two cases, a transition is made between combustion that is completely premixed and that which has both premixed and diffusion combustion. The transient takes place the most slowly in this case, as dictated by the engine command. Upon the onset of the load sweep, the premixed burning becomes more intense and becomes slightly more retarded. By cycle 42, however, it becomes apparent that the combustion is no longer purely premixed, as diffusion combustion is present. Unlike the other two load sweeps, this one takes place with a significant amount of EGR and residual in the cylinder, which acts to lengthen ignition delays and slow down combustion. Presence of these stoichiometric combustion products in the cylinder are most likely the cause of the slower combustion rates and diffusion combustion.

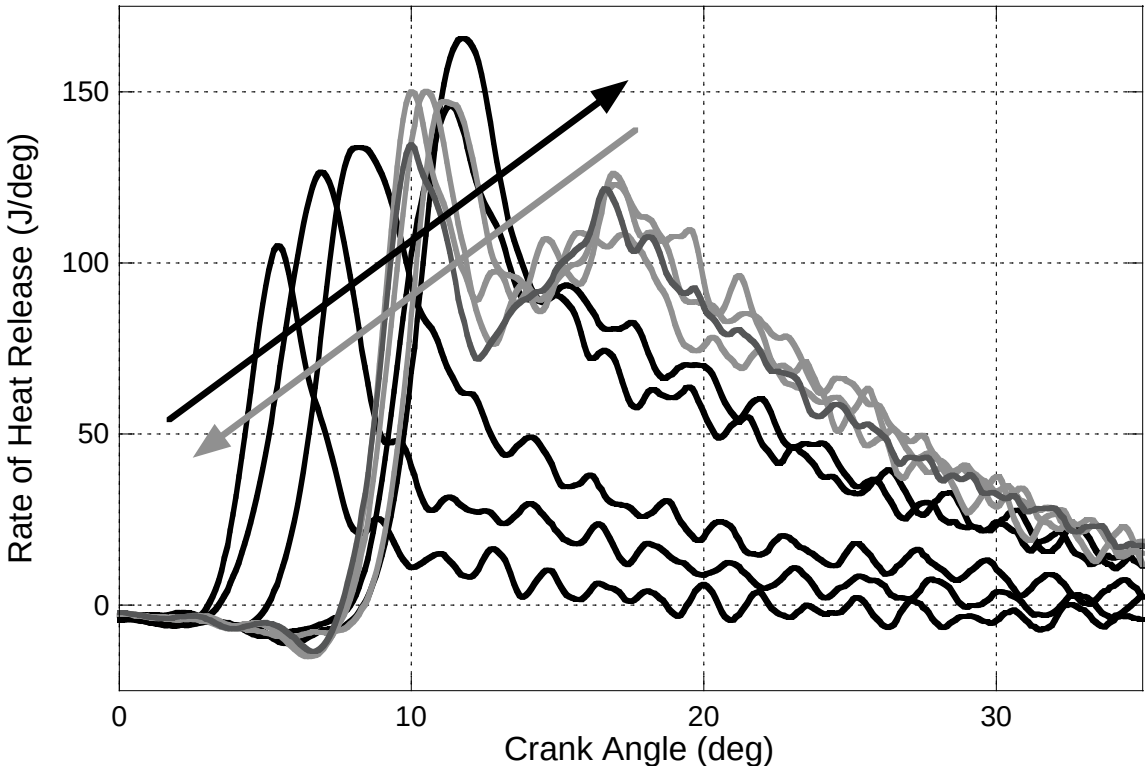

Figure 7.22: Rate of Heat Release for Cycles -12-142 during 5 Second Transient Load Sweep from 1 to 9 Bar BMEP at 2000 rpm

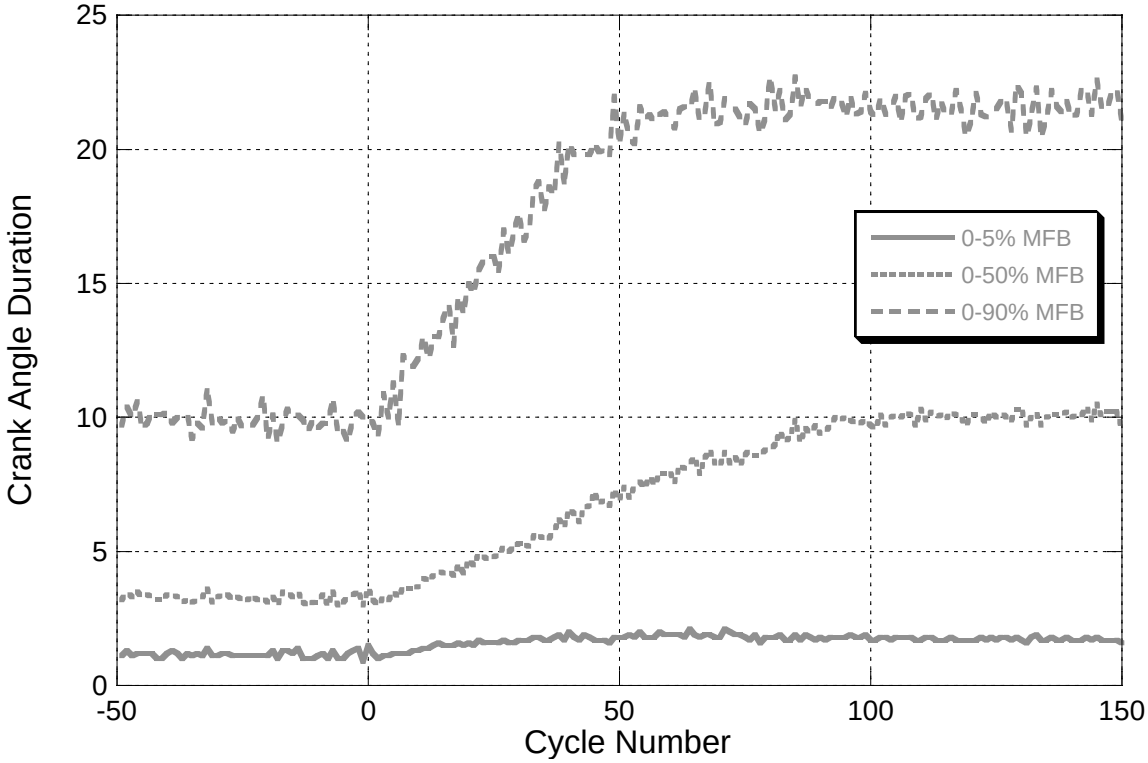

Figure 7.23: Mass Fraction Burn Durations: 0-5%, 0-50%, and 0-90% during 5 Second Transient Load Sweep from 1 to 9 Bar BMEP at 2000 rpm

As the premixed spike grows in intensity, its located relative to TDC becomes more retarded due to more late fuel injections, as shown in Figure 7.17. This contributes to the growth of the premixed combustion, and by cycle 81 has reached a maximum. From this point forward, the combustion process gradually becomes more advanced with less premixed burning and more diffusion burning.

Combustion phasing for the 5 Second sweep is shown in Figure 7.23. This plot shows that the durations for combustion transition very smoothly and gently from their initial conditions to their final ones. Therefore consecutive cycles have very little difference in combustion rates.

7.2.9 NO Emissions

NO emissions are formed in localized areas of the combustion chamber where the temperatures are high and plenty of oxygen is available. Temperatures are typically highest during combustion where the air/fuel ratio is near the stoichiometric value. Even though spatially-resolved in-cylinder data is not available, a wealth of information about in-cylinder conditions is known and is used to understand NO emissions trends. The factors that contribute to NO formation are divided into four major categories: injection parameters, in-cylinder gas composition, combustion characteristics, and localized in-cylinder conditions.

The NO emissions measured during the transient load sweeps are shown in Figure 7.24, and there are some similarities and some marked differences between the three cases. All three cases begin the load sweep with a very constant NO concentration of around 90 ppm. After the transient sweeps take place, the NO concentration for all three conditions averages about 260 ppm, but is fluctuating ±70 ppm of the mean. The differences in the three cases occur during the transition from one steady-state condition to the other.

The 0 Second case experiences a large burst in NO emissions to concentrations above 400 ppm during the first 25 cycles of the sweep, while the other two cases exhibit a more gradual change in NO emissions throughout the sweep.

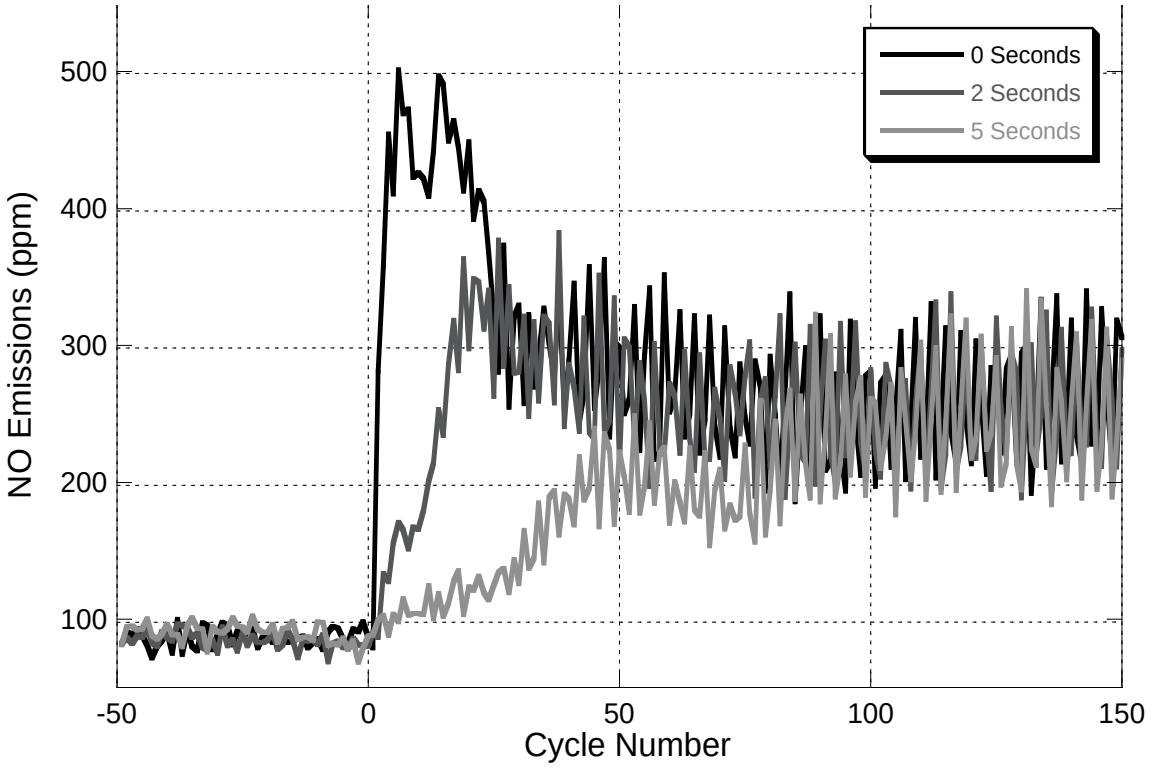

Figure 7.24: NO Emissions during Transient Load Sweep from 1 to 9 Bar BMEP at 2000 rpm

NO Emissions and Injection Parameters

The injection parameters that impact NO emissions are injection timing and injection pressure. Injection timing during the sweeps for all three cases is presented above in Figure 7.17. For all three cases, the injection timing retards as the load sweep occurs. Retarding of the injection timing typically leads to lower NO emissions [49, 50], so the injection timing is not the cause of the discrepancies.

The maximum injection pressure for each cycle is shown in Figure 7.25. It is well accepted that higher injection pressures typically lead to higher NO emissions [51, 52].

While these pressures spike upwards quickly for the 0 Second case, they do not exceed the injection pressures experienced by the other operating conditions. Therefore it is unlikely that injection pressure is the cause for the higher NO emissions. These high fuel injection pressures in the 0 Second sweep do occur, however, when cylinder pressures and temperatures are lower than in the other cases, which would enhance fuel jet penetration.

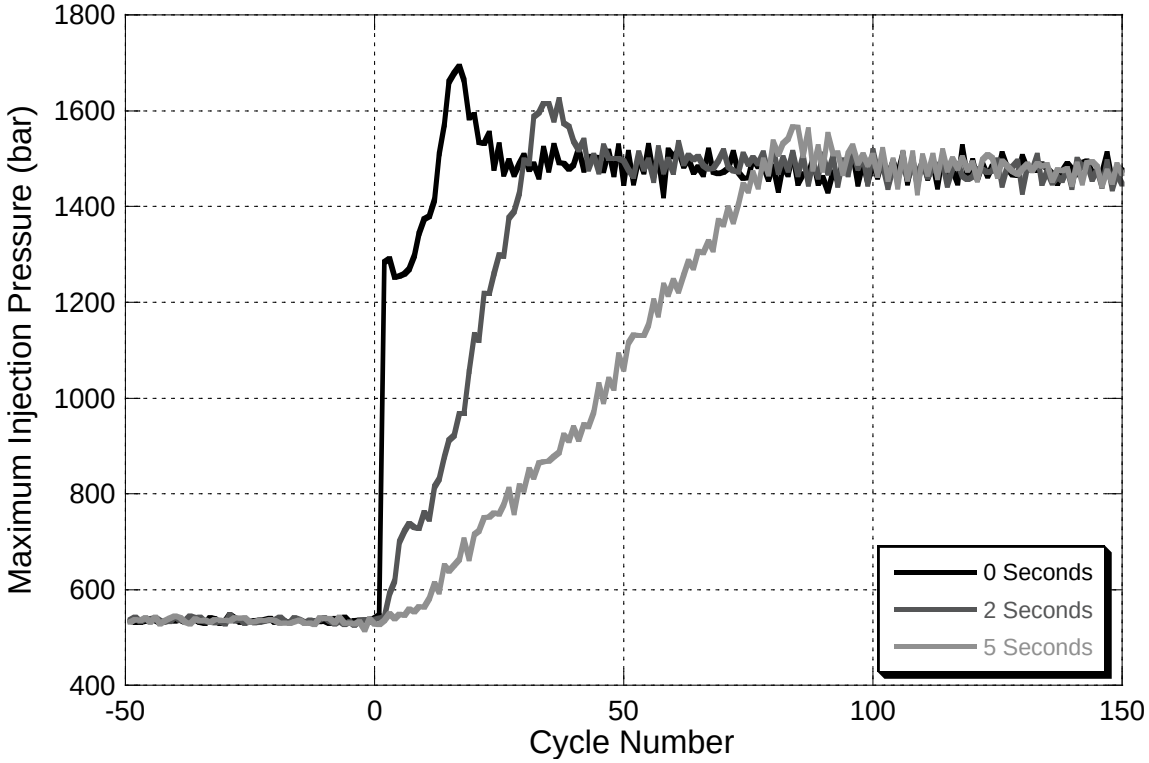

Figure 7.25: Maximum Injection Pressure during Transient Load Sweep from 1 to 9 Bar BMEP at 2000 rpm

NO Emissions and In-Cylinder Gas Composition

In Section 6.3 it is demonstrated that the quantity of oxygen in the cylinder prior to combustion has a significant impact on the steady-state emissions formed. This quantity is shown in Figure 7.26 for all three load sweeps. It is apparent that the 0 Second case experiences in-cylinder O_2 concentrations that are quite different than the

other two conditions. The most significant variances occur at cycles 2 and 3, which have less oxygen than the other two cases. NO emissions for these cycles are actually right around the final steady-state value. Since these combustion cycles are relatively rich, the amount of O_2 in the cylinder is greatly reduced. Another variance occurs between cycles 18 and 75, in which the 0 Second case has more O_2 than the other two sweeps. These deviations could lead to the higher NO emissions measured between cycles 18 and 25, but does not explain why NO emissions are at maximum values between cycles 4-18.

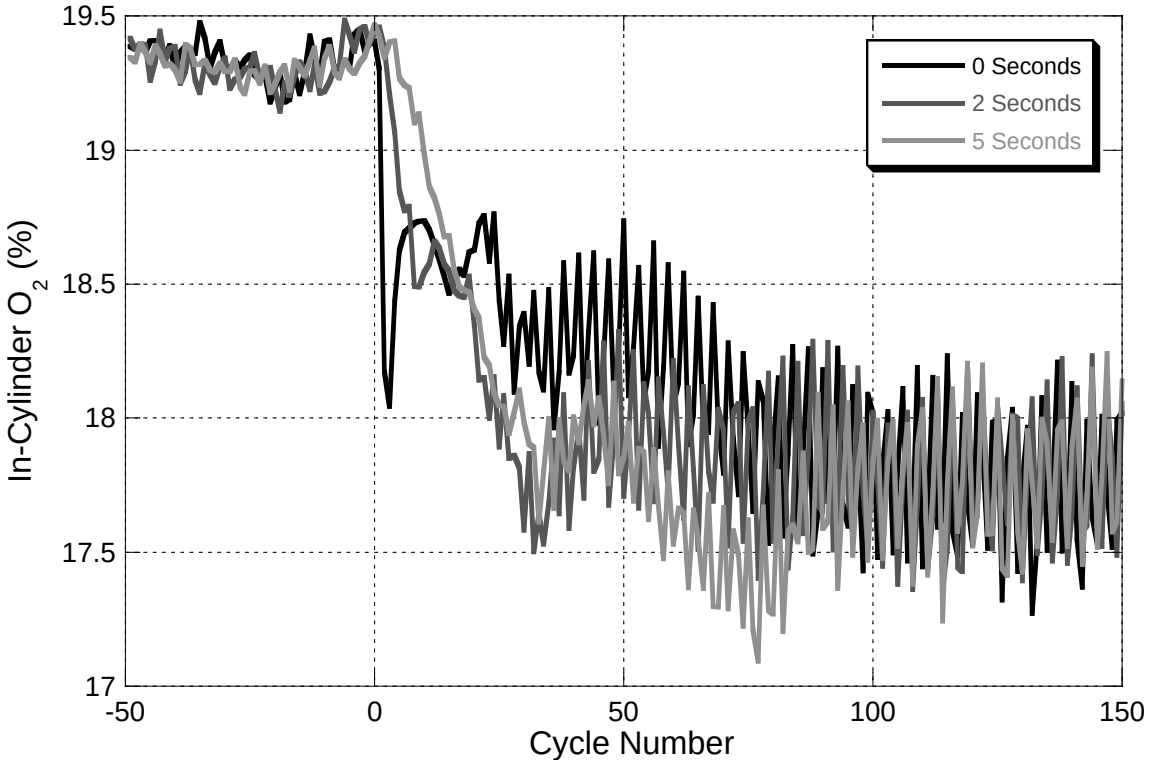

Figure 7.26: In-Cylinder Pre-Combustion O_2 Concentration during Transient Load Sweep from 1 to 9 Bar BMEP at 2000 rpm

NO Emissions and Combustion Characteristics

Rate of heat release curves are analyzed to understand how combustion characteristics differ for the three investigated transient load sweep cases. Figure 7.27 displays four rate of heat release curves for each of the three cases during the cycles in

which the 0 Second case produces a burst of NO emissions. All three cycles are exhibiting combustion that is primarily premixed in nature, and the 0 Second cases have premixed spikes that are much more intense than the other two sweeps. This type of combustion produces higher temperatures in the cylinder, as larger quantities of heat are released in a narrow crank angle window. These higher temperatures generated during stronger premixed spikes tend to produce higher levels of NO [53, 54]. Beyond the cycles shown here, the 2 Second and 5 Second sweeps do increase in premixed intensity. Their peak levels are much lower, however, and they occur when there is significantly less oxygen in the cylinder, which leads to lower NO emissions.

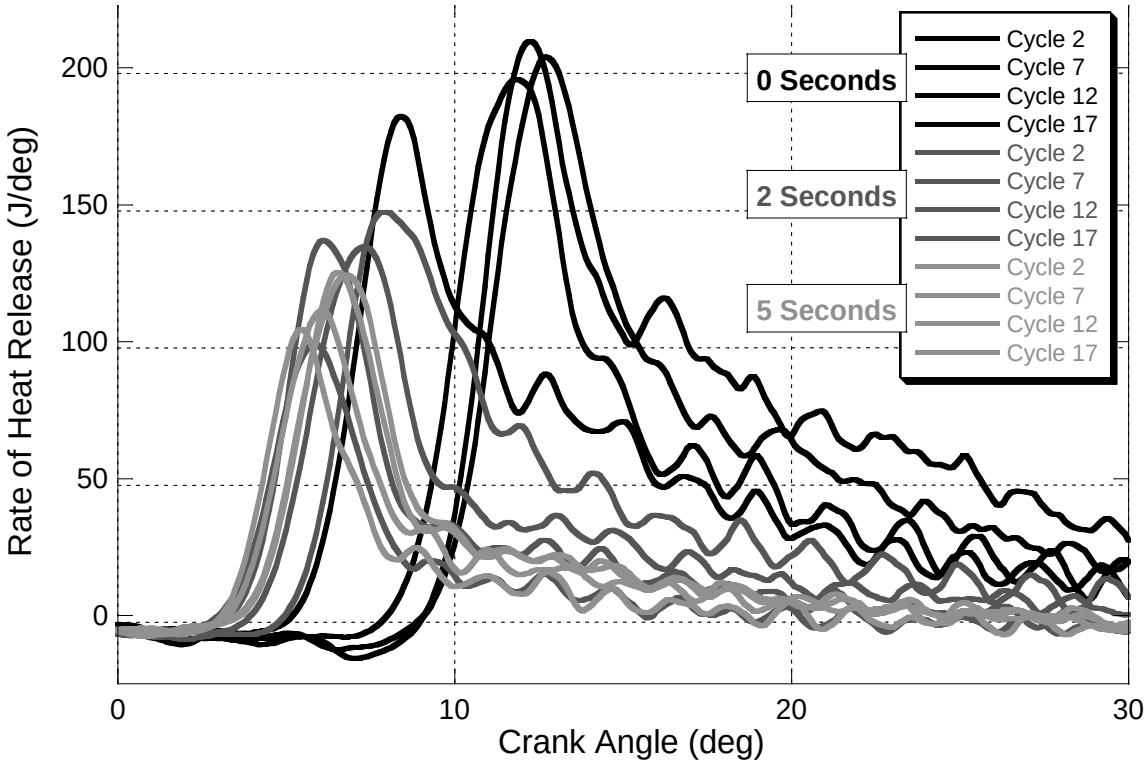

Figure 7.27: Rate of Heat Release for Four Cycles Near Beginning of 0 Second, 2 Second, and 5 Second Transient Load Sweeps from 1 to 9 Bar BMEP at 2000 rpm

NO Emissions and Localized In-Cylinder Conditions

The influence of spatially-resolved in-cylinder conditions undoubtedly has a large impact on NO emissions. Changing fuel injection parameters, in-cylinder gas constituents, and combustion characteristics will significantly influence how combustion proceeds in the cylinder. This experimental technique has no way to account for spatial resolution in the cylinder, and further simulation work is necessary to quantify its effect on NO production.

7.2.10 Particulate Emissions

Particulate values are provided at 10 Hz by a device that has a response time of 200 ms, which is on the order of 3 engine cycles at 2000 rpm. This adds a significant lag to the instrument and allows mixing of the sample, which distorts the reading enough so that it is impossible to link a particular particulate measurement to a specific cycle. The data can be analyzed, however, to understand the trends of particulate emissions that occur during a transient load sweep.

Particulate formation is a very complicated process that is highly dependent upon spatially-resolved in-cylinder conditions. While these variations cannot be quantified with the experimental technique, a number of different metrics are measured that significantly influence particulate emissions, such as: injection parameters, air/fuel ratio, the quantity of stoichiometric combustion products, and combustion characteristics.

Figure 7.28 shows the particulate emissions for all three sweeps. Particulate concentrations before and after the transient load sweep are very similar for all three cases. Large variances occur during the transient load sweep, however. A significant spike in particulates is measured upon the onset of the transient in the 0 Second case. The magnitude of the peak concentration is roughly 30 times greater than the initial steady-state particulate level. At the beginning of the 0 Second sweep, the injection

pressure increases sharply, as shown in Figure 7.25. This tends to decrease particulate emissions [55, 56]. Some particulates may be formed, however, if the increased injection pressure is causing liquid fuel impingement on the piston surface.

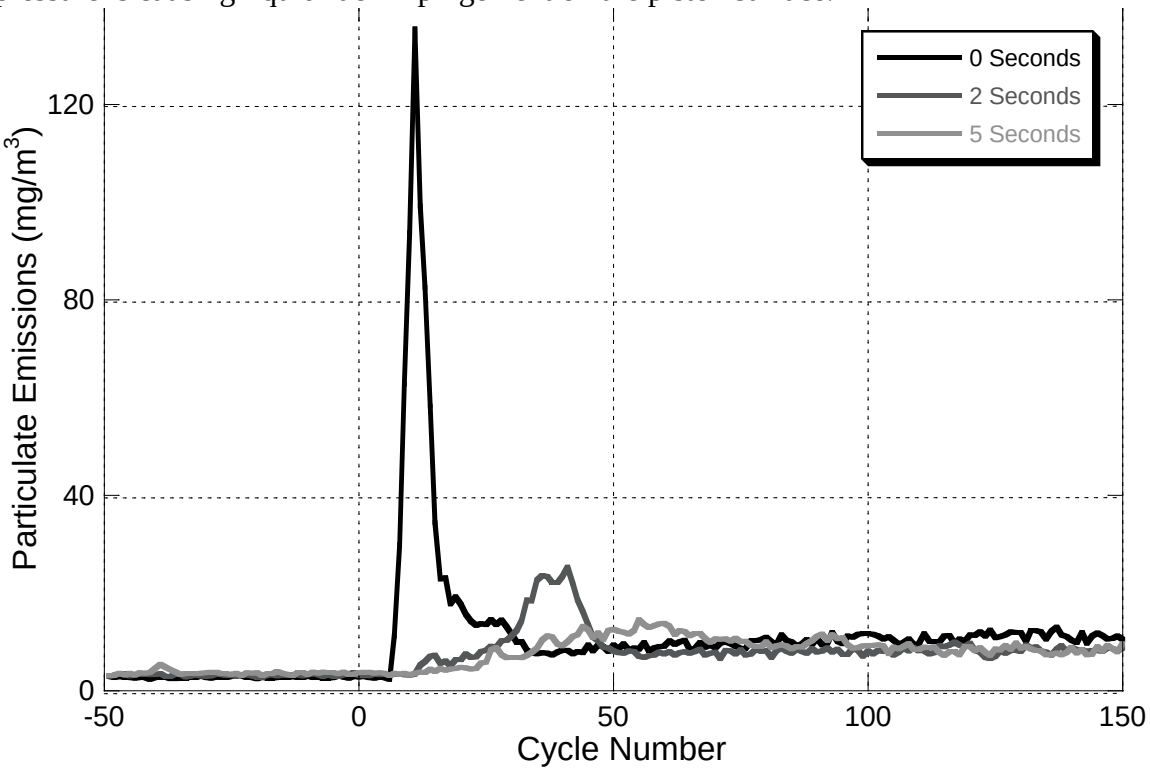

Figure 7.28: Particulate Measurement during Transient Load Sweep from 1 to 9 Bar BMEP at 2000 rpm

The 0 Second load sweep experiences a few extremely low air/fuel ratios, as shown in Figure 7.13, at the onset of the transient due to an overshoot in the fueling rate. One cycle in particular has an air/fuel ratio of 14.8, a level that is so near stoichiometric that it undoubtedly produces a significant level of particulate.

Excessively high manifold pressure ratios could also contribute to particulate formation if internal residual levels are high. The manifold pressure ratios throughout the sweeps are shown in Figure 7.9. In the 0 Second sweep, the manifold pressure ratio during the valve overlap period increases from 1.08 to over 1.8 in just five cycles. But considering that the percentage of stoichiometric combustion products trapped in the cylinder goes down upon the onset of the transient as shown in Figure 7.7, the effect of

increased internal residual is minimal and does not impact particulate formation during this transient process.

Combustion prior to the 0 Second sweep is purely premixed. When the load sweep begins, the premixed combustion becomes more intense. It is during this period of the sweep that the large spike in particulate emissions occurs. Premixed combustion does not produce such large levels of particulate and therefore the combustion characteristics do not contribute to this burst of particulate.

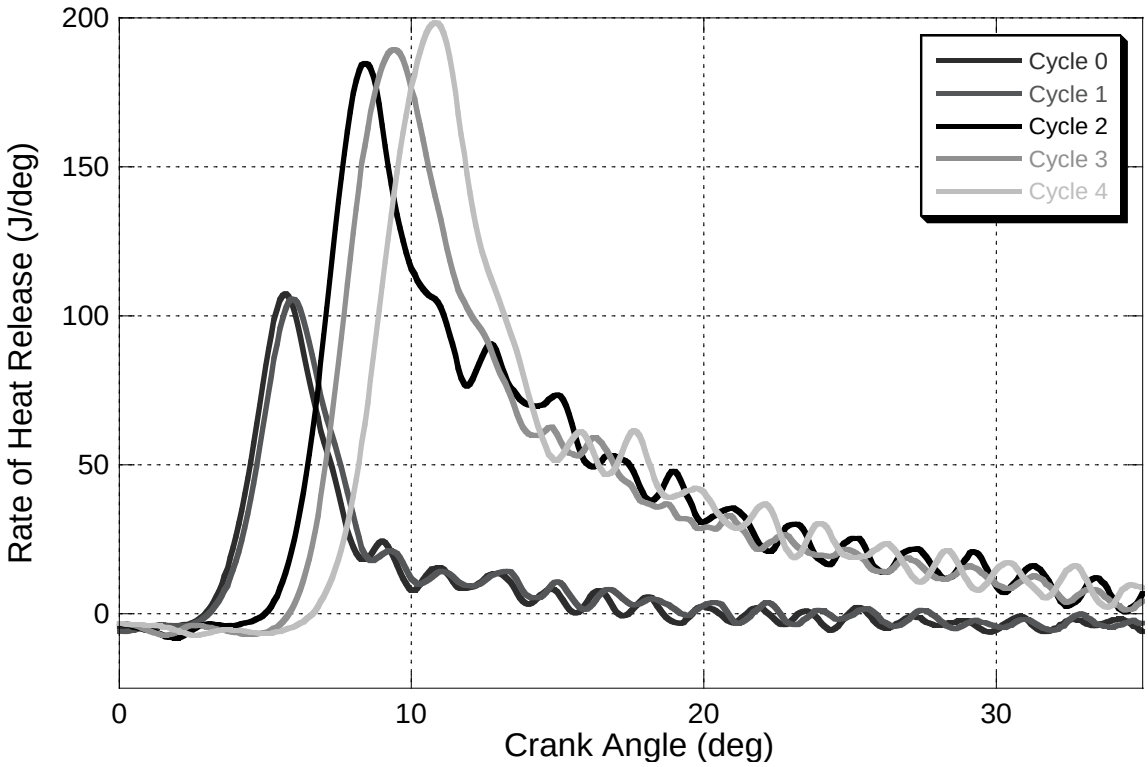

Figure 7.29: Rate of Heat Release for Five Cycles at the Beginning of the 0 Second Transient Load Sweep from 1 to 9 Bar BMEP at 2000 rpm

The heat release process for cycle 2, the richest combustion cycle, is examined carefully because it differs so significantly from the other cycles in this load sweep. The heat release for this cycle (black line), as well as the two preceding and following it, is shown in Figure 7.29. The injection for cycle 2 is 10 degrees longer than the cycles that precede it and has a combustion duration of 26.5º, which is 5 degrees longer than any

other cycle. When coupled with the low air/fuel ratio of 14.8, these three characteristics suggest that this combustion cycle very likely produces a large amount of particulate.

The 2 Second transient experiences a 25.4 mg/m^3 hump in particulate emissions that begins around cycle 25 in Figure 7.28. Fuel injection pressures and timings near this point do not act in ways that would produce this hump. The percentage of stoichiometric combustion products during this part of the transient are not changing significantly and probably do not cause the particulate hump. Combustion during this part of the transient is almost completely premixed and does not exhibit the characteristics of a combustion cycle that produces significant amounts of particulate. Of the metrics quantified by this experimental technique, the only one that is changing in ways that contribute to larger particulate emissions is air/fuel ratio. The lowest air/fuel ratio experienced in this sweep is 17.7 at cycle 32 and is probably be the root cause of the particulate hump.

A small 14.6 mg/m^3 hump is present in the 5 Second case around cycle 50 is discernable. Examination of the fuel injection parameters at this point in the load sweep reveals no characteristics that would cause larger particulate emissions. Combustion events around this cycle are mostly premixed with a small proportion of diffusion burning, and probably do not contribute to the particulate hump. The air/fuel ratios fall gradually throughout the transient sweep, and around this point are around 30; alone this is not a condition that would produce significant particulates. During this same period, however, the proportion of stoichiometric combustion products reaches around 10% of the cylinder mass, as shown in Figure 7.7. The combination of the falling air/fuel ratios and the high mass percentage of stoichiometric combustion products probably are the cause of the small particulate hump in the 5 second case.

7.3 Constant-Speed Load Sweep Summary

Significant differences are observed when the engine experiences constant-speed load sweeps with different rates of change of engine command. The variance that causes by far the largest impact is the overshooting of the mass of fuel injected in the 0 Second load sweep. The presence of this one cycle significantly impacts the combustion and emissions process throughout the sweep. The 2 Second and 5 Second sweeps experienced no such phenomenon and fuel injection masses behave as the engine desires.

The quantity of stoichiometric combustion products trapped in the cylinder in the 0 Second case goes to very low levels because of the closing of the EGR valve at the onset of the load sweep, before opening back up later in the transient. The 2 Second case also closes the EGR valve, but not nearly as quickly or as far as in the 0 Second sweep. The net result is that the proportion of stoichiometric combustion products remains relatively constant throughout the 2 Second sweep. In the 5 Second case, the EGR valve opens at the onset of the transient, causing the percentage of stoichiometric combustion products to double before settling down to the final steady-state value.

Air mass trapped in the cylinder is governed by the intake manifold pressure and the behavior of the EGR valve. In the 0 Second and 2 Second sweeps, intake manifold pressure dominates the first part of the transient as air masses increase, but then EGR valve opening displaces fresh air flow and reduces the trapped air masses by the end of the sweep. In the 5 Second sweep, air ingested from the lean exhaust gases through the open EGR valve augments the amount of total trapped air during the first part of the cycle. Once the EGR valve begins to close, trapped air masses decrease and are then controlled by intake manifold pressures.

Air/fuel ratios in the 0 Second sweep plunge sharply at the beginning of the transient to levels far below what is normally observed due to the excessive mass of fuel injected. As the turbocharger builds boost and the fuel injection system follows demand

values, the air/fuel ratio settles to its final value. Air/fuel ratios in the 2 Second case fall more gradually, with only a small dip in air/fuel ratio below the final value that is present due to turbocharger lag. The 5 Second sweep air/fuel ratio falls smoothly from its initial value to its final value, demonstrating that the air charging system is able to provide the proper amount of air for each cycle.

Combustion events transition significantly throughout the transient sweep. Initially the engine is experiencing completely premixed combustion. At the end, a combination of premixed and diffusion burning is present. The 0 Second sweep makes the transition the quickest, with the premixed spike doubling in intensity and retarding in timing due to later injection timings and relatively cool in-cylinder conditions. Slowly as the chamber begins to warm, ignition delays decrease, the intensity of the premixed spike decreases, and diffusion burning grows in strength. The same type of transition occurs during the 2 Second sweep, but over more cycles and with less intense premixed combustion. During the 5 Second sweep, the strength of the premixed burn increases slightly for a few cycles, and then simultaneously diffusion burning appears and grows in intensity from cycle to cycle.

The 0 Second sweep experiences about 25 cycles with abnormally high NO emissions. Intense premixed combustion, coupled with a combustion chamber devoid of stoichiometric combustion products and flush with oxygen contribute to the high levels of NO. Both the 2 Second and 5 Second cases transitioned smoothly from one condition to another, with the amount of NO produced strongly a function of the amount of stoichiometric combustion products in the cylinder.

Particulate emissions during the 0 Second sweep experienced a large spike about 30 times greater than the steady-state condition. The presence of this burst of particulate is attributed to a few, maybe even one, cycle of combustion with near-stoichiometric air/fuel ratios and lengthened combustion durations. The 2 Second case produces a particulate hump that is one-fifth the size of the 0 Second spike. Low air/fuel ratios are

probably the cause. The 5 Second sweep produces a very small hump of particulates that occur probably because of lower air/fuel ratios and the presence of a significant amount of stoichiometric combustion products.

CHAPTER 8

CYCLE-RESOLVED MEASUREMENTS DURING IN-VEHICLE TRANSIENT OPERATION

The experimental technique presented in this study is used to analyze engine behavior during realistic in-vehicle transients. This is accomplished by using the test cell's engine-in-the-loop capability, where a vehicle model and a driver model are linked to the test cell and run in parallel with the system. The engine therefore experiences equivalent driver inputs and speed and load combinations to what it encounters when operating in an actual vehicle. This chapter is broken into three sections: a description of the experimental procedure, a discussion of the results, and presentation of the summary.

8.1 In-Vehicle Transient Operation Experimental Procedure

The engine is able to be tested as though it is in a vehicle by using the engine-in-the-loop capability [40]. The vehicle model used simulates an AM General High-Mobility Multipurpose Wheeled Vehicle (HMMWV) 1097 A2 4x4. Known as the Hummer, this vehicle has been used by the United States Military for personnel and light cargo transport for over 20 years. The transmission is a four-speed automatic with a lockup torque converter. Vehicle mass is 5112 kg, which represents a fully-loaded condition. Frontal area is 3.5 m^2 and the aerodynamic drag coefficient is 0.7.

This vehicle is operated over an FTP 75 driving cycle, which simulates an urban route with frequent stops. The average speed for the driving cycle is 31.5 km/hr and the maximum speed during the cycle is 91.2 km/hr. This cycle is used by the US EPA for the emissions certification of light-duty vehicles. Figure 8.1 demonstrates the first 1370 seconds of the FTP 75. The portion of the test not shown involves repeating the speed profiles from the first 505 seconds.

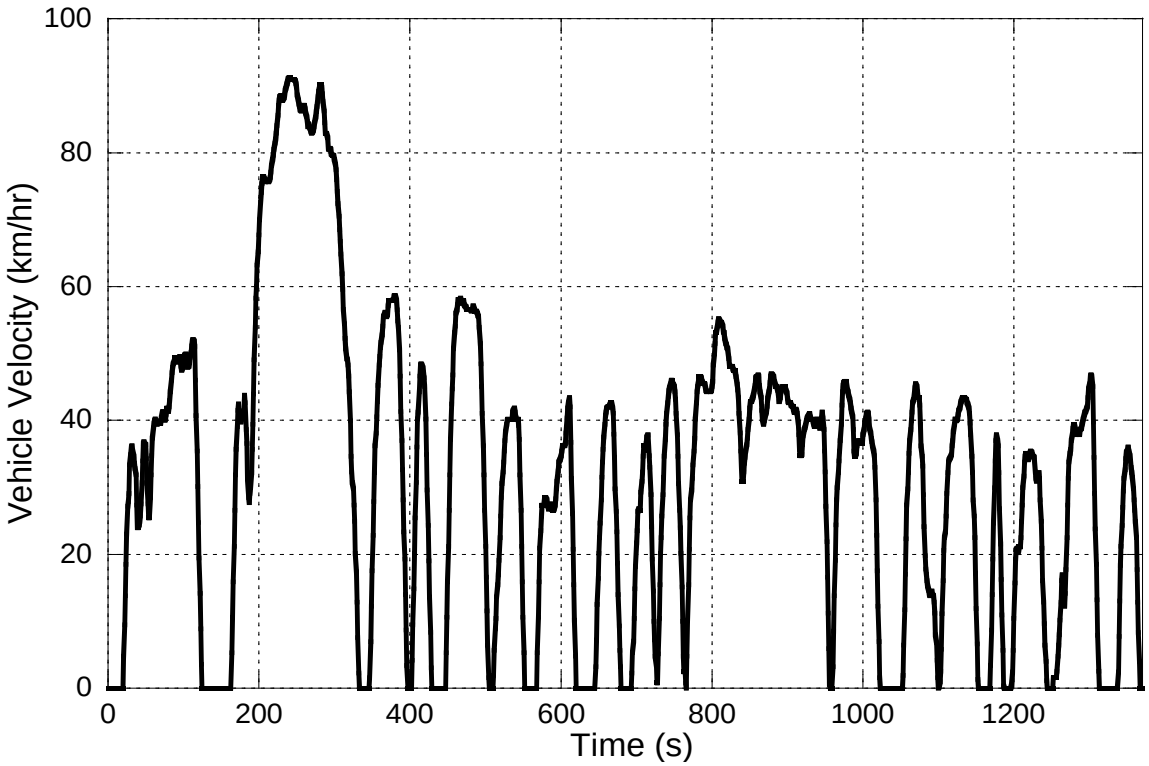

Figure 8.1: First 1370 Seconds of FTP 75 Driving Cycle

8.2 In-Vehicle Transient Operation Experimental Results

While data has been collected and analyzed over the entire cycle, the discussion addresses the engine behavior over the first two velocity profiles of the FTP 75. These profiles encompass the first 340 seconds of the driving cycle and contain the most aggressive portions of the cycle. The data is further broken down into sections that represent a specific kind of vehicle behavior, namely accelerations. Since steady-state

engine operation is discussed at length in Chapter 6, the portions of the drive cycle that exhibit near steady-state conditions are not discussed in this document unless unexpected behavior is observed. Vehicle decelerations are not examined in this document because fueling rates and emissions go to near-zero values.

The discussed accelerations are divided into three categories: 1. Accelerations from zero vehicle velocity, 2. Accelerations from moderate vehicle velocity, and 3. Accelerations from high vehicle velocity. Two accelerations from zero vehicle velocity are identified and discussed: between cycles 160-310 and between cycles 1640-1790. Two accelerations that begin at a moderate vehicle velocity are also identified; one that encompasses cycles 540-1340 and another that spans cycles 1920-2320. One acceleration that begins at high vehicle velocity is studied and it occurs between cycles 2350 and 2950. These periods in the driving cycle are demonstrated in Figure 8.2.

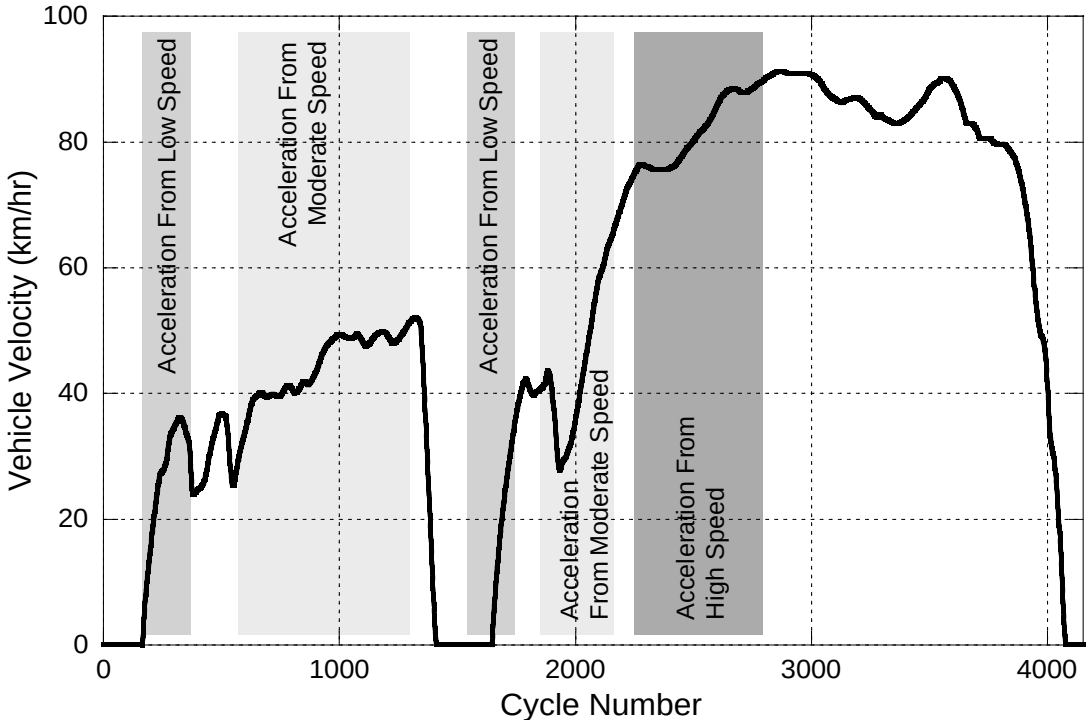

Figure 8.2: Portions of Accelerations during FTP 75 that are Examined in Results Discussion

To fully characterize the accelerations, more information about engine and vehicle behavior prior to the event is necessary. The accelerations from zero velocity are essentially standing starts to a moderate speed beginning with the vehicle in gear. Therefore prior to acceleration the engine is near idle speeds and has a load on it from the drag of the torque converter. The acceleration between cycles 160-310 has an average intensity of 3.4 km/hr/s and the one between cycles 1640-1790 has an average intensity of 4.4 km/hr/s. The two accelerations from a moderate vehicle velocity occur after a vehicle deceleration; therefore the beginning engine speed is low and the initial load is zero. This kind of acceleration simulates the transition of a vehicle from coasting-down at residential speeds to speeding-up to near highway speeds. One of the accelerations is very mild as the vehicle speeds up at a rate of 0.36 km/hr/s; the second is more aggressive at 2.1 km/hr/s. The final acceleration investigated replicates acceleration at highway speeds. Initial engine speeds and loads are mid-range, and the overall acceleration rate is 0.43 km/hr/s.

Table 8.1: Characteristics of Investigated FTP 75 Accelerations

Cycles	Vehicle Velocity (km/hr)		Vehicle Velocity Change Prior to Acceleration	Initial Engine Speed (rpm)	Initial Load (bar BMEP)	Elapsed Time (s)
	Initial	Final				
160-310	0	34	None, Vehicle is Stationary	750	2.1	10.0
1640-1790	0	44	None, Vehicle is Stationary	749	2.2	10.2
540-1340	28	50	Decreasing	774	0	60.9
1920-2320	32	76	Decreasing	935	0	21.4
2350-2950	76	91	None, Vehicle is Moving at Constant Velocity	1799	4.5	34.6

To reduce the number of graphs presented, data from similar accelerations are consolidated onto one graph. Specifically, the accelerations from zero velocity and are placed on one graph and referred to in the text and on the graphs as, “Low-Intensity from Zero Vehicle Velocity” between cycles 160-310 and “High-Intensity from Zero Vehicle Velocity” between cycles 1640-1790. Data from the remaining three accelerations are placed on one graph and the accelerations between cycles 540-1340 is referred to as “Low-Intensity from Moderate Vehicle Velocity”, between cycles 1920-2320 is called “High-Intensity from Moderate Vehicle Velocity”, and between cycles 2350-2950 is denoted “Low-Intensity from High Vehicle Velocity”. These three final accelerations all encompass a different number of cycles, and are graphed together with the same x-axis. For the two accelerations that encompass a fewer number of cycles, no data is reported for the cycles after which the defined accelerations have ended.

8.2.1 Engine Command

Engine command quantifies the driver demand for vehicle velocity change. Figure 8.3 shows the engine command for the accelerations from zero vehicle velocity. The engine command for the high-intensity acceleration from zero goes from 14% to 100% in the span of 15 cycles and remains wide-open for 30 cycles. From this point, the engine command drops gradually down to zero by the end of the acceleration. Engine command for the low-intensity acceleration from zero goes from the initial value of 14% up to about 60% at cycle 180 before dropping off to 0% around cycle 250 before rising up to 100% and back down to 0% by the end of the acceleration.

Figure 8.4 demonstrates the engine command for the accelerations when the vehicle is initially moving. The two accelerations from moderate velocity both jump from 10% to 100% in the span of 12 cycles and remain there for about 22 cycles. From there, the low-intensity acceleration drops to average around 20% for the remainder of

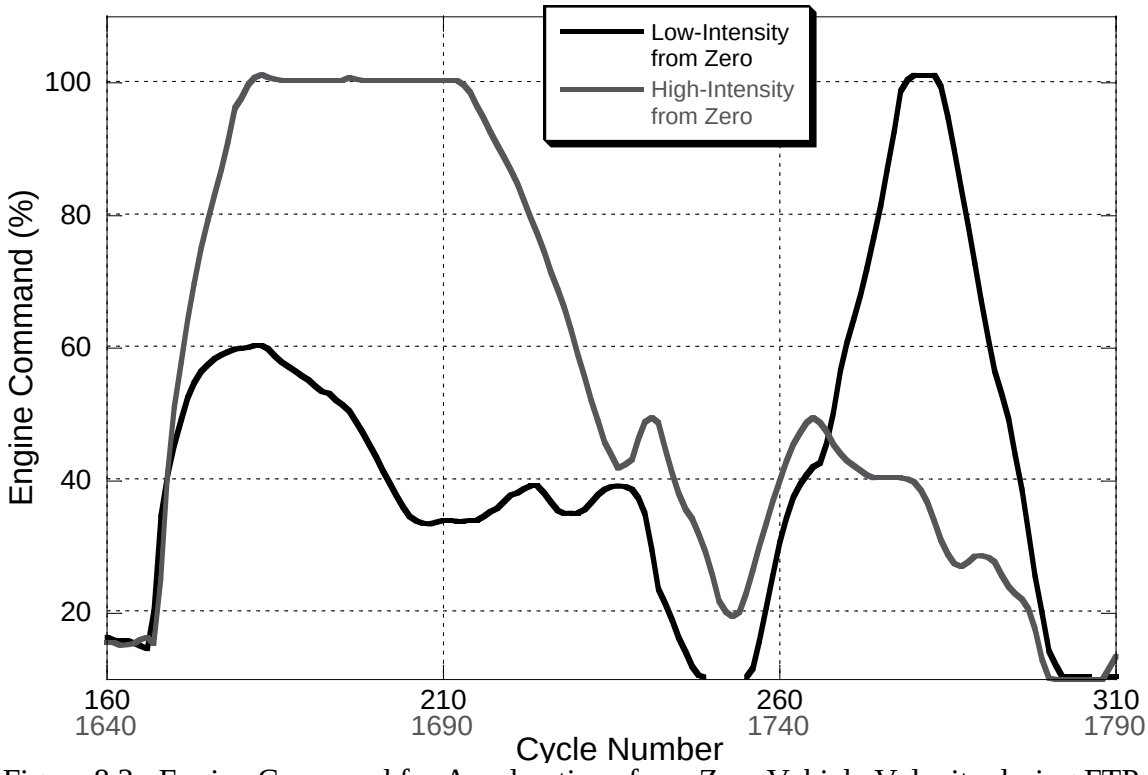

Figure 8.3: Engine Command for Accelerations from Zero Vehicle Velocity during FTP 75

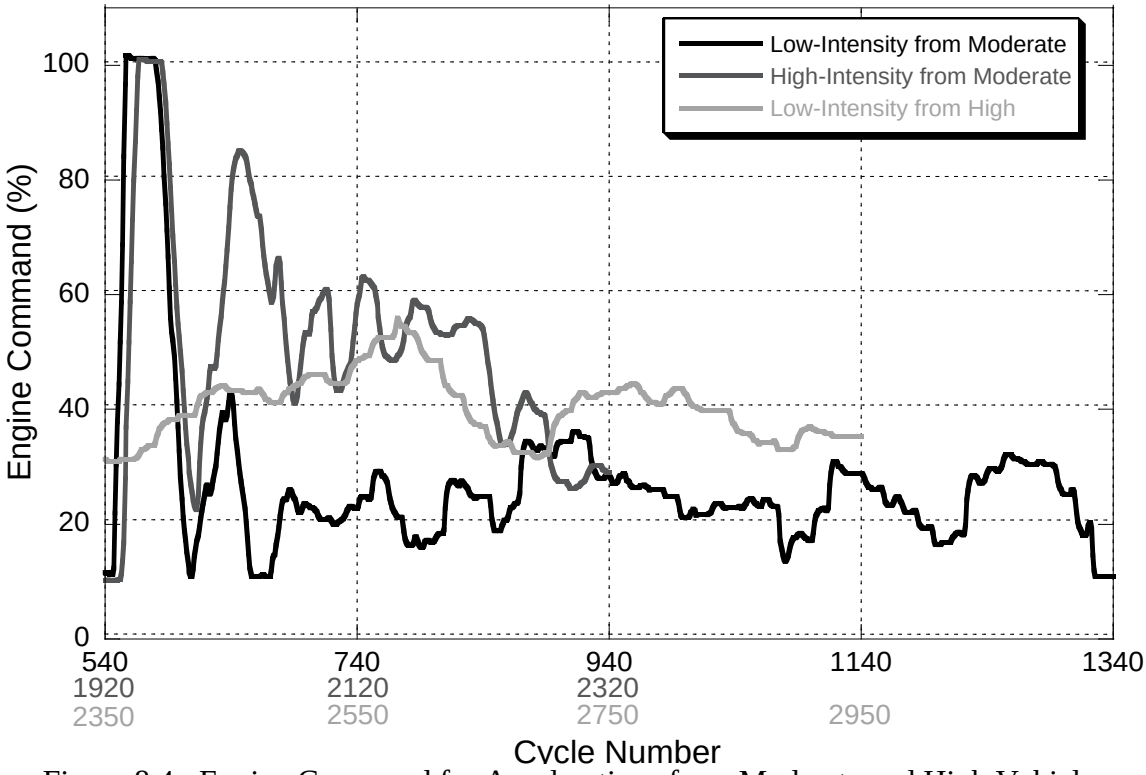

Figure 8.4: Engine Command for Accelerations from Moderate and High Vehicle Velocities during FTP 75

the event and the high-intensity acceleration decreases to average 50% for the rest of the speed increase. The engine command for the low-intensity acceleration from high initial vehicle velocity begins at 30% and moves gradually upward to around 55% before dropping down to average about 40% until the acceleration is over.

8.2.2 Engine Speed, Torque, and Power

The engine responds to changes in command by generating torque and changing speed, and the combination of these two is engine power. The speed, torque, and power response of the engine during the accelerations from zero vehicle velocity are displayed in Figure 8.5, Figure 8.6, and Figure 8.7, respectively. Engine speed and torque for the two cases move up gradually together for the first 40 cycles of the accelerations. From there, the two lines diverge, as the high-intensity acceleration experiences higher speeds and torques due to the larger engine command. The behavior of the engine power output is generally a greater function of engine torque output, as these two graphs are nearly identical in the relative motion of the two lines with some magnitude variations occurring due to the influence of engine speed.

Figure 8.8, Figure 8.9, and Figure 8.10 demonstrate the engine speed, torque, and power during the accelerations that occur from moderate and high velocities. During the first portion of the accelerations from moderate velocities, the first 80 cycles are nearly identical. Engine speed spikes up immediately, but torque remains low for about 20 cycles as the engine's speed increases to that of the transmission. After this initial period, the lines diverge as the more intense acceleration experiences speeds, torques, and powers that are much higher than the low-intensity acceleration. The acceleration at high speeds experiences consistently-high engine speeds, torques, and powers throughout. As with the accelerations from zero, power trends are more closely associated with torque behavior and in general rise and fall with the engine command.

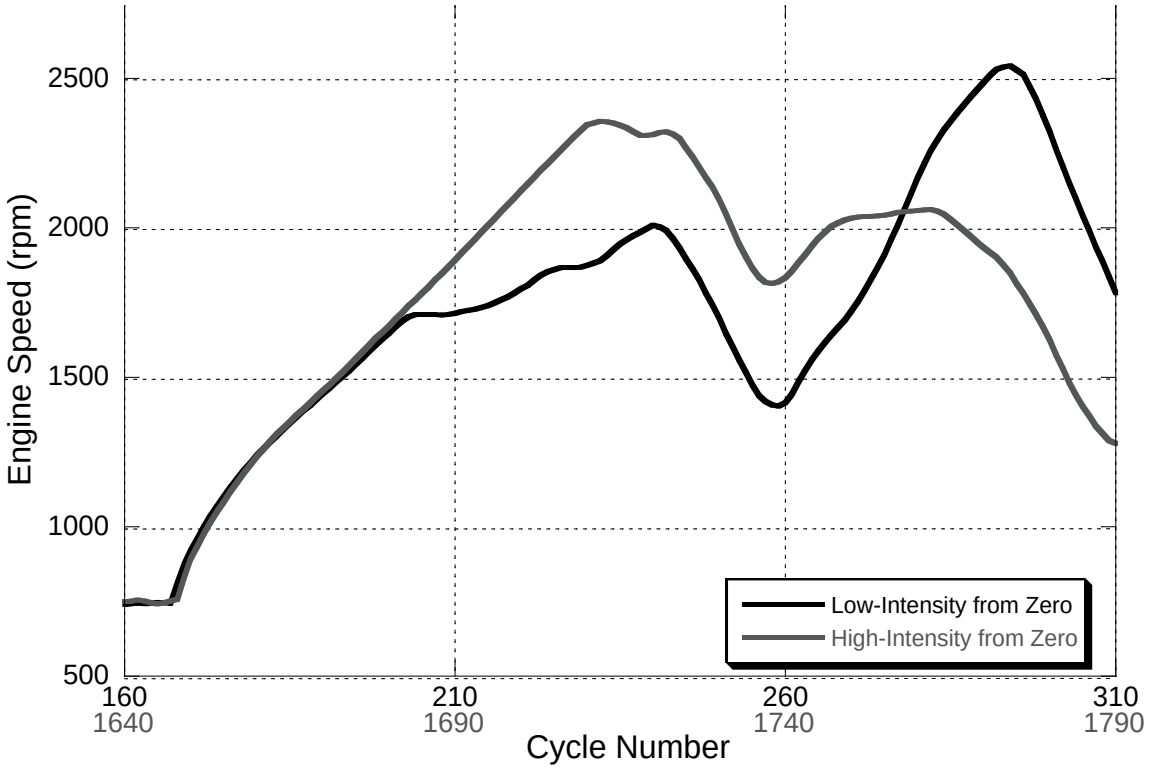

Figure 8.5: Engine Speed for Accelerations from Zero Vehicle Velocity during FTP 75

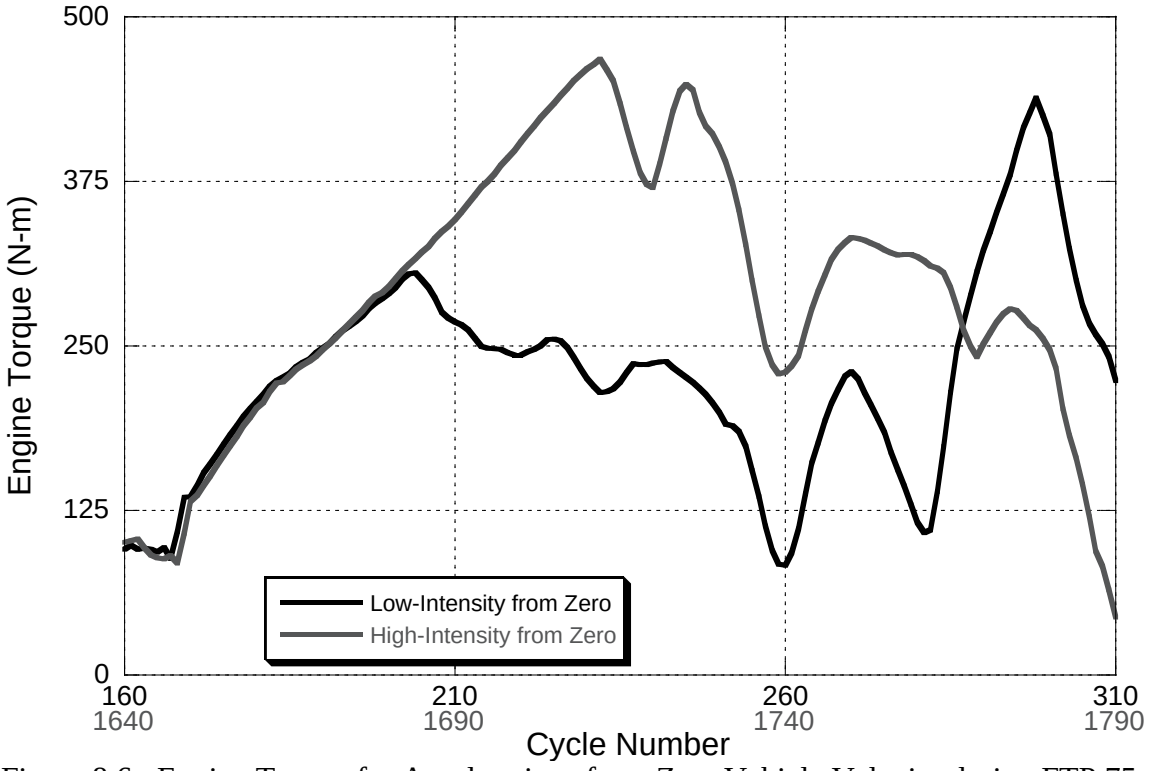

Figure 8.6: Engine Torque for Accelerations from Zero Vehicle Velocity during FTP 75

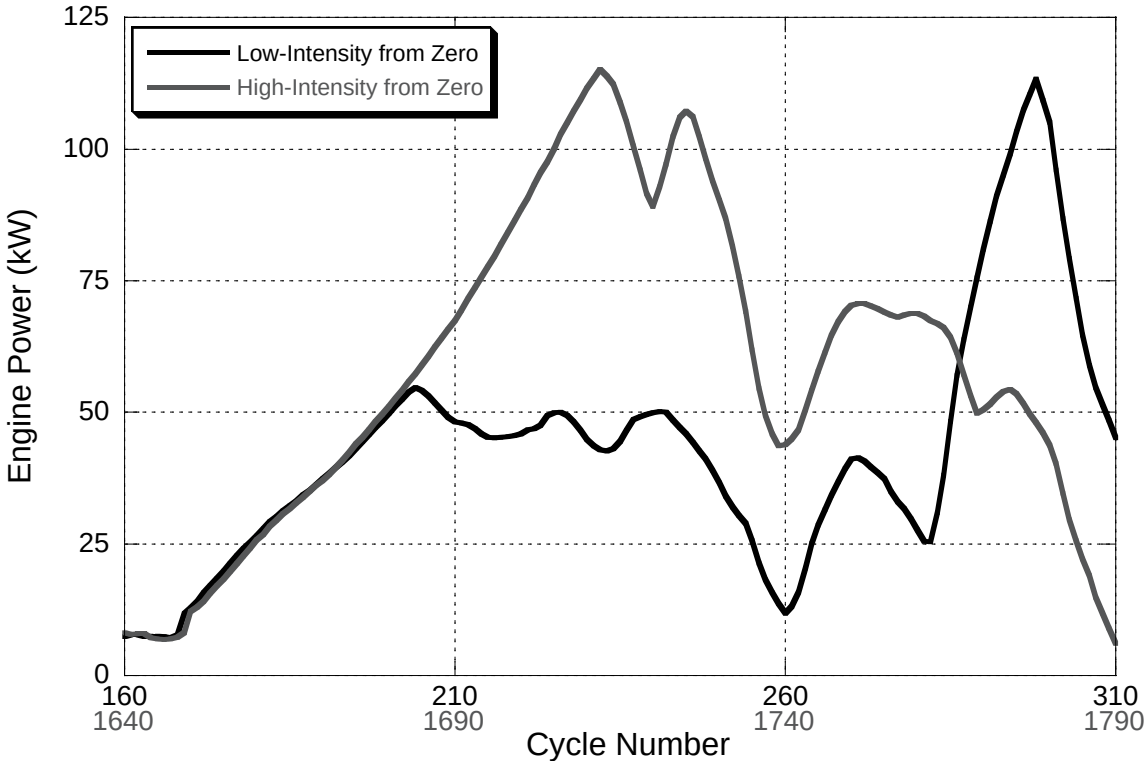

Figure 8.7: Engine Power for Accelerations from Zero Vehicle Velocity during FTP 75

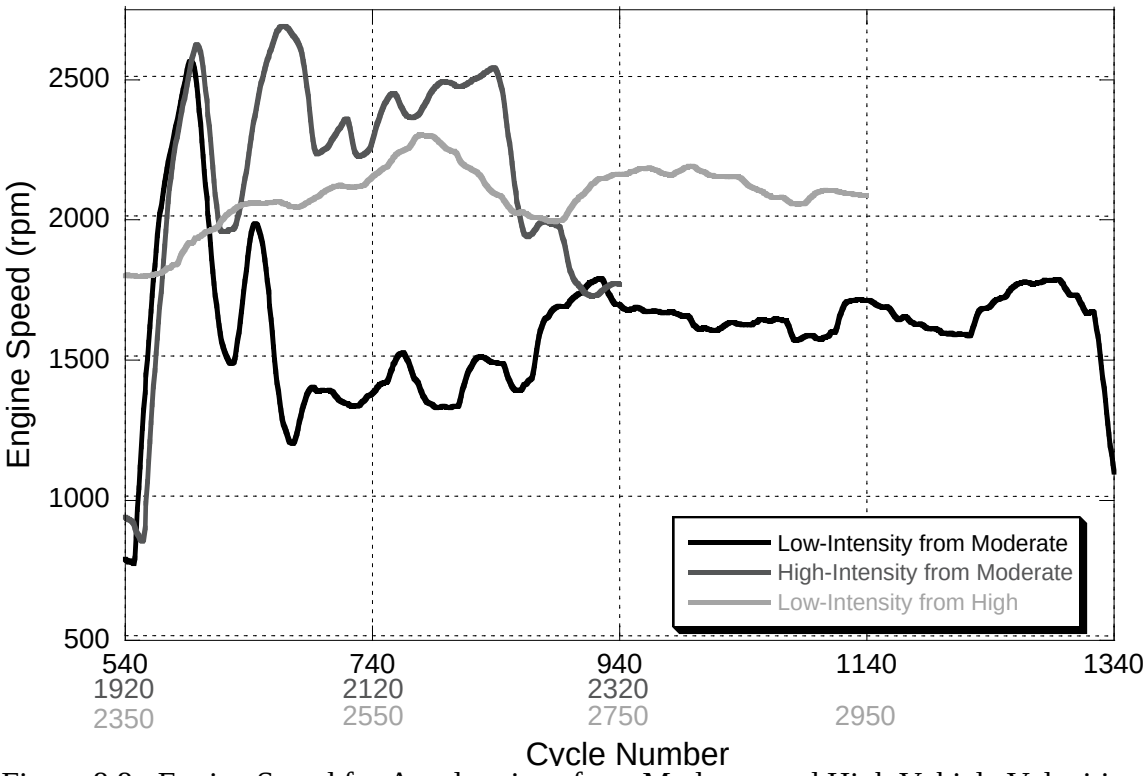

Figure 8.8: Engine Speed for Accelerations from Moderate and High Vehicle Velocities during FTP 75

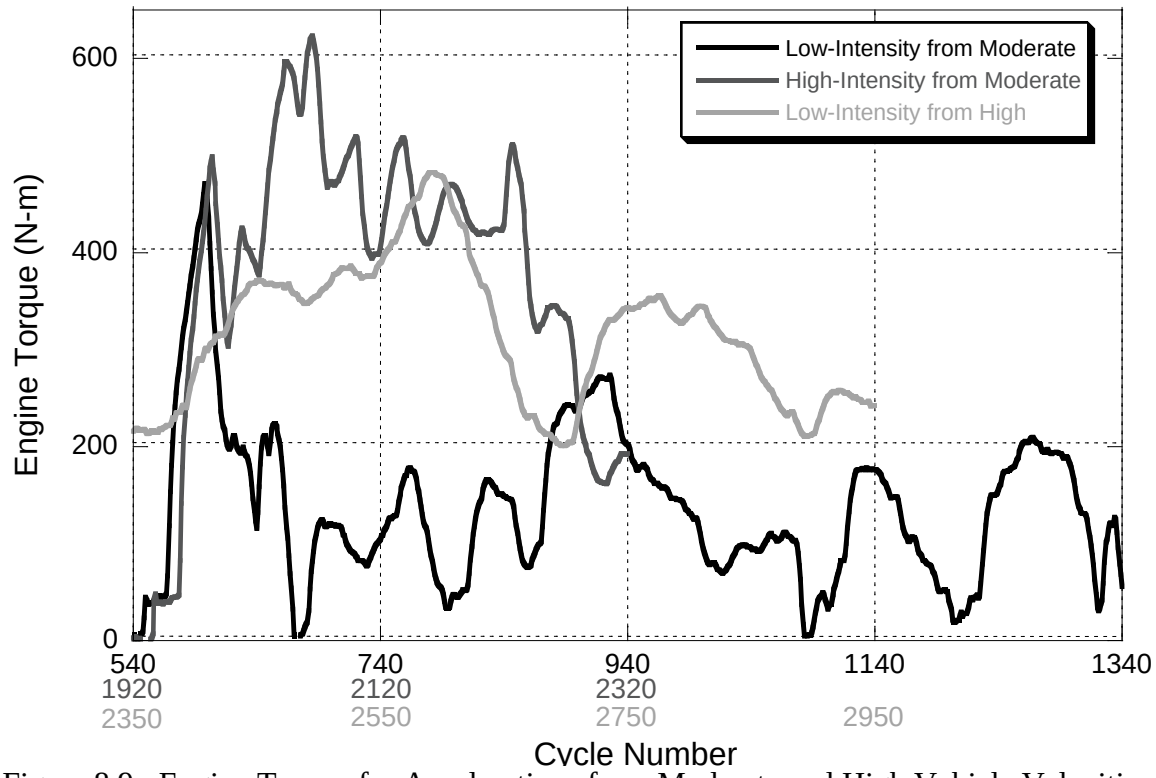

Figure 8.9: Engine Torque for Accelerations from Moderate and High Vehicle Velocities during FTP 75

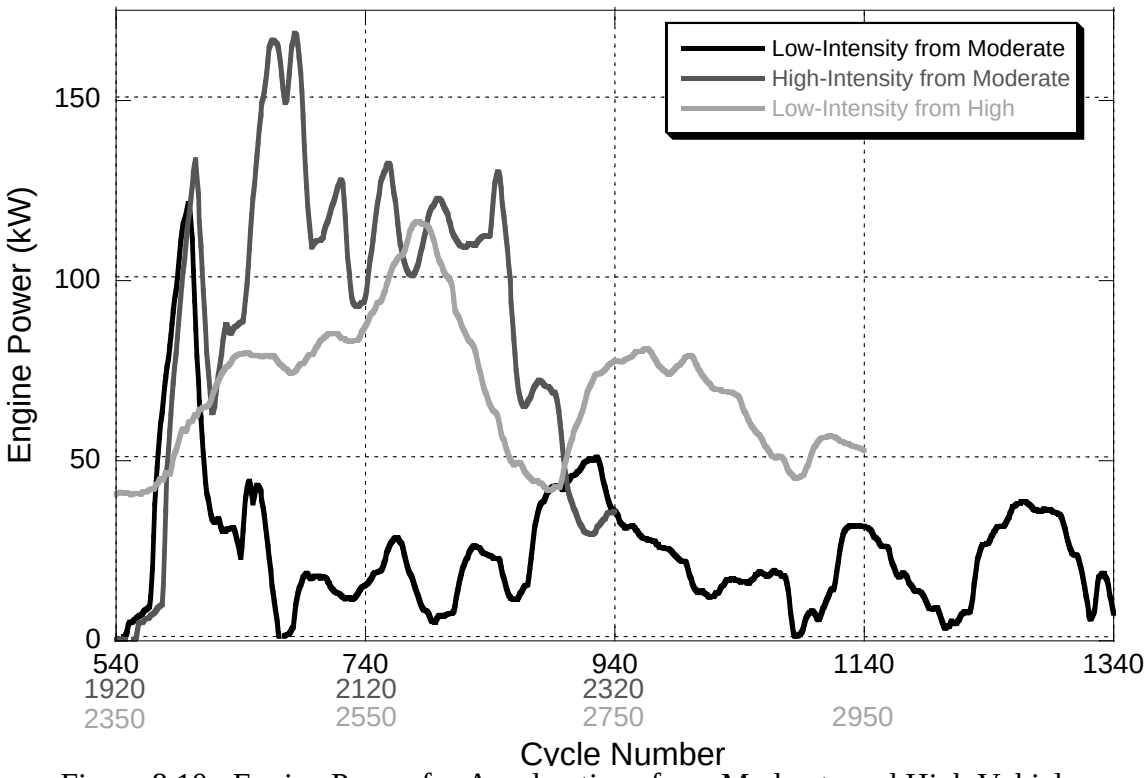

Figure 8.10: Engine Power for Accelerations from Moderate and High Vehicle Velocities during FTP 75

8.2.3 Fuel Injection Timing

Fuel injection timings and engine command for the accelerations from zero vehicle velocity are shown in Figure 8.11. The injection timings are equivalent during the periods where the engine command is increasing rapidly. This is especially evident during the first 40 cycles and between the 90th and 110th cycles. In general, the injection timing tends to be a function of engine command, and high levels of engine command have more retarded timings. The most advanced timings are around 6º before TDC and the most retarded timings are about 4º after TDC.

Behavior of the injection timing during the accelerations that occur when the vehicle is already in motion is similar to what it is during the accelerations from zero vehicle velocity. This relationship is shown in Figure 8.12, where higher engine commands have more retarded timings and vice versa.

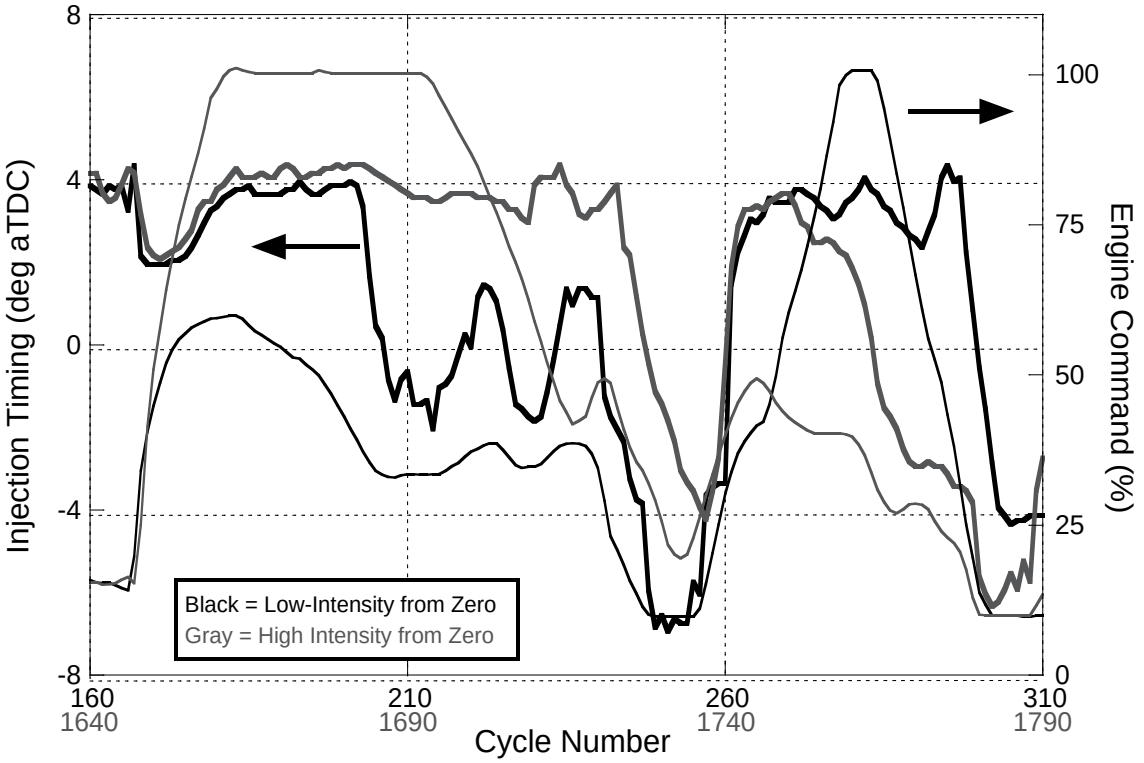

Figure 8.11: Fuel Injection Timing and Engine Command for Accelerations from Zero Vehicle Velocity during FTP 75

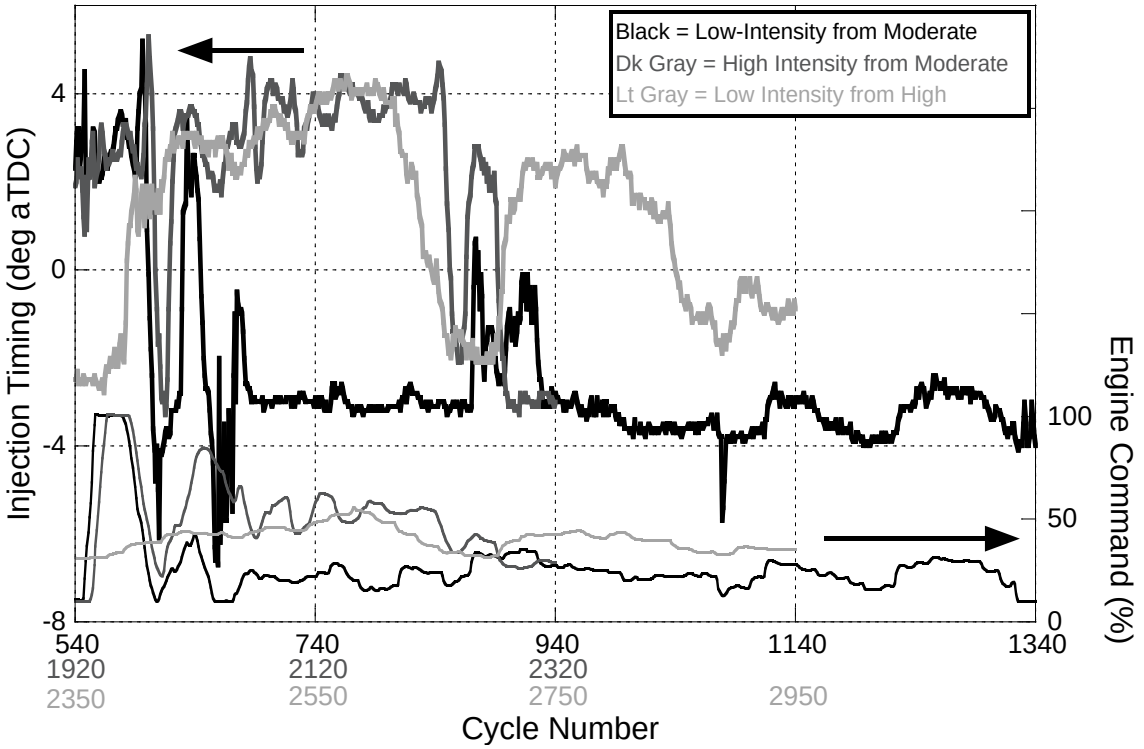

Figure 8.12: Fuel Injection Timing and Engine Command for Accelerations from Moderate and High Vehicle Velocities during FTP 75

8.2.4 Fuel Injection Pressure

Fuel injection pressure and engine command for the accelerations from zero vehicle velocity are shown in Figure 8.13 and for the accelerations from moderate and high vehicle velocities are displayed in Figure 8.14. High engine commands result in high fuel injection pressures and vice versa; this relationship is evident in both graphs. Under intense accelerations, the injection pressure does not move up as quickly as the engine command. This is visible during the beginning of the low-intensity acceleration from zero, where engine command rises from around 14% up to 100% in about 15 cycles, but fuel injection pressure takes more than 50 cycles to reach its maximum value. The shape of this injection pressure curve very closely resembles the behavior of the power curve as shown in Figure 8.7. Injection pressure is therefore governed by the amount of engine command, but its rate of increase is subject to the engine's power level.

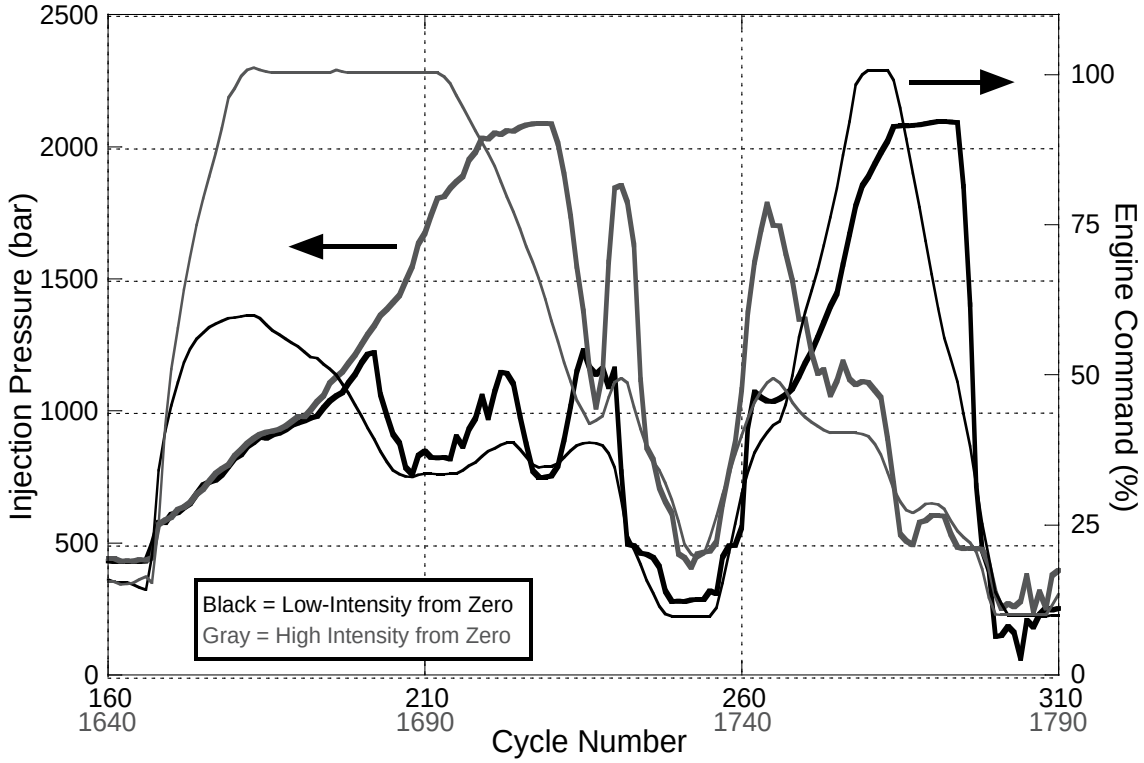

Figure 8.13: Fuel Injection Pressure and Engine Command for Accelerations from Zero Vehicle Velocity during FTP 75

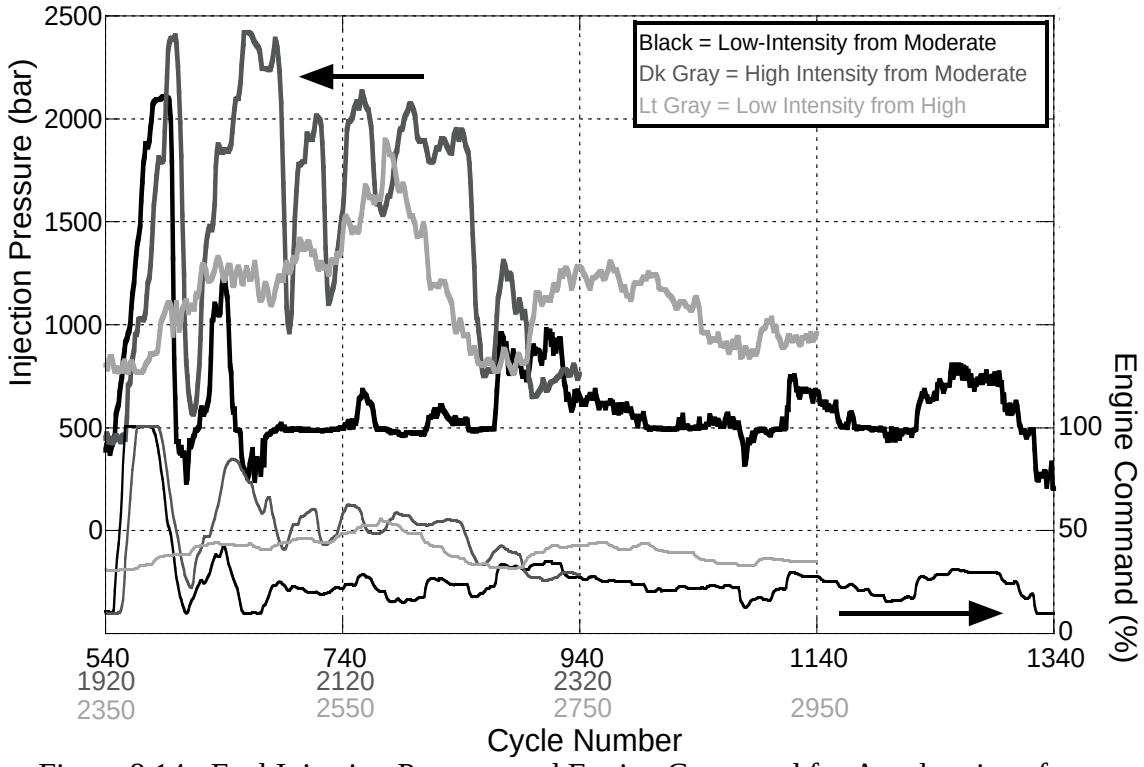

Figure 8.14: Fuel Injection Pressure and Engine Command for Accelerations from Moderate and High Vehicle Velocities during FTP 75

8.2.5 EGR Valve Position

EGR valve behavior during the accelerations from zero is shown in Figure 8.15. During the most intense portions of the accelerations, the EGR valve remains completely closed. As the engine command reduces, the EGR valve opens. As engine command drops moderately, the valve only cracks open, as in cycles 210-235 of the low-intensity acceleration from zero vehicle velocity. During this stage of relatively constant engine command, the EGR valve opens progressively. When the engine command is falling drastically, as in cycles 1690-1715 and 1760-1780 of the high-intensity acceleration from zero, the valve opens significantly.

The EGR valve position and the engine command during the accelerations from moderate and high vehicle velocities are shown in Figure 8.16. Valve behavior at these conditions are similar to those observed in Figure 8.15; with EGR valve openings taking place anytime that the engine command is reduced. The valve openings, however, are much larger during these decelerations, as the valve opens up fully on more than one occasion. The degree to which the valve opens seems to correlate well with the engine power being produced at that time. As engine power levels increase, so too does the amount that the EGR valve opens when the engine command is reduced. Periods of extended cycles when the EGR valve remains open are present during the latter portions of the low-intensity acceleration from moderate vehicle velocity and the low-intensity acceleration from high vehicle velocity. During these conditions, engine command is relatively constant, and engine behavior is more similar to steady-state. Any time a small increase in engine command is experienced, however, the EGR valve moves closed.

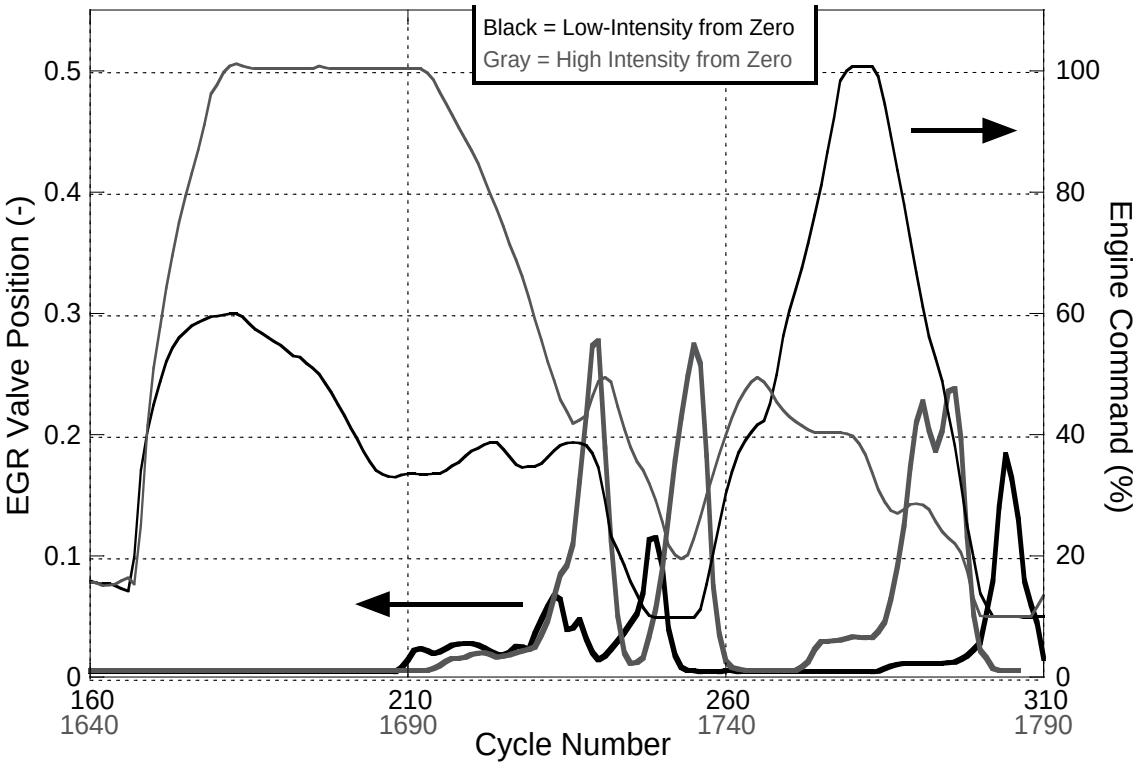

Figure 8.15: EGR Valve Position and Engine Command for Accelerations from Zero Vehicle Velocity during FTP 75

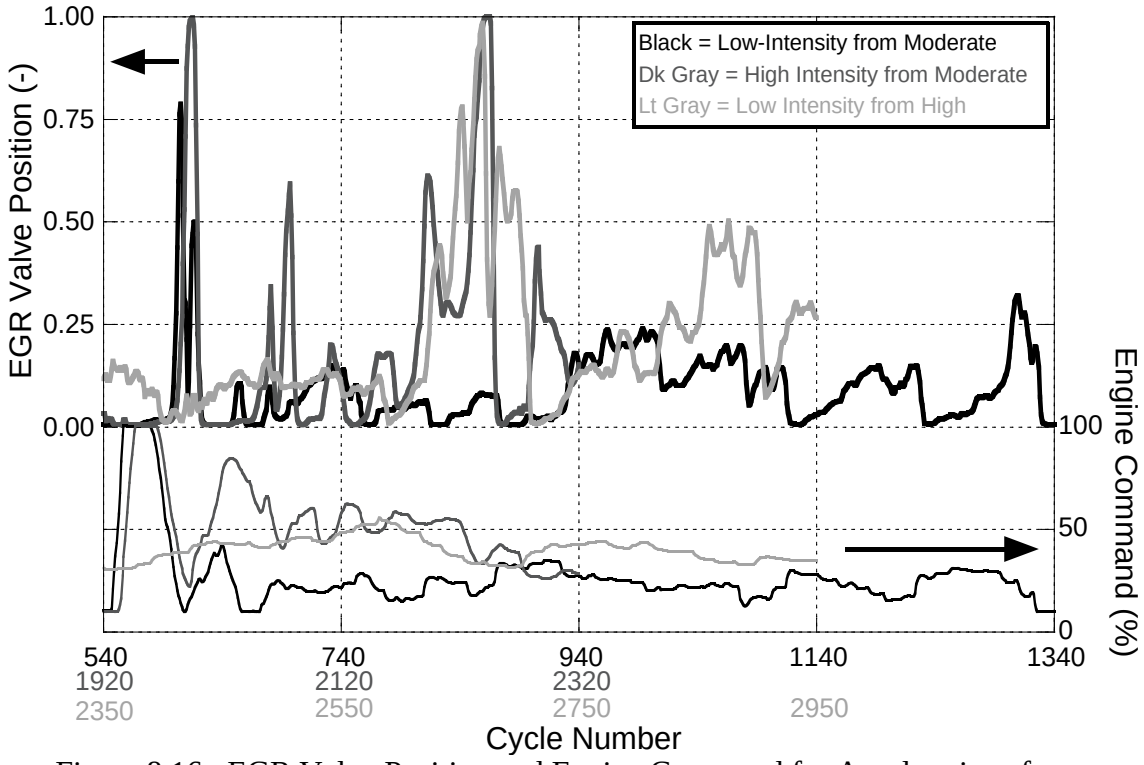

Figure 8.16: EGR Valve Position and Engine Command for Accelerations from Moderate and High Vehicle Velocities during FTP 75

8.2.6 VGT Vane Position

VGT vane position and engine command for the accelerations from zero vehicle velocity are shown in Figure 8.17. At the beginning of these intense accelerations, the VGT vanes close immediately to spin the turbocharger up faster in order to build boost. As the engine increases in speed and load, the VGT vanes gradually open up to regulate turbocharger speed and to increase its flow capacity. When engine command drops drastically and engine speed and load are relatively high, as in cycles 235, 1745, and 295 the VGT vanes open even further to reduce the back pressure on the cylinder.

Behavior of the VGT during accelerations from moderate and high vehicle velocities is similar to those described above, which is demonstrated in Figure 8.18. Higher engine speeds and torques, however, lead to closing and opening values that are more extreme than those observed in Figure 8.17

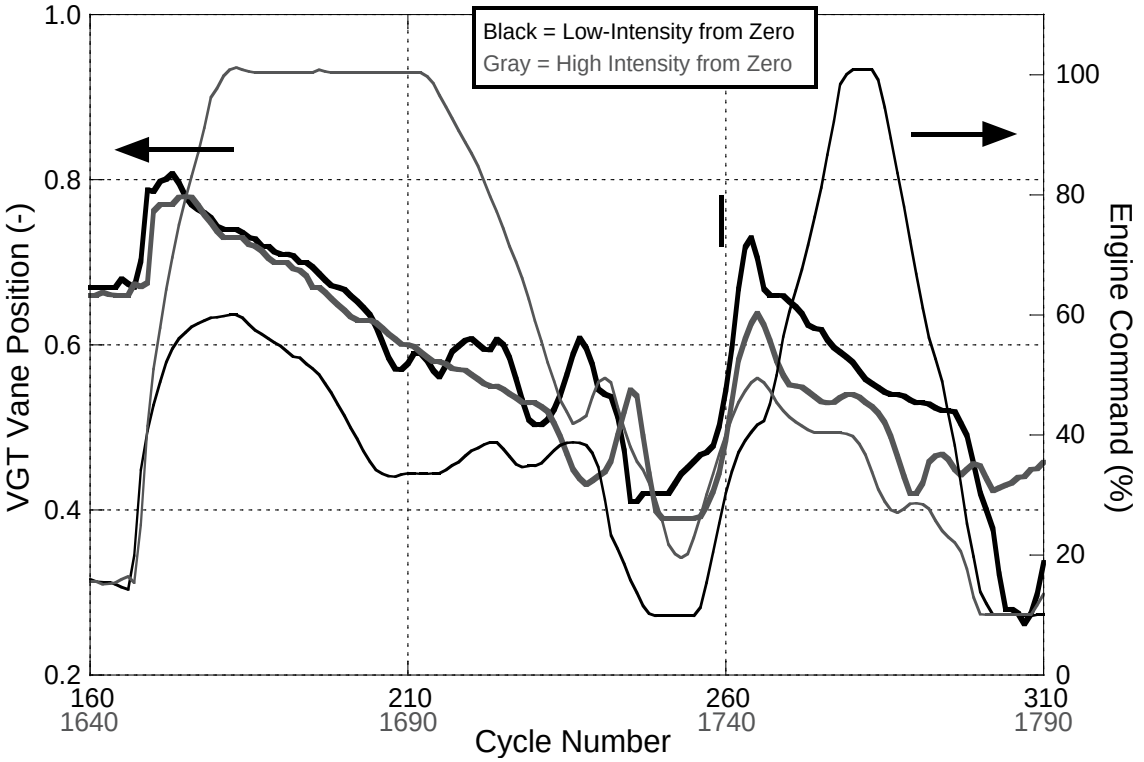

Figure 8.17: VGT Vane Position and Engine Command for Accelerations from Zero Vehicle Velocity during FTP 75

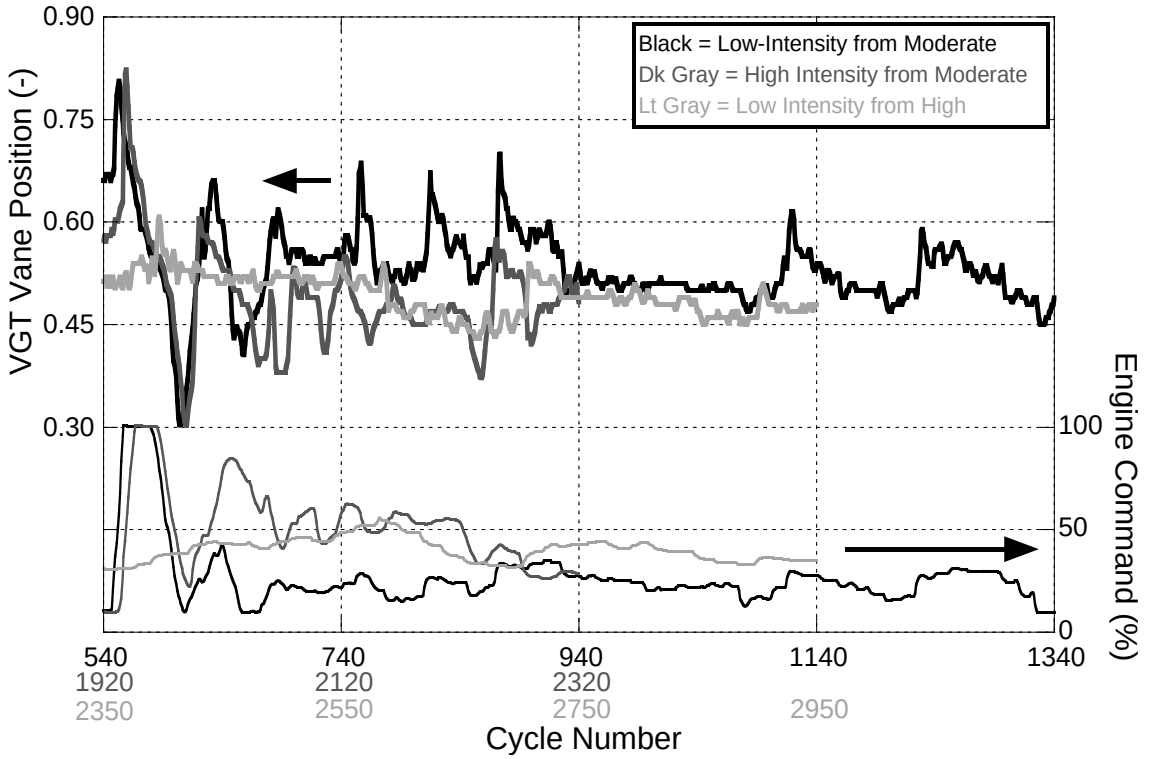

Figure 8.18: VGT Vane Position and Engine Command for Accelerations from Moderate and High Vehicle Velocities during FTP 75

8.2.7 Intake Manifold Pressure

Intake manifold pressure for the accelerations from zero vehicle velocity is shown in Figure 8.19 and the accelerations from moderate and high vehicle velocities is displayed in Figure 8.20. Increases in engine command cause intake manifold pressures to go up and vice versa. In high power cases, such as in cycles 2010-2045 of the high-intensity acceleration from a moderate velocity, intake manifold pressure gets high enough to saturate the pressure transducer. The engine power during these cycles is around 150 kW. Also observed is the noticeable lag that exists between engine command and intake manifold pressure, which is present in both figures, but especially predominant in Figure 8.19. The behavior of the intake manifold pressure tracks very well with engine power, as higher engine speeds and loads have the capacity to produce more boost.

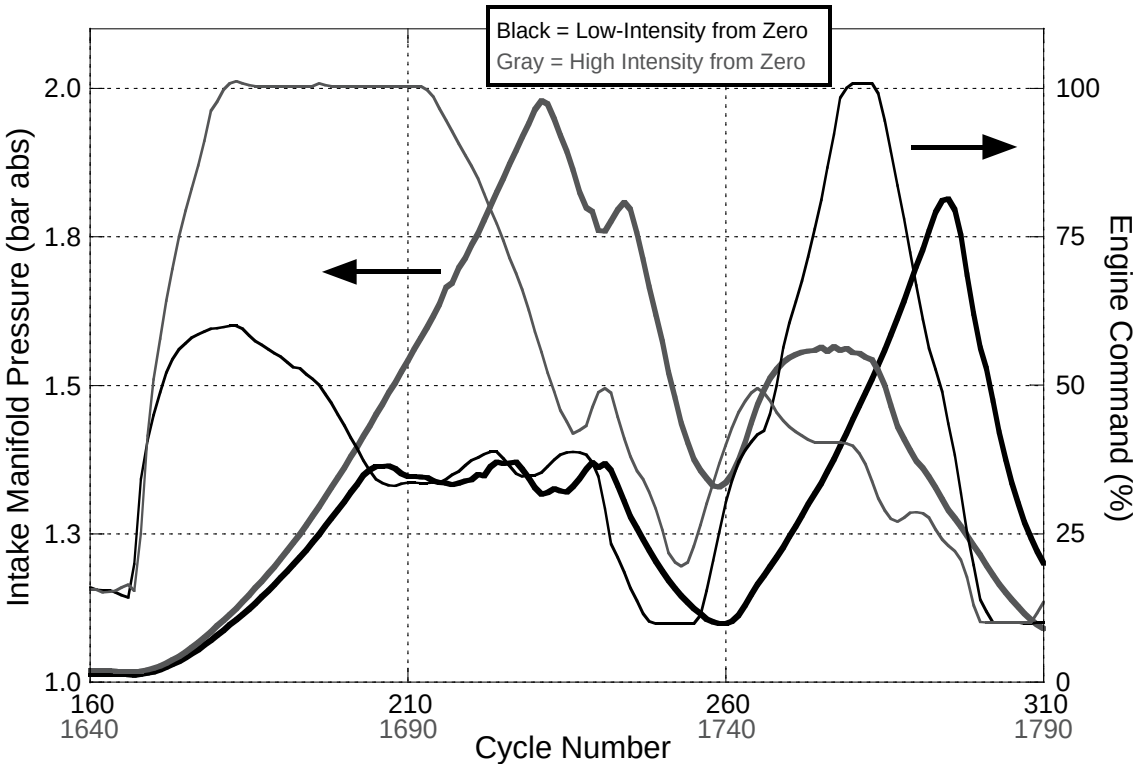

Figure 8.19: Intake Manifold Pressure and Engine Command for Accelerations from Zero Vehicle Velocity during FTP 75

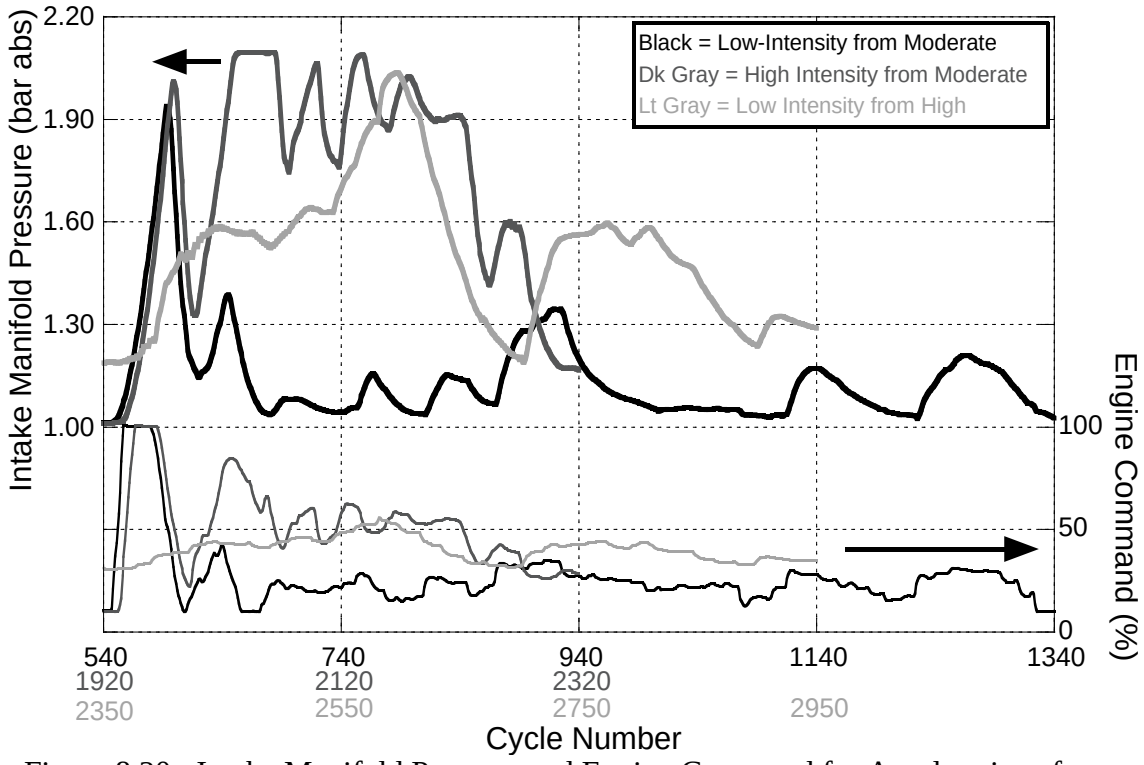

Figure 8.20: Intake Manifold Pressure and Engine Command for Accelerations from Moderate and High Vehicle Velocities during FTP 75

8.2.8 Measured and Desired Fuel Mass

Fuel mass injected for each cycle is determined via the technique described in Section 4.4. This quantity, along with the mass of fuel desired by the engine's PCM is graphed in Figure 8.21 for the accelerations from zero vehicle velocity. The measured value of injected fuel agrees very well with the demanded mass of fuel except during rapid increases or decreases in the engine command.

If engine command increases by a large amount over a short period of cycles, the measured fuel injection mass will overshoot the demand value for a cycle or two. This behavior is evident when considering the onset of the accelerations from zero vehicle velocity as shown in greater detail in Figure 8.22, which displays the first 20 cycles of both accelerations. Under these conditions, the measured mass of injected fuel overshoots the desired mass by 135% for the low-intensity acceleration and 100% for the high-intensity acceleration. For both cases, this occurs because the injection duration is lengthened by a factor of 4.3 for the low-intensity acceleration and 2.6 for the high-intensity acceleration over the span of consecutive cycles. Injection pressures during this period remain unchanged. Some fuel overshoot is present in the accelerations around cycles 260 and 1740, but these are not nearly as large. At these cycles, engine speeds and torques are elevated and overall fuel injection mass is much higher. This suggests that this particular fuel injection system is more controllable at higher fueling rates.

Measured and desired fuel injection mass for the accelerations from moderate and high vehicle velocities are shown in Figure 8.23. Aside from some discrepancies that occur in absolute values, the agreement between the measured and desired fuel masses is much better during these accelerations than in those that take place from zero vehicle velocity. Detailed examination of the initial portion of the accelerations, displayed in Figure 8.24, shows that while some overshoot in fuel mass is present, the measured value is only 50% more than the desired value.

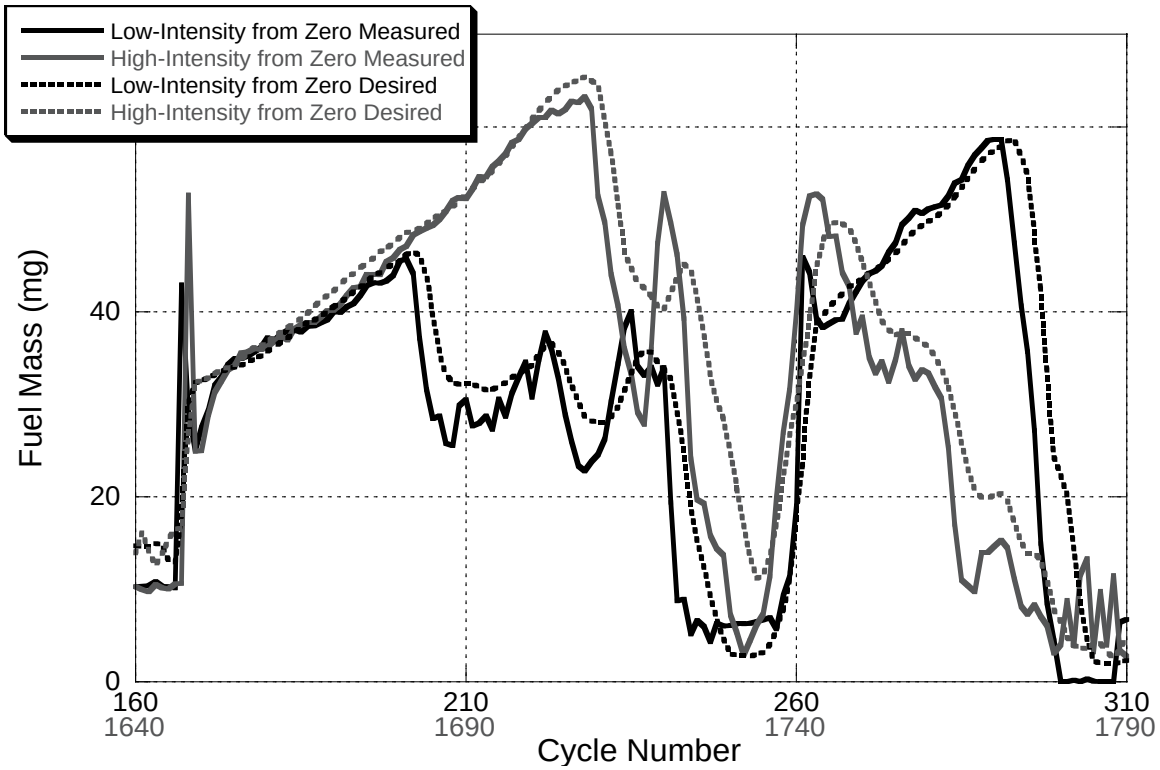

Figure 8.21: Measured and Desired Fuel Mass for Accelerations from Zero Vehicle Velocity during FTP 75

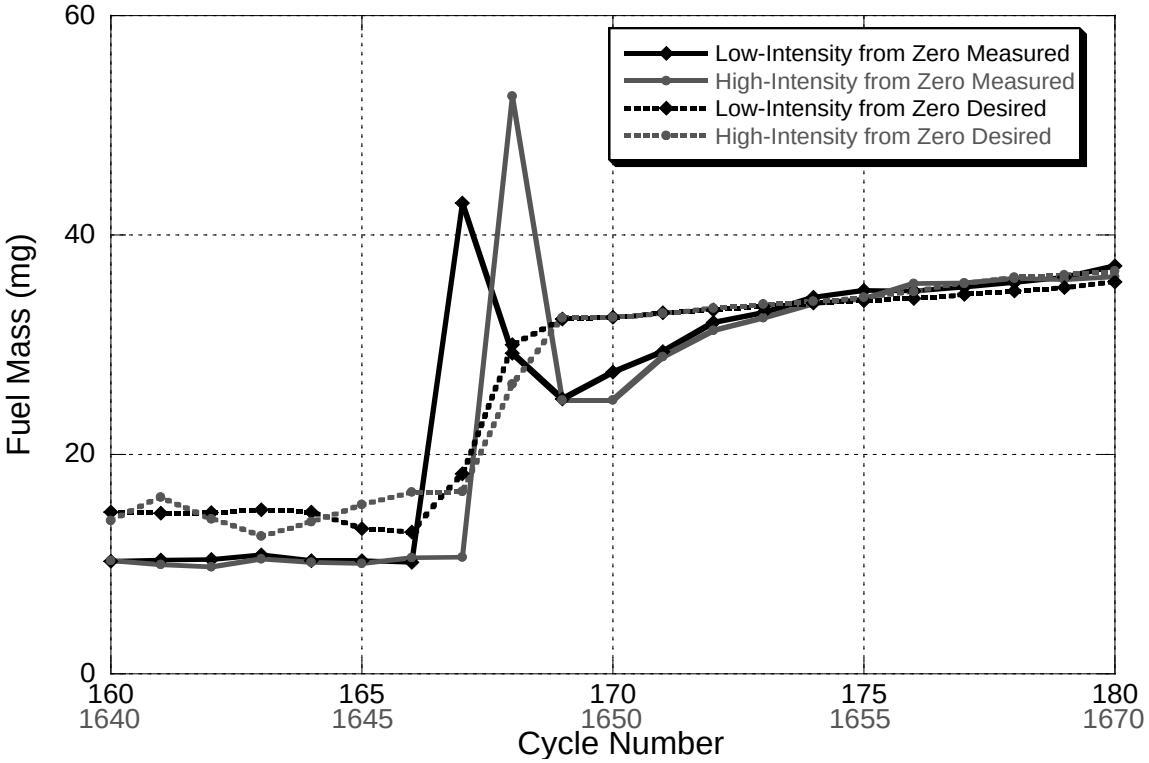

Figure 8.22: Measured and Desired Fuel Mass for the First 20 Cycles of Accelerations from Zero Vehicle Velocity during FTP 75

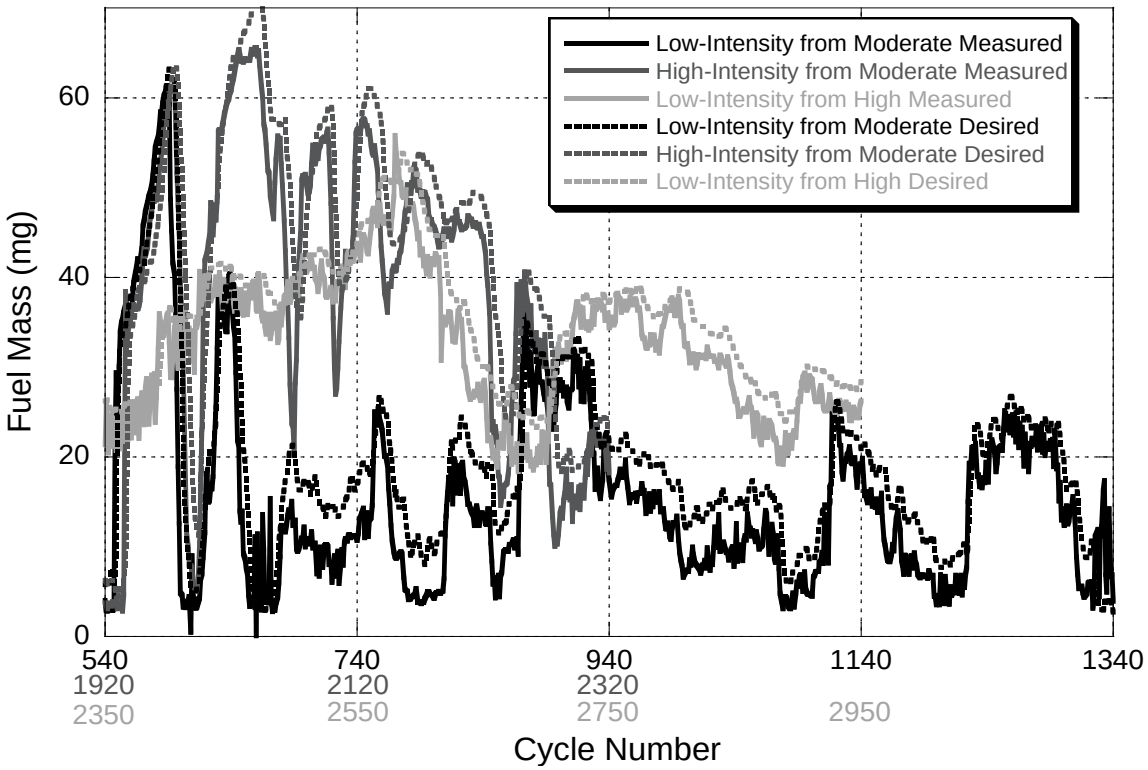

Figure 8.23: Measured and Desired Fuel Mass for Accelerations from Moderate and High Vehicle Velocities during FTP 75

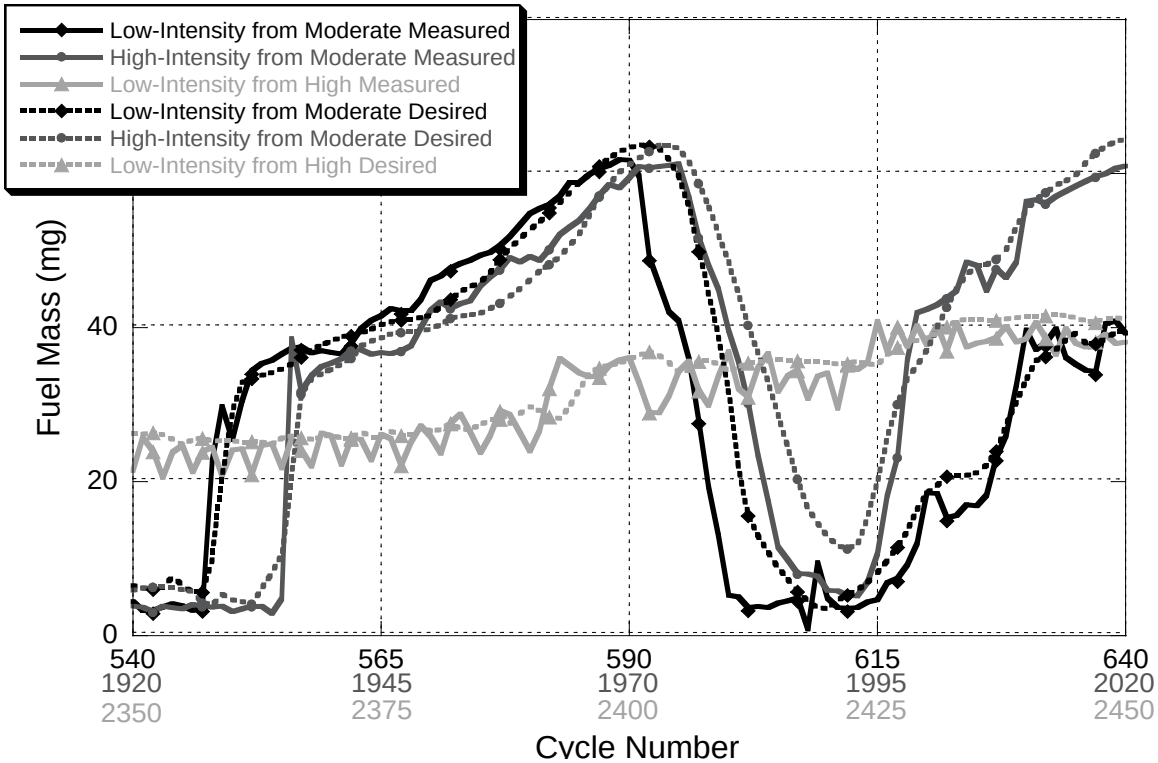

Figure 8.24: Measured and Desired Fuel Mass for the First 100 Cycles of Accelerations from Moderate and High Vehicle Velocities during FTP 75

8.2.9 In-Cylinder CO_2 Measurements

Carbon dioxide in the cylinder prior to combustion comes from residual gases trapped from the previous combustion cycle and from the presence of EGR. The concentration of CO_2 present is dependent upon the mass of residual and EGR trapped as well as the proportion of CO_2 in these gases. This section discusses the in-cylinder CO_2 trends observed but does not explain why these differences occur. These trends are explained in Section 8.2.11, which explores the mass of stoichiometric combustion products trapped in the cylinder prior to combustion.

Figure 8.25 shows the amount of CO_2 in-cylinder and engine command during the accelerations from zero vehicle velocity. These two metrics are closely related and their relationship is similar for both accelerations. When engine command levels are increasing and above 50%, in-cylinder CO_2 levels are low. As engine command decreases or falls below around 50%, the in-cylinder CO_2 levels increase. The maximum observed values are around 0.9% and occur during periods when engine command is dropping rapidly. The lowest values of in-cylinder CO_2 are observed when engine command reaches a minimum of around 10%.

Figure 8.26 displays in-cylinder CO_2 concentration and engine command during the accelerations from moderate and high vehicle velocities. As in the previous case, in-cylinder CO_2 values are low during increases in engine command and high when engine command is decreasing. For the latter part of the low-intensity acceleration from moderate vehicle velocity and the entire portion of the low-intensity acceleration from high vehicle velocity, engine command remains elevated but below 50%. During these periods, in-cylinder CO_2 levels remain relatively high and only decrease when engine command increases. The peak value for in-cylinder CO_2 is around 2.2% and is observed in the latter portion of the high-intensity acceleration when engine command is constant, engine speed is around 2500 rpm, and engine load is around 9 bar BMEP.

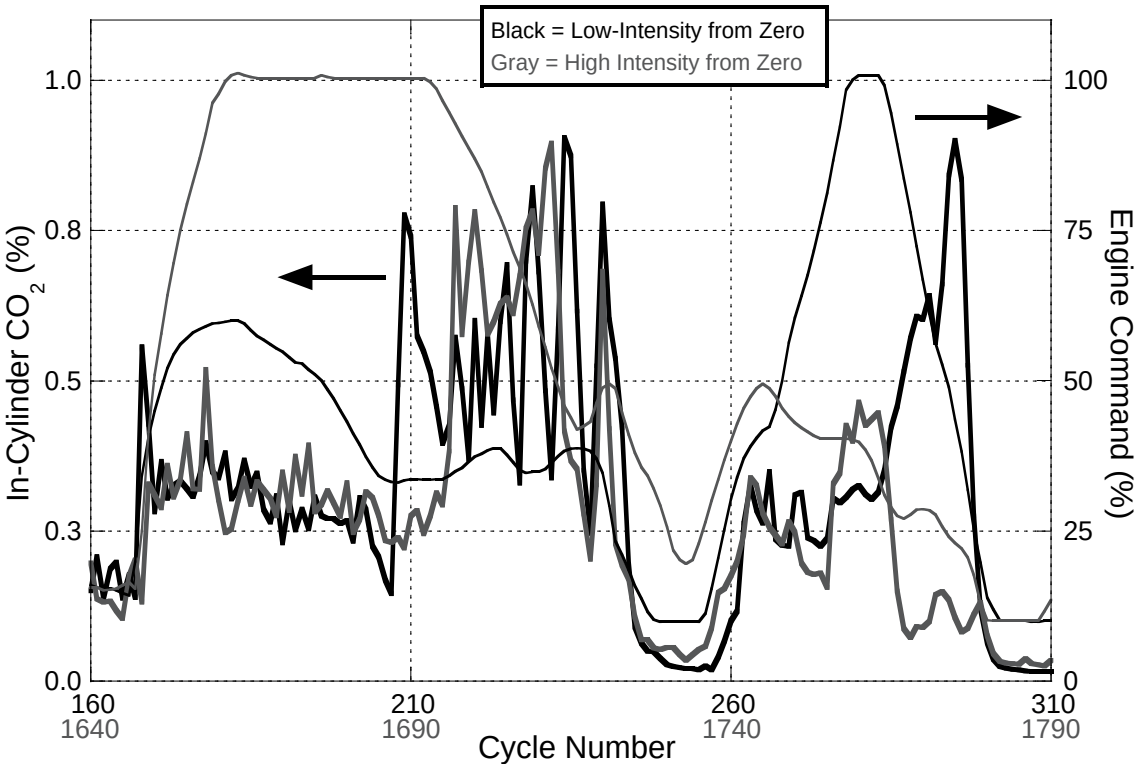

Figure 8.25: In-Cylinder CO_2 Concentration and Engine Command for Accelerations from Zero Vehicle Velocity during FTP 75

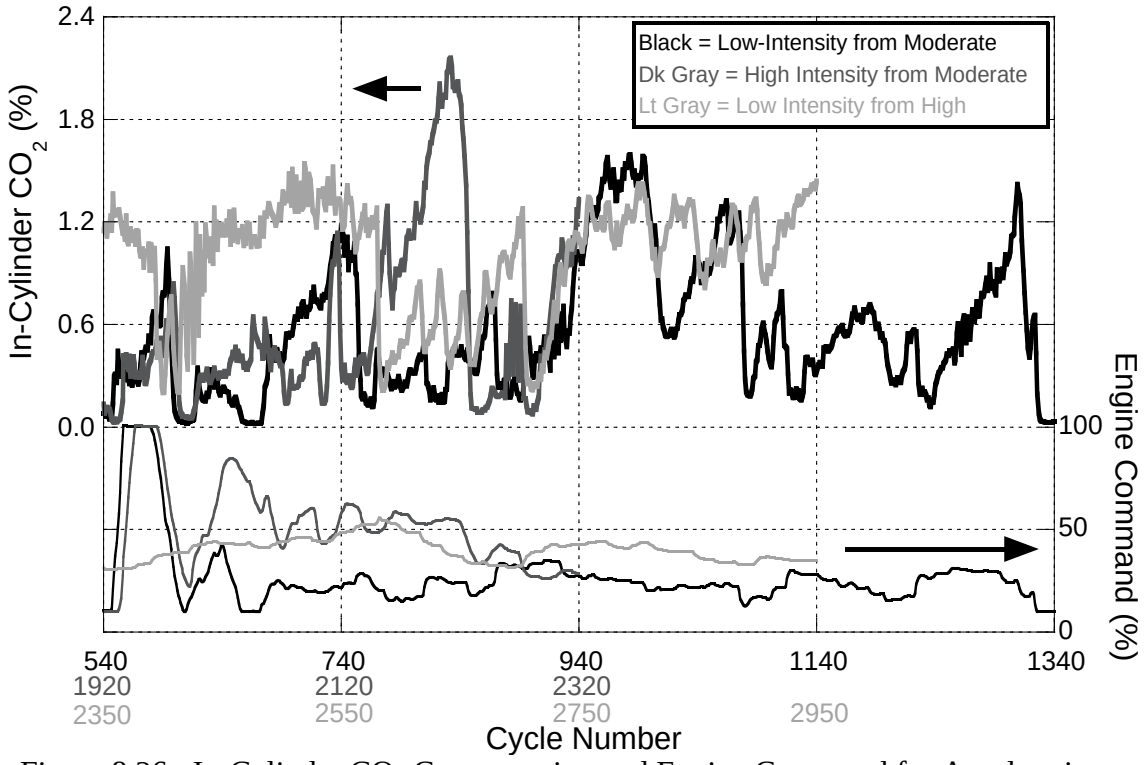

Figure 8.26: In-Cylinder CO_2 Concentration and Engine Command for Accelerations from Moderate and High Vehicle Velocities during FTP 75

8.2.10 Exhaust Manifold CO_2 Measurements

Carbon dioxide measured in the exhaust manifold has two origins: CO_2 that is generated during combustion, and CO_2 that comes from the stoichiometric combustion products that are trapped in the cylinder prior to combustion. Exhaust manifold CO_2 concentration measurements during the accelerations from zero vehicle velocity are shown in Figure 8.27. Prior to the accelerations CO_2 levels are quite low, but once engine command begins to increase, exhaust manifold CO_2 concentrations spike upward immediately, drop down for a few cycles and then continue moving upward until engine command drops off. As engine command modulates up and down, so does the CO_2 concentration. In-cylinder CO_2 concentrations prior to combustion are generally so low that their influence is difficult to identify when examining the exhaust manifold CO_2 concentrations. When engine command drops to its lowest levels and the engine is not generating any torque, as in cycles 250-255, no virtually no CO_2 in the exhaust manifold is detected, indicating lack of combustion. In conditions such as this, the engine is in a free-wheeling coast-down period, which occurs frequently during the FTP 75. The highest observed CO_2 levels are over 12% and occur during the large increase in engine command around cycles 260 and 1740.

Figure 8.28 demonstrates CO_2 measurements in the exhaust manifold during the accelerations from moderate and high vehicle velocities. Much of the behavior here is similar to that observed in the accelerations from zero vehicle velocity. As engine command increases, the amount of CO_2 goes up, and as engine command goes down, CO_2 falls—sometimes to levels near enough to zero to indicate that no combustion is occurring. For cases in which engine command is elevated and relatively constant, as it is in the later portions of the low-intensity acceleration from moderate vehicle velocity and the low-intensity acceleration from high vehicle velocity, CO_2 concentrations also remain elevated and relatively high.

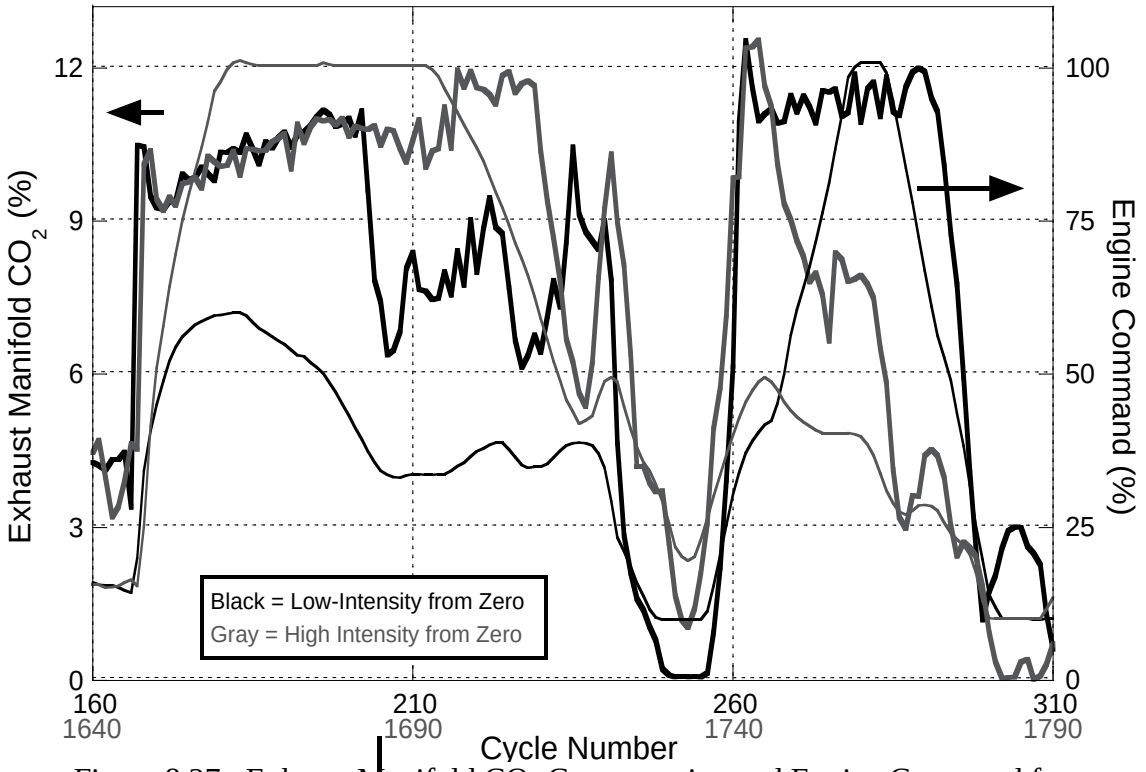

Figure 8.27: Exhaust Manifold CO_2 Concentration and Engine Command for Accelerations from Zero Vehicle Velocity during FTP 75

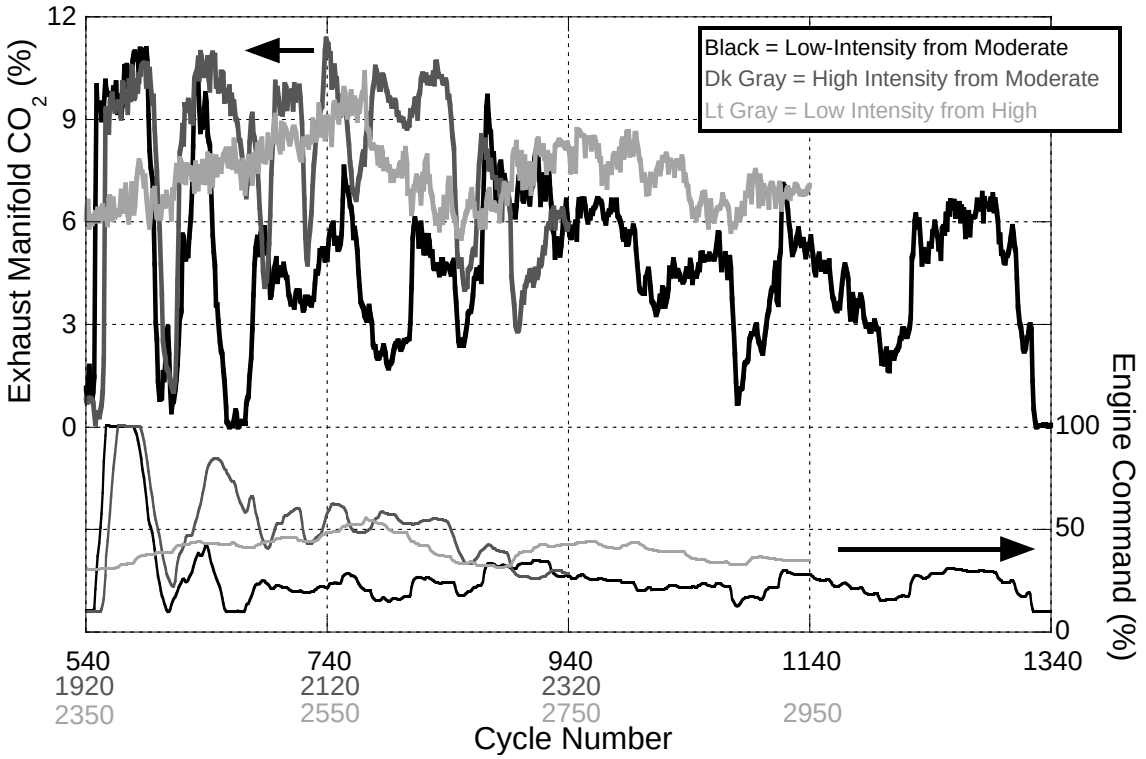

Figure 8.28: Exhaust Manifold CO_2 Concentration and Engine Command for Accelerations from Moderate and High Vehicle Velocities during FTP 75

8.2.11 Stoichiometric Combustion Product Mass Percentage

The mass percentage of stoichiometric combustion products in the cylinder prior to combustion is a direct calculation from the in-cylinder CO_2 concentration. Therefore the trends in the stoichiometric combustion product mass are the same as those observed in the in-cylinder CO_2 concentration. These behaviors were explored in Section 8.2.9, so they are not repeated here. This section focuses on why the stoichiometric combustion product mass fluctuates as it does. The presence of stoichiometric combustion product in the cylinder prior to combustion is due to residual trapped from the previous combustion cycle and EGR. Three main factors contribute to the amount of residual and EGR: the ratio of exhaust manifold pressure to intake manifold pressure, which serves to cause more residual to be trapped and provides the pressure differential to drive EGR flow, the opening of the EGR valve, and the CO_2 concentration in the exhaust.

Figure 8.29 demonstrates the proportion of stoichiometric combustion products in the cylinder for accelerations from zero vehicle velocity. Maximum values experienced in these cases are around 7% of the total trapped mass. The regions in which the stoichiometric combustion product mass goes to zero represent those cycles where fuel injection mass and exhaust manifold CO_2 concentrations are so low that inaccurate values are reported. Air and stoichiometric combustion product masses are not calculated, so the percentage of stoichiometric combustion product mass goes to zero. These conditions were discussed in Section 5.4. Figure 8.30 shows the proportion of stoichiometric combustion products in the cylinder for accelerations from moderate and high vehicle velocities. The maximum and overall levels of stoichiometric combustion products are higher during these accelerations than the accelerations from zero.

To fully examine why each acceleration's stoichiometric combustion mass behaves as it does, individual graphs are made for each condition with information about the EGR valve position, the manifold pressure ratio, and the exhaust CO_2 concentration.

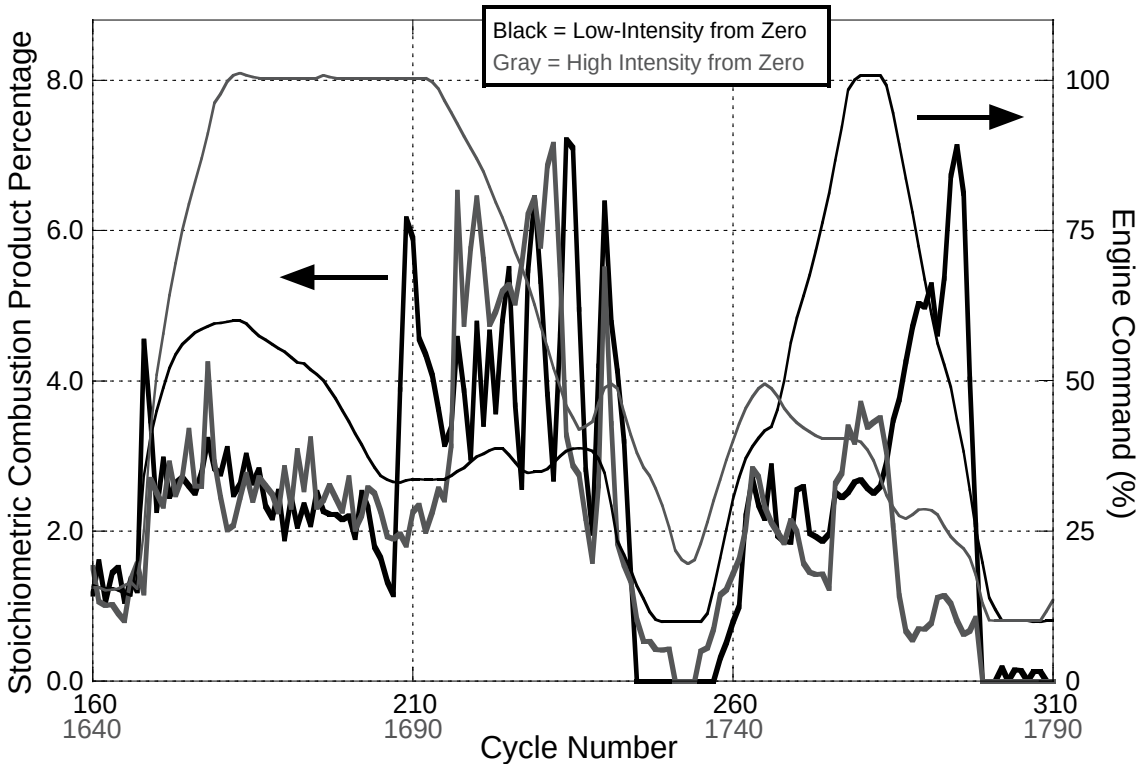

Figure 8.29: Stoichiometric Combustion Product Mass Percentage and Engine Command for Accelerations from Zero Vehicle Velocity during FTP 75

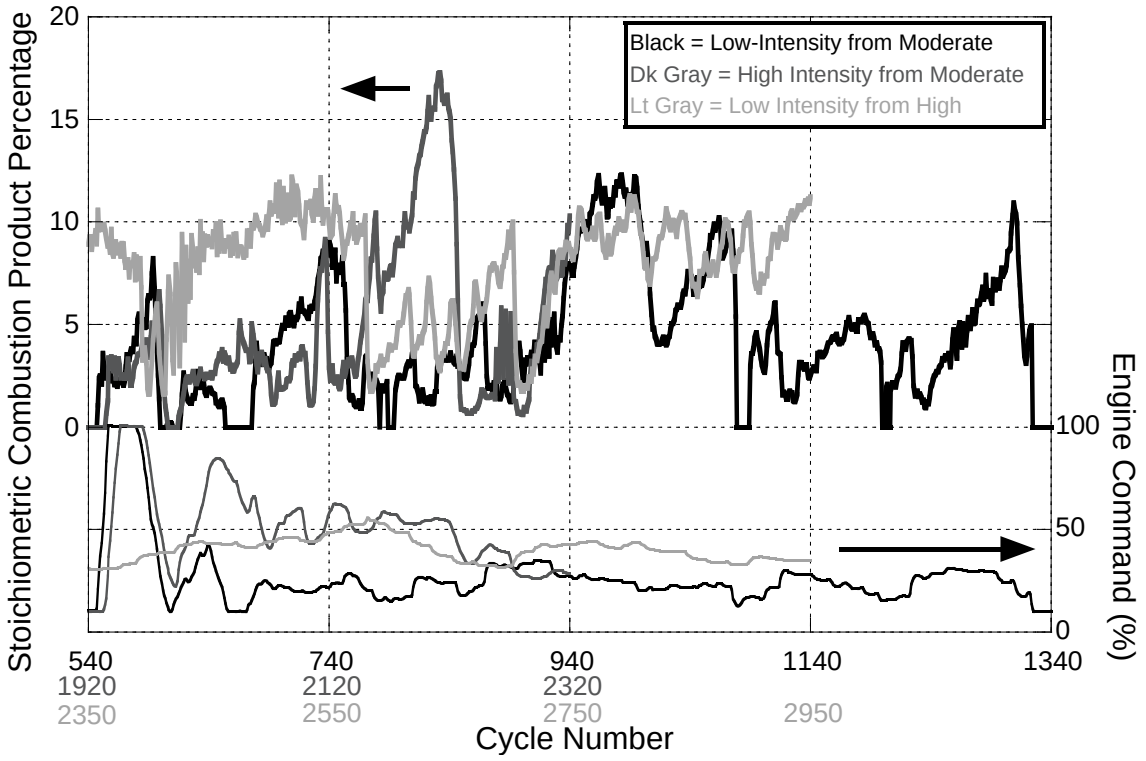

Figure 8.30: Stoichiometric Combustion Product Mass Percentage and Engine Command for Accelerations from Moderate and High Vehicle Velocities during FTP 75

Low-Intensity Acceleration from Zero Vehicle Velocity, Cycles 160-310

The trapped mass percentage of stoichiometric combustion products, exhaust manifold CO_2 concentration, EGR valve position, and manifold pressure ratio during the low-intensity acceleration from zero vehicle velocity is shown in Figure 8.31. During cycles 160-205, the EGR valve is completely closed and CO_2 in the cylinder prior to combustion is a function of manifold pressure ratio and CO_2 concentration in the exhaust manifold. Around cycle 205, the EGR valve opens, causing the percentage of stoichiometric combustion products to triple. This behavior continues until around cycle 243, when the concentration of CO_2 in the exhaust decreases drastically to near-zero and manifold pressure ratio drops as a response to the engine free-wheeling during a vehicle deceleration. As engine command increases for the second portion of the acceleration, CO_2 levels in the exhaust manifold and manifold pressure ratios jump up, resulting in a larger proportion of stoichiometric combustion products in the cylinder.

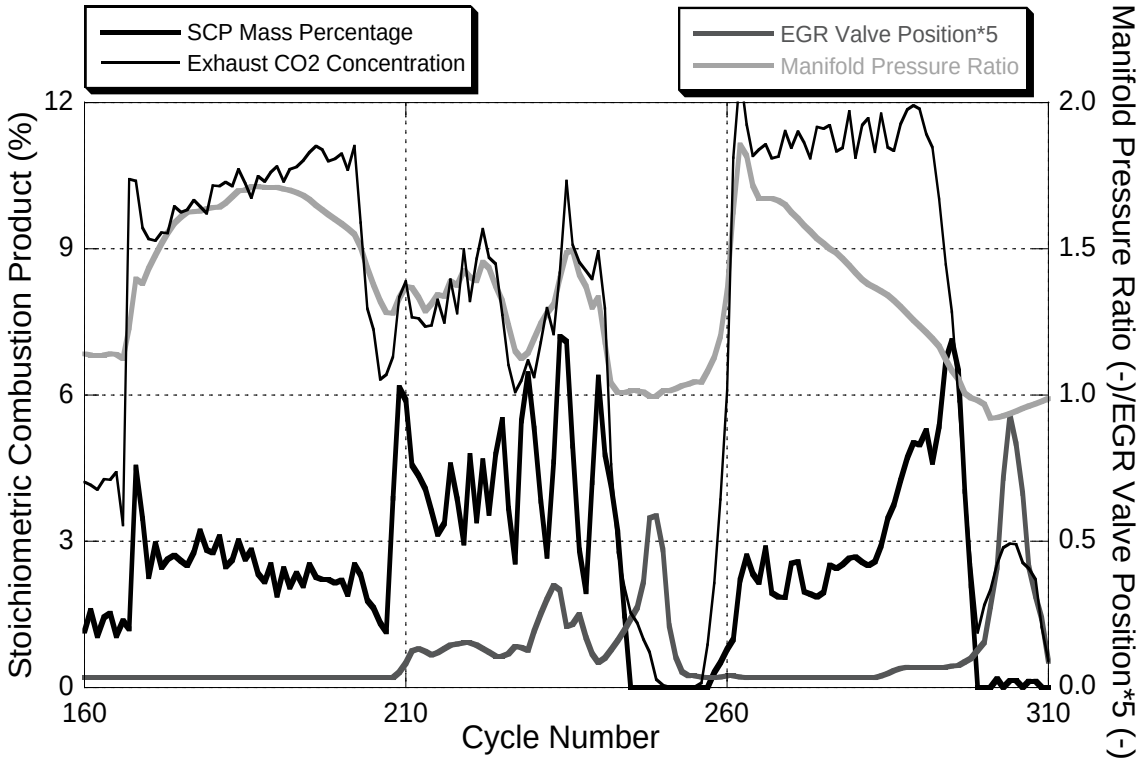

Figure 8.31: Stoichiometric Combustion Product Percentage, Exhaust CO_2 Concentration, EGR Valve Position, and Manifold Pressure Ratio for Low-Intensity Acceleration from Zero Vehicle Velocity, Cycles 160-310 of FTP 75

High-Intensity Acceleration from Zero Vehicle Velocity, Cycles 1640-1790

Figure 8.32 displays the stoichiometric combustion product percentage, exhaust CO_2 concentration, EGR valve position, and manifold pressure ratio during the high-intensity acceleration from zero vehicle velocity. During the initial and most intense part of the acceleration, the EGR valve remains closed and all the CO2 in the cylinder is due to trapped residual and the influence of manifold pressure ratio and exhaust CO2 percentage. Around cycle 1695, the EGR valve begins to open slightly, and the presence of EGR doubles the percentage of stoichiometric combustion product in the cylinder. During the deceleration around cycle 1710, the EGR valve opens even more fully, but the amount of CO2 in the exhaust is very low; therefore the exhaust is mostly air. The same kind of behavior is observed for the EGR valve, manifold pressure ratio, and exhaust CO2 concentration during cycles 1740-1790, the second portion of the acceleration.

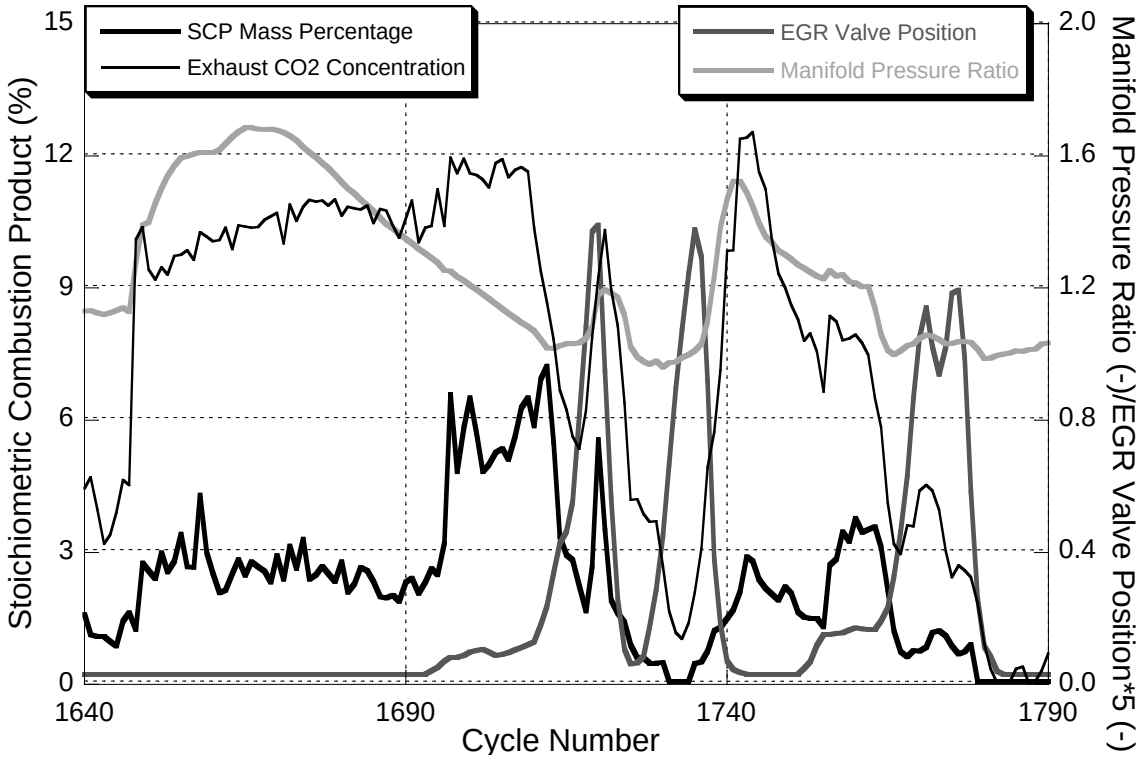

Figure 8.32: Stoichiometric Combustion Product Percentage, Exhaust CO_2 Concentration, EGR Valve Position, and Manifold Pressure Ratio for High-Intensity Acceleration from Zero Vehicle Velocity, Cycles 1640-1790 of FTP 75

Low-Intensity Acceleration from Moderate Vehicle Velocity, Cycles 540-1340

The percentage of stoichiometric combustion products, exhaust CO_2 concentration, EGR valve position, and manifold pressure ratio for the low-intensity acceleration from moderate vehicle velocity is displayed in Figure 8.33. This figure demonstrates that the engine behavior during this acceleration is composed of one strong acceleration at the beginning followed by many shorter low-intensity accelerations. Each time engine power increases, CO_2 in the exhaust and manifold pressure ratio increases and the EGR valve closes. During these portions, the proportion of stoichiometric combustion products in the cylinder is purely a function of CO_2 concentration in the exhaust and manifold pressure ratio. The result is stoichiometric combustion product proportions that are rather low—typically below 3%. During more steady engine operation or decelerations, the EGR valve opens up, raising stoichiometric combustion product percentages to values above 3% and in some cases over 12%.

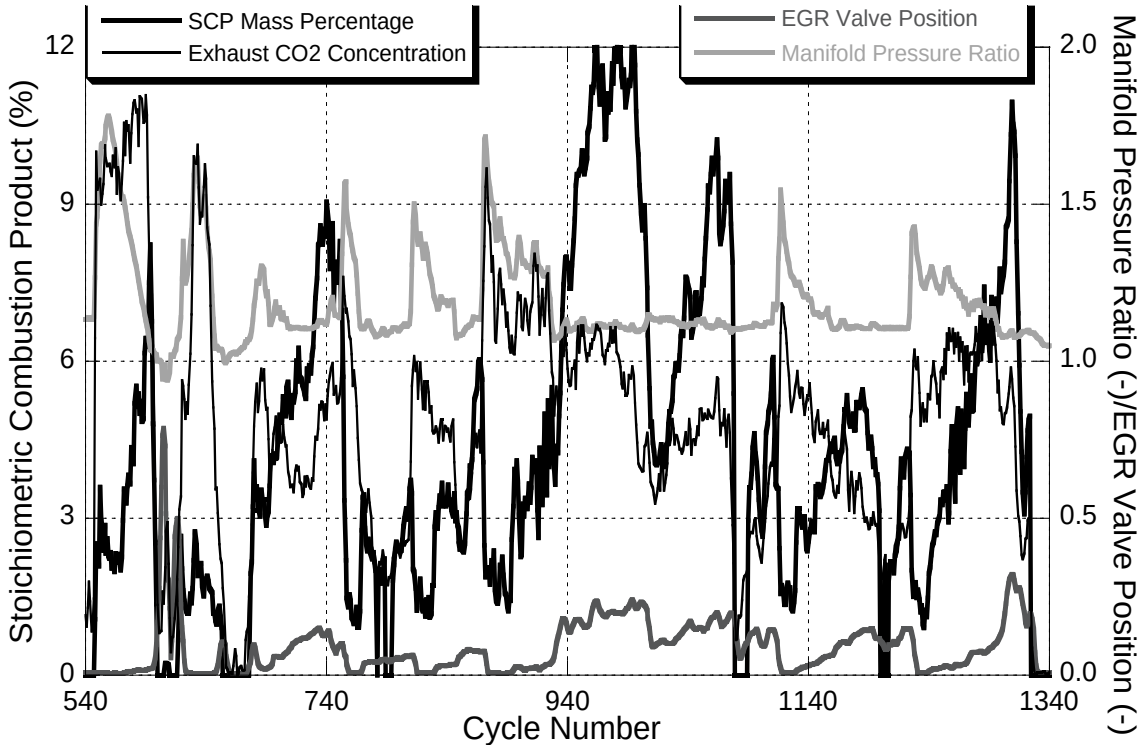

Figure 8.33: Stoichiometric Combustion Product Percentage, Exhaust CO_2 Concentration, EGR Valve Position, and Manifold Pressure Ratio for Low-Intensity Acceleration from Moderate Vehicle Velocity, Cycles 540-1340 of FTP 75

High-Intensity Acceleration from Moderate Vehicle Velocity, Cycles 1920-2320

Figure 8.34 demonstrates the percentage of stoichiometric combustion products, exhaust CO_2 concentration, EGR valve position, and manifold pressure ratio for the high-intensity acceleration from moderate vehicle velocity. This event consists of sustained periods of high-intensity accelerations interspersed with a few periods of decelerations. During the cycles in which the accelerations are occurring, the EGR valve remains closed and the proportion of stoichiometric combustion products remains low. In the instances where the EGR valve does open during these high engine loads, such as around cycle 2200, the amount of stoichiometric combustion products can exceed 15%. During rapid decelerations, such as around cycles 1990 and 2230, the EGR valve opens significantly, but low manifold pressure ratios have little potential to drive EGR and residual flow. Any exhaust gases that are trapped in the cylinder, however, come from very lean combustion events that have very small concentrations of CO_2.

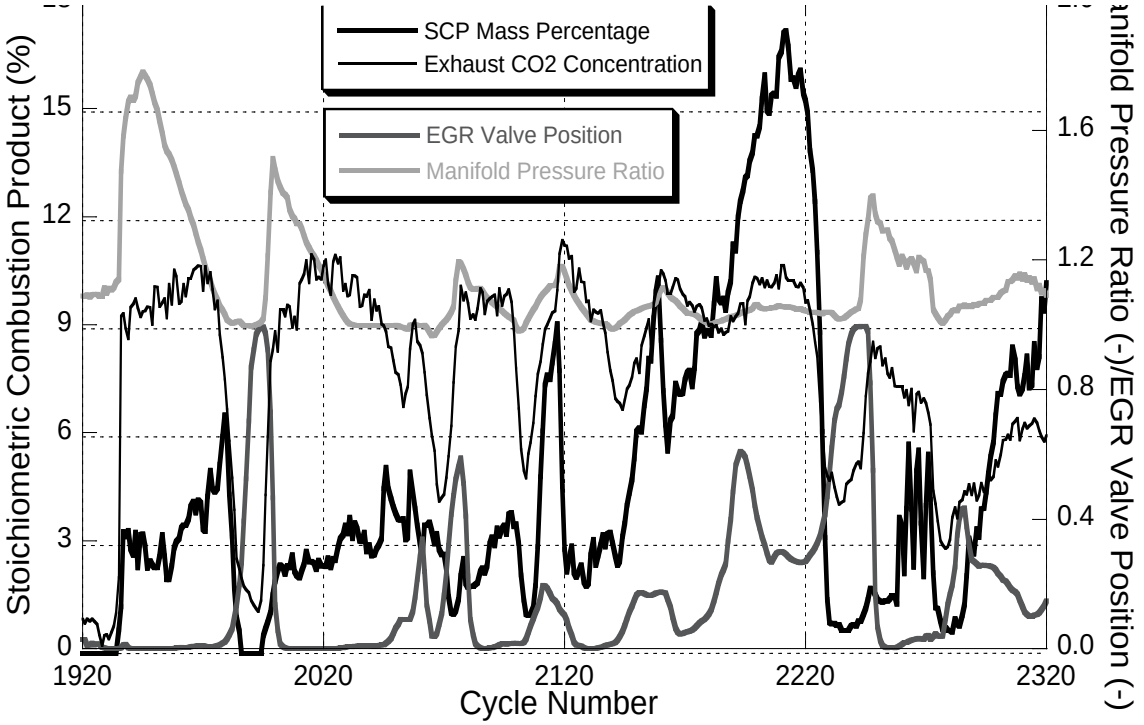

Figure 8.34: Stoichiometric Combustion Product Percentage, Exhaust CO_2 Concentration, EGR Valve Position, and Manifold Pressure Ratio for High-Intensity Acceleration from Moderate Vehicle Velocity, Cycles 1920-2320 of FTP 75

Low-Intensity Acceleration from High Vehicle Velocity, Cycles 2350-2950

Figure 8.35 displays the percentage of stoichiometric combustion products, exhaust CO_2 concentration, EGR valve position, and manifold pressure ratio for the low-intensity acceleration from high vehicle velocity. Engine behavior during this transient is characterized by steady increases in engine power with one significant deceleration around cycle 2560. The EGR valve is open during most of the acceleration, resulting in overall much higher proportions of stoichiometric combustion products. Prior to cycle 2550, about 10-12% of the trapped mass in the cylinder consists of stoichiometric combustion products. Around cycle 2560, however, the EGR valve closes, the manifold pressure ratio decreases, and the concentration of CO_2 in the exhaust manifold goes down. These three all work to reduce the stoichiometric combustion product fraction to one-fourth of its original value. As the acceleration continues, conditions return to their previous orientations and the SCP percentage rises back to around 9%.

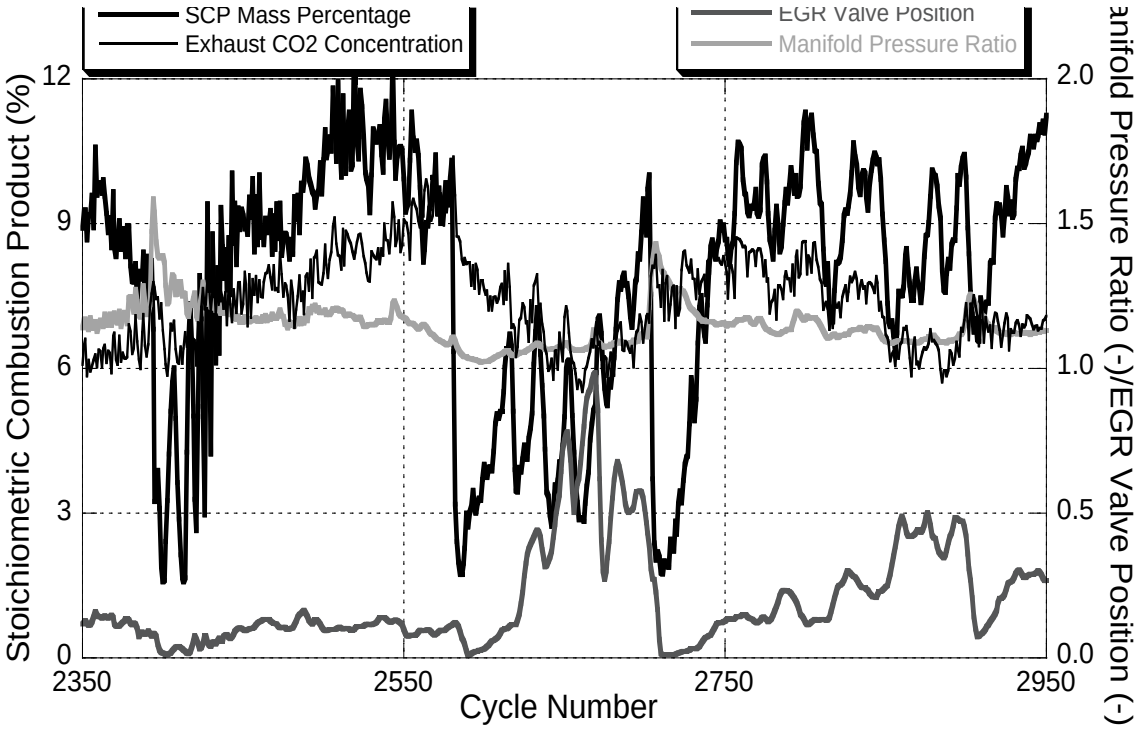

Figure 8.35: Stoichiometric Combustion Product Percentage, Exhaust CO_2 Concentration, EGR Valve Position, and Manifold Pressure Ratio for Low-Intensity Acceleration from High Vehicle Velocity, Cycles 2350-2950 of FTP 75

Stoichiometric Combustion Product Mass Percentage Summary

Five separate accelerations are analyzed to understand the factors that drive the proportion of stoichiometric combustion products trapped in the cylinder during realistic engine behavior. While all of these accelerations are very different when studied from a higher level, closer examination reveals consistent behavior of engine systems that produce the observed fraction of stoichiometric combustion products.

During any time at which engine command is increasing and more power is being demanded from the engine, the EGR valve closes and the amount of stoichiometric combustion products is governed solely by the manifold pressure ratio and the concentration of CO_2 in the exhaust gases. During these periods of acceleration, CO_2 concentrations are high and manifold pressure ratios are at their highest. But in this engine, compression ratios are quite high (18.0:1), clearance volumes are quite low (5.6% of total volume), and the valve overlap period is relatively short (13.4º) leaving little room for trapped residual. Typical stoichiometric combustion products mass fractions are around 3% during these conditions.

When engine behavior is steadier and engine power is neither increasing nor decreasing rapidly, the EGR valve begins to open, which greatly increases the proportion of stoichiometric combustion products trapped in the cylinder. Under such conditions, the ratio of stoichiometric combustion products can be anywhere between 3-17% depending on engine operating conditions.

During conditions in which the engine command is decreasing rapidly, the EGR valve opens, the manifold pressure ratio drops, and the concentration of CO_2 in the exhaust falls to near zero. Any exhaust gases trapped in the cylinder consist mostly of air, resulting in very small proportions of stoichiometric combustion products in the cylinder.

8.2.12 Air Mass

The calculated trapped air mass and engine command for each combustion cycle during the accelerations from zero vehicle velocity is shown in Figure 8.36. During the beginning portions of these accelerations, the mass of air trapped in the cylinder is equivalent. This is no surprise, as all other engine metrics investigated confirm that engine behavior during these initial 40 cycles is very similar. From this point, air mass during the high-intensity acceleration continues to climb, while the air mass for the low-intensity acceleration remains relatively unchanged.

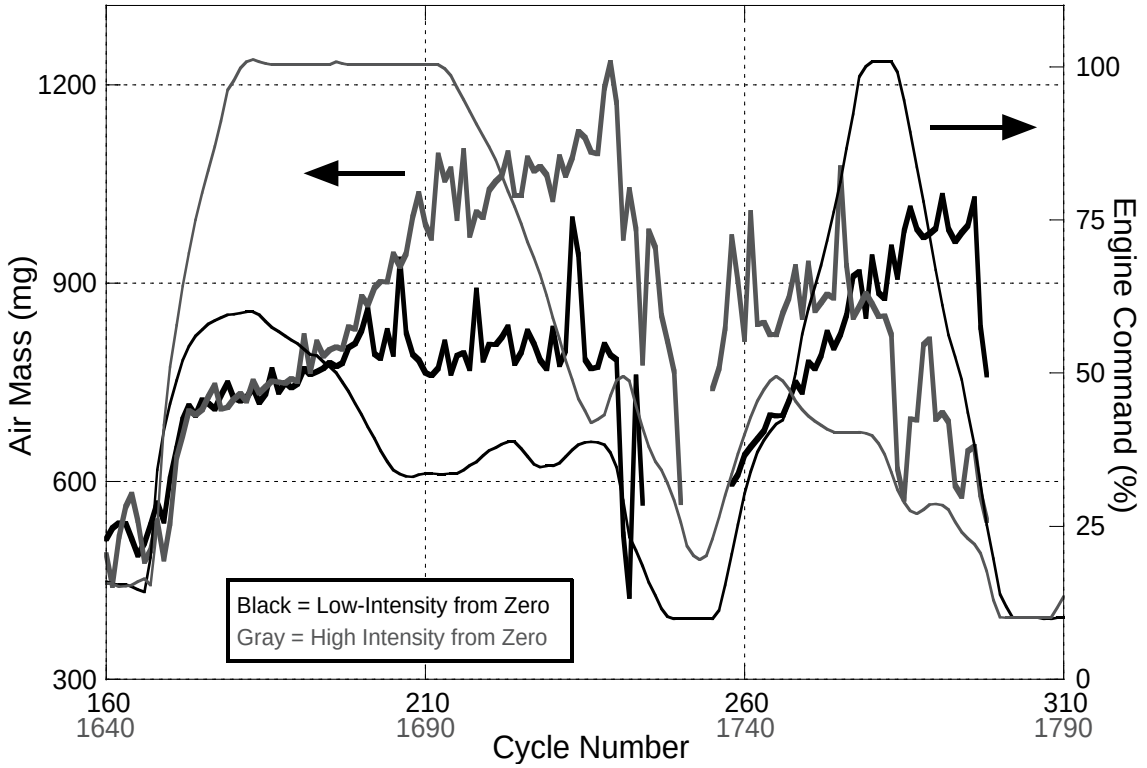

Figure 8.36: Air Mass and Engine Command for Accelerations from Zero Vehicle Velocity during FTP 75

This discrepancy is due to two factors: the intake manifold pressure and the engine speed. As intake manifold pressure increases, the amount of air that flows into the cylinder during the intake stroke increases. Conversely, as engine speed goes up, the amount of time available for air to enter the cylinder goes down and air mass decreases.

Thus the net result of the mass of air trapped in the cylinder is the outcome of these two counter-acting factors. To understand this interaction during the accelerations from zero vehicle velocity, the air mass is graphed with engine speed and intake manifold pressure in Figure 8.37. During the first 40 cycles of the transient, engine speed and intake manifold pressure are equivalent for both accelerations. After this, the two accelerations diverge, with the higher intensity case continuing to increase in engine speed and intake manifold pressure. While the intake manifold pressure is much higher and contributes to greater trapped air mass, its influence is tempered by the increase in engine speed. The net result of these two factors dictate trapped air mass for the remainder of the accelerations. For cycles in which the technique produces meaningless air mass results, data is omitted.

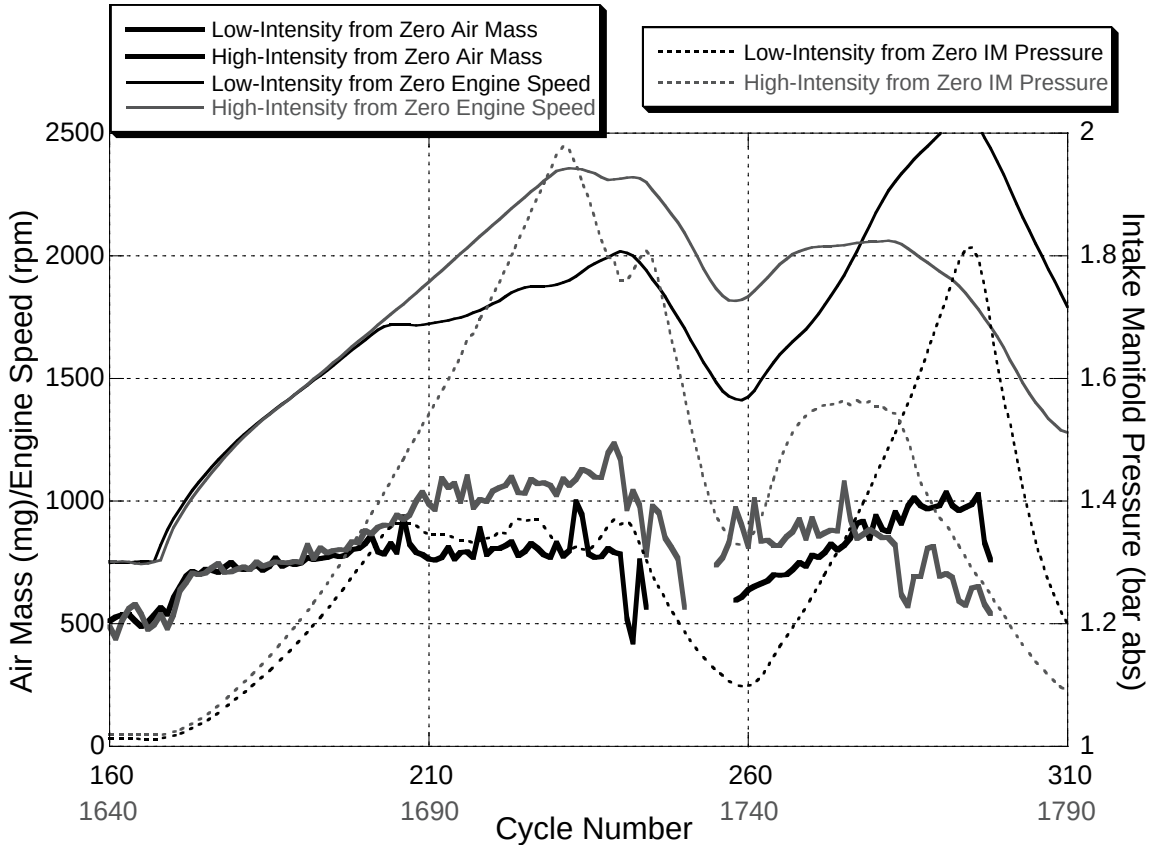

Figure 8.37: Air Mass, Engine Speed, and Intake Manifold Pressure for Accelerations from Zero Vehicle Velocity during FTP 75

Air mass and engine command for the accelerations from moderate and high vehicle velocities are displayed in Figure 8.38. As in the case of the accelerations from zero vehicle velocity, the amount of air ingested into the cylinder is a function of intake manifold pressure and the engine speed. Higher engine speeds and loads produce more turbocharger boost, and increase the amount of air trapped in the cylinder. This is especially apparent when considering the level of engine power produced, as the conditions in which the engine is producing the most power are also those which have the greatest mass of trapped air.

There are a few regions in which the experimental technique provides erroneous data due to extremely low fuel injection mass and exhaust manifold CO_2 concentrations. They occur during portions of the cycle in which the engine is free-wheeling so that virtually no fuel is injected and combustion is negligible. In Figure 8.38, these regions occur around cycles 570, 590, and 1950.

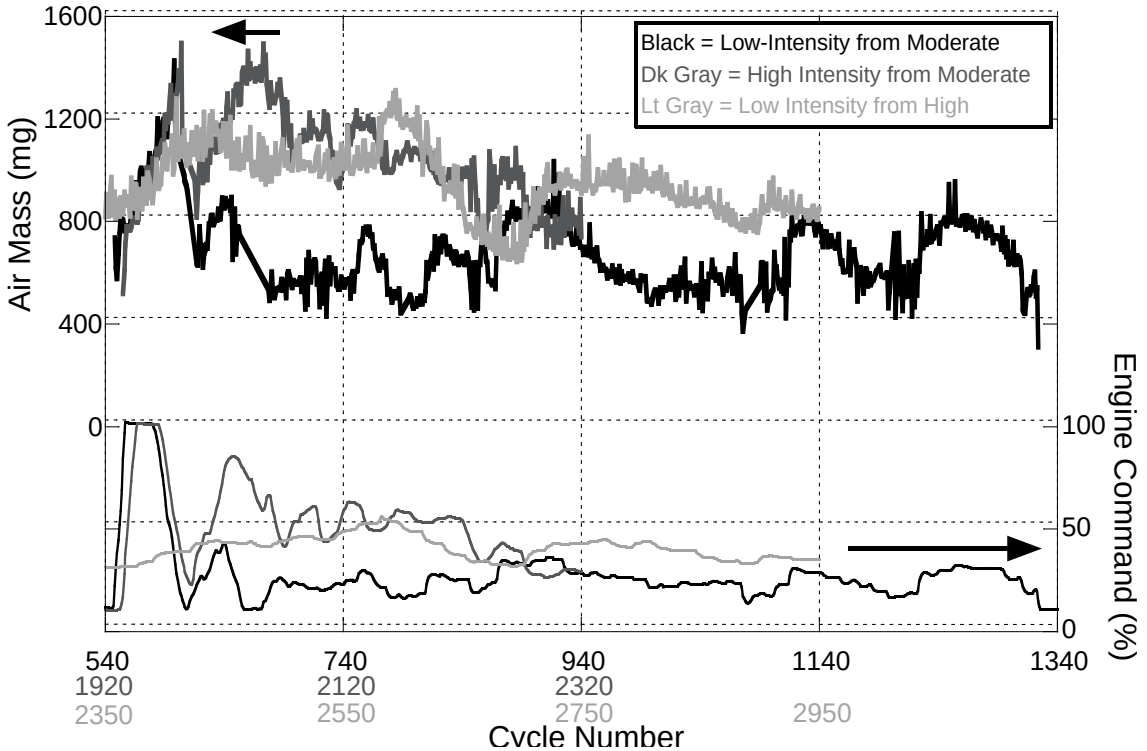

Figure 8.38: Air Mass and Engine Command for Accelerations from Moderate and High Vehicle Velocities during FTP 75

8.2.13 Air/Fuel Ratio

The air/fuel ratio is the ratio of the air mass to the fuel mass in the cylinder and is an important metric when studying engine behavior. Figure 8.39 shows the air/fuel ratios and engine command during the accelerations from zero vehicle velocity. Most notable is the extremely low air/fuel ratios that are encountered during the initial stages of the accelerations. During these cycles, engine speed and torque are near idling conditions and in the span of one cycle, a large increase in the mass of injected fuel occurs into a cylinder with air and stoichiometric combustion product masses that are unchanged from previous cycles. Absolute values for the mass of air and fuel during these cycles are contained in Figure 8.22 and Figure 8.36. This causes a drastic drop in air fuel ratio, and the lowest values are 12.5 in the low-intensity case and 10.3 in the high-intensity acceleration. These values are below the level of stoichiometric combustion and indicate that the air/fuel mixture is actually rich for these cycles.

When the second portions of the transients occur around cycles 260 and 1740, air fuel ratio plunges again, but the levels are not as low as the values near the beginning of the accelerations. The lowest values are 14.2 in the low-intensity case and 15.7 in the high-intensity acceleration. This is because the magnitude of the amount of fuel overshoot is much less in these conditions than in the initial cycles of the accelerations. The remainder of the air/fuel ratios experienced throughout the acceleration are well within expected values.

Figure 8.40 displays the air/fuel ratios and engine command during the accelerations from moderate and high vehicle velocities. At the beginning of the high-intensity acceleration from moderate vehicle velocity, one cycle occurs when the air/fuel ratio is 13.4 and is due to fuel overshoot. All other cycles, however, experience air/fuel ratios that are well within the range expected values.

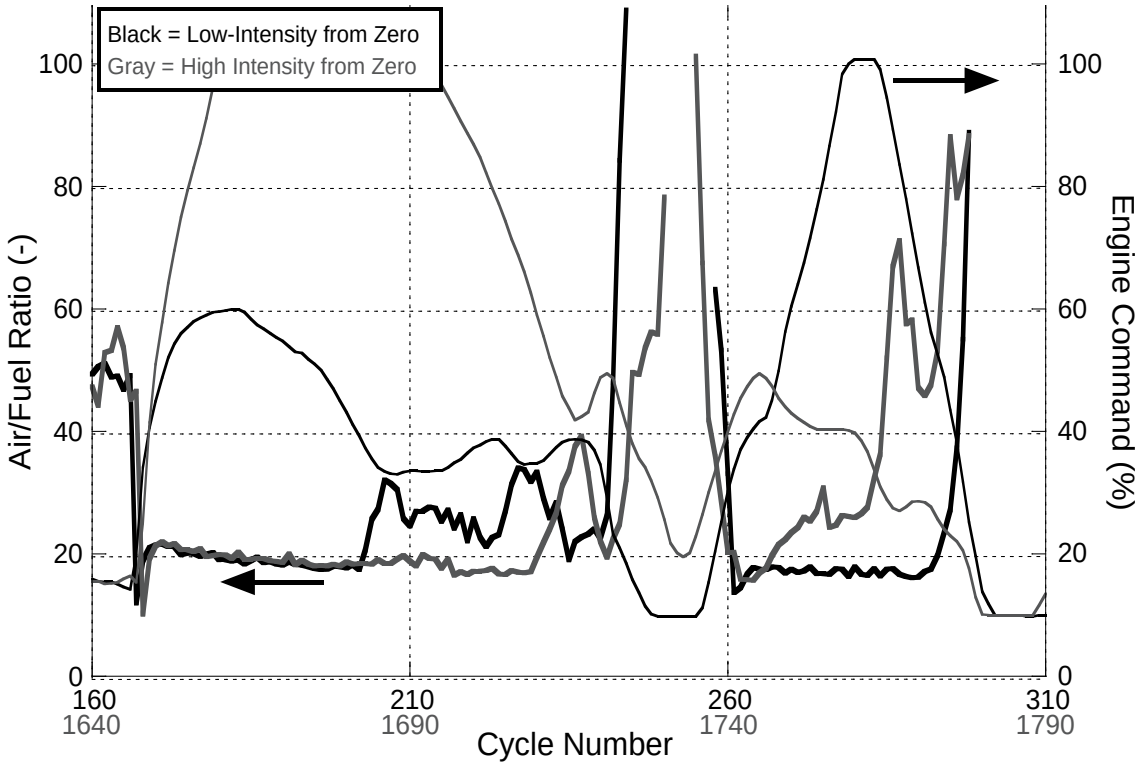

Figure 8.39: Air/Fuel Ratio and Engine Command for Accelerations from Zero Vehicle Velocity during FTP 75

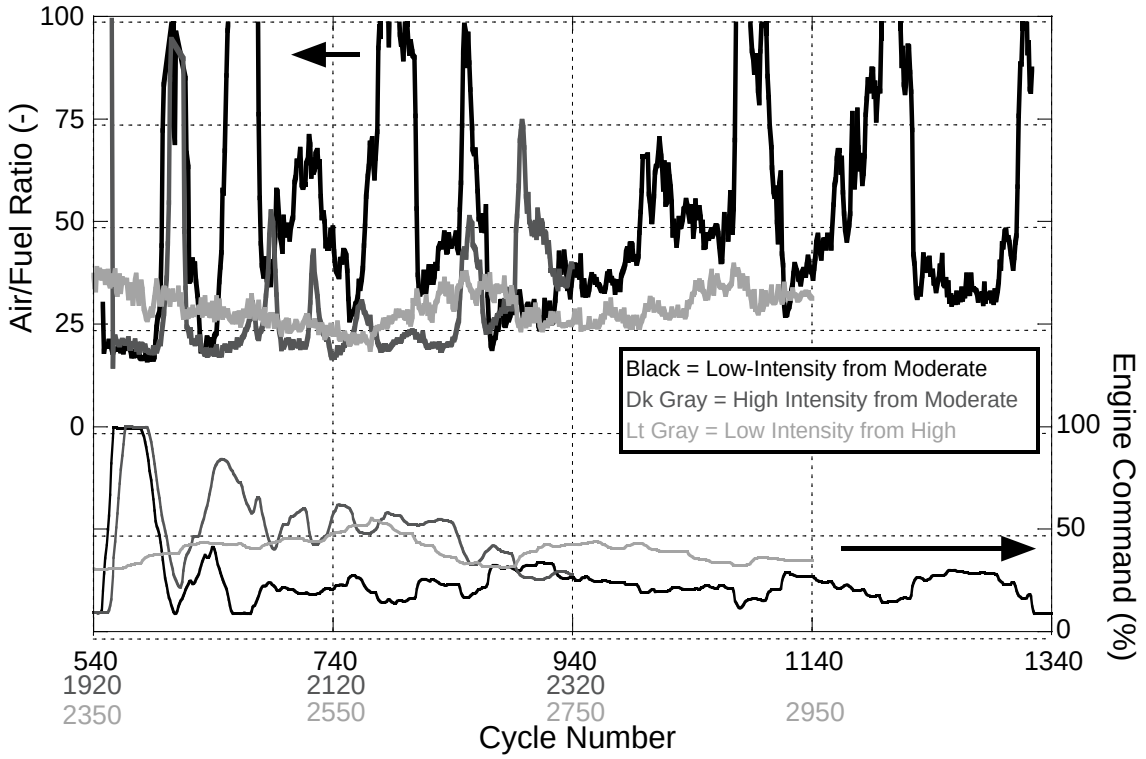

Figure 8.40: Air/Fuel Ratio and Engine Command for Accelerations from Moderate and High Vehicle Velocities during FTP 75

8.2.14 Combustion Analysis

To better understand the nature of combustion during transient engine behavior, rate of heat release analysis is conducted for every cycle during the FTP 75. To minimize redundancy, detailed discussions of three of the five accelerations are included: the high-intensity acceleration from zero vehicle velocity, the high-intensity acceleration from moderate vehicle velocity, and the low-intensity acceleration from high vehicle velocity.

High-Intensity Acceleration from Zero Vehicle Velocity, Cycles 1640-1790

The combustion evolution during this acceleration process is broken into sections to permit more detailed analysis of specific engine behavior, and these sections are marked by the divisions shown in Figure 8.41. Cycles 1642-1708 are grouped together because they encompass the very intense acceleration at the onset of the transient. The period of decreasing engine command and fueling rate following the initial acceleration is contained in cycles 1708-1730, and the period of increasing and then decreasing engine command and fuel mass is grouped together during cycles 1735-1778.

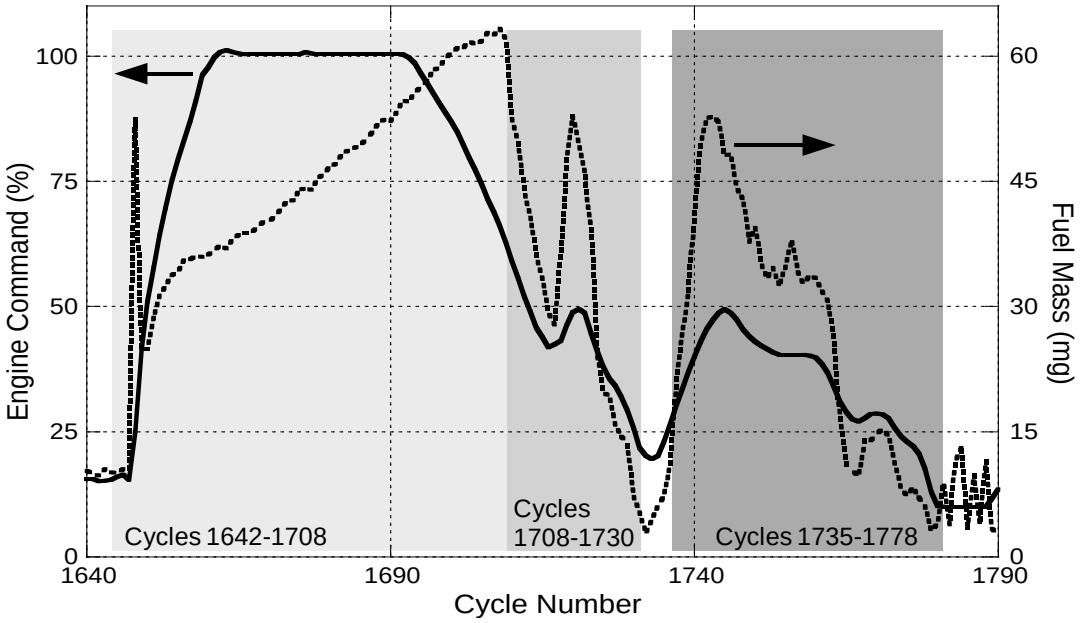

Figure 8.41: Engine Command, Fuel Mass, and Divisions Created for Heat Release Analysis in Cycles 1640-1790 of High-Intensity Acceleration from Zero Vehicle Velocity during FTP 75

Figure 8.42 displays heat release curves from the initial portion of acceleration when engine command and fueling rates are increasing. Combustion prior to the acceleration is represented by cycles 1642 and 1647 which show conditions of completely premixed combustion. There is a step change in fuelling rate in cycle 1648, as the fuel mass in this cycle is nearly five times the fuel mass of cycle 1647 and over twice the amount of fuel as cycle 1649. The combustion in cycle 1648 has a huge spike in premixed combustion which is 1.7 times the value observed in cycle 1647, and is nearly two times higher than any other premixed spike observed during any steady-state engine operation. After the premixed spike, the presence of some weak diffusion combustion is detectable. Since the premixed spike is completed by 10º after TDC and the fuel injection event for this cycle lasts until 13.7º after TDC, the fuel injected later must combust in a diffusive manner. The following cycle, 1649, has a much shorter injection duration, and the combustion for this cycle returns back to being completely premixed.

Following cycle 1649, the combustion modes transition from being fully premixed to having both premixed and diffusion aspects. This is first discernable around cycle 1668. By cycle 1708, the cycle at the zenith of the fueling rate and engine power, the heat release has a relatively mild premixed component and is strongly diffusive in nature.

From cycle 1647 to 1648, the start of injection timing advances by 2.2º, as seen in Figure 8.43, but the ignition delay remains the same, as shown in Figure 8.44. During the period following cycle 1649, the engine retards engine timing back to the original setting of around 4º after TDC, which contributes to the retarding location of the premixed spike as the acceleration takes place. Also playing a role is changing timescales. As the engine speed increases, the time elapsed for each crank angle goes down, resulting in longer combustion events on a crank angle basis. This is also noticeable when considering the trend of ignition delay between cycles 1640-1680. The

injection timing remains relatively unchanged through the remainder of this portion of the load increase. During the cycles following 1685, decreased ignition delays and an advance in the combustion timing is observed and is most likely due to hotter in-cylinder conditions prior to combustion which accelerate the time necessary to prepare fuel for combustion.

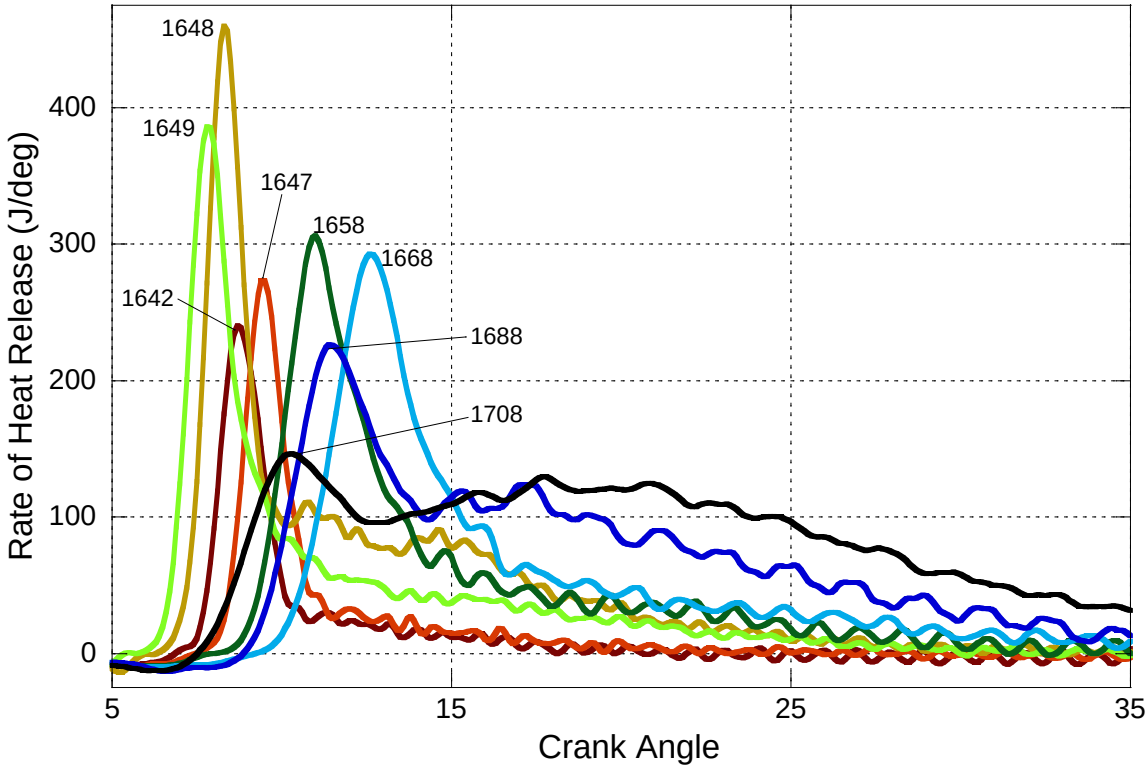

Figure 8.42: Rate of Heat Release Curves for Cycles 1642-1708 of High-Intensity Acceleration from Zero Vehicle Velocity during FTP 75

The mass fraction burned durations for the high-intensity acceleration from zero vehicle velocity is shown in Figure 8.45. As the fuelling step occurs, all three displayed durations increase, as the number of crank angles to release the energy goes up. As the engine speeds up, injects more fuel, and transitions into combustion that has both premixed and diffusion portions, the burn durations increase significantly. In fact, the number of crank angles required to reach 50% MFB and 90% MFB, also known as the combustion duration, goes up by a factor of five.

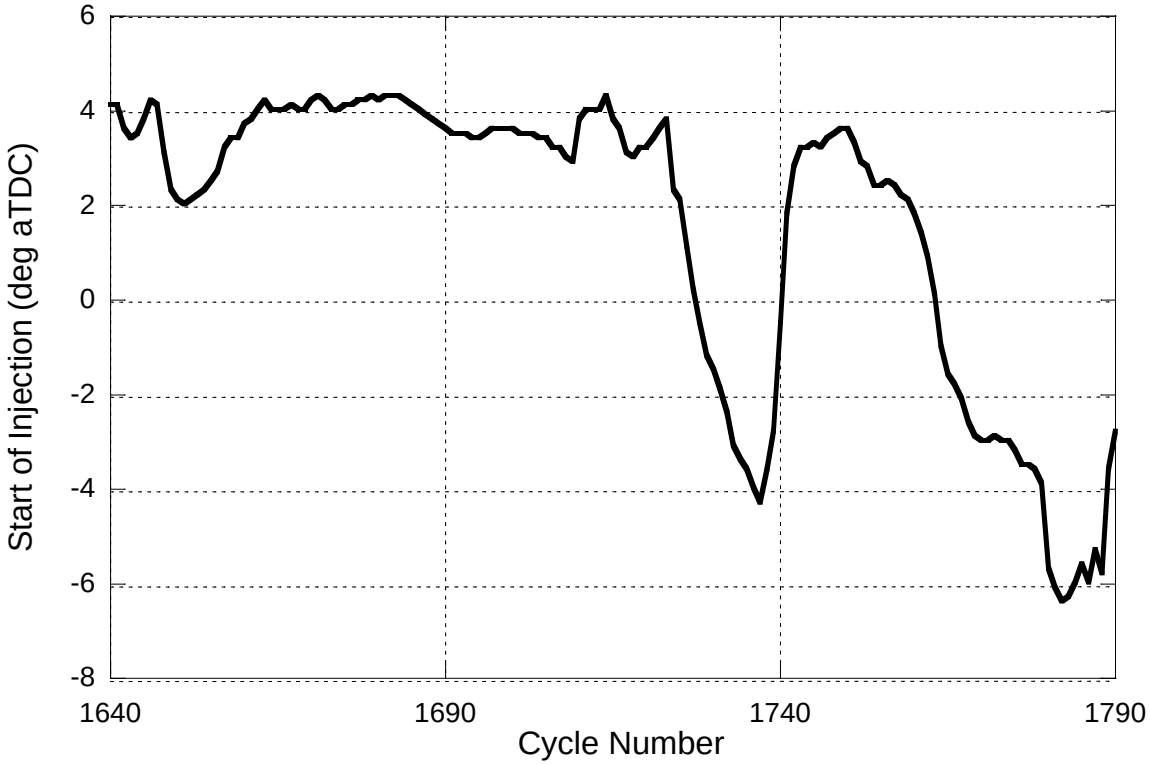

Figure 8.43: Start of Fuel Injection Timing for High-Intensity Acceleration from Zero Vehicle Velocity during FTP 75

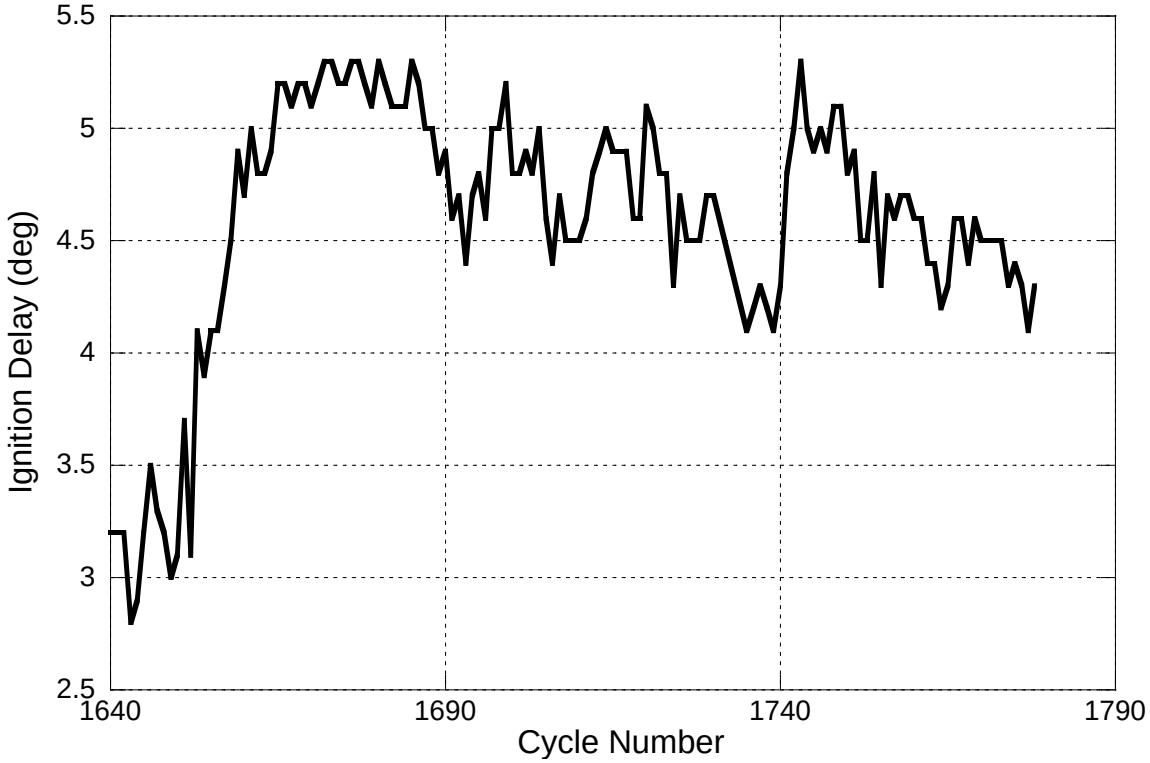

Figure 8.44: Ignition Delay for High-Intensity Acceleration from Zero Vehicle Velocity during FTP 75

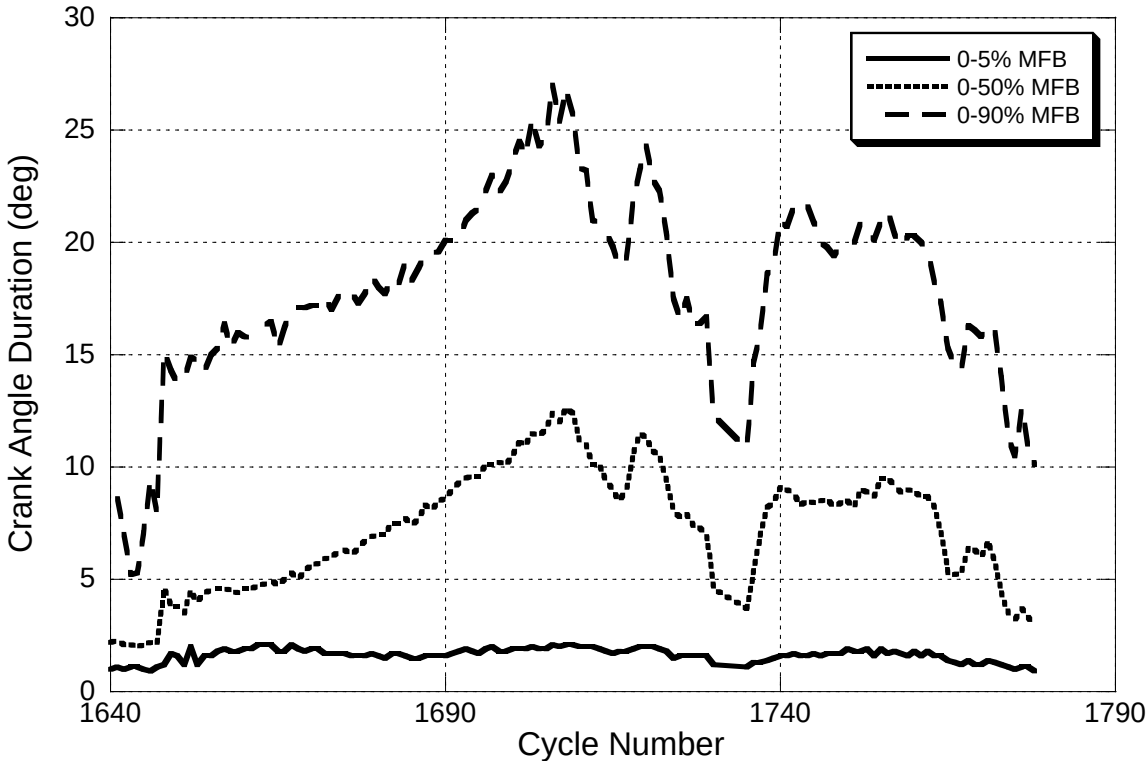

Figure 8.45: Mass Fraction Burned Durations for High-Intensity Acceleration from Zero Vehicle Velocity during FTP 75

Behavior of the combustion process during the fall in engine command, injected fuel mass, and power during cycles 1708-1730 is shown in Figure 8.46. In cycle 1712, as load begins to fall from the levels of cycle 1708, the premixed spike remains unchanged, but the quantity of diffusion combustion is reduced. Cycle 1717 demonstrates heat release that is much lower in intensity, but retains the relative proportions of premixed and diffusion burning as the previous cycles. The blip in engine command and fuel mass during the deceleration causes an increase in heat release, and this is visible in cycle 1722. Continued reduction in the engine command and fueling rate lead to weaker and weaker combustion events, as demonstrated by cycles 1727 and 1730, and the heat release is transitioning back into purely premixed combustion. Injection timings during the period advances and ignition delay remains constant, resulting in more advanced combustion as the engine reaches lower speeds and loads. Crank angle durations for MFB points also become shorter, reflecting the presence of premixed combustion.

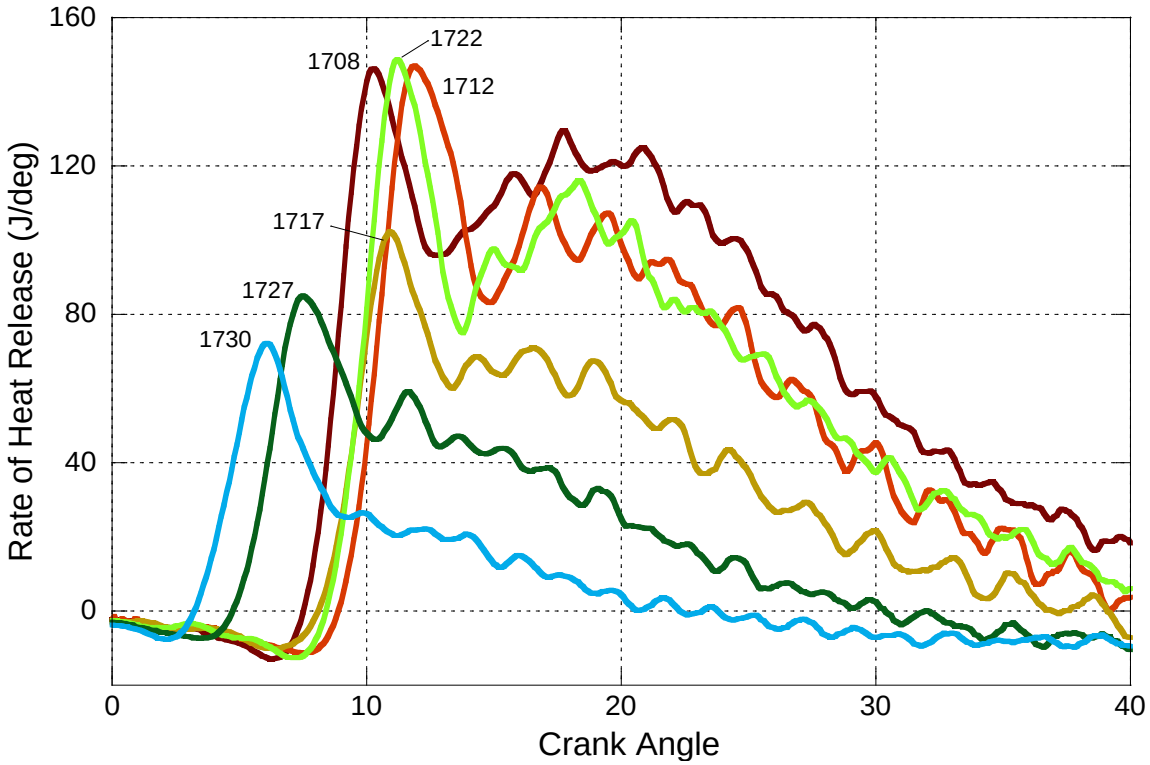

Figure 8.46: Rate of Heat Release Curves for Cycles 1708-1730 of High-Intensity Acceleration from Zero Vehicle Velocity during FTP 75

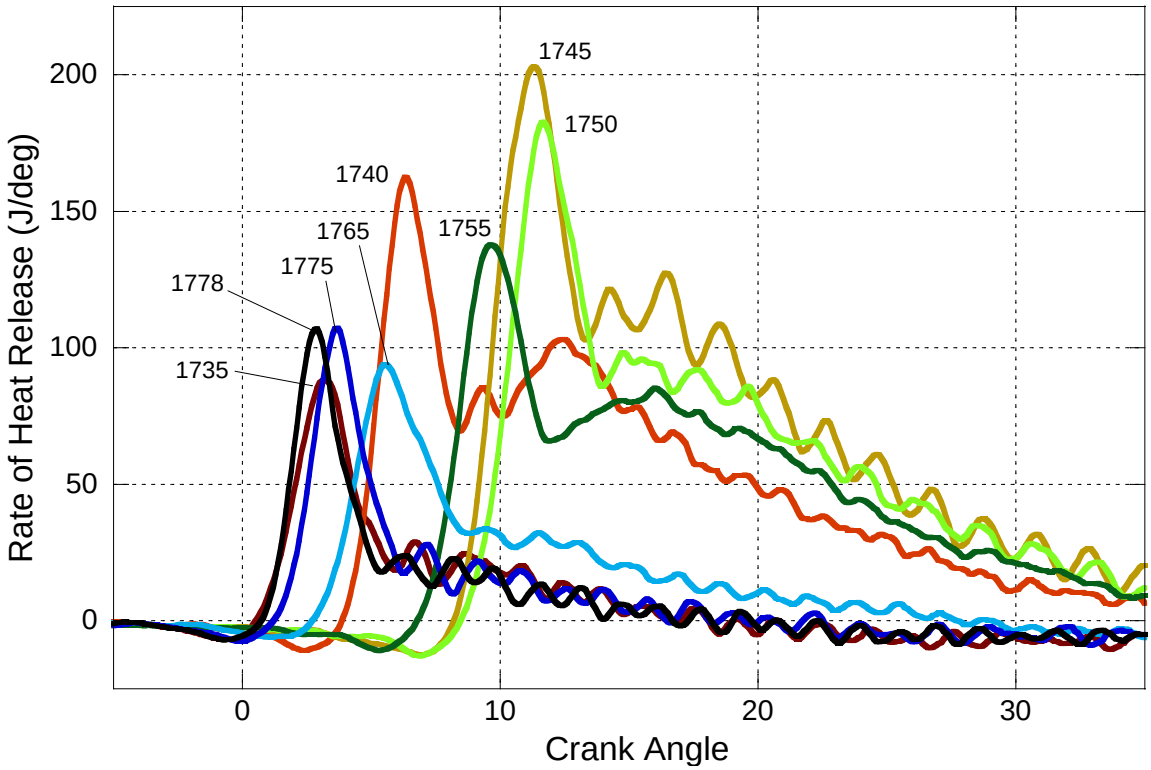

Figure 8.47: Rate of Heat Release Curves for Cycles 1735-1778 of High-Intensity Acceleration from Zero Vehicle Velocity during FTP 75

For the final period of this high-intensity acceleration from zero vehicle velocity during cycles 1735-1778, engine load first increases and then decreases. This is reflected in the rate of heat release curves from this period shown in Figure 8.47. As engine load increases, the combustion goes from completely premixed in cycle 1735 to a combination of premixed and diffusion combustion by cycle 1740. Cycle 1745 occurs very near the peak fueling levels and the rate of heat release reaches highest premixed and diffusion levels as well. As engine load decreases in cycles 1750-1765, the strength of diffusion combustion goes down until it completely disappears by cycle 1775. The combustion process returns to its original state by cycle 1778, which is completely premixed.

Prior to the beginning of this final period of increasing engine command, injection timings are quite advanced at 4º before TDC. Once the load begins increasing, the start of injection retards to near 4º after TDC within the span of a few cycles. This causes the significant rightward shift of the location of the premixed combustion spike seen in cycles 1335-1745. Ignition delay is increased during this period; partly due to the later injection timings and partly due to the reduced timescales from higher engine speeds. Injection timings remain at this retarded state until engine command is decreased around cycle 1760, when they move back to their advanced condition.

Mass fraction burned curves behave as expected, with longer combustion durations under higher engine load and speed. The presence of a significant portion of diffusion combustion contributes to the amount crank angles necessary to consume the fuel. As the engine command decreases and combustion shifts back to a purely premixed phase, combustion duration, as well as the 0-5% MFB and 0-50% MFB durations decrease.

High-Intensity Acceleration from Moderate Vehicle Velocity, Cycles 1920-2320

This acceleration is broken into sections of cycles to facilitate a clearer understanding of combustion evolution. Three major divisions are made and are similar to the partitions made in the high-intensity acceleration from zero vehicle velocity; they are represented in Figure 8.48. Cycles 1935-1973 encompass the cycles during the initial portion of the acceleration, where engine speeds and torques go from very low moderately high values. Cycles 1973-1985 contain combustion events while the engine command, fueling rate, and power are decreasing. Finally, cycles 1995-2040 are analyzed to evaluate combustion as the engine undergoes acceleration to a high-power condition. Rate of heat release analysis is conducted on cycles within these regions, and the transitions from one operating state to another are scrutinized to understand how combustion evolves during such engine behavior.

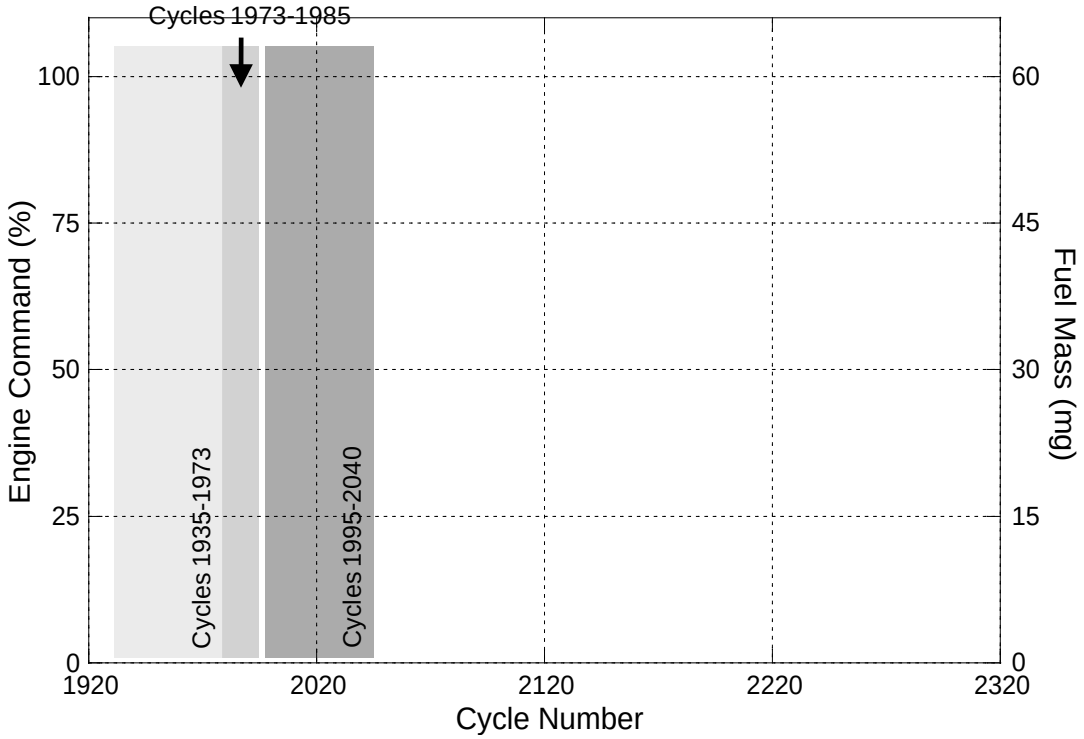

Figure 8.48: Engine Command, Fuel Mass, and Divisions Created for Heat Release Analysis in Cycles 1920-2320 of High-Intensity Acceleration from Moderate Vehicle Velocity during FTP 75

Heat release curves for cycles 1935-1973 are displayed in Figure 8.49. Three consecutive cycles from 1935-1937 are plotted to demonstrate how combustion evolves during this rapid increase in engine command. Cycle 1935 represents combustion behavior prior to the increase in load, and is fully premixed in nature. Heat release from cycle 1936 is the result of a step change in fuel mass which is 8.2 times greater than cycle 1935. The combustion is mainly premixed, and the intensity of the premixed burn spike increases by a factor of 1.5. Some diffusion combustion is present in this combustion event as well. Cycle 1937 fuel mass is slightly lower, but the strong intensity of the premixed spike and the presence of diffusion burning remains. Cycle 1942 is almost completely premixed in nature, and the intensity of the spike is equivalent to cycle 1937. After cycle 1942, the combustion modes transition smoothly to a combination of premixed and diffusion combustion. By cycle 1973 at the end of the increasing fueling rates, the combustion is characterized as predominantly diffusive.

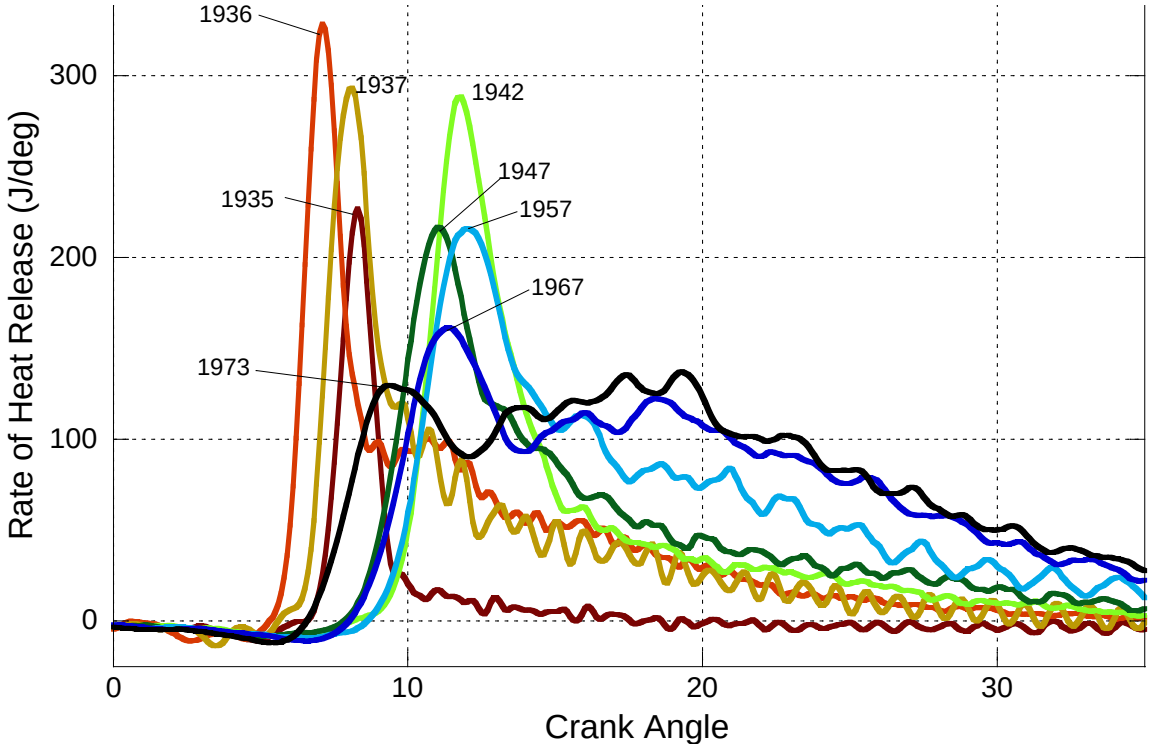

Figure 8.49: Rate of Heat Release Curves for Cycles 1935-1973 of High-Intensity Acceleration from Moderate Vehicle Velocity during FTP 75

Injection timing during cycles 1935-1973 retards about 1º overall, as displayed in Figure 8.50. Cycles 1936 and 1937 have injection timings right around 2º after TDC, which is earlier than the cycles around them and contributes to these cycles being more advanced than others. As the acceleration progresses, the phasing of cycle 1942 and others following is later than previous cycles due to higher engine speeds and longer crank angle-based ignition delays as shown in Figure 8.51. By cycle 1960, the ignition delay climbs to over 6º. As more heat is generated from the more intense combustion, though, ignition delay begins to shorten and by cycle 1973 it drops to 4.4º.

Mass fraction burned trends for this acceleration are shown in Figure 8.52. As in the previous case, the onset of the acceleration lengthens the crank angle burn durations. The transition from purely premixed combustion to a mixture of premixed and diffusion contributes to this, as does the shortening timescales with higher engine speed.

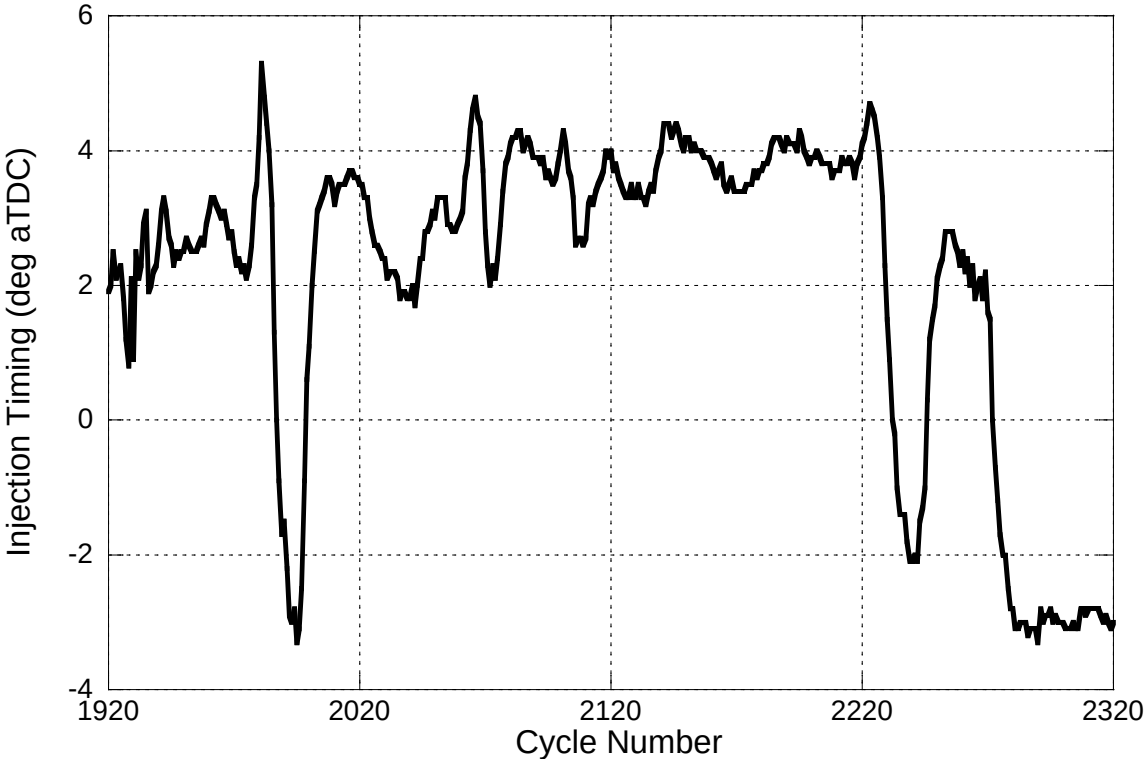

Figure 8.50: Start of Fuel Injection Timing for High-Intensity Acceleration from Moderate Vehicle Velocity during FTP 75

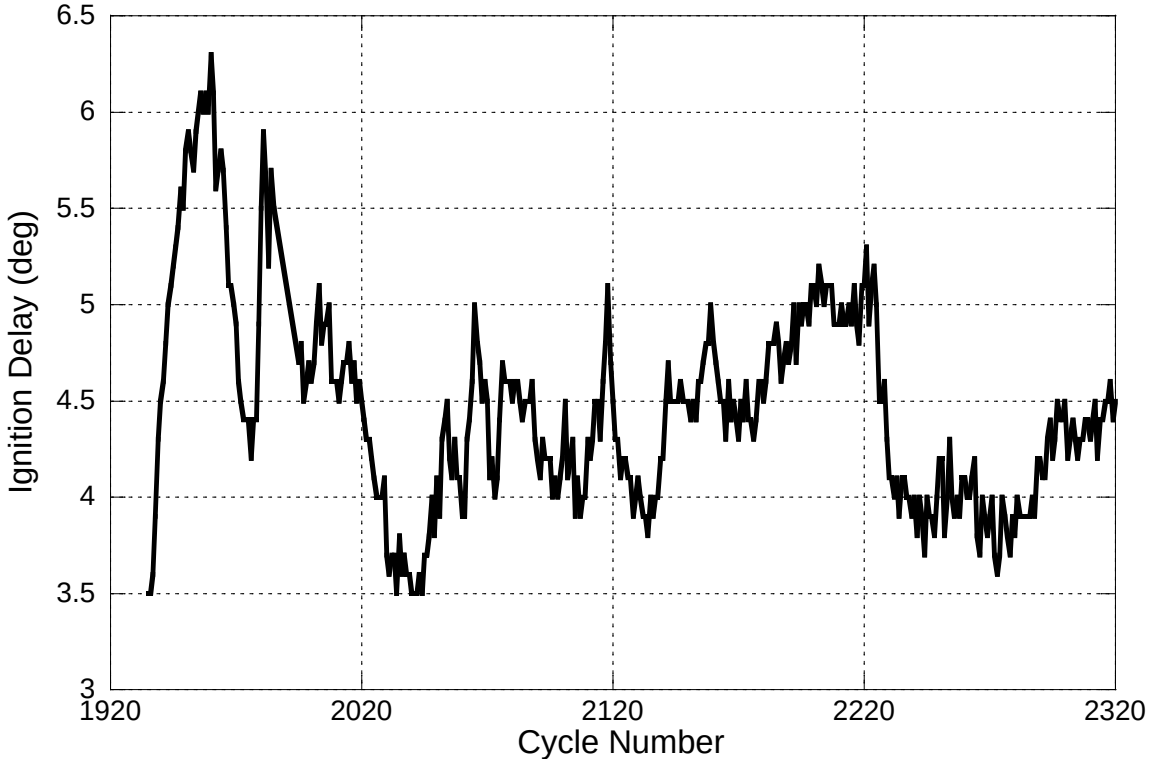

Figure 8.51: Ignition Delay for High-Intensity Acceleration from Moderate Vehicle Velocity during FTP 75

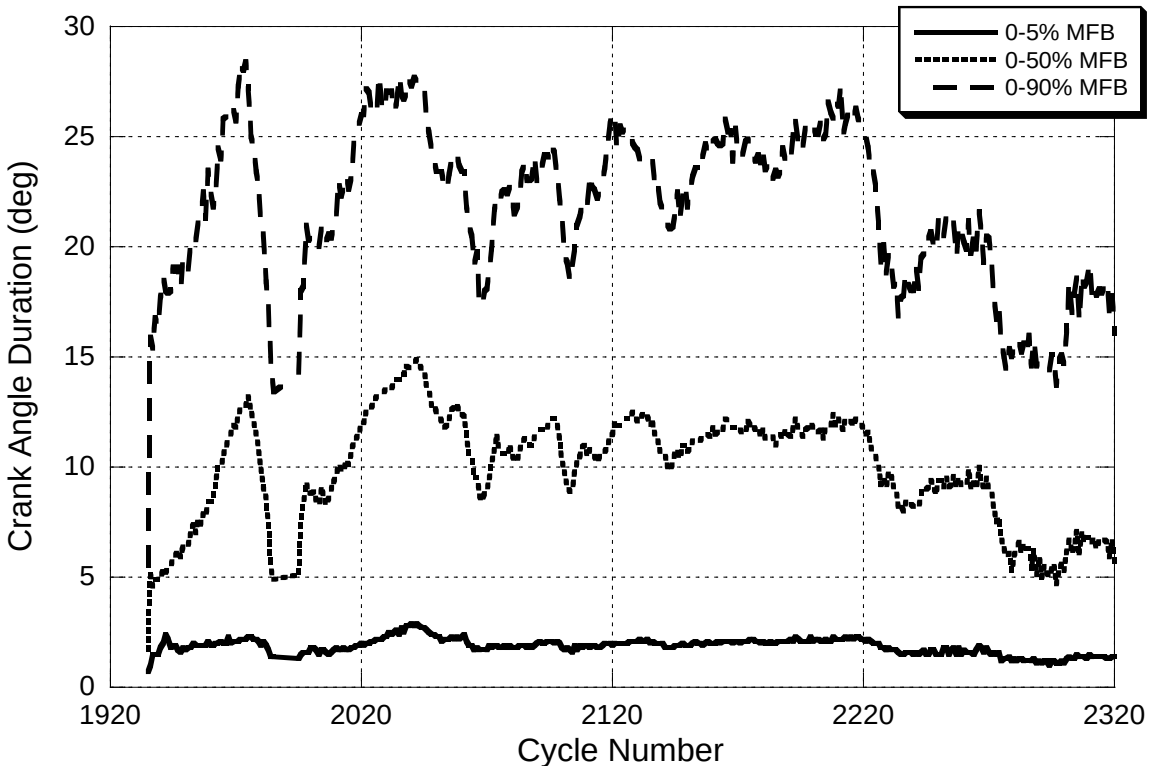

Figure 8.52: Mass Fraction Burned Durations for High-Intensity Acceleration from Moderate Vehicle Velocity during FTP 75

Rate of heat release curves for the cycles 1973-1985, in which engine command and fueling rate are falling, are shown in Figure 8.53. Fuel mass rates are falling progressively and lead to the continual reduction in the area enclosed by these curves. During this period, combustion begins as a combination of premixed and diffusion combustion. Transitioning from cycles 1973 to 1981 there is a significant retardation in injection timing from 2.1º after TDC to 5.3º after TDC, which lengthens ignition delay and consequently increases the relative proportion of premixed combustion and decreases the relative amount of diffusion combustion. From cycles 1981 to 1985, the injection timing advances back to around 2º after TDC, which shortens the ignition delay and advances the combustion phasing. By this stage, little fuel is injected and premixed burning dominates the combustion process.

Figure 8.54 demonstrates the evolution of combustion during cycles 1995-2040, in which the engine transitions from a low speed and load condition to a high power operating point. Cycle 1995 is completely premixed, but in the span of 10 cycles, the engine smoothly transitions into premixed and diffusion burning. During these cycles, the injection timing changes from -3.3º to 3.5º after TDC, the ignition delay increases on a crank angle basis, and the engine speed goes up. These contribute to the progressively later combustion from cycles 1995 to 2005. Combustion remains relatively unchanged between cycles 2005 and 2020. After this, the injection timing begins to advance, reducing the ignition delay and the time required to prepare the fuel and air for combustion. Combustion starts earlier in the cycle when less fuel is present, which results in much more mild premixed combustion and increases the proportion of diffusion combustion. This is evident when observing the progress of the rate of heat release curves from cycle 2015-2040. By cycle 2040, the combustion appears to have very little premixed behavior and is mostly diffusion combustion. This transition to more diffusion combustion is evident from the lengthening mass fraction burned durations in Figure 8.52 during these cycles.

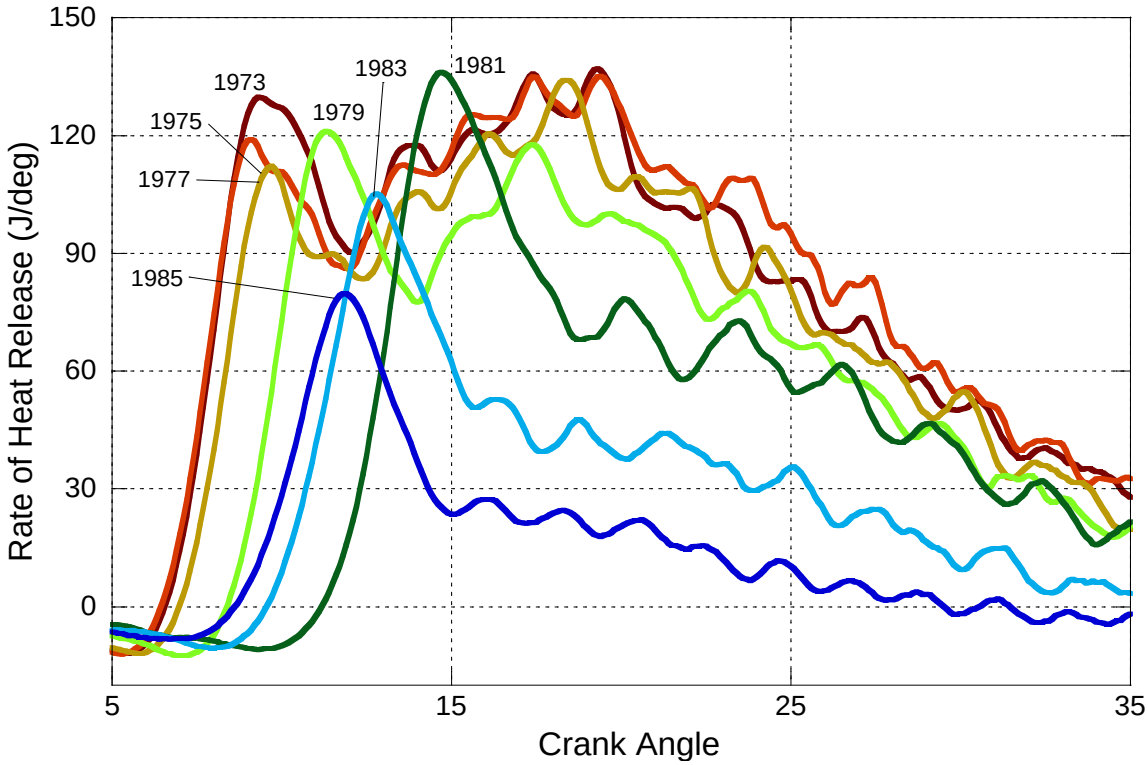

Figure 8.53: Rate of Heat Release Curves for Cycles 1973-1985 of High-Intensity Acceleration from Moderate Vehicle Velocity during FTP 75

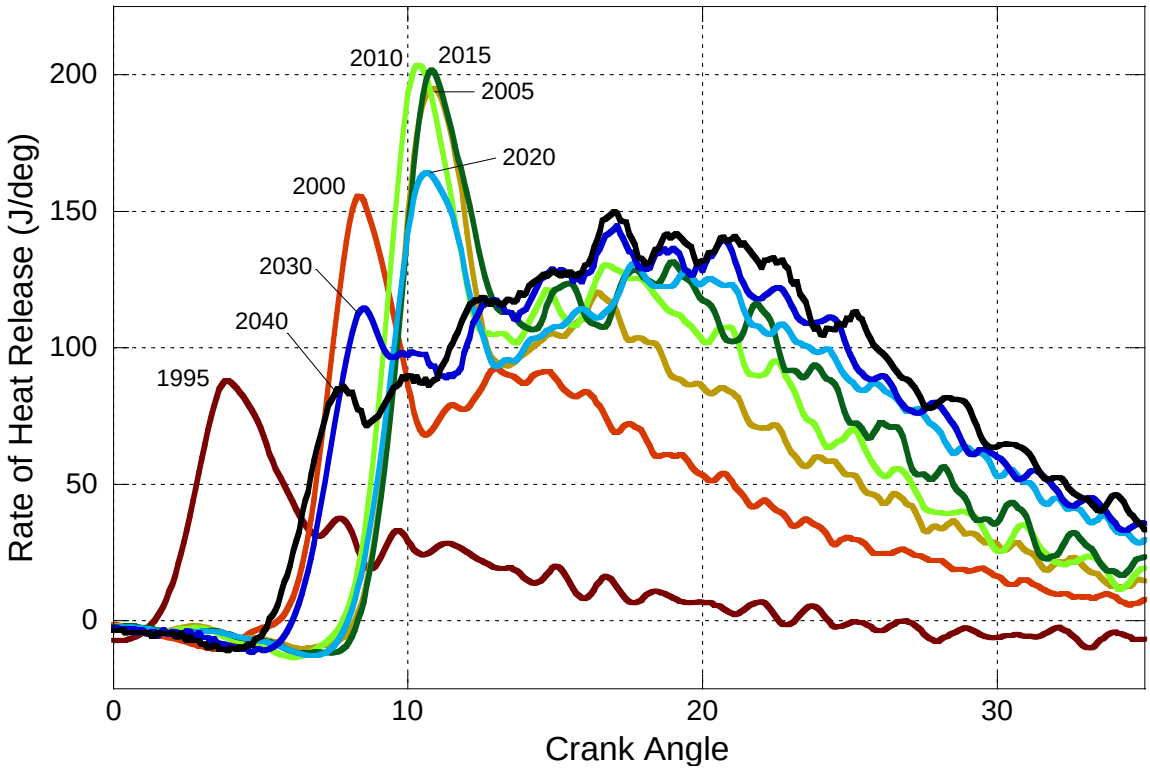

Figure 8.54: Rate of Heat Release Curves for Cycles 1995-2040 of High-Intensity Acceleration from Moderate Vehicle Velocity during FTP 75

Low-Intensity Acceleration from High Vehicle Velocity, Cycles 2350-2950

The period of vehicle acceleration between cycles 2350-2950 is characterized by constant engine behavior that is quite smooth when compared to the other accelerations. Because of this, only two divisions are made during this acceleration, and these regions are denoted in Figure 8.55. Cycles 2350-2581 encompass a period in which engine command and fuel mass are rising steadily. Between cycles 2581-2931, engine command falls gradually and then gradually goes up and down again before ending the acceleration with engine command and fuel mass at relatively constant levels.

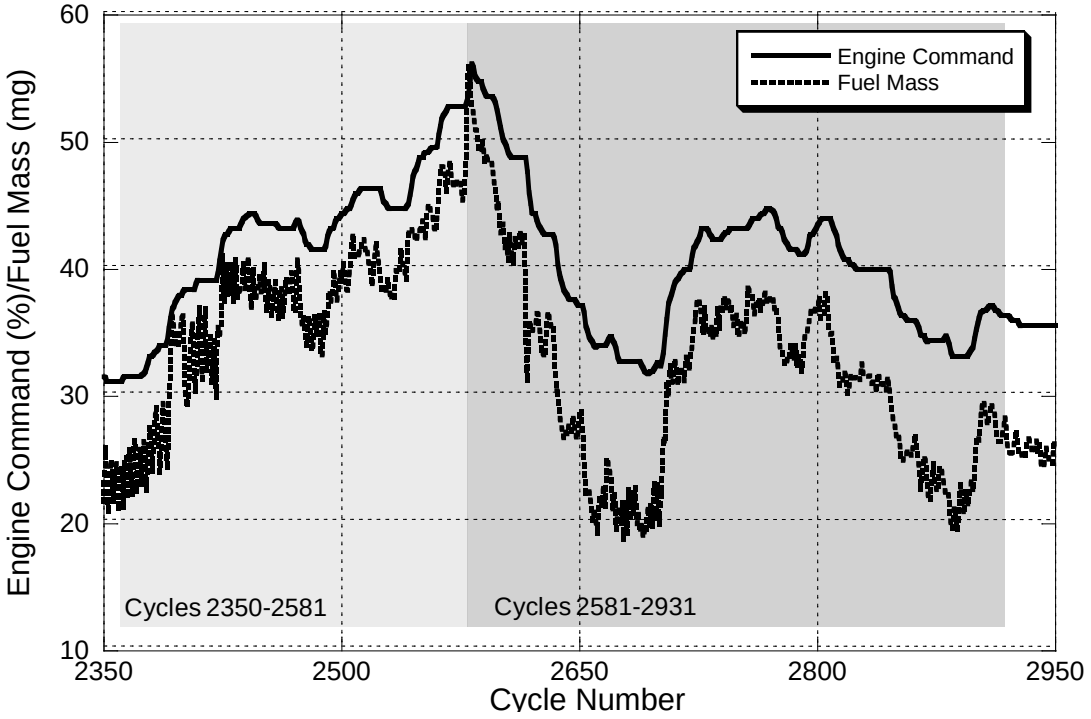

Figure 8.55: Engine Command, Fuel Mass, and Divisions Created for Heat Release Analysis in Cycles 2350-2950 of High-Intensity Acceleration from Moderate Vehicle Velocity during FTP 75

Rate of heat release curves are shown for cycles 2350-2581 in Figure 8.56. At the onset of the acceleration at cycle 2350, combustion consists of combustion that has premixed and diffusion burning characteristics. Between cycles 2350 and 2482, combustion becomes steadily more intense, with significant growth in the proportion of

diffusion combustion. The premixed portion of combustion is quantitatively unchanged during this period. Combustion phasing does retard steadily during this period, and is attributed to the later injection timings that occur during these cycles and relatively unchanged values of ignition delay. The start of fuel injection is shown in Figure 8.57 and demonstrates that from cycle 2350 to 2482, the injection timing retards from -2.5º to 2.2º after TDC. During this same period, ignition delay does not change significantly, as shown in Figure 8.58.

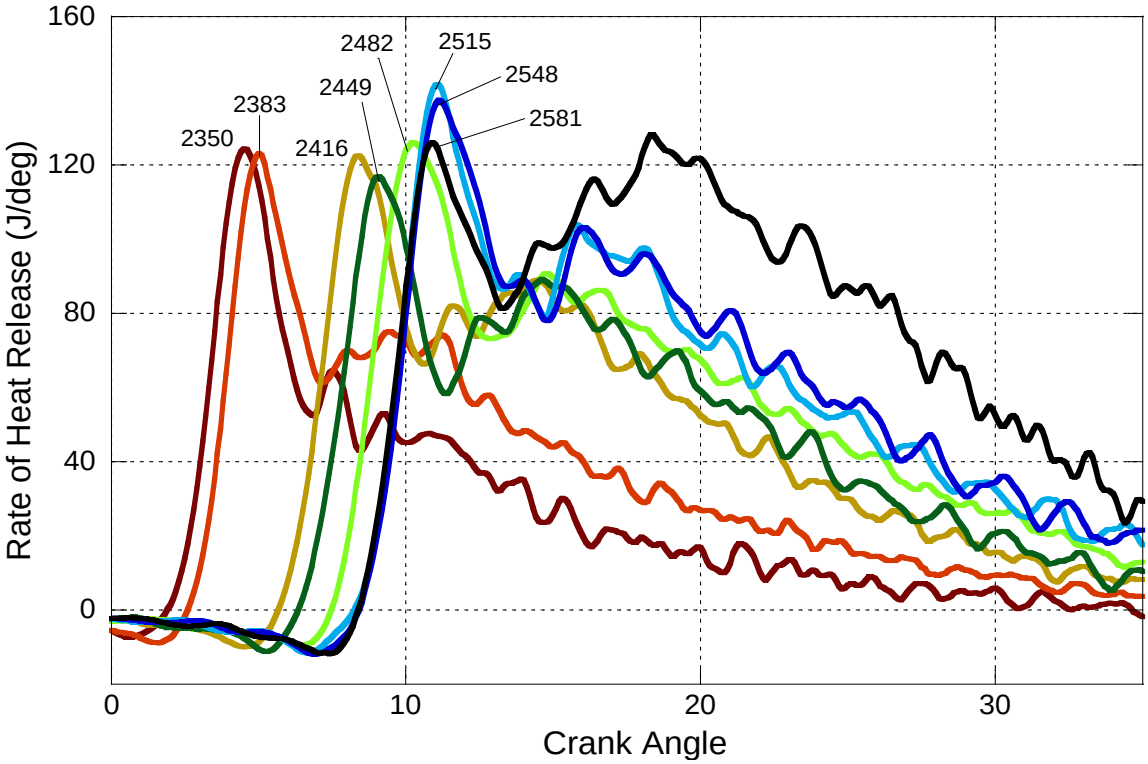

Figure 8.56: Rate of Heat Release Curves for Cycles 2350-2581 of Low-Intensity Acceleration from High Vehicle Velocity during FTP 75

Cycles 2515 and 2548 experience a proportionately higher level of premixed combustion, which is most likely due to the longer ignition delays at this condition. Injection timings here are more retarded than in previous cycles (3.7º and 3.6º after TDC) and the proportion of stoichiometric combustion products is over 10%, both of which contribute to longer times necessary to begin combustion. Cycle 2581, the event with the

largest amount of heat release in this acceleration, has an injection timing that is very late at 4º after TDC. The ignition delay for this cycle, however, is less than in cycles 2515 and 2548, resulting in a premixed spike that is similar in size to cycles 2350-2482. The most likely reason for this shorter ignition delay is the lower concentration of stoichiometric combustion products in the cylinder at this condition. The diffusion portion of cycle 2581 is quite large, which reflects the large quantity of energy released during this combustion event.

Mass fraction burned durations are shown in Figure 8.59. During the transition from cycle 2350 to 2581, the increasing mass of fuel, growing proportion of diffusion combustion, and increasing engine speed all contribute to the lengthening of the combustion duration on a crank angle basis. This is especially evident after cycle 2550, where the added fuel greatly contributes to the larger fraction of diffusion combustion.

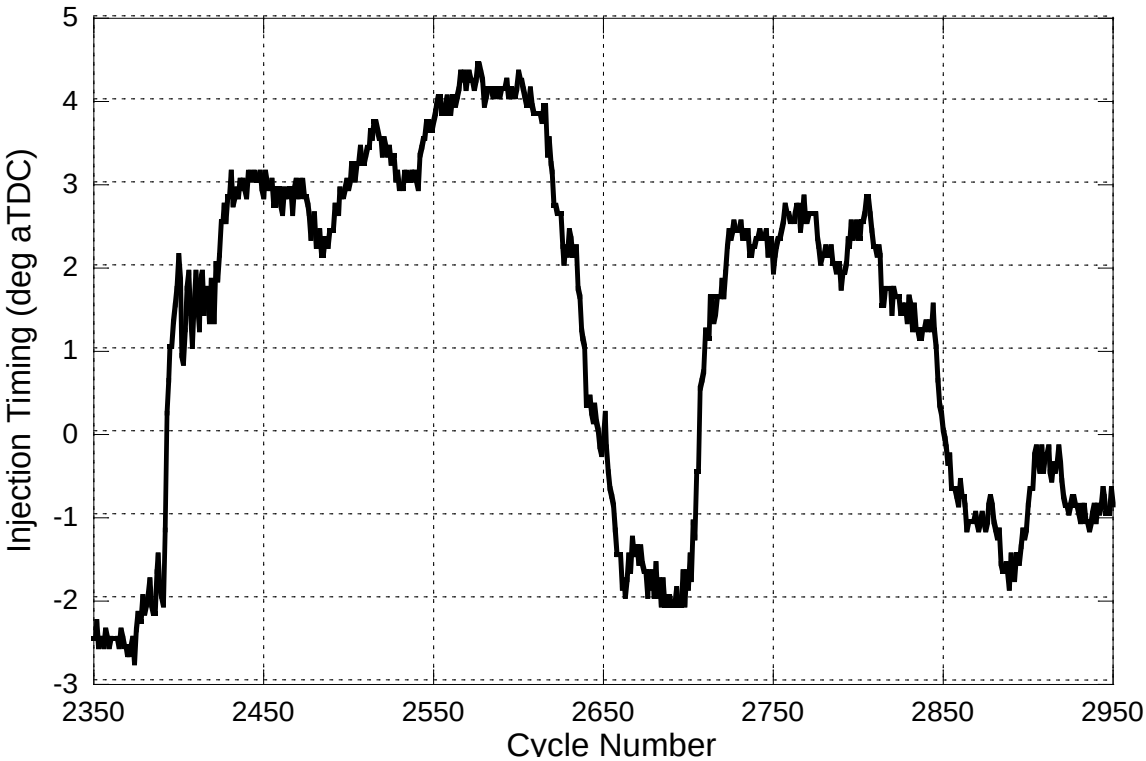

Figure 8.57: Start of Fuel Injection Timing for Low-Intensity Acceleration from High Vehicle Velocity during FTP 75

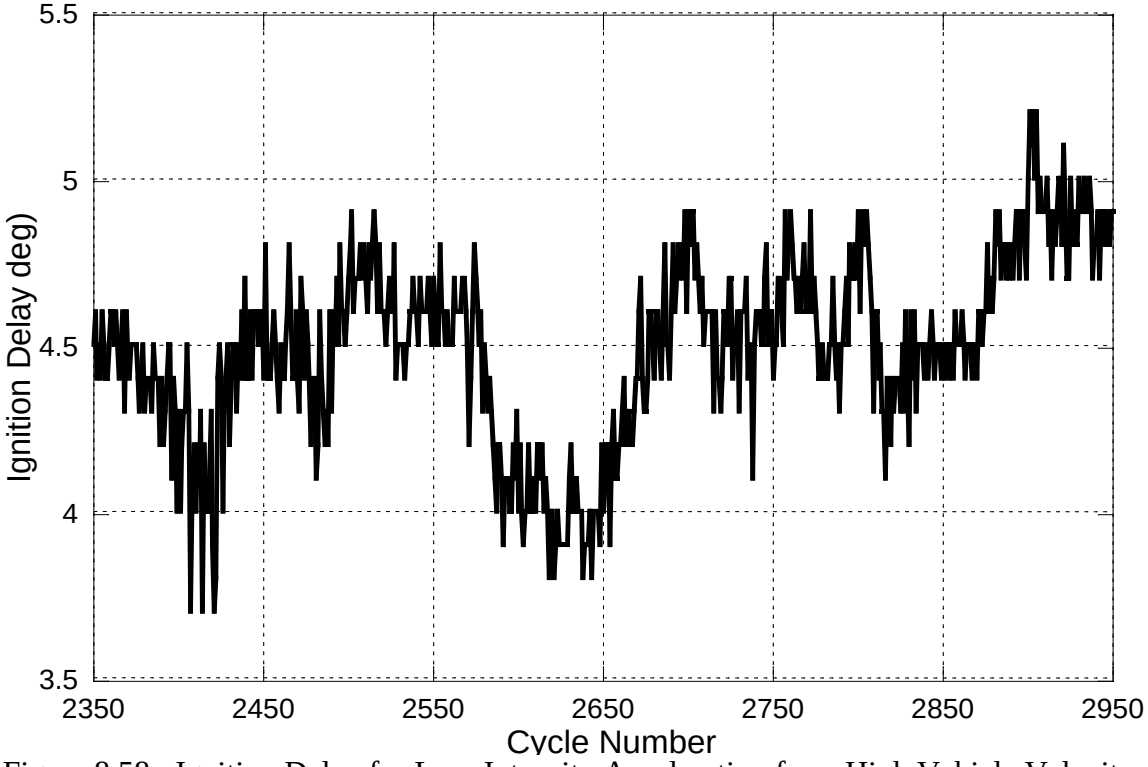

Figure 8.58: Ignition Delay for Low-Intensity Acceleration from High Vehicle Velocity during FTP 75

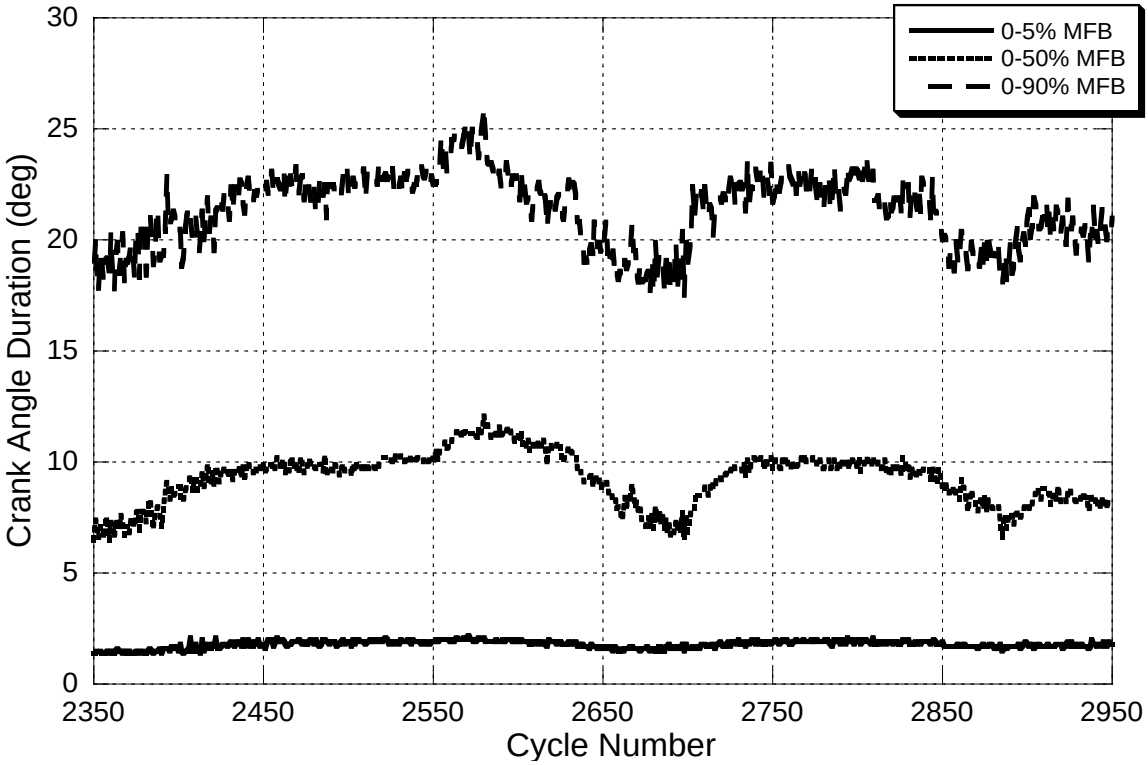

Figure 8.59: Mass Fraction Burned Durations for Low-Intensity Acceleration from High Vehicle Velocity during FTP 75

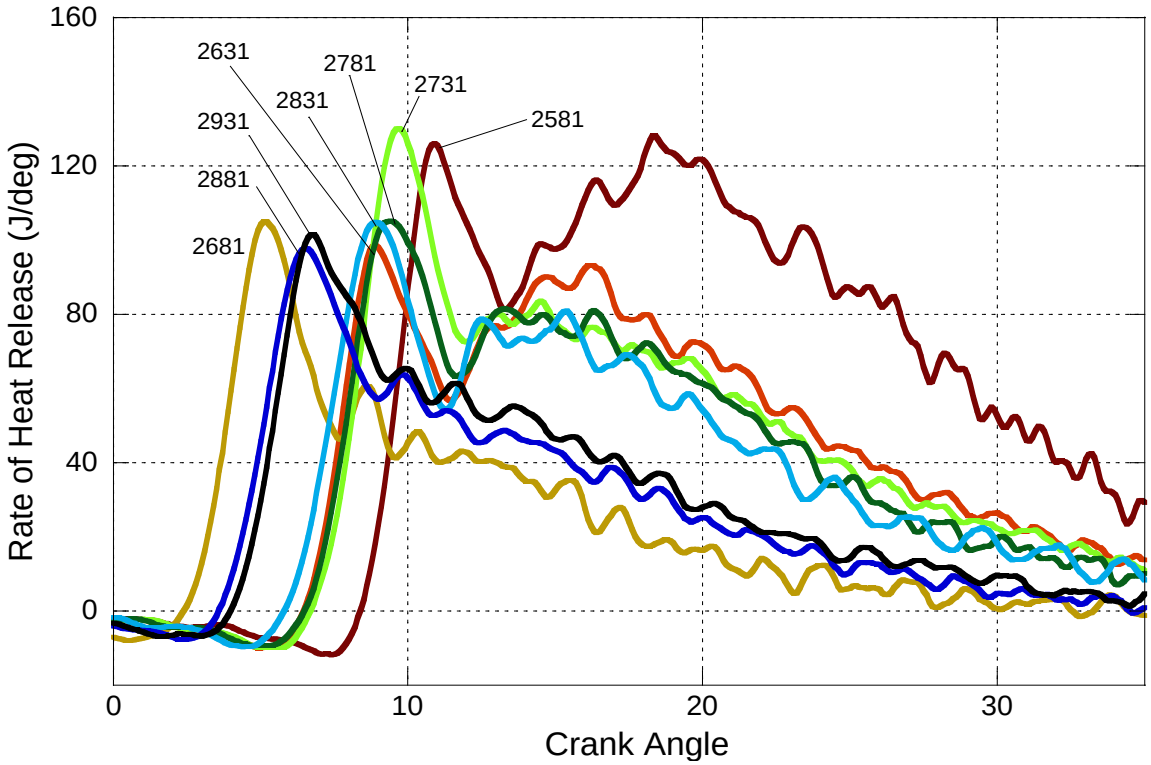

Figure 8.60: Rate of Heat Release Curves for Cycles 2581-2931 of Low-Intensity Acceleration from High Vehicle Velocity during FTP 75

Rate of heat release curves for the remainder of the low-intensity acceleration from high speed are shown in Figure 8.60. The starting cycle in this figure is 2581, which represents the cycle with the greatest quantity of heat release in this acceleration. Between cycles 2581 and 2681, the fuel mass drops by a factor of 2.4 and the injection timing advances by 5.6º, resulting in combustion that is completely premixed in nature and occurs at a much earlier crank angle. From there, engine command gradually increases. As it does, injection timing retards and the quantity of fuel mass increases, resulting in the heat release observed in cycles 2731 and 2781, which have higher levels of both premixed and diffusion combustion. Reductions in engine command and fueling rate, coupled with more advanced injection timings, produce the heat release curves for cycles 2831, 2881, and 2931, which are primarily premixed in nature. Mass fraction burn duration curves demonstrate that those combustion events that occur under higher load last longer; this is due to greater fractions of diffusion combustion.

Combustion Analysis Summary

Combustion analysis is performed on all the cycles contained within three accelerations: high-intensity from zero vehicle velocity, high-intensity from moderate vehicle velocity and low-intensity from high vehicle velocity. It is observed that the transitions that take place from cycle-to-cycle are very similar in all three cases when investigated at this level. Under low-load conditions, engine combustion is primarily premixed. As engine command is increased and the amount of fuel injected goes up, the intensity of the premixed spike increases. The degree to which this occurs is commensurate with the mass of fuel added.

For cases in which a large step change in fuel mass is made from one cycle to another, such as in cycle 1648 or 1936, the intensity of the premixed spike is nearly two times greater than ever observed during steady state conditions. During such cycles, the large amount of injected fuel is typically facilitated by extra-long injection durations which exceed the burn duration of the premixed spike. Therefore the additional fuel burns in a weak form of diffusion combustion.

If engine command is increased in such a manner that the fuel mass change from cycle-to-cycle does not involve an overshoot in the fuel mass, the level of premixed combustion grows first. Diffusion combustion development is secondary. The faster the rate at which fuel energy is added, the greater the extent of premixed growth before the appearance of diffusion combustion. Slower rates of fuel energy addition experience simultaneous growth in premixed and diffusion combustion. If enough fuel energy is added and enough time is permitted, the proportion of diffusion combustion can grow larger than the fraction of premixed combustion.

When the engine is operating at a high load condition, combustion consists of both premixed and diffusion burning. When engine command is increased under such

conditions and all other inputs remain the same, the level of diffusion burn grows larger and the premixed portion remains unchanged.

A decrease in engine command from a high-load condition results first in a reduction in the intensity of diffusion combustion, followed by a decrease in the premixed spike. If the amount of fuel injected reduces to the point where the combustion is completely premixed, then the level of the premixed combustion may either be lower or higher than the premixed intensity prior to the reduction in engine command.

8.2.15 NO Emissions

The formation of NO during constant-speed load sweeps is discussed in Section 7.2.9. Results of these experiments reveal that NO formation is strongly a function of in-cylinder composition, combustion mode, and localized in-cylinder conditions. While this work cannot quantify the influence of spatially-resolved in-cylinder variations, it can assess the impact of in-cylinder composition and combustion mode on NO production.

Accelerations from Zero Vehicle Velocity

The NO emissions for the accelerations from zero vehicle velocity are shown in Figure 8.61and Figure 8.62. Also displayed are the engine command and concentration of O_2 in the cylinder prior to combustion. It is apparent from these graphs that NO concentrations are closely tied to engine command. Any time the engine command increases, the concentration of NO jumps upward. Conversely, falling rates of engine command result in a reduction of NO emissions.

The cycles with the highest NO concentrations observed during the FTP 75 occur during the onset of acceleration from zero vehicle velocity. Initially, engine speed is near idle and load is present but small. The first few cycles of the transient are relatively rich, as the fuel system injects an excess amount of fuel. This causes the O_2

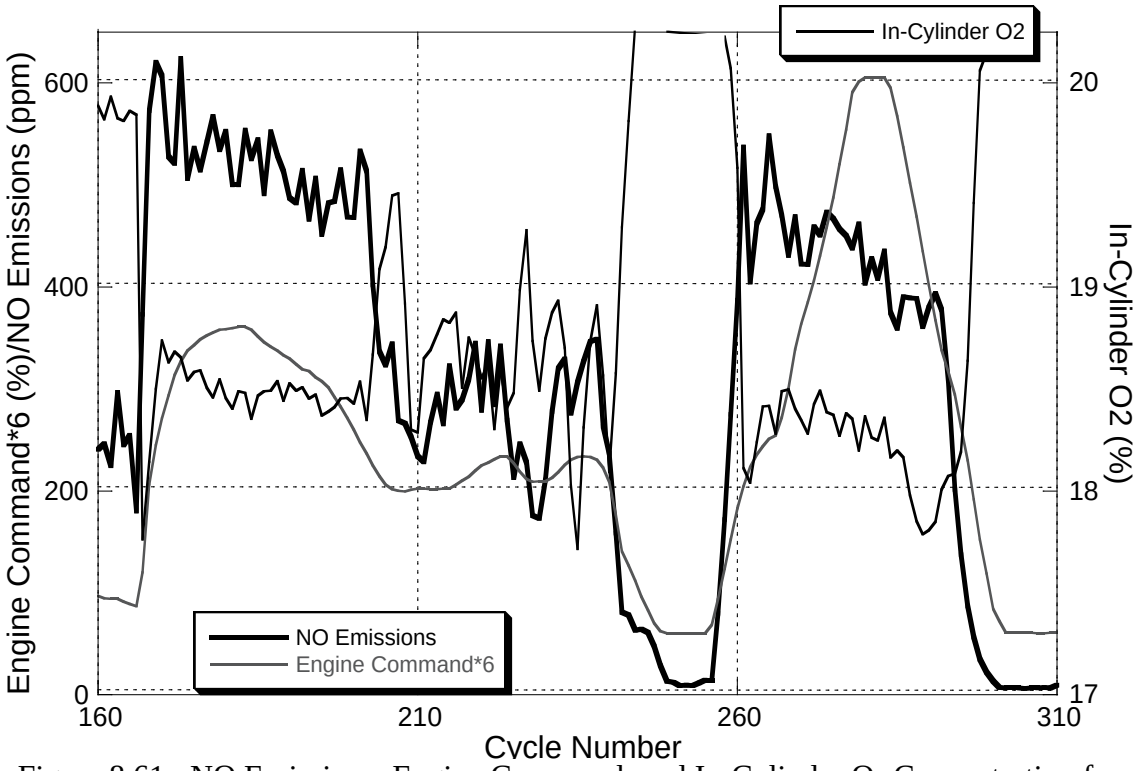

Figure 8.61: NO Emissions, Engine Command, and In-Cylinder O_2 Concentration for Low-Intensity Acceleration from Zero Vehicle Velocity, Cycles 160-310 of FTP 75

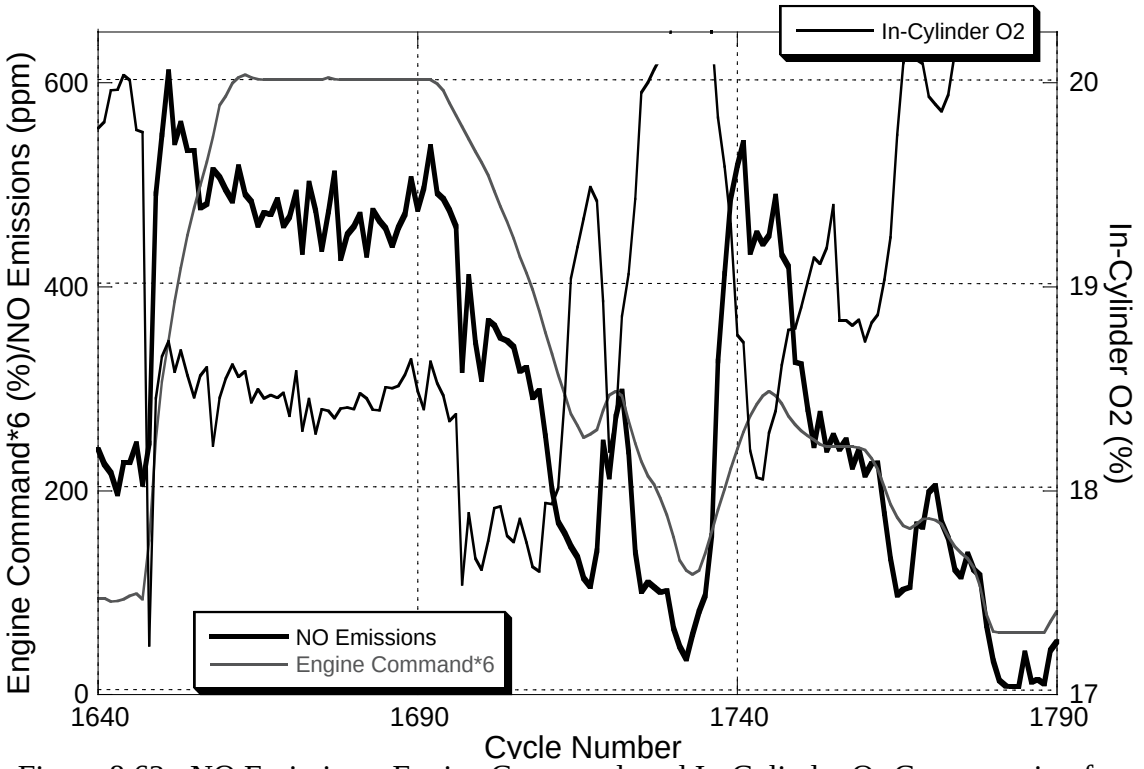

Figure 8.62: NO Emissions, Engine Command, and In-Cylinder O_2 Concentration for High-Intensity Acceleration from Zero Vehicle Velocity, Cycles 1640-1790 of FTP 75

concentration in these cycles to be very low, as evidenced by data from cycles 167 and 1648. NO emissions in these cycles are quite low and remain practically unchanged from the values prior to the acceleration. After a few cycles, however, in-cylinder O_2 levels rise, and NO emissions spike upwards. During these cycles, the combustion mode is intensely premixed (see Figure 8.42), which results in very high localized temperatures in the cylinder. The combination of this premixed combustion and relatively high levels of O_2 in the cylinder contribute to the high NO levels observed a few cycles into the acceleration from zero vehicle velocity.

In the periods following the first few cycles after the beginning of the acceleration, NO levels trend downward gradually as the combustion transitions to more premixed and less diffusion burning. The amount of stoichiometric combustion products in the cylinder also plays a role, as NO tends to be reduced with lower levels of O_2 in the cylinder.

The transitions observed around cycle 250 and 1730 begin with essentially zero-combustion cycles as the engine coasts down in speed and load. When engine command is increased, combustion begins again and transitions quickly into a combination of premixed and diffusion combustion as shown in Figure 8.47. This tempers the amount of NO formed during the transition, and as NO spikes upwards it does not reach the levels observed in the first portions of the accelerations.

Accelerations from Moderate Vehicle Velocity

Figure 8.63 and Figure 8.64 demonstrate NO emissions trends, along with engine command and in-cylinder O_2 concentration prior to combustion for the accelerations from moderate vehicle velocity. When considered at a fundamental level, much of the engine behavior in these accelerations mimics those that occur in the accelerations from zero vehicle velocity. The low-intensity acceleration from moderate vehicle velocity consists

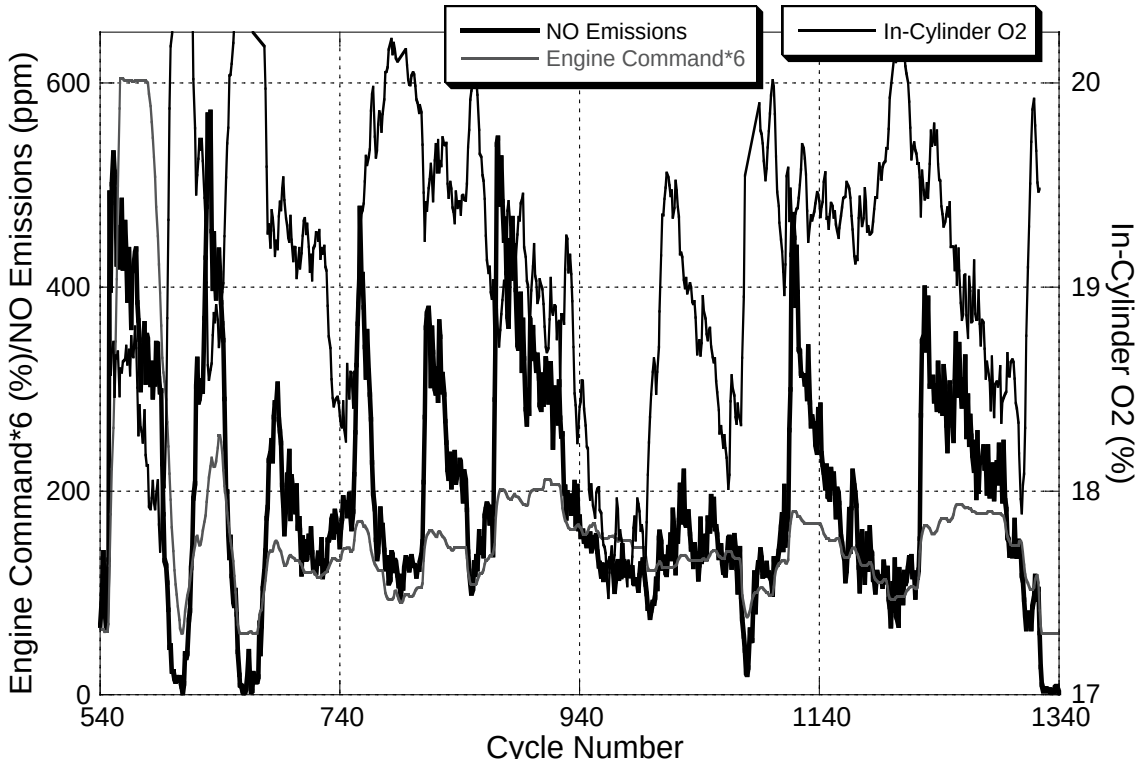

Figure 8.63: NO Emissions, Engine Command, and In-Cylinder O_2 Concentration for Low-Intensity Acceleration from Moderate Vehicle Velocity, Cycles 540-1340 of FTP 75

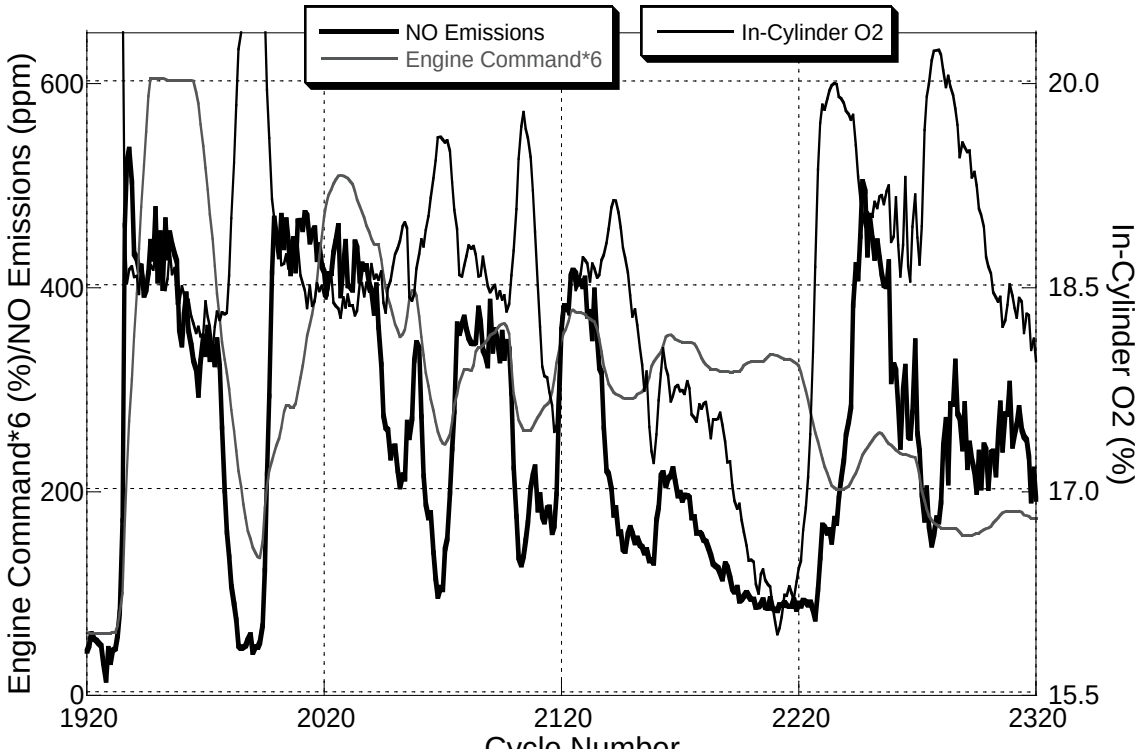

Figure 8.64: NO Emissions, Engine Command, and In-Cylinder O_2 Concentration for High-Intensity Acceleration from Moderate Vehicle Velocity, Cycles 1920-2320 of FTP 75

essentially of one strong engine command increase, followed by a drop to near zero and then a series of minor undulations in engine command. The high-intensity acceleration from moderate vehicle velocity is nearly identical, except that the series of repeating engine command oscillations are more intense and less frequent. This has a significant impact on NO emissions, as engine command and NO formation are so closely linked.

The first portion of these accelerations is similar to the conditions observed in the second part of the accelerations from zero vehicle velocity. Combustion transitions gradually from premixed combustion to premixed-diffusion burning, tempering the NO emissions of the initial cycles, and O_2 concentration in the cylinder dictates NO production in the latter part of the engine command increase. As engine command drops such that the engine is coasting down, lack of fuel injection results in cycles where combustion and NO formation do not occur.

The remainder of the accelerations follow this same trend, with engine command either increasing or decreasing and NO formation mimicking the behavior. Rapid increases in engine command result in high levels of in-cylinder O_2 and NO emissions, as shown around cycle 860. Slower increases in engine command have stoichiometric combustion products present throughout, resulting in lower in-cylinder O_2 levels and reduced NO emissions, as displayed near cycle 720.

One period during these accelerations experiences a relatively constant engine command for a number of cycles. Just prior to cycle 2200, engine speed is increasing gently while load remains relatively constant. At this condition, the EGR valve opens significantly and floods the intake manifold with a large quantity of stoichiometric combustion products. This results in much lower levels of in-cylinder O_2 prior to combustion and a marked reduction in NO emissions.

Accelerations from High Vehicle Velocity

The acceleration from high vehicle velocity is much different from the other accelerations studied because the engine command changes much more slowly. Rather than oscillating up and down frequently, it gently trends upward and downward through throughout the acceleration event. Figure 8.65 demonstrates the NO emissions, the engine command, and in-cylinder O_2 prior to combustion for this acceleration.

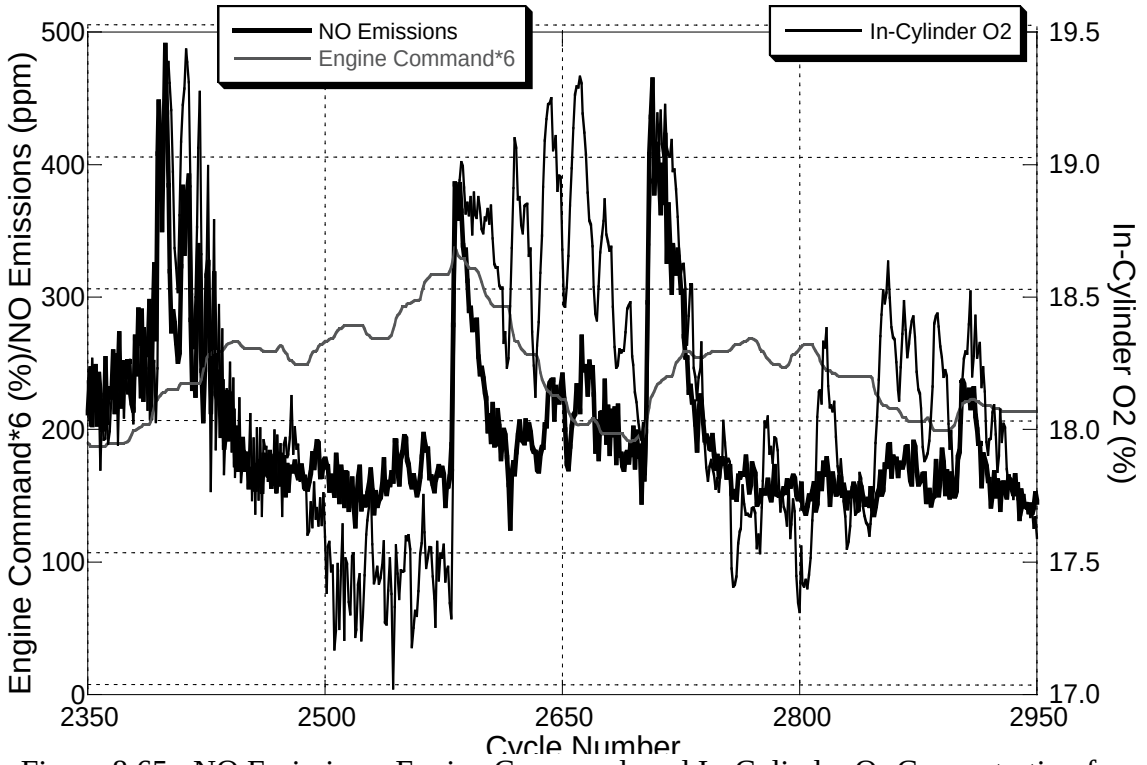

Figure 8.65: NO Emissions, Engine Command, and In-Cylinder O_2 Concentration for Low-Intensity Acceleration from High Vehicle Velocity, Cycles 2350-2950 of FTP 75

NO production during this acceleration is governed by the presence of stoichiometric combustion products in the cylinder. Through most of the acceleration, the EGR valve remains open and the mass fraction of stoichiometric combustion products in the cylinder is above 6%, and NO emissions are under 200 ppm. The only times the EGR valve closes are around cycles 2400, 2580, and 2700. During these periods, the fraction of stoichiometric combustion products falls by a factor of 3, the amount of O_2 in

the cylinder rises, and NO emissions go up by a factor of 2.5. Following the EGR valve closure in cycle 2580, the engine begins a gentle deceleration that spans cycles 2600-2700. During the first part of this period the EGR valve reopens, but O_2 levels in the cylinder are not affected due to falling exhaust CO_2 levels (see Figure 8.28) and small manifold pressure ratios. Despite of this, NO emissions fall; this is attributed to a reduction in injected fuel mass during this period of reducing engine command. This trend continues until the engine command increases again round cycle 2700.

8.2.16 Particulate Emissions

Particulates generated during the investigated accelerations are shown in Figure 8.66 and Figure 8.67. Production of particulates follows a very repeatable pattern: any time there is a large change in engine command in terms of both magnitude and rate that cause air/fuel ratios to fall below 20, particulate bursts are formed. The largest spikes in terms of concentration are observed at the beginning of the accelerations from zero vehicle velocity. For the low-intensity case, cycles 167 and 168 have air/fuel ratios of 12.5 and 19.4 and the highest particulate concentration is 97.2 mg/m^3. For the high-intensity case, cycles 1648 1649 have air/fuel ratios of 10.3 and 19.3 and a peak particulate spike of 432.0 mg/m^3. These extremely low air/fuel ratios are undoubtedly the cause of the huge bursts of particulate at these conditions. Overshooting of the desired fuel injection mass for just a cycle or two results in these low air/fuel ratios. During cycles 260-300, the engine undergoes an intense acceleration, and air/fuel ratios are consistently below 18 and cause an extended period of high particulate emissions.

Similar results are observed when considering the particulates from the accelerations from moderate vehicle velocities. Particulates reach their highest levels near the beginning of the accelerations, when engine command goes from minimum to maximum values in the span of a few cycles, causing air/fuel fuel ratios to remain around

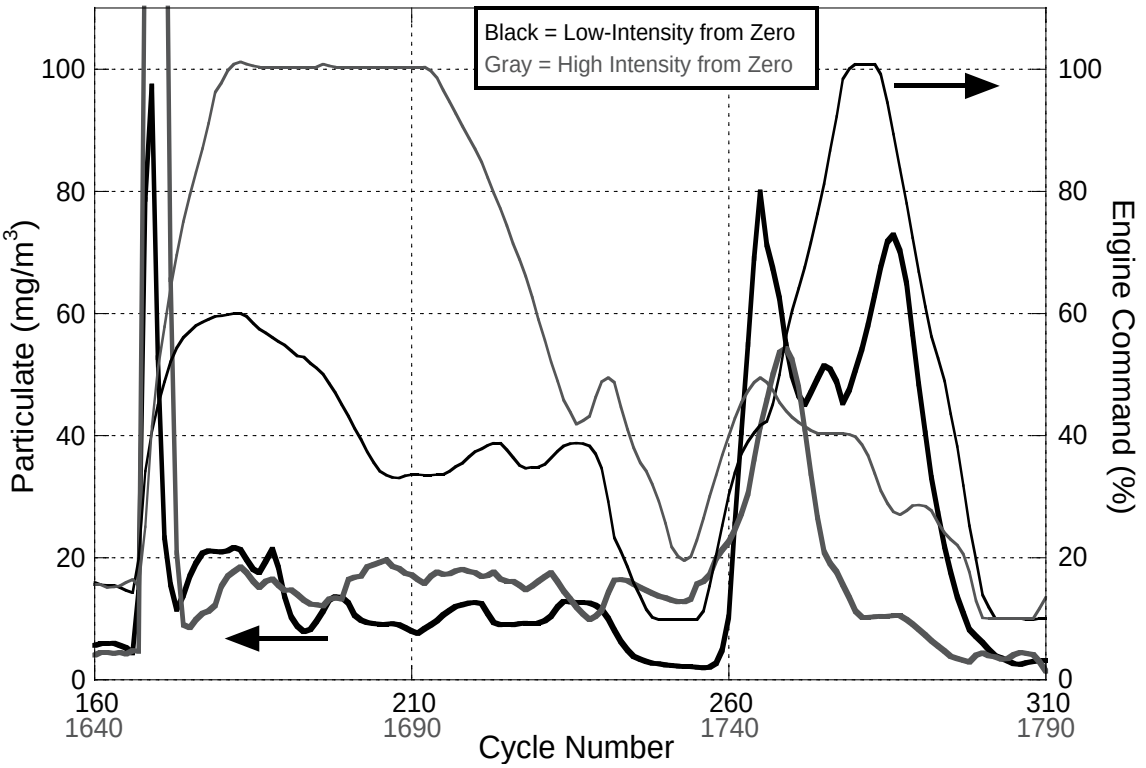

Figure 8.66: Particulate Emissions and Engine Command for Accelerations from Zero Vehicle Velocity during FTP 75

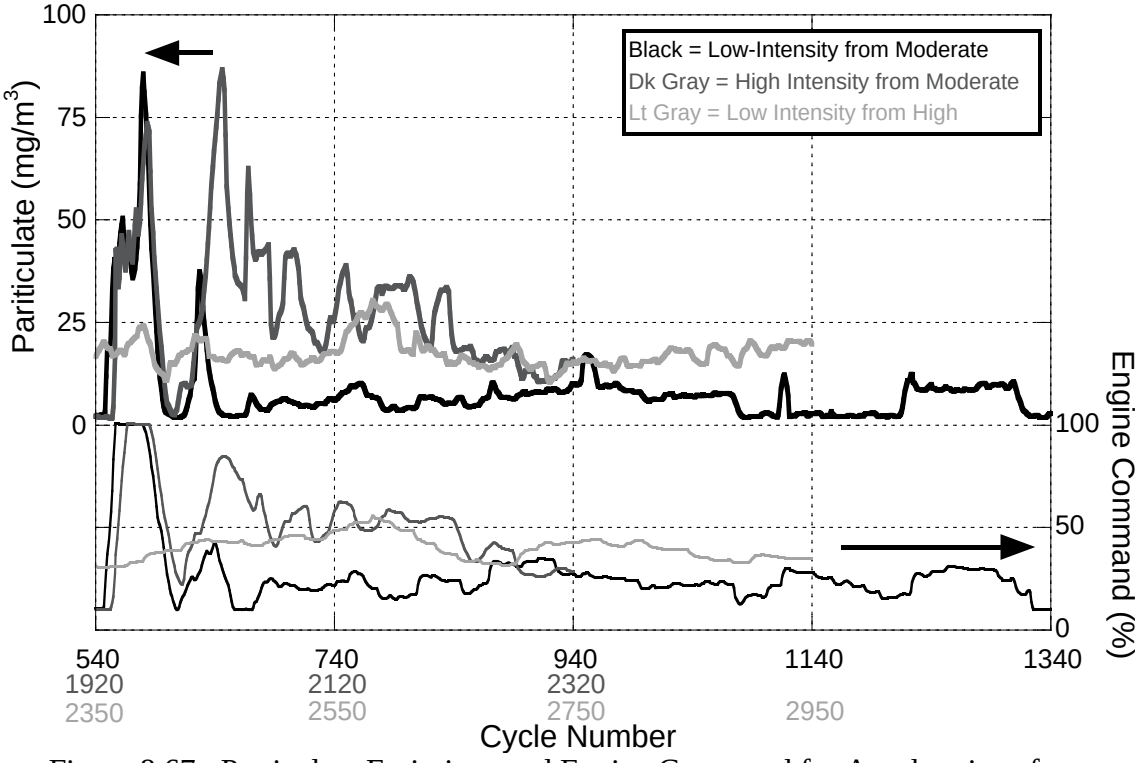

Figure 8.67: Particulate Emissions and Engine Command for Accelerations from Moderate and High Vehicle Velocities during FTP 75

twenty or less. Little fuel overshoot is present in these cycles, as the engine transitions more smoothly in these cases. After the large initial engine command increases, the level of particulate production is proportional to the absolute value and degree of change of the engine command. The high-intensity acceleration experiences numerous particulate spikes of moderate intensity due to engine command changes that are more drastic and a baseline air/fuel ratio right around 20. Conversely, the low-intensity acceleration experiences very few particulate spikes, as its changes in engine command are relatively smoother and occur at air/fuel ratios of about 30.

The low-intensity acceleration at high speed experiences a constant particulate concentration throughout. This is due to the smooth behavior of engine command and the average air/fuel ratio of 30. The peak level of particulate during this acceleration occurs right around cycle 2580, where the air/fuel ratio reaches its minimum value of just below 20.

8.2.17 Emissions Insight

Deeper insight into emissions formation is obtained when closely considering the fuel injection events and rate of heat release curves that occur during the beginning of an intense vehicle acceleration. Figure 8.68 shows such data from three cycles: one before the onset of the transient, the cycle in which the overfuelling occurs, and the cycle following it.

The excess amount of fuel in cycle 1648 is caused by an elongated injection event. Fuel injection pressure in this case is relatively low and unchanged from previous cycles. This results in a fuel injection that has poor penetration, atomization, entrainment and mixing. A huge premixed combustion spike occurs, but the lengthened fuel injection event continues until well after the premixed combustion is concluded and the remainder of the fuel combusts in a weak diffusion burn.

With a global equivalence ratio of 1.4, the overall cylinder conditions are extremely rich and therefore the availability of oxygen in the cylinder is reduced. When combined with the poor mixing from the low injection pressures, the result is a combustion event with lower localized temperatures and higher localized equivalence ratios. Additionally, the fuel injection takes place through the duration of the premixed burn and lasts well into the weak diffusion burn. Such an environment is ideal for particulate production and the antithesis of particulate oxidation.

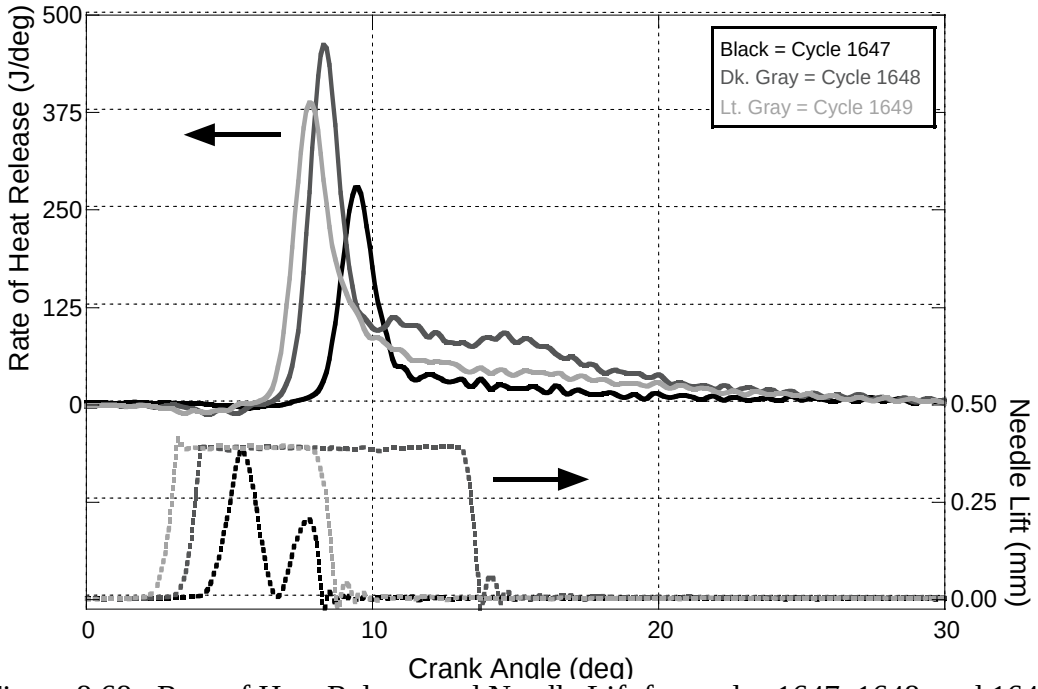

Figure 8.68: Rate of Heat Release and Needle Lift for cycles 1647, 1648, and 1649 during High-Intensity Acceleration from Zero Vehicle Velocity during FTP 75

The cycles that serve as ideal for particulate production are not conductive to NO formation. Lack of oxygen and excess fuel lead to lower in-cylinder temperatures and more rich combustion, which are conditions not suitable for NO production. Indeed, examination of the NO emissions from cycles 1647 and 1648 reveal a negligible change in NO emissions.

Following the cycle with an excess of injected fuel, however, NO emissions quickly rise to roughly triple their original value. Cycle 1649 is the beginning of this trend. In this cycle, the equivalence ratio has fallen to 0.75 and the combustion is purely premixed in nature. The oxygen concentration has also risen from 17.2% to 18.4%. The conditions result in higher localized temperatures with more available oxygen, which is perfect for NO formation. For cycles 1650-1655, the mixture conditions in the cylinder remain unchanged, but fuel injection pressures are increasing which enhances the mixing and entrainment processes. During the same period, the intensity of the premixed combustion is reducing but remains very strong. The net result of all of these trends are extremely high NO concentrations. As the engine transitions into combustion with both premixed and diffusion burning with lower overall oxygen concentrations, NO emissions are reduced.

8.3 In-Vehicle Transient Operation Summary

This chapter closely examines engine behavior over an FTP 75 driving cycle. The experimental technique presented in Chapter 4 is used to quantify the fuel mass, air mass, and stoichiometric combustion product mass for every combustion cycle. Cycle-resolved NO emissions are also measured, as is particulate concentration at a rate of 10 Hz. These data are then analyzed to create a link between the inputs to combustion and the outputs from combustion. The discussion focuses on five specific portions of the driving cycle, all of them accelerations: two from zero initial vehicle velocity, two from a moderate initial vehicle velocity, and one from a high initial vehicle velocity.

Engine command is found to be a very important metric when analyzing engine behavior over a transient driving cycle. It represents what is being demanded of the engine and its level and rate of change significantly impact engine operation. All accelerations investigated have continuously-increasing vehicle velocities. The engine,

however, experiences frequent loading and unloading. For accelerations that are more aggressive, the engine command increases and decreases at rapid rates, but does so at a low frequency. Less aggressive accelerations often put the engine through the same initial engine command increase as a more severe acceleration, but then the engine experiences periods of relatively high-frequency transitions between increasing and decreasing engine command. The frequency and intensity of the engine's transitions from speed and load conditions to higher ones is a significant driving force in the production of emissions.

Performance of the fuel injection system has a significant impact on engine operation. When transitioning from a low-load condition to a high one, the engine generates more torque by increasing the mass of fuel injected. For accelerations that take place from zero vehicle velocity, this often involves an overshoot in the amount of fuel mass, where the first cycle of the acceleration has much more fuel than the cycle before or after it. For the cases studied, one overshoot cycle had 4.2 times the fuel mass of the cycle before it and 1.5 times the fuel mass of the cycle after it. These factors were 5.0 and 2.1 for the other acceleration from zero. When an acceleration takes place while the vehicle is already in motion, the fuel injection system does not have such a severe overshoot in the fuel mass.

The trapped mass of stoichiometric combustion products is governed by the behavior of the EGR valve, the manifold pressure ratio, and the concentration of CO_2 in the exhaust. During periods in which the engine command is increasing at a substantial rate, the EGR valve remains closed, and the only CO_2 in the cylinder comes from residual. Under such conditions, the proportion of stoichiometric combustion products in the cylinder is less than 3%. When engine command is relatively constant under moderate load, the EGR valve opens and greatly increases the amount of stoichiometric combustion products. Depending on engine operation, this proportion spans anywhere from 3-17%. During periods of decreasing engine command, the EGR valve opens,

permitting the flow of exhaust gases into the intake manifold. Under such conditions, however, manifold pressure ratios are typically small and CO_2 concentrations in the exhaust are low, resulting in very small proportions of stoichiometric combustion products in the cylinder during periods of decreasing engine command.

Air flow into the cylinder is dictated by intake manifold pressure and engine speed. As engine speed and load increase the amount of turbocharger boost goes up, which increases intake manifold pressure. At the same time, the time during which air can flow into the cylinder is decreased due to increasing engine speeds. Therefore the amount of air in the cylinder generally trends with intake manifold pressure, but its value is tempered by the influence of engine speed.

Air/fuel ratios are naturally the outcome of the behavior of the two independent systems that provide fuel and air to the cylinder. This ratio is an important metric when studying combustion and emissions formation. The most significant air/fuel ratio values found in this portion of the study occur during the onset of an aggressive transient. In these cases, the amount of fuel increases drastically with no change in air mass. The result is a cycle or two with extremely low ratios—the lowest observed is 10.3, which represents a combustion event with an equivalence ratio of 1.4. Aside from these conditions where the engine injects an excess of fuel, air/fuel ratios are well within the range of those observed during steady-state operation.

Combustion analysis is conducted to assess how the transitions from one operating state to another occur. Under light-load conditions, the combustion is purely premixed. If engine command is increased, the intensity of the premixed combustion grows and diffusion combustion appears. The faster the transition, the greater the extent to which the premixed combustion grows before the appearance of diffusion burning. A very slow transition results in the gradual appearance in diffusion combustion and simultaneous growth in the intensity of both phases. As load is increased from an operating condition that consists of both premixed and diffusion combustion, the

diffusion combustion grows in intensity while the premixed combustion remains unchanged. Reduction of load from premixed and diffusion combustion results in first a decrease in diffusion combustion, followed by a decrease in premixed combustion. During the cycles in which an excess amount of fuel is injected, premixed combustion occurs such that the intensity of the premixed spike is nearly two times larger than any observed during steady-state operation. Any remaining fuel that is not burned at the end of the premixed phase is consumed by a weak form of diffusion combustion.

NO emissions are found to be strongly a function of the amount of injected fuel, and in general, the higher the fueling rate, the greater the NO emissions. The highest NO concentrations measured are over 600 ppm and occur 3-4 cycles after the onset of an acceleration from zero vehicle velocity. Intense premixed combustion during these cycles cause high localized temperatures within the cylinder, and when coupled with relatively high in-cylinder O_2 levels prior to combustion, they provide an environment very conductive to NO formation. If engine command values remain steady for long enough periods, the EGR valve opens and increases the proportion of stoichiometric combustion products in the cylinder, which reduces NO emissions.

Particulate emissions experience a burst in concentration whenever engine command increases a significant amount at a fast rate. Study of the particulate spikes reveals that if engine command changes by over 30% at a rate of 30% per second, the likelihood of forming particulate in excess of 50 mg/m^3 (Bosch 1.3) is very high. If the air/fuel ratio is below 25, engine command changes in excess of 10% at a rate of 20% per second will likely produce particulate spikes. Causes of these particulate bursts are most likely the few cycles that occur with extremely low air/fuel ratios and rate of heat release curves that exhibit a strong premixed spike followed by weak diffusion burning. Outside of changes in engine command that exceed the rough boundaries presented here, particulates throughout the remainder of the FTP 75 were present but at a very low value overall.

CHAPTER 9

SUMMARY AND CONCLUSIONS

An experimental technique to determine cycle-resolved in-cylinder composition prior to combustion is introduced in this study. This chapter first summarizes the motivations for this work and reiterates its objectives. The technique itself is then reviewed and the validity of its results is discussed. Major findings from application of the technique to steady-state and transient engine behavior are presented, followed by the conclusions of the study. Finally, recommendations for future work are suggested.

9.1 Motivation and Objectives

Increasingly stringent emissions standards are forcing diesel engine manufacturers to produce cleaner engines. Many methods are being evaluated to achieve these ends. One such approach is the reduction of emissions that arise from transient engine operation, which constitute a significant portion of total vehicle emissions. Transient engine behavior is characterized by a transition between operating states such that quantities of in-cylinder components and their mixing processes are not well-controlled.

Currently not much is known about transient emissions and why they form. This is due to two reasons. First, diesel combustion is incredibly complex and involves turbulent mixing, three-dimensional heterogeneity, and unsteadiness. Therefore modeling the physics and developing the equations that describe emissions formation is extremely difficult. Current physics-based models that accurately predict emissions

formation in during realistic engine operation do not exist. Second, typical test cell instrumentation does not possess the capability to quantify engine behavior during transient engine operation. These devices do not respond quickly enough to the changes that occur within the engine. By using traditional test cell measurement techniques, it is impossible to understand why and how emissions are formed during transient engine behavior.

Thus there is a need to establish a better understanding of why and how emissions are formed during transient engine operation. In order to do this experimentally, knowledge of the inputs and outputs of each combustion process is vital. Such methods, however, do not exist. It is therefore the goal of this work to develop an experimental technique to aid in the understanding of emissions formation during transient engine operation. The objectives of this study are four-fold:

1. To develop an experimental technique that can quantify the amount of fuel, air, EGR, and residual trapped for each combustion cycle and to measure cycle-resolved NO and particulate emissions during realistic engine behavior.
2. To validate the experimental technique by performing a comprehensive error and sensitivity analysis and by comparing its results to those obtained with traditional test cell instrumentation.
3. To apply the technique by using it to investigate transient engine behavior in which high concentrations of emissions are formed and explain why these occur in light of knowledge of the amount of fuel, air, EGR, and residual that went into each cycle.
4. To provide insight into how to manage the engine during transients to reduce emissions production.

9.2 Experimental Technique Development

Fuel mass in the cylinder is quantified by first assuming that fuel behaves according to the Bernoulli equation as it flows through the injector into the cylinder. The problem thus simplifies to the equation for fluid flow through an orifice. To calculate fuel flow the cylinder pressure, fuel injection pressure, crank angle location of the beginning and ending of injection must be known. These values are all tractable through use of an instrumented fuel injector and a cylinder pressure transducer. Discharge coefficient is determined through use of a lookup table that is generated by steady-state data.

Air/fuel ratio is determined through use of a carbon-balance across the cylinder, which is made possible by quantifying of the amount of CO_2 generated during each combustion process. To accomplish this, fast-responding CO_2 probes are inserted into the engine so that one probe measures in-cylinder CO_2 during the compression stroke and the other samples exhaust CO_2. The air mass is calculated via the fuel mass and the air/fuel ratio. Knowledge of the concentration of in-cylinder CO_2 prior to combustion leads to the determination of the mass of stoichiometric combustion products, which consist of any CO_2, H_2O, and excess N_2 that is recycled into the cylinder through EGR or residual gases.

9.3 Experimental Technique Validation

Validation of the experimental technique is conducted by four methods: assessing how it impacts combustion, performing an error and sensitivity analysis to establish 95^{th} percentile confidence intervals on the data it reports, comparing typical results to those obtained with traditional test cell instrumentation, and examining those engine conditions in which the technique produces results with high levels of uncertainty.

Instrumentation of the cylinder to permit the sampling of gases adds volume and thereby decreases compression ratio by 0.41%. This acts to reduce pre-combustion temperatures and pressures, and its impact is compounded by the removal of mass for the measurement of CO_2 concentration during the compression stroke. The maximum amount of mass removed from the cylinder is estimated to be 1.9% at engine idle. The influence of instrumenting the cylinder and removing mass on combustion is assessed by performing rate of heat release analysis. Of all engine operating conditions investigated, idle is affected the most, as ignition delay is increased from 2º to 3º. At this condition, the rate of heat release curve does not change shape but is shifted to occur one crank angle degree later. At other engine operating conditions, combustion does not change significantly. As speed and load increase, the impact of the measurement technique goes down.

Sampling of exhaust gases prior to the turbocharger reduces exhaust flow and impacts boost pressure. The greatest percentage of exhaust volume sampled is 1.0% at engine idle. Boost pressures are reduced the most at high engine loads and low speeds; at 750 rpm and 5.7 bar BMEP, the removal of the exhaust gases reduces boost pressures by 1.5%.

An error and sensitivity analysis is performed to assess the accuracy of the reported masses of fuel, air, and stoichiometric combustion products from this experimental technique. Error in the fuel mass is incurred from two sources: determination of the value of the discharge coefficient and the use of the composite trapezoid rule to approximate an integral. When considering all the factors involved, 95% of the reported fuel mass values have an error of less than ±0.74%.

In the development of the method to determine the mass of air and stoichiometric combustion products from emissions measurements, the emissions of carbon monoxide and unburned hydrocarbons is neglected. This assumption incurs error in the calculation of air/fuel ratio and is quantified by assessing engine data from transient driving cycles.

The emissions from these realistic conditions are used to calculate two air/fuel ratios: one by using and the other by neglecting CO and HC emissions to establish a standard deviation of error in the air/fuel ratio. It is found that by ignoring CO and HC emissions, the reported air/fuel ratio has an error of ±2.0% with a 95^{th} percentile confidence interval.

Error in air mass and the stoichiometric combustion product mass is incurred through fuel mass error, neglecting the presence of CO and HC in the exhaust, and the impact of errors in the in-cylinder and exhaust manifold CO_2 measurements. The errors in the first two factors have already been developed, but the relationship of air mass and stoichiometric combustion product mass to CO_2 error is more complex. Therefore a sensitivity analysis is conducted to assess how errors CO_2 measurements impact the air mass and stoichiometric combustion product mass. Of all engine operating conditions investigated, the highest sensitivity CO_2 measurements is found at high-speed and low-load conditions. At such points, a simultaneous 95^{th} percentile error in both in-cylinder and exhaust manifold CO_2 results in an air mass that deviates ±1.84% and stoichiometric combustion product mass that varies ±3.30% from the true values. When combined with the other sources of error, the mass of air is reported with an error of ±2.82% and the mass of stoichiometric combustion product mass is determined to have error of ±3.93%, both with a 95^{th} percentile confidence interval.

Data from transient engine operation is obtained simultaneously using both the developed experimental technique and traditional test cell instrumentation. The traditional test cell instrumentation is unable to quantify data variation at the cyclic level due to slow device response times, transport delay, and the loss of resolution that occurs because of mixing during the transport delay. The proposed experimental technique, however, is capable of capturing cycle-resolved values of the inputs to and outputs from combustion over a broad range of engine operation.

The information provided by the technique has high levels of uncertainty at engine operation near the outer edges of its performance envelope. As the engine is

coasting down in speed so that no power is being generated, the needle lift signal disappears, causing errors in the reported start and end of injection timings. This leads to erroneous fuel mass values. The amount of CO_2 in the exhaust during engine coast down practically zero, and small absolute errors in CO_2 concentration lead to large relative errors in air and stoichiometric combustion product mass calculations. Under certain low-speed low-load conditions, the fuel injector needle has a significant amount of bounce when it closes. This makes the determination of the end of injection difficult, which strongly impacts the fuel mass calculation. Such coast-down periods and low-speed, low-load conditions occur frequently during the FTP 75 driving cycle used to test the engine. But because little to no fuel is being consumed at these conditions, the formation of emissions due to transient engine behavior is not present and the data from such conditions are neglected.

As engine loads increase such that the exhaust manifold pressure exceeds about 200 kPa absolute, the exhaust manifold Fast CO_2 probe is unable to maintain a constant chamber pressure. When these chamber pressures fluctuate to values other than the value used during calibration, errors are created in CO_2 measurement, which propagate through to air and stoichiometric combustion product masses. Fortunately, during the FTP 75 driving cycle used to test the engine in this study, such high-load conditions are experienced infrequently. Therefore these inaccuracies have little to no bearing on the results obtained.

9.4 Results from Application of Experimental Technique

The experimental technique proposed in this study is used to analyze engine behavior during steady-state conditions, constant-speed load sweeps, and during realistic engine behavior during an FTP 75 driving cycle. Major findings from these three investigations are summarized separately in the following sections.

9.4.1 Steady-State Engine Operation

Two operating conditions are investigated to analyze engine behavior at steady-state conditions. Engine speed and engine command are held constant at 2000 rpm, 1 bar BMEP and 2000 rpm, 9 bar BMEP. Electronically-controlled engine parameters, such as start of injection, injection pressure, mass of injected fuel, EGR valve position, and VGT vane position perform according to the engine's standard calibration. Findings from this portion of the study are summarized below.

- When the engine operates at a steady speed with a constant engine command signal, the injection timing, injection pressure, EGR valve position, and VGT vane position are not constant. These inconsistencies result in larger relative variances in the trapped mass of fuel, air, stoichiometric combustion products.
- The fuel injection system performs more consistently when nominal fuel injection pressures are higher and fuel injection events are longer.
- The engine experiences a high level of heterogeneity in the intake manifold due to poor mixing of EGR and fresh air, as evidenced by significant cycle-to-cycle variations in the mass of stoichiometric combustion products.
- Larger variances in the mass of fuel, air, and stoichiometric combustion products lead to greater inconsistencies in combustion processes.
- NO emissions on a cyclic level are strongly a function of injection parameters and oxygen concentration in the cylinder. At the lighter load condition, injection parameters have a larger influence. At the higher load condition, cyclic fluctuations in pre-combustion in-cylinder O_2 result in cyclic changes in NO formation, with higher levels of O_2 corresponding to higher values of NO.
- Instrumentation limitations prevent resolution of particulate emissions into cyclic values.

9.4.2 Constant-Speed Load Sweeps

Transient load sweeps are conducted from 1 bar BMEP to 9 bar BMEP at a constant speed of 2000 rpm. The time elapsed during the increase of engine command is varied to simulate accelerations of different intensities. The investigated time sweeps over which the engine command increases last 0, 1, 2, 3, and 5 seconds. While the results of all five cases are analyzed, only the results of the 0, 2, and 5 second cases are included in the discussion. Major findings of this portion of the study are summarized below.

- Rate of engine command significantly impacts engine behavior during transient operation.
- In the first cycle in which the engine responds to a change in engine command during the 0 Second load sweep, the amount of fuel injected overshoots the desired value by a factor of 2.4. The result is a combustion event with an air/fuel ratio of 14.8, or an equivalence ratio of 0.98, which is 25% more rich than any observed standard calibration operating point. Three more cycles of fuel overshoot take place before the amount of injected fuel agrees with the desired value. All other cycles in all other sweeps did not experience this fuel mass overshooting behavior.
- The proportion of stoichiometric combustion product mass during the transient sweeps is governed by EGR valve position. Manifold pressure ratio also plays a role, but its influence is secondary.
- EGR valve behavior during the load sweeps is different in all investigated cases and significantly impacts the mass of stoichiometric combustion products trapped in the cylinder during the transition. The more rapid the rate of engine command increase, the more the EGR valve closes, which causes a reduction in the mass of stoichiometric combustion products.
- Air mass during constant-speed transients is controlled by intake manifold pressure and EGR valve position.

- During these transients, combustion transitions from purely premixed to a combination of premixed and diffusion burning. The load sweeps that take place the quickest initially experience a significant growth in the magnitude of premixed combustion. Diffusion burning appears later as the engine approaches steady-state conditions. As the pace of the load sweep slows, the premixed burning does not reach such high levels, but diffusion burning appears sooner. For the slowest sweep, diffusion burning appears just a few cycles into the transition.
- NO emissions formed during the load sweep are highly-dependent on the rate of change of the engine command. Faster changes in engine command results in larger spikes in NO concentration. Intense premixed combustion near TDC causes high in-cylinder temperatures and when coupled with a combustion chamber devoid of stoichiometric combustion products and flush with oxygen, an environment ideal for NO production is created. Slower engine command increases occur with higher levels of stoichiometric combustion products in the cylinder, which causes the combustion rates to slow and transition to diffusion burning more quickly. Thus cylinder temperatures are lower, O_2 concentration is reduced, and NO production is smaller.
- Particulate emissions are strongly related to the rate of change of engine command at the onset of the transient. The few cycles near the beginning of the 0 Second engine command sweep that had very high levels of fueling and low air/fuel ratios are most likely the cause of the large spike in particulate emissions observed at the start of the load sweep. Slower engine command transitions experience particulate response, and are most likely due to a combination of the presence of stoichiometric combustion products and low air/fuel ratios. These levels of particulates, however, are an order of magnitude lower than the spike in the 0 Second sweep.

9.4.3 In-Vehicle Transient Operation

Using the engine-in-the-loop capability of the test cell, the engine is operated as though it is in a U. S. Military Humvee over the FTP 75 driving cycle. The proposed experimental technique is used to assess engine behavior throughout the cycle and used to identify those conditions in which high levels of emissions are formed. Discussion focuses on five specific acceleration procedures: two from zero initial vehicle velocity, two from a moderate initial vehicle velocity, and one from a high vehicle velocity. The results of this investigation are summarized below.

- Behavior of engine command during in-vehicle operation is the single largest determiner of engine behavior. Vehicle velocities and accelerations that are very different from one another can result in engine behavior that is very similar and therefore vehicle behavior alone is not sufficient to characterize engine operation.
- Rate of change of engine command during the first few cycles of a vehicle acceleration largely determines the degree to which excess emissions are formed.
- The operation of the fuel injection system has a significant impact on engine performance. Fuel mass overshoots that occur for only one cycle are observed in the accelerations from zero vehicle velocity. In the most intense acceleration from zero vehicle velocity, this cycle has 3.1 times the mass of injected fuel that the engine commands. This cycle has an air/fuel ratio of 10.3, which corresponds to an equivalence ratio of 1.4; this cycle is 79% more rich than any cycle observed at steady-state conditions. When accelerations occur while the vehicle is already in motion, fuel overshoots do take place, but not to the levels observed when the accelerations take place from zero vehicle velocity.
- Cycles in which excess fuelling occurs is caused by injection events that have much longer durations than other cycles. Injection pressures remain similar to adjacent engine cycles.

- The mass of stoichiometric combustion products in the cylinder during vehicle accelerations is a function of EGR valve position, manifold pressure ratio, and the concentration of CO_2 in the exhaust products. EGR valve position has the most significant impact. Under intense accelerations, the EGR valve remains closed and internal residual levels result in stoichiometric combustion product fractions to remain below 3%. As engine command increases become less severe, the EGR valve remains partially open, and the proportion of stoichiometric combustion products ranges from 6-17% depending on engine operation.
- Trapped air mass is proportional to intake manifold pressure and inversely proportional to engine speed.
- Air/fuel ratios during accelerations are only outside engine calibration limitations during the first few cycles of engine command increase. The degree to which this occurs is a function of the level of fuel mass overshoot. All other air/fuel ratios observed during the driving cycle tests are above the values observed during steady-state engine operation.
- During an acceleration, the mode of combustion transitions from being completely premixed to a combination of premixed and diffusion burning. As engine speed and load increase, the intensity of the premixed combustion grows and diffusion burning appears gradually. The more aggressive the engine command change, the greater the intensity of the premixed spike and the later the appearance of diffusion combustion. More moderate changes in engine command result in lower overall premixed intensity and a more rapid appearance of diffusion combustion.
- During cycles in which an excess amount of fuel in injected, the heat release is intensely premixed followed by weak diffusion burning. The strength of the premixed combustion can exceed 400 J/deg, which is over twice the value typically seen at any steady-state condition. The diffusion burn occurs because of extended injection events that last longer than the duration of the premixed burning. Cycles

that follow such events transition back to purely premixed, as fuel rates are much lower. The intensity of the premixed combustion during these cycles remains above the strength of premixed combustion observed at steady state conditions.

- NO emissions typically are governed by the mass of injected fuel, and larger fuel masses lead to higher NO concentrations.
- The highest NO concentrations occur during the accelerations from zero vehicle velocity and begin 3-4 cycles after the fueling rate begins to increase. At these conditions, in-cylinder O_2 levels are high and the combustion is intensely premixed, which results in high cylinder temperatures and conditions ideal for NO formation.
- NO concentrations are high during the beginning of an acceleration while the vehicle is moving, but do not reach the levels of NO observed in the accelerations from zero vehicle velocity. In general, these cases have lower levels of in-cylinder O_2 and less intense premixed combustion, and therefore are not as favorable for NO formation.
- High concentrations of particulate are formed whenever an engine command increases by a large amount at a rapid rate. For this engine, this condition can be summarized as an absolute change in engine command that exceeds 30% and lasts for one second or longer. The closer the engine is to an air/fuel ratio of 20 or below, the less engine command has to change to form a particulate burst.
- The highest concentrations of particulate are observed during the beginning of an acceleration from zero vehicle velocity. These most likely occur due to the existence of one combustion cycle that has an equivalence ratio that exceeds one and then exhibits weak diffusion combustion. This is an environment that is ideal for soot formation and awful for soot oxidation.

9.5 Accomplishments and Conclusions

The accomplishments of this research effort to develop and validate a new engine experimental technique and the conclusions drawn from the application of the technique to steady-state and transient engine operation are summarized in the list below.

- An experimental technique is developed in this study that quantifies cycle-resolved values of fuel mass, air mass, and stoichiometric combustion product mass over a broad range of engine operation.
- Engine modifications that permit the necessary instrumentation are non-invasive and the devices during data acquisition are configured in a manner such that the combustion events of the instrumented cylinder are minimally impacted. Therefore the data acquired is representative of engine operation from an uninstrumented cylinder.
- Errors in the mass of fuel, air and stoichiometric combustion products are very low over a broad range of engine operating conditions and provide high levels of confidence in the results obtained by the experimental technique.
- The technique provides information about fuel, air, and stoichiometric combustion product masses that cannot be obtained with traditional test cell instrumentation and methodologies.
- Knowledge of the cycle-resolved behavior of the mass of fuel, air, and stoichiometric combustion products provides unique insight into the causes of emissions formation due to transient engine operation.
- Large increases in engine command from low-speed low-load operating conditions cause the fuel injection system to inject an excess amount of fuel in one or two cycles. These cycles can have equivalence ratios over one and exhibit combustion modes that are significantly different from those observed at steady state.

- Abnormally-high concentrations of NO are produced after 3-4 cycles of a large increase in engine command because the cylinder is flush with oxygen and the combustion mode is intensely premixed. This leads to high localized in-cylinder temperatures and provides ideal conditions for NO formation.
- Particulate bursts are created whenever a large increase in engine command occurs over a sustained period of time. This most likely results due to the first few combustion cycles that occur immediately after the engine command begins increasing. The lower the air/fuel ratios encountered, the higher the concentration of particulate formed. Cycles in which the mass of fuel greatly exceeds the desired amount have ultra-low air/fuel ratios and cause the largest observed concentrations in particulate emissions.
- To reduce the formation of both NO and particulate during transient engine operation, the fuel injection system must be able to precisely control injection pressure as well as the start and end of injection for every cycle. These fuel injection events must be accurate and repeatable at every possible engine operating condition.
- NO emissions produced during transient engine operation can be mitigated through introduction of stoichiometric combustion products into the cylinder during periods of increasing engine command.

9.6 Recommendations for Future Work

This research effort introduces an experimental technique and demonstrates how it can be used to better explain engine behavior during transient operation. There exist a number of ways to improve the technique and to apply it to new topics. Suggestions for future research are provided in the following list.

- Perform simulation studies with KIVA to better understand how and why NO and particulate form as they do and identify the role of local in-cylinder conditions in transient emissions formation.
- Acquire or develop the hardware and software necessary to control injection parameters, EGR valve, and VGT vane position during transient engine operation. This permits the development of engine control strategies to mitigate the emissions formed due to transient phenomenon.
- Incorporate Fast CO and Fast HC measurements in the exhaust manifold into the technique in order to assess the extent to which these emissions are formed during the combustion cycles with excessive fueling.
- Improve the fuel injection system so that fuel mass overshoot does not occur during the most aggressive transient engine behavior.
- Develop an advanced algorithm for the EGR valve position such that the concentration of exhaust CO_2 and manifold pressure ratio are used as inputs to better control the mass of stoichiometric combustion products trapped in the cylinder.
- Use data obtained with this experimental technique to aid in the development of physics-based and phenomenological models of transient engine behavior, especially those that focus on emissions formation.
- Investigate how multiple injections can be used during transient engine operation to maintain driveability but avoid excessive emissions.
- Develop a method to use in-cylinder CO_2 measurements during the compression stroke in conjunction with cylinder pressure to create a closed-loop engine control strategy.

APPENDICES

APPENDIX A

MATLAB PROGRAM TO POST-PROCESS DATA

The data obtained in this investigation to determine cycle-resolved in-cylinder composition is done so on a crank-angle basis, and tests that last any longer than a few seconds generate enough data to warrant a post-processing routine. MATLAB is chosen to perform these calculations because of its flexibility and functionality. This section serves to explain the algorithms used to process the data, as well as the structure of the code itself.

A.1 Code Structure

The algorithm is broken into subroutines to simplify modification and interpretation. The main program is called Transient_Calculations and serves to input data, call subroutines, and output the data. Fuel mass is then determined with fuel injector data, cylinder pressure, and engine speed by the aptly-named Fuel_Mass routine and its subroutines. Then the fuel mass and in-cylinder and exhaust manifold CO_2 measurements are used to determine the air mass and mass of stoichiometric combustion products in the cylinder prior to combustion in the Air_and_Inert_Mass subroutine. Heat release is then performed with the outputs of the preceding routines and the Heat_Release_Call subroutine. A schematic of the code structure is shown in Figure A.1. In this figure, code hierarchy is represented by nested rectangles, while order of execution represented by vertical orientation. The specifics of each of these subroutines are explored in the following sections.

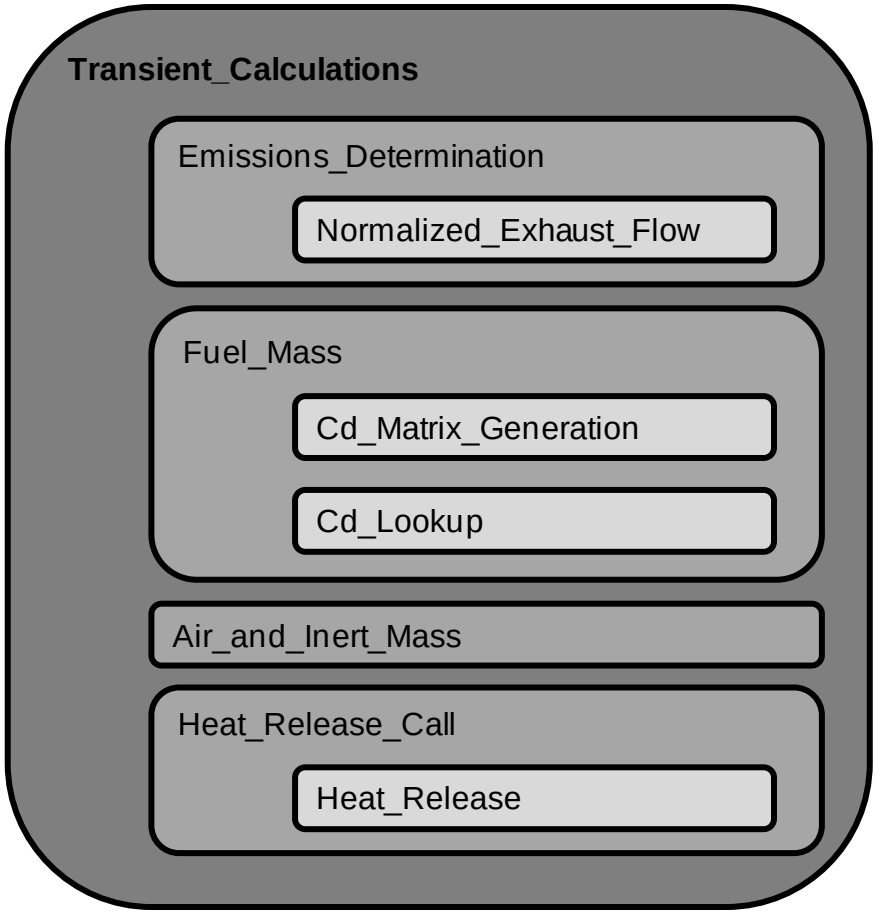

Figure A.1: Structure of MATLAB Program Used to Post-Process Crank Angle Resolved Data

A.2 Subroutine Functions

While earlier chapters focus on development of the assumptions, methods, and equations necessary to determine the mass of fuel, air, and stoichiometric combustion products for each engine cycle, this section presents a higher-level overview of raw and processed data as it flows through the calculation routines.

A.2.1 Transient_Calculations

The first task of this parent routine is to load all of the raw data and place it into appropriate variables. Crank angle resolved cylinder pressure, intake and exhaust manifold pressure, and injection pressure are each assigned their own variable name and

then divided into 720-degree increments which are written into consecutive columns so that the n^{th} column of a particular variable represents the n^{th} cycle of the data. In a similar fashion, cycle-resolved data, such as the start and end of injection, are transposed so that each column represents data from a different cycle. For cycle-resolved data, however, there is only one piece of information per cycle and n cycles of data is represented by a 1-by-n matrix.

Cylinder pressure and fuel injection pressure are then filtered with a 2^{nd} order low pass Butterworth filter to remove noise from these signals. The cutoff frequency used is a function of engine speed, as higher engine speeds result in a greater sampling frequency and require a stronger filter to remove an equivalent amount of noise. This filter is applied using MATLAB's *filtfilt* command, which first filters the data in a forward direction and then backwards, which results in output data with zero phase shift.

At this point, the data pre-processing is completed and then the subroutines shown in Figure A.1 are called in the order presented. Once these values have been determined and all outputs have been generated, the Transient_Calculations routine then organizes the data into a logical order with appropriate units before generating arrays that are user-friendly and able to be saved. Eighty-four pieces of cycle-resolved data, some measured and some calculated, are saved in an Excel format. Selected crank-angle resolved data, such as rate of heat release and integrated heat release, are saved in individual text files because of the sheer volume of data involved.

A.2.2 Emissions_Determination

This subroutine is called to interpret the crank angle resolved in-cylinder CO_2 data, exhaust manifold CO_2 data, and exhaust manifold NO data and translate it into cycle-resolved data. This data is first broken into 720-degree sections so that each increment contains the data from one cycle. Algorithms are then used to locate the

beginning of the blowdown process for the exhaust manifold measurements. The average cycle-resolved value of exhaust CO_2 and NO are determined through use of an exhaust flow model that serves as a weighting function to the measured concentrations. In-cylinder concentrations are determined by finding an average around the peak value of the signal for each cycle. Details of these algorithms are explored further in Appendix B.

A.2.3 Fuel_Mass

Injector and cylinder pressure data, as well as fuel properties are then used to calculate the mass of fuel injected for each cycle in the Fuel_Mass subroutine. The first part of this process is accomplished by calling the Cd_Matrix_Generation routine which uses steady-state engine speed, peak injection pressure, and injection duration, to create a three-dimensional matrix that has an injector discharge coefficient value at each data point. To equalize the weighting of engine speed, peak injection pressure, and injection duration, these values are first normalized relative to the peak values the engine can produce. Therefore these values all range from zero to one. Once the matrix is created, the *delaunay3* function is used to take this three-dimensional, sparse, non-uniform data and divide it into tetrahedrons such that the vertices of each tetrahedron consist of the steady-state data points and no other data point is contained within any tetrahedron. A visualization of this process is shown in Figure A.2 and A.3, which demonstrate how the interpolation space looks before and after the tetrahedrons are created.

After the injector discharge coefficient is created, the Cd_Lookup subroutine is called to interpolate the cyclic engine data. For each engine cycle, an engine speed, maximum injection pressure, and injection duration are specified. These values are first normalized and then used in the *tsearch* function that determines the indices of the tetrahedron in which the data is contained and the relative proximity to each vertex. The

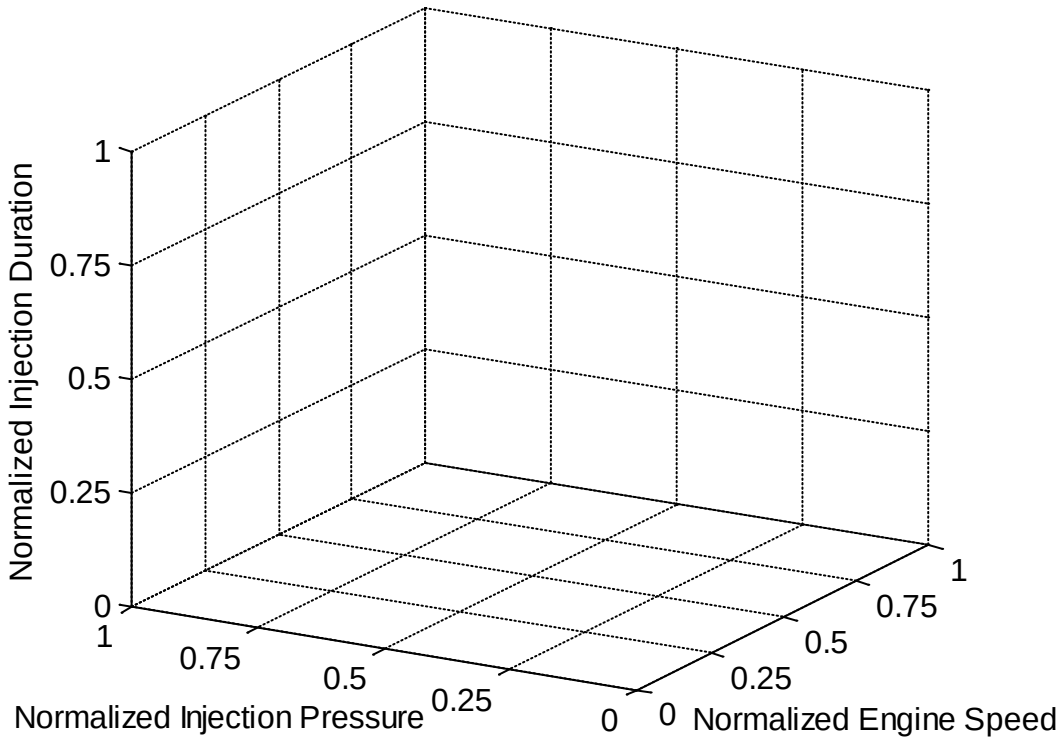

Figure A.2: Discharge Coefficient Data Points Plotted as a Function of Engine Speed, Injection Duration, and Maximum Injection Pressure

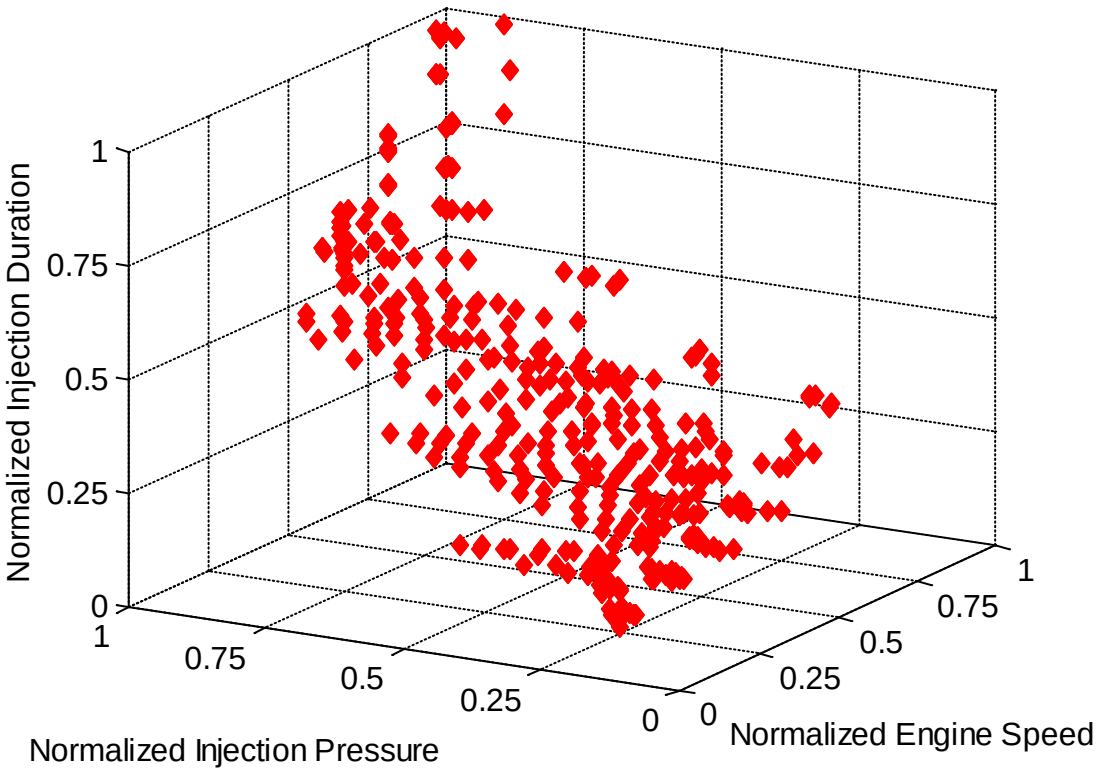

Figure A.3: Visualization of Tetrahedrons Created by the delaunay3 Function in MATLAB

discharge coefficient of that point is the weighted average of the coefficients of the tetrahedron's vertices in which it is contained.

Once the injector discharge coefficient is interpolated, the calculation of fuel mass is completed by the Fuel_Mass subroutine. It uses injection pressure and cylinder pressure, along with fuel density and the interpolated discharge coefficient to calculate the fuel injection velocity and then the instantaneous fuel flow rate. This value is then integrated with the *trapz* function to yield the overall injected fuel mass. The equations used in this scheme are fully developed in Section 4.4.

A.2.4 Air_and_Inert_Mass

Once the fuel mass and in-cylinder and exhaust manifold CO_2 concentrations are calculated, the Air_and_Inert_Mass subroutine is called to determine the mass of air and stoichiometric combustion products trapped in the cylinder prior to combustion by executing the iterative steps described in Section 4.5. When the mass of air and stoichiometric combustion products prior to combustion are calculated, all the components of the cylinder charge are known. The routine then determines the mixture molar and mass fractions of each compound before and after combustion, including: oxygen, nitrogen, carbon dioxide, water, and fuel.

A.2.4 Heat_Release_Call

Now that the amount of fuel, air, and stoichiometric combustion products in each cycle are known, the Heat_Release_Call subroutine is used to prepare input data and call the heat release code. Three distinct steps are taken here: defining the proper inputs, calling the code, and post-processing the heat release data.

Inputs to the heat release code are broken into two categories: those that are independent of engine operating condition, and those that are dependent on engine

operating conditions. First defined are those that remain fixed; these values include engine geometry and specifications about which assumptions or models the code uses. Then a loop is constructed for each engine cycle, and the variables that change with engine operation (speed, mass flows, and cylinder pressure) are assigned. These values are then used to write a text file that is used as an input to the heat release code.

The heat release code itself, which exists in a MATLAB-created subroutine, is then called. Its outputs are written to another text file, which are immediately read in by the MATLAB code where they are post-processed. Rate of heat release, integrated heat release, rate of work, rate of heat transfer, rate of internal energy, and bulk gas temperature are all important heat release outputs that are recorded in this analysis.

These outputs are then used to determine important combustion characteristics, such as start of combustion, mass fraction burned curves, and combustion duration. Once these have been determined, they are sent back to the main Transient_Calculations routine to be saved with the rest of the output data. Further details about the heat release code and how combustion characteristics are defined are explored in Appendix C.

APPENDIX B

DETERMINATION OF CYCLE-RESOLVED EMISSIONS VALUES

Data from both channels of the Fast CO/CO_2 analyzer and the Fast NO analyzer are recorded continuously on a crank-angle basis. These data must be interpreted to yield a single value of in-cylinder CO_2, exhaust manifold CO_2, and exhaust NO for each cycle. This section demonstrates representative in-cylinder and exhaust manifold data and describes the procedures employed to calculate cycle-resolved emissions values.

B.1 In-Cylinder CO_2

Operation of the CSV500 and how it provides an in-cylinder sample to a channel of the Fast CO_2 sensor was described in detail in Section 3.2.12. Because this channel of the Fast CO_2 analyzer typically samples ambient air, its output during the majority of the cycle is essentially zero. When in-cylinder gases are sampled, the presence of EGR and residual gas causes a once-per-cycle plateau. Sensor response time dictates that enough in-cylinder gas be provided to the analyzer to produce an accurate reading of the true concentration of CO_2 in the sample. This is accomplished through careful tuning of the CSV, which was described in Section 5.1.2.

A typical trace of in-cylinder CO_2 measurement with appropriate CSV settings is shown in Figure B.1. The Fast CO_2 sensor updates its output signal every 3 ms; IndiCom, however, records the output of the sensor every crank angle. These in-between points that are recorded by IndiCom are a result of signal modulation by the integrated

RC circuit in the analyzer, and are manifested in the hooks in the curve that are evident in Figure B.1.

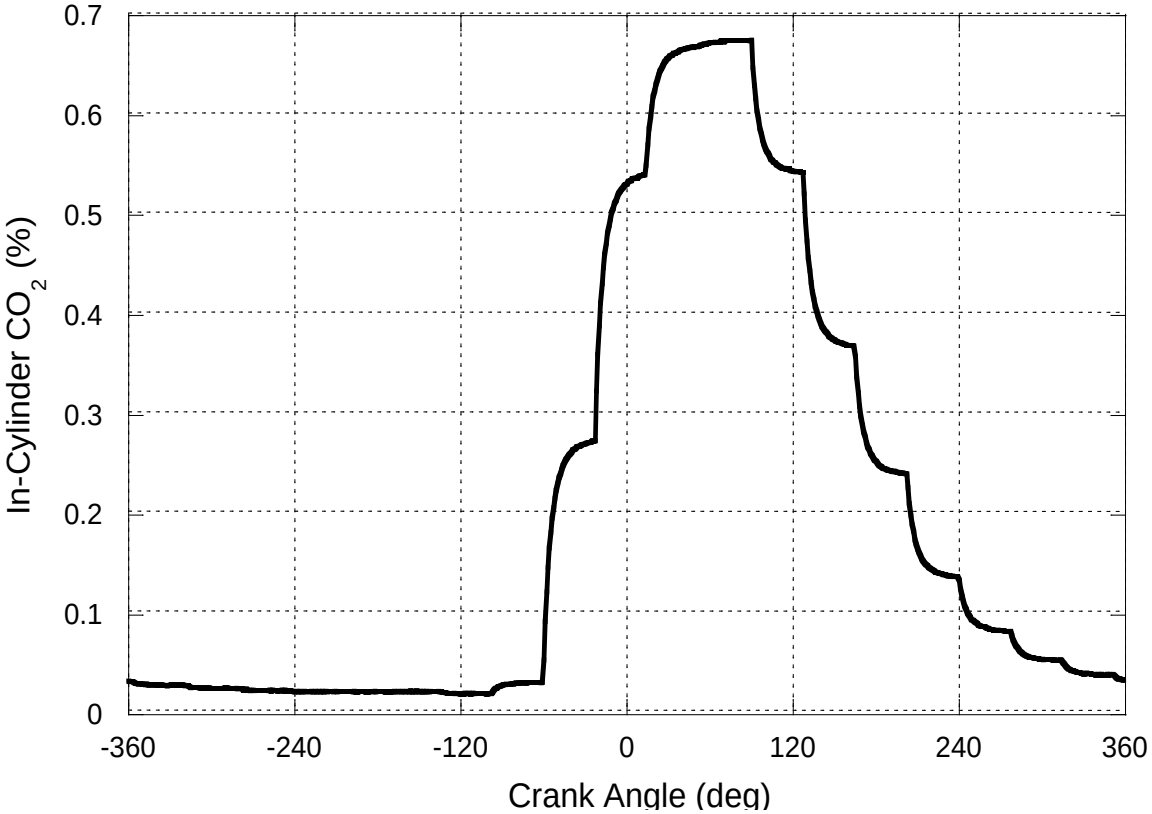

Figure B.1: Crank-Angle Resolved In-Cylinder CO_2 Data

The value of this curve that matters is the peak level of the plateau, which is defined by two consecutive data points from the analyzer that are within 5% of one another. In the particular example shown here, the engine speed is 2000 rpm, which translates to the analyzer providing data every 36 degrees of crankshaft rotation and a plateau that is at least 72 crank angle degrees long. Because the settings of the CSV are appropriate for the operating condition, the plateau shown contains two distinct data points.

To interpret these data and provide a single in-cylinder CO_2 concentration for each cycle, a MATLAB code is developed that divides the data into segments that are each 720 crank angle degrees long. Within each segment is contained one CO_2 plateau

for each cycle. Transport delay within the system skews the data with respect to crank angle and varies as a function of speed and load, which dictates careful examination of the data to ensure that one plateau is contained in each segment for all operating conditions.

Once the data is segmented, the maximum CO_2 concentration in each division is located and any point within 5% of that value is used to average the signal. In this particular case, the in-cylinder concentration is calculated to be 0.66%.

B.2 Exhaust Manifold Emissions Measurements

Both CO_2 and NO are sampled in the exhaust manifold near the exhaust valves of the instrumented cylinder and recorded on a crank angle basis. These signals must be interpreted to yield a single cycle-resolved concentration for CO_2 and NO. Because thousands of non-uniform cycles must be evaluated, a MATLAB code is developed to perform this calculation. The process of interpreting these data is equivalent for both sensors, and from henceforth the discussion will focus on the example of the CO_2 signal. Figure B.2 demonstrates three cycles of typical CO_2 concentration signal taken from the exhaust manifold. Two distinct tasks must be completed: locating the beginning of the each exhaust process, and then interpreting the signals from EVO to TDC to yield a single concentration value for each combustion cycle.

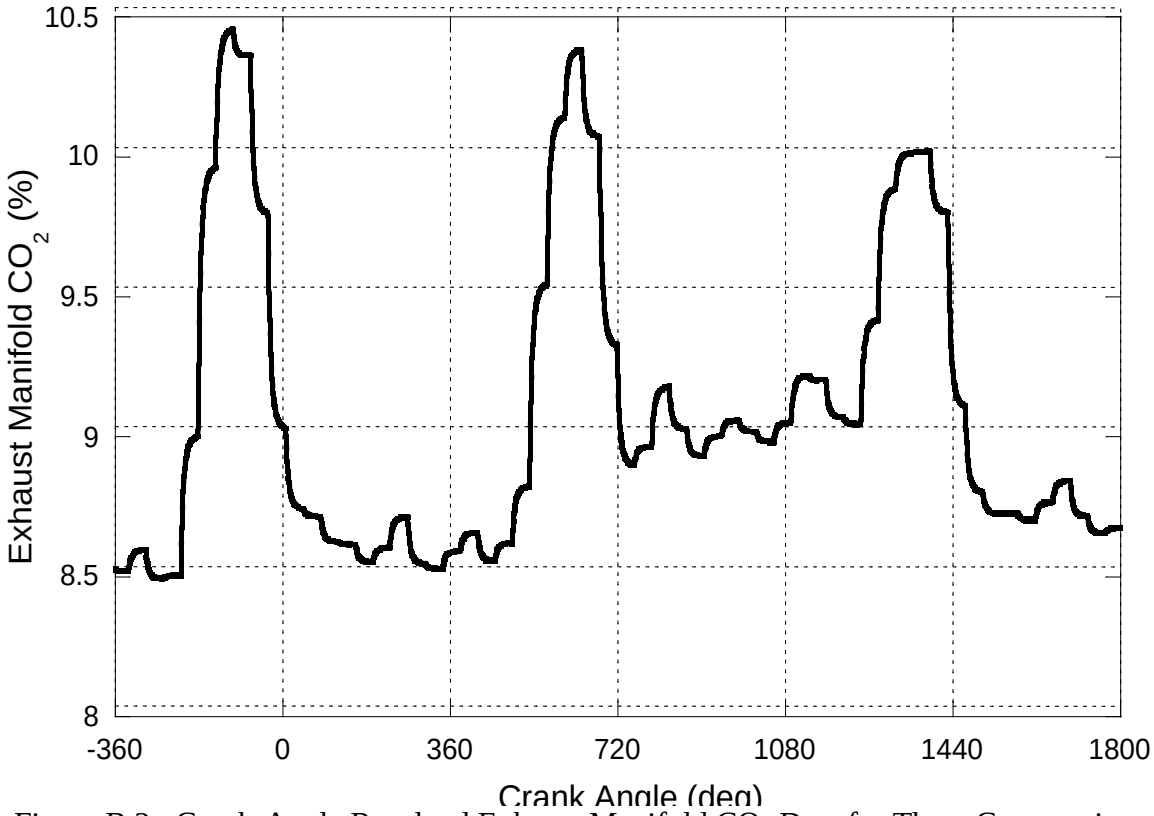

Figure B.2: Crank-Angle Resolved Exhaust Manifold CO_2 Data for Three Consecutive Engine Cycles

B.2.1 Determination of the Beginning of the Exhaust Process

Emissions concentration data is obtained on a crank angle basis and the first step of interpreting the data is to break it into 720 degree increments that represent each cycle. Care must be taken to ensure that the data is divided so that each increment contains the start of blowdown and the end of the exhaust process for one cycle over the entire range of engine operating conditions. One such division is shown in Figure B.3, which is the first cycle from Figure B.2.

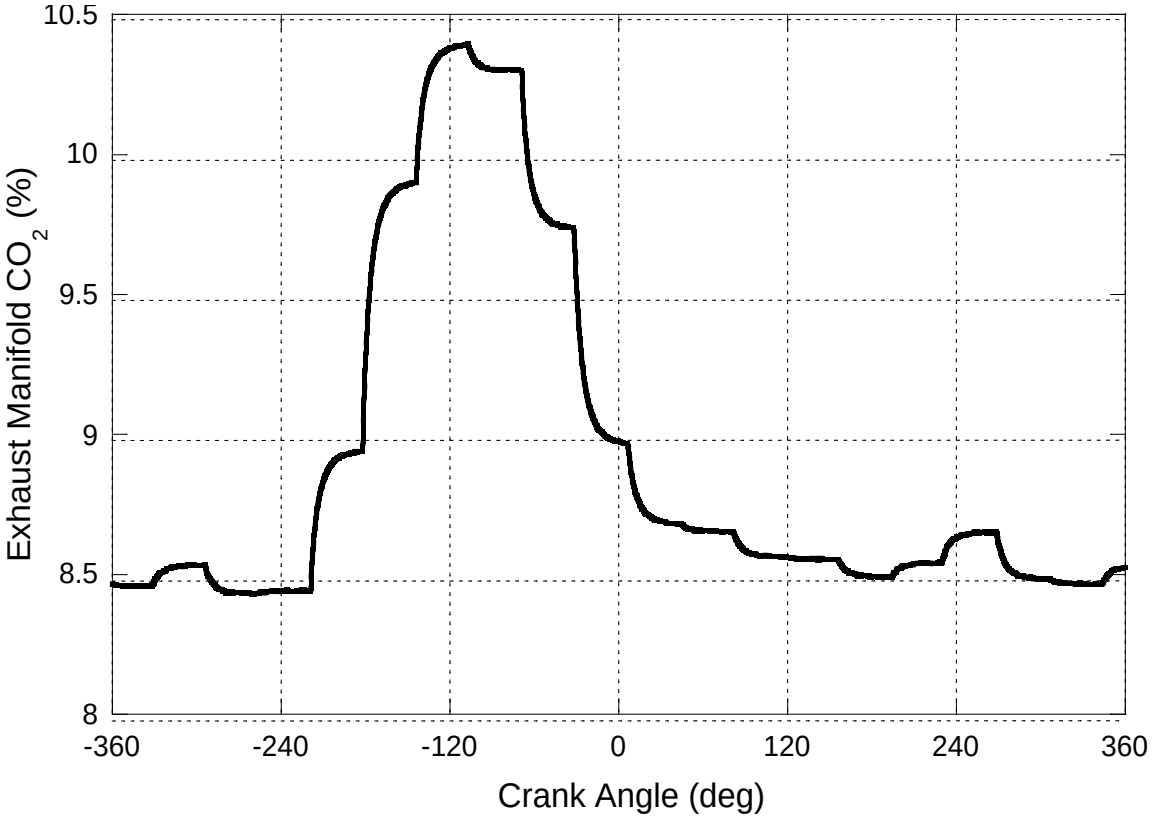

Figure B.3: Crank-Angle Resolved Exhaust Manifold CO_2 Data for One Engine Cycle

As engine speed and load change, so too does the exhaust gas flow rate and the backpressure in the exhaust manifold. This results in varying transport times of exhaust gas to the emissions sensors and consequently differing times at which the blowdown process is detected. Therefore the data from onset of the blowdown will occur at a wide range of crank angles. Fortunately, the presence of exhaust blowdown is readily identifiable, and is marked by a drastic change in concentration.

Considering the data shown in Figure B.3, the CO_2 level between -360º and -240º is relatively unchanged. At about -220º, however, the concentration of CO_2 increases significantly, which denotes the beginning of the exhaust process. Since the exhaust valve opens at 134.9º aTDC, the data shown in Figure B.3 actually represents the CO_2 signal that was generated from the previous combustion cycle and indicates that at this load and speed (2000 rpm and 9 bar bmep) the transport and sensor delay result in a signal shift of 445º.

To locate the beginning of blowdown, the MATLAB code first locates the maximum concentration in each segment and then the minimum concentration between the beginning of the segment and the maximum. For this particular cycle, the maximum CO2 concentration is 10.42% and is found at -107º. The minimum between the beginning of the segment and the maximum is 8.45% at -260º. Then 5% of the difference between these two values is computed and added to the minimum, which is 8.55%. The code then starts looking backwards from the maximum toward the minimum for the crank angle at which this value occurs. For this cycle, that value occurs at -218.2º, and this crank angle is considered to be the beginning of the exhaust process. Figure B.4 demonstrates this process.

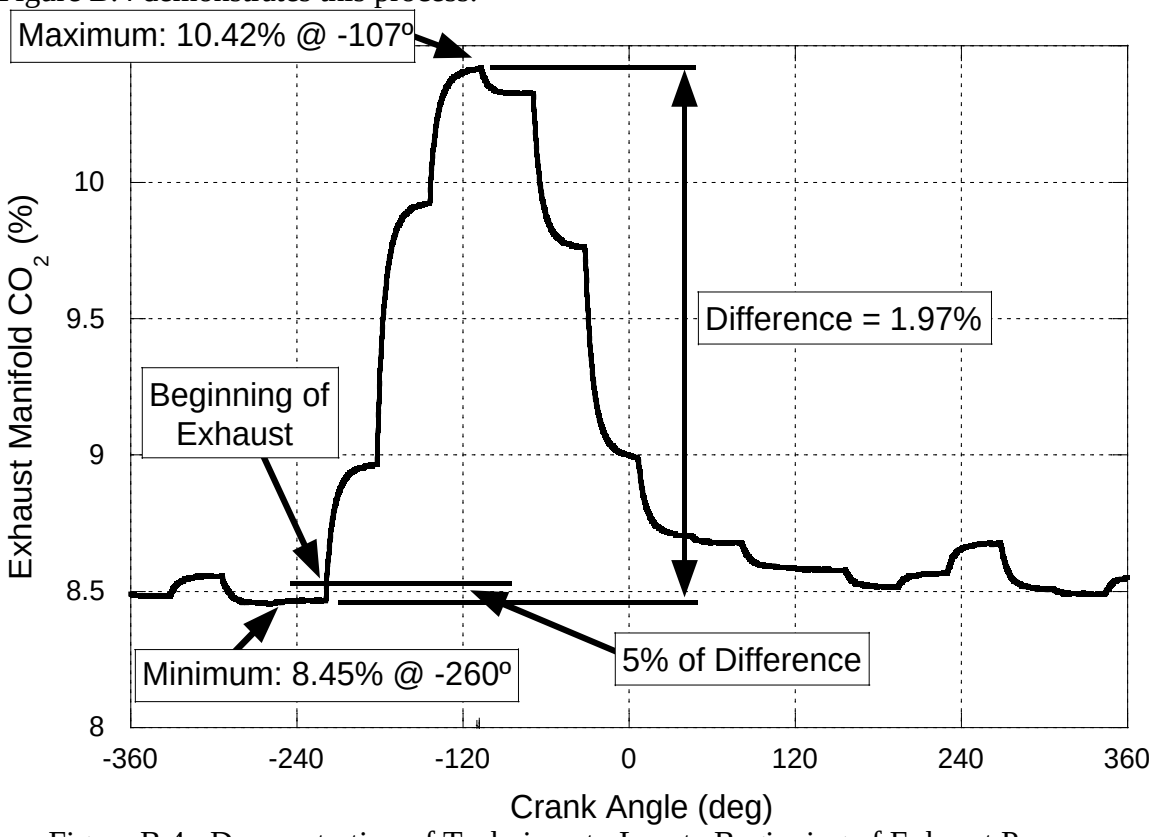

Figure B.4: Demonstration of Technique to Locate Beginning of Exhaust Process

B.2.2 Cycle-Resolved Emissions Results

Determination of cycle-averaged values from the exhaust manifold is complicated by the variation of exhaust mass flow and exhaust properties throughout the exhaust process. While the concentration of CO_2 is measured directly, the amount of mass flowing through the exhaust associated with each concentration is not known. To account for these variations, a blowdown-displacement model introduced by Heywood [43] is used to assume an exhaust mass flow profile over the exhaust process.

The blowdown-displacement exhaust flow model breaks the exhaust process into two distinct components: blowdown, which is governed by pressure differential across the exhaust valve and uses orifice flow equations, and displacement, which assumes that the gas is incompressible as the piston pushes it out of the cylinder during the exhaust stroke.

During blowdown, the flow is assumed to be compressible and is maximum when the gas velocity at the minimum flow area equals the velocity of sound. To determine if the flow has reached this critical point, the following criterion is evaluated: if

$$\frac{P_{Exh}}{P_{Cyl}} \leq \left(\frac{2}{\gamma+1}\right)^{\frac{\gamma}{\gamma-1}} \tag{B.1}$$

Where: P_{Exh} = Exhaust manifold pressure (kPa)

P_{Cyl} = Cylinder pressure (kPa)

γ = Ratio of specific heats (-)

then the flow is choked. Cylinder pressure and exhaust manifold pressure are both measured on a crank angle basis and used here. The ratio of specific heats is dependent upon gas composition and is determined with heat release. If the flow is choked, the exhaust flow rate is calculated by evaluating

$$\dot{m}_{Exh,B} = \frac{C_d A_T P_{Cyl} \sqrt{\gamma}}{\sqrt{R T_{O,Exh}}} \left(\frac{2}{\gamma+1}\right)^{\frac{\gamma+1}{2(\gamma-1)}} \tag{B.2}$$

Where: $\dot{m}_{Exh,B}$ = Exhaust mass flow rate from blowdown (kg/s)

$C_d A_T$ = Effective flow area of exhaust valves (m^2)

P_{Cyl} = Cylinder pressure (kPa)

γ = Ratio of specific heats (-)

R = Gas constant (kJ/kg/K)

$T_{O,Exh}$ = Stagnation temperature of the exhaust flow (K)

If Equation (B.1) is not satisfied, then the flow is not choked and the blowdown flow is given by

$$\dot{m}_{Exh,B} = \frac{C_d A_T P_{Cyl}}{\sqrt{R T_{O,Exh}}} \left(\frac{P_{Exh}}{P_{Cyl}}\right)^{\frac{1}{\gamma}} \sqrt{\left(\frac{2\gamma}{\gamma-1}\right)\left[1-\left(\frac{P_{Exh}}{P_{Cyl}}\right)^{\frac{\gamma-1}{\gamma}}\right]} \tag{B.3}$$

The effective flow area of the exhaust valves is a function of valve lift and is obtained from tabulated engine data provided by the engine manufacturer. The gas constant is a function of mixture molecular weight and is determined by heat release. The stagnation temperature of the exhaust flow is estimated by using the heat release-derived temperature at exhaust valve opening and then expanding the gas isentropically from the cylinder pressure to the exhaust manifold pressure and is calculated with

$$T_{O,Exh} = T_{EVO}\left(\frac{P_{Cyl}}{P_{Exh}}\right)^{\frac{\gamma-1}{\gamma}} \tag{B.4}$$

Where: $T_{O,Exh}$= Stagnation temperature of the exhaust flow (K)

T_{EVO}= Temperature at exhaust valve opening (K)

P_{Cyl} = Cylinder pressure (kPa)

P_{Exh}= Exhaust manifold pressure (kPa)

γ = Ratio of specific heats (-)

Once the blowdown process has subsided, the exhaust is assumed to be incompressible and the flowrate of the exhaust is governed by the motion of the piston and is given by

$$\dot{m}_{Exh,D} = \rho_{Exh}\left(\frac{dV_{Cyl}}{dt}\right) \tag{B.5}$$

Where: $\dot{m}_{Exh,D}$ = Exhaust mass flow rate (kg/s)

ρ_{Exh} = Exhaust gas density (kg/m^3)

$\frac{dV_{Cyl}}{dt}$ = Rate of cylinder volume change (m^3/s)

Density of the exhaust gas is determined with the ideal gas law and is defined as

$$\rho_{Exh} = \frac{P_{Cyl}}{RT_{O,Exh}} \tag{B.6}$$

The values of cylinder pressure, gas constant, and temperature are the same as those defined above. Rate of change of the cylinder volume is a function of crank angle and is directly calculated via engine geometry and engine speed with

$$\frac{dV_{Cyl}}{dt} = \frac{B^2\pi^2 SN}{240} sin\theta\left[1 + \frac{cos\,\theta}{\sqrt{\left(\frac{2l}{S}\right)^2 - sin^2\theta}}\right] \tag{B.7}$$

Where: $\frac{dV_{Cyl}}{dt}$ = Rate of cylinder volume change (m^3/s)

B = Bore (m)

S = Stroke (m)

N = Engine speed (rpm)

l = Connecting rod length (m)

θ = Crank angle (deg)

When using the displacement-blowdown model, exhaust flow at each crank angle step is calculated using both the blowdown approximation and the displacement model. When estimating the blowdown flow the critical ratio in Equation (B.1) is checked first to determine whether Equation (B.2) or (B.3) should be used to calculate blowdown flow. Displacement flow is approximated by Equation (B.5), and then the larger of the displacement flow and blowdown flow is used to determine the exhaust flow. Once the

exhaust flow has been calculated for each crank angle step, the concentration of CO_2 at the corresponding points are used to determine a mass-averaged CO_2 concentration using

$$\overline{\chi_{CO_2}} = \frac{\sum_i \chi_{CO_{2_i}} \cdot \dot{m}_{Exh_i}}{\sum_i \dot{m}_{Exh_i}} \tag{B.8}$$

Where: $\overline{\chi_{CO_2}}$ = Mass averaged concentration of CO_2

$\chi_{CO_{2_i}}$ = Concentration of CO_2 in i^{th} crank angle step

$\dot{m}_{Exh_i}$ = Mass flow rate of exhaust in i^{th} crank angle step

Figure B.5 demonstrates typical results from the blowdown-displacement flow model. Both crank angle and cycle-resolved values of CO_2 are shown, as are flow rate estimations from the model for three consecutive cycles. At this engine condition, the flow during the blowdown period is roughly 50% greater than the peak flow during the displacement phase. Over the entire exhaust event, the blowdown typically accounts for about 30% of the total mass flow. These results are in good qualitative agreement with the data shown in Heywood. [43].

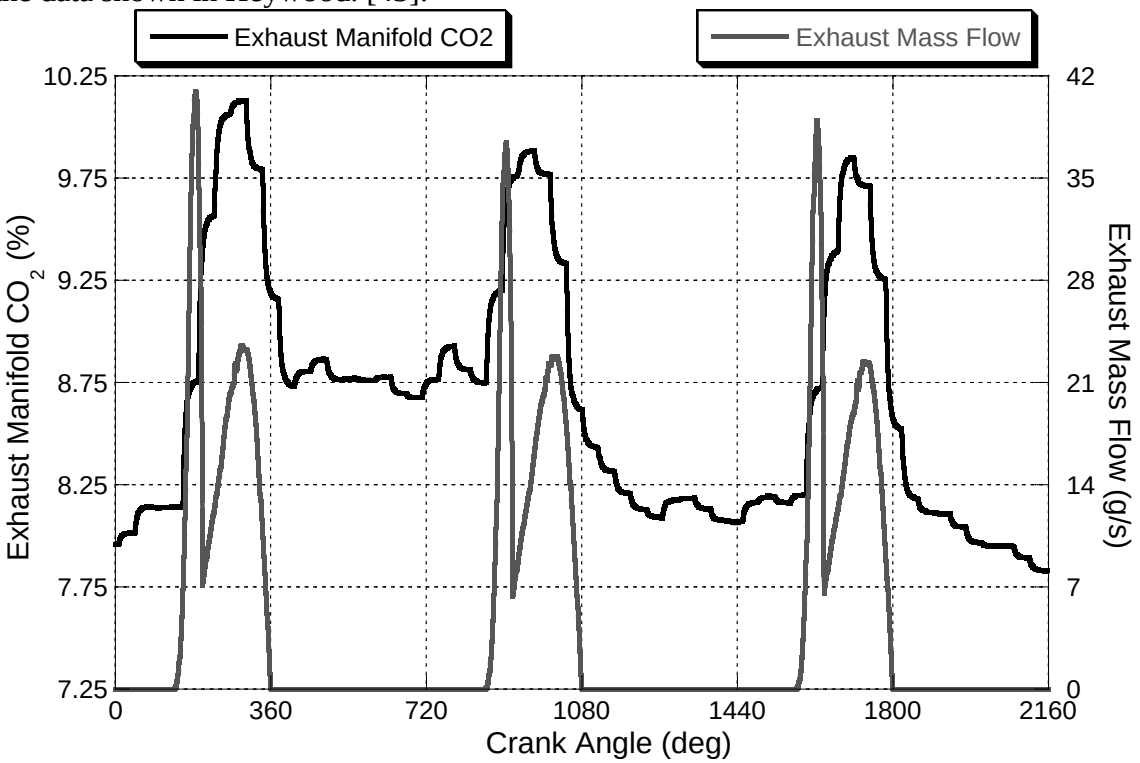

Figure B.5: Measured CO_2 Concentration from Exhaust Manifold and Approximated Exhaust Mass Flow Rate from Blowdown-Displacement Model

A number of different simplifications are used in the blowdown-displacement exhaust flow model that serve to decrease its accuracy. The effects of heat transfer and unsteady flow are completely neglected, and the inaccuracy of pressure measurements greatly alter estimated flow rates. But because the exhaust flow rate is used to weight the values of CO_2 concentration, it is irrelevant if the absolute values of the calculated flow rates are correct on an absolute basis. What matters is that the flow profiles accurately represent the relative flow of exhaust gas throughout the exhaust process.

To assess the influence of using the blowdown-displacement exhaust flow model to weight the CO_2 concentration curve, a comparison is made between using it and a straight average. Considering all of the data obtained, the largest deviation between the two cases is 3.4%. It is important to note, however, that in all cases the use of the blowdown-displacement model results in a cycle-resolved CO_2 values that are greater than those obtained with a straight average. Figure B.6 shows a sample of 30 cycles of weighted and unweighted CO_2 data during a load transition from 1 to 9 bar BMEP at 2000 rpm. The largest deviation occurred during the cycle in which the largest load transition occurred. At steady-state conditions, however, deviations are typically below 2%.

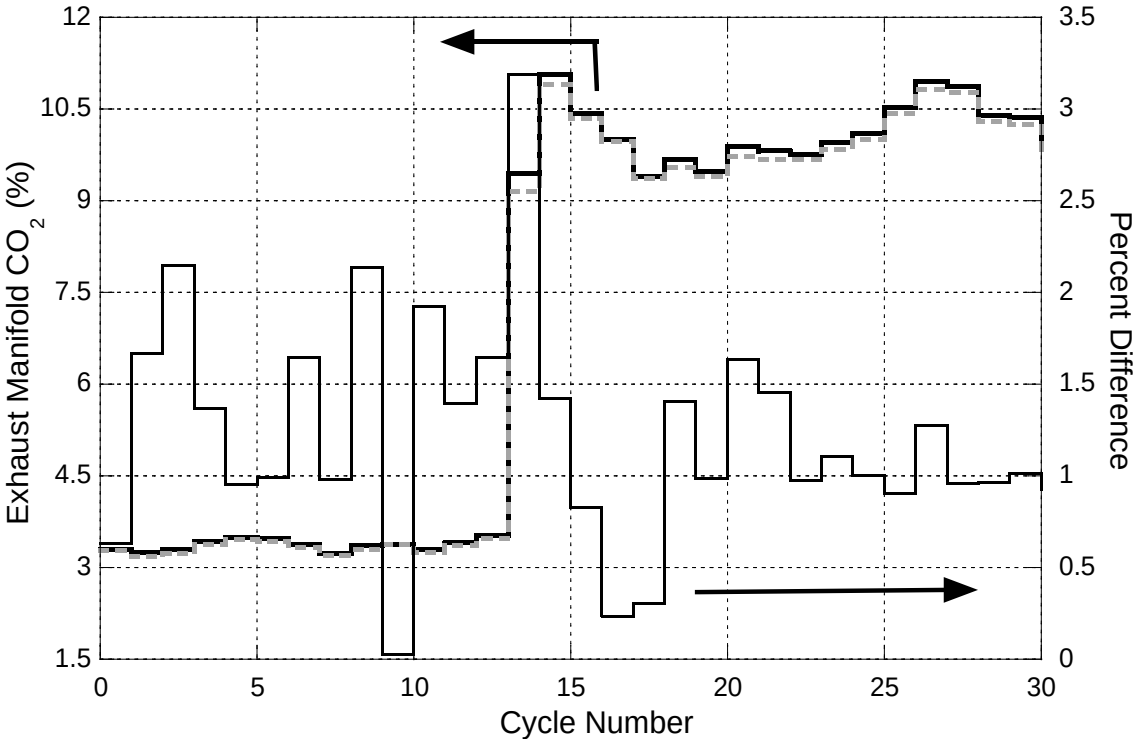

Figure B.6: Cycle-Resolved CO_2: Weighted Average with Exhaust Flow, Straight Average, and Percent Difference

A comparison of weighted and unweighted NO in the exhaust manifold for the same 30 cycles as in the previous figure is shown in Figure B.7. Unlike CO_2, NO the exhaust flow-weighted values are sometimes lower than the unweighted averages. Typically, though, by using the exhaust flow model to weight the cycle-resolved concentration, NO values are increased above the straight average. Maximum deviations between the methods of averaging in all cases is 6.0%. Similar to the CO_2 case, the NO averages are in closer agreement during steady-state engine operation.

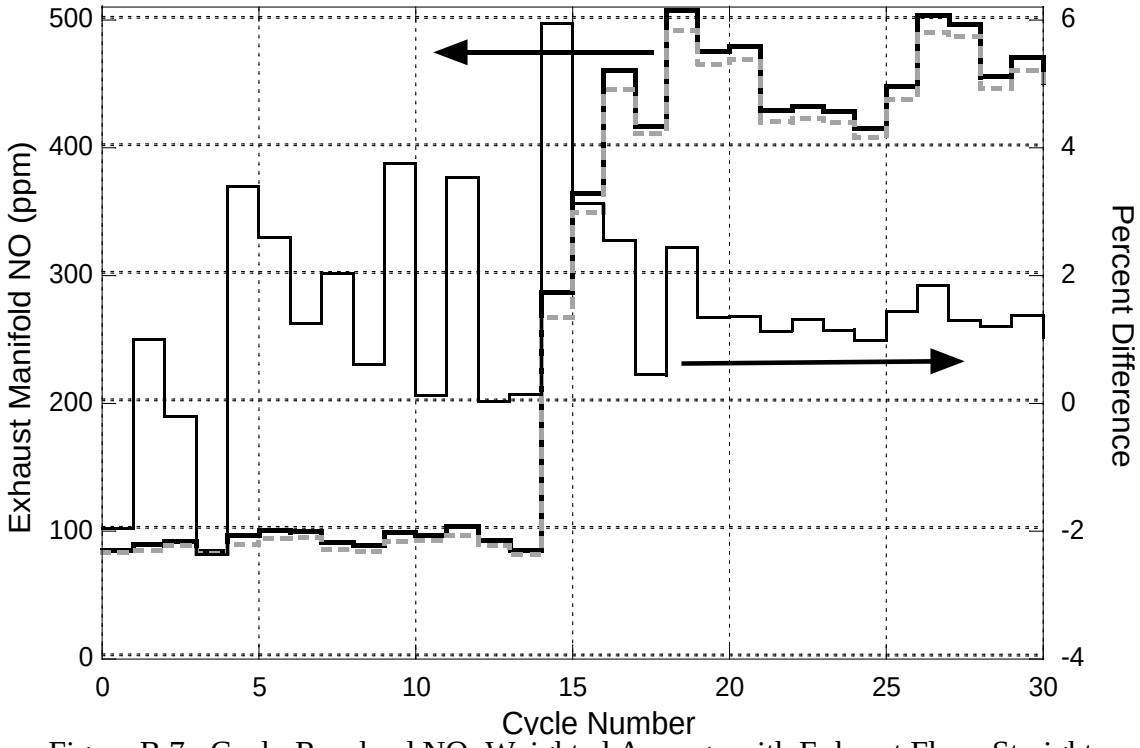

Figure B.7: Cycle-Resolved NO: Weighted Average with Exhaust Flow, Straight Average, and Percent Difference

APPENDIX C

HEAT RELEASE

When evaluating the performance of an internal combustion engine, numerous metrics are considered: power, fuel economy, exhaust gas pollutant formation, and noise. In order to fully characterize engine performance, simply measuring the amount of each output produced is insufficient; an understanding of in-cylinder processes is necessary. Much of this knowledge is facilitated through study of the amount of energy released by the fuel. This so-called heat release analysis involves quantifying the fuel heat release rate and total amount of heat release at each crank angle increment.

C.1 Heat Release Overview

Heat release cannot be directly obtained; it must be calculated from other measured parameters. The most critical measured component of heat release analysis is the cylinder pressure at each crank angle. Engine geometry, engine operating conditions, and cylinder charge properties also influence the heat release calculation.

To calculate the heat release from cylinder pressure data, the First Law of Thermodynamics is written in differential form on a per crank angle basis for the engine cylinder.

$$\frac{dQ_{Ch}}{d\theta} = \frac{dU_{CV}}{d\theta} + \frac{dW_{CV}}{d\theta} + \frac{dQ_{HT}}{d\theta} + \sum \left[h_{Out} \frac{dm_{Out}}{d\theta} \right] \tag{C.1}$$

Where: $\frac{dQ_{Ch}}{d\theta}$ = Rate of heat release from fuel during combustion (kJ/CA)

$\frac{dU_{CV}}{d\theta}$ = Rate of internal energy change (kJ/CA)

$\frac{dW_{CV}}{d\theta}$ = Rate of work done on the piston (kJ/CA)

$\frac{dQ_{HT}}{d\theta}$ = Rate of heat transfer into the cylinder (kJ/CA)

h_{Out} = Enthalpy of crevice flows and blowby (kJ/kg)

$\frac{dm_{Out}}{d\theta}$ = Rate of mass loss via crevice flow and blowby (kg/CA)

This equation essentially states that the energy released from the fuel is divided amongst: heating up the gases in the cylinder, boundary work through piston motion, heat transfer through the combustion chamber walls and the piston, and mass losses past the piston rings.

To accurately determine the amount of heat release from the fuel, each of the four terms on the right hand side must be accounted for. The complex and unsteady nature of these components requires that numerical methods or models of physical processes be used to approximate them. Thus the heat release calculation itself is an approximation and highly dependent upon the assumptions made. Numerous authors have investigated accurate calculation methods of heat release [43, 49-67].

C.1.2 Internal Energy

The internal energy of a system is related to its degree of molecular activity and its molecular structure; this involves both the kinetic and potential energies of the molecules. Any motion of a molecule relative to itself or its surroundings is included in molecular kinetic energy. Translation, rotation, and vibration are all types of molecular motion that contribute to molecular kinetic energy. Molecular internal energy consists of binding forces between individual molecules, between the atoms of one molecule, and between the particles within an atom and its nucleus.

The amount of internal energy contained within a control volume of molecules is dependent upon the total mass present. Thus the internal energy, U_{CV} is an extensive property and can be written as

$$U_{CV} = mu_{CV} \tag{C.2}$$

Where: m = Mass of the system (kg)

u_{CV} = Internal energy (kJ/kg)

Differentiating Equation (C.2) with respect to crank angle gives

$$\frac{dU_{CV}}{d\theta} = m\frac{du_{CV}}{d\theta} + u_{CV}\frac{dm}{d\theta} \tag{C.3}$$

Generally, cylinder gas components are modeled as an ideal gas that behaves according to the ideal gas law, given by

$$PV = mRT \tag{C.4}$$

Where: P = Cylinder pressure (kPa)

V = Cylinder volume (m^3)

m = Mass of the system (kg)

R = Specific gas constant (kJ/kg-K)

T = Temperature (K)

It has been shown experimentally and demonstrated mathematically that internal energy is a function only of temperature for an ideal gas $\left(u = u(T)\right)$ and therefore

$$\frac{du_{CV}}{d\theta} = c_V\frac{dT}{d\theta} \tag{C.5}$$

Where: c_V = Constant-volume specific heat (kJ/kg-K)

Substituting Equation (C.5) into Equation (C.3) yields

$$\frac{dU_{CV}}{d\theta} = mc_V\frac{dT}{d\theta} + u_{CV}\frac{dm}{d\theta} \tag{C.6}$$

The temperature profile of the mixture is derived through use of the ideal gas law shown in Equation (C.4), along with the measured cylinder gas pressure, volume, trapped mass, and gas constant. Volume is determined by knowing the crank angle and engine geometry. The trapped mass and gas constant are accounted for by using the mass flow rates of air, fuel, residual, and EGR into the cylinder. This calculated temperature is a bulk value for the entire cylinder contents. Previous work [43,61] has shown that this single temperature value is close to the mass-averaged temperature of all cylinder gas components because burned and unburned molecular weights are nearly the same. Therefore using a single temperature to characterize the cylinder charge is a reasonable approximation.

The constant volume specific heat of a mixture is a function of its temperature, pressure, and composition. As the combustion process occurs, the temperature and pressure fluctuate and the mixture composition varies continuously making the computation of the actual mixture specific heat very difficult. Therefore, numerous methods have been suggested to approximate the c_V of a mixture [49,58,61,65,68]. The simplest is to assume that c_V is constant throughout the combustion process. Greater accuracy is obtained by defining c_V as a function of temperature. More sophisticated approximations determine the concentrations of the individual species and incorporate temperature-dependant specific heat correlations for each component [69,70].

The constant volume specific heat of a mixture can be written in terms of the gas constant as

$$c_V = c_P - R \tag{C.7}$$

Where: c_P = Constant-pressure specific heat (kJ/kg-K)

No simplification is made here because c_P is also dependant on mixture temperature, pressure, and composition. But by defining the ratio of specific heats, γ, as

$$\gamma = \frac{c_P}{c_V} \tag{C.8}$$

and combining this relationship with Equation (C.7), the constant volume specific heat can be written as

$$c_V = \frac{R}{\gamma - 1} \tag{C.9}$$

It has been found experimentally that the ratio of specific heats is easier to relate to temperature and composition than c_V or c_P. Thus c_V can be defined by fixing R and using a correlation for γ [58,59,61].

The complex nature of the combustion process and the reliance of critical parameters on continually-changing values of mixture temperature, pressure, and composition make the internal energy estimation difficult. Different engines will require various levels of approximation sophistication to yield sufficiently accurate results.

C.1.3 Work

The second term on the right hand side of Equation (C.1) accounts for the energy transferred into piston motion. This form of work is known as boundary work because of a changing volume and is expressed as

$$\frac{dW_{CV}}{d\theta} = P\frac{dV}{d\theta} \tag{C.10}$$

Where: $\frac{dW_{CV}}{d\theta}$ = Rate of work done on the piston (kJ/CA)

P = Cylinder pressure (kPa)

$\frac{dV}{d\theta}$ = Rate of change of cylinder volume (m^3/CA)

The cylinder pressure is measured directly with the cylinder pressure transducer. Cylinder volume is calculated through engine geometry, where the volume at any crank angle is given by Equation (C.11) from Heywood [43].

$$V(\theta) = V_C \left\{ 1 + \frac{1}{2}(r_c - 1) \left[\frac{l}{2S} + 1 - cos\,\theta - \sqrt{\left(\frac{l}{2S}\right)^2 - sin^2\theta} \right] \right\} \quad \text{(C.11)}$$

Where: $V(\theta)$ = Cylinder volume at any given crank angle (m^3)

V_C = Cylinder clearance volume (m^3)

r_C = Compression ratio (-)

l = Connecting rod length (m)

S = Engine stroke (m)

θ = Crank angle

Compression ratio is determined by

$$r_C = \frac{V_C + V_D}{V_C} \quad \text{(C.12)}$$

Where: V_D = Cylinder displaced volume (m^3)

Displaced cylinder volume is calculated by

$$V_D = \frac{\pi B^2}{4} S \quad \text{(C.13)}$$

Where: B = Cylinder bore (m)

S = Cylinder stroke (m)

Work calculation in this manner is very accurate because of the direct measurements of cylinder pressure and cylinder volume. It is therefore widely used to determine the amount of work that the piston extracts from the cylinder components.

C.1.4 Heat Transfer

Energy flow due to a temperature gradient is known as heat transfer. In an engine, large temperature differences exist between the cylinder gases and the combustion chamber walls. Two forms of heat transfer are prevalent within the combustion chamber: convection and radiation. These phenomena are quantified by

$$\frac{dQ_{HT}}{d\theta} = \left[h_c(T - T_w) + h_r\left(T^4 - {T_w}^4\right)\right]\frac{dA_s}{d\theta} \quad \text{(C.14)}$$

Where: $\frac{dQ_{HT}}{d\theta}$ = Rate of heat transfer into the cylinder (kJ/CA)

h_c = Convective heat transfer coefficient (kJ/m^2-K)

h_r = Radiative heat transfer coefficient (kJ/m^2-K^4)

T = Cylinder gas temperature (K)

T_w = Wall temperature of combustion chamber (K)

$\frac{dA_s}{d\theta}$ = Rate of change of surface area for heat transfer (m^2/CA)

The surface area is a function of engine geometry and is given by Equation (C.15) which is obtained from Heywood [43].

$$A_S(\theta) = A_{Cylhd} + A_{Pstn} + \frac{\pi BS}{2}\left[\frac{l}{2S} + 1 - cos\,\theta - \sqrt{\left(\frac{l}{2S}\right)^2 - sin^2\theta}\right] \quad \text{(C.15)}$$

Where: $A_S(\theta)$ = Cylinder surface area at any given crank angle (m^2)

A_{Cylhd} = Cylinder head area (m^2)

A_{Pstn} = Piston crown area (m^2)

B = Cylinder bore (m)

S = Engine stroke (m)

l = Connecting rod length (m)

θ = Crank angle

The determination and use of h_c and h_r has been investigated by several authors [68,71-84]. These coefficients must account for numerous complex phenomena including charge motion, changing cylinder gas composition, and fluctuating cylinder conditions. Consequently, the suggested correlations are highly empirical and very specific to engine geometry and operating condition. For spark ignition engines h_r is generally neglected, while in diesel engines the heat transfer due to radiation is significant due to the luminous, radiating flame.

Wall temperatures include the temperatures of the surfaces of the cylinder head, piston crown, and cylinder walls that are indirect contact with the cylinder gases. These temperatures fluctuate both temporally and spatially due to heterogeneity in the combustion process and cooling passages around the cylinder. Cylinder-to-cylinder variation will also occur because the coolant itself changes temperature as it flows through the block and heads.

C.1.5 Blowby and Crevice Flow

The final term on the right hand side of Equation (C.1) accounts for crevice flow and blowby effects. As the combustion process occurs, high pressures are generated which force some cylinder gas components into the region of or past the piston rings. This phenomenon reduces the overall mass trapped in the cylinder and therefore the heat release calculation. Numerous researchers have examined crevice flow and blowby and have developed models to predict its impact on engine heat release.

C.2 University of Michigan Heat Release Code

From the above discussion, it is evident that heat release analysis is not an exact science. The use of numerous approximations to physical processes and sensitivity of correlations to engine geometry and operating conditions can lead to significant inaccuracies in heat release values. To perform proper analysis, the models used for each component of the right hand side of Equation (C.1) must be selected and implemented carefully.

Members of the W.E. Lay Automotive Laboratory at the University of Michigan have developed a computer program to aid researchers in heat release analysis. The program allows the user to define engine geometrical parameters, input a cylinder

pressure curve, select the appropriate thermodynamic and heat transfer models, and evaluate the impact of these models on the heat release calculation.

C.2.1 Program Description (Adapted from [85])

The University of Michigan Heat Release (UMHR) Program contains two distinct components: the Graphical User Interface (GUI) written in Visual C++ and the heat release code itself written in FORTRAN. The GUI serves as a straight-forward means by which the user inputs data, selects the operation parameters, and views the program output. Once the user has defined the desired inputs to the program, the GUI will call the heat release code just as a computer program will call a subroutine. All of the computation work is done by the FORTRAN portion of the program and when the final results have been calculated, they are sent back to the GUI to be reported to the user. The FORTRAN portion of the code is stand-alone, and can be run by various means. This characteristic of the code gives it the flexibility to adapt to the needs of a variety of users. The GUI was selected as the interface between the user and heat release code because of its simplicity and familiarity as it uses Windows-based menus, commands, and graphics.

The FORTRAN heat release code has a modular structure and the bulk of the main program consists of subroutine call commands. Most of the computation in the UMHR code takes place in the subroutines. This architecture allows the code to be understood and modified easily by future contributors. The flowchart shown in Figure C.1 represents how the UMHR code functions. Each box represents a subroutine that is called by the main program. To initialize a heat release calculation, the operational parameters must be defined through the Input/Output Parameters window. Here, the location of the source data (pressure versus crank angle) is identified, as well as the destination of the UMHR output. Crank angle resolution and the number of points in the input file are also defined. The subroutines that are first called by the main program are

used to either prepare the input data for calculation or to determine important parameters that are used in the heat release calculation. Once these parameters have been calculated, the cylinder heat transfer, work, and internal energy are determined and then summed together to arrive at the heat release. Additional subroutines compute the mass fraction burned (MFB), mass of fuel burned, and equivalence ratio.

The UMHR program uses iteration methods to converge on final heat release values. To initialize the procedure, constant gas properties γ, R, c_P, c_V are assumed to generate values for MFB at each step of crank angle resolution. Once the initial values are obtained, the program then uses either the MIXTURE subroutine (using chemical equilibrium) or the SMPLPROP subroutine (using empirical equations) to account for variable working fluid properties if so specified. The program then recalculates the MFB at each crank angle and then checks the MFB at exhaust valve opening (EVO) with the MFB at EVO from the previous iteration. If the difference between the two is greater than some user-defined value of epsilon, the program will go through the process again. However, if the new MFB value is within epsilon of the old MFB value, the program ceases to iterate and the final output is reported.

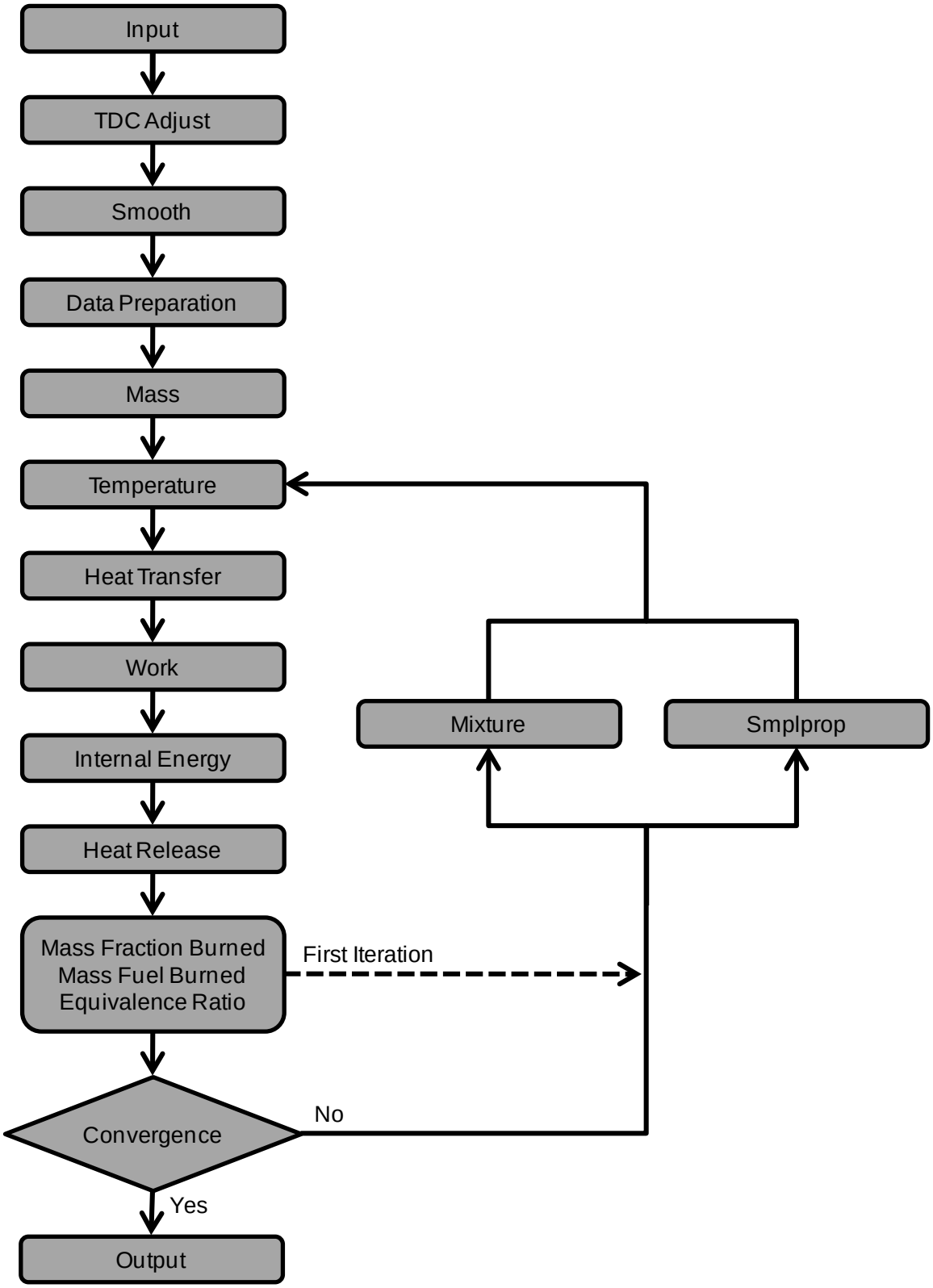

Figure C.1: Original UMHR Architecture

C.3 UMHR Program Modifications

In its original form the UMHR program was intended to be used for one cycle at a time, and the user would enter in new data for every case investigated. For this study, thousands of cycles of data need to be processed, so a routine is developed to call the program recursively. Fortunately, the code was written in a modular and flexible manner to permit straight-forward modification. Also, because additional inputs are known due to the cycle-resolved measurements, some calculations within the heat release code are either altered or removed altogether.

Significant changes are made to the MASS subroutine. Since the cycle-resolved measurement of in-cylinder and exhaust manifold CO_2 results in knowledge of exactly how much fuel, air, and stoichiometric combustion products are in the cylinder prior to combustion, trapped cylinder mass does not need to be calculated. In accordance with this change, heat release does not use EGR rate as an input. Additionally, the MIXTURE and SMPLPROP subroutines are used only as weighting functions to calculate the cylinder's thermodynamic properties. Equilibrium routines are no longer needed because the cylinder contents are known.

To permit recursive calling of the UMHR program, the FORTRAN code is transformed using the MEX command in MATLAB. This command compiles and links source files into a MEX-file, which is executable in MATLAB. Essentially, the FORTRAN code and all its support files are compiled in a once-and-for-all manner such that in order to run the code, the inputs must be defined and then the executable is called from the MATLAB command window. When placed inside of a loop structure, this executable is called recursively.

To reduce the degree to which the code is altered, most subroutines and input/output data processes remain unchanged. The UMHR still reads in a *.txt data file and outputs its information in a *.csv format. When placed inside of a loop, however, the

inputs are first defined for a particular cycle and then the proper HR_Input.txt file is written. The input parameters selected when running the modified UMHR code strongly influence the output rate of heat release values. They must be chosen carefully to guarantee meaningful results. Table C.1 shows the settings and values used as inputs to the modified code. These settings are used throughout this investigation.

Table C.1: Input Parameters to Heat Release Code

Order of Differentiation	4
Data Smoothing	None
Number of Data Points	7200
Flow Rate Specification	All flows defined by user
Gas Constant Determination	Based on mixture molecular weight
Specific Heat Determination	Based on mixture
Constant Volume Specific Heat Calculation	From Gas Constant and Ratio of Specific Heats
Maximum Number of Iterations	100
Use of Equilibrium Routines	N/A
Fuel Specification	Diesel
Crank Angle Resolution	One Tenth Degree
Bore (m)	0.095
Stroke (m)	0.105
Compression Ratio	18
Connecting Rod Length (m)	0.176
Cylinder Head Surface Area (m^2)	0.00708822
Piston Crown Surface Area (m^2)	0.0104197
Engine Speed (rpm)	Cycle-Dependent
Air Flow Rate (mg/cycle)	Cycle-Dependent
Fuel Flow Rate (mg/cycle)	Cycle-Dependent
Mass of Stoichiometric Combustion Products (mg/cycle)	Cycle-Dependent
Wall Temperature (K)	460
Intake Valve Closing (deg aTDC)	-145.3

Initial Guess for Gas Constant (J/kg/K)	300
Initial Guess for Ratio of Specific Heats (-)	1.3
Stoichiometric Air/Fuel Ratio (-)	14.4855
Lower Heating Value of Fuel (kJ/kg)	42657
Heat Transfer Correlation	Hohenberg
Convergence Criterion	0.0001
Exhaust Valve Opening (deg aTDC)	134.9
Mole Fraction of Oxygen in Air	0.21
Mole Fraction of Nitrogen in Air	0.79
Mole Fraction of Argon in Air	0
Mole Fraction of Carbon Dioxide in Air	0
Moles of Carbon in Fuel	14.4
Moles of Hydrogen in Fuel	25.8048
Moles of Oxygen in Fuel	0
Moles of Nitrogen in Fuel	0
Start of Injection (deg aTDC)	Cycle-Dependent

After the UMHR code is executed, it writes all of its outputs to a HR_Output.csv file. This file is then read into MATLAB, where important metrics, such as rate of heat release, integrated heat release, bulk gas temperature, rate of work, rate of heat transfer, and rate of internal energy are recorded. The rate of heat release curve is then interpreted to yield important combustion characteristics, like start of combustion and the mass fraction burned curves. A typical rate of heat release curve is shown in Figure C.2.

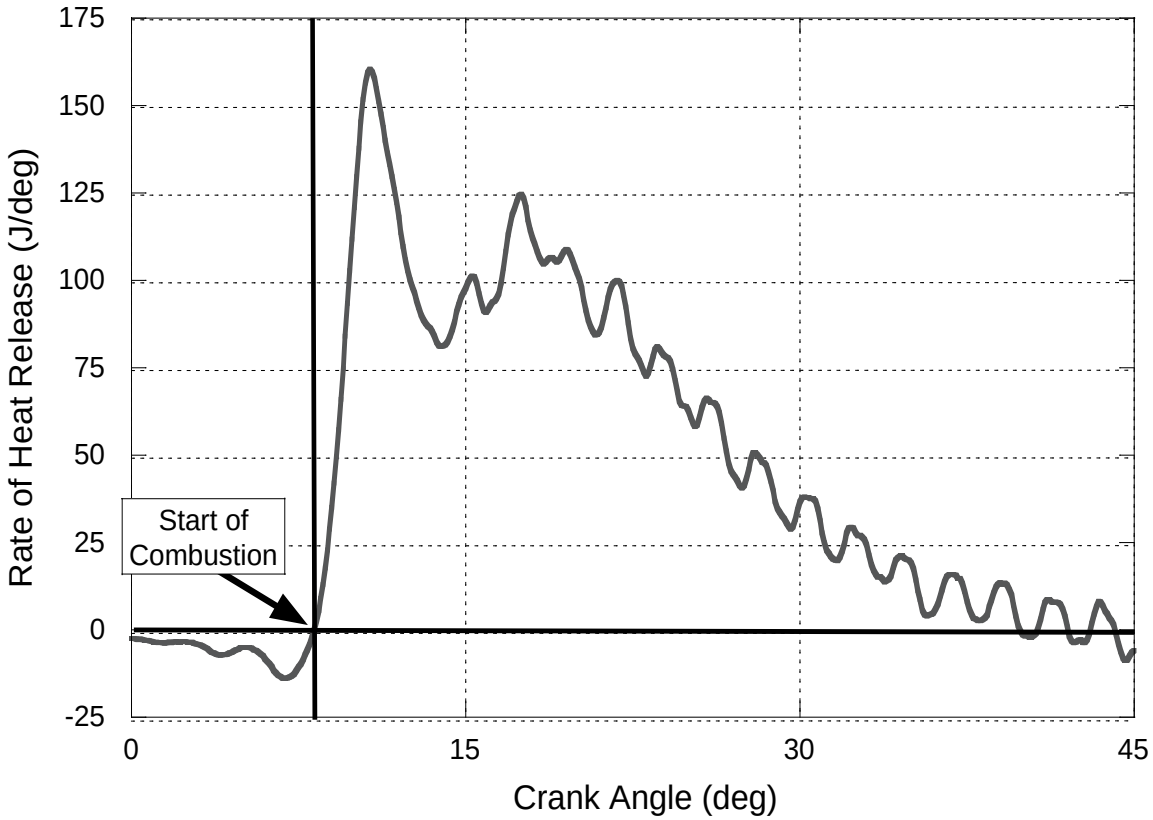

Figure C.2: Typical Rate of Heat Release Curve at 2000 rpm and 9 Bar BMEP

After fuel injection has begun and before combustion begins, the high temperatures in the cylinder vaporize the injected fuel. This phenomenon is evidenced by negative rates of heat release. As combustion begins, fuel energy is released and the rate of heat release becomes positive. Because the exact point of beginning of combustion is difficult to locate, a common convention is to define combustion start as the crank angle at which the rate of heat release curve becomes positive [43]. These features are demonstrated in Figure C.2.

The total quantity of energy released in this analysis is determined by considering the heat release curve, which is the integral of the rate of heat release and shown in Figure C.3. This metric, also known as the mass fraction burned curve, is used to analyze the relative speed and duration of the combustion process. The difference between the minimum heat release value (at the start of combustion) and the maximum heat release value is total amount of fuel energy released. The crank angles at which 10%, 50%, and

90% of this difference occur give important insight about the rate of combustion. End of combustion is defined to occur at 90% mass fraction burned. This definition is used because the 90% MFB crank angle is much more consistent than the 100% MFB crank angle. Combustion duration is therefore defined as the elapsed crank angle from the start of combustion to the 90% MFB crank angle.

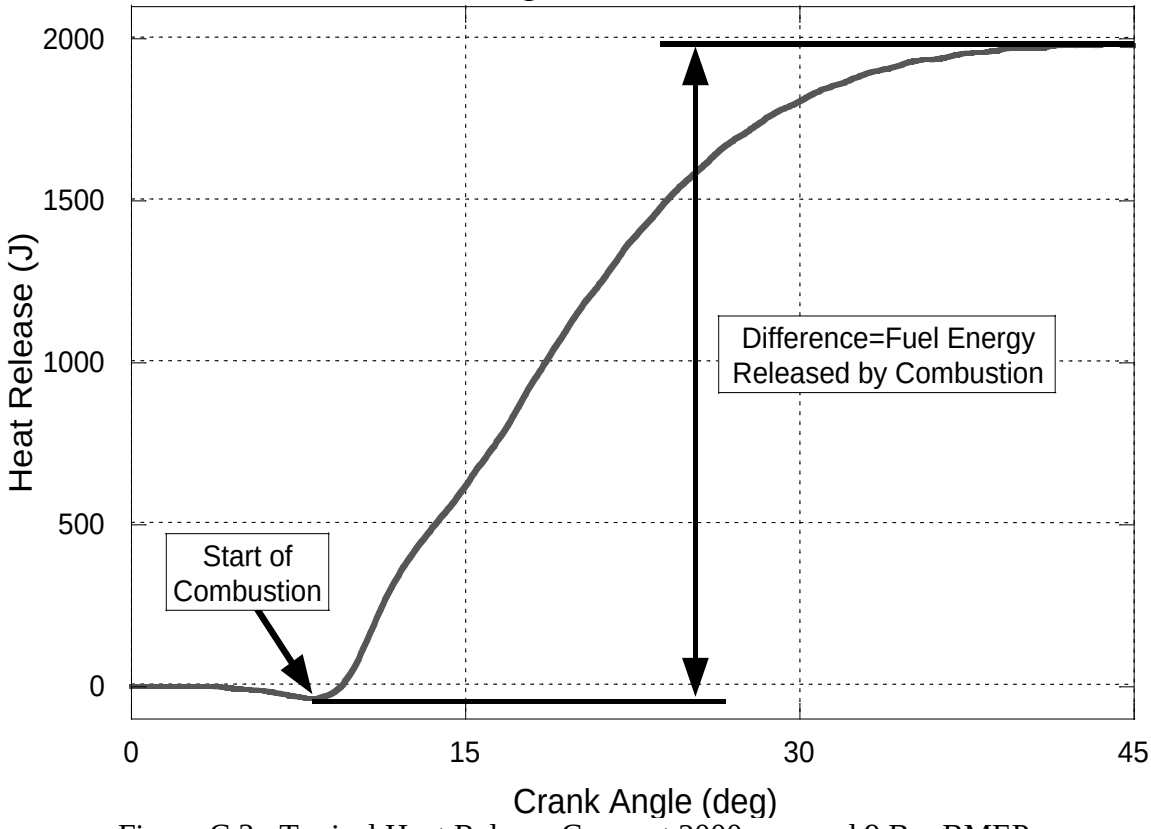

Figure C.3: Typical Heat Release Curve at 2000 rpm and 9 Bar BMEP

Incorporating cycle-resolved emissions measurements and a recursive heat release program permits the detailed study of combustion during transient engine processes. This is unique because the masses of fuel, air, and stoichiometric combustion products is known for each cycle, and the researcher can evaluate how combustion evolves over realistic engine operation. Typical results are shown in Figure C.4, which displays twenty consecutive rate of heat release curves during constant-speed load step.

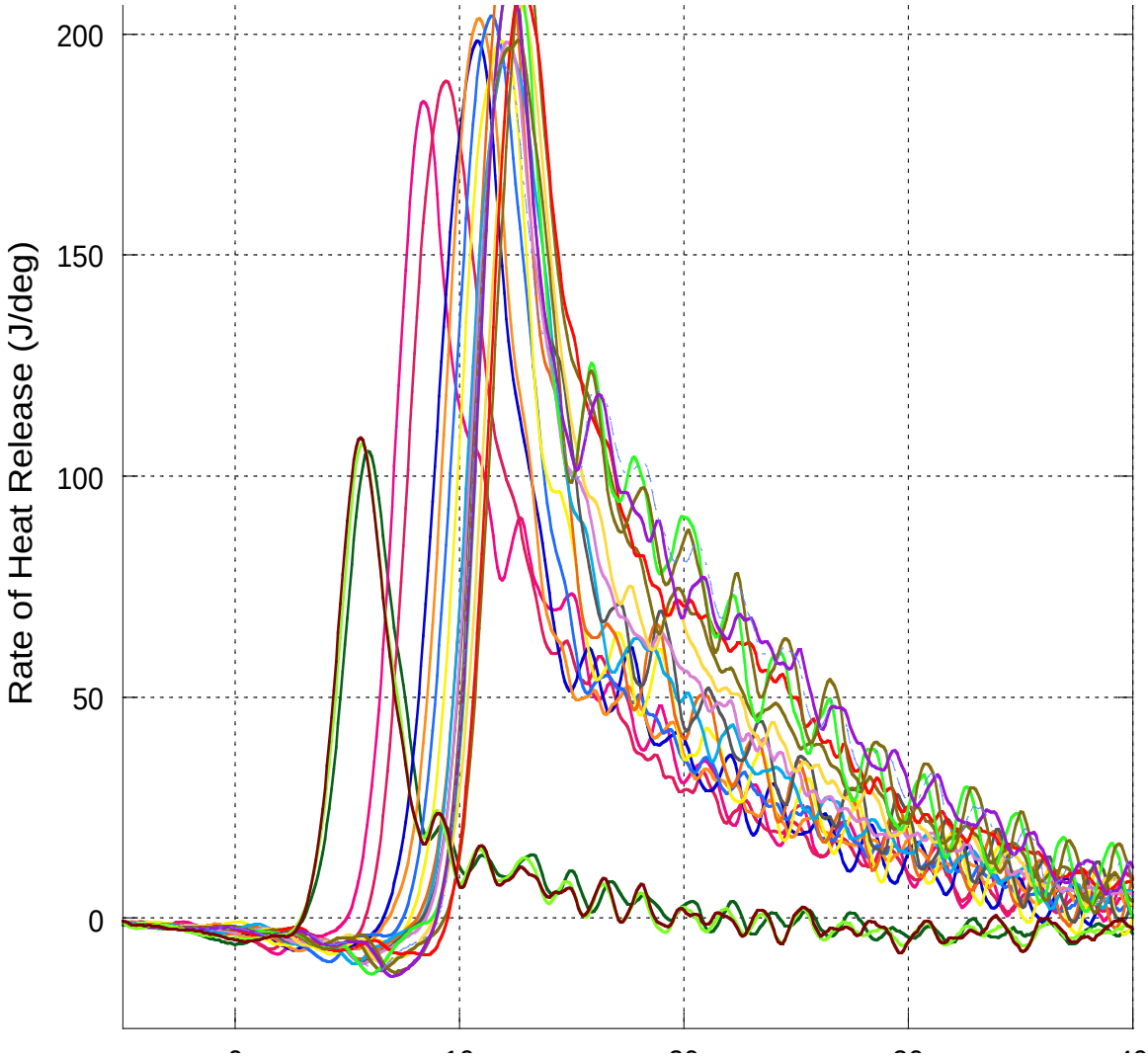

Figure C.4: Rate of Heat Release for Twenty Consecutive Cycles During 1 to 9 bar BMEP Instantaneous Load Step at 2000 rpm

APPENDIX D

SIMUATION CODE TO MODEL FLOW THROUGH CSV

Cambustion, Incorporated, the manufacturer of the CSV 500, has developed a simulation code the models flow through the CSV with the goal of guiding researchers as they configure the CSV to suit their needs. Assumptions used to model the gas flow through the system and into the analyzers, as well as the equations incorporated into the code have graciously been provided by Cambustion. Equations that are used in the simulation are presented and not rigorously developed.

Four separate components are modeled in the simulation: the sample line, the orifice valves, the storage tube, and the analyzer tube. The sample line is treated with a one-dimensional isothermal compressible flow. From here the gases pass through either the sample or purge valve, and their behavior is approximated by conventional orifice flow equations that are isentropic up to the throat. The storage tube flow is modeled by using one-dimensional isothermal incompressible equations. As with the sample line, the analyzer tube is treated with one-dimensional isothermal compressible flow assumptions. To make nomenclature more clear, a schematic of the CSV 500 that demonstrates the locations of the modeled components is shown in Figure D.1.

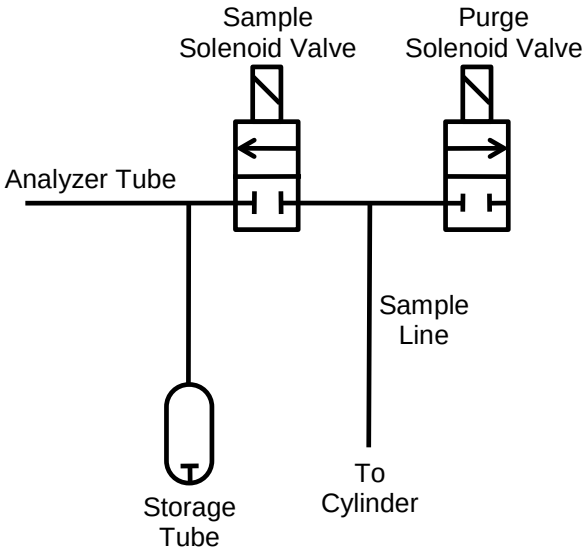

Figure D.1: Flow Schematic of CSV 500

The driving force behind the gas flow through the system is cylinder pressure, which is input by the user. Also required are the physical characteristics of the sampling system, including line and tube lengths and diameters. The pressures in the storage tube and at the outlet of the purge solenoid valve are both set to be atmospheric. Temperature in the sample line is defined to be fixed at 500 K as recommended by Cambustion. Gas analyzer information, such as sample rate, analyzer tube length and diameter, and temperature and pressure are also estimated. Opening and closing crank angles of the purge solenoid valve and sampling solenoid valve are input and define the crank angles over which sample flows through the system.

For the sample line, storage tube, and the analyzer tube, the flow is modeled as Fanno flow, which is isothermal and may be either compressible or incompressible. The first step using this model is to assume that the flow is not choked and then to calculate a mass flow using the relationship shown in Equation D.1.

$$\left(\frac{\dot{m}}{A}\right)^2 = \frac{({p_i}^2 - {p_e}^2)}{4RTf\frac{L}{d}} \tag{D.1}$$

Where: $\dot{m}$ = Mass flow rate of gas (kg/s)

A = Flow cross-sectional area (m^2)

p_i = Pressure at the inlet of the line (N/m^2)

p_e = Pressure at the exit of the line (N/m^2)

R = Gas constant (J/kg/K)

T = Temperature (K)

f = Friction factor (-)

L = Line length (m)

d = Line diameter (m)

The value of the friction factor, f, is dependent upon whether the flow is laminar or turbulent. If the Reynolds number is greater than 4000, the flow is considered turbulent. For the laminar case, the value of the friction factor is

$$f = \frac{16}{Re} \tag{D.2}$$

Where: f = Friction factor (-)

Re = Reynolds Number

If the flow is turbulent, the friction factor is given by

$$f = 0.079Re^{-\frac{1}{4}} \tag{D.3}$$

The Reynolds Number for flow in a duct is given by

$$Re = \frac{\dot{m}d}{A\mu} \tag{D.4}$$

Where: Re = Reynolds Number (-)

$\dot{m}$ = Mass flow rate of gas (kg/s)

d = Flow diameter (m)

A = Flow cross-sectional area (m^2)

μ = Gas dynamic viscosity (N-s/m^2)

If the flow is laminar, then Equation D.2 simplifies to

$$\left(\frac{\dot{m}}{A}\right) = \frac{({p_i}^2 - {p_e}^2)d^2}{64RTL\mu} \tag{D.5}$$

Iterations are then used with Equations D.1-D.5 to determine if the flow is laminar or turbulent and to calculate a final mass flow rate. The value obtained is then used to check if the flow is choked or not by using

$$M_e = \frac{\dot{m}\sqrt{RT}}{Ap_e} \tag{D.6}$$

Where: M_e = Mach Number at the exit of the line (-)

$\dot{m}$ = Mass flow rate of gas (kg/s)

R = Gas constant (J/kg/K)

T = Temperature (K)

A = Flow cross-sectional area (m^2)

p_e = Pressure at the exit of the line (N/m^2)

If the value of Equation D.6 is greater than one, then the flow is choked and the mass flow must be recalculated using choked flow equations. If the flow is laminar and choked, then the relationship between the inlet and exit pressures is given by

$$p_e = \frac{-k + \sqrt{k^2 + 4{p_i}^2}}{2}$$

Or (D.7)

$$p_i = \sqrt{p_e(k + p_e)}$$

Where: $$k = \frac{64L\mu\sqrt{RT}}{d^2}$$

Equation D.5 can then be used to calculate the laminar flow choked mass. If the flow is turbulent, then the friction factor is constant and the relationship between the inlet and outlet pressures is

$$p_e = \frac{p_i}{\sqrt{4\gamma f\frac{L}{d} + 1}} \tag{D.8}$$

With this relationship, Equation D.1 is then used to calculate flow rate. Conditions at any axial position along the length of the tube can also be determined. The pressure at any axial location in the line is given by

$$p_x = \sqrt{{p_i}^2 - \frac{x}{L}({p_i}^2 - {p_e}^2)} \tag{D.9}$$

Where: p_x = Pressure at axial location x (N/m^2)

p_i = Pressure at the inlet of the line (N/m^2)

p_e = Pressure at the exit of the line (N/m^2)

x = Axial location (m)

L = Length of line (m)

The velocity at any axial location in the line is given by

$$u_x = \sqrt{\frac{RTd}{4fL\left(\frac{{p_i}^2}{{p_i}^2 - {p_e}^2} - \frac{x}{L}\right)}} \tag{D.10}$$

Where: u_x = Velocity at axial location x (m/s)

R = Gas constant (J/kg/K)

T = Temperature (K)

d = Flow diameter (m)

f = Friction factor (-)

L = Length of line (m)

p_i = Pressure at the inlet of the line (N/m^2)

p_e = Pressure at the exit of the line (N/m^2)

x = Axial location (m)

The mass in an isothermal tube is given by

$$m = \frac{2AL({p_i}^3 - {p_e}^3)}{3RT({p_i}^2 - {p_e}^2)} \tag{D.11}$$

Where: m = Mass contained in tube (kg)

A = Flow cross-sectional area (m^2)

L = Length of line (m)

p_i = Pressure at the inlet of the line (N/m^2)

p_e = Pressure at the exit of the line (N/m^2)

R = Gas constant (J/kg/K)

T = Temperature (K)

For an axial distance along the length of the tube, the cumulative mass is stated as

$$m = \frac{2AL}{3RT({p_i}^2 - {p_e}^2)}\left[{p_i}^3 - \left({p_i}^2 - \frac{x}{L}({p_i}^2 - {p_e}^2)\right)^{\frac{3}{2}}\right] \tag{D.12}$$

Where: m = Mass contained in tube (kg)

A = Flow cross-sectional area (m^2)

L = Length of line (m)

R = Gas constant (J/kg/K)

T = Temperature (K)

p_i = Pressure at the inlet of the line (N/m^2)

p_e = Pressure at the exit of the line (N/m^2)

x = Axial location (m)

Next flow through the solenoid valves must be simulated, which is accomplished with conventional orifice flow equation with a discharge coefficient of 0.6 and by assuming that the flow is isentropic. First the pressure ratio across the orifice is determined by checking the following relationship.

$$\frac{p_u}{p_d} \geq \left(\frac{2}{\gamma+1}\right)^{\frac{\gamma}{\gamma-1}} \tag{D.13}$$

Where: p_u = Upstream pressure of orifice (N/m^2)

p_d = Downstream pressure of orifice (N/m^2)

γ = Ratio of specific heats (-)

If this statement is false and the pressure ratio is less than the term on the right hand side, then the flow is unchoked and mass flow rate through the orifice is given by

$$\dot{m} = \frac{C_d A p_u}{\sqrt{RT}} \left(\frac{p_d}{p_u}\right)^{\frac{1}{\gamma}} \sqrt{\frac{2\gamma}{\gamma-1}\left[1 - \left(\frac{p_d}{p_u}\right)^{\frac{\gamma-1}{\gamma}}\right]} \tag{D.14}$$

Where: $\dot{m}$ = Mass flow rate of gas (kg/s)

C_d = 0.6, Orifice discharge coefficient (-)

A = Orifice cross-sectional area (m^2)

p_u = Pressure upstream of the orifice (N/m^2)

p_d = Pressure downstream of the orifice (N/m^2)

R = Gas constant (J/kg/K)

T = Temperature (K)

γ = Ratio of specific heats (-)

If the statement in Equation D.9 is true, then the flow is choked and the mass flow rate through the orifice is stated as

$$\dot{m} = \frac{C_d A p_u}{\sqrt{RT}} \sqrt{\gamma} \left(\frac{2}{\gamma+1}\right)^{\frac{\gamma+1}{2(\gamma-1)}} \tag{D.15}$$

Where: $\dot{m}$ = Mass flow rate of gas (kg/s)

C_d = 0.6, Orifice discharge coefficient (-)

A = Orifice cross-sectional area (m^2)

p_u = Pressure upstream of the orifice (N/m^2)

R = Gas constant (J/kg/K)

T = Temperature (K)

γ = Ratio of specific heats (-)

Flow dynamics and unsteadiness during the operation of the CSV are accounted for by considering transit times and time constants. The transit time is given by

$$\tau_t = \sqrt{\frac{16L^3 f(p_i{}^3 - p_e{}^3)^2}{9RTd(p_i{}^2 - p_e{}^2)^3}} \tag{D.16}$$

Where: τ_t = Time constant (-)

L = Length of line (m)

f = Friction factor (-)

p_i = Pressure at the inlet of the line (N/m^2)

p_e = Pressure at the exit of the line (N/m^2)

R = Gas constant (J/kg/K)

T = Temperature (K)

d = Flow diameter (m)

When the flow is laminar, the friction coefficient is given by Equation D.2 and Equation D.16 simplifies to

$$\tau_t = \frac{128L^2\mu(p_i{}^3 - p_e{}^3)}{3d^2(p_i{}^2 - p_e{}^2)} \tag{D.17}$$

Where: τ_t = Time constant (-)

L = Length of line (m)

μ = Friction factor (-)

p_i = Pressure at the inlet of the line (N/m^2)

p_e = Pressure at the exit of the line (N/m^2)

μ = Gas dynamic viscosity (N-s/m^2)

The laminar time constant for the flow is given by

$$\tau_{lc} = \sqrt{\frac{1.54L^2(p_i{}^2 + p_e{}^2)}{RT(p_i{}^2 - p_e{}^2)}} \tag{D.18}$$

Where: τ_{lc} = Laminar time constant (-)

L = Length of line (m)

p_i = Pressure at the inlet of the line (N/m^2)

p_e = Pressure at the exit of the line (N/m^2)

R = Gas constant (J/kg/K)

T = Temperature (K)

The turbulent time constant is stated as

$$\tau_{tc} = \sqrt{\frac{66.2f^{\frac{3}{2}}L^2(p_i{}^2 + p_e{}^2)}{RT(p_i{}^2 - p_e{}^2)}} \tag{D.19}$$

Where: τ_{tc} = Turbulent time constant (-)

f = Friction factor (-)

L = Length of line (m)

p_i = Pressure at the inlet of the line (N/m^2)

p_e = Pressure at the exit of the line (N/m^2)

R = Gas constant (J/kg/K)

T = Temperature (K)

BIBLIOGRAPHY

1. United States Energy Information Administration Website. www.eia.doe.gov. November 4, 2007.

2. Annual Energy Review 2006. Energy Information Administration. United States Department of Energy. Document Number DOE/EIA-0384(2006). 2007.

3. PennWell Corporation. *Oil & Gas Journal.* Volume 104.47. December 18, 2006.

4. United States Energy Information Administration. *U.S. Crude Oil, Natural Gas, and Natural Gas Liquids Reserves, 2005 Annual Report.* Document Number DOE/EIA-0216(2005). November 2006.

5. Centre International d'Information sur le Gaz Naturel et tous Hydrocarbures Gazeux (CEDIGAZ). *Natural Gas in the World.* July 2006.

6. Annual Energy Review 2005. Energy Information Administration. United States Department of Energy. Document Number DOE/EIA-0384(2005). 2006.

7. United States Energy Information Administration. International Energy Outlook 2007. Document Number DOE/EIA-0484(2007). 2007.

8. R. S. Wijetunge, C. J. Brace, J. G. Hawley, N. D. Vaughan, R. W. Horrocks, and G. L. Bird. Dynamic Behavior of a High Speed Direct Injection Diesel Engine. *SAE Transactions—Journal of Engines.* Volume 108. Paper Number 1999-01-0829. 1999.

9. C. D. Rakopoulos, E. G. Giakoumis, D. T. Hountalas, and D. C. Rakopoulos. The Effect of Various Dynamic, Thermodynamic, and Design Parameters on the Performance of a Turbocharged Diesel Engine Operating Under Transient Load Conditions. SAE Paper Number 2004-01-0926. 2004.

10. M. J. Samulski and C. C. Jackson. Effects of Steady-State and Transient Operation on Exhaust Emissions from Nonroad and Highway Diesel Engines. *SAE Transactions—Journal of Engines.* Volume 107. Paper Number 982044. 1998.

11. N. N. Clark, M. Gautam, B. L. Rapp, D. W. Lyons, M. S. Graboski, R. L. McCormick, T. L. Alleman, and P. Norton. Diesel and CNG Transit Bus Emissions Characterization by Two Chassis Dynamometer Laboratories: Results and Issues. SAE *Transactions—Journal of Fuels and Lubricants.* Volume 108. Paper Number 1999-01-1469. 1999.

12. R. M. Green. Measuring the Cylinder-to-Cylinder EGR Distribution in the Intake of a Diesel Engine During Transient Operation. *SAE Transactions—Journal of Engines.* Volume 109. Paper Number 2000-01-2866. 2000.

13. Environmental Protection Agency Website. http://www.epa.gov/otaq/invntory/overview/solutions/milestones.htm. November 10, 2007.

14. Environmental Protection Agency Website. http://www.epa.gov/history/org/origins/reorg.htm. November 10, 2007.

15. Dieselnet Website. http://www.dieselnet.com/standards/us/light.html. November 10, 2007.

16. J. E. Dec. A Conceptual Model of DI Diesel Combustion Based on Laser-Sheet Imaging. *SAE Transactions—Journal of Engines.* Volume 106. Paper Number 970873. 1997.

17. J. E. Dec and C. Espey. Ignition and Early Soot Formation in a DI Diesel Engine Using Multiple 2-D Imaging Diagnostics. SAE *Transactions—Journal of Engines.* Volume 104. Paper Number 950456. 1995.

18. J. E. Dec and E. B. Coy. OH Radical Imaging in a DI Diesel Engine and the Structure of the Early Diffusion Flame. *SAE Transactions—Journal of Engines.* Volume 105. Paper Number 960831. 1996.

19. J. E. Dec and R. E. Canaan. PLIF Imaging of NO Formation in a DI Diesel Engine. *SAE Transactions—Journal of Engines.* Volume 107. Paper Number 980147. 1998.

20. P. F. Flynn, R. P. Durrett, G. L. Hunter, A. O. zur Loye, O. C. Akinyemi, J. E. Dec, and C. K. Westbrook. Diesel Combustion: An Integrated View Combining Laser Diagnostics, Chemical Kinetics, and Empirical Validation. *SAE Transactions—Journal of Engines.* Volume 108. Paper Number 1999-01-0509. 1999.

21. J. E. Dec and P. L. Kelly-Zion. The Effects of Injection Timing and Diluent Addition on Late-Combustion Soot Burnout in a DI Diesel Engine Based on Simultaneous 2-D Imaging of OH and Soot. SAE Paper Number 2000-01-0238. 2000.

22. J. Galindo, V. Bermudez, J.R. Serrano, and J. J. Lopez. Cycle-to-Cycle Diesel Combustion Characterization During Engine Transient Operation. *SAE Transactions—Journal of Engines.* Volume 110. Paper Number 2001-01-3262. 2001.

23. C. J. Brace, A. Cox, J. G. Hawley, N. D. Vaughan, F. W. Wallace, R. W. Horrocks, and G. L. Bird. Transient Investigation of Two Variable Geometry Turbochargers for Passenger Vehicle Diesel Engines. *SAE Transactions—Journal of Engines.* Volume 108. Paper Number 1999-01-1241. 1999.

24. R. S. Wijetunge, J. G. Hawley, and N. D. Vaughan. Application of Alternative EGR and VGT Strategies to a Diesel Engine. SAE Paper Number 2004-01-0899. 2004.

25. H. Yokomura, S. Kouketsu, S. Kotooka, and Y. Akao. Transient EGR Control for a Turbocharged Heavy Duty Diesel Engine. SAE Paper Number 2004-01-0120. 2004.

26. M. J. van Nieuwstadt, I. V. Kolmanovsky, and P. E. Moraal. Coordinated EGR-VGT Control for Diesel Engines: and Experimental Comparison. *SAE Transactions—Journal of Engines.* Volume 109. Paper Number 2000-01-0266. 2000.

27. J. R. Serrano, H. Climent, F. J. Arnau, and G. Traumat. Global Analysis of the EGR Circuit in a HSDI Diesel Engine in Transient Operation. SAE Paper Number 2005-01-0699. 2005.

28. S. K. Chen and O. Yanakiev. Transient NO_X Emission Reduction Using Exhaust Oxygen Concentration-Based Control for a Diesel Engine. SAE Paper Number 2005-01-0372. 2005.

29. D. Assanis, Z. Filipi, S. Fiveland, and M. Syrimis. A Methodology for Cycle-by-Cycle Transient Heat Release Analysis in a Turbocharged Direct Injection Diesel Engine. *SAE Transactions—Journal of Engines.* Volume 109. Paper Number 2000-01-1185. 2000.

30. M. Muller, P. Olin, and B. Schreurs. Dynamic EGR Estimation for Production Engine Control. *SAE Transactions—Journal of Engines.* Volume 110. Paper Number 2001-01-0553. 2001

31. N. Clark, J. Daley, R. Nine, and C. Atkinson. Application of the New City-Suburban Heavy Duty Vehicle Route to Truck Emissions Characterization. SAE Paper Number 1999-01-1467. 1999.

32. Y. Takada, N. Takada, and N. Iida. Transient NO_X Characteristics of Freight Vehicles with EGR Systems in Real Traffic Conditions. SAE Paper Number 2005-01-1619. 2005.

33. R. S. Benson, J. D. Ledger, N. D. Whitehouse, and S. Walmsley. Comparison of Experimental and Simulated Transient Responses of a Turbocharged Diesel Engine. *SAE Transactions.* Volume 82. Paper Number 730666. 1973.

34. Z. Filipi, Y. Wang, and D. Assanis. Effect of Variable Geometry Turbine (VGT) on Diesel Engine and Vehicle System Transient Response. SAE Paper Number 2001-01-1247. 2001.

35. J. Benajes, J. M. Luján, and J. R. Serrano. Predictive Modeling Study of the Transient Load Response in a Heavy-Duty Turbocharged Diesel Engine. SAE Paper Number 2000-01-0583. 2000.

36. G. Theotokatos and N. P. Kyrtatos. Diesel Engine Transient Operation with Turbocharger Compressor Surging. SAE Paper Number 2001-01-1241. 2001.

37. C. D. Rakopoulos and E. G. Giakoumis. Parametric Study of Transient Turbocharged Diesel Engine Operation from the Second-Law Perspective. SAE Paper Number 2004-01-1679. 2004.

38. C. D. Rakopoulos, G. C. Mavropoulos, and D. T. Hountalas. Modeling the Structural Thermal Response of and Air-Cooled Diesel Engine Under Transient Operation Including a Detailed Thermodynamic Description of Boundary Conditions. SAE Paper Number 981024. 1998.

39. F. Payri, E. Reyes, and J. R. Serrano. A Model for Load Transients of Turbocharged Diesel Engines. *SAE Transactions—Journal of Engines.* Paper Number 1999-01-0225. Volume 108. 1999.

40. Z. Filipi, H. Fathy, J. Hagena, A. Knafl, R. Ahlawat, J. Liu, D. Jung, D. Assanis, H. Peng, and J. Stein. Engine-in-the-Loop Testing for Evaluating Hybrid Propulsion Concepts and Transient Emissions—HMMWV Case Study. *SAE Transactions—Journal of Commercial Vehicles.* Volume 115. Paper Number 2006-01-0443. 2006.

41. K. Park, F. Cao, D. B. Kittelson, and P. H. McMurry. Relationship Between Particle Mass and Mobility for Diesel Exhaust Particles. *Environmental Science and Technology.* Volume 37. Number 3. Pages 577-583. 2003.

42. D. L. Stivender. Development of a Fuel-Based Mass Emission Measurement Procedure. SAE Paper Number 710604. 1971.

43. J. B. Heywood. *Internal Combustion Engine Fundamentals*. McGraw-Hill. New York. 1988.

44. C. von Kuensberg Sarre, S. C. Kong, and R. D. Reitz. Modeling the Effects of Injector Nozzle Geometry on Diesel Sprays. *SAE Transactions—Journal of Engines*. Volume 108. Paper Number 1999-01-0912. 1999.

45. K. H. Goney and M. L. Corradini. Isolated Effects of Ambient Pressure, Nozzle Cavitation and Hole Inlet Geometry on Diesel Injection Spray Characteristics. *SAE Transactions—Journal of Fuels and Lubricants*. Volume 109. Paper Number 2000-01-2043. 2000.

46. H. Chaves, M. Knapp, A. Kubitzek, F. Obermeier, and T. Schneider. Experimental Study of Cavitation in the Nozzle Hole of Diesel Injectors Using

Transparent Nozzles. *SAE Transactions—Journal of Engines*. Volume 104. Paper Number 950290. 1995.

47. L. C. Ganippa, S Andersson, and J. Chomiak. Transient Measurements of Discharge Coefficients of Diesel Nozzles. *SAE Transactions—Journal of Engines*. Volume 109. Paper Number 2000-01-2788. 2000.

48. M. T. Heath. Scientific Computing, An Introductory Survey. 2nd Edition. McGraw-Hill. New York. 2002.

49. H. Schulte, M. Duerholz, and K. Wuebbeke. The Contribution of the Fuel Injection System to Meeting Future Demands on Truck Diesel Engines. *SAE Transactions—Journal of Commercial Vehicles.* Volume 99. Paper Number 900822. 1990.

50. T. Aoyama, J. Mizuta, and Y. Oshima. NO_X Reduction by Injection Control. *SAE Transactions—Journal of Engines*. Volume 99. Paper Number 900637. 1990.

51. K. Oberlander, K. Kollmann, M. Kramer, and I. Kutschera. The Influence of High Pressure Fuel Injection on Performance and Exhaust Emissions of a High Speed Direct Injection Diesel Engine. *SAE Transactions—Journal of Engines.* Volume 98. Paper Number 890438. 1989.

52. J. R. Needham, M. P. May, D. M. Doyle, S. A. Faulkner, and H. Ishiwata. Injection Timing and Rate Control—A Solution for Low Emissions. *SAE Transactions—Journal of Engines*. Volume 99. Paper Number 900854. 1990.

53. T. Shimada, T. Shoji, and Y. Takeda. The Effect of Fuel Injection Pressure on Diesel Engine Performance. *SAE Transactions—Journal of Engines*. Volume 98. Paper Number 891919. 1989.

54. M. Bakenhus, and R. D. Reitz. Two-Color Combustion Visualization of Single and Split Injections in a Single-Cylinder Heavy-Duty D.I. Diesel Engine Using an Endoscope-Based Imaging System. *SAE Transactions—Journal of Engines*. Volume 108. Paper Number 1999-01-1112. 1999.

55. Y. Chi, J. Cheong, C. Kim, and K. Choi. Effects of VGT and Injection Parameters on Performance of HSDI Diesel Engine with Common Rail FIE System. *Diesel Fuel Injection and Sprays 2002*. Special Publication Number SP-1696. SAE Paper Number 2002-01-0504. 2002.

56. D. J. Timoney, and W. J. Smith. Correlation of Injection Rate Shapes with D.I. Diesel Exhaust Emissions. *SAE Transactions—Journal of Fuels and Lubricants*. Volume 104. Paper Number 950214. 1995.

57. M. F. J. Brunt and A. L. Emtage. Evaluation of Burn Rate Routines and Analysis Errors. SAE Paper Number 970037. 1997.

58. M. F. J. Brunt, H. Rai and A. L. Emtage. The Calculation of Heat Release Energy from Engine Cylinder Pressure Data. *SAE Transactions—Journal of Engines.* Volume 107. Paper Number 981052. 1998.

59. M. F. J. Brunt and K. C. Platts. Calculation of Heat Release in Direct Injection Diesel Engines. SAE Paper Number 1999-01-0187. 1999.

60. F. G. Chmela, and G. C. Orthaber. Rate of Heat Release Prediction for Direct Injection Diesel Engines Based on Purely Mixing Controlled Combustion. SAE Paper Number 1999-01-0186. 1999.

61. J. A. Gatowski, E. N. Balles, K. M. Chun, F. A. Nelson, J. A. Ekchian, and J. B. Heywood. Heat Release Analysis of Engine Pressure Data. *SAE Transactions.* Volume 93. Paper Number 841359. 1984.

62. B. M. Grimm and R. T. Johnson. Review of Simple Heat Release Computations. SAE Paper Number 900445. 1990.

63. S. C. Homsy and A. Atreya. An Experimental Heat Release Rate Analysis of a Diesel Engine Operating Under Steady State Conditions. *SAE Transactions—Journal of Engines.* Volume 106. Paper Number 970889. 1997.

64. T. K. Jensen and J. Schramm. A Three-Zone Heat Release Model for Combustion Analysis in a Natural Gas SI Engine. Effects of Crevices and Cyclic Variations on UHC Emissions. SAE Paper Number 2000-01-2802. 2000.

65. R. B. Krieger and G. L. Borman. The Computation of Apparent Heat Release for Internal Combustion Engines. ASME Paper No. 66-WA/DGP-4. *ASME Proceedings of Diesel Gas Power*. 1966.

66. C. D. Rakopoulos and D. T. Hountalas. Net and Gross Heat Release Rate Calculations in a DI Diesel Engine Using Various Heat Transfer Models. *Thermodynamics and the Design, Analysis, and Improvement of Energy Systems.* Vol. 33. 1994.

67. P. J. Shayler, M. W. Wiseman, and T. Ma. Improving the Determination of Mass Fraction Burnt. SAE Paper Number 900351. 1990.

68. G. F. Hohenberg. Advanced Approaches for Heat Transfer Calculations. *SAE Transactions.* Volume 88. Paper Number 790825. 1979.

69. C. Olikara and G. L. Borman. A Computer Program for Calculating Properties of Equilibrium Combustion Products with Some Applications to I.C. Engines. SAE Paper Number 750468. 1975.

70. M. K. Martin and J. B. Heywood. Approximate Relationships for the Thermodynamic Properties of Hydrocarbon-Air Combustion Products. *Combustion Science and Technology*. Vol. 15. Pages 1-10. 1977.

71. W. J. D. Annand. Heat Transfer in the Cylinders of Reciprocating Internal Combustion Engines. *Proceedings of the Institution of Mechanical Engineers*. Volume 177(36). Pages 973-990. 1963.

72. W. J. D. Annand and T. H. Ma. Instantaneous Heat Transfer Rates to the Cylinder Head Surface of a Small Compression-Ignition Engine. *Proceedings of the Institute of Mechanical Engineers*. Volume 185(72/71). Pages 976-987. 1970-1971.

73. W. J. D. Annand and D. Pinfold. Heat Transfer in the Cylinder of a Motored Reciprocating Engine. SAE Paper Number 800457. 1980.

74. J. C. Dent and S. J. Suliaman. Convective and Radiative Heat Transfer in a High Swirl Direct Injection Diesel Engine. *SAE Transactions*. Volume 86. Paper Number 770407. 1977.

75. G. Eichelberg. Some New Investigation on Old Combustion Engine Problems. *Engineering*. Volume 148. Pages 463-446, 547-560. 1939.

76. K. Elser. Instationare Warmeubertragung bei Periiodisch Adiabater Berdichung Turbulenter Gase. *VDI Forsch. Ing-Wessen*. Volume 21(3). Pages 65-74. 1955.

77. S. B. Han, Y. J. Chung, Y. J. Kwon and S. Lee. Empirical Formula for Instantaneous Heat Transfer Coefficient in Spark Ignition Engine. SAE Paper Number 972995. 1997.

78. A. A. Kornhauser and J. L. Smith Jr. Application of a Complex Nusselt Number to Heat Transfer During Compression and Expansion. *ASME*. Volume 116. Pages 536-542. 1994.

79. T. Lefeuver, P. A. Myers, and O. A. Uyehara. Experimental Instantaneous Heat Fluxes in a Diesel Engine and Their Correlation. *SAE Transactions*. Volume 78. Paper Number 690464. 1969.

80. W. Nusselt. Der Warmeubergang in der Verbrenungskraftmaschene. *Z. Verdt. Ing.* Volume 67. Pages 692, 708. 1923.

81. T. Oguri. On the Coefficient of Heat Transfer Between Gases and Cylinder Walls of the Spark-Ignition Engine. *Bull. JSME*. Volume 3(11). Pages 363-369. 1960.

82. V. D. Overbye, J. E. Bennethum, O. A. Uyehara, and P. A. Myers. Unsteady Heat Transfer in Engines. *SAE Transactions*. Volume **69.** Pages 461-494. 1961.

83. C. F. Taylor and T. Y. Toong. Heat Transfer in Internal Combustion Engines. *ASME*. 1957.

84. G. Woschni. A Universally Applicable Equation for the Instantaneous Heat Transfer Coefficient in the Internal Combustion Engine. *SAE Transactions*. Volume 67. Paper Number 670931. 1967.

85. C. Depcik, T. J. Jacobs, J. R. Hagena, and D. N. Assanis. Instructional Use of a Single Zone, Pre-Mixed Spark-Ignition Heat Release Simulation. *International Journal of Engineering Education.* Volume 35. Number 1. January 2007.